



COAL AND PEAT FIRES

A Global Perspective

VOLUME 1

COAL – GEOLOGY AND COMBUSTION

Edited by
GLENN B. STRACHER, ANUPMA PRAKASH,
ELIINA V. SOKOL



Coal and Peat Fires: A Global Perspective

Captions for Front Cover Photos

Top Photo: An underground coal fire being manually excavated in the Sungai Wain Nature Reserve on the Island of Borneo. Underground coal beds were ignited here in 1998 by forest fires in East Kalimantan. Photo by Alfred E. Whitehouse, 1999.

Bottom-Left Photo: A gob-pile fire started by spontaneous combustion in the Kleinkopje Colliery located in the Witbank Coalfield, South Africa. The vertical field of view is 3 m and the foreshortened horizontal field of view is 9 m. Photo by Robert B. Finkelman, 2004.

Bottom-Middle Photo: Surface expression of an underground coal fire in the Carbonera Formation; burning in the Lobatera Mine in Táchira State, western Venezuela. The horizontal field of view is about 120 cm. Photo by Manuel Martínez, 2007; courtesy of Gonzalo Márquez and Manuel Martínez.

Bottom-Right Photo: Bituminous coal in the Raniganj Formation, ignited by spontaneous combustion; burning in the opencast Kajora Mine, Raniganj Coalfield, Burdwan, West Bengal, India. The maximum thickness of the exposed seam is approximately 2 m. Most coal seams in the Raniganj Formation are 4-5 m thick. Photo by Prasun Gangopadhyay, 2006.

Coal and Peat Fires: A Global Perspective

Volume 1: Coal – Geology and Combustion

Edited by

Glenn B. Stracher

*Division of Science and Mathematics, University System of Georgia, 131 College Circle,
Swainsboro, Georgia 30401 USA*

Anupma Prakash

*Geophysical Institute, University of Alaska Fairbanks, 903 Koyukuk Drive, Fairbanks,
Alaska 99775 USA*

Ellina V. Sokol

*Institute of Geology and Mineralogy, Siberian Branch of the Russian Academy of Sciences,
pr. Koptyuga, 3, Novosibirsk 630090 Russia*



ELSEVIER

Amsterdam – Boston – Heidelberg – London – New York – Oxford – Paris
San Diego – San Francisco – Singapore – Sydney – Tokyo

Elsevier
Radarweg 29, PO Box 211, 1000 AE Amsterdam, The Netherlands
The Boulevard, Langford Lane, Kidlington, Oxford OX5 1GB, UK

First edition 2011

Copyright © 2011 Elsevier B.V. All rights reserved

No part of this publication may be reproduced, stored in a retrieval system or transmitted in any form or by any means electronic, mechanical, photocopying, recording or otherwise without the prior written permission of the publisher

Permissions may be sought directly from Elsevier's Science & Technology Rights Department in Oxford, UK: phone (+44) (0) 1865 843830; fax (+44) (0)1865 853333; email: permissions@elsevier.com. Alternatively you can submit your request online by visiting the Elsevier web site at <http://elsevier.com/locate/> permissions, and selecting Obtaining permission to use Elsevier material

Library of Congress Cataloging-in-Publication Data

A catalog record for this book is available from the Library of Congress

British Library Cataloguing in Publication Data

A catalogue record for this book is available from the British Library

ISBN: 978-0-444-52858-2

For information on all Elsevier publications
visit our website at elsevierdirect.com

Printed and bound in United Kingdom

10 11 10 9 8 7 6 5 4 3 2 1

Working together to grow
libraries in developing countries

www.elsevier.com | www.bookaid.org | www.sabre.org

ELSEVIER

BOOK AID
International

Sabre Foundation

Dedication

We dedicate this four-volume book to Janet L. Stracher whom we love and admire for her kindness to strangers, devotion to family and friends, and her love of nature. Her inspiration and guidance throughout our undertaking of this monumental project assured its completion.

This page intentionally left blank

Preface

COAL AND PEAT FIRES: A GLOBAL PERSPECTIVE, Volumes 1–4, is a comprehensive collection of diverse and pioneering work in coal and peat-fires research conducted by scientists and engineers around the world. It contains hundreds of magnificent color photographs, tables, charts, and multimedia presentations. Explanatory text is balanced by visually impressive graphics.

This work is devoted to all aspects of coal and peat fires. It contains a wealth of data for the research scientist, while remaining comprehensible to the general public interested in these catastrophic fires. Amateur and professional mineralogists, petrologists, coal geologists, geophysicists, engineers, environmental and remote sensing scientists, and anyone interested in coal and peat mining and coal and peat fires will find these four volumes useful. Although the technical level varies, the science-attentive audience will be able to understand and enjoy major portions of this work.

The four volumes are also a valuable source of information about the socioeconomic and geoenvironmental impacts of coal and peat fires. As an example, the mineral, creosote, and select-gas analyses presented will be of great interest to environmental scientists, academicians, people employed in industry, and anyone interested in pollution and the by-products of combustion.

The contents of this work can be used to design and teach courses in environmental science and engineering, coal geology, mineralogy, metamorphic processes, remote sensing, mining engineering, fire science and engineering, etc. A variety of case studies on a country by country basis, including prehistoric and historic fires, encompass a wide range of geoscience disciplines including mineralogy, geochemical thermodynamics, medical geology, numerical modeling, and remote sensing, making this work a cutting edge publication in “global coal and peat-fires science.”

Volume 1 before you contains 19 chapters illustrated in full color. Chapter 1 discusses the origin of coal and coal fires. Chapter 2 discusses the techniques used for mining coal in addition to coal fires that occur in association with such mining. In Chapter 3, the connection between spontaneous combustion and coal petrology is discussed. Chapter 4 is about the utilization of coal by ancient man. Geotechnical and environmental problems associated with burning coal are discussed in Chapter 5. The general effects of coal fires that are burning around the world are discussed in Chapter 6, and Chapter 7 examines the environmental and human-health impacts of coal fires. Chapter 8 is devoted to explaining the analytical method of gas chromatography used to analyze samples of coal-fire gas collected in the field. Numerous complex processes associated with the nucleation of minerals from coal-fire gas are presented in Chapter 9, and in Chapter 10 the analytical methods used to identify such minerals are discussed. Chapter 11 presents a synopsis of the analytical procedures used to identify the semivolatile hydrocarbons that nucleate from coal-fire gas. In Chapter 12, the magnetic signatures recorded by rocks and soils affected by the heat energy from burning coal are examined. Chapter 13 presents a synopsis of the historical utilization of airborne thermal infrared imaging for examining coal fires, and in Chapter 14 a more in-depth synopsis of the use of remote sensing technology for studying coal fires is presented. In Chapter 15, the historical and political implications for US government policy regarding coal fires are presented. The former US Bureau of Mines role in controlling coal fires in abandoned mines and spoils piles is presented in Chapter 16. Chapters 17 and 18, respectively, present engineering fire-science studies of combustion phenomena and the suppression of smoldering coal fires. Volume 1 concludes with Chapter 19, in which the use of compressed-air-foam injection for extinguishing coal fires is discussed.

Volume 2 presents hundreds of color photos of coal and peat fires burning around the world as well as multimedia presentations that include movies, radio talk shows, and presentations given at professional meetings. Volume 3 presents case studies about fires on a country by country basis. Volume 4 is devoted to all aspects of peat and peat fires. An online interactive world map of coal and peat fires is designed to complement all four volumes.

The editors of this four-volume book believe that scientists and engineers as well as the general public will find that the information presented herein reveals the complexity of coal and peat-fires science, the effects of these fires, and useful methods for investigating them. We hope that the information presented will create global awareness about these fires and trigger new research ideas and methods for studying them, accelerate efforts to mitigate and extinguish them, and build a better-living environment in mining areas around the world.

Acknowledgments

We thank all contributors to *Coal and Peat Fires: A Global Perspective*, Volumes 1–4, for the submission of their research results, photos, and multimedia materials for publication. We are grateful for the necessary permission granted for publication by select institutions that some of our contributors work for. The valuable assistance of Guest Editor Rudiger Gens with developing the interactive online world map of coal and peat fires and Guest Editor Guillermo Rein with developing Volume 4 is much appreciated. We also thank all our colleagues who helped with peer review of the contents. In addition, we thank Anita Koch, Linda Versteeg, Mageswaran Babusivakumar, Greg Harris, Mónica Mendoza, and others at Elsevier who assisted in the publication of this work.

Glenn B. Stracher
Anupma Prakash
Ellina V. Sokol

This page intentionally left blank

Contents

Volume 1: Coal – Geology and Combustion

Volume 2: Photographs and Multimedia Tours

Volume 3: Case Studies – Coal Fires

Volume 4: Peat – Geology, Combustion, and Case Studies

On Line: Interactive World Map of Coal and Peat Fires by Rudiger Gens

Captions for Front Cover Photos	ii
Dedication	v
Preface	vii
Acknowledgments	ix
List of Contributors	xix
Chapters	
1. Coal Formation and the Origin of Coal Fires	1
<i>Ann G. Kim</i>	
1.1. The Formation of Coal	2
Introduction	2
Geologic Distribution of Coal Seams	3
Coal Swamps	5
Cyclothem	5
Coalification	6
Coal Composition	10
1.2. Origin of Coal Fires	15
Introduction	15
Incidence of Coal Fires	16
Ignition and Propagation of Coal Fires	16
Control of Coal Fires	19
Conclusions	22
Acknowledgments	23
Important Terms	23
References	24
WWW Addresses: Additional Reading	28
2. Coal-Mining Techniques and Coal Fires	29
<i>Stanley R. Michalski</i>	
2.1. Brief History of Coal Mining	30
Introduction	30
Evolution of Coal Mining	30
Coal-Mining Techniques	31
Coal-Mining Machines	32
2.2. Underground Coal Mining	33
Underground Mining	33
Methods of Coal Mining	34
The Special Case of Anthracite Mining	36
Ventilation	36
2.3. Surface Coal Mining	37
Surface Mining	37

Contour Mining	37
Area Mining	38
Auger Mining	38
Mountain Top Removal	38
2.4. Coal Mining and Coal Fires	39
Discovery and Investigation	39
Monitoring	39
Mine Atmosphere	40
Abatement	41
Acknowledgments	42
Important Terms	43
References	44
WWW Addresses: Additional Reading	45
3. Spontaneous Combustion and Coal Petrology	47
<i>Maria Mastalerz, Agnieszka Drobniak, James C. Hower, Jennifer M.K. O'Keefe</i>	
3.1. Spontaneous Combustion and Coal Petrology	48
Introduction	48
Maceral Composition of Coal	48
Inorganic Matter in Coal	50
Microlithotypes	54
Lithotypes	54
Coal Rank	55
Coal Petrology and Spontaneous Combustion	56
Important Terms	60
References	61
WWW Addresses: Additional Reading	62
4. Coal and Ancient Man: Cremation at the Tschudi Burn, Chan Chan, Northern Peru	63
<i>William E. Brooks, Cesar G. Mora, John C. Jackson, John P. McGeehin, Darden G. Hood</i>	
4.1. Coal and Ancient Man	64
Introduction	64
Coal in Peru	64
Chan Chan	65
Metallurgical Furnace or Crematorium	66
Temperature of the Tschudi Burn	66
Calcium in the Soil	67
Sulfur in the Soil	68
Fuel Ash Chemistry	68
Oxide and Trace Element Data	69
¹⁴ C Date	74
Cremation in Society	74
Fuel for Cremation	75
Cremation at the Tschudi Burn	76
Discussion	77
References	78
WWW Addresses: Additional Reading	81
5. Geotechnical and Environmental Problems: Coal and Spontaneous Combustion	83
<i>Laurance J. Donnelly, Fred G. Bell</i>	
5.1. Geotechnical and Environmental Problems	84
Introduction	84
Origin of Spontaneous Combustion	85
Spontaneous Combustion: Life and Human Health	85
Coal Seam and Colliery-Spoil Heap Fires	86
Control and Prevention of Spontaneous Combustion and Coal Fires	86
Examples of Spontaneous Combustion and Coal Fires	89
Conclusions	98
Acknowledgments	99
Important Terms	99
References	99

6. The Effects of Global Coal Fires	101
<i>Glenn B. Stracher, Tammy P. Taylor</i>	
6.1. The Global Catastrophe	102
Introduction	102
The Mining Hazard	103
Catastrophic Coal Fires	105
Discussion	109
Acknowledgments	110
Important Terms	110
References	110
WWW Addresses: Additional Reading	113
7. Environmental and Health Impacts of Coal Fires	115
<i>Robert B. Finkelman, Glenn B. Stracher</i>	
7.1. Environmental and Health Impacts of Coal Fires	116
Introduction	116
Environmental Consequences	118
Health-Related Effects	121
Discussion	122
Important Terms	123
References	123
WWW Addresses: Additional Reading	125
8. Analysis of Coal-Mine-Fire Gas	127
<i>Timothy R. Blake, Simone Meinardi, Donald R. Blake</i>	
8.1. Trace Gas Analyses	128
Introduction	128
Gas Collection	128
Sample Analyses	129
Methane System	129
CO/CO ₂ System	130
VOC System	130
Quality Control: Standards	132
Modifying	133
Important Terms	133
References	133
WWW Addresses: Additional Reading	134
9. Gas Vent Mineralization and Coal Combustion	135
<i>Glenn B. Stracher</i>	
9.1. The Origin of Gas Vent Minerals	136
Introduction	136
Mineral-Forming Processes	136
Isochemical Mineralization	136
Mass Transfer Mineralization	138
Discussion	142
9.2. Sample Collecting and Field Data	143
Introduction	143
Safety Precautions	143
GPS and Temperature Measurements	144
Mineral and Rock-Collecting Techniques	145
Gas-Collecting Techniques	147
In Situ Chemical Analyses	148
Discussion	150
Acknowledgments	151
Important Terms	151

References	151
WWW Addresses: Additional Reading	152
10. Sample Identification and Imaging of Gas-Vent Mineral Assemblages	155
<i>Paul A. Schroeder, Chris Fleisher, Glenn B. Stracher</i>	
10.1. Sample Identification and Imaging	156
Introduction	156
X-Ray Diffraction	157
Electron Microprobe	159
Short-Wave Infrared Spectroscopy	163
Other Analytical Methods	165
Comments	166
Acknowledgments	166
Important Terms	166
References	169
WWW Addresses: Additional Reading	171
11. Semivolatile Hydrocarbon Residues of Coal and Coal Tar	173
<i>Stephen D. Emsbo-Mattingly, Scott A. Stout</i>	
11.1. Source Identification	174
Source Signatures	174
Fossil Fuels	175
Carbonization	175
Lines of Evidence	177
11.2. Sample Preparation	178
Collection	178
Extraction	178
Cleanup	179
11.3. Sample Analysis	180
Introduction	180
Total Organic Carbon	180
Total Extractable Material	180
High-Resolution Hydrocarbon Scan	181
Polycyclic Aromatic Hydrocarbons	184
Saturated Hydrocarbons	188
Geochemical Biomarkers	191
11.4. Coal-Fire Residues	193
Semivolatile Hydrocarbons	193
Dominant Hydrocarbons	193
PAH Transformations	195
Saturated Hydrocarbon Residues	198
Biomarker Stability	201
Conclusions	205
Acknowledgments	205
Important Terms	205
References	207
12. Magnetic Signatures of Rocks and Soils Affected by Burning Coal Seams	209
<i>Robert S. Sternberg</i>	
12.1. Magnetic Signatures	210
Introduction	210
Field Work	211
Magnetic Anomalies	212
Magnetic Properties	214
Discussion	215
Acknowledgments	216
Important Terms	216
References	216
WWW Addresses: Additional Reading	218

13. Historical Use of Airborne Thermal Infrared Imaging for Detecting and Studying Coal Fires	219
<i>Daniel H. Vice</i>	
13.1. Airborne Thermal Infrared Imaging	220
Introduction	220
Thermal Infrared Imaging	220
Color Infrared Imaging	222
Early Use	222
Later Use	225
Depth Estimation	226
Discussion	226
Acknowledgments	227
Important Terms	227
References	227
WWW Addresses: Additional Reading	229
14. Remote Sensing of Coal Fires	231
<i>Anupma Prakash, Rudiger Gens</i>	
14.1. Remote Sensing	232
Introduction	232
14.2. Principles of Remote Sensing	233
Electromagnetic Energy and Spectrum	233
Visible and Near-Infrared Regions	234
Shortwave and Thermal Infrared Regions	235
Microwave Region	237
14.3. Remote Sensing Platforms and Sensors	239
Overview and Significance	239
14.4. Coal-Fire Parameter Extraction from Remote Sensing Images	242
Introduction	242
Crack-Density Mapping	242
Reflection-Aureole Mapping	242
Land-Cover (Coal Area) Mapping	243
Fire-Area Estimation	244
Fire-Depth Estimation	245
Subsidence Mapping	246
Greenhouse-Gas Emissions	247
14.5. Time Series Analysis and Integrated Interpretation in a GIS	248
Introduction	248
Important Terms	248
References	250
WWW Addresses: Additional Reading	252
15. The Policy Setting for Coal Fires: Indicators for Government Action	255
<i>Karen M. McCurdy</i>	
15.1. The Policy Setting for Coal Fires	256
Introduction	256
Phases in the Policy Cycle	257
Policy Innovation in the Nineteenth Century	259
Lessons for Coal Fires	264
Acknowledgments	264
Important Terms	265
References	265
16. United States Bureau of Mines—Study and Control of Fires in Abandoned Mines and Waste Banks	267
<i>Ann G. Kim</i>	
16.1. United States Bureau of Mines	268
Introduction	268
Mine-Fire Control	268
16.2. Fire-Control Projects in Abandoned Mines and Waste Banks	271
Introduction	271

Eastern Bituminous Region	271
Western United States and Alaska	272
Anthracite Coalfields	273
16.3. Characteristics of Fires in Abandoned Coal Mines and Waste Banks	277
Introduction	277
Initiation of Coal-Mine Fires	277
Geologic and Mining Factors	279
Natural Barriers	280
Discontinuous Fire Propagation	281
16.4. Locating Abandoned Mine Fires	282
Introduction	282
Mine-Fire Diagnostics	282
Geophysical Methods	288
Temperature Monitoring	290
16.5. Controlling Abandoned Mine Fires	293
Introduction	293
Burnout Control	293
Water Injection	295
Foam Injection	297
Cryogenic Slurry Injection	297
Summary	299
Acknowledgments	299
Important Terms	300
References	302
WWW Addresses: Additional Reading	304
17. Smoldering Combustion Phenomena and Coal Fires	307
<i>Guillermo Rein</i>	
17.1. Smoldering and Coal Combustion	308
Introduction	308
Overall Characteristics	308
Structure of a Smoldering Front	311
Smoldering-Coal Fires	312
Smoldering Wildfires	313
Acknowledgments	314
Important Terms	314
References	314
WWW Addresses: Additional Reading	315
18. Burning and Water Suppression of Smoldering Coal Fires in Small-Scale Laboratory Experiments	317
<i>Rory Hadden, Guillermo Rein</i>	
18.1. Burning and Suppression Experiments	318
Introduction	318
Suppression of Smoldering Coal Fires	318
Small-Scale Experimental Work	320
Conclusions	324
Acknowledgments	324
Important Terms	325
References	325
WWW Addresses: Additional Reading	326
19. Modern-Foam-Injection Technology for Extinguishing Coal Fires	327
<i>Lisa LaFosse', Mark Cummins</i>	
19.1. Modern-Foam-Injection Technology	328
Introduction	328
New Method of Foam Generation	329
Experimental Fires	329
Fire Science	331
Compressed Foam	331

Quality Control	331
New Developments	331
What the Future Holds	332
The Grand Finale	332
Important Terms	332
References	332
WWW Addresses: Additional Reading	333
Author Index	335
Subject Index	343

This page intentionally left blank

List of Contributors

Fred G. Bell, British Geological Survey, Keyworth, NG12 5GG Nottinghamshire, United Kingdom

Donald R. Blake, Department of Chemistry, University of California, Irvine, California 92697, USA

Timothy R. Blake, Department of Chemistry, University of California, Irvine, California 92697, USA

William E. Brooks, Geology and Environmental Science-5F2, George Mason University, Fairfax, Virginia 22030, USA

Mark Cummins, CAFSCO Fire Fighting Service, P.O. Box 403, Joshua, Texas 76058, USA; 135 Conveyor, Joshua, Texas 76058, USA

Laurance J. Donnelly, Wardell Armstrong LLP, 2 The Avenue, Leigh, Greater Manchester, WN7 1ES, United Kingdom

Agnieszka Drobniak, Indiana Geological Survey, Indiana University, 611 North Walnut Grove, Bloomington, Indiana 47405, USA

Stephen D. Emsbo-Mattingly, NewFields Environmental Forensics Practice, LLC., 300 Ledgewood Place, Suite 305, Rockland, Massachusetts 02370, USA

Robert B. Finkelman, Department of Geosciences, University of Texas at Dallas, Richardson, Texas 75090, USA

Chris Fleisher, Department of Geology, University of Georgia, Athens, Georgia 30602, USA

Rudiger Gens, Alaska Satellite Facility, Geophysical Institute, University of Alaska Fairbanks, Fairbanks, Alaska 99775, USA

Rory Hadden, BRE Centre for Fire Safety Engineering, School of Engineering, The University of Edinburgh, Edinburgh, EH9 3JL, United Kingdom

Darden G. Hood, MicroAnalytica, LLC, 4989 SW 74 Court, Miami, Florida 33156, USA

James C. Hower, University of Kentucky Center for Applied Energy Research, 2540 Research Park Drive, Lexington, Kentucky 40511, USA

John C. Jackson, US Geological Survey, 926A National Center, Reston, Virginia 20191, USA

Ann G. Kim, National Energy Technology Laboratory, 626 Cochran Mill Road, P.O. Box 10940, United States Department of Energy, Pittsburgh, Pennsylvania 15236, USA

Lisa LaFosse, CAFSCO Fire Fighting Service, P.O. Box 403, Joshua, Texas 76058, USA; 135 Conveyor, Joshua, Texas 76058, USA

Maria Mastalerz, Indiana Geological Survey, Indiana University, 611 North Walnut Grove, Bloomington, Indiana 47405, USA

Karen M. McCurdy, Department of Political Science, Georgia Southern University, Statesboro, Georgia 30460, USA

John P. McGeehin, US Geological Survey, 926A National Center, Reston, Virginia 20191, USA

Simone Meinardi, Department of Chemistry, University of California, Irvine, California 92697, USA

Stanley R. Michalski, GAI Consultants, 4101 Triangle Lane, Export, Pennsylvania 15632, USA

Cesar G. Mora, Instituto Nacional de Cultura, Trujillo, Peru

Jennifer M.K. O’Keefe, Department of Physical Sciences, Morehead State University, Morehead, Kentucky 40351, USA

Anupma Prakash, Geophysical Institute, University of Alaska Fairbanks, Fairbanks, Alaska 99775, USA

Guillermo Rein, BRE Centre for Fire Safety Engineering, School of Engineering, The University of Edinburgh, Edinburgh, EH9 3JL, United Kingdom

Paul A. Schroeder, Department of Geology, University of Georgia, Athens, Georgia 30602, USA

Robert S. Sternberg, Department of Earth and Environment Science, Franklin & Marshall College, Lancaster, Pennsylvania 17604, USA

Scott A. Stout, NewFields Environmental Forensics Practice, LLC., 300 Ledgewood Place, Suite 305, Rockland, Massachusetts 02370, USA

Glenn B. Stracher, Division of Science and Mathematics, East Georgia College, University System of Georgia, Swainsboro, Georgia 30401, USA

Tammy P. Taylor, Los Alamos National Laboratory, P.O. Box 1663, MS F650, Los Alamos, New Mexico 87544, USA

Daniel H. Vice, Science Department, Hazleton Campus, Hazleton, Pennsylvania 18202, USA

Volume 1

Coal – Geology and Combustion



Boyce Park, Pennsylvania



Witbank, South Africa

The Earth's crust preserves evidence for prehistoric-coal fires. Since the industrial revolution in Europe, the proliferation of such fires the world over has created numerous environmental catastrophes.



Jharia, India



Wuda Coalfield, Inner Mongolia

Photos: Steve Jones (Boyce Park Mine Fire, Pennsylvania, USA, 2002, horizontal field of view is about 1.2 m), Robert B. Finkelman (Witbank Coalfield, South Africa, 2004, horizontal field of view is about 9 m), Prasun Gangopadhyay (Jharia, Jharkhand State, India, 2006), Claudia Kuenzer (Wuda Coalfield, Inner Mongolia, 2002, horizontal field of view is about 30 cm).

This page intentionally left blank

CHAPTER 1

Coal Formation and the Origin of Coal Fires

CHAPTER CONTENTS

1.1 The Formation of Coal

- Introduction
- Geologic Distribution of Coal Seams
- Coal Swamps
- Cyclothems
- Coalification
- Coal Composition

1.2 Origin of Coal Fires

- Introduction
- Incidence of Coal Fires
- Ignition and Propagation of Coal Fires
- Control of Coal Fires
- Conclusions
- Acknowledgments
- Important Terms
- References
- WWW Addresses:
Additional Reading



Evidence for an underground coal-mine fire in Renton, Pennsylvania includes this sinkhole and the anomalous snow melt, smoke, and fumes. As pillars of coal that support the roof of an underground mine burn, the roof collapses, forming a sinkhole visible at the surface. *Photo: US Bureau of Mines, 1985.*



1.1. The Formation of Coal

Ann G. Kim

Coal seam (photo center) exposed in the New River Gorge, West Virginia.

Photo: National Park Service, <http://nps.gov/neri/NatureScience/geologicformations.htm>

Introduction

Coal formation has been described as “an inefficiency in the carbon cycle,” (Barghoorn, 1952) when carbon from plants remains in terrestrial sediments and is not recycled to the atmosphere (Figure 1.1.1). Coal is, by definition, a readily combustible rock containing more than 50% by weight and 70% by volume of carbonaceous material (Schopf, 1966). Another definition describes coal as a combustible solid, usually stratified, which originated from the accumulation, burial, and compaction of partially decomposed vegetation in previous geologic ages (Hendricks, 1945).

Coal has been used for over 3000 years, in China, in Bronze Age Europe, and by Plains Indians in America (Cassidy, 1973). During the Middle Ages, coal use became more common, for forges, kilns, and breweries, as well as domestic heating (EIA, 2002). In 1306, King Edward issued a royal decree banning the use of coal in London, but the ban was ineffective because charcoal made from wood was in short supply. The development of brick chimneys 100 years later alleviated the problem to some extent (Hessley et al., 1986). In the United States, wood was the primary fuel used by the colonists. It was abundant and relatively easy to obtain. In 1850, coal was used to fuel the steam engine and became the principal source of energy until 1950 when it was surpassed by petroleum for use in automobiles and by natural gas for home heating (Figure 1.1.2). Since 1984, coal has produced about one third of the energy consumed in the United States (EIA, 2002). And 92% of the coal mined in the United States is used to produce over 50% of our electricity (EIA, 2006). Projections by the US Department of Energy indicate that coal consumption will continue to increase as demand for electricity increases (EIA, 2008).

As of 2005, world coal consumption was 5883 million mt (metric tons) of which China consumed 2339 million mt, the United States—1086 million mt, and India—493 million mt (EIA, 2008). World coal consumption is projected to grow by 2.5% per year to 9583 million mt (EIA, 2006). In spite of the environmental problems associated with coal mining and coal use (acid mine drainage, coal fires, greenhouse gas emission, air pollution, etc.), it seems that coal will continue to be a major source of energy for the foreseeable future.

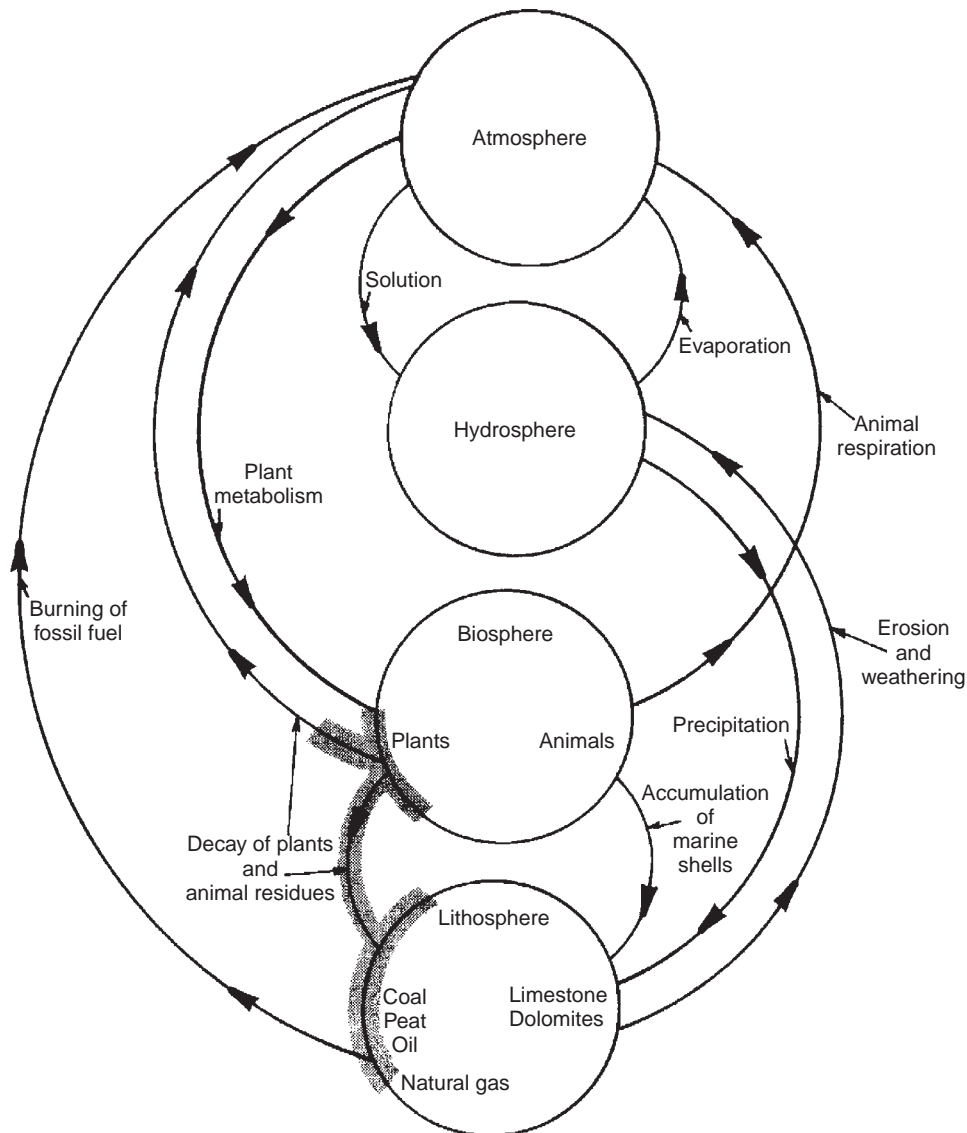


Figure 1.1.1. The carbon cycle. From Kim and Kissell 1988, p. 18.

Geologic Distribution of Coal Seams

Although coal deposits are known to have formed in every geologic period, the development of land plants in the Silurian and Devonian provided source material for peat and coal. The periods of greatest coal formation were the Carboniferous and the Cretaceous/Tertiary (Cooper and Murchison, 1969; van Krevelen, 1963).

Carboniferous Coals

The formation of coal deposits required abundant plant material, a suitable climate, areas for accumulating peat and means of preserving the carbonaceous sediment. These conditions were prevalent over large areas during the Carboniferous (Pennsylvanian in the United States) period. During this period, large areas of what is now the Eastern USA, Europe, Asia, and Australia were located near the equator and had a climate that was tropical to subtropical with mild temperatures, high humidity and heavy rainfall, without cold winters, or extended dry periods (White, 1925).

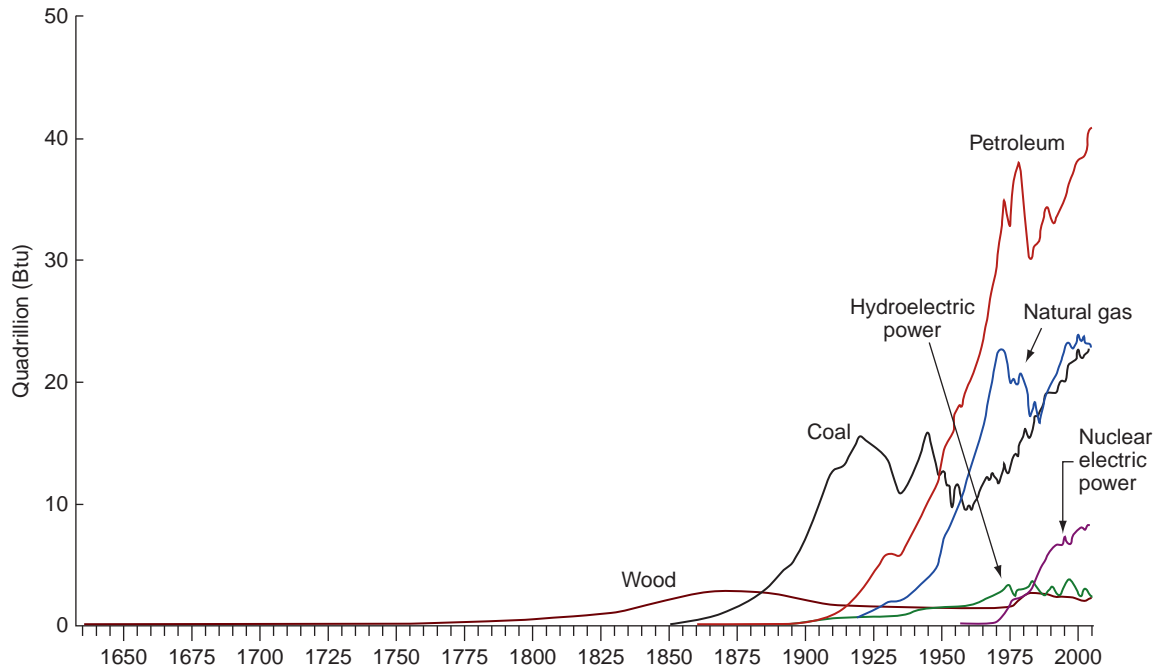


Figure 1.1.2. Energy consumption from 1635 to 2006. From EIA 2006, Figure 5.

In the early Carboniferous, coal swamps were found primarily in the low-latitude areas. In the later Carboniferous, a belt of coal swamps extended from the mid-western United States through Europe to Africa. Another coal belt extended from the Donets Basin of Russia to Morocco. In China and Mongolia, coals and interbedded marine sediments are related to the mid-Carboniferous transgression and regression of a broad seaway (Tatsch, 1980).

Terrestrial plants had been developing for 100 million years, and by the Carboniferous, plants adapted to semiaquatic or marshy areas were abundant. The majority of coal-forming plants were fern-like pteridophytes, such as the calamites (Figure 1.1.3), smaller plants, 4.5–12 m high that formed dense jungles, similar to canebrakes. The lycopodia or club mosses, lepidodendra and sigillaria, grew to over 30 m and had diameters in excess of 1.2 m. Spermatophytes of the period included cordaites, a tall slender tree that may have been an upland plant whose leaves were carried by streams into the peat swamp (Edmunds, 2002; Janssen, 1939; Kummel, 1961).

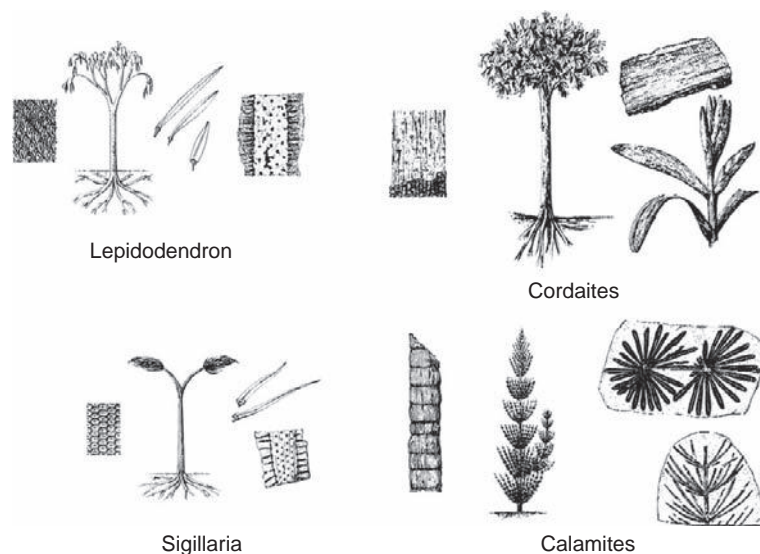


Figure 1.1.3. Carboniferous coal-forming plants. From Edmunds 2002, with permission.

Cretaceous/Tertiary Coals

Extensive deposits of Cretaceous and Tertiary coals are found in the western North America, Northeastern Russia and Siberia. They are also found in Europe, Japan, Africa, China, New Zealand, Australia, and South America. In the Western United States, a seaway extended periodically from the Arctic Ocean to the Gulf of Mexico. A seaway also connected the Barents Sea with the Tethys Ocean. In the late Cretaceous, the Tethys Seaway was also connected to the South Atlantic through the Niger Trough. An interior sea existed in central Australia in the mid-Cretaceous (McCabe and Parrish, 1992).

Cretaceous coals developed in areas where the annual precipitation exceeded evaporation. In tropical areas, rainfall was high and the humid climate preserved sediments. In higher mid-latitudes, evaporation was constrained by the cooler climate (McCabe and Parrish, 1992). In the Western United States, which has the largest volume of Cretaceous coal, wetlands developed along the margin of the retreating sea. The rising Rocky Mountains created intermontane valley swamps. A warm humid climate and isolation from the Cretaceous sea produced extremely thick, low-sulfur coals (Smith et al., 1994; WSGS, 2001).

During the early Cretaceous, conifer forests with ferns, gingophytes, and Czekanowskiales were the prevalent in the coal-forming swamps. In the middle Cretaceous, although forests remained dominated by conifers, **angiosperms** diversified and became an important component of the vegetation. In the late Cretaceous, conifers continued to dominate the coal-forming swamps, but angiosperm trees and shrubs were also important (Saward, 1992).

Coal Swamps

A site in which carbonaceous sediments could accumulate was created by erosion and the retreat of shallow seas. Broad level areas at or very near sea level, such as coastal plains, deltas, or a partially filled basins, could readily develop the marshy conditions needed for the growth of a carbonaceous swamp or mire. The consistent gradual rise in sea level or continuous slow land subsidence was required for between 1000 and 100 000 years in order to form a 10 m peat deposit which would be converted to a 1.5 m coal seam (Ashley, 1928). **Eustatic** rise in sea level, due to the melting of glaciers in the southern hemisphere, or **epeirogenic** sinking of the land would facilitate continual deposition of plant residues (Bennett, 1963; Kay and Colbert, 1965; Wanless et al., 1969).

Marshy conditions fostered the formation of peat and the preservation of the organic sediment. Under aerobic conditions, plants are rapidly decomposed to cell carbon, carbon dioxide (CO₂), and water (H₂O). In a marshy area, the movement of fresh H₂O is inhibited, and an anaerobic environment develops, slowing the rate of microbial decay and allowing carbonaceous sediments to accumulate. Toxic products also accumulate in the slow moving H₂O, decreasing microbial activity and preserving the sediments from further alteration. A rapid rise in sea level or increase in the rate of subsidence would flood the swamp, halting growth, and burying the peat under inorganic sediment.

In contrast to the slow deposition of peat, the deposition of inorganic sediments was relatively rapid, turbulent, and variable. The rocks associated with coal seams are usually fine grained clastics, particularly shales, mudstones, and siltstones. Black shales overlying many coal seams represent a gradational change as more sediment was carried into the peat swamp. Sandstones immediately above a coal seam may be related to erosion and subsequent deposition within an existing seam. Channel sands can be seen as stream erosion of an existing coal or peat deposit and deposition of sediments within the stream channel (McCullogh et al., 1975). The rate of sediment deposition within or immediately above the peat would affect the concentration of **syngenetic** minerals, while sandstones deposited above a coal seam could increase the concentration of **epigenetic** minerals.

Cyclothems

A cyclothem is a series of repeating sediments representing the transgression and regression of H₂O or the submergence and emergence of land. In coal-bearing strata, changes in depositional environment produced a cyclic repetition of beds. The cyclothem is defined as a series of beds deposited during a single sedimentary cycle.

Several “ideal” cyclothems have been defined (Kosanke et al., 1960; Weller, 1931), but, in a top-down sequence, they basically consist of shale, limestone, shale, coal, underclay, limestone, shale, and sandstone. The ideal cyclothem is typically associated unstable shelf or interior basin conditions. It represents maximum alteration of marine and nonmarine conditions, typical of western Illinois. The Southern Appalachian or Piedmont-type cyclothem is characterized by dominant continental clastic sediments, well-developed coals, and few marine beds. Alternating limestone and shale are representative of marine cyclothems, with thin sandstones and subordinate underclays and coals (Krumbein and Sloss, 1963).

Several mechanisms have been proposed for the formation of cyclothems. Diastrophic theories attribute them to sinking basins and rising source areas. Climactic theories propose that glaciations produced sea level oscillations, rainfall cycles, and variable erosion. Sedimentation theories attribute the formation of cyclothems to differential deposition related to depth of H₂O, strength of currents, distance from a river’s mouth, and compaction of sediments. It is unlikely that a single mechanism operating on a limited time span can adequately explain the development of multiple types of sedimentary cycle (Weller, 1931, 1964). In the Appalachian area, the sedimentary rocks are similar to deltaic deposits. Coal, ironstones and limestones are the chemical deposits formed in nonmarine, brackish, or marine environments. Episodes of detrital or clastic sedimentation interrupted the development of chemical deposits. The detrital rocks have a finite horizontal limit and grade laterally into chemical sediments (Ferm and Cavaroc, 1969).

Coalification

Peat formation is considered the biochemical stage of coal formation, during which plant residues are partially decomposed. The geochemical stage of **coalification** is a continuous and irreversible process that produces a rock from the organic sediment. In the long term, coalification produces progressively higher **rank** coals (ASTM, 2005) from lignite through subbituminous, high-volatile bituminous, medium-volatile bituminous, low-volatile bituminous to anthracite. Heat and pressure are the primary agents of coal metamorphism, rather than time (Figure 1.1.4). Temperature and pressure increase as a function of depth; high temperature is also related to folding and faulting and to the presence of igneous intrusions.

The first step in coalification is the removal of H₂O due to the weight of overlying sediments (Figure 1.1.5). An increase in the carbon concentration and a decrease in the hydrogen and oxygen concentrations are noted in higher rank coals (Hessley et al., 1986).

Coal macromolecules are formed from altered biopolymers in plants (Hatcher and Clifford, 1997). **Dehydroxylation**, **ether cleavage**, and **demethylation** are proposed mechanisms by which brown coal and lignite are produced from **lignin**. The removal of alkyl side chains and condensation reactions are assumed to account for increasing aromatic character. Coalification to the bituminous rank involves the reduction in oxygen content through

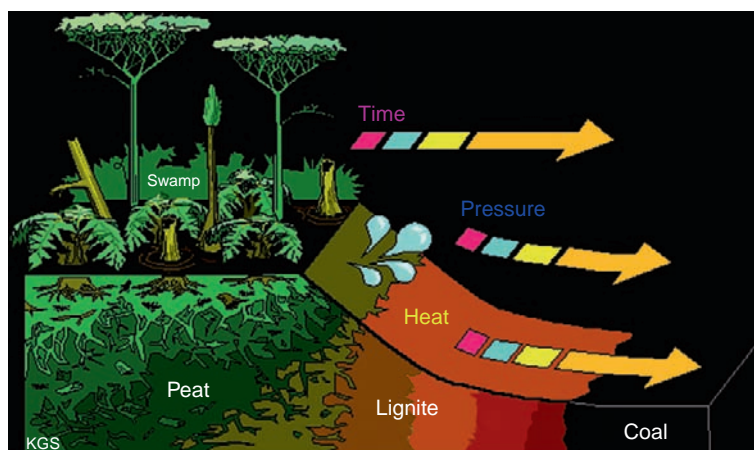


Figure 1.1.4. The transition from peat to hard coal, due primarily to heat at elevated pressures and extended periods of time. From Kentucky Geological Survey, University of Kentucky, <http://www.uky.edu/KGS/coal/>, with permission.

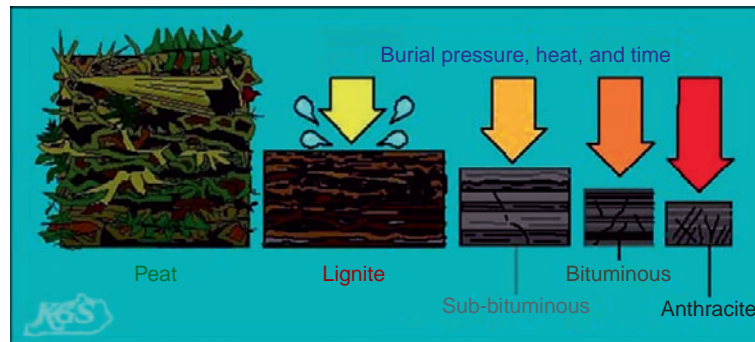


Figure 1.1.5. Increasing rank of coal due to pressure, heat, and time. From Kentucky Geological Survey, University of Kentucky, <http://www.uky.edu/KGS/coal/>, with permission.

pyrolytic condensation to form polycyclic aromatic ring structures with the loss of side chain carbons. During geochemical coalification, there is an increase in carbon content, and a decrease in the concentration of oxygen and hydrogen. Humic structures become more aromatic, and alkyl chains are split off to form CO_2 and CH_4 (Teichmuller and Teichmuller, 1967).

The increase in coal rank with increasing depth (**Hilt's Rule**) was assumed to be a function of increasing overburden pressure. Also, folding was assumed to accelerate coalification by tangential pressure. However, experimental evidence suggests that static pressure actually inhibits the chemical processes of coalification. The increase of rank with depth is as readily explained by increasing rock temperature. Increases in rank along thrust planes can be related to the frictional heating during tectonic movements. Magmatic contacts also produce local increases in rank. The maximum depth of burial and the maximum temperature to which the coal was exposed for long periods of time determine the rank of the coal. An estimate of the maximum temperature required to produce different coal ranks is given in Table 1.1.1. Coalification is a function of time only if the temperature is sufficiently high. Coals of the same rank can be produced either by short intense heating or by heating at lower temperatures for longer periods of time.

It is relatively well established that age is not a primary determinant of coal rank and that tectonic events increase the rank of coal beds. Most Pennsylvanian age coals in the Appalachian Basin and in the Interior Basin are bituminous in rank (Figure 1.1.6). The folded and faulted coals affected by the Alleghenian orogeny are anthracites. The Cretaceous coals of the Powder River Basin (PRB) in the Western United States are primarily subbituminous, while the younger Paleogene and Neogene coals affected by the formation of the Alps are bituminous to anthracite.

Table 1.1.1
Estimated temperature, depth of burial, and time required for metamorphism in normal coal series.

Coal rank	Temperature ($^{\circ}\text{C}$)		Depth of burial (m)			Time (10^6 years/transition)*
	Range*	Maximum [†]	Maximum*	Maximum [‡]	Maximum [†]	
Peat	10–20	15				67
Lignite	20–40	45	<1000	1500	1750	28
Subbituminous	40–50	80		2300	2400	4
Bituminous	50–100	175	<2100	6100	>6000	6
Anthracite	100 to >150	205	>2700	7600		1.7

* Francis (1961).

[†] White (2002).

[‡] Smith et al. (1994).

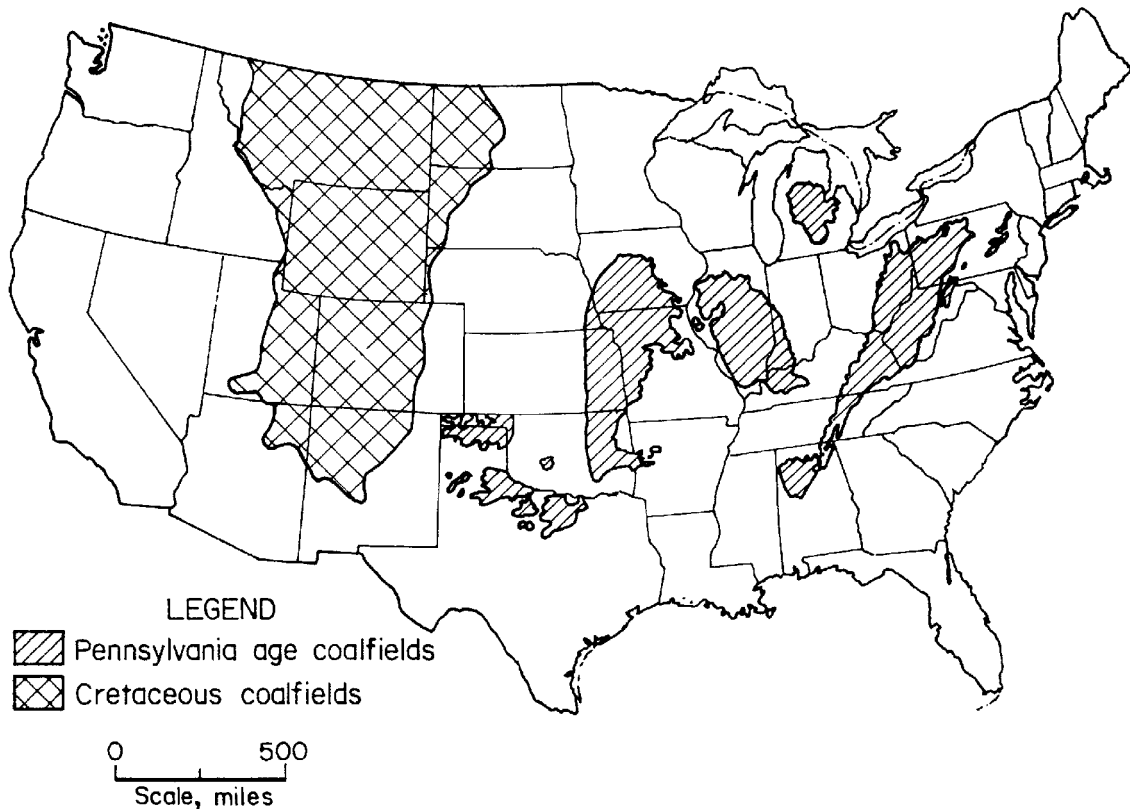


Figure 1.1.6. Location of Pennsylvanian and Cretaceous/Tertiary coalfields in the United States. Based on Kim and Chaiken (1993, p.3)

Possible Mechanisms for Increasing Coal Rank

The increased temperature necessary to increase rank is assumed to be related to depth of burial (Francis, 1961). The increased pressure and deformation during tectonic activity are presumed to have little effect on coal rank (Teichmuller and Teichmuller, 1982). The hydrothermal brines expelled from tectonic belts are currently postulated as a mechanism of anomalous heat transfer (Copard et al., 2000).

A number of authors have described increases in the maturation of coal-bearing rocks as related to a particular mechanism, i.e., depth of burial, magmatic intrusion, tectonic activity, and more recently, hydrothermal fluids. The following examples demonstrate the variety of plausible mechanisms and are not intended to be a comprehensive catalog of such studies.

Depth of Burial Paleo heat flow values and the thickness of eroded sediments in the Saar basin were evaluated with one-dimensional thermal models based on **vitrinite reflectance** and temperature data (Hertle and Littke, 2000). The thermal maturity of the sediments is explained by deep burial and moderate heat flow. The calculated heat flows imply a maximum burial of 30–40 km. The effect of volcanism on heat distribution was considered to be much less than the effect of deep burial.

In the southern part of the Lower Saxony Basin, areas of high thermal maturation had previously been attributed to magmatic intrusions (Petmecky et al., 1999). Based on numerical modeling, only deep burial and relatively low heat flow produced a satisfactory fit between measured and calculated data. The low gradient in vitrinite reflectance with depth and sedimentation rates of 170 m/m.y. support depth of burial rather than magmatic intrusion as the coalification mechanism.

Although coalification patterns in the Upper Silesian Coal Basin generally followed Hilt's Rule, deviations from it were also observed (Sivek et al., 2002). Most of the localized variations can be explained by igneous intrusions and tectonic deformation. Heat flow effects related to hydrothermal fluid migration are rare.

In a study of four widely separated coal basins, Hower and Gayer (2002) determined that coal metamorphism is generally controlled by increased temperature related to depth of burial. However, there are sufficient exceptions to this to attribute some increases in coal rank to other causes, such as igneous and tectonic activity, and to the movement of hydrothermal fluids.

Igneous Activity and Tectonism In the Illinois basin, Damberger et al. (1999) correlated the rank of most of the coal seams with maximum depth of burial. A rank increase in the coal seams of SE Illinois that exceeds the expected increase was attributed to a heating event related to a paleo-geothermal anomaly.

In Indonesia, Paleogene coals are generally bituminous in rank, while Neogene coals are subbituminous (Daulay and Cook, 2000). However, in some areas Neogene coals in geologically young basins are bituminous. In this area, increased rank is attributed to uplift and igneous intrusions.

Tectonic displacement of coal seams in China has resulted in comminution of coal in the footwall (Cao et al., 2000). Only slight differences in reflectance and other chemical properties were observed in bituminous and anthracite samples collected from undisturbed and from deformed layers. However, lower molecular weight hydrocarbon fragments were concentrated in the deformed samples, indicating that there was some modification of chemical structure due to exposure to tectonic pressure.

Isotopic ratios of authigenic clay minerals indicated that two episodic, short-lived thermal events were responsible for increases in the rank of coals in the Bowen Basin of Australia (Uysal et al., 2001). Rather than gradual temperature increase due to progressive burial, the increased maturity of the coals is related to igneous activity associated with the breakup of Gondwana.

Hydrothermal Fluids Anomalous variations in rank unrelated to depth of burial or igneous heat flow have been attributed to the transient geothermal gradients due to the migration of hydrothermal fluids (Hower and Gayer, 2002). This model suggests that coal maturation is due to long term (>10 my) burial and to short lived (1–2 my) regional high-temperature fluid flow. However, a simple causal relationship between coal metamorphism and fluid flow has not yet been demonstrated; rather a variety of parameters have been cited to support the increase in coal rank by hydrothermal fluids.

Numeric heat flow models of a transition zone between the Alps and the Pannonian Basin were used to evaluate heat flow in Paleogene and Neogene sediments (Sachsenhofer et al., 2001). Oligocene vulcanism was the main heat source for the Paleogene sediments, and magmatic activity was partially responsible for Miocene heat flow. But igneous rocks were absent in at least one area of very high heat flow, and local increases in the rank of coals may be due to migrating fluids expelled from sediments beneath the Alpine front (Sachsenhofer and Rantitsch, 1999).

Pyrite from 14 samples of lower Pennsylvanian coals of northwestern Alabama was examined by ion microprobe/SEM (Kolker et al., 1999). Epigenetic pyrite was found to be enriched with arsenic. Arsenic-rich coals are prevalent in fault zones, implying that hydrothermal fluids were limited to fault zones and that the hydrothermal activity was post coalification.

The vertical distribution of coal rank in the South Wales coalfield was found to deviate from the relationship of Hilt's Law (Fowler and Gayer, 1999). Variations in vitrinite reflectance were correlated with the intensity of tectonic deformation. The complexity of a detailed model of faults necessary to explain the vertical rank profile by post coalification faulting renders this model improbable. Shear stress, frictional heating, and localized fluid flow are considered more probable mechanisms for this vertical rank profile.

Daniels et al. (1990) collected 15 coal samples from the anthracite fields of Pennsylvania and analyzed minerals from three distinct locations with the coal: in the coal matrix, in the systematic cleat, and in a poorly mineralized nonsystematic joint set. Mineral assemblages in the three were significantly different; the differences are attributed to differences in the composition of fluids during late stage diagenesis. Enrichment in Mg and Na suggests that the minerals were derived from migrating hydrothermal fluids in the higher permeability systematic joint sets of the coal seams which acted as regional aquifers. The authors suggest that the hydrothermal fluids at temperatures between 250 and 300°C caused the increase in coal rank. Depth of burial is discounted as the primary mechanism due to the necessity of assuming that the coal was covered by 6 km of overburden, an unusually large value. Since igneous activity is absent in this region, the heat flow necessary to produce anthracite would have to have come from another source.

Experimental Studies of Coalification

Vitrinite reflectance ($R_{v\max}\%$, $R_0\%$) is the percentage of light reflected from the surface of polished vitrinite. It is a standard measurement used to classify organic rocks, and standard values are associated with various ranks of coal (Table 1.1.2).

According to Cooper (1996), the time–temperature index (TTI method), based on both laboratory studies and observations of reflectance and temperature in drill holes, assumes that vitrinite reflectance doubles for every 10°C increase in temperature. The reflectance of vitrinite is affected by the chemical reorganization of aromatic groups associated with the liberation of reactants (namely, O and H). From these experiments, Burnham and Sweeney (1989) have derived the following equation relating changes in vitrinite reflectance to changes in major element concentration:

$$R_0\% = 12 \exp \left[-3.3 \left(\frac{H}{C} \right) \right] - \left(\frac{O}{C} \right).$$

In artificial maturation experiments on one humic coal, samples were heated isothermally for 24 h at temperatures between 200 and 800°C (Han et al., 2001). Based on vitrinite reflectance, the sample maturity increased from high-volatile bituminous ($R_{v\max} = 0.77\%$) to anthracite ($R_{v\max} = 5.02\%$). The process is characterized by two fast reaction phases and two slow reaction phases. The first fast phase occurs at 0.9% vitrinite reflectance and is associated with the removal of attached fragments from aromatic rings. The second fast phase coincides with the late anthracite increase in reflectance. The increase in maturity was attributed to the temperature dependent breakage of C–C bonds and the generation of gaseous hydrocarbons.

In another laboratory experiment, the change in vitrinite reflectance was determined over a pressure range of 0.5–20.0 kbar at temperatures between 200 and 350°C (Dalla Torre et al., 1997). The results indicated that applied pressure suppressed increases in vitrinite reflectance.

Coal Composition

The composition of coal can be described by its components, by the elemental concentrations, and by macroscopic and microscopic composition.

Table 1.1.2
Coals by rank and vitrinite reflectance (% R_0).

Coal rank		Range*	Random†	Maximum†	Minimum‡
Class	Group				
Anthracite	Meta-anthracite				
	Anthracite		6.55	7.00	2.50
	Semianthracite		2.65	2.83	1.92
Bituminous	Low volatile		1.85	1.97	1.51
	Medium volatile	1.00–1.40	1.49	1.58	1.12
	High volatile	0.3–1.00			0.5
Subbituminous		<0.40–0.6	0.60	0.63	0.42
Lignite			0.40	0.42	

* Pearson Coal Petrography.

† White. (2002).

‡ Smith et al. (1994).

Proximate Composition

On a **proximate** basis, coal is composed of moisture, mineral matter, volatile matter, and fixed carbon (Table 1.1.3) (ASTM, 2007; Hessley et al., 1986). Although one of the first effects of coalification is removal of H₂O, some physically and chemically bound H₂O remains in coal. Volatile matter includes gases that are released by thermal decomposition (pyrolysis) of coal, such as hydrogen, carbon monoxide (CO), methane, and other hydrocarbons, tar vapors, ammonia, CO₂, and H₂O vapor other than residual moisture. The fixed carbon is the solid combustible material in coal, the nonvolatile organic portion. It is estimated by difference, subtracting the percentages of moisture, ash, and volatile matter from 100. The heating value and rank of the coal increase with increased fixed carbon content (Figure 1.1.7). On a practical basis, coals are usually compared on a moisture and mineral matter-free (mmmf) or dry ash-free (daf) basis.

Table 1.1.3
Examples of variation in proximate composition (wt.%) and calorific value (MJ/kg) of coal by rank.

Coal rank	Moisture*	Ash*	Volatile Matter	Fixed Carbon	Calorific value†
Lignite‡	35.43	8.06	29.86*	26.5*	23.0
Subbituminous‡	14.74	10.97	36.42*	37.8*	33.5
Bituminous‡	6.97	7.87	43.14*	41.0*	36.0
High-volatile bituminous	6.9§	5.1	>31	<69	35.6
Medium volatile bituminous	1.5§	0.2§	31	69	36.0
Low-volatile bituminous	0.8§	1.2§	22	78	36.4
Semianthracite	0.6§	8.32 §	14	86	36.0
Anthracite	1.4§	1.6§	8	92	35.2
Meta-anthracite			<2	>98	

Note: The data should not be considered representative.

* As received.

† White (2002).

‡ White and Theisen (1913).

§ Kosanke (1952).

|| ASTM (2005).

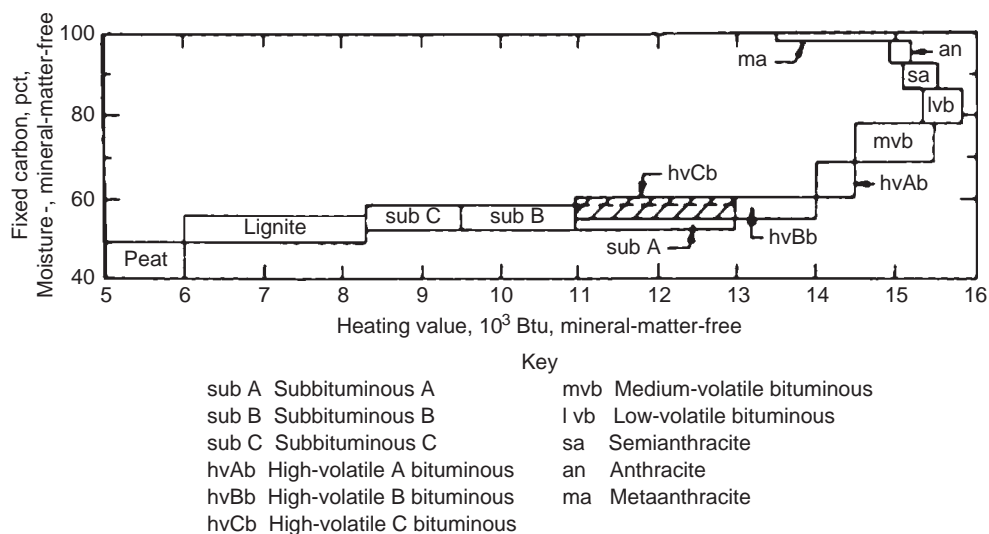


Figure 1.1.7. Progressive increase in fixed carbon and heating value for ranks of coal from peat to anthracite. From Kim and Kissell 1988, p. 19.

The mineral matter in coal, determined by low-temperature ashing or by dissolution in HF, is emplaced during or after coal formation. Minerals that are an integral part of the organic matrix are considered included minerals, while those in the cleats and fractures are termed excluded minerals. Although some of the inorganic compounds originate in the plant material, most are deposited during (**syngenetic**) or after (**epigenetic**) coalification. Syngenetic minerals can be formed by precipitation in an anoxic, aqueous medium during the biochemical stage of coalification, or they may be detrital clastics transported into the peat swamp by wind or H₂O. Epigenetic minerals are deposited within the coal seam, in cracks, fractures, and bedding planes, by migrating fluids. They may also be produced from syngenetic minerals by increased temperature and pressure. Mackowsky (1968) indicated that most of the silicates, quartz, and phosphates had been transported into the peat swamp. Carbonates, sulfides, and chalcedony from the weathering of feldspar and mica, were formed within the swamp. These minerals tended to be intimately intergrown with the organic matrix, as included minerals. Some carbonates, sulfides, and oxides were deposited in cleats and fractures; these excluded minerals are independent of the organic portion.

The quartz in 40 samples of a PRB coal was primarily detrital, but trace amounts of β -form quartz, with apatite and zircon, were attributed to air-fall and reworked volcanic ash deposited in the peat swamp (Brownfield et al., 1999). In a study of Gulf Coast lignites, enrichment of some elements was attributed to proximity to igneous rocks or to deposition of volcanic ash (Warwick et al., 1997).

Coal–mineral matter includes a variety of minor or trace elements. The concentration of these elements in coal may be greater than their average concentration in the earth’s crust (Table 1.1.4). The distribution of trace elements varies too widely to be described by a general statement. Coals from different areas may show distinctive trace element characteristics (Table 1.1.5), and within a single coal seam, the trace element distribution may not be consistent. This suggests that no single process has been responsible for the accumulation of trace elements in coal. When compared to the overlying **carbonaceous shale**, the concentration of trace elements is lower in coal, reflecting the influx of detrital inorganic sediments that eventually terminated the formation of the peat swamp (Kim, 2002).

Ultimate Composition

Ultimate analysis of coal is the determination of the carbon, hydrogen, sulfur, nitrogen, and oxygen (Table 1.1.6) (ASTM, 2002; Hessley et al., 1986). Carbon includes organic and any mineral carbonate. Hydrogen is present in the organic portion of the coal and as H₂O. Nitrogen is assumed to be part of the organic matter, and sulfur may be

Table 1.1.4
Distribution of trace elements in coal ash compared to the average concentration in the earth’s crust and shales (mg/kg).

Element	Crust	Shale	Coal	Coal ash, minimum	Coal ash, maximum
Ag	0.7	.07	<0.05	1	10
As	1.8	13	<100	100	900
B	10	100	58	86	5800
Ba	425	580	92	300	3500
Be	2.8	3	1	1	30
Co	25	19	9	30	300
Cr	100	90	20	50	400
Cu	55	45	12	20	500
Mn	950	830	85	200	1000
Mo	1.5	2.6	3	10	200
Ni	75	68	22	50	800
Pb	12.5	20	40	5	700
Sr	375	300	110	80	3500
V	135		5	100	1000
Zn	70	95	34	100	1000

Source: Based on Nicholls (1968).

Table 1.1.5
Minerals identified in coal.

Sample	Bituminous	PRB
Units	wt.% mm*	wt.% mm
No. of Samples	3	1
Quartz	12	27
Kaolinite	13	19
Illite	13	8
Montmorillonite	<1	2
Feldspar	<1	2
Silicates	27	29
Pyrite	16	1
Sulfides	<1	1
Siderite	<1	<1
Calcite	3	–
Carbonates	2	<1
Rutile/anatase	<1	3
Phosphates	<1	6

Source: After Senior et al. (2000).

PRB, Powder River Basin.

* wt.% mm = weight % of mineral matter.

Table 1.1.6
An estimate of the average ultimate composition of coal by rank (wt.%).

Coal rank	C	H	N	O
Peat	56	5.8	1.4	36
Lignite	69	4.6	1.2	25
Bituminous	86	5.4	1.6	7.5
Anthracite	94	2.5	1.0	2.3

Source: After Tatsch (1980) and Mott (1942).

organically bound, in pyrites and in inorganic sulfates. Oxygen, which can be in the organic and inorganic portions of the coal, is determined by difference. The ultimate composition of coal on a moisture and mineral matter-free (mmmf) basis is the hypothetical pure coal substance.

Macroscopic and Microscopic

On a macroscopic scale, most large coal deposits are described as banded, exhibiting layers which represent variations in the plant material or its degree of biochemical alteration. These coals are termed **autochthonous** and were formed in situ. **Allochthonous** or drift coals are those in which plant material was carried into the area of deposition. Two types of drift coals are cannel coal formed from plant spores and boghead coal formed from the remains of algae. **Drift coals** tend to be smaller deposits and have a higher concentration of mineral matter (>10%). (Hessley et al., 1986)

Stopes (1919) described banded coals by what he called **lithotypes**. Vitrain was a bright glassy band, formed from wood or bark. Clarain was a smooth interlaminated band of bright and dull coal; no specific origin was postulated. Durain was a dull black band and was very hard. In contrast, fusain was a charcoal-like band, porous, friable, and frequently containing mineral matter.

On a microscopic scale, three **macerals**, the organic equivalent of minerals (Stopes, 1935), were identified: vitrinite, exinite, and inertinite. Vitrinite, typically shiny and glassy, is the coalified remains of cell walls, woody tissue of stems, branches, leaves and roots of plants, and the precipitated gels from these materials. In white light, vitrinite is a pale-gray to white. It is the predominant maceral in coal, and is the only important component of vitrain. It has a relatively high concentration of oxygen and a moderate amount of hydrogen and volatile matter. Exinite was formed from waxy resinous debris, and is divided into sporinite, alginite, resinite, and cutinite. It is rich in hydrogen and is primarily aliphatic. Inertinite, the third maceral, is formed from oxidized wood or bark. It is aromatic and has low-volatile matter content. The relatively unreactive inertinite which forms fusain is made up of macrinite and micrinite, massive or granular residues of protoplasm. Also, fusinite is oxidized woody tissue in which the cell structure is still visible, semifusinite is less oxidized, and sclerotinite is formed from fungal remains (Petraakis and Grandy, 1980).

The preceding information on coal, how it is formed and its composition, is intended as a general overview. For more detailed information, consult the listed references.



1.2. Origin of Coal Fires

Sinkholes such as this one due to an underground mine fire in Renton, Pennsylvania may develop without warning, resulting in injury or death.

Photo: US Bureau of Mines, 1985.

Introduction

Coal fires in abandoned mines, in waste banks, and in unmined outcrops constitute serious safety and environmental hazards. Subsidence, the emission of toxic fumes, and deterioration in air quality create an unsafe and unpleasant atmosphere that can consume resources and depress property values for affected land and for adjacent areas. Fires in abandoned mines and waste banks often affect people who had no connection with the original mining.

Coal fires occur in almost every coal-bearing area and have been a problem for hundreds of years. In 1765, a fire was started in the Pittsburgh seam in Pennsylvania. This fire was active until at least 1846 (Eavenson, 1938, 1942). In the Western United States, coal-outcrop fires were a natural feature of the landscape. In 1805, Lewis and Clark, in their exploration of the Missouri River, reported that coal seams were plainly visible in the bluffs along the river and that some of the veins were burning, ignited by spontaneous combustion or by grass fires (Lavender, 1988, pp. 190, 196). In southeastern Montana, an outcrop fire in a 6 m (~20 ft) thick seam has propagated ~1524 m (5000 ft) along a small drainage basin. The fire has affected a total area of 500 acres and has been burning for an estimated 400–600 years (Shellenberger and Donner, 1979). Hundreds of natural coal-bed fires are burning in the PRB. The age of zircons in associated clinker indicates that such fires have been occurring in this area for thousands of years (Heffren et al., 2007). Coal fires associated with the abandoned or inactive coal mines are reported from mining areas around the world (Prakash and Gupta, 1999; Stracher and Taylor, 2004). Surface expressions of underground coal fires observable in the field include baked rocks, areas of dead vegetation, land subsidence, and gas vents and fissures with encrusted minerals (Gupta and Prakash, 1998; Stracher, 2007).

Incidence of Coal Fires

Recent studies have indicated that uncontrolled coal fires are a global problem. In addition to the inherent health and safety problems, such fires are believed to contribute to greenhouse gas emissions. Over 1% of the global emission of CO₂ from fossil fuels is believed to be generated by coal fires in China (Rosema et al., 1999; Stracher and Taylor, 2004; Voigt et al, 2004).

In the United States, fires in abandoned mines and in outcrops, termed wasted coal fires, have occurred during the past 200 years. Since 1950, there have been over 600 coal-related fires in the United States (Johnson and Miller, 1979). As of 2005, 141 fire-control projects on abandoned mine lands (AMLs) were listed on the Office of Surface Mining Reclamation and Enforcement's Inventory (OSMRE, 2005). This is an underestimate of the actual number of fires because many that occur are not associated with coal mining. In the United States, most underground mine fires are in the eastern coal-producing states. The characteristics of eastern fires vary depending upon whether they are in bituminous or anthracite seams. Waste bank fires occur in the eastern and central states where the majority of coal-preparation plants were located. Outcrop fires in inactive or unmined deposits are more prevalent in the Western United States.

Currently, coal fires are a serious problem in the Jharia coalfield of India and the Wuda coalfield in Inner Mongolia. Fires are also a problem in Indonesia, New Zealand, South Africa, Australia, Siberia, and other parts of the world (Masalehdani et al., 2007; Michalski, 2004; Sokol and Volkova, 2007; Stracher, 2007; Whitehouse and Mulyana, 2004). In addition to the loss of energy resources, coal fires are a source of CO₂ and other air pollutants. They may cause subsidence, ignite forest fires, and can create a health hazard due to airborne dust, acid gases, and potentially toxic trace elements and organic compounds (Finkelman, 2004). Uncontrolled burning of coal can create problems from an unpleasant atmosphere to the destruction of property to the devastation of ecosystems.

Ignition and Propagation of Coal Fires

As with any fire, coal fires require three elements: fuel, oxygen, and an ignition source (Figure 1.2.1). In coal combustion, the fuel is the carbon in the coal. If combustion is considered the **exothermic** reaction of carbon and oxygen to form CO₂, written as



the amount of heat liberated is 93.7 kcal/mol.

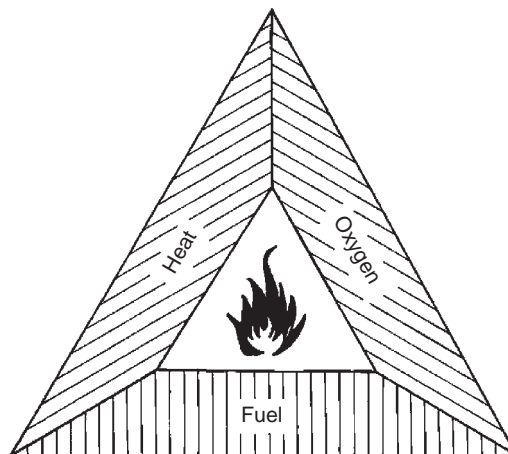


Figure 1.2.1. Fire triangle showing the three essential elements for any fire: fuel, oxygen, ignition source. From Kim and Chaiken 1993, p. 6.

However, coal is not composed of elemental carbon. On a dry, mineral matter free basis, coal contains between 60 and 90% carbon. The rest of the coal “molecule” is composed of hydrogen, oxygen, nitrogen, and sulfur. For example, the stoichiometric combustion of coal can be written as (Chaiken, 1977):



This reaction produces 138.4 kcal/mol. Combustion reactions are exothermic. Depending on the rank of the coal, combustion produces from 5 to 10 kcal/g of coal or between 6 and 16 000 Btu/lb.

The oxidation of coal occurs constantly. The temperature of the coal is a function of the rate of heat generation versus the rate of heat loss. Since the rate of heat generation is an exponential function of temperature and the rate of heat loss is a linear function of temperature, as the temperature increases, the reaction rate increases faster than the heat loss (Kanury, 1975). Ignition is a function of the amount of energy released by a reaction and the rate at which it is released, as well as the rate at which energy is transferred from the reacting mass to the surroundings. The reaction rate is a function of the concentration of reactants, carbon and oxygen, the surface area, particle size, temperature, and activation energy.

Sources of Ignition

There are two types of ignition: forced and spontaneous. Forced ignition sources include lightning, brush and forest fires, improperly controlled man-made fires and spontaneous combustion in adjacent materials like trash. Spontaneous combustion in coal or coal refuse is related to the oxidation of the coal to form CO_2 , CO , and H_2O (Kim, 1977). Spontaneous combustion may be the initial cause of a fire which is then spread by conduction or convection to other areas of a mine (Banerjee, 1985; CMRS, 1991).

The oxidation of pyrite and the adsorption of H_2O on the coal surface also are exothermic reactions that increase the probability of spontaneous combustion. Thermophilic bacteria may also contribute to raising the temperature of the coal (Chaiken et al., 1983).

Factors Favoring Propagation of Coal Fires

An abandoned mine or waste bank is a physical environment that favors the accumulation of heat. In bituminous-coalfields, the depth of overburden, the degree of fracturing, and the nature of the overlying strata are the primary geologic factors (Dalverny and Chaiken, 1991).

In underground mines that used a **room-and-pillar mining system**, a relatively large proportion (30–50%) of the coal is left in place. The **roof coals** and carbonaceous shales are also left in the mine. The tonnage of combustible material remaining in the mine may exceed that extracted during mining. Older mines had several entries at the outcrop for drainage, ventilation, and access. Fires usually started at the outcrop and propagated along the outcrop or through interconnected workings. Heat could move by convection through the mine or by conduction into the overburden. The overburden served as an insulator, preventing the transfer of heat away from the combustible material. As the overburden became warmer or as the coal pillars failed, the overburden subsided, creating a system of cracks and fractures through which smoke and fumes left the mine and fresh air entered the mine (Figure 1.2.2). Under these conditions, most abandoned mine fires exhibit smoldering combustion, involving relatively small amounts of coal at any given time, with little visible flame. They can continue to burn in an atmosphere with as little as 2% oxygen (Scott, 1944). Such fires can burn for extended periods of time (10–80 years) and are difficult to extinguish (Dalverny and Chaiken, 1991; Kim et al., 1992; Leitch, 1940).

In abandoned surface mines, the coal outcrop may be left exposed when stripping operations are terminated, or coal refuse may be left in contact with the outcrop. In either case, fires are not unusual. If a stripping operation involved the **barrier pillar** of an abandoned mine, it is possible for a fire to propagate into the mine (Kim and Chaiken, 1993).

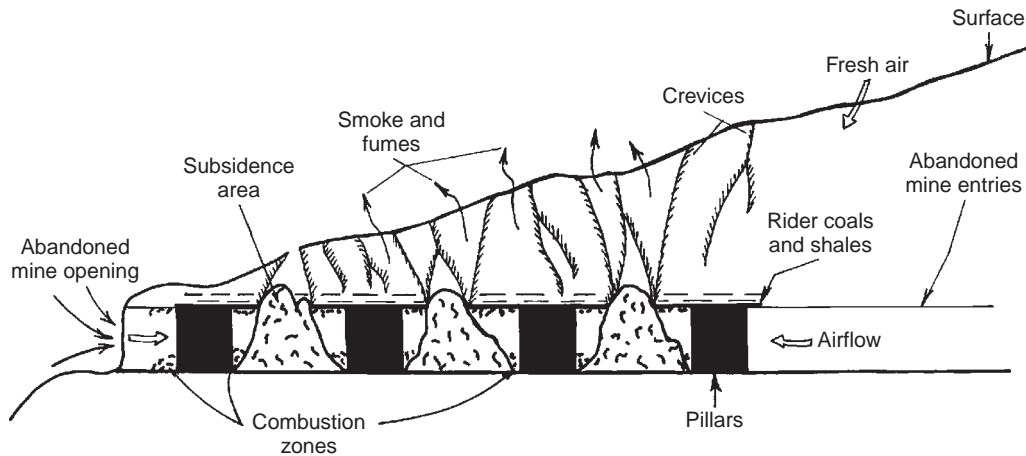


Figure 1.2.2. Wasted-coal fire in an abandoned mine showing emission of smoke and fumes through cracks and fractures and intake of fresh air through openings and overburden. From Kim and Chaiken 1993, p. 3.



Figure 1.2.3. Glenburn anthracite waste bank at Shamokin, Pennsylvania. From Kim and Chaiken 1993, p. 5.

Surface disposal of coal waste, from mines, and from preparation plants, is also a source of wasted-coal fires (McNay, 1971). Approximately 25% of the coal removed from the mine in the United States was rejected and disposed of on the surface (Doyle, 1976). Over the past 200 years, over three billion tons of refuse has accumulated in 3000–5000 active and abandoned waste piles and impoundments in the eastern coalfields alone. It has been estimated that a billion m^3 of anthracite waste has been disposed of in surface piles in the anthracite region (Figure 1.2.3). The refuse consists of waste coal, slate, carbonaceous shales, pyritic shales, and clay associated with the coal seam. The combustible content of this material averages between 2000 and 6000 Btu/lb. Material with a combustible content above 1500 Btu/lb will support combustion (Chaiken, 1980; Kim, 1995).

In anthracite mines and in some western mines, the **dip** or **pitch** of the beds also influences the propagation of fires. On steep pitches, differences in temperature and elevation are sufficient to control the circulation of air and fumes. The movement of hot gases can transfer heat to other areas of a mine. The distance between coal beds and their connection by fractures or tunnels determines the transfer of heat between beds and the possibility of propagation of a fire from the source bed to adjacent beds (White, 1973).

The rank of a coal is also a factor in the incidence of coal fires. Generally, lower rank coals tend to be more susceptible to spontaneous combustion. Although lignites and subbituminous coals are more prone to spontaneous

combustion, spontaneous combustion in higher rank coals can be supposed from the number of fires in which no other cause is suggested (Kim and Chaiken, 1993).

Natural barriers to subsurface fire propagation include faults where vertical displacement disrupts the continuity of the coal bed. Boundary pillars are considered natural barriers to fire propagation because solid coal seams do not burn readily. The H₂O table serves as a barrier by limiting the amount of oxygen and by absorbing energy released by the fire. In the absence of these natural barriers, a subsurface fire can, in an extended time period, burn from outcrop to outcrop (Kim and Chaiken, 1993).

Hazards

The primary hazards of coal fires are toxic fumes and subsidence. These fires also can affect the conservation of coal resources, ignite surface fires, and affect the value of adjacent property. Fumes from a fire zone frequently contain coal distillates, mercaptans carbonyl sulfides, which create noxious and unpleasant odors in addition to CO₂ and CO. Subsidence occurs when a fire consumes a portion of the coal, removing support from the overlying strata. The surface expression of the subsurface fire may be a small vent, a fracture line, a slight depression or a relatively large sinkhole. At least 60 deaths have been attributed to accidents at burning-coal refuse piles (McNay, 1971).

The potentially most serious problem associated with coal fires is the migration of toxic fumes from the fire through overlying strata into homes or other enclosed surface structures. A fire produces CO, CO₂, H₂O, and consumes oxygen. CO is the most serious hazard. This colorless, odorless gas readily combines with the hemoglobin of the blood, which normally transports oxygen; it replaces oxygen and forms carboxyhemoglobin. The effect of CO exposure increases with duration of exposure, higher humidity, and lower barometric pressure. The rate of effect also increases with increased physical exertion. Other factors in individual response to CO exposure are age (very old and very young), pregnancy, heart disease, poor circulation, anemia, asthma, lung impairment, or the presence of drugs/alcohol in the blood (Plunkett, 1976).

The hazards of mine fires are insidious. They are not like hurricanes, tornados, earthquakes, or floods, in which a single catastrophic event affects a large number of people. Fires in abandoned mines and waste banks are protracted events; they can have a moderate effect on people for 20 years or more. The most widespread effect is the environmental degradation caused by noxious odors and fumes. A more serious, but less prevalent, effect is subsidence and/or fume migration into surface structures (Kim and Chaiken, 1993).

Control of Coal Fires

In order to to extinguish a fire, one of the three elements, fuel, oxygen, or energy, must be removed. Fuel is removed when it is consumed or when it is physically separated from the burning mass. Oxygen removal depends on either the introduction of an inert atmosphere or on the isolation of the fire zone from sources of fresh air. Heat removal can be accomplished by moving a heat-absorbing agent (usually an inert gas or H₂O) through the mine. To prevent reignition of the fire, all coal and heated rock must be cooled below the reignition temperature. Even very small isolated areas where the coal is oxidizing at a high rate can serve as reignition points if the control measure fails and oxygen becomes available. It is generally assumed that if the temperature is below 100° C, the chance of reignition is small (Kim and Chaiken, 1993).

Conventional Methods of Extinguishing Subsurface Fires

Excavation (loading out, daylighting, dig and quench, stripping) is a fuel-removal method that is the most successful of the AML fire-control techniques (Chaiken, 1984). It involves physically removing the burning material and cooling it to extinguish the fire. The hot material is cooled either by spraying it with H₂O or by spreading it out on the ground and allowing it to cool in air. H₂O is preferred as the heat removal medium. It is also used to protect equipment from high temperatures and to suppress dust. If properly applied, excavation is the surest method of extinguishing wasted-coal fires. However, exposure of smoldering coal to an unlimited supply of oxygen can produce a sudden increase in fire activity (Figure 1.2.4). Excavation also involves exposure of men and equipment to a hazardous environment (Figure 1.2.5) The recurrence of excavated fires is usually due the failure to



Figure 1.2.4. Combustion enhanced by excavating hot coal in the presence of an unlimited supply of oxygen. Photo courtesy of the West Virginia Department of Natural Resources.



Figure 1.2.5. Excavation involves the hazards of working in hot material and toxic fumes. US Bureau of Mines photo 1982, Calamity Hollow Burnout Control Project.

completely excavate the fire or to the failure to lower the temperature of backfilled material beyond the reignition point (Kim and Chaiken, 1993).

Inundation methods of extinguishing wasted-coal fires involve the underground use of H_2O to lower the temperature of the burning material (heat removal). Covering the burning material with H_2O also stops the combustion reaction by oxygen exclusion. To raise the H_2O level, dams are constructed underground. The H_2O level must cover not only the burning coal, but must also reach the overlying heated rock. This method is limited to use on fires that are small, fairly accessible, at or near the H_2O table and have been burning for a relatively short time to minimize the amount of stored heat. Another inundation method provides for the continuous flow of H_2O through the hot material. This can be accomplished by continuous pumping or by gravity flow from a surface impoundment. The volume of H_2O required, the cost of high-capacity pumps, and time considerations have limited the utility of continuous pumping.

The gravity flow method has apparently been tried on waste banks by excavating a reservoir on the top of the bank and allowing H₂O to flow naturally downward (Bruhn and Michalski, 1989). The constraint on either of these methods is that the H₂O is not uniformly distributed. It may flow through channels and may bypass the fire zone. Even if the H₂O fails to cool a small amount of material, the probability of reignition is high.

Flushing is designed to fill the voids in an underground fire zone with fine, noncombustible solids. The noncombustible material is intended to cover the burning material and fill the interstices in adjacent rock, limiting the amount of oxygen in the system and absorbing heat. The high percentage of incombustible material, if properly emplaced, is expected to form a barrier to further propagation of the fire. Flushing can be effective where deposition of the noncombustible material can be controlled, where the voids have a relatively simple geometry, and where the injected material will remain in place.

Sand, silt, **red dog**, crushed limestone, and fly ash are the most commonly injected materials. Air or H₂O is usually used to carry the material through a borehole into the mine. With pneumatic (air) flushing, the noncombustible material is deposited at the bottom of the borehole. It forms a conical pile that theoretically reaches to the roof of the mine. Material is pumped into the hole to rejection, when it is assumed that the void is filled.

Pneumatic injection has two constraints: the material does not penetrate rubbleized strata and the material tends to slump which reduces the contact with overlying strata (Figure 1.2.6). This allows air to flow near the roof. In hydraulic flushing, H₂O is used to produce a slurry of the incombustible material. When the material is emplaced in the mine, the solids settle as the H₂O drains down dip. This method is believed to carry material further than dry flushing and to have some penetration through rubbleized material.

Grout slurries have been pumped underground to form fire control barriers. Cement in the grout slurry solidifies to form a competent seal, which also adds support to collapsed strata. The addition of foaming agents and incombustible materials, like sand or soil, has been used to produce a lower density foam grout that hardens to a cellular concrete (Colaizzi, 2004). The grout encapsulates the burning coal and limits combustion by limiting exposure to oxygen. The foamed grout has a low thermal conductivity, between 80 and 228 cal/min/m²/°C/cm and acts as an insulator, retaining heat within the coal. To remove heat, a thermal aggregate like small metal particles can be added to the grout (Terry, 1987). To be effective, the remotely emplaced grout seal must be complete, encapsulating all burning material and isolating it from other combustible materials (Figure 1.2.7), and the grout barrier must be stable for extended periods of time while the material cools.

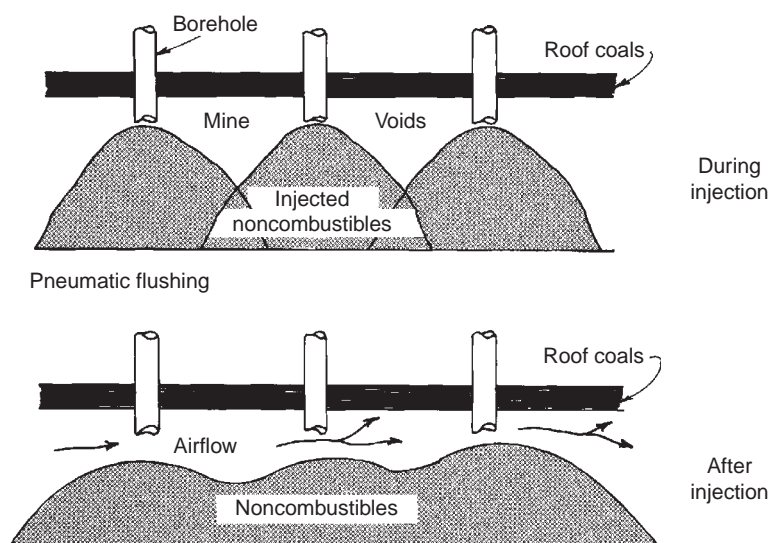


Figure 1.2.6. Sketch of pneumatic injection through boreholes, allowing slump of injected material and continued airflow near roof coals. From Kim and Chaiken 1993, p. 36.

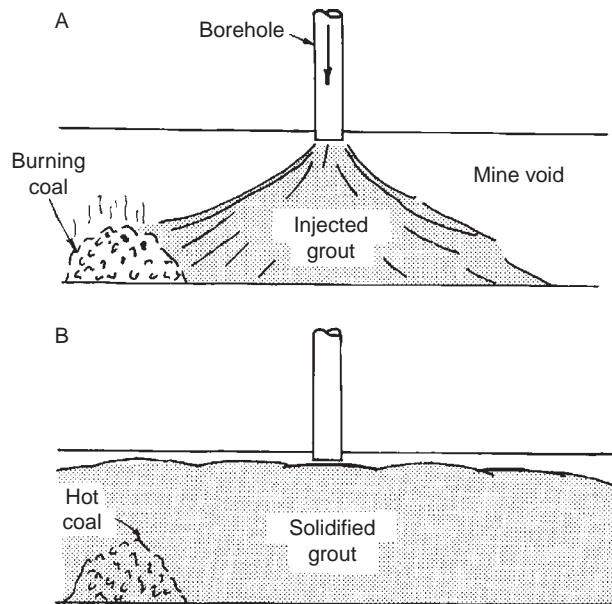


Figure 1.2.7. Sketch of the use of grout with concrete to encapsulate burning coal. A: Injection to encapsulate burning coal; B: Solidified grout for O₂ exclusion while hot material cools to below the reignition point. From Kim and Chaiken 1993, p. 36.

Surface sealing is a relatively inexpensive method of controlling abandoned mine fires. It is intended to inhibit ventilation of the fire zone. The exclusion of air and the accumulation of combustion products suppress the rate of fire propagation. If the seal can be maintained while all the stored heat dissipates, the fire may eventually be extinguished. During this period, the seal must be maintained. In general, most surface seals can be expected to fail between 1 and 3 years after construction. Failure may be related to settling, shrinkage, drying, or increased fire activity.

In the Western United States, 85% of fire abatement projects were surface seals. This is due to the relatively low cost, the topography of the area, and the lack of H₂O needed to implement other methods (Shellenberger and Donner, 1979).

Surface sealing suppresses surface evidence of a fire. If the seal is maintained for a sufficient length of time (10–20 years), the fire may be extinguished. Surface seals adequately control subsidence, inhibit unsightly venting and limit the emission of noxious fumes. In these circumstances, surface seals with regular and periodic maintenance provide an adequate control mechanism (Kim and Chaiken, 1993).

Conventional methods of controlling and/or extinguishing AML fires comprise a limited arsenal of dealing with the problem. None of the methods are routinely successful. Most of the methods involve some degree of hazard, have varying costs and may disrupt more surface area than the fire threatens.

Conclusions

The problem of coal fires is a serious one. Such fires can involve a high degree of hazard and can be less amenable to solution. Given the nature of these fires, it is unlikely that the extent of the problem or the cost of solutions will decrease in the near future. Although new techniques for locating fires and for controlling and extinguishing fires may be developed, the majority of current fire control projects utilize conventional methods and techniques.

Coal fires have occurred in the United States for over 200 years and, they may continue to occur. Experience has shown that they are difficult and expensive to control. Currently available technology used to control them is less than 70% effective. Research in new technology and in the adaptation of technology available in other fields may significantly improve the effectiveness of fire-control methods.

Acknowledgments

I wish to acknowledge Maurice Deul and Robert F. Chaiken, my supervisors at the US Bureau of Mines, who generously shared their extensive knowledge of coal geology and coal-mine fires.

Important Terms

Angiosperms	A flowering seed plant, as opposed to nonflowering seed plants (gymnosperms), such as conifers.
Allochthonous	Formed or produced elsewhere than in its present place; applied to coal or peat that originated from plant material transported from its place of growth.
Autochthonous	Formed or produced in its current location; applied to coal or peat that originated at the place where its constituent plants grew and decayed.
Barrier pillar	A solid block or rib of coal, etc., left unworked between two mines for security against an influx of H ₂ O. The unmined block of coal between adjacent mines or between the mine workings and the outcrop.
Carbonaceous shale	A coal-like material containing too much mineral matter to be considered coal, frequently formed by an influx of inorganic sediment into the coal swamp.
Coalification	Processes in response to diagenetic and metamorphic agents that determine the genetic and metamorphic history of coalbeds.
Dehydroxylation	Removal of hydroxyl ions (OH ⁻) from a compound or radical.
Demethylation	Removal of a methyl group (CH ₃) from a compound.
Dip	The angle at which a stratum or any horizontal feature is inclined to the horizontal.
Drift coal	Coal that originates from an accumulation of plant material that has been transported from its place of growth, allochthonous coal.
Epeirogenic	Pertaining to the uplift and subsidence of extensive areas of the earth's crust.
Epigenetic	Pertaining to a mineral deposit formed later than the enclosing rock; in ore petrology, mineral deposits of later origin than the enclosing rocks or to the formation of secondary minerals by alteration.
Ether cleavage	The reaction of an ether (CH ₃ -O-CH ₃) containing molecule with a strong acid (HBr) to form an alkyl halide (CH ₃ Br) and an alcohol (CH ₃ OH).
Eustatic	Pertaining to worldwide changes of sea level that affect all the oceans.
Exothermic	A chemical reaction producing heat.
Hilt's Rule	In a vertical sequence at any given point in a coalfield, the rank of the coal of the successive seams increases with increasing depth.
Lignin	The major noncarbohydrate portion of wood, an amorphous polymeric substance that cements the fibrous portions (cellulose) together.
Lithotype	A macroscopically visible band in humic coals.
Maceral	An elementary microscopic constituent of coal, analagous to mineral as used in petrography; organic units composing the coal mass, having the termination -inite; i. e., vitrinite, exinites, and inertinites.
Pitch	In structural geology, the angle that a line in a plane makes with a horizontal line in that plane.
Proximate composition	The compounds contained in a mixture, particularly the concentrations of moisture, volatile matter, mineral matter and fixed carbon in coal.

Pyrolytic condensation	A reaction at high temperature in which two molecules combine with the elimination of H ₂ O or other small molecule.
Rank	Describes the stage of coalification attained by a given coal; the place occupied by a coal in a classification of coals according to their degree of metamorphism, or progressive alteration, in the order: lignite, subbituminous, bituminous, anthracite.
Red dog	Material of a reddish color resulting from the combustion of carbonaceous shale and other mine waste in surface mine dumps or waste banks.
Roof coal	The layer immediately over the main-coal seam. It may be coal of poor quality or carbonaceous shale, and is frequently left in place.
Room-and-pillar mining	A system of mining in which typically flat-lying beds of coal are mined in rooms separated by pillars of undisturbed coal left for roof support.
Syngenetic	A mineral formed contemporaneously with the enclosing rocks.
Ultimate composition	The elements contained in a compound, as distinguished from proximate analysis, which is the determination of the compounds contained in a mixture. In the case of coal and coke, the determination of carbon, hydrogen, sulfur, nitrogen, and oxygen.
Vitrinite reflectance	As coal rank increases, the vitrinite macerals become increasingly reflective. The percentage reflection of a beam of normal incident white light from the surface of polished vitrinite is a function of the rank (maturity) of the maceral. The reflectivity (<i>R</i>) may either be recorded as <i>R_v</i> max% or <i>R_o</i> %. Both are measurements of the percentage of light reflected from the sample, calibrated against a material which shows ~100% reflectance.
Wasted-coal fires	Wasted coal is that left in mines or disposed of on the surface. Wasted-coal fires occur in inactive or abandoned coal mines and coal-waste banks. Also called “Abandoned Mined Lands” fires.

References

- Ashley, G.H., 1928. Bituminous Coal Fields of Pennsylvania. Pennsylvania Geological Series, Fourth Series, Bulletin M6, Part 1.
- ASTM, 2002. D3176-89(2002) Standard Practice for Ultimate Analysis of Coal and Coke. American Society for Testing and Materials, Book of Standards v 05.06—Gaseous Fuels; Coal and Coke. ASTM, West Conshohocken, PA.
- ASTM, 2005. D388-05 Standard Classification of Coals by Rank. American Society for Testing and Materials, Book of Standards v 05.06—Gaseous Fuels; Coal and Coke. ASTM, West Conshohocken, PA.
- ASTM, 2007. D3172-07 A Standard Practice for Proximate Analysis of Coal and Coke. American Society for Testing and Materials, Book of Standards v 05.06—Gaseous Fuels; Coal and Coke. ASTM, West Conshohocken, PA.
- Banerjee, S.C., 1985. Spontaneous Combustion of Coal and Mine Fires. Oxford and IBH Publishing Company, New Delhi, 168 p.
- Barghoorn, E.S., 1952. Degradation of plant materials and its relation to the origin of coal. Second Conference on the Origin and Constitution of Coal, Nova Scotia Department of Mines, Crystal Cliffs, NS, pp. 181–203.
- Bennett, A.J.R., 1963. Origin and formation of coal seams. Australia CSIRO, Division of Coal Research, Miscellaneous Report No. 239.
- Brownfield, M.E., Affolter, R.H., Cathcart, J.D., Brownfield, I.K., Hower, J.C., Stricker, G.D., 1999. Dispersed volcanic ash in feed coal and its influence on coal combustion products. International Ash Utilization Symposium, Lexington, KY, October 18–20, 1999. Center for Applied Energy Research, University of Kentucky, 8 p., CD-ROM.
- Bruhn, R.W., Michalski, S.R., 1989. Control of an underground mine fire in Pennsylvania’s anthracite region. Proceedings of 11th Annual Association of Abandoned Mine Land Programs Conference, Williamsburg, VA, October 16–19, 1989, pp. 56–62.

- Burnham, A.K., Sweeney, J.J., 1989. A chemical kinetic model of vitrinite maturation and reflectance. *Geochim. Cosmochim. Acta* 53, 2649–2657.
- Cao, Y., Mitchell, G.D., Davis, A., Wang, D., 2000. Deformation metamorphism of bituminous and anthracite coals from china. *Int. J. Coal Geol.* 43, 227–242.
- Cassidy, S.M., 1973. History of coal mining. In: Cassidy, S.M., (Ed.), *Elements of Practical Coal Mining*. Coal Division, SME-AIME, New York, pp. 1–10.
- Chaiken, R.F., 1977. Heat balance in in-situ combustion. US Bureau of Mines, RI 8221, 11 p.
- Chaiken, R.F., 1980. Controlled burnout of wasted coal on abandoned coal mine lands. US Bureau of Mines, RI 8478, 23 p.
- Chaiken, R.F., 1984. Extinguishment of wasted coal fires: a critical review—new directions. Proceedings of the National Symposium and Workshops on Abandoned Mine Land Reclamation, Bismarck, ND, May 21–24, 1984, pp. 457–484.
- Chaiken, R.F., Brennan, R., Heisey, B., Kim, A.G., Malenka, W., Schimmel, J., 1983. Problems in the control of anthracite mine fires: a case study of the Centralia mine fire. US Bureau of Mines, RI 8799, 93 p.
- CMRS, 1991. Assessment of status and control of underground coal mine fires. Central Mining Research Station, Dhanbad, India, 108 p.
- Colaizzi, G.J., 2004. Prevention, control and/or extinguishment of coal seam fires using cellular grout. In: Stracher, G.B. (Ed.), *Coal fires burning around the world: a global catastrophe*. *Int. J. Coal Geol.* 59 (1–2), 75–81.
- Cooper, G., 1996. *Vitrinite Reflectance*: Petroleum Exploration Society of Australia.
- Cooper, B.S., Murchison, D.G., 1969. Organic geochemistry of coal. In: Eglinton, G., and Murphy, M.T.J. (Eds.), *Organic Geochemistry*. Springer-Verlag, New York, pp. 699–726.
- Copard, Y., Disnar, J.R., Becq, G., Giraudon, J.F., Boussafir, M., 2000. Evidence and effects of fluid circulation on organic matter in intramontane coalfields (Massif Central, France). *Int. J. Coal Geol.* 44, 49–68.
- Dalla Torre, M., Mahlmann, R.F., Ernst, W.G., 1997. Experimental study on the pressure dependence of vitrinite maturation. *Geochim. Cosmochim. Acta* 61, 2921–2928.
- Dalverny, L.E., Chaiken, R.F., 1991. Mine fire diagnostics and implementation of WIFE at Renton, PA. US Bureau of Mines, RI9363, 42 p.
- Damberger, H.H., Demir, I., Pine, J., 1999. Age relationships between coalification and geothermal events in the Illinois Basin: abstracts with programs. *Geol. Soc. Am.* 31, 403.
- Daniels, E.J., Altaner, S.P., Marshak, S., 1990. Hydrothermal alteration in anthracite from Eastern Pennsylvania: implication for mechanisms of anthracite formation. *Geology* 18, 247–250.
- Daulay, B., Cook, A., 2000. Coalification of Indonesian coal. *AAPG Bull.* 84, 1417.
- Doyle, W.S., 1976. *Deep Coal Mining Waste Disposal Technology*. Noyes Data Corporation, Park Ridge, NJ, 392 p.
- Eavenson, H.H., 1938. The Pittsburgh coal bed—its early history and development. *Trans. AIME* 130, 9–10.
- Eavenson, H.H., 1942. *The first century and a quarter of American coal industry*. Privately printed, Pittsburgh, PA, 701 p.
- Edmunds, W.E., 2002. *Coal in Pennsylvania*, second ed. Pennsylvania Geological Survey, 4th Series, Educational Series 7, PA Dept. of Conservation and Natural Resources, Harrisburg, PA, 28 p.
- EIA, 2002. *Energy in the United States: 1635–2000*. Energy Information Administration, US Department of Energy, <http://www.eia.doe.gov/emeu/aer/eh> (accessed May 2008).
- EIA, 2006. *Annual energy outlook*. Energy Information Administration, US Department of Energy, http://www.eia.doe.gov/oiaf/ieo/pdf/ieoreftab_6.pdf (accessed May 2008).
- EIA, 2008. *Recent coal consumption*. Energy Information Administration, US Dept of Energy, <http://www.eia.doe.gov/emeu/international/coalconsumption.html> (accessed May 2008).
- Ferm, J.C., Cavaroc, V.V., 1969. *A field guide to Allegheny deltaic deposits in the Upper Ohio Valley*. Ohio Geological Society and Pittsburgh Geological Society.
- Finkelman, R.B., 2004. Potential health impacts of burning coal beds and waste banks. In: Stracher, G.B. (Ed.), *Coal fires burning around the world: a global catastrophe*. *Int. J. Coal Geol.* 59 (1–2), 19–24.
- Fowler, P., Gayer, R.A., 1999. The association between tectonic deformation, inorganic composition and coal rank in the bituminous coals from the South Wales coalfield, United Kingdom. *Int. J. Coal Geol.* 42, 1–31.
- Francis, W., 1961. *Coal, its Formation and Composition*, second ed. Edward Arnold Publishers, Ltd, London.
- Gupta, R.P., Prakash, A., 1998. Reflection aureoles associated with thermal anomalies due to subsurface mine fires in the Jharia Coalfield, India. *Int. J. Remote Sens.* 19 (14), 2619–2622.
- Han, Z., Yang, Q., Pang, Z., 2001. Artificial maturation of a humic coal and torbanite. *Int. J. Coal Geol.* 46, 133–143.
- Hatcher, P.G., Clifford, D.J., 1997. The organic geochemistry of coal: from plant materials to coal. *Org. Geochem.* 27, 251–274.

- Heffren, E.L., Reiners, P.W., Naesner, C.W., Coates, D., 2007. Geochronology of clinker and implications for evolution of the Powder River Basin Landscape, Wyoming and Montana. In: Stracher, G.B. (Ed.), *Geology of Coal Fires: Case Studies from around the World. Reviews in Engineering Geology XVIII*. Geological Society of America, Boulder, CO, pp. 155–175.
- Hendricks, T.A., 1945. The origin of coal. In: Lowry, H.H. (Ed.), *Chemistry of Coal Utilization*. John Wiley and Sons Inc., New York, pp. 1–24.
- Hertle, M., Littke, R., 2000. Coalification pattern and thermal modeling of the Permo-Carboniferous Saar Basin. *Int. J. Coal Geol.* 42, 273–296.
- Hessley, R.K., Reasoner, J.W., Riley, J.T., 1986. *Coal Science*. John Wiley and Sons, New York, 269 p.
- Hower, J.C., Gayer, R.A., 2002. Mechanisms of coal metamorphism: case studies from Paleozoic coalfields. *Int. J. Coal Geol.* 50, 215–245.
- Janssen, R.E., 1939. Leaves and stems from the fossil forests. *Illinois State Museum Popular Science Series*.
- Johnson, W., Miller, G., 1979. Abandoned coal-mined lands: nature, extent and cost of reclamation. *US Bureau of Mines Special Publication 6-79*, 29 p.
- Kanury, A.M., 1975. *Introduction to Combustion Phenomena*. Gordon and Breach Science Publishers, New York, 411 p.
- Kay, G.M., Colbert, E.H., 1965. *Stratigraphy and Life History*. John Wiley and Sons, Inc., New York.
- Kim, A.G., 1977. Laboratory studies on spontaneous heating of coal: a summary of information in the literature. *US Bureau of Mines, IC 8756*, 13 p.
- Kim, A.G., 1995. Relative self-heating tendencies of coal, carbonaceous shales, and coal refuse. *US Bureau of Mines, RI 9537*, 21 p.
- Kim, A.G., 2002. Physical and chemical characteristics of CCB. In: Vories, K., and Throgmorton, D. (Eds.), *Coal Combustion By-Products and Western Coal Mines: A Technical Interactive Forum*. Golden, CO, April 16–18, 2002. US Department of the Interior, Office of Surface Mining, and Coal Research Center, Southern Illinois University at Carbondale, CD ROM, 25 p.
- Kim, A.G., Chaiken, R.F., 1993. Fires in abandoned coal mines and waste banks. *US Bureau of Mines, IC9352*, 58 p.
- Kim, A.G., Justin, T.R., Miller, J.F., 1992. Mine fire diagnostics applied to the Carbondale mine fire. *US Bureau of Mines, RI 9421*, 16 p.
- Kim, A.G., Kissell, F.N., 1988. Methane formation and migration in coalbeds. In: Deul, M., and Kim, A.G. (Eds.), *Methane Control Research: Summary of Results, 1964–1980*. US Bureau of Mines, Bulletin 687.
- Kolker, A., Goldhaber, M.B., Hatch, J.R., Meeker, G.P., Koeppen, R.P., 1999. Arsenic-rich pyrite in coals of the warrior field, northwestern Alabama: mineralogical evidence for a hydrothermal origin. *Abstr. Progr. Geol. Soc. Am.* 31, 402.
- Kosanke, R.M., 1952. Petrographic and microchemical studies of coal. *Second Conference on the Origin and Constitution of Coal*, Crystal Cliffs, Nova Scotia, June 1952, p. 251.
- Kosanke, R.M., Simon, J.A., Wanless, H.R., Wilman, H.B., 1960. Classification of the Pennsylvanian strata of Illinois. *Illinois Geological Survey, Report of Investigations No. 214*.
- Krumbein, W.W., Sloss, L.L., 1963. *Stratigraphy and Sedimentation*. W.H. Freeman and Company, San Francisco.
- Kummel, B., 1961. *History of the Earth*. W.H. Freeman and Company, San Francisco.
- Lavender, D., 1988. *The Way to the Western Sea, Lewis and Clark across the Continent*. University of Nebraska Press, Lincoln, NE, 444 p.
- Leitch, R.D., 1940. Some information on extinguishing refuse-bank fires near Mahanoy City, PA. *US Bureau of Mines, IC 7104*, 16 p.
- Mackowsky, M.W., 1968. Mineral matter in coal. In: Murchison, D.G., and Westoll, T.S. (Eds.), *Coal and Coal Bearing Strata*. American Elsevier Publishing Co., New York, p. 311.
- Masalehdani, M.N., Black, P.M., Kobe, H.W., 2007. Mineralogy and petrology of iron-rich and paralavas formed by spontaneous combustion, Rotowaro coalfield, North Island, New Zealand. In: Stracher, G.B. (Ed.), *Geology of Coal Fires: Case Studies from around the World. Reviews in Engineering Geology XVIII*. Geological Society of America, Boulder, CO, pp. 117–132.
- McCabe, P.J., Parrish, J.T., 1992. Tectonic and climatic controls on the distribution and quality of cretaceous coals. In: McCabe, P.J., and Parrish, J.T. (Eds.), *Controls on the Distribution and Quality of Cretaceous Coals*. Geological Society of America, Boulder, CO, Special Paper 267, pp. 1–15.
- McCullogh, C.M., Diamond, W.P., Bench, B.M., Deul, M., 1975. Selected geologic factors affecting mining of the Pittsburgh coalbed. *US Bureau of Mines, RI 8093*, 72 p.
- McNay, L.M., 1971. Coal refuse fires, an environmental hazard. *US Bureau of Mines, IC 8513*, 50 p.
- Michalski, S.R., 2004. The Jharia mine fire control technical assistance project: an analysis. In: Stracher, G.B. (Ed.), *Coal fires burning around the world, a global catastrophe*. *Int. J. Coal Geol.* 59 (1–2), 83–90.
- Mott, R., 1942. The origin and composition of coal. *Fuel in Sci. Pract.* 22, 20–26.

- Nicholls, G., 1968. The geochemistry of coal-bearing strata. In: Murchison, D.G., and Westoll, T.S. (Eds.), *Coal and Coal Bearing Strata*. American Elsevier Publishing Co., New York, pp. 271–272.
- OSMRE (Office of Surface Mining Reclamation and Enforcement), 2005. MINE FIRES, <http://www.techtransfer.osmre.gov/nttmainsite/Initiatives/MineFires/minefires.htm> (accessed October 2009).
- Pearson Coal Petrography, Vitrinite Reflectance, <http://www.coalpetrography.com> (accessed June 2008).
- Petmecky, S., Meier, L., Reiser, H., Littke, R., 1999. High thermal maturity in the lower Saxony basin: intrusion or deep burial. *Tectonophysics* 304, 317–344.
- Petrakis, L., Grandy, D.W., 1980. Coal analysis, characterization and petrography. *J. Chem. Educ.* 57, 689–694.
- Plunkett, E.R., 1976. *Handbook of Industrial Toxicology*. Chemical Publishing Co., Easton, PA, pp. 85, 88–89.
- Prakash, A., Gupta, R.P., 1999. Surface fires in Jharia Coalfield, India—their distribution and estimation of area and temperature from TM data. *Int. J. Remote Sens.* 20, 1935–1946.
- Rosema, A., Guan, H., van Genderen, J.L., Veld, H., Vekerdy, Z., Ten Katen, A.M., Prakash, A.P., 1999. Manual of coal fire detection and monitoring. Report of the Project ‘Development and implementation of a coal fire monitoring and fighting system in China’. Netherlands Institute of Applied Geoscience, Utrecht, NITG 99-221-C, ISBN 90-6743-640-2, 245 p.
- Sachsenhofer, R.F., Jelen, B., Hasenhuettl, C., Dunkl, I., 2001. Thermal history of tertiary basins in Slovenia. *Tectonophysics* 334, 77–99.
- Sachsenhofer, R.F., Rantitsch, G., 1999. Heat Flow in the Eastern Alps during Tertiary times. 4th Workshop on Alpine Geological Studies, Tübingen, Federal Republic of Germany, pp. 50–51.
- Saward, S.A., 1992. A global view of cretaceous vegetation patterns. In: McCabe, P.J., and Parrish, J.T. (Eds.) *Controls on the Distribution and Quality of Cretaceous Coals*. Geological Society of America, Special Paper 267, Boulder, CO, pp. 17–35.
- Schopf, J.M., 1966. Definitions of peat and coal and of graphite that terminates the coal series (graphocite). *J. Geol.* 74, 584–592.
- Scott, G.S., 1944. Anthracite mine fires: their behavior and control. US Bureau of Mines, RI 455, 206 p.
- Senior, C.L., Zeng, T., Che, J., Ames, M.R., Sarofim, A.F., Olmez, I., Huggins, F.E., Shah, N., Huffman, G.P., Kolker, A., Mroczkowski, S., Palmer, C., Finkelman, R., 2000. Distribution of trace elements in selected pulverized coal as a function of particle size and density. *Fuel Process. Technol.* 63, 215–241.
- Shellenberger, F.H., Donner, D.L., 1979. Controlling fires in unmined coal deposits and abandoned coal mines in the Western United States and Alaska. US Bureau of Mines, Progress Report 10047, 150 p.
- Sivek, M., Caslavsky, M., Jirasek, J., 2002. Applicability of Hilt’s law to the Czech part of the Upper Silesian Coal Basin (Czech Republic). *Int. J. Coal Geol.* 73, 185–195.
- Smith, G.G., Cameron, A.R., Bustin, R.M., 1994. Coal resources of the Western Canada Sedimentary Basin. Chapter 33 in *Atlas of the Western Canada Sedimentary Basin*, Alberta Geological Survey, http://www.ags.gov.ab.ca/publications/wcsb_atlas/atlas.html (accessed June 2008).
- Sokol, E.V., Volkova, N.I., 2007. Combustion metamorphic events resulting from natural coal fires. In: Stracher, G. B., ed., *Geology of Coal Fires: Case Studies from around the World: Reviews in Engineering Geology XVIII*. Geological Society of America, Boulder, CO, pp. 97–116.
- Stopes, M.C., 1919. On the four visible ingredients in banded bituminous coal. *Proc. R. Soc.* 90, 470–487.
- Stopes, M.C., 1935. On the petrology of banded bituminous coal. *Fuel in Sci. Pract.* 14, 4–13.
- Stracher, G.B., 2007. The origin of gas-vent minerals: isochemical and mass-transfer processes. In: Stracher, G.B. (Ed.), *Geology of Coal Fires: Case Studies from around the World: Reviews in Engineering Geology XVIII*. Geological Society of America, Boulder, CO, pp. 91–96.
- Stracher, G.B., Taylor, T.P., 2004. Coal fires burning out of control around the world: thermodynamic recipe for environmental catastrophe. In: Stracher, G.B. (Ed.), *Coal fires burning around the world, a global catastrophe*. *Int. J. Coal Geol.* 59 (1–2), 7–17.
- Tatsch, J.H., 1980. *Coal Deposits: Origin, Evolution and Present Characteristics*. Tatsch Associates, Sudbury, MA, 590 p.
- Teichmüller, M., Teichmüller, R., 1967. Diagenesis of coal (coalification). In: Larson, G., and Chilingar, G.V. (Eds.), *Diagenesis in Sediments*. Elsevier, Amsterdam, pp. 391–415.
- Teichmüller, M., Teichmüller, R., 1982. The geological basis of coal formation. In: Stach, E. (Ed.), *Stach’s Textbook of Coal Petrology*, third ed. Lubrecht and Cramer Ltd, Port Jervis, NY, pp. 5–87.
- Terry, R.C., 1987. Terminating persistent underground coal fires. US Patent No. 4,641,711, February 10, 1987.
- Uysal, T., Golding, S.D., Thiede, D.S., 2001. K-Ar and Rb-Sr dating of authigenic illite-smectite in late Permian coal measures, Queensland, Australia: implications for thermal history. *Chem. Geol.* 171, 195–211.
- Van Krevelen, D.W., 1963. Geochemistry of coal. In: Breger, I. (Ed.), *Organic Geochemistry*. Pergamon Press, Oxford, pp. 183–247.
- Voigt, S., Tetzlaff, A., Jianzhong Zhang, Künzer, C., Zhukov, B., Strunz, G., Oertel, D., Roth, A., Dijk, P.M. van, Mehl, H., 2004. Integrating satellite remote sensing techniques for detection and analysis of uncontrolled coal

- seam fires in North China. In: Stracher, G.B. (Ed.), Coal fires burning around the world: a global catastrophe. *Int. J. Coal Geol.*, 59 (1-2), 121–136.
- Wanless, H.R., Baroffio, J.R., Trescott, P.C., 1969. Conditions of deposition of Pennsylvanian coal beds. In: Dapples, E.C., and Hopkins, M.E. (Eds.), *Environment of Coal Deposition*. Geological Society of America, Boulder, CO, Special Paper No. 114, pp. 105–142.
- Warwick, P.D., Crowley, S.S., San Filipo, J.R., 1997. Geologic influences on the distribution of potentially hazardous elements in lignites, Gulf Coast Province, USA. *Proceedings of the 14th International Pittsburgh Coal Conference*, Taiyan, Shanxi, P.R. China, CD-ROM, 3 p.
- Weller, J.M., 1931. The conception of cyclical sedimentation during the Pennsylvanian period. In: Merriam, D.F. (Ed.), *Studies Relating to the Order of and Conditions of Accumulation of the Coal Measures*. Illinois State Geological Survey, Bulletin No. 60, pp. 163–177.
- Weller, J.M., 1964. Development of the concept and interpretation of cyclic sedimentation. In: Merriam, D.F. (Ed.), *Symposium on Cyclic Sedimentation*. State Geological Survey of Kansas, Bulletin 169, vol. 2, pp. 607–621.
- White, D., 1925. Environmental conditions of deposition of coal. *Trans. Am. Inst. Min. Metall. Eng.* 71, 3–34.
- White, E.M., 1973. Fires and explosions. In: Cassidy, S.M. (Ed.), *Elements of Practical Coal Mining*. Coal Division, SME-AIME, New York, pp. 227–258.
- White, L., 2002. *Coal Geology*. John Wiley and Sons Ltd, Chichester, UK, 384 p.
- White, D., Thiessen, R., 1913. The origin of coal. US Bureau of Mines, Bulletin 38.
- Whitehouse, A.E., Mulyana, A.A.S., 2004. Coal fires in Indonesia. In: Stracher, G.B. (Ed.), *Coal fires burning around the world: a global catastrophe*. *Int. J. Coal Geol.* 59 (1–2), 91–97.
- WSGS, 2001. Coal: Wyoming State Geological Survey, <http://www.wsgs.uwyo.edu/coalweb/> (accessed September 12, 2008).

WWW Addresses: Additional Reading

- (1) **Dictionary of Mining, Mineral, and Related Terms**
<http://www.maden.hacettepe.edu.tr/dmmrt>
- (2) **Kentucky Geological Survey**
http://www.uky.edu/KGS/coal/coal_information.htm
- (3) **Electronic Field Trip to a Coal Mine**
<http://www.ket.org/Trips/Coal/AGSMM/agsmmintro.html>
- (4) **Office of Surface Mining Search Engine**
<http://www.wrcc.osmre.gov/GLAS/Search/BrowseList.asp>
- (5) **Office of Surface Mining Technical Library**
<http://www.techtransfer.osmre.gov/NTTMainSite/osmlibrary.htm>
- (6) **National Institute of Occupational Safety and Health.**
<http://www.cdc.gov/niosh/mining/pubs>
- (7) **United States Geological Survey Coal Resources.**
<http://www.usgs.gov/science/science.php?term=172>
- (8) **Energy Information Administration**
<http://www.eia.doe.gov/>
- (9) **Coal Fires - a natural or man made hazard?**
<http://www.gi.alaska.edu/~prakash/coalfires/coalfires.html>
- (10) **The Encyclopedia of Earth: Coal Fires**
http://www.eoearth.org/article/Coal_fires
http://www.eoearth.org/article/Natural_and_anthropogenic_coal_fires
- (11) **Smithsonian Magazine: Fire in the Hole**
<http://www.smithsonianmag.com/travel/firehole.html>

CHAPTER 2

Coal-Mining Techniques and Coal Fires



CHAPTER CONTENTS

2.1 Brief History of Coal Mining

- Introduction
- Evolution of Coal Mining
- Coal-Mining Techniques
- Coal-Mining Machines

2.2 Underground Coal Mining

- Underground Mining
- Methods of Coal Mining
- The Special Case of Anthracite Mining
- Ventilation

2.3 Surface Coal Mining

- Surface Mining
- Contour Mining
- Area Mining
- Auger Mining
- Mountain Top Removal

2.4 Coal Mining and Coal Fires

- Discovery and Investigation
- Monitoring
- Mine Atmosphere
- Abatement
- Acknowledgments
- Important Terms
- References
- WWW Addresses:
Additional Reading



Photo by Stanley R. Michalski, 1994.

2.1. Brief History of Coal Mining

Stanley R. Michalski

Dragline removing overburden in the Jharia Coalfield, state of Jharkhand, India.

Introduction

Man has mined coal from the time he learned to control and use fire as a source of heat for cooking and keeping warm. There is no clear point in time when coal was first used. Early man, however, was in tune with his environment and to survive he had to use what the environment offered. The black rock that burned was first collected by scraping it from the rocky outcrops where it was exposed. This was the first method of mining coal. Coal's use, however, was limited. Wood was the principal source of energy for heating and cooking as it was available just about anywhere man settled.

Evolution of Coal Mining

The use of coal for energy was slow to develop. In Europe "sea coal" was mined by simply picking it off the beaches where it was deposited after being eroded from coal outcrops both above and below sea level (Lindbergh and Provorse, 1980, p. 18). Since wood was much easier to acquire and utilize, coal was largely ignored until the Industrial Revolution. Coal's first industrial use was for smelting and working metals. Coal could achieve the heat required to work metals where charcoal from wood by itself could not. In the early 1700s, there was an increasing need for fuel for heating and to drive small burgeoning industries. Wood was still the universal fuel, but, by the eighteenth century, wood was becoming scarce and expensive and in England was even being imported (Oosthoek, 2008). Early industry used coal that was extracted from near the ground surface where it was easy to mine. Initially, coal exposed on a hillside was mined by following the coal seam, horizontally into the ground. This became the **drift mine** which followed the coal for hundreds of meters leaving behind blocks of coal to support the roof of the mine. Another form of mining developed where the coal seam occurred below the ground surface and a shallow shaft was dug to reach the coal. This became the **bell pit** (Lindbergh and Provorse, 1980, p. 36). The bell pit would be expanded within the coal seam until the erstwhile miners were threatened by collapsing walls. Then a new bell pit would be created adjacent to the old one. In the 1700s, drift mines and bell pits were small-scale, coal-mining operations where the coal was close to the surface and used locally for home heating and small scale industry.

As the mines got deeper by following the coal seam into the hill or down an incline, flooding of the mine workings and suffocation of the workers as well as explosive, combustible, and poisonous gases became very real dangers. A spark from a pick axe, a flame from a candle, or from a miner lamp could trigger a disastrous underground explosion. Pockets of gas rich in carbon dioxide or low in oxygen content could render a miner unconscious. Consequently, removing water and dangerous gases from a working mine became a necessity. Despite these improvements in safety, coal mining became more and more dangerous for those who went into the pits and underground mines. The deepening mines also had to cope with the increasing weight of the **overburden**. The underground network of passages within the mines was supported with blocks of coal left in place and wooden poles or props cut from a nearby wood lot. A thin line often existed between the quantity of coal to leave behind for

supporting the roof and the quantity of coal to extract for profit. As a result, underground collapses of the workings which often took the lives of the miners, were common.

The areal extent of the early underground mines was further limited by the seepage of ground water into the workings. As the mines dipped below the natural ground water level, seepage and subsequent flooding was soon to follow. Large-scale, coal mining would not begin until improvement in the steam engine allowed water to be efficiently pumped from the mine workings.

As coal became more important as a fuel, and as its production increased, so did the difficulty and complexity of extracting it. Despite the problems, the mining industry grew very rapidly with the Industrial Revolution. Eventually, experience and technological advancement led to the development of various mining methods and techniques to safely maximize coal production. These methods evolved over the years in response to a variety of geological, environmental, economic and engineering considerations. Every **coalfield** has its own set of physical constraints that govern the mineability of its coal. As a result, specialized variations in mining techniques evolved to optimize coal recovery for a given set of conditions or constraints. Optimizing coal recovery requires a mining plan. The goal of any mining plan is to recover the maximum amount of coal in the safest possible manner at the lowest possible cost. Before a mining plan is implemented, the mineability of a particular coal seam must be determined. The mineability, methods of coal recovery, and potential profits can be estimated by providing definitive answers to the following:

- What is the coal thickness?
- What is the grade or **coal rank**?
- What is the potential net recovery?
- What is the thickness of overburden or cover and how does it vary?
- What will be the preferred method of mining?
- What are the environmental impacts and consequences of mining?
- What is the cost of implementing an optimized-mining scheme?; and
- Where is the coal market?

Of these considerations, only the methods of mining are considered in the following paragraphs.

Coal-Mining Techniques

There are only two mining techniques for recovering coal from the earth; underground mining and surface mining. Many variations of the underground and surface mining methods exist, but the ones discussed in the following paragraphs account for nearly all the coal mined world wide (World Coal Institute, 2005).

Underground mining is a process whereby coal is recovered from within its underground position. Surface mining is to remove the earth and rock strata overlying the coal. The coal can then be recovered. The method is normally dependent on the geology of the coal seam and the nature and thickness of overburden above the coal, as well as the **geomorphology** of the land surface. At depths greater than 61 m (200 ft) and with a uniform overburden consisting of rock strata, underground mining methods are generally used (Hansen, 1990, p. 28). If the coal lies at shallower depth or the overburden consists of unconsolidated materials or the geomorphology allows for easy removal of overburden, then surface mining methods are employed. Other factors contributing to the selection of an appropriate mining method are the uniformity and attitude or pitch of the seam. Steeply pitching coal seams are mined quite differently than seams that are relatively flat lying and of uniform thickness.

Underground mining methods access the coal through drift openings, inclined tunnels, or **slopes** and vertical **shafts**. Only the drift opening permits access directly to the coal face without having to dig through overlying rock strata. Whatever type of access to the coal seam, its purpose is to facilitate entry of men and equipment to the mine, provide egress from the mine for the mined coal, and provide ventilation to the underground workings which are often far removed from the original opening to the coal seam (mine). Mining through slopes and vertical shafts requires a conveyor (slope) or an elevator (shafts) to transport men, materials, and coal into and out of the mine.

Coal-Mining Machines

Surface Coal Mining

The ever-expanding surface mining industry and dramatic increases in productivity have been the direct result of increase in size and efficiency of the equipment used. Surface mining operations employ equipment similar to that used in the construction industry. This includes bulldozers, drilling machines, front-end loaders, hydraulic backhoes, giant draglines, power shovels, bucket wheel excavators, scrapers, and off-road haulage trucks.

Bulldozers are self-propelled track-mounted machines equipped with a large steel blade attached to their front. Bulldozers are used to push, level, and grade soil and rock over short distances during the mining and reclamation phase of an operation.

Borehole drilling machines are used to drill numerous boreholes through the overburden to load with explosives which loosen the overlying rock to facilitate excavation. Drilling machines are diesel or electrically powered.

Front-end loaders are rubber tired tractors equipped with a large bucket that is used to load soil, rock, and coal into trucks to be transported to a spoil disposal area or to a **coal preparation plant** for further processing. Hydraulic backhoes are equipped with a bucket at the end of a large boom and are used for a multitude of tasks in a surface mining pit.

Draglines are machines that have a very large bucket hanging by a cable from a long boom attached to the front of the machine, as shown in the introductory figure of this section. The bucket is cast a considerable distance from the dragline by swinging and dropping the bucket in one motion. The bucket is filled with overburden by retracting the cable which pulls the bucket back towards the dragline. The filled bucket is then lifted and rotated to the disposal area and dumped by lifting the rear of the bucket, again by retracting cables. Draglines can be giant mining machines such as the “Big Muskie” weighing in at over 13 000 tons with a bucket capacity of 220 cubic yards or 325 tons (American Electric Power, 2008). These machines efficiently excavate and cast overburden in one cyclical motion from a location on the top of the overburden. The large draglines are called walking draglines because they are moved by being lifted on large pads and moved forward by rotating large cams. Smaller draglines can move on crawler tracks.

The development of steam power shovels was the primary technology that created the large-scale surface mining industry. The steam power shovel loaded the overburden into the off road haulage trucks to be transported to a spoil disposal site. The steam power shovel has been replaced with large electric or diesel powered shovels.

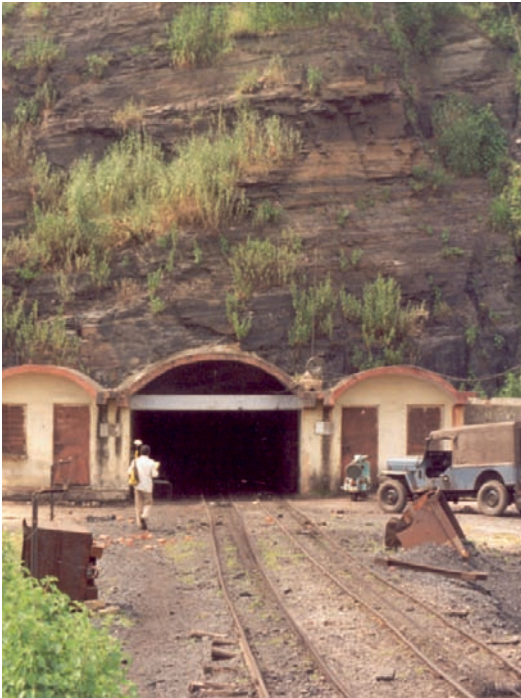
Bucket-wheel excavators are large excavating machines equipped with a long boom on which is mounted a rotating wheel encircled with buckets along its outer edge. The boom is directed into the material to be excavated and the buckets rotate into the overburden scooping up the material which is then dumped onto a conveyor system for transport to a disposal site. Bucket-wheel excavators are best suited to removing unconsolidated overburden that does not contain large rocks or require blasting.

Scrapers are self-propelled rubber tired vehicles that can be used to remove and transport unconsolidated overburden. They are self-loading by pushing forward and lowering a metal plate to scrape and lift dry-unconsolidated overburden into a hopper located in the center of the vehicle. After hauling, the overburden is unloaded by opening the bottom of the hopper while moving forward and using gravity to place a thin layer of overburden at the disposal site or an area being restored.

Off-road haulage trucks are used to transport the overburden to the designated disposal sites. The capacity and size of the off-road haulage trucks increased concurrently with the development of high-capacity power shovels. Today’s modern off-road haulage trucks are truly gigantic, some capable of carrying loads of 300 tons or more.

Underground Coal Mining

Unlike machines used in surface mining, machines used to mine coal in the underground are specifically designed for that single purpose. Such machines include continuous miners equipped with tungsten carbide cutting teeth that rip the coal from the working face to form the rooms in room-and-pillar mining. Coal shearing machines and hydraulically operated roof support systems are used in the longwall setting. In addition, ventilation equipment, rock dusters, roof bolters, shuttle cars, personnel vehicles, scoops, underground rail, coal conveying, and water pumping systems are employed in underground mining.



2.2. Underground Coal Mining

Drift mine opening into an underground mine complex in the Jharia Coalfield, state of Jharkhand, India.

Photo by Stanley R. Michalski, 1994.

Underground Mining

Underground coal mining is comprised of two basic systems; the conventional mining system and the continuous mining system. Conventional deep mining is a systematic procedure whereby the coal, through a series of sequential events, is drilled, blasted, excavated, and hauled from the mine. Intermediate steps include rock dusting for health and safety reasons and roof bolting for insuring roof support in mines. In past mining practice, manual labor was used to achieve these ends. Modern mechanization has increased productivity by mechanizing the sequential utilization of machines to perform these operations. In the modern conventional mine, individual machines are used at the working face to undercutting the coal face, drill the blast holes into the coal seam, load and haul the coal from the mine, and bolt the roof (Schmidt, 1979, p. 164).

The continuous mining system differs from the conventional system by eliminating the need for the sequential steps of drilling, blasting, and manually loading coal from the working face. These operations have been optimized by replacing manual methods with mechanized, mining machines.

Conventional and continuous mining systems continue to be used in various types of underground mining. These two systems of underground mining account for about 60% of world coal production (World Coal Institute, 2005).

Today's modern underground mines are extensions or variations of the early drift and bell pit mines. Regardless of whether they are drift, slope, or vertical shaft mines or use the conventional or continuous mining system, the development of an underground mine employs either the "room-and-pillar" method, also known as "board-and-pillar" mining or the longwall-mining method. Variations of the two principal mining methods exist in the industry. For example, room-and-pillar mine development in horizontal bituminous coal seams is quite different from the room-and-pillar method used to mine steeply pitching anthracite coal seams. Room-and-pillar mining had been the mainstay of underground mining in the United States whereas the longwall method had been well established in Europe. Reasons for this difference include shallower seams in the United States and deeper seams in Europe. In the case of the deeper seams, the required pillar support of the room-and-pillar mining method would leave too much coal in the ground. Less pillar support would result in the crushing of pillars under the weight of the overburden. In the 1970s longwall mining in the United States began to rapidly gain acceptance as a mining method of choice when conditions favor its use (Energy Information Administration, 2008).

Methods of Coal Mining

The principal methods of conventional and continuous methods of mining are discussed in the following paragraphs.

Room-and-Pillar Coal Mining

The room-and-pillar method of mining has changed little throughout the years since its development. The mining method can apply to drift, slope, or vertical shaft mines. In room-and-pillar mining, coal seams are mined by developing a network of “rooms” in the coal seam. Between the “rooms” are “pillars” (walls) of coal left in place to support the roof of the mine. The “pillars” left behind can account for as much as 40% of the total coal in the seam, although much of this can be recovered during later stages of **retreat mining** (World Coal Institute, 2005). In early conventional mining, the “rooms” were excavated by using hand tools (picks and shovels). Then hand drills and explosives were used to loosen the coal and the coal was then hauled from the mine. Today, mechanized equipment undercuts the coal, drilling machines make the drill holes for explosives, and scoops load the blasted coal into shuttle cars or conveyor systems to bring the coal to the surface. In continuous mining, the “rooms” and “pillars” are the same, but differ in the type of mechanization used to mine the coal. Modern advances in technology have led to the development of the **continuous miner**, a machine that cuts into the full thickness of the coal seam. The self-propelled continuous mining machine rips the coal from the working face, in a preplanned pattern of room-and-pillars, with an array of hardened steel cutting teeth mounted on rotating wheels. The excavated coal passes through the continuous mining machine onto a conveyor system or into shuttle cars that transport the coal from the mine (Schmidt, 1979, p. 168). The continuous mining machine has increased the tonnage of coal mined per man shift enormously (Lindbergh and Provorse, 1980, p. 68). Room-and-pillar mining accounts for about 49% of all the underground coal mined in the United States today (American Coal Council, 2008). A significant disadvantage of the room-and-pillar method is that it can leave 50–60% of the coal underground in the supporting “pillars” (World Coal Institute, 2005), but much of this coal can later be recovered by retreat mining (Figure 2.2.1).

Longwall Coal Mining

The **longwall-mining** method is a continuous mining system that was developed for mining coal deposits uniform in thickness and slope or where the overburden pressures may crush support pillars or for improving productivity. This method relies on the complete extraction of the coal in a designated area referred to as a **panel** (of solid coal). As the panel is mined, complete subsidence or caving of the overlying rock strata occurs into the mined-out area behind the working mine face.

Longwall mining can be conducted as advance longwall mining or retreat longwall mining. In either method of longwall mining, the production of coal takes place along a face (wall of coal) that is blocked-out between the two parallel panel entries. The panel in the area designated to be mined can be 305 m (~1000 ft) wide by 3050 m (~10 000 ft) or more deep (Energy Information Administration, 2008). Steel arches and hardwood packs provide the parallel panel entries with roof support. Coal is removed from the face which is perpendicular to the parallel entries. Mining is accomplished by a shearer or cutting tool forced against the face of the coal seam hydraulically and pulled laterally across the width of the panel. The shearer consists of rotating drums studded with cutting bits that are raised or lowered depending on seam thickness. The shearer operator moves with the machine as it advances along the face. The broken coal is deposited on a conveyor system running parallel to the face which carries the coal to the parallel entries and out of the mine.

The roof of the mine is supported by hydraulically powered, self-advancing roof supports attached to the mining machine. As the mining machine advances into the solid coal panel, the roof supports also advance keeping overburden from collapsing into the exposed face of the coal. At the same time, the roof left unsupported is allowed to break and cave immediately behind the support line with each face advance. This permits most of the weight of the overburden to rest on the broken, caved spoil material as mining advances. The longwall-mining machine, conveying system, roof support, and guidance systems are advanced hydraulically after each pass of the coal shearer.

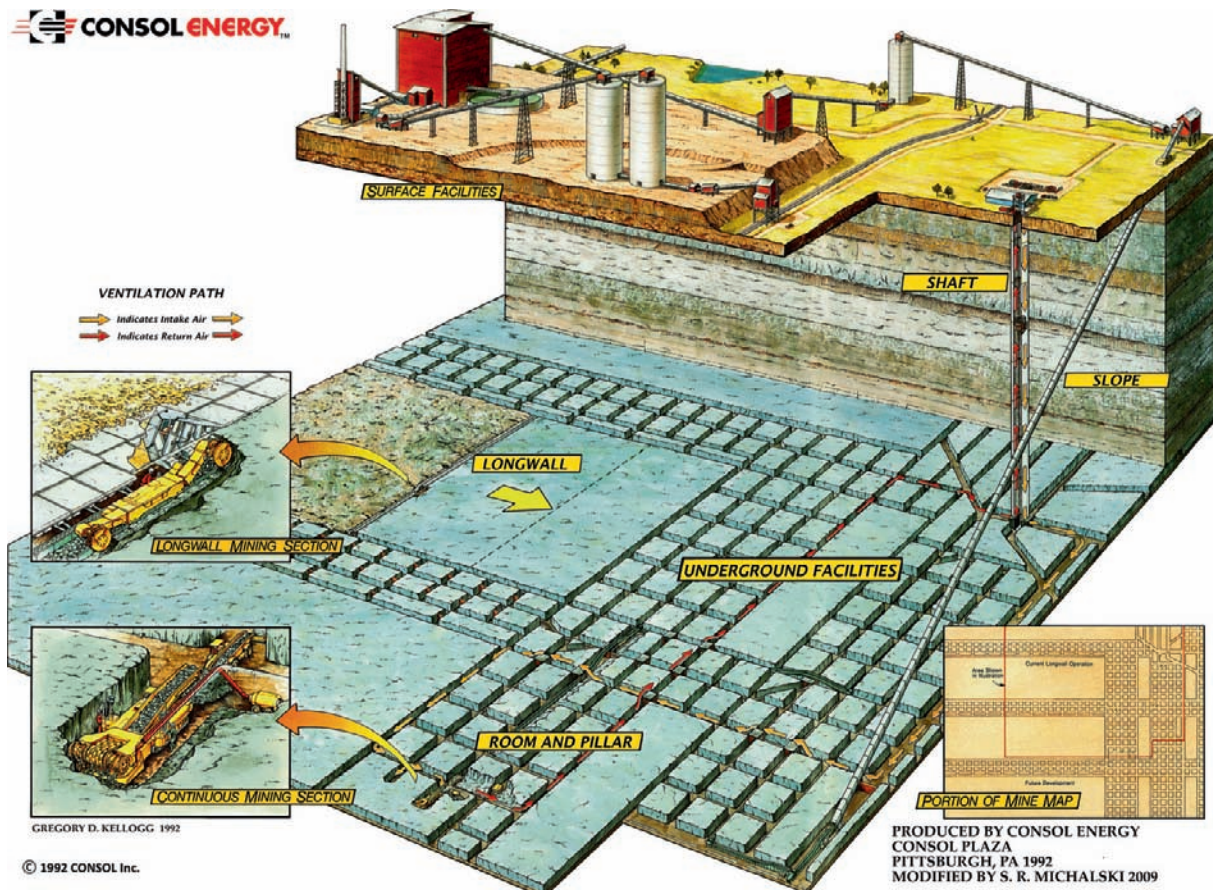


Figure 2.2.1. Figure illustrating the general layout of a modern coal mine. Although incomplete in every detail, it illustrates the mining methods and technology employed. Modified with permission from Consol Energy Inc. 1992 poster by Stanley Michalski, 2009.

As the title suggest, the advance longwall system mines the panel by advancing into the coal seam and simultaneously developing the parallel entries moving farther away from the main entry. Retreat longwall mining is the reverse of the advance longwall method and is used where unstable roof and floor conditions exist throughout the mine. In retreat longwall mining, the parallel entries are first driven to the farthest limit of the designated mining panel and a connection is made between the parallel entries before production begins. Longwall mining then begins at the farthest or outer end of the panel and “retreats” back to the main entry. The principal disadvantage of the retreat system is that lead time between driving the parallel entries and coal production is much greater than in the advance longwall system in which coal production can begin almost immediately. The tools, support system, and coal conveyance out of the mine are the same for both methods. Mining is completed when the panel between the parallel entries has been completely extracted.

Production costs per ton of coal are generally lower with the longwall method than with the room-and-pillar method, due to fewer roof-control problems, lower roof-support costs, reduced maintenance costs, minimal dust control cost, and a higher tonnage yield per man. Ventilation problems are also greatly reduced, as the air must be coursed over only one working area. The room-and-pillar method of mining requires air to be passed through several areas requiring a complex network of ventilation control devices. In addition, the training of personnel for longwall mining can be accomplished more quickly than the training required for the room-and-pillar method. About 50% of the underground coal mined in the United States today is by the longwall-mining system (American Coal Council, 2008).

The Special Case of Anthracite Mining

Although anthracite coal mining is of relatively minor importance today, the methods of recovering anthracite coal include surface mining, room-and-pillar, and longwall mining when the coal beds are relatively flat lying. The excavation of very deep strip-mining pits (surface mining) and the unique method of steep-pitch mining (underground mining) are used when the anthracite coal seam slopes into the ground at a steep angle. Steep-pitch mining requires driving **gangways** perpendicular to the slope of the coal that begin at the base of a slope or shaft mine entry. The gangways usually contain mine car tracks that are used to haul the mined coal to the slope or shaft, deliver men and equipment to the working faces, and provide a conduit for ventilating the mine (Rhone, 2008, p. 3). Gangways are followed by chute-and-pillar mining (a variation of room-and-pillar) upslope of the gangways. The method allows the mined coal to fall by gravity from the room being mined through a chute and into coal shuttles that move into and out of the mine along a network of gangways (Otto, 1925, p. 712). The method of driving gangways and the chute-and-pillar method of steep-pitch mining was highly developed in the anthracite coal basins of the eastern United States (Buch and Corgan, 1956, p. 44; Otto, 1925, p. 711). The introductory figure of Section, 2.3 is a photograph of the Centralia Basin, a part of the Western Middle Field of the anthracite coal fields of the eastern United States where steep-pitch underground mining and surface mining techniques were used to maximize recovery.

As in most forms of mining, anthracite surface mining methods recover the most coal. Anthracite underground methods, particularly the room-and-pillar method, result in substantial coal left in the ground. The remaining coal is in the form of pillars that support the mine or as barrier pillars to control water or separate one mining operation from another. These remaining pillars also support surface features such as highways, towns, railroads, streams, and rivers.

Ventilation

Proper ventilation of active underground workings is an integral part of the conventional and continuous mining systems. Without it, underground coal mining cannot proceed since the proper movement of air throughout the mine brings fresh air to the working face so miners can breathe. Proper ventilation also carries away explosive and poisonous gases and prevents the accumulation of heat in areas prone to **spontaneous combustion**. Ventilation is accomplished by using the existing tunnels, galleries, cross-cuts, and haulage ways to create a ventilation circuit. The ventilation circuit is driven by large fans that exhaust the mine air from the mine while fresh air inflow is directed to the area to be ventilated. The quantity (volume) and velocity of air flowing through a mine are a function of the rate at which gases are liberated at the working face (Schmidt, 1979, p. 179). Since the mining operation continuously creates new tunnels and an advancing working face, the ventilation system becomes dynamic and must constantly change as the mining progresses and underground conditions change.



2.3. Surface Coal Mining

Surface and steep pitch underground mining in the Centralia Basin, Centralia, Pennsylvania. The Centralia Mine Fire underlies a portion of Centralia Borough, visible at the top of the photograph.

Photo by Robert W. Bruhn, 1983.

Surface Mining

The surface-mining method is commonly referred to as strip, open-cast, or open-cut mining and is employed in flat to moderately rolling terrain. Modern day surface mines tend to be very large, extensively engineered and highly mechanized operations. With this method, an economical thickness of overburden is removed down to a coal seam by following a coal contour along or around a hill or by removing the entire hill top above the coal seam. Mining begins by removing the topsoil and subsoil which are reserved for final reclamation. Then large-scale excavating, drilling, and hauling equipment is employed to remove the rock overlying the coal which is transported to a spoil disposal site. Once the overburden is removed, smaller equipment, including front-end loaders and power shovels, loads the coal into large trucks that transport the coal from the pit and deliver it to a coal preparation plant. Approximately 90% of the coal can be recovered by surface mining. Surface-mining techniques include contour mining, area mining, auger mining, and mountain top removal, all of which account for about 40% of the coal mined in the world and about 67% of the coal mined in the United States (World Coal Institute, 2005). These methods are discussed in more detail in the following sections.

Contour Mining

Contour mining is used when the coal may actually outcrop on the flanks of hillsides in steep, hilly, or mountainous terrain. The technique involves the removal of overburden by following the contour of the outcropping coal and extending the excavation into the hillside to the point where the **overburden ratio** makes further mining unprofitable. This results in a wedge of overburden that is removed and stockpiled. The excavated area becomes a level bench on top of the coal seam. The coal is then mined and the overburden is placed back on the bench to return the hill to its approximate natural slope and contour. In past years, the overburden was cast onto the slope below the exposed coal where it was permanently left which resulted in fill on the outside slope and a highwall on the inside slope with the coal seam exposed at the base of the highwall. Remaining coal behind the exposed high wall was left since it would not have been economical to remove the overburden. This coal was partially recovered by another surface-mining procedure known as auger mining.

In modern day contour mining, once the coal is removed, the land is returned to the approximate original contour with the removed overburden being returned to the mined pits in roughly the same order in which it was removed. Topsoil and subsoils, the first materials to be removed, are then spread over the restored surface and re-vegetated.

Area Mining

Area mining is performed where the ground surface is relatively flat and the overburden is economical to remove. The typical area mine requires the excavation of a series of pits or cuts. The overburden is cast into stockpiles. Overburden from the first cut is usually reserved whereas overburden removal in subsequent cuts is cast into the previous completed cut after the coal is removed. In each cut the overburden is removed until the underlying coal seam is exposed. The coal is then mined in its entirety by large power shovels or front end loaders and hauled from the open cut by trucks. All of the coal seam is recovered by this method of mining. The process of excavation, coal recovery and cut backfilling continues until no additional cuts can be made at which time the reserved first cut overburden is used to fill the last cut.

Auger Mining

Auger mining requires boring large diameter, closely spaced horizontal holes into the coal seam that is exposed at the base of a previously prepared highwall. A horizontal boring machine, equipped with large diameter auger boring tools drills a pattern of horizontal boreholes into the exposed coal seam removing the coal as the bore advances into the coal seam. Augers can bore 61 m (200 ft) or more into a solid coal seam that would otherwise require recovery by developing an underground mine (Schmidt, 1979, p. 199).

The coal bed thus mined must be relatively uniform in thickness and relatively flat lying. The method is not so commonly practiced today as the auger holes left in the coal seam open a very large surface area of coal exposed to air and ground water infiltration resulting in significant production of **acid mine drainage (AMD)**. This results because auger holes are rarely backfilled in their entirety. Typically they are sealed at the exposed end with a low permeability soil backfill that is placed a short distance into the auger hole. After each auger hole is filled in this manner, the length of the exposed coal face is backfilled (buried) with a low permeability soil to seal the coal seam and reclaim the mined area. This method is applicable when no additional overburden can be economically removed.

Mountain Top Removal

The mountain top removal method of surface mining may be the mining method of choice in regions where the rock strata are relatively flat lying and the landscape is punctuated by numerous hills and stream valleys exposing multiple coal seams in the valley walls. Where multiple seams occur and where the overburden to the highest elevation is within an economical overburden stripping ratio, the entire mountain top above the coal seams may be removed. The mountain top is progressively lowered by drilling and blasting the overburden. The overburden is pushed by dozer or cast by dragline into the adjacent valleys surrounding the mountain top. Many hundreds of meters of overburden may be removed in this manner, depending on the number and thickness of the potential coal seams to be recovered. Upon reaching the first layer of coal, drilling and blasting stops while the coal is removed. Drilling and blasting then resumes until the next seam of coal is exposed. The spoil is not used to restore the mountain top, but rather a relatively flat landscape is created with buried stream valleys connecting the flattened mountain tops. While reclamation efforts such as stabilization and revegetation are required for mountaintop removal, the remaining landscape is far different from what it was before mining. The nature of the mountain top removal method of mining so drastically alters the landscape that many oppose its use (McQuaid, 2009).



2.4. Coal Mining and Coal Fires

Abandoned illegal mining and small-scale coal coking operation along a coal outcrop in the state of West Bengal, India.

Photo by Stanley R. Michalski, 1994.

Discovery and Investigation

No single mining technique can claim responsibility for causing coal-mine fires. In the underground methods of coal mining, coal fires can be initiated by accident or, given the proper conditions, by spontaneous combustion. A successful recovery from a fire in an active mine is possible only if fire abatement methods are quickly implemented. In surface mining, fires may be minimized since, theoretically, all the coal is removed which precludes a fire. In some regions of the world where subbituminous and lignite coals are highly susceptible to spontaneous combustion, surface mining cannot be successfully carried to completion if procedures are not in place to deal with the spontaneous eruption of fire that is caused by exposing these coal seams to the atmosphere (Blazek, 2001).

Many technologies are available to determine the location, extent, and rate of spread of coal fires both underground and on the ground surface. Some of these technologies include satellite imagery, airborne thermal infrared imagery (TIR), and historical geologic and mining data and reports. Drilling programs can sample overburden and coal and provide an access to the mine to monitor fire conditions with temperature and gas sampling equipment and to conduct ventilation studies.

Monitoring

A network of monitoring devices in an active mine can provide an early warning and location of an impending fire, help isolate an existing fire, and provide a means of evaluating the effectiveness of fire abatement measures. Monitoring gases that accumulate in active underground workings provides an early warning of spontaneous combustion.

Existing fires in underground mines, where access to the workings is prohibited, can be located and monitored through a network of boreholes drilled to mine level and equipped with appropriate gas- and temperature-sensing devices. Such equipment can be used to determine the intensity, the rate, and direction in which a fire progresses. These boreholes drilled to mine level can normally be left in place for monitoring over the longer term to monitor the effectiveness of abatement measures.

Airborne TIR is a process where a low flying aircraft, flying in the predawn hours, scans the ground surface with an on-board thermal infrared scanner. The method is most often used to diagnose the surface extent of underground burning over large areas of abandoned mined lands. The TIR product is a pictorial representation on a photographic medium of temperature differences between objects at the ground surface. TIR primarily highlights the area where heated gases escape or vent at the ground surface. These vents or “hot spots” may be distant from the actual source of underground burning in a mine. Properly interpreted in the context of the local geology and mine plans, the

general source area of the fire can be estimated. Such surveys are useful when repeated periodically under similar weather conditions, the same time of day (typically in the predawn hours) and in the same season. Repeat surveys will show new as well as retired areas of hot gas venting. TIR surveys most prominently highlight the area of venting gases and may not capture the total spatial extent of an underground mine fire.

Mine fires in active surface or subsurface workings typically are located quickly and abatement measures implemented in a timely manner. Underground mine fires in abandoned mines are more difficult to locate, track, and abate. These mine fires require integrating a host of technologies to effectively locate and assess the scope of the fire problem. Where little is known about an underground fire other than smoke exiting an entry or vent, the first task is to determine the potential limits of the fire. These limits can be determined through an understanding of the coal geology, mining history, pattern of mine workings, and known barriers to the spread of fire both above and below ground. A TIR survey will quickly locate the limits of venting along an outcrop or from fissures extending into the mine workings.

Mine Atmosphere

On a volumetric basis, normal (fresh) air consists of 20.94% oxygen (O₂), 78.08% nitrogen (N₂), 0.93% argon (Ar), 0.03% carbon dioxide (CO₂), and 0.02% other gases, including neon (Ne), methane (CH₄), helium (He), and other trace gases (Weast, 1986, p. F-156). Mine atmosphere compositions may depart from this norm due to a variety of underground phenomena, including mine fires. The composition of the mine atmosphere varies within a mine due to a variety of underground conditions, and these variations, in conjunction with temperatures can assist in differentiating areas that are burning from those that are not. The composition of the mine atmosphere can change with time and present conditions will not necessarily last indefinitely. Roof falls and other ground adjustments may redirect air flow so as to dilute or drive off areas of low O₂ content so flaming combustion cannot occur. Reactions – some of them subtle, others violent – may chemically alter the constituents of the mine atmosphere. Like temperature, the composition of the mine atmosphere is transient and must be monitored on a periodic basis to obtain useful information.

Oxidation is a chemical process that is widespread in mine workings and involves the combination of oxygen with another substance to form a compound. The composition and properties of the compound may vary depending upon the rate and temperature of the oxidation process. Here, oxidation refers to slow, low-temperature processes, such as the weathering of coal or pyrite or the decay of wood whereas the term **combustion** refers to the rapid chemical combination of oxygen with the combustible elements of a fuel wherein appreciable heat is given off, sometimes with light.

Oxidation of coal can result in the phenomenon of spontaneous combustion where the coal is not exposed to an external heat source, but environmental conditions allow for the accumulation of heat and the continued oxidation of the coal. The oxidation process releases CO₂, CO, and heat. In addition, the oxidation of pyrite and the **adsorption** of water on the coal surface are also heat-generating processes and add to the accumulating heat. As the temperature rises, sustainable self-heating of coal begins when the rate of heat gain increases faster than the rate of heat loss. Once self-heating begins and the environmental conditions that induce the process are maintained, the temperature of the coal will continue to rise until the ignition temperature is reached whereby flaming combustion is initiated. Figure 2.4.1 shows the cross-over point whereby accumulating heat leads to accelerated oxidation which results in ignition and flaming combustion. As long as the heat of oxidation is removed faster than it can accumulate or the oxygen content is insufficient to support combustion, then there will be no fire.

The sustainable self-heating temperature of coal can vary substantially, but mostly depends on the rank of the coal and conditions that favor the retention of heat. The minimum temperature in which a coal will self-heat is about 35°C (95°F) for lignite, subbituminous, and high-volatile bituminous coal (Smith and Lazzara, 1987, p. 25), 135°C (275°F) for bituminous coal and 140°C (284°F) for anthracite coal (Kim and Chaiken, 1990, p. 3). Kim and Chaiken (1993) report that normal ignition temperature of coals they investigated range between 400 and 500°C (753–932°F), though some poorer quality coals in Asia have also reported to ignite well below the boiling point of water (Chakrabarty, 2009, p. 3 and Coalfire.org, 2009). The ignition temperature is influenced by pressure, velocity, geometry of the burning zone, catalysts, air–fuel mixture, ignition source, and moisture content. In combustion, a portion of the fuel may remain unburned, leaving carbon in the ash; or the carbon may burn incompletely to form CO as well as CO₂. The quantity of air theoretically required for complete combustion is

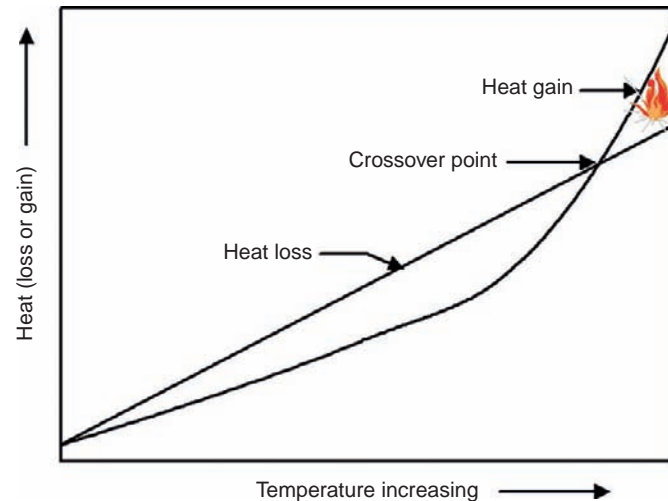


Figure 2.4.1. Rate of heat loss and rate of heat gain versus temperature. From Kim et al. 1993.

termed 100% total air. Because the conditions for combustion are never wholly ideal, the theoretical air requirement must generally be augmented to achieve complete combustion. Analyses of the gases leaving a combustion process can indicate the relationship between excess air and the types of fuel being burned. A variety of fuels can participate in the combustion process including coal, wood, tar, pitch, and coke, among others. Day-to-day and hole-to-hole variations in gas composition may reflect actual differences in fuel type, but may also reflect variations in mine level ventilation and other factors.

A number of other parameters and indices have been devised by physical chemists to express relationships between combustion products derived from mine fires. Although largely developed in a controlled laboratory environment, these relationships have been successfully employed in determining the status of fires in active mines. The application of these parameters and indices to abandoned mines is more tenuous. Yet, much useful information can come from these gas analyses, particularly when used in conjunction with borehole temperature data. It is beyond the scope of this chapter to delve into the details of these various parameters.

Abatement

Mine fire control is comprised of two components: isolation (containment) and extinguishment. Isolation entails blocking or severing all potential avenues for the spread of fire. Extinguishment entails eliminating the fire. To extinguish a fire, either the fuel or the oxygen supply must be removed or the temperature (of the fuel) must be reduced below the limits required to support combustion. Removing any one of these legs of the fire triangle will result in extinguishment. Depending on the particular situation, these components constitute the three legs of the fire triangle illustrated in Figure 2.4.2 and may be addressed singly or in combination.

The components of the fire triangle can be further subdivided into conventional mine fire control techniques and more or less unconventional or unproven mine fire control techniques. The former includes conventional construction procedures such as total excavation (of the burning seam), isolation trenches, and mine void filling. The latter may include less conventional or novel techniques including chemical treatment (including nitrogen entrainment in foam), in situ coal gasification, and **burn-out control** (Michalski et al., 1997).

The success of a fire abatement measure often depends on whether the mine is active or abandoned, regardless of the method of mining. Fires in active underground mines are often discovered quickly, through an explosion or through detection by monitoring which results in quickly implemented abatement measures. It is important that abatement in an active mine is attended to in a timely manner so as to prevent loss of life and to minimize lost coal production. The sudden emergence of a young fire is slow to heat the overburden and condition the coal that enhances susceptibility to ignition. Fire abatement measures in an active mine

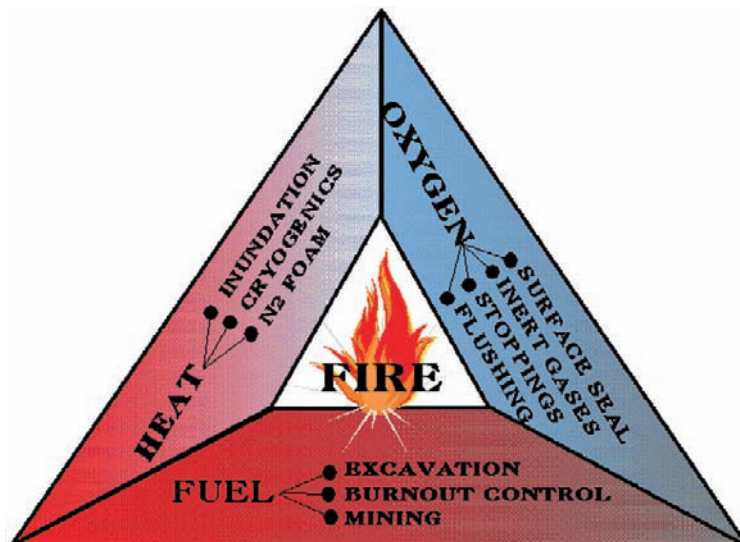


Figure 2.4.2. The fire triangle. From Kim et al. 1993.

may include isolating the burning portion of the mine through controlled ventilation and flooding the area with inert gases or nitrogen entrained foam extinguishing agents which are often successful. Inert gas usage may include the introduction of cryogenic nitrogen or carbon dioxide or even combustion gases with a low O_2 content that will not support combustion.

Fires in abandoned mines are quite another matter. Often they reside in the abandoned room-and-pillar workings for many years before they are detected. Such long residence time heats the surrounding overburden and rock strata, conditions the coal and dries the underground workings resulting in an ever-increasing rate of fire progression. These fires become intractable and may require heroic efforts and staggering cost to bring them under control, usually with no guarantee of success. More often than not, the cost and effort required for mitigation strains both government and industry resulting in a policy to do little or nothing (Michalski, 2004, p. 90).

The Centralia Mine Fire, located in the steep pitch, room-and-pillar mines in the anthracite coal fields of eastern Pennsylvania, is an example of an underground mine fire on abandoned mined lands. The fire began in 1962 in an abandoned strip mine pit made into a landfill dump (Dekok, 1986, p.20). The Buck Mountain coal seam was exposed at the bottom of the pit underlying the landfill. As the trash in the landfill burned, the fire came in contact with the coal seam and quickly spread into the underground workings. Eventually, the fire spread from the Buck Mountain seam into the workings of other, overlying, mined coal seams (Bruhn, et al., 1983, v. 1, p. 3.35). Over the years, numerous investigation and abatement projects were initiated that had either too little funding or were implemented too late. As the fire spread, abatement cost escalated. Consequently, in 1983, the United States Congress appropriated 42 million dollars to buy out the Borough of Centralia (Dekok, 1986, p. 276) and relocate its 1000 residents and more than 600 buildings (Krajick, 2005, p. 52, 59). This was considered to be the most cost-effective measure to distance the population from the dangers of the mine fire (Tietz, 2004, p. 42) since a total excavation of the burning zone in 1983 would have cost 663 million dollars (Bruhn, et al., 1983, v. 2, p. 6.36). This final buyout was in addition to the 200 buildings and 178 houses that were demolished in the 1960s due to the fire's encroachment on the Borough (Krajick, 2005, p. 60). The cost of all abatement measures over the years and the final buyout, did nothing to abate the fire which has expanded from ~195 acres in 1983 (Bruhn, et al., 1983, v. 2, p. 6.5) to ~400 acres in 2005 (Krajick, 2005, p. 60) to a potential ultimate spread of 3700 acres (Bruhn, et al., 1983, v. 2, p. 6.29).

Acknowledgments

The author thanks Tomas A. Gray, P.E., Tetra Tech, Inc., Pittsburgh, Pennsylvania for his review of this chapter.

Important Terms

Acid mine drainage (AMD)	Acid mine drainage (AMD) is the runoff produced when water comes in contact with exposed rocks containing sulfur-bearing minerals that react with water and air to form sulfuric acid and dissolved iron. This acidic run-off dissolves heavy metals including copper, lead, and mercury which pollute ground and surface water.
Adsorption (on coal)	A process that occurs when water accumulates on the surface of coal, forming a film.
Airborne thermal infrared imagery (TIR)	A remote sensing technology used to scan the earth's surface from a low flying aircraft for the purpose of detecting heat emissions at the ground surface. Data are presented in a photographic format.
Bell pit	The bell pit is an obsolete form of mining whereby a vertical shaft was dug into the ground to the level of the coal seam. That portion of the pit that was in the coal seam would be expanded laterally and the coal removed through the central shaft. The room at the bottom of the shaft would be enlarged to the point of collapse at which point a new bell pit would be dug.
BTU (British thermal unit)	The quantity of heat required to raise the temperature of one pound of water one degree Fahrenheit.
Burn-out control	An experimental technology that accelerates the in situ combustion of coal within a defined area in an inactive underground mine that provides some measure of control over the rate and direction of the underground burn. The technology can recover useful heat in the process that can be used to generate electricity or heat water.
Coalfield	An area of land underlain by one or more coal seams.
Coal preparation plant	A facility where the coal coming from a mine is processed or cleaned in order to enhance its properties to be made more suitable for its ultimate use. The process removes unwanted noncombustible materials such as rock and unwanted minerals such as pyrites, resulting in the enhancement of the heat value per ton of coal.
Coal rank	A classification scheme based on the moisture, carbon, and ash content of a coal, and to a lesser extent on additional associated minerals. Coals are classified into four principal ranks: lignite, subbituminous, bituminous coal, and anthracite. Lignite, being the lowest rank of coal contains 0.6 wt.% sulfur, 38% moisture, 27% volatile matter, 29% fixed carbon, and about 6% ash and has the lowest heating value (about 6800 BTU/lb) and the lowest carbon content. Subbituminous is next in rank being composed of 0.6 wt.% sulfur, 25% moisture, 35% volatile matter, 35–45% fixed carbon, and about 7% ash and has a heating value at about 8250 BTU/lb. Bituminous is the most common type of coal and is comprised of 3.0 wt.% sulfur, 5% moisture, 38% volatile matter, 45–86% fixed carbon, and about 9% ash with a heating value of 12 900 BTU/lb. Anthracite is the highest rank of coal, containing 1.5 wt.% sulfur, 4% moisture, 7% volatile matter, 86–97% fixed carbon, and about 10% ash and has a heating value of about 13 500 BTU/lb (G.E. Dolbear & Associates, Inc., 2009).
Combustion	The rapid chemical combination of oxygen with the combustible elements of a fuel (coal) wherein heat is produced (burning), sometimes accompanied with light.
Continuous miner	The continuous miner is a mining machine with a large rotating steel drum equipped with tungsten carbide teeth that cut coal from an exposed coal seam. The machine typically operates in a room-and-pillar-type underground mine. Continuous miners work in conjunction with conveyor systems to move the mined coal out of the mine.
Drift mine	A type of underground mine where an opening or entry is made into an exposed coal seam, usually in the side of a hill.
Gangway	A permanent heavily supported tunnel constructed at the bottom of an entry slope or shaft that is driven in two directions through a steeply pitching coal seam. Gangways

	usually contain mine car tracks that are used to haul the mined coal to the slope or shaft, deliver men and equipment to the working faces, and to provide a conduit for ventilating the mine.
Geomorphology	The scientific study of landforms and the processes that shape them.
Longwall mining	A form of underground coal mining where a longwall (typically about 250–400 m long) of coal is mined in a single slice (typically 1–2 m thick). The longwall “panel” (the block of coal that is being mined) is typically 3–4 km long and 250–400 m wide.
Overburden	In mining, overburden is the material that lies above the area to be mined. The cast overburden then becomes mine spoil.
Overburden ratio	The ratio of the amount of soil and rock overburden excavated to the coal recovered. A break-even stripping ratio is reached when the value of the mined coal is the same as the cost to remove the overburden.
Oxidation	The interaction between oxygen molecules and other substances, including coal.
Panel	The term is used in longwall mining where a panel is a rectangular block, or pillar, of coal, the size of which is determined by the surrounding workings which is ultimately completely mined.
Retreat mining	The systematic removal of all or parts of the pillars left following completion of a room-and-pillar mining operation. Retreat mining begins at the rear of the mine and progresses toward the mine entry. As the coal in the remaining pillars is extracted, pillar support is reduced, and the roof of the mine collapses. About half again of what was originally left in the mine can be recovered by this very hazardous mining technique. Following retreat mining, the mined area is abandoned.
Slopes and shafts	A slope is an inclined excavation extending from the ground surface to the coal seam, whereas a shaft is a vertical excavation from the ground surface to the coal seam.
Spontaneous combustion (of coal)	Self-heating and burning of coal in contact with air.

References

- American Coal Council, 2008. http://www.clean-coal.info/pubs/coal_basics.pdf (accessed December 15, 2008).
- American Electric Power, Inc., 2008. <http://www.aep.com/newsroom/newsreleases/?id=517> (accessed December 15, 2008).
- Blazek, C., 2001. The influence of moisture on the spontaneous combustion of coal. Benetech, Inc., <http://www.benetechusa.com/pdf/article/SpontaneousCombOfPRBCoal.pdf> (accessed October 15, 2008).
- Bruhn, R.W., Michalski, S.R., Winschel, L.J., Yeasted, J.G., 1983. Engineering analysis and evaluation of the Centralia Mine Fire. Contract Report No. J5130057, GAI Consultants, Inc., Pittsburgh, PA for the U.S. Department of the Interior, Office of Surface Mining Reclamation and Enforcement, Eastern Technical Center, Pittsburgh, PA., vols. 1 and 2.
- Buch, J.W., Corgan, J.A., 1956. Anthracite: mineral facts and problems. U.S. Department of the Interior, U.S. Bureau of Mines, Bulletin 556, United States Government Printing Office, Washington, DC, 1259 p.
- Chakrabarty, G., 2009. Coalfires: an environmental hazard. Msc Geo-informatics, BIT Mesra, Ranchi, India, 21 p. Coalfire.org. http://www.coalfire.org/image/pdf/b_dmt_bam.pdf (accessed May 30, 2010).
- DeKok, D., 1986. Unseen danger: a tragedy of people, government, and the Centralia Mine Fire. University of Pennsylvania Press: Philadelphia, 299 p.
- Energy Information Administration, Coal production in the United States. U.S. Department of Energy, 2008. http://www.eia.doe.gov/cneaf/coal/page/coal_production_review.pdf (accessed February 13, 2008).
- G.E. Dolbear & Associates, Inc., 2009. The science and technology of coal. Diamond Bar, CA, <http://www.coalscience.com/rank.htm> (accessed January 8, 2009).
- Hansen, M.C., 1990, Coal. How It Is Found and Used. An Earth Resources Book. Enslow Publishers, Inc., Hillside, NJ, USA, 64 p.

- Kim, A.G., Chaiken, R.F., 1990. Relative self-heating tendencies of coal, carbonaceous shales, and coal refuse. Proceedings of the 1990 Mining and Reclamation Conference, Charleston, WV, April 23–25, 1990. WV University Publishing Services, Morgantown, WV, pp. 535–542.
- Kim, A.G., Chaiken, R.F., 1993. Fires in abandoned coal mines and waste banks. U.S. Department of the Interior, Bureau of Mines, Information Circular IC9352, Washington, DC, 58 p.
- Krajick, K., 2005. Fire in the hole. Smithsonian Magazine, May 2005. pp. 52–61.
- Lindbergh, K., Provorse, B.L., 1980. Coal. A Contemporary Energy Story. Scribe Publishing Corporation, Seattle, WA, 207 p.
- McQuaid, J., 2009. Mining the mountains. Smithsonian Magazine, January 2009, <http://www.smithsonianmag.com/science-nature/Mining-the-Mountain.html?c=y&page=6> (accessed January 19, 2009).
- Michalski, S.R., Custer, E.S., Jr. and Munshi, P.L., 1997. Investigation of the Jharia Coalfield Mine Fires-India, Proceedings of the American Society for Surface Mining and Reclamation, Austin, Texas, May 10-16, 1997.
- Michalski, S.R., 2004. The Jharia mine fire control technical assistance project: an analysis, International Journal of Coal Geology, 59, Issues 1-2, July 2004, pp. 83–90.
- Oosthoek, K.J.W. 1998. The role of wood in world history. <http://www.eh-resources.org/wood.html> (accessed February 2008).
- Otto, H.H., 1925. Ultimate recovery from anthracite beds. Am. Inst. Min. Eng. Trans. 72, pp. 710–729.
- Rhone, R.D., 2008. Anthracite coal mines and mining. eHistory@The Ohio State University, <http://ehistory.osu.edu/osu/mmh/gildedage/content/AnthraciteRhone.cfm> (accessed September 2008).
- Schmidt, R.A., 1979. Coal in America. An Encyclopedia of Reserves, Production, and Use. Coal Week/McGraw-Hill Publications Co., New York, 458 p.
- Smith, A.C., Lazzara, C.P., 1987. Spontaneous combustion studies of U.S. coals. U.S. Department of the Interior, Bureau of Mines, Report of Investigations RI9079, Washington, DC, 28 p.
- Tietz, J., 2004. The great Centralia mine fire. Harpers Magazine, February 2004, pp. 47–57.
- Weast, R.C. (Ed.), 1986. CRC Handbook of Chemistry and Physics, 67 ed. CRC Press, Inc., Boca Raton, FL, 2424 p.
- World Coal Institute, 2005. The coal resource: a comprehensive overview of coal. World Coal Institute, London, UK, 46 p.

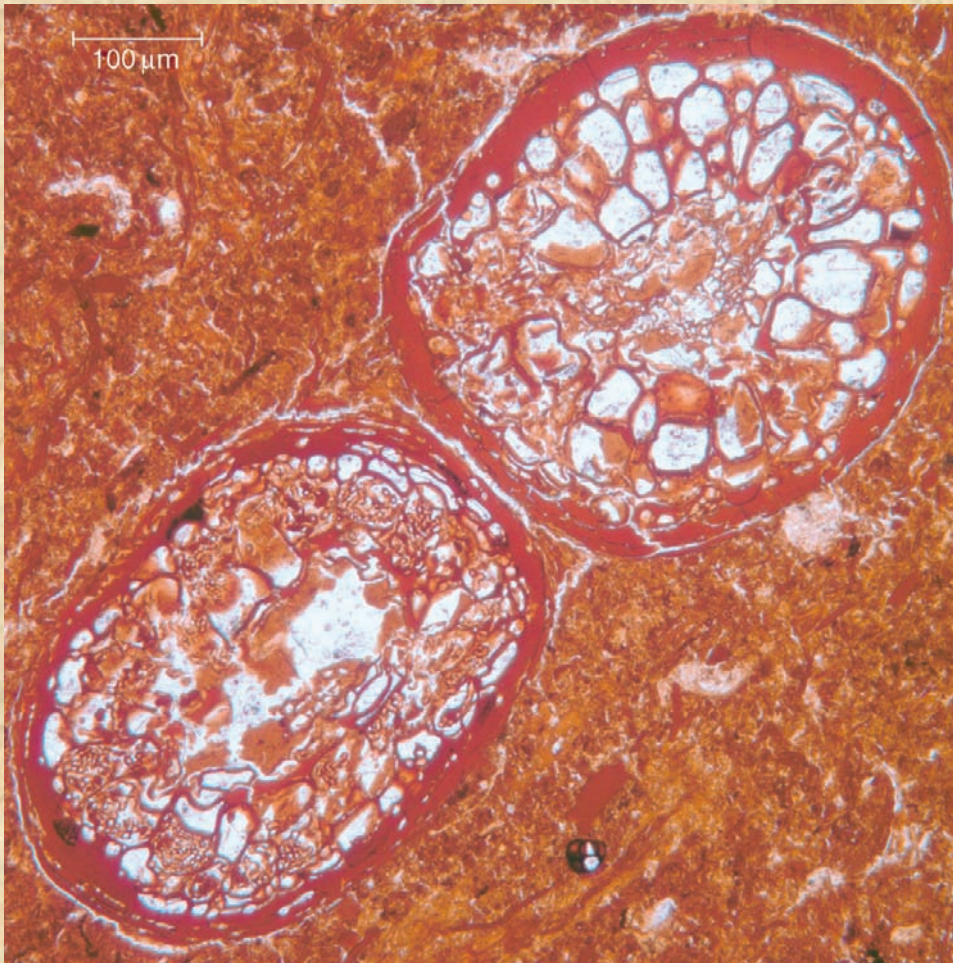
WWW Addresses: Additional Reading

- (1) **American Coal Council**
http://www.clean-coal.info/pubs/coal_basics.pdf
- (2) **American Electric Power, Inc.**
<http://www.aep.com/newsroom/newsreleases/?id=517>
- (3) **Coal, Wikipedia, The Free Encyclopedia**
<http://en.wikipedia.org/wiki/coal>
- (4) **BCS, Inc., 2002. Mining industry of the future: energy and environmental profile of the U.S. mining industry.** U.S. Department of Energy, Office of Energy Efficiency and Renewable Energy, pp. 2–21, 2–26, <http://www1.eere.energy.gov/industry/mining/pdfs/coal.pdf> (accessed February 2008).
- (5) Clark, G., Jacks, D., 2007. Coal and the industrial revolution, 1700–1869. Eur. Rev. Econ. Hist. 11, 39–72.
- (6) Doyle, W.S., Strip mining of coal. Environmental Solutions. Noyes Data Corp., Park Ridge, NJ, 352 p.
- (7) Eavenson, H.N., 1942. The First Century and a Quarter of American Coal Industry. Pittsburgh. Privately printed (Waverly Press, Baltimore), 701 pp.
- (8) **Energy Information Administration, U.S. Department of Energy**
<http://www.eia.doe.gov/neic/aboutEIA/aboutus.html>
- (9) Freese, B., 2003. Coal. A Human History. Perseus Publisher Cambridge, MA, 308 p.
- (10) Fung, R., 1981. Surface Coal Mining Technology Engineering and Environmental Aspects. Energy Technology Review, No. 71. Noyes Data Corp., Park Ridge, NJ, 380 p.
- (11) **History of Coal Mining, Wikipedia, The Free Encyclopedia.**
http://en.wikipedia.org/wiki/History_of_coal_mining
- (12) Jones, D.C., Hunt, J.W., 1949. Coal Mining, 3rd ed. School of Mineral Industries, Pennsylvania State College, State College, PA.
- (13) Keystone Coal Industry Manual, 2005. Intertec Publishing, Chicago, 832 pp.
- (14) Majumdar, S.K., Miller, E.W., Pennsylvania Coal Resources, Technology, and Utilization. Pennsylvania Academy of Science, Easton, PA, 594 p.
- (15) Quigley, J., The Day The Earth Caved IN. Random House, NY, 237 pp.

- (16) Rhone, R.D., 1902. Anthracite Coal Mines and Mining. Review of Reviews, NY.
- (17) Schobert, H.H., 1987. Coal, The Energy Source of The Past and Future. American Chemical Society, Washington, DC, 298 p.
- (18) Stefanko, R., Bise, C.J. (Eds.), 1983. Coal Mining Technology Theory and Practice. Society of Mining Engineers of the American Institute of Mining, Metallurgical, and Petroleum Engineers, New York, NY, 410 p.
- (19) **When Coal was King: Coal Mining in Western Canada**, Heritage Community Foundation.
<http://www.coalking.ca/>
- (20) **World Coal Institute**
<http://www.worldcoal.org>

CHAPTER 3

Spontaneous Combustion and Coal Petrology



Cross-section of a Neogene plant root (?) in a high volatile A coal, south Urals, Russia.

CHAPTER CONTENTS

3.1 Spontaneous Combustion and Coal Petrology

- Introduction
- Maceral Composition of Coal
- Inorganic Matter in Coal
- Microlithotypes
- Lithotypes
- Coal Rank
- Coal Petrology and Spontaneous Combustion
- Important Terms
- References
- WWW Addresses: Additional Reading

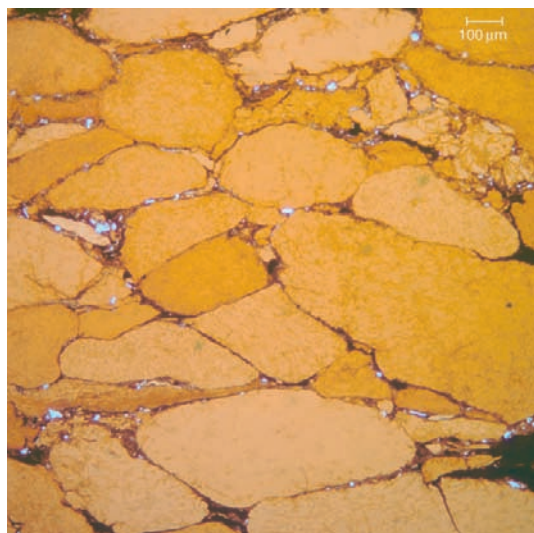


Photo by James C. Hower, 2008.

3.1. Spontaneous Combustion and Coal Petrology

Maria Mastalerz
Agnieszka Drobniak
James C. Hower
Jennifer M.K. O'Keefe

Assemblage of Cretaceous resinite in a high volatile A Liposzii coal, Russia.

Introduction

Macerals, the microscopically identifiable organic constituents of coal, are one of three basic parameters that define coal. The other two parameters are the **coal rank**, the measure of metamorphism of the organic constituents, and the **inorganic content of the coal**, most visibly seen as the minerals associated with coal. Below we briefly present the basic concepts of **coal petrology** and discuss coal parameters that have been noted as potential triggers for spontaneous combustion.

Maceral Composition of Coal

Macerals are microscopically recognizable organic entities in coal and sedimentary rocks. They were introduced by analogy to minerals in rocks. There is, however, a major difference between the concept of minerals and macerals. In contrast to minerals that have homogeneous composition and unchangeable internal structure, macerals consist of a mixture of organic compounds that, in addition, undergo both physical and chemical changes during coalification. Macerals in coal are distinguished microscopically by color, shape, morphology, and degree of preservation of cell structure, reflectance level, and the intensity of fluorescence. These differences between macerals result from different parent material (e.g., different plant parts), different depositional environment, or preservation.

Macerals are classified into three groups: **vitritinite/huminitite**, **inertinite**, and **liptinitite** (Table 3.1.1). These maceral groups are each subdivided into maceral subgroups and macerals. Several standardized systems of nomenclature exist worldwide. These classification systems are variations of the system established by the International Committee for Coal and Organic Petrology (ICCP, 1998, 2001; Sykorova et al., 2005), the organization that develops and revises coal petrology terminology and nomenclature.

The **vitritinite** group (Figure 3.1.1) represents woody plant material (e.g., stems, trunks, roots, and branches), derived from lignin and cellulose of plant tissues. **Telovitritinite** represents intact compressed fragments of woody material of varying degree of compaction. The remains of the cell structure must be visible to distinguish this maceral subgroup. **Detrovitritinite** results from smaller fragments, shows higher degree of degradation, and usually forms groundmass for other macerals. Gelified material produced before or during coalification becomes **gelovitrinitite**, a relatively rare maceral in the coal.

The **liptinitite** group (Figure 3.1.2) includes components that are chemically more resistant to physical and chemical degradation than other macerals such as pollen, spores, cuticles, waxes, and resins. Liptinitite

Table 3.1.1

Classification of macerals into subgroups and groups, based on the international committee for coal and organic petrology (ICCP, 1998, 2001), the Australian Standard System of nomenclature (AS, 1995), and the American Society for Testing and Materials (ASTM, 1996).

Maceral group	Maceral subgroup	Maceral (ICCP, 1998, 2001)	Maceral (AS 3856-1986)	Maceral (ASTM D 2799)
Vitrinite	Telovitrinite	Telinite	Textinite*	Vitrinite
		Collotelinite	Texto-ulminite* Eu-ulminite* Telocollinite	
	Detrovitrinite	Vitrodetrinite Collodetrinite	Attrinite* Densinite* Desmocollinite	
	Gelovitrinite	Gelinite Corpogelinite	Corpogelinite Porigelinite* Eugelinite	
Liptinite		Sporinite	Sporinite	Sporinite
		Cutinite	Cutinite	Cutinite
		Resinite	Resinite	Resinite
		Exsudatinite	Liptodetrinite	
		Chlorophyllinite	Alginite	Alginite
		Suberinite	Suberinite	
		Alginite (var. lamalginite, telalginite)	Fluorinite	
		Bituminite	Exsudatinite	
		Liptodetrinite	Bituminite	
Inertinite	Telo-inertinite	Fusinite	Fusinite	Fusinite
		Semifusinite	Semifusinite	Semifusinite
		Funginite	Sclerotinite	Sclerotinite
		Secretinite		
		Inertodetrinite	Inertodetrinite	Inertodetrinite
	Detro-inertinite	Micrinite	Micrinite	Micrinite
		Macrinite	Macrinite	Macrinite
	Gelo-inertinite			

*Refers to brown coal (low-rank) macerals, otherwise the vitrinite classification is for medium and high-rank coals.

macerals are enriched in hydrogen, owing to a greater amount of aliphatic components. Therefore, **alginite** (the remains of algae) and other hydrogen-rich components such as **bituminite** are also included in this group. Liptinite is fluorescent at lower coal ranks, and the fluorescent color and the intensity of fluorescence help identify individual macerals of this group. In higher rank coals, liptinite loses its fluorescence and is generally indistinguishable from vitrinite due to the convergence of reflectances of the maceral groups.

The **inertinite** maceral group (Figure 3.1.3) originates from the same material as the vitrinite group and the liptinite group, but has a higher degree of aromatization and condensation. Inertinite macerals have a greater carbon content than vitrinite group macerals at the same rank because they were carbonized, oxidized, or subjected to chemical or bacterial attacks prior to coalification, usually in the peat stage. Under reflected light microscope, macerals of inertinite group are lighter (higher reflectance) compared to vitrinite macerals. Cell structure is very well preserved in **fusinite** and significantly less preserved in **semifusinite**. Other macerals of this group are distinguished based on their gelification degree (**macrinite**) or their high reflectance (**micrinite**). The fusinite and semifusinite macerals of this group are formed, in part, as a result of wildfires, and their reflectance is directly related to the fire temperature.

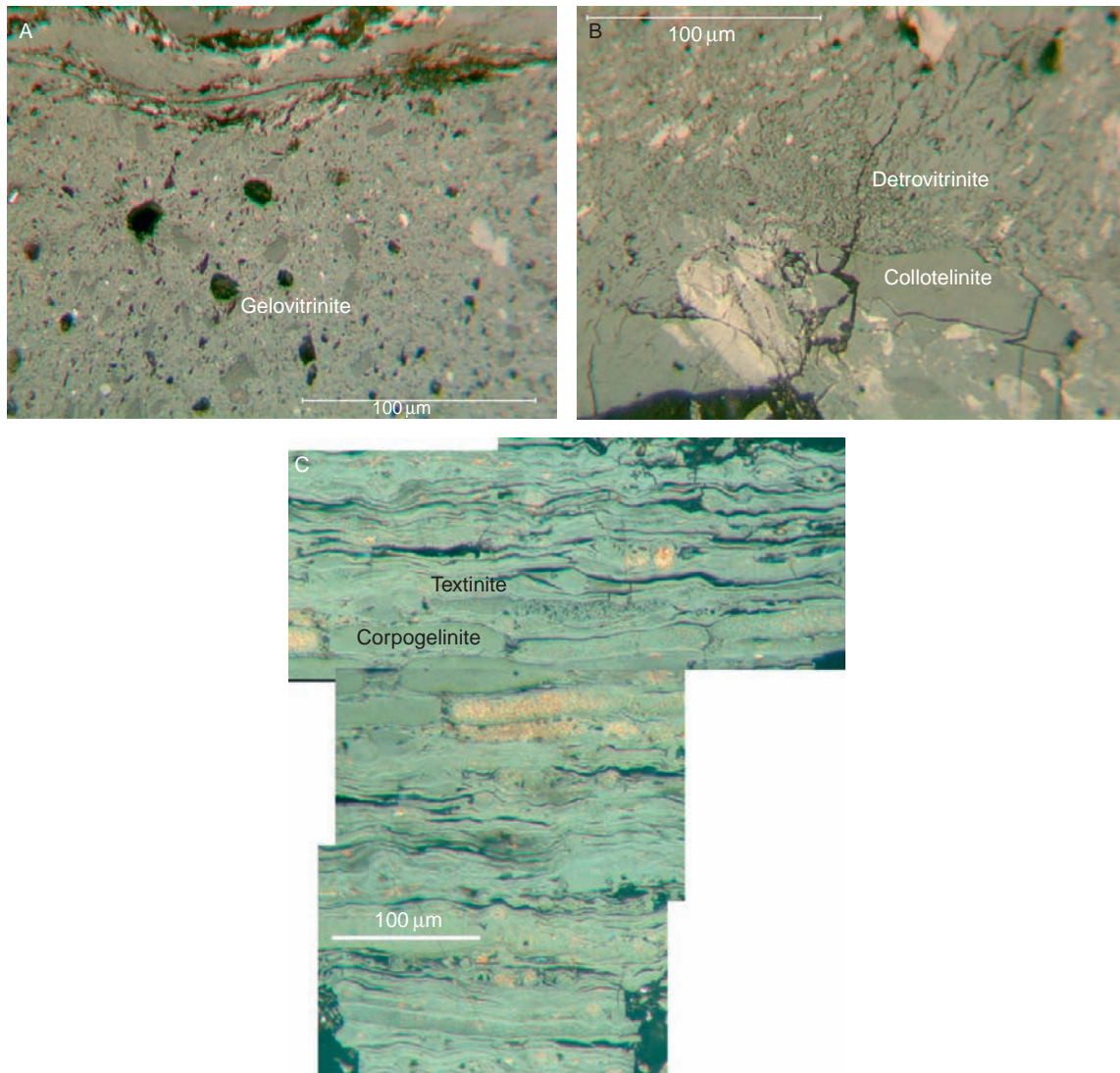


Figure 3.1.1. (A) Gelovitrinite with liptodetrinite and inertodetrinite, (B) Detrovitrinite with fragments of collotelinite and inertinite, (C) Textinite and corpohuminite.

Inorganic Matter in Coal

Mineral matter (Figure 3.1.4) in coal could be of syngenetic origin (minerals incorporated or formed during peat deposition or present in the inorganic compounds and organometallic complexes of the original plant material) or epigenetic origin (formed postdepositionally during diagenesis, coalification, etc.).

The most abundant minerals in coal are **clays** and the most common are kaolinite, illite, montmorillonite, and smectite. **Carbonates** are the next most common minerals in coal and they include calcite, siderite, ankerite, and dolomite. Sulfides (e.g., pyrite, sphalerite, galena), silicates (e.g., quartz, zircon), and oxides (e.g., rutile) are also found in coal and locally can occur in high concentrations. Table 3.1.2 (from Stach et al., 1982; Taylor et al., 1998) lists some of the minerals identified in coal and their approximate abundance. Texturally, minerals may occur in thin layers, as fillings of cleats and fractures in coal, as fillings of cell lumens in macerals, or intimately associated with macerals or other minerals. Minerals such as siderite or pyrite can also replace cell walls. Minerals can also occur finely dispersed within the coal matrix.

The content of mineral matter in coal is often proxied by ash yield. However, there are important differences between mineral matter content and ash yield. Ash yield, as determined for the proximate and ultimate analyses, results from the combustion of organic fraction and minerals and, therefore, presents lower quantity than mineral

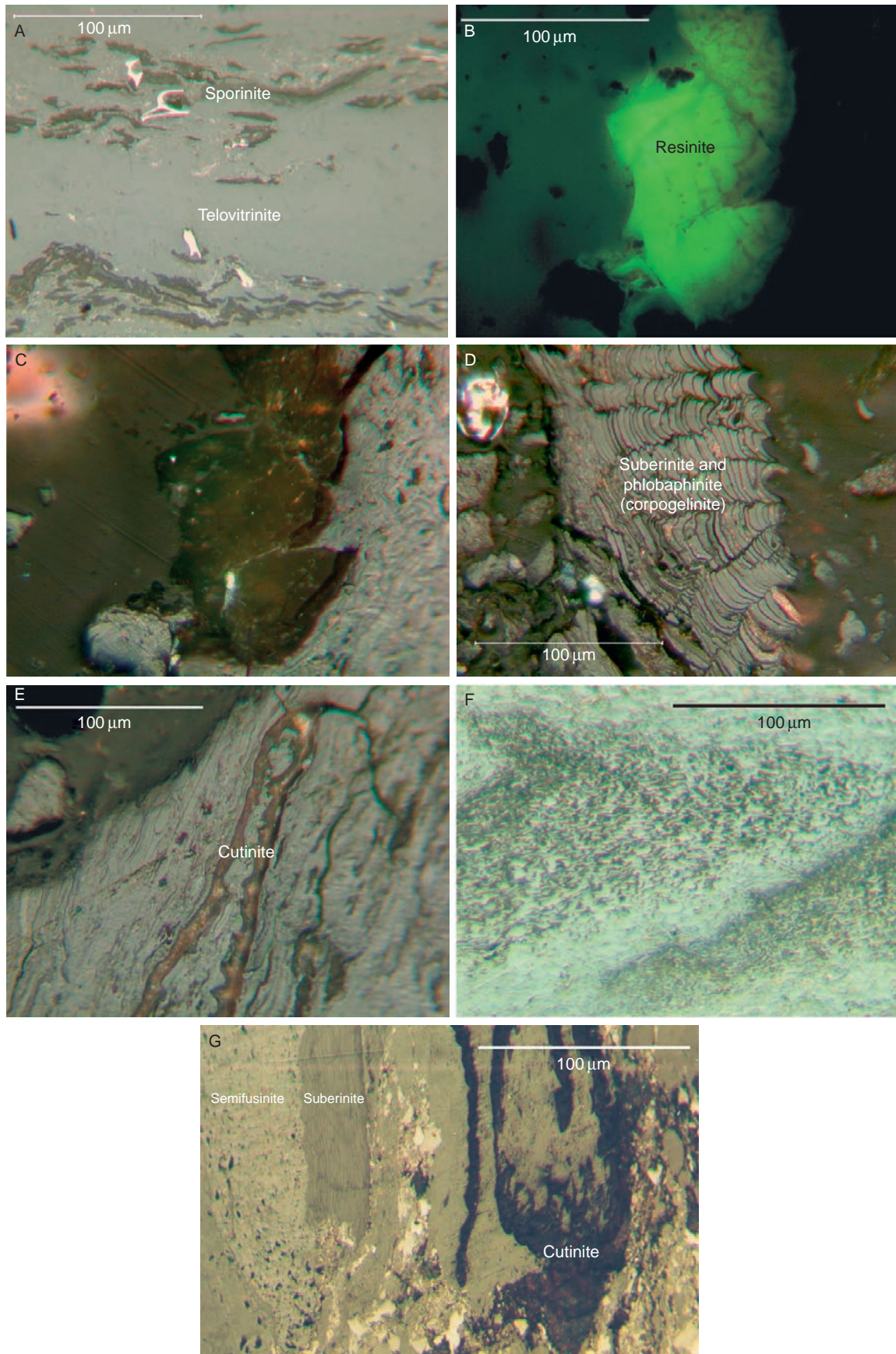


Figure 3.1.2. (A) Sporinite and telovitrinite, (B) Blue-light image of resinite, (C) white-light image of resinite, (D) Suberinite and phlobaphinite, (E) Cutinite, (F) Suberinite, (G) Suberinite, cutinite, and semifusinite.

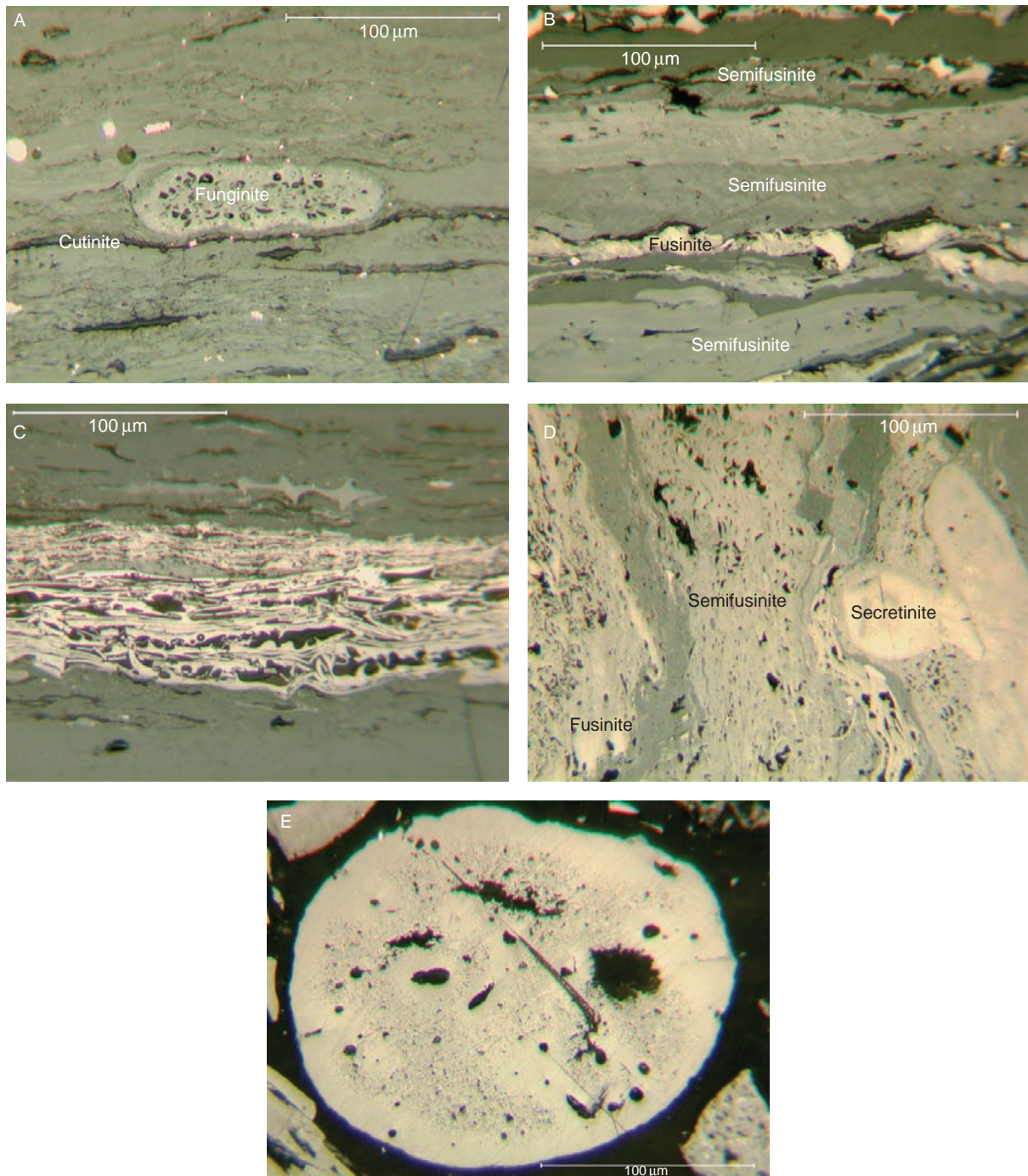


Figure 3.1.3. (A) Funginite in center, (B) Fusinite and semifusinite, (C) Fusinite and semifusinite, (D) Fusinite, semifusinite, and secretinite, (E) Secretinite.

matter because hydrous, and other, minerals are altered during the ashing process. Frequently, the **Parr formula** is used to calculate mineral matter content from the ash yield. In this formula, mineral matter by weight is calculated as $1.08 (\text{ash yield}) + 0.55 (\text{sulfur})$. This quantity can be further converted to a volume percent by formulae in ASTM 2799 (ASTM, 1996).

The major, minor, and trace elements comprising minerals, and elements in organic association, are important in coal utilization. Ten elements are routinely determined and expressed as oxides and these are SiO_2 , Al_2O_3 , CaO , Na_2O , K_2O , Fe_2O_3 , TiO_2 , MgO , P_2O_5 , and SO_3 .

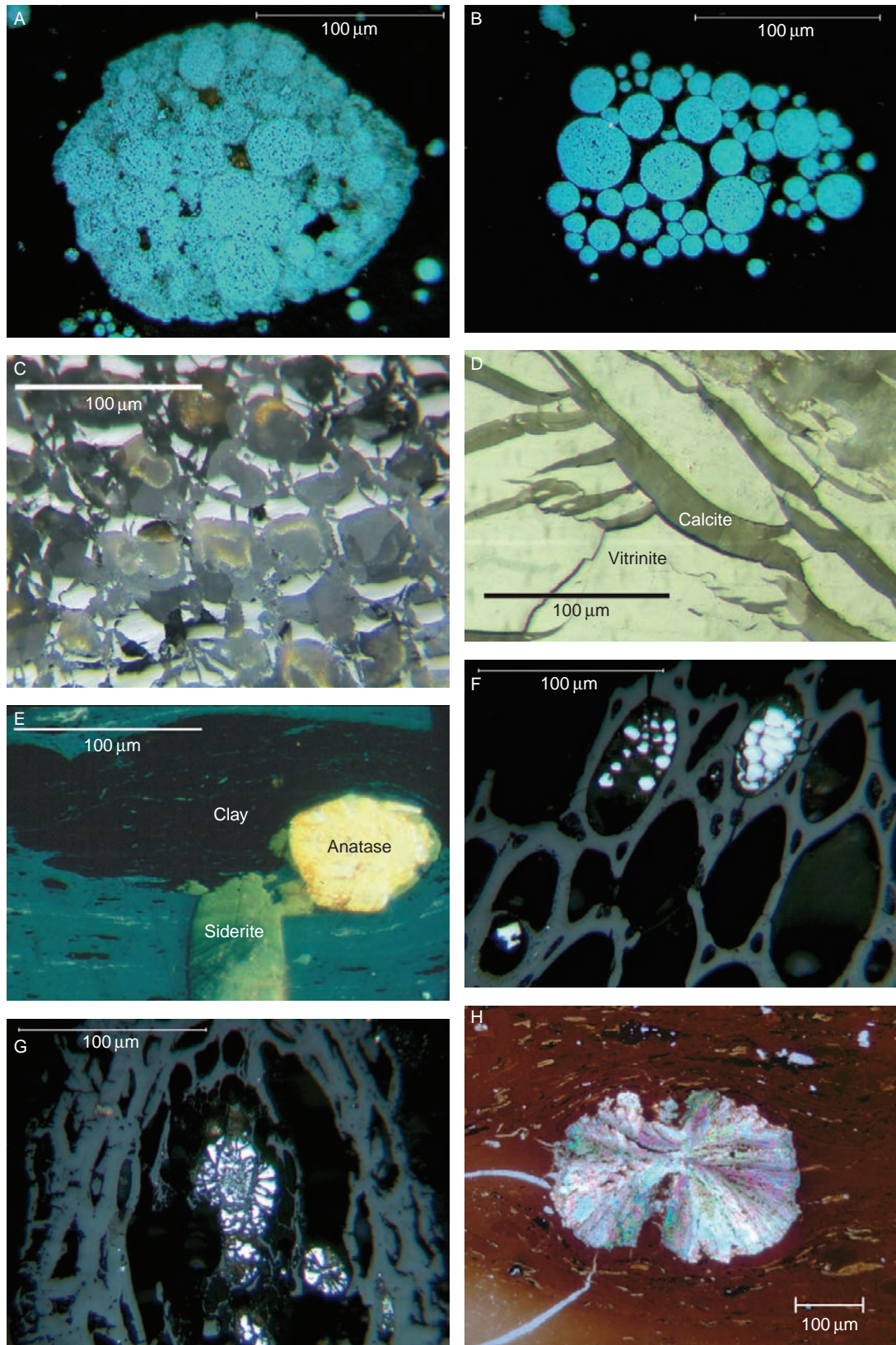


Figure 3.1.4. (A) Pyrite framboids, (B) Pyrite framboids, (C) Siderite with fusinite, (D) Calcite in fractures in vitrinite, (E) Clay, siderite, anatase in coal, (F) Sulfide in fusinite, (G) Sulfide (?) in fusinite, (H) Siderite in vitrinite (thin section).

Table 3.1.2
Minerals found in coal.

Mineral Group	Mineral	Composition	Occurrence
Clay	Illite–sericite	(K, H ₃ O) (Al, Mg, Fe) ₂ (Si, Al) ₄ O ₁₀ (OH) ₂ · nH ₂ O	dom–ab
	Montmorillonite	Al ₄ Si ₄ O ₁₀ (OH) ₂ · nH ₂ O	r–c
	Kaolinite	Al ₄ Si ₄ O ₁₀ (OH) ₈	c–vc
	Halloysite	Al ₂ Si ₂ O ₅ (OH) ₄	r
Iron disulfides	Pyrite	FeS ₂	r–c
	Marcasite	FeS ₂	r
	Melnikovite	FeS ₂	r
Carbonates	Siderite	FeCO ₃	c–vc
	Ankerite	CaFe(CO ₃) ₂	c–vc
	Calcite	CaCO ₃	c–vc
	Dolomite	CaMg(CO ₃) ₂	r–c
Oxides	Hematite	Fe ₂ O ₃	r
	Magnetite	FeFe ₂ O ₄	vr
	Rutile	TiO ₂	vr
Hydroxides	Limonite	HFeO ₂	r–c
	Goethite	HFeO ₂	r
	Diaspore	HAIO ₂	r
Sulfides/selenides	Sphalerite	ZnS	r
	Galena	PbS	r
	Chalcopyrite	CuFeS ₂	vr
	Pyrrhotite	FeS	vr
	Clausthalite	PbSe	vr
Phosphates	Apatite	Ca ₅ (PO ₄) ₃ (F, Cl, OH)	r
	Crandallite group	(Ba, Ca, Ce, Nd, Pb, Sr, Th)(Al, Fe) ₃ [(P, As)O ₄] ₂ (OH) ₅ with or without H ₂ O	r
Sulfates	Barite	BaSO ₄	r
	Gypsum	CaSO ₄ ·2H ₂ O	r

Source: Modified after Stach et al., 1982; other minerals are possible.

Note: Chemical compositions are variable and may include trace elements. ab, abundant; dom, dominant; c, common; r, rare; vc, very common; vr, very rare.

Microlithotypes

Microlithotypes (Table 3.1.3) are associations of macerals that occur in bands at least 50- μ m thick. There are three main classes of microlithotypes:

- (1) **Monomaceral microlithotypes** contain one maceral or maceral group, for example, **liptite** (dominated by liptinite (L) macerals) or **vitrite** (dominated by vitrinite (V) macerals).
- (2) **Bimaceral microlithotypes** are composed of macerals of two maceral groups, each accounting for >5%, for example, **clarite** (dominated by vitrinite and liptinite) or **durite** (dominated by liptinite and inertinite (I)).
- (3) **Trimaceral microlithotypes** are composed of macerals of three maceral groups, each accounting for at least 5%, namely **duroclarite** (V > L or I), **clarodurite** (I > V or L), and **vitrinertoliptite** (L > V or I).

Associations of microlithotypes rich in mineral matter are called **carbominerites**. In carbominerites, the mineral matter accounts for at least 20% (volume) in case of silicates or carbonates or 5% (volume) of sulfides.

Lithotypes

Lithotypes are megascopically identified layers in coal seams (Figure 3.1.5). Lithotype variations in the coal reflect changes in organic input and depositional conditions in the mire.

Table 3.1.3
Classification and composition of microlithotypes found in coal.

Microlithotype	Maceral composition	Group
Vitrite	Vitrinite (V) > 95%	Monomaceralic
Liptite	Liptinite (L) > 95%	
Inertite	Inertinite (I) > 95%	
Clarite	V + L > 95%	Bimaceralic
Durite	I + L > 95%	
Vitrinertite	V + I > 95%	
Duroclarite	V > L, I (each > 5%)	Trimaceralic
Vitrinertoliptite	L > V, I (each > 5%)	
Clarodurite	I > V, L (each > 5%)	
Carbargilite	Coal + 20–60% (vol.)	Carbominerite*
Carbopyrite	Clay	
Carbankerite	Coal + 5–20% (vol.)	
Carbosilicate	Sulfides	
Carbopolyminerite	Coal + 20–60% (vol.)	
	Carbonates	
	Coal + 20–60% (vol.)	
	Quartz	
	Coal + 20*–60% (vol.)	
	Various minerals	

Source: Adapted from Stach et al., 1982; Taylor et al., 1998.

* 5% (vol.), if pyrite is high.

There are several systems of megascopic classification. Classification of brown coal lithotypes is based on color, texture, desiccation pattern, strength, and degree of gelification (Table 3.1.4; after Hagemann, 1980; see Bustin et al., 1983, for description of use of system). Two systems of the classification of black coal lithotypes are given in Table 3.1.3 (from Diessel, 1992 and Hower et al., 1990). For black coal (**subbituminous** rank and higher), texture, luster, type of fracture, proportion of bright versus dull bands, and mineral matter content are used to distinguish the coal lithotype. Each individual lithotype must be thicker than 5 mm for the Australian system or 3 mm for the US system. Consequently, thinner bands become part of a thicker lithotype unit.

Coal Rank

Coal rank is the measure of the degree of organic metamorphism (coalification) of a coal, ranging from low-rank **peat** to high-rank **meta-anthracite** (Table 3.1.5). Rank can be determined through a number of chemical and physical parameters. In general, no single parameter can be used throughout the entire rank range. For example, **equilibrium moisture** is one of the most appropriate parameters at low ranks, but gives way to **heating value** and **volatile matter** at intermediate ranks and hydrogen at the highest ranks. **Vitrinite reflectance** is a good parameter for many coal ranks, although it is of questionable value at the lowest ranks where interspecies differences in wood types and their varying preservation could greatly influence individual values. For **bituminous** coals, vitrinite reflectance is a commonly used rank parameter and has advantages over chemical parameters in being based on one maceral, eliminating the chemical differences between macerals and the interfering effects of mineral matter.

The initial stage of **coalification** is biochemical degradation which involves the chemical decomposition of plant material aided by microorganisms. Whereas this process may be rapid in tropical environments, where conditions are ideal for the bacteria and fungi, rapid plant growth may balance the increased rate of decomposition. This early decomposition and degradation of organic matter is followed by humification. **Humification**, the biochemical path from woody peat to the huminite macerals, affects the preservation of **cellulose**, **hemicellulose**, and **lignin** (the most-resistant compound of the three) compounds in plant cell walls. Humification begins with the oxidation of plant matter and attack by aerobic organisms such as fungi, insects, and aerobic bacteria; with consequent extraction of hydrocarbon-rich functional groups and enrichment of the

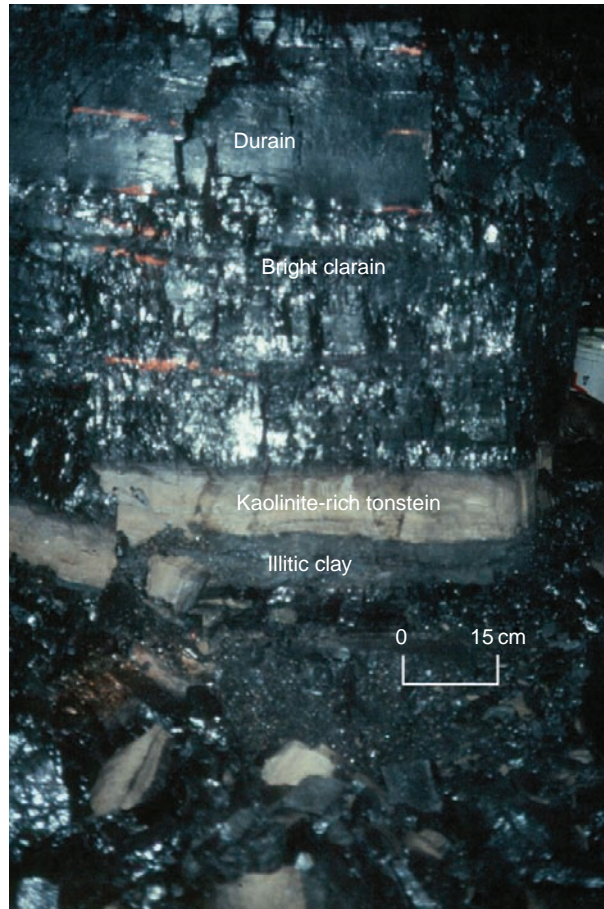


Figure 3.1.5. In-mine profile of portion of Fire Clay coal bed, eastern Kentucky, with bright clarain and durain above illitic clay and tonstein partings.

refractory organic material in oxygen and carbon. Humic acids are formed during this process. Burial of the plant material or degraded plant material below the groundwater table effectively stops oxidation or attack from aerobic organisms. Anaerobic bacteria may continue to decompose the plant matter until it reaches a depth or conditions unsuitable for their viability. Biochemical degradation ends with the polymerization of humic acids at the rank of subbituminous coal.

Physicochemical coalification that follows biochemical degradation is caused by the amount of heating of the coal and, to a lesser extent, the pressure conditions during the coal's history. Temperature increase has been traditionally thought of as the product of greater depth of burial (and the prevailing geothermal gradient) (Hilt, 1873), but recent studies have led to the recognition that the flow of hydrothermal fluids through coal seams can account for the heating (Hower and Gayer, 2002; Harrison et al., 2004). Physicochemical coalification causes major changes in the coal properties, including changes in the thermal and mechanical properties (details in Taylor et al., 1998).

Coal Petrology and Spontaneous Combustion

Among many factors that trigger spontaneous combustion, oxidation of coal at ambient temperature is the major one (Banerjee et al., 1990; Goodarzi and Gentzis, 1990). The oxidation of coal is an exothermic reaction, the exact mechanisms of which are not fully understood. At very low temperatures, reaction between coal and oxygen is physical (adsorption), and it changes into chemisorptions starting at ambient temperature (Postrzednik et al., 1988). The rate of oxygen consumption is very high during the first few days, following exposure of a fresh coal to the atmosphere. Afterwards, it decreases slowly unless generated heat is allowed to accumulate in the environment.

Table 3.1.4a
Macropetrographic classification of brown coal lithotypes.

Categories	Lithotype classes	Lithotypes	Lithotype varieties (determined on dried material in laboratory)			
Quality parameter	Structure: presence of xylite and/or contamination by mineral matter	Texture: ratio between groundmass and plant remains	Intensity and hue of color	Evidence of gelification	Inclusions	Additional features
Macro-petrographic description	(1) Pure coal, non-xylitic Pure coal, xylitic Fibrous xylite Brittle xylite	(1) Unbanded coal	(1) Pale yellow	(1) Gelified groundmass (+, ++, +++)	(1) Resin bodies (+, ++, +++)	(a). Surface texture Extensive cracking Moderate cracking No cracking
	(2) _____ Tree stumps, tree trunks, etc. Impure coal, non-xylitic	(2) Moderately banded coal	(2) Medium light yellow	(2) Gelified tissues (+, ++, +++)	(2) Cuticles (+, ++, +++)	(b) Fracture Even imbricated
	(3) Clayey coal, sandy coal, calcareous coal, iron sulfides, etc.	(3) Banded coal	(3) Pale brown	(3) Microgranular humic gel particles (+, ++, +++)	(3) Charcoal (+, ++, +++)	(c) Size degradation Coarse fragmentation Fine fragmentation Crumbling
	(4) Impure coal, xylitic	(4) Highly banded coal	(4) Medium light brown (5) Dark brown (6) Black			

Source: Lithotypes after Hagemann, 1980.

Table 3.1.4b
The classification of bituminous coal lithotypes.

Lithotype and corresponding symbol (Diessel, 1992)	Lithotype (Hower, et al., 1990)*	Description
Bright coal (vitrain) B	Vitrain	Vitreous to subvitreous luster; even to conchoidal fracture; brittle; may contain up to 10% dull bands less than 5 mm (3 mm [†])
Banded bright coal Bb	Bright clarain	Mainly vitrain containing 10–40% dull bands less than 5 mm (3 mm [†])
Banded coal (duroclarain) Bd	Clarain	Contains 40–60% dull bands less than 5 mm (3 mm*)
Banded dull coal (clarodurain) Db	Dull clarain	Mainly dull coal containing 10–40% thin (less than 5 mm (3 mm [†])) bright bands
Dull coal (durain) D	Durain	Matt luster and uneven fracture; contains less than 10% vitrain less than 5 mm (3 mm [†])
Fibrous coal (fusain) F	Fusain	Dull with satin sheen; friable; may contain up to 10% of other coal lithotypes less than 5 mm (3 mm ^{*†})
Shaly coal Cs	Bone	Contains between 30–60% of clay and silt either in intimate mixture with coal or in separate bands each less than 5 mm (3 mm ^{*†})
Coaly shale, coaly mudstone, etc. Shale, mudstone, etc.		Any sediment containing 60–90% finely disseminated carbonaceous matter* Any sediment containing less than 10% carbonaceous matter*

Source: From Diessel, 1992; Hower et al., 1990.

* Noted in lithologic description at any recognizable thickness (Hower et al., 1990).

† Stopes, 1919.

Table 3.1.5
The maximum value of rank parameters (after Diessel, 1992) with further subdivisions of lower rank coals after Teichmüller (in Stach et al., 1982).

Rank stage	Carbon (daf) (%)	Volatile matter (daf) (%)	Gross-specific energy (MJ/kg)	<i>In situ</i> moisture (%)	Vitrinite reflectance (%) (Oil, 546 nm) (Teichmüller, 1982)		Vitrinite reflectance (%) (Oil, 546 nm) (Diessel, 1992)	
					R_{random}	R_{max}	Rank subclass	R_{random}
Wood	50	>65						
Peat	60	>60	14.7	75	0.20	0.20		0.26
Lignite	71	52	23	30	0.40	0.42		0.38
Subbituminous	80	40	33.5	5	0.60	0.63	C B	0.42 0.49
High volatile bituminous	86	31	35.6	3	0.97	1.03	A C B A	0.65 0.65 0.79 1.11
Medium volatile bituminous	90	22	36	<1	1.47	1.58		1.50
Low volatile bituminous	91	14	36.4	1	1.85	1.97		1.92
Semianthracite	92	8	36	1	2.65	2.83		2.58
Anthracite	95	2	35.2	2	6.55	7.00		5.00

Note: Overlap of subbituminous A and high volatile C bituminous ranks as expressed in vitrinite reflectance. Distinction between subbituminous and high volatile bituminous coals must be made on other parameters: e.g., agglomerating properties of high volatile bituminous coals and solubility of subbituminous coals in KOH solutions. daf: dry, ash free.

In general, the following, often interrelated, properties of coal affect spontaneous combustion (e.g., Güney, 1968; Kaymakçi and Didari, 2002):

- (1) moisture content and volatile matter content,
- (2) particle size and available surface area,
- (3) mineral matter type and pyrite content in particular,
- (4) coal rank, and
- (5) petrographic composition (coal type)

Chakravorty and Kolada (1988) and Morris and Atkinson (1988) reviewed the factors which contribute to the potential for spontaneous combustion of coal. Among the intrinsic factors which cannot be controlled, Chakravorty and Kolada (1988) noted high volatile matter and high moisture, both indicative of low-rank coals; high pyrite; and high liptinite as the important coal properties. Chandra and Prasad (1990) found that the higher volatile matter Indian coals in their study had the highest susceptibility to spontaneous combustion.

Particle size and available surface area are important because adsorption is an important process in coal oxidation. Higher adsorption, and the monolayer capacity in particular, influences the amount of moisture that can be retained in the coal and moisture is frequently cited as the main control on spontaneous combustion (Allardice and Evans, 1971). The larger the monolayer capacity, the smaller is the rate of increase of wetting the outer core of the particle during condensation of moisture. It appears that there is a range of values for monolayer capacity that may lead to ignition; at higher and lower values, the particle does not ignite.

Fractured and faulted thick coal seams with pyrite and organic shale partings are particularly susceptible to spontaneous combustion. Falcon (1986) and Misra and Singh (1994) also considered open-structure fusinite to be a factor owing to the enhanced surface area. Beamish et al. (2001), Beamish and Blazak (2005), Beamish and Hamilton (2005), and Beamish (2005) correlated R_{70} , the average rate of temperature rise from 40°C to 70°C in an adiabatic oven with O₂ flow of 50 mL/min, with a number of properties for New Zealand and Australian coals. Beamish and Blazak (2005) and Beamish and Hamilton (2005) found R_{70} to decrease with an increase in mineral matter, with the mineral matter acting as a heat sink, and an increase in the moisture content. Subbituminous coals have the highest self-heating rate (Beamish et al., 2001; Beamish, 2005). In general, it has been widely recognized that lower rank coals are more susceptible to spontaneous combustion than higher rank coals because they have high percent of reactive macerals (vitrinite and liptinite).

Coal type (maceral and microlithotype composition) influences (1) the reactivity between oxygen and coal and (2) the adsorption behavior of the coal, two processes very important during coal oxidation. Higher reactivity of coal results in a sharper increase in particle temperature and thus the ignition delay is shorter. If the coal reactivity is lower than a critical value, the rate of heat generation remains lower than the rate of heat dissipation; the coal particle fills up with moisture and ignition is not achieved. Therefore, coal rich in reactive macerals (liptinite and vitrinite) has higher susceptibility to spontaneous combustion.

These and other parameters have been used in modeling of spontaneous combustion (Bhattacharyya, 1971; Arisoy and Akgün, 1994; Bhat and Agarwal, 1996; Krishnaswamy et al., 1996a, b, c). These studies provide valuable information about significance of the used parameters for various coals.

Important Terms

alginite
ankerite
bimaceral microlithotypes
bituminite
bituminous
colcite
carbominerites
carbonates
cellulose
clarite
clarodurite

liptite
lithotypes
macerals
macrinite
meta-anthracite
micrinite
microlithotypes
mineral matter
monomaceral microlithotypes
montmorillonite
oxides

clays	Parr formula
coal petrology	peat
coal rank	pyrite
coalification	quartz
detrovitrinite	rutile
dolomite	semifusinite
durite	siderite
duroclarite	silicates
equilibrium moisture	smectite
fusinite	sphalerite
galena	subbituminous
gelovitrinite	sulfides
heating value	telovitrinite
hemicellulose	trimaceral microlithotypes
humification	vitriertoliptite
illite	vitritine/huminite
inertinite	vitritine
inorganic content of the coal	vitritine reflectance
kaolinite	vitrite
lignin	volatile matter
liptinite	zircon

References

- Allardice, D.J., Evans, D.G., 1971. The brown coal/water system: Part 2. Water sorption isotherms on bed-moist Yallourn brown coal. *Fuel* 50 (3), 236–253.
- Arisoy, A., Akgün, F., 1994. Modelling of spontaneous combustion of coal with moisture content included. *Fuel* 73 (2), 281–286.
- American Society for Testing and Materials, 1996. Standard test method for microscopical determination of volume percent of physical components of coal (D2799-94): 1996 Annual Book of ASTM Standards, 5.05, 279–281.
- Australian Standards, 1995. Standard for Reflectance: AS 2486-1989.
- Banerjee, S.C., Nandy, D.K., Ghosh, S.K., Banerjee, D.D., Sen, S.K., Singh, B., 1990. Approach to assessing the status of sealed-off fires by examination of fire indices. *Min. Sci. Tech.* 10, 37–51.
- Beamish, B.B., Hamilton, G.R., 2005. Comparison of the R_{70} self-heating rate of New Zealand and Australian coals to Suggate rank parameter. *Int. J. Coal Geol.* 64, 139–144.
- Beamish, B.B., Barakat, M.A., St. George, J.D., 2001. Spontaneous-combustion propensity of New Zealand coals under adiabatic conditions. *Int. J. Coal Geol.* 45, 217–224.
- Beamish, B.B., Blazak, D.G., 2005. Relationship between ash content and R_{70} self-heating rate of Callide coal. *Int. J. Coal Geol.* 64, 126–132.
- Beamish, B.B., Hamilton, G.R., 2005. Effect of moisture content on the R_{70} self-heating rate of Callide coal. *Int. J. Coal Geol.* 64, 133–138.
- Bhat, S., Agarwal, P.K., 1996. The effect of moisture condensation on the spontaneous combustibility of coal. *Fuel* 75 (13), 1523–1532.
- Bhattacharyya, K.K., 1971. The role of sorption of water vapour in the spontaneous heating of coal. *Fuel* 50 (4), 367–380.
- Bustin, R.M., Cameron, A.R., Grieve, D.A., Kalkreuth, W.D., 1983. Coal petrology: its principles, methods, and applications. *Geol. Assoc. Can. Short Course Notes* 3, 230 p.
- Chakravorty, R.N., Kolada, R.J., 1988. Prevention and control of spontaneous combustion in coal mines. *Min. Eng.* 4, 952–956.
- Chandra, D., Prasad, Y.V.S., 1990. Effect of coalification on spontaneous combustion of coals. *Int. J. Coal Geol.* 16, 225–229.
- Diessel, C.F.K., 1992. Coal-bearing depositional systems. Springer-Verlag, Berlin, 721.
- Falcon, R.M., 1986. Spontaneous combustion of the organic matter in discards from the Witbank Coalfield. *JS Afr. Inst. Min. Metall.* 86, 243–250.

- Goodarzi, F., Gentzis, T., 1990. The lateral and vertical reflectance and petrological variation of a heat-affected bituminous coal seam from southeastern British Columbia, Canada. *Int. J. Coal Geol.* 15, 317–339.
- Gouws, M.J., Wade, L., 1989b. Self-heating liability of coal: predictions based on composite indices. *Min. Sci. Tech.* 9, 81–85.
- Güney, M., 1968. Oxidation and spontaneous combustion of coal—review of individual factors. *Colliery Guardian*, 216, 105–110.
- Hagemann, H.W., 1980. Part I. Identification of lithotypes in lignites of southern Saskatchewan, Part II. Macro-petrographic examination and collecting samples from cores stored at the Hat Creek mine site, British Columbia: Geological Survey of Canada Open File Report, 67 p.
- Harrison, M.J., Marshak, S., Onasch, C.M., 2004. Stratigraphic control of hot fluids on anthracitization, Lackawanna synclinorium, Pennsylvania. *Tectonophysics* 378 (1), 85–103.
- Hilt, C., 1873. Die Beziehungen zwischen der Zusammensetzung und den technischen Eigenschaften der Steinkohle. *Verein Deutscher Ingenieure Zeitschriften* 17, 194–202.
- Hower, J.C., Esterle, J.S., Wild, G.D., Pollock, J.D., 1990. Perspectives on coal lithotype analysis. *J. Coal Quality* 9, 48–52.
- Hower, J.C., Gayer, R.A., 2002. Mechanisms of coal metamorphism: case studies from Paleozoic coalfields. *Int. J. Coal Geol.* 50, 215–245.
- International Committee for Coal and Organic Petrology (ICCP), 1998. New vitrinite classification (ICCP system 1994). *Fuel*, 77, 349–358.
- International Committee for Coal and Organic Petrology (ICCP), 2001. New inertinite classification (ICCP system 1994). *Fuel*, 80, 459–471.
- Kaymakçi, E., Didari, V., 2002. Relations between coal properties and spontaneous combustion parameters. *Turkish J. Eng. Env. Sci.* 26, 59–64.
- Krishnaswamy, S., Bhat, S., Gunn, R.D., Agarwal, P.K., 1996a. Low-temperature oxidation of coal. 1. A single-particle reaction-diffusion model. *Fuel* 73 (3), 333–343.
- Krishnaswamy, S., Gunn, R.D., Agarwal, P.K., 1996b. Low-temperature oxidation of coal. 2. An experimental and modeling investigation using a fixed-bed isothermal flow reactor. *Fuel* 75 (3), 344–352.
- Krishnaswamy, S., Agarwal, P.K., Gunn, R.G., 1996c. Low-temperature oxidation of coal. 3. Modelling spontaneous combustion in coal stockpiles. *Fuel* 75 (3), 353–362.
- Misra, B.K., Singh, B.D., 1994. Susceptibility to spontaneous combustion of Indian coals and lignites: an organic petrographic autopsy. *Int. J. Coal Geol.* 25, 265–286.
- Morris, R., Atkinson, T., 1988. Seam factor and the spontaneous heating of coal. *Min. Sci. Tech.* 7, 149–159.
- Postzednik, S., Bialecki, R., Novak, A., Scholz, R., Specht, E., 1988. Zur Problematik der Selbsterwärmung fester Brennstoffe (1): Erdöl-Erdgas Kohle, Heft 2, 79–85
- Stach, E., Mackowsky, M.-Th., Teichmüller, M., Taylor, G.H., Chandra, D., Teichmüller, R., 1982. *Stach's Textbook of Coal Petrology*, third ed. Gebrüder Borntraeger, Berlin, 535 p.
- Stopes, M., 1919. On the four visible ingredients in banded bituminous coal. *Proc. R. Soc. Lond. B* 90, 470–487.
- Sykorova, I., Pickel, W., Christanis, K., Wolf, M., Taylor, G.H., Flores, D., 2005. Classification of huminite—ICCP system 1994. *Int. J. Coal Geol.* 62, 85–106.
- Taylor, G.H., Teichmüller, M., Davis, A., Diessel, C.F.K., Littke, R., Robert, P., 1998. *Organic Petrology*. Gebrüder Borntraeger, Berlin, 704 p.

WWW Addresses: Additional Reading

(1) Coal Petrology

http://topics.scirus.com/Coal_petrology.html

CHAPTER 4

Coal and Ancient Man: Cremation at the Tschudi Burn, Chan Chan, Northern Peru



Exterior of calcined cranial vault fragment from the coal-fueled Tschudi burn, Chan Chan, northern Peru. Fracture pattern typical of bone that was fleshed when burned
Photo by William E. Brooks, 2006.

CHAPTER CONTENTS

4.1 Coal and Ancient Man

- Introduction
- Coal in Peru
- Chan Chan
- Metallurgical Furnace or Crematorium
- Temperature of the Tschudi Burn
- Calcium in the Soil
- Sulfur in the Soil
- Fuel Ash Chemistry
- Oxide and Trace Element Data
- ^{14}C Date
- Cremation in Society
- Fuel for Cremation
- Cremation at the Tschudi Burn
- Discussion
- References
- WWW Addresses: Additional Reading



Photo by William E. Brooks, 2006.

4.1. Coal and Ancient Man

William E. Brooks

Cesar G. Mora

John C. Jackson

John P. McGeehin

Darden G. Hood

Calcined cranial-vault fragment from the Tschudi burn, Chan Chan, northern Peru

Introduction

Underground coal fires, which have occurred for millions of years, are caused by, among other things, lightning strikes or spontaneous combustion and may have given ancient man the idea to use the black rock as an energy fuel. Perhaps these underground fires were seen as fiery, smoldering gateways to the underworld.

These fires are common in coal-producing regions of the world such as China, India, Peru, South Africa, Venezuela, and the United States (Stracher and Taylor, 2004). In Venezuela, an ongoing, underground coal fire earned the name “Paso Diablo” and underground fires are also known at Cerrejon, Colombia, and Goyllarisquiza, Peru (Washington Group International, 1982 Hackley and Martinez, 2007). And, in the western United States, the Powder River Basin, Wyoming, received its descriptive name because of the odor of sulfur, a component of coal and gunpowder, from the ever-burning, underground coal fires in the region.

Ancient man first used coal as an energy source 73 500 years ago in Les Canalettes, southern France, and archaeologists initially thought that the coal was deformed charcoal (They et al., 1995, 1996). Coal was used to fuel cremation pyres during the Bronze Age in southern Wales. Underground coal seams to have burned in China for centuries (Stracher and Taylor, 2004) and the Chinese were the first to record their use of coal sometime during the Han dynasty (200 BC to AD 220) (Cassidy, 1973, p. 1; Raymond, 1986, p. 150). Coal was used by the ancient Greeks and described as a substance that “burned and continued to burn with a troublesome and disagreeable smell” (Agricola, 1556, p. 34). In the southwestern United States, coal was mined and used by the Hopi for firing pottery at approximately AD 1100 (Hodge, 1904; Hack, 1942). At about the same time, “sea-coale” was found on the beaches of England. This discovery led to widespread coal mining as coal replaced wood as an energy source and became the energy fuel of the Industrial Revolution.

Coal in Peru

Coal is widely available in South America with occurrences in Argentina, Brazil, Chile, Colombia, Peru, and Venezuela (Alvarado, 1980). In the late 1800s, it was estimated that a major new coal field in northern Peru’s La Libertad Department could supply coal needed for copper smelting and even drive imported English coal from the market (The Manufacturer and Builder, 1878).

In northern Peru’s Santa Valley, there are a number of coal mines such as Baños de Chimú, Callacuyán, Cocobal, La Galgada, Goyllarisquiza, La Limeña, La Victoria, and numerous smaller occurrences. Of these, Goyllarisquiza is the most well known because it supplied coal to the copper smelters at Cerro de Pasco. Mines are included in northern Peru’s extensive Alto Chicama coal field, which is also referred to as the Northern Anthracite



Figure 4.1.1. Modern brick from Trujillo, Peru brickyard showing bubbling, vitrification, and flow features caused by the 1300–1600°C coal-fired, curing process. Photo by William E. Brooks, 2006.

Field (Escudero, 1978; Samamé Boggio, 1979b, p. 1414; Petersen, 1983; Dunin-Borkowski, 1996; Carrascal et al., 2000).

Prior to the Industrial Revolution in Europe, “sea-coale” found on the beaches of England indicated the regional abundance of a fuel that would soon replace wood. In northern Peru, the regional abundance of coal is indicated by sea-coale which may be found on the beach at Huanchaco, near Trujillo, and the archaeological site of Chan Chan. This sea-coal was transported by streams from outcrops in the Santa Valley to the Pacific Ocean and then was rounded by abrasion as longshore drift brought the coal northward along the coast to Huanchaco (Brooks et al., 2004).

Coal is widely available in northern Peru and was used by ancient Peruvians, such as the Moche (approximately 100 BC to AD 700) and Chimu (approximately AD 800–1450), for metallurgy (Pfordte, 1893; Agramonte and Diaz, 1983), mirrors, and jewelry (Mujica Gallo, 1959; Hyams and Ordish, 1963; Petersen, 1970; Burger, 1992; Morris and von Hagen, 1993; Larco Hoyle, 2001, p. 133). At Huancavelica, coal was one of several local fuels used for retorting mercury in the late 1800s (Arana, 1901, p. 102).

Coal is now mined in northern Peru on a small scale and is used locally for curing bricks (Figure 4.1.1), making coal briquettes, cooking, and as a fuel to calcine limestone for making cement (Mucho, 1992; Wax, 2000; Brooks and Willett, 2004; Brooks et al., 2004). However, despite the regional abundance of coal, large-scale mining of coal in Peru is difficult because the coal has been tectonized and is present mainly in steeply dipping and faulted units. Therefore, even though Peru has coal reserves of approximately one billion metric tons (Carrascal et al., 2000, p. 103), coal is imported for large-scale uses (Bowen, 2001).

Chan Chan

Chan Chan is in the Moche Valley, northern Peru, approximately 5 km from the modern city of Trujillo, and was the most extensive adobe city in South America before the arrival of the Europeans in the 1500s (Hardoy, 1973). It was the administrative, commercial, and metallurgical center of the Chimu Empire (approximately AD 800–1450). However, by the late 1400s, Chan Chan’s craftsmen and metalworkers had been absorbed into the Inca Empire.

Chan Chan’s ruins now cover as much as 20 km² and include 10 rectilinear *ciudadelas*, or compounds, outlined by adobe walls that were once as high as 10 m. Burial practices at Chan Chan were simple to elaborate and one royal burial platform, Laberinto, contained the bodies of 200–300 adolescents and young adult females (Conrad, 1982).

Metallurgical Furnace or Crematorium

In 1865, George Squier, an American writer and diplomat, visited Chan Chan and included descriptions of four large burned areas. One of these was the 25 × 70 m Tschudi burn, which is only a few meters northeast of *Cuidadela* Tschudi, one of the major *ciudadelas* at Chan Chan. The Tschudi burn is outlined by crumbled, blackened, and deeply scorched adobe walls. Because of the great quantity of silver and gold objects that were produced by Chimu craftsman and the discovery of a chamber “filled with utensils of gold and silver” found close to the burned area, Squier interpreted the vesiculated adobe as copper- or silver-bearing slag and the burned walls as evidence of a large Chimu metallurgical furnace.

Squier was an experienced journalist and diplomat; however, he had no training in metallurgy, mining, or geology (Hollowell, 2003) with which to substantiate his interpretation. Colonel La Rosa, Squier’s Peruvian colleague who was from nearby Trujillo and familiar with local history, told Squier that the sites had been used for burning of the dead. Squier acknowledged that “... a few traces of bones were to be found at the time of my visit,” and that he “...found no traces elsewhere, nor do we hear of it among the traditions of the ancient occupants of the region.” He was, therefore, “disposed to regard this as a furnace connected with ancient metallurgical operations” (Squier, 1877). Even though chemical analyses of the scoria, which Squier interpreted to be metallurgical slag, showed no gold, silver, or copper (Hollister in Petersen, 1970, p. 51), the Tschudi burn came to be known as a large metallurgical center (Caley and Easby, 1959; Petersen, 1970, p. 51; Samamé Boggio, 1979a).

If the Tschudi burn had been a Chimu metallurgical site, then it would have been the largest ever described in the Andean region. Therefore, the burned sites at Chan Chan were researched by Lechtman and Moseley (1975) and their chemical analyses of the scoria indicated that the burned material contained 57.0–64.0 wt% (weight percent) SiO₂ and was identical in SiO₂ content to the unburned adobe—the scoriaceous material was not metallurgical slag as interpreted by Squier, but only deeply burned adobe. Analyses further showed that the copper content of samples from the Tschudi burn was too low to be considered a copper slag when compared to the copper content of slags from several European, Middle Eastern, and South American metallurgical sites (Lechtman and Moseley, 1975, Table II). Similarly, no copper pellets or “prills,” which are common in copper slags from ancient smelters, such as at Timna, Israel (Milton et al., 1973, p. 24), have been described from the Tschudi burn.

Even after field and laboratory studies proved that metallurgy had not taken place at the site, the purpose of the Tschudi burn remained unknown (Lechtman and Moseley, 1975, p. 162). However, the absence of evidence for metallurgy, La Rosa’s commentary, and Squier’s acknowledgment of calcined human remains at the site all indicated the possibility of human cremation at the Tschudi burn.

Temperature of the Tschudi Burn

Petersen (1970, p. 51) estimated the temperature of the Tschudi burn to have been approximately 1,300°C. Lechtman and Moseley (1975, pp. 161–162) later reported that the burn was caused during a single, high-temperature (1,320°C) burn that lasted from 16–40 hours and that the fuel was a local desert plant, *Tillandsia latifolia*. Their estimated temperature of the burn, was based on step heating of an unburned test brick until bubbling, vitrification, and flowage of the brick, comparable to the characteristics of the burned adobe at Tschudi, took place (Lechtman and Moseley, 1975, pp. 154–155). The textures on the test brick and the adobe at the Tschudi burn may be replicated by curing a modern brick in an ~24-hour-long, coal-fueled fire (Figure 4.1.1).

Controlled burning temperatures, with locally obtained coal as a fuel for brick making, range from 1000°C to 1200°C (Sr. Merardo Castillo Cruz, owner, Ladrillera Castillo, Trujillo, Peru, written communication, January 2007); however, some curing fires may get out of control and these temperatures may be exceeded which will result in scoriated, vesiculated brick. He also indicated that wood burns at lower temperatures, approximately 500°C, and some anthracite may burn as hot as 2800°C.

Therefore, the textural features of the ancient, vesiculated adobe brick at Tschudi, when compared with the modern, vesiculated brick from the Trujillo brickyard, suggest that a similarly high-heat, high-BTU fuel (a British thermal unit is the energy needed to raise the temperature of 1 pound of water 1°F), such as coal, was available and used to fuel the Tschudi burn. Anthracite, the higher rank coal commonly found in northern Peru, is compact, with only 10% water, high carbon content, no recognizable plant matter, and may contain up to 15 500 BTU/lb (Craig

et al., 2001, p. 143). Peat, which is a commonly used fuel with recognizable plant material and high water content, contains only 5400 BTU/lb.

The burning temperature for specific plants, such as *Tillandsia*, is not available; however, wood burns at approximately 600°C (Vogel, 2003), and, because of its carbon content, coal burns at higher temperatures, from 1300°C to 1600°C, depending on rank (IEA Clean Coal Centre, 2006). Therefore, the 1320°C temperature of the Tschudi burn (Lechtman and Moseley, 1975, pp. 161–162) is more consistent with the higher temperatures and higher BTUs of a coal-fueled fire and not the lower temperatures and BTUs of a plant-fueled fire.

Calcium in the Soil

Previous geochemical studies of the deeply burned adobe walls at the Tschudi burn showed no anomalous metal content and hand samples contained no copper prills that would be evidence of copper processing. However, the soil within the burn had not been similarly studied. If metallurgy had taken place at the site at any time in the past, then analyses of soil samples would have elevated metal content with respect to the background. Therefore, eight reconnaissance soil samples were taken at ~10 m intervals at 10–20 cm depth across the Tschudi burn—four sieved samples were taken outside the burned area to establish background metal concentrations and four sieved samples were taken within the burned area. Samples were collected with a plastic trowel and plastic sieves were used to avoid any metal contamination. These soil samples were submitted to a commercial exploration assay laboratory for multielement, induced coupled plasma (ICP) analysis. The analyses showed uniformly low gold (<5 ppm) and silver (<0.05 ppm) content of the soil samples from inside and outside the burned area (Table 4.1.1). There was no difference between the copper content of the soil outside the burned area (11–15 ppm) and the copper content of the soil within the burned area (11–16 ppm). The analyses from this soil survey confirmed, as previous studies had shown (Lechtman and Moseley 1975, Table III; Brooks et al., 2004) that there was no geochemical evidence for metallurgy at the site.

However, the soil data showed that the calcium content of the soil inside the burned area (8300–18 000 ppm) was higher than the calcium content of the soil outside the burned area (7200–10 000 ppm) (Table 4.1.1). This indicated that calcium was present, either during or after the burn, in the soil samples. Possible sources included human bone from reported cremation (La Rosa in Squier, 1877, p. 141); shell fragments used in the adobe, which contained 1–6 wt% CaO (Lechtman and Moseley, 1975, Table III); mouse bones or osseous inclusions (Lechtman and Moseley, 1975, p. 149); or, perhaps, the fuel used for the burn.

Table 4.1.1
Analyses from soil geochemical traverse across the Tschudi burn, Chan Chan, northern Peru.
ICP analyses from American Assay Laboratories, Sparks, Nevada.

Trace elements in soil, inside and outside of burned area

Element concentration	Ag (ppm)*	Au (ppm)	Cu (ppm)	Ca (ppm)	P (ppm)	K (ppm)	B (ppm)	S (ppm)
Sample number								
SS 1	<0.05	<5	15.3	7257	1254	3514	11	166
SS 2	<0.05	<5	13.6	7557	1157	3653	14	184
SS 3	<0.05	<5	14.1	8357	1395	4395	21	1202
SS 4A	<0.05	<5	16.2	18186	1916	6120	32	9733
SS 4B	<0.05	<5	10.8	10947	2260	5867	30	2635
SS 5	<0.05	<5	13.1	17960	1696	5763	38	6981
SS 6	<0.05	<5	11.0	10274	1141	3092	15	193
SS 7	<0.05	<5	11.4	9752	1401	3244	11	463

Note: Samples 1, 2, 6, and 7 were taken outside the burned area to establish background. Samples 3, 4A, 4B, and 5 were taken inside the burned area.ppm, parts per million.

Given Colonel La Rosa's explanation of human cremation at the Tschudi burn, then calcium and other elements found in the reconnaissance geochemical traverse were of interest. This is because human bone, or hydroxapatite, contains mainly calcium and lesser amounts of phosphorus, potassium, and boron. Concentrations of these elements are elevated within the burned area as compared to background concentrations from the soil outside the burned area (Table 4.1.1). And, of these elements, phosphorus is especially significant because, as shown in a court case, chemical analyses of disputed human remains contained calcium, which is consistent with human bone, but did not contain phosphorus, a definitive element in the bone (Warren and Van Rinsvelt, 2000). However, as previously discussed, there were several possible sources for the above-background concentrations of calcium and phosphorus.

Sulfur in the Soil

Sulfur, which is not a normal component of bone or adobe, was also higher in the soil samples from the burned area (Table 4.1.1.); its presence suggested that coal may have been used as a fuel. In a modern example of the significance of sulfur as a component of coal, acid rain is produced when sulfur, contained in pyrite (FeS_2) in coal, is volatilized from coal burned in a coal-fired power plant. The volatilized sulfur then combines with atmospheric water to produce sulfuric acid (H_2SO_4) which slowly attacks marble or other carbonate dimension stone. In order to reduce acid rain and the pollution caused by the sulfur released during coal burning at power plants, it is a common industry practice to add calcium, as limestone, to the burning coal so that the sulfur combines with the calcium to precipitate synthetic gypsum ($\text{CaSO}_4 \cdot 2\text{H}_2\text{O}$), which thereby reduces the release of sulfur to the atmosphere. Therefore, a coal-fueled fire with calcium from an as yet unknown source becomes a reasonable explanation for the elevated sulfur content of the Tschudi burn soil samples.

In studies of fuels used for metallurgy, coal is not a preferred fuel for smelting because of its sulfur content, whereas wood charcoal was preferred because of its low sulfur content. In China, coal was used for smelting because of limited timber for charcoal production combined with the regional availability of low-sulfur coal (Tylecote, 1980, p. 204; Craddock, 1995, p. 196). Chemical analysis of some primitive European iron artifacts contained sulfur, demonstrating that coal had been used, though rarely, as a smelting fuel (Tylecote, 1962, p. 191). The presence of sulfur in the soil samples from the Tschudi burn pointed to coal as the fuel.

Fuel Ash Chemistry

Carbonized plant material at the Tschudi burn and subsequent compaction calculations led Lechtman and Moseley (1975, pp. 140, 156) to conclude that a local plant, *T. latifolia*, was the fuel for the Tschudi burn. However, the lab temperature of 1320°C inferred for the Tschudi burn suggested a fuel that burned much hotter than plant material.

Charcoal was the preferred fuel for ancient metallurgy and, in ancient Peru, charcoal from the algarrobo tree was the most commonly used fuel for smelting (Shimada et al., 1983, p. 38; Shimada and Merkel, 1991, p. 81). However, whatever is locally available, whether it is wood, coal, or plant material, may also have been used as a fuel (Needham, 1980, p. 521).

The use of coal, wood, charcoal, or plant material as a fuel is inherently a destructive process, and therefore, only chemical analysis of the remaining ash or burned residue provides direct evidence of the fuel that was burned. Ash from several commonly used ancient fuels such as coal, charcoal, and peat was analyzed by Tylecote (1980, p. 205), but locally used plant fuels, such as *Tillandsia*, were not included. By using SiO_2 and other oxides, Tylecote easily differentiated coal ash (25–53 wt% SiO_2) from plant/charcoal ash (8.0 wt% SiO_2) and other fuels (Table 4.1.2).

Major oxide and trace element data from 14 coal ash samples, collected as part of a regional coal quality inventory (Finkelman et al., 2001; Brooks and Willett, 2004; Brooks et al., 2006) served as a database (Table 4.1.3) for comparison of known Peruvian coal ash composition with the unknown ash from the Tschudi burn. Three samples from the 10–20 cm ash exposed in the research trench were analyzed (Table 4.1.4). An average of the data for the 14 samples in Table 4.1.3 and the data from samples of algarrobo-wood ash are also included in Table 4.1.4.

Table 4.1.2
Analyses of fuel ash compositions.

Weight percent oxides in ash in ancient fuels			
Fuel	Charcoal	Coal ash	Peat
Oxide in fuel ash			
SiO ₂	8.0	25–53	3–30
Al ₂ O ₃	0.9	20–40	0.3–5
Fe ₂ O ₃	tr	9–26	12–19
MnO ₂	31.6	0–0.2	–
MgO	7.6	0–10	1–7
CaO	25.0	2–12	24–30
Na ₂ O + K ₂ O + CO ₂	22.0	1.0–2.0	0.6–4.0
P ₂ O ₅	4.9	0.2–2.0	0.2–2.5

Source: From Tylecote (1980, p. 205) tr, trace amount.

Tillandsia was collected in Peru for analysis, but was not permitted into the United States; therefore, chemical data on plant ash, also in Table 4.1.4, is from Kabata-Pendias and Pendias (1992).

Oxide and Trace Element Data

Data for a number of oxides and trace elements from regional coal samples are presented in Table 4.1.3. However, only specific oxides (bold-faced data in Table 4.1.3) such as SiO₂, Al₂O₃, CaO, and K₂O (Tylecote, 1980, p. 205), and trace element data, specifically zirconium, compiled in this study provide key information for determination of the original material used as fuel at the Tschudi burn. This is because only a few elements form refractory compounds: for example, the melting point of SiO₂ is 1713°C, CaO is 2570°C, Al₂O₃ is 2050°C, and ZrO₂ is 2710°C (Norton, 1968, p. 230). During coal burning, or ashing for geochemical analysis, some elements, such as arsenic, lead, mercury, or silver, are volatilized. Other elements and their oxides, such as aluminum, calcium, silicon, and zirconium, are not volatilized (Fletcher and Skeen, 1995) and therefore, are especially useful for comparison and determination of the original composition of the unknown fuel material.

The geological environment of coal formation is also an important factor in understanding and interpreting the analytical data. Coal formation begins in a warm, humid region, in a basin that acts as a catch-all for plant material as well as a variety of intercalated stream-transported, detrital or airborne, volcanogenic minerals in varying amounts that are included in the coal. Over tens of thousands of years, coal forms from the accumulation, burial, and compaction of plant and other intercalated material. Carbon becomes concentrated during this process and water is expelled until a higher rank, such as bituminous or anthracite coal, is attained. Plants, in contrast, use and accumulate specific minerals from local soils for their growth and development.

The most distinctive of several oxides and elements used to differentiate coal ash from other ash compositions are discussed below:

SiO₂, Al₂O₃—Tylecote (1980, p. 205) established 25–53 wt% as the range of SiO₂ content of coal compared with 8 wt% SiO₂ for charcoal. Similarly, the Al₂O₃ content of coal is much higher (20–40 wt%) than in plants (<1.0 wt%). This is directly related to the accumulation of detrital grains of quartz (SiO₂) and feldspar (Al₂O₃ is an important constituent of this mineral series) in the coal-forming basin. In general, these elements are not as abundant in trees and the SiO₂ content of common plants is 0.3–1.2 wt% (Kabata-Pendias and Pendias, 1992, p. 151).

CaO, K₂O—Tylecote (1980, p. 205) indicates that the CaO content of charcoal ash is 25.0 wt% and peat ash is 24–30 wt%, compared with only 2–12 wt% in coal ash. In this study, the CaO content of wood ash is 41.0–53.0 wt% compared with 1.0–7.0 wt% in coal ash (Table 4.1.4). Calcium would bioaccumulate in plants as an element

Table 4.1.3

Major oxide and selected trace element content of coal ash samples, northern Peru. SiO₂, Al₂O₃, Fe₂O₃, MgO, CaO, Na₂O, K₂O, TiO₂, P₂O₅, SO₃, Cl, S, ash, and moisture reported in weight percent, all others in parts per million. Analyses are “as determined, ash basis”; Energy Team, US Geological Survey, Reston, VA and Denver, CO; ultimate-proximate data, BTU/lb, forms of sulfur, Free Swelling Index (FSI), ash fusion temperature, and sample locations are available in Brooks et al. (2006).

Major oxides and trace elements in Peruvian coal ash.*

Mine	Alto Chicama 1	Alto Chicama 2	Alto Chicama 3	Banos de Chimu	Caraz	Cocabal	La Galgada	La Limena	La Limena	La Victoria	La Victoria	Sta. Julia	San Roque	Villon	Average
Field no.	BP2300	BP3100	BP3200	BP2900	B0106	B0104	B0101	B0102	B0103	BP2400	BP2500	B0108	B0107	B0105	Average
Lab no.	E-178577	E-178582	E-178583	E-178581	E-186584	E-186582	E-186579	E-186580	E-186581	E-178578	E-178579	E-186586	E-186585	E-186583	
SiO₂	56.9	38.9	50.9	38.2	62.2	69.7	63	61.8	59.3	40.3	30.1	45.1	59.6	45.7	51.3
Al₂O₃	28	32.4	38.9	32.8	25.9	18.5	28.2	24.6	17.8	34	33	18.6	30.9	31.8	28.2
Fe ₂ O ₃	2.3	4.2	1.1	1.8	3.5	4.6	4.5	5.6	5.4	1.5	5.6	10.4	2.2	4.1	4.6
MgO	0.29	2.8	0.41	1.4	0.9	0.93	1.3	0.87	5.6	1.4	5.4	5.7	0.43	0.53	2
CaO	1.3	3.4	0.04	2.2	0.38	0.69	0.97	1.2	1.6	2.2	7.5	1.2	0.2	2.3	1.8
Na ₂ O	1.7	0.49	0.22	2.3	0.48	2	1.7	1.9	1.3	1.3	1.3	4.8	0.14	0.1	1.41
K₂O	2.3	1.5	0.89	1.6	3.2	1.6	2.8	4.5	1.6	1.5	0.81	5.4	0.73	0.54	2.7
TiO ₂	1.5	2.2	1.9	1.7	1.6	1.1	1.4	1.1	1.4	1.9	1.6	1.1	1.9	1.8	1.59
P ₂ O ₅	0.05	1.5	0.06	0.54	0.34	0.16	0.1	0.02	0.08	0.42	0.58	0.69	0.06	2.4	0.5
SO ₃	NA	NA	NA	NA	0.82	1.1	1.2	2	4.5	NA	NA	9.1	0.31	0.54	2.45
Ash	31.5	3.9	63.4	8.9	27.5	10.4	30.7	31.1	23.8	6.8	2.4	29	17	12	21.3
Moisture	5.8	2	1	2.2	0.8	1.4	2.1	2.3	2.5	1.5	1.3	4.2	0.8	0.6	2.4
Cl	0.052	0.023	<<0.015	0.018	0.10	0.03	0.30	0.50	0.04	<<0.015	<<0.015	1.84	<<0.01	0.14	0.30
S	NA	NA	NA	NA	0.47	0.70	0.51	0.75	0.38	NA	NA	1.74	0.66	0.99	0.77
Sc	42.9	61.5	13.3	122	23.5	18.3	24	17.8	28.3	60.4	48.4	25.7	34.6	37.9	40
Cr	70.6	141	27.6	280	68.9	64.6	63.1	36.4	28.1	150	118	37.9	72.9	71.6	87.9
Co	10.6	69.8	29.3	121	22.7	17.6	23.4	23.2	26.3	48.7	73.4	54.9	77.2	20.7	44.2
Zn	52.6	207	81.4	567	359	8690	90.2	218	90.1	171	326	1080	83.7	228	875
As	50.9	12.5	4.3	84.3	26.7	21.8	26.7	57.2	19.5	15.8	24.2	3220	87.4	33.6	263
Rb	132	44.9	60.9	144	118	53.1	128	148	48.8	80.1	27	244	37.4	23	92.1
Sr	321	1380	215	2020	404	240	344	290	96.2	802	771	436	176	2010	679
Zr	301	460	392	311	411	219	410	535	391	328	346	409	754	560	416
Mo	22	11	2.2	14	2	6.1	5.4	5	6.3	7.3	6.9	4.5	10.3	3.2	7.59
Sb	10.5	4.5	1.1	21.9	7.4	3.4	3.6	10.9	7.2	3.9	6.6	17.6	7.3	1.6	7.68

Cs	15.6	4.8	78.8	60.5	24	11.1	23.6	13.1	22	11.5	2.8	12.2	20.8	13.9	22.5
Ag	<<1	<<1	<<1	<<1	<<2	<<2	<<2	<<2	<<2	<<1	<<1	2	<<2	<<2	2
Be	6	10.5	1.9	21.9	2.1	2.5	3.3	3.5	<<1	10.1	9	3.2	2.8	4.9	6.28
Bi	0.76	1.6	0.73	2.5	<<0.1	<<0.1	<<0.1	0.59	<<0.1	1.1	1.6	5.2	0.56	0.5	1.51
Ga	33.8	48.7	53.8	104	31.5	24.3	34.3	28.2	23.4	50.9	39.7	31.1	41.5	45.2	42.2
Sn	18.3	33	11.8	33.7	6.7	12.9	11.5	10.4	5.8	23.8	106	28.4	11.8	3.8	22.7
Au	<<10	<<10	<<10	<<10	<<10	<<10	<<10	<<10	<<10	<<10	<<10	<<10	<<10	<<10	<<10
Th	16.2	39.8	10	69.1	11.7	11	19	14.8	11.8	40.3	32.5	17.8	28.7	29.2	25.1
U	2.2	11.9	2.6	17.7	2.1	1.9	2.4	2.4	2.1	11.4	10.1	3.6	5.2	6.5	5.86
Mn	37.3	261	63	866	218	229	298	455	1040	166	753	689	40.5	41.2	368
Hg	0.04	0.13	0.19	0.31	0.49	0.07	0.21	0.31	0.51	0.04	0.04	0.24	0.45	0.27	0.23
Cu	96.6	85	49.6	631	71.1	55.8	79.1	102	72.7	216	258	466	204	679	219
Li	32.3	187	150	463	140	47.8	101	72.4	45.3	167	197	39.5	140	216	143
Ni	12.9	185	32	162	31.2	51.9	52.4	31.6	28.8	84.3	113	62.4	55.2	48.6	68
V	451	509	97.5	1070	215	206	215	145	188	477	406	143	470	364	354
Y	18.9	91.4	<<1	93.1	9.4	10.1	17.9	11.3	27.1	65.6	84.8	28.3	24.4	73.9	42.8
B	27	66.2	383	124	82	81.3	241	139	87	108	198	550	72.8	35.9	157
Cd	0.54	0.76	0.43	1.4	7.3	5.1	0.6	3.1	1.2	1.1	1.9	21.1	0.38	0.35	3.23
Ge	3.6	8.9	3.8	7.8	0.47	4.8	1.8	4.5	3.1	2.3	5.7	2.6	5.5	3	4.13
Nb	6.6	37.4	18.2	51.7	13.5	11.1	14.3	10.5	12.6	26.8	27.7	8.4	21.2	7.9	19.1
Pb	140	45.9	10	104	75.3	45	30.9	140	142	38.5	53.8	1120	70.7	168	156
Te	1.8	2.3	0.65	3.1	0.19	1.4	0.5	1.2	1	0.69	2.5	3.1	1.3	1.3	1.5
Tl	3.1	0.44	0.36	1.3	1.3	0.77	1.1	2	0.52	0.9	0.36	1.2	1.2	1.4	1.14
Se	2.6	0.34	3.1	0.41	0.54	0.27	1	0.81	0.27	<<0.10	<<0.10	0.94	1.7	1.7	1.14
Ba	940	840	234	620	381	1080	382	1160	160	633	706	412	62.6	810	601

Note: Bold-faced data are necessary for determining the original fuel.

NA, not available.

* Oxides are in weight percent (wt %); trace elements are in parts per million (ppm).

Table 4.1.4

Comparison of known ash compositions and unknown ash from the Tschudi burn, Chan Chan, northern Peru. SiO₂, Al₂O₃, Fe₂O₃, MgO, CaO, Na₂O, K₂O, TiO₂, P₂O₅, SO₃, Cl, S, ash, and moisture reported in weight percent, all others in parts per million. Analyses are “as determined, ash basis”; Energy Team, US Geological Survey, Reston, VA and Denver, CO; ultimate–proximate data, BTU/lb, forms of sulfur, FSI, ash fusion temperature, and sample locations are available in Brooks et al. (2006). Plant data from Kabata-Pendias and Pendias (1992).

Major oxides and trace elements of materials in study area *							
Material	Ash	Ash	Ash	Ash	Algorrobo wood	Charcoal	Plant data
	Peru coal	Tschudi burn	Tschudi burn	Tschudi burn	Chao valley	Trujillo market	
Field no.	Average	BP0701	BP0801	BP0901	BP0101	BP0601	
Lab no.	(Table 3)	E-199457	E-199458	E-199459	E-199743	E-199456	
SiO ₂	51.3	54.7	51.8	52.3	3.1	5.8	0.3-1.2
Al ₂ O ₃	28.2	12.5	11.9	11.8	0.82	2	NA
Fe ₂ O ₃	4.6	5.4	5.2	4.8	0.97	4.2	NA
MgO	2	3	2.8	2.1	1.6	1.3	NA
CaO	1.8	4.5	4.2	3.8	53	41	NA
Na ₂ O	1.41	6.7	6.7	5.8	1.1	0.44	NA
K₂O	2.7	2.2	2.1	1.8	1.9	7.5	NA
TiO ₂	1.59	0.68	0.67	0.6	0.08	0.09	NA
P ₂ O ₅	0.5	0.69	0.65	0.53	0.31	2.3	NA
SO ₃	2.45	1.5	1.2	0.36	2.1	4.8	NA
Ash	21.3	98.1	100	99.5	1.1	4.93	NA
Moisture	2.4	0.928	0.945	0.417	6.04	1.93	NA
Cl	0.30	0.051	0.075	<<0.015	NA	0.074	NA
S	0.77	0.606	0.476	0.163	NA	0.061	NA
Sc	40	13.3	13.4	13.7	<<4	<<4	NA
Cr	87.9	33.7	35.5	33.4	31.8	42	NA
Co	44.2	15.2	20.4	15.4	4.1	5.7	NA
Zn	875	147	129	98.6	404	316	NA
As	263	20	20.5	15	5	9.7	NA
Rb	92.1	74.6	76.6	62.6	11.4	38.9	NA
Sr	679	377	402	411	1960	3080	NA
Zr	416	206	212	182	19.9	18.5	10-20
Mo	7.59	1.6	2	1.3	25.6	7.6	NA
Sb	7.68	2.4	2.2	2	18.4	0.43	NA
Cs	22.5	5.1	4.5	2.7	0.38	0.96	NA
Ag	2	<<2	<<2	<<2	<<2	<<2	NA
Be	6.28	2	2	1.8	<<1	1.1	NA
Bi	1.51	0.28	0.16	<<0.1	0.62	0.13	NA
Ga	42.2	11.6	11.9	11.2	1.3	2	NA
Sn	22.7	<<3	<<3	<<3	38	6.7	NA
Au	<<10	<<10	<<10	<<10	<<10	<<10	NA
Th	25.1	12	13.1	12.2	<<8	<<8	NA
U	5.86	3.7	3.2	2.9	0.44	0.48	NA
Mn	368	758	818	734	366	244	NA
Hg	0.23	0.03	0.02	<<0.02	<<0.02	0.03	NA
Cu	219	26.6	38.7	15.2	101	93.5	NA
Li	143	38.6	36	40.2	112	15.7	NA
Ni	68	<<4	<<4	<<4	7.5	140	NA
V	354	128	131	116	3.3	12	NA

Table 4.1.4
(continued)

Major oxides and trace elements of materials in study area*							
Material	Ash	Ash	Ash	Ash	Algorrobo wood	Charcoal	Plant data
	Peru coal	Tschudi burn	Tschudi burn	Tschudi burn	Chao valley	Trujillo market	
Field no.	Average	BP0701	BP0801	BP0901	BP0101	BP0601	
Lab no.	(Table 3)	E-199457	E-199458	E-199459	E-199743	E-199456	
Y	42.8	13.4	14	13.2	10.1	8	NA
B	157	102	55.8	<<20	306	284	NA
Cd	3.23	0.21	0.25	<<0.1	7	0.1	NA
Ge	4.13	1.9	2	1.9	0.52	1	NA
Nb	19.1	7.6	11.3	8	0.76	4.1	NA
Pb	156	10	11.4	12.5	598	7.2	NA
Te	1.5	0.11	0.18	<<0.1	<<0.1	0.36	NA
Tl	1.14	0.37	0.23	0.11	0.23	0.11	NA
Se	1.14	0.63	0.62	<<0.10	<<0.05	<<0.10	NA
Ba	601	378	360	348	112	174	NA

Note: Bold-faced data are necessary for determining the original fuel.

NA, not available.

* Oxides are in weight percent (wt %); trace elements are in parts per million (ppm).

necessary for plant cell manufacture and development (Tucker, 1995). Analyses of charcoal, coal, and peat ash by Tylecote (1980, p. 205) (Table 4.1.4) showed that the combined content of CO₂, K₂O, and Na₂O was 22 wt% for charcoal, 1.0–2.0 wt% for coal ash, and 0.6–4.0 wt% for peat ash, and those oxides can be used to chemically differentiate the fuels.

The abundance and importance of potassium, sometimes referred to as the compound “potash” (K₂O), is indicated by the use of ashed hardwood trees to provide an abundant source of potash for fertilizer (Craig et al., 2001, p. 339). The principal elemental components of wood ash are calcium, potassium, and nitrogen—potassium is one of the chief components of fertilizer. In general terms, wood charcoal and plant or peat ash would have higher CaO and K₂O content relative to coal ash.

Zr—This element is commonly found in the mineral zircon (ZrSiO₄) and may enter the coal basin as a detrital grain weathered from igneous, metamorphic, or sedimentary rocks or as wind-blown material from a volcanic eruption. Zircon is a heavy mineral (specific gravity 4.6–4.7) with a hardness of 7.5 and, therefore, would resist abrasion in streams and would not degrade during the coal-forming process. The zirconium signature of coal ash is high and may range from 130 ppm to 2400 ppm (Finkelman, 1981, p. 269). But equally important, the mineral zircon is geologically stable and highly refractory to temperatures of 2500°C (Blumenthal, 1995, p. 860) and is used as foundry sand. Therefore, because of its refractory nature, the zirconium content of wood or coal would not be affected by ashing in the laboratory or by burning, for example, at the 1320°C Tschudi burn, and, therefore, would provide an important elemental signature of the unburned fuel.

There is a paucity of data on zirconium in plants and not much agreement among the reported values for zirconium plant data; however, a concentration of 10–20 ppm zirconium was given by Kabata-Pendias and Pendias (1992, p. 2001). Zirconium data on plants in the United States showed that beans and corn contained <20 ppm zirconium and some trees contained <20 ppm to 60 ppm zirconium (Connor and Shacklette, 1973, p. 167). Land plants have little tendency to use zirconium and 70% of plants analyzed had no zirconium present (Lenntech, 1995).

The results indicate, that in relative terms, the zirconium content of an ashed plant fuel would be low, approximately 20 ppm, relative to the higher zirconium content of coal ash, from 130 ppm to as high as 2400 ppm. The data in Table

4.1.4 indicate that the geochemical signature for the three samples of ash from the Tschudi burn is consistent with coal ash and, therefore, indicate the use of coal, and not plant material, as the fuel at the Tschudi burn.

¹⁴C Date

Carbonized plant material is herein interpreted to have been used as tinder to start the coal and not the primary fuel. Even though widely distributed, Peruvian coal is very difficult to ignite because it has been tectonized to a very dense, shiny, mirror-like form of anthracite, locally called *cisco* and, therefore, does not have a large domestic or international market. Dried plant material, *Tillandsia*, would have been ideal tinder with which to ignite the coal. Fragments of this plant material exposed in the upper part of the research trench (Figure 4.1.2) were submitted for ¹⁴C dating. The calibrated result indicated that the *Tillandsia* was closed to ¹⁴C uptake AD 1312–1438 (Table 4.1.5) and was likely used as tinder shortly thereafter. The ¹⁴C date indicates that (1) the Tschudi burn took place before European contact and (2) toward the end of Chimu control and the onset of Inca domination of the region.

The sulfur content of the coal is also considered to be high which may contribute to pollution and fouling of the burners. The total sulfur content of coal from Callacuyan, for example, may be as high as 23 wt% (Carrascal et al., 2000, p. 54). The type of fuel used at the Tschudi burn had been resolved by ash chemistry, temperatures, and supportive data. Timing of the Tschudi burn had been bracketed by isotopic data; however, another important question, “Que cosa queman?” (What was burned?), remained.

Cremation in Society

No geochemical evidence for metallurgy had been found in the analyses of the vespicular adobe or the soil samples from the Tschudi burn. Therefore, Colonel La Rosa’s description of “calcined human bones ... burning of



Figure 4.1.2. Carbonized plant material (*Tillandsia latifolia*) to the right of scale, interpreted as tinder to start the Tschudi burn, gave a ¹⁴C date of AD 1312–1438. Melted, vespicular adobe is above the plant material and poorly sorted gravels are below. Photo by William E. Brooks, 2005.

Table 4.1.5
¹⁴C date on carbonized plant material (*Tillandsia latifolia*) from the Tschudi burn,
 Chan Chan, northern Peru.

Calibrated C-14 dates of carbonized plant material					
		¹⁴ C	¹³ C/ ¹² C [†]	Calibrated (AD)	Calibrated (AD)
Sample	Description	Years (BP)	Ratio	± 1 Sigma	± 2 Sigma
B0401	Carbonized Plant Material	1467 AD +/-	-25%	1326–1343	1312–1358
	plant material	34 years		1394–1426	1387–1438

[†] ¹³C/¹²C is deviation in parts per thousand of the sample relative to the standard. BP, before present.

the dead” and the elevated calcium and phosphorus content of the soil pointed to evaluation of cremation as the next working hypothesis (Brooks, 2004).

Cremation is a global mortuary practice that dates to 40 000 years ago at the Mungo Man site in the coal-producing region of New South Wales, Australia (Bowler et al., 2003). As early as 3000 years ago, providing niches for cremated ashes was a profitable business in Greece and Rome. The Romans reserved cremation for Julius Caesar, Nero, and others of high social standing; however, the Israelites considered cremation as befitting only the despicable (Prothero, 2002, p. 6). Cremations were described in the Iberian Peninsula at the beginning of the first millennium (Universidad Complutense Madrid, 2001). And by AD 400, earth burial had replaced cremation in Europe except in instances of widespread disease; for example in 1656, in Naples, when 60 000 victims of the Black Death were cremated in 1 week (Australian Museum, 2003).

Cremation, which has been used throughout the world, is not considered to have been a mortuary practice in ancient Peru (Rowe, 1991, p. 29). Secondary cremations of human skeletal remains in ancient Peru have been described; these are cremations of bone that were not covered with flesh at the time of burning as indicated by cracking or “checking” on the surface and longitudinal splitting (Ubelaker, 1978, p. 35; Verano, 1991, p. 200).

Fuel for Cremation

Coal or wood are the common cremation fuels used throughout history—both are available in northern Peru. In Great Britain, coal is abundant and was used by inhabitants of southern Wales to cremate their dead during the Bronze Age. Coal was also used to fuel the first legal cremation in South Wales in 1884 (Cassidy, 1973, p. 1; Freese, 2003, p. 16). In North America, the Tolkotins, a Native American group in Oregon, practiced open-air, wood-fueled cremation long before the first US crematorium, which used coal, opened in 1876 in the coal-producing region of Washington, Pennsylvania (Prothero, 2002, p. 28). During World War II, coal from nearby mines was used to fuel the crematoriums at Auschwitz (Mattogno and Deana, 1993). Coal is used for cremation in the coal mining regions of China.

The decomposing bodies of many of the victims of the deadly tsunami that struck southeast Asia in 2004 were cremated in wood-fueled pyres (Nakashima, 2003, p. A17). In 1960, three lives were lost to a 9 m, earthquake-generated tsunami that struck near Chimbote, northern Peru. Then, in 1996, 12 people, some of whom were children, were killed by a 5 m tsunami that struck the same area (Tsunami Research Group, 2005). Natural hazards such as El Niño floods, mudflows (huaycos or aluviones), and earthquakes have affected Peru for centuries (Stillwell, 1992; Brooks et al., 2005) and the victims of these ancient disasters may have been cremated using locally available fuel. But regardless of the reason for cremation, soil and ash chemical data and temperatures from the Tschudi burn all pointed to coal as the fuel.

Cremation at the Tschudi Burn

Colonel La Rosa's commentary and, now, elevated calcium and phosphorus were very suggestive that cremation may have occurred at the Tschudi burn—yet, the anomalous calcium and phosphorus content of the soil could be explained as coming from other sources. Therefore, if the Tschudi burn had actually been used for cremation, only the presence of calcined human bone would be definitive.

Calcined bone generally survives longer in the soil than unburnt bone. This is due to a case-hardening effect and increased density brought on by heating, recrystallization, and conversion of the bone material (hydroxapatite) to β -tricalcium phosphate. Then, upon cooling, water is absorbed and the bone reverts to a more coarsely crystalline hydroxapatite which may contribute to its survival in the soil. Heating also destroys the organic component of bone which would attract organisms that would ultimately destroy the bone (Mays, 1998, p. 209).

Since cremation is a destructive process, it is important to consider which bones and how much material might remain. At the Museo Arqueológico Nacional in Madrid, a diorama showed that at the prehistoric Necropolis de Medellín, after cremation took place, bone was recovered and placed in a stone receptacle. In another example, Bronze Age cremation studies in Europe showed that no more than 60% of the bone weight may be recovered (McKinley, 1998). Some of the more commonly occurring bone fragments that remain after cremation include parts of the vertebra, the mandible, or temporal bone and most fragments are small, in the 2–4 mm range (Mays, 1998, pp. 210–213). After a modern cremation, which takes place at temperatures of 800–1200°C for only 2–3 hours, the larger, more-dense, weight-bearing bones, such as femur, hip, jaw, and perhaps a part of the skull, will remain somewhat intact. Depending on bone structure, only 5–7 lb of bone will remain after cremation and this material must be uniformly crushed before the cremains or “ashes” are returned to the family (Bloomquist, 1996). Any of these bones, if still present at the Tschudi burn, would have been conspicuous, found, and described by previous researchers. However, given the duration of the Tschudi burn, some bones may have been completely consumed in the 16–40 hour, 1320°C fire. Or, bone may have been removed after cremation for secondary burial, scattered by scavengers or looters, or simply degraded after more than 600 years of exposure.

In May 2005, a 5 gm, 4.5 cm bone fragment was found. The fragment had weathered out of excavated material from the research trench that was dug in the 1970s. The bone fragment was angular and considered in-place as any rounded edges would have indicated that it washed in among the sediments that underlie the burned material. The fragment was described as consistent with calcined bone from the cranial vault, likely the subparietal bone, of a youth and showed meningeal vessel grooves on the interior surface (Figure 4.1.3). Protein radioimmuno assay (pRIA) was recommended to confirm its human or other origin (Douglas H. Ubelaker, Ph.D., anthropologist, Smithsonian Institution, Washington, DC, oral communication, June 20, 2005). The fracture pattern on the surface is irregular and shows splitting, all consistent with the fracture pattern of bone that was fleshed when burned (Ubelaker, 1978, p. 38). The fragment was denser than unburned bone because of heating and recrystallization (Mays, 1998, p. 207).

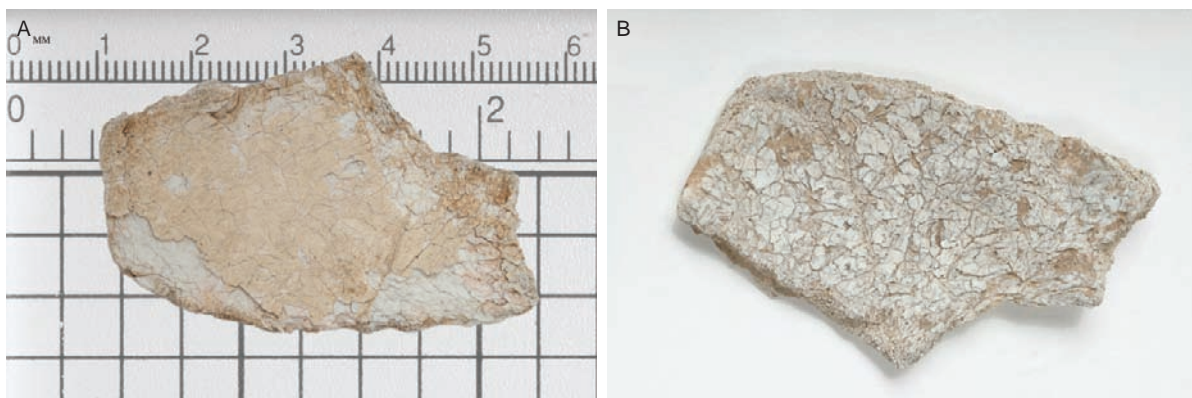


Figure 4.1.3. Calcined cranial vault fragment (B0502) from the Tschudi burn. (A) exterior, showing fracture pattern typical of bone that was fleshed when burned and (B) interior, showing meningeal vessel grooves. Photo by William E. Brooks, 2005.

Table 4.1.6

Results of protein radioimmuno assay (pRIA) analysis on calcined cranial vault fragment recovered from the Tschudi burn, Chan Chan, northern Peru. (A) pRIA results; (B) percent correlations. Original field number for calcined fragment from the Tschudi burn is B0502, MicroAnalytica lab number is MA-1929; analysis by MicroAnalytica, LLC, Miami, Florida.

Analysis of bone fragment sample MA-1929						
A	Comparison of sera standards					
		Human	Bison	Dog	Rat	Sample MA-1929
	Human	27	1	3	9	5
	Bison	7	21	3	21	0
	Dog	3	1	26	1	0
	Rat	19	3	4	45	1
B	Correlation coefficients					
		Human	Bison	Dog	Rat	
	Human					
	Bison	-22				
	Dog	22	2			
	Rat	-61	-63	-29		
	MA-1929	76	-48	-40	-16	

Note: The high value of 5 for sample MA-1929 in part A of the table and the 76% correlation coefficient in part B indicate a human origin.

A 1 g sample of the bone fragment was submitted for pRIA and details of the analysis are shown in Table 4.1.6. This technique is based on protein extraction from small skeletal fragments and has been used to distinguish human from nonhuman samples in forensic studies (Ubelaker et al., 2004). To determine human/nonhuman origin, the sample was tested using antisera standards of human, bison, dog, and rat. In Table 4.1.6, part A, the highest value for the sample from the Tschudi burn indicates “human origin” and in part B, the correlation coefficient is 76%, confirming the human origin of the bone fragment.

The gray-brown color of the bone fragment indicated that it had been heated to temperatures in the range of 440–525°C (Mays, 2003, pp. 207, 217). Previous studies by Shipman et al. (1982, p. 319) showed that the temperatures of cremated bone could be more precisely determined from X-ray diffraction patterns. Therefore, a cremated human bone standard and a fragment of the bone recovered from the Tschudi burn were analyzed (Figure 4.1.4) by X-ray diffraction. Based on comparison with X-ray diffraction data on cremated bone standards in Shipman et al. (1982, p. 319), it was inferred that the bone fragment from the Tschudi burn had been heated to 525°C.

Discussion

Algorrobo charcoal is the acknowledged fuel for metallurgy in northern Peru, but the world-wide, centuries-old use of coal, its regional availability, and its use for jewelry and mirrors in ancient Peru suggest that it may have been used for other purposes, such as for an energy fuel, in the archaeological record of Latin America.

The use of only one fuel is probably rare and other materials, such as grass, wood, bone, or dung, may have also been used at different times in multiuse fires. Non fuel materials such as broken ceramics, bits of food, or cloth may have been disposed of in a multiuse fire. The Tschudi burn, however, was an exceptionally large, single-use fire, apparently for a specific purpose or ritual, and the fuel for this event was possibly chosen for a specific characteristic such as its property as a burning rock or its sulfurous, brimstone smell. Underground coal fires, such as those in China, Colombia, Peru, or Paso Diablo, Venezuela, may have been interpreted by ancient people as fiery, sulfurous, smoldering gateways to the underworld. Therefore, perhaps this burning rock with a strong smell was a highly regarded resource that was to be used carefully which might explain the absence of unburned coal at the site.

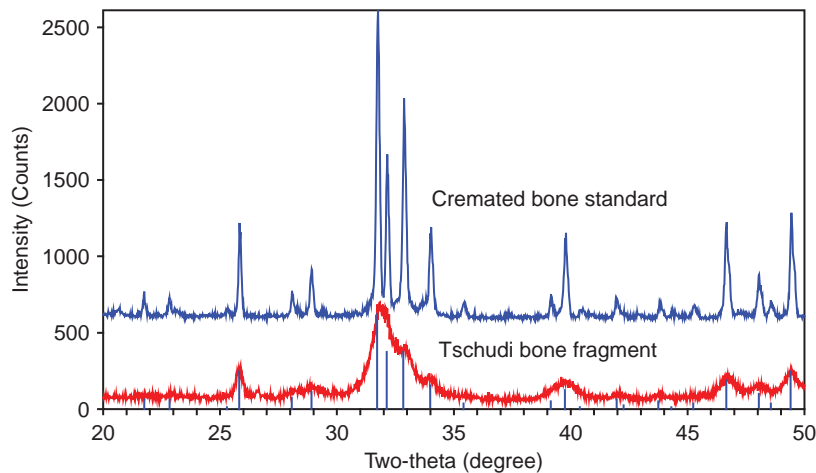


Figure 4.1.4. X-ray diffraction patterns of a cremated human bone standard (top) and calcined cranial vault fragment (bottom) from the Tschudi burn, Chan Chan, northern Peru. The standard was heated to 940°C in a modern crematory furnace and the Tschudi fragment (B0502) was heated to 525°C. The temperatures are inferred from comparison with X-ray diffraction patterns on cremated bone standards in Shipman et al. 1984, p. 319. Vertical lines indicate peaks for hydroxapatite.

How many individuals were cremated is unknown. Given that mass burials are common in ancient northern Peru, 200–300 bodies were found in burial platforms at Chan Chan, and the large size of the Tschudi burn, it is possible that a number of individuals may have been cremated at the Tschudi burn. The data provided herein lead to questions and speculation as to why cremation took place at Tschudi.

Cremation appears to have been a rare occurrence in ancient Andean funeral customs. Examples of cremation in other parts of the world suggest that disease control, as was done in Europe during the Black Death, may have been a possible explanation for cremation at the Tschudi burn. Tsunamis, earthquakes, debris flows, El Niño flooding, and other natural disasters have affected northern Peru for centuries. Cremation may have been used, as it was in southeast Asia after the 2004 tsunami, to dispose of the decomposing bodies of the victims of a natural disaster.

Cremation has also been used as a punishment, a threat, and a statement of power over the victim's life and body after death. In the early 1400s, Joan of Arc was convicted of heresy and was then burned at the stake. In the 1530s, Atahualpa, the Inca king, was threatened with strangulation or being burned to death by his Spanish captors. During World War II, cremation destroyed the body and was a violation of the funeral rites of the Auschwitz victims.

The reason for cremation at the Tschudi burn remains unknown. A coal-fueled fire is indicated by the elevated content of refractory compounds and elements, such as SiO_2 , Al_2O_3 , and zirconium, from the completely combusted ash horizon at the Tschudi burn; sulfur content of the soil; and 1320°C temperature of the burn which resulted in vesiculation and flowage of the adobe. A ^{14}C date on carbonized plant material, interpreted as tinder, indicates that the Tschudi burn was pre-European contact and took place AD 1312–1438, toward the end of Chimú domination of the region. The presence of a calcined, human skull fragment that was heated to 525°C confirms, as Colonel La Rosa said in 1877, that the site was used for burning of the dead.

References

- Agramonte, J., Diaz, A., 1983. *Inventario Preliminar del Carbon Mineral en el Peru*. Instituto Geológico, Minero y Metalúrgico, Lima.
- Agricola, G., 1950. *De Re Metallica* (H.C. Hoover and L.H. Hoover, Trans.). Dover Publications, New York (Original work published 1556).
- Alvarado, B., 1980. Recursos de carbon en Suramerica. *Revue de L'Institut Francais du Petrole* 35 (2), 387–421.
- Arana, P.P., 1901. *Las Minas de Azogue del Peru*. Imprenta El Lucero, Lima, 107p.

- Australian Museum, 2003. Death the last taboo, disposal of the body. <http://www.maxdesign.com.au> (accessed June 2005).
- Bloomquist, R., 1996. Keeper of the flame. *Washington City Paper* 16 (11), 20–26.
- Blumenthal, W.B., 1995. Zirconium and zirconium compounds. In: Howe-Grant, M. (Ed.), *Kirk-Othmer Encyclopedia of Chemical Technology*, fourth edition, vol. 25. John Wiley and Sons, New York, pp. 853–896.
- Bowen, S., 2001. Cheap energy—Belgian company opens Peru's first coal utility plant. *Latin Trade*, February, 29–30.
- Bowler, J.M., Johnston, H., Olley, J.M., Prescott, J.R., Roberts, R.G., Shawcross, W., Spooner, N.A., 2003. New ages for human occupation and climatic change at Lake Mungo, Australia. *Nature* 412 (6925), 837–840.
- Brooks, W.E., 2004. Coal and cremation at Chan Chan, northern Peru: Geological Society of America, Abstracts with Programs, 36, 2, 65.
- Brooks, W.E., Willett, J.C., 2004. Update, World Coal Quality Inventory-Peru: U.S. Geological Survey Open-File Report 2004-1023. <http://pubs.usgs.gov/of/2004/1023/index.html> (accessed June 2004).
- Brooks, W.E., Kent, J.D., Willett, J.C., 2004. Mineral, energy, and fertilizer resources of the north coast of Peru, perspective from the Santa Rita B archaeological site: U.S. Geological Survey Open File Report 2004-1024. <http://pubs.usgs.gov/of/2004/1024/index.html> (accessed June 2004).
- Brooks, W.E., Finkelman, R.B., Willett, J.C., Gurmendi, A.C., Yager, T.R., Carrascal, R., Mucho, R., 2006. World Coal Quality Inventory-Peru: Chapter 6 of World Coal Quality Inventory, South America, U.S. Geological Survey Open-File Report 2006-1241. <http://pubs.usgs.gov> (accessed December 2006).
- Burger, R.L., 1992. *Chavin and the Origins of Andean civilization*. Thames and Hudson, New York, 225p.
- Caley, E.R., Easby, D.T., 1959. The smelting of sulfide ores of copper in preconquest Peru. *Am. Antiquity* 25 (1), 59–65.
- Carrascal, R., Matos, C., Silva, O., 2000. Carbon en el Peru. Instituto Geológico, Minero y Metalúrgico, Boletín 7, Lima.
- Cassidy, S.M., 1973. *Elements of Practical Coal Mining*. American Institute of Mining, Metallurgical, and Petroleum Engineers, New York.
- Connor, J.J., Shacklette, H.T., 1973. Background geochemistry of some rocks, soils, plants, and vegetable in the conterminous United States. U.S. Geological Survey Professional Paper 574-F, 45p.
- Conrad, G.W., 1982. The burial platforms of Chan Chan, some social and political implications. In: Moseley, M.E., Day, K.C. (Eds.), *Chan Chan, Andean Desert City*, University of New Mexico Press, Albuquerque, pp. 87–117.
- Craddock, P.T., 1995. *Early metal mining and production*, Smithsonian Institution, Washington, DC, 245p.
- Craig, J.R., Vaughan, D.J., Skinner, B.J., 2001. *Resources of the Earth—Origin, Use and Environmental Impact*, Prentice-Hall, Upper Saddle River, New Jersey, 520p.
- Dunin-Borkowski, E., 1996. *Minerales industriales del Peru*, Instituto Geológico, Minero y Metalúrgico, Lima, 164p.
- Escudero, J., 1978. El carbon del Alto Chicama, Instituto Geológico, Minero y Metalúrgico, Boletín 2, Lima, 87p.
- Finkelman, R.B., 1981. Modes of occurrence of trace elements in coal. U.S. Geological Survey Open-File Report 81-99, 220p.
- Finkelman, R.B., Warwick, P.D., Pierce, B.S., 2001. The World Coal Quality Inventory. U.S. Geological Survey Fact Sheet 155-00.
- Fletcher, J.D., Skeen, C.J., 1995. Determination of 18 elements in 5 whole Argonne premium coal samples by qualitative direct-current arc atomic emission spectrography, In: Palmer, C.N. (Ed.), *The Chemical Analysis of Argonne Premium Coal Samples*. U.S. Geological Survey, Bulletin 2144, Reston, pp. 13–17.
- Freese, B., 2003. *Coal, a Human History*. Perseus Publishing, Cambridge, 225p.
- Hack, J.T., 1942. *Prehistoric Coal Mining in the Jeddito Valley, Arizona: Reports of the Awatovi Expedition*, Peabody Museum, Harvard University, Cambridge, MA.
- Hackley, P.C., Martínez, M., 2007. Organic petrology of Paleocene Marcelina Formation coals, Paso Diablo mine, western Venezuela: Tectonic controls on coal type: *International Journal of Coal Geology*, 71, 505–526.
- Hardoy, J.E., 1973. *Pre-Columbian Cities*. Walker and Company, New York, 106p.
- Hodge, F.W., 1904. Hopi fired pottery with coal. *Am. Anthropologist* 6, 581–582.
- Hollowell, J.L., 2003. Ephraim G. Squier 1821–1888, the energy, the tragedy: abstract presented at the 22nd Annual Northeast Conference on Andean Archaeology and Ethnohistory, November 1–2, Harvard University, Cambridge, MA.
- Hyams, E., Ordish, G., 1963. *The Last of the Incas*. Barnes and Noble, New York.
- IEA Clean Coal Centre, 2006. *Coal Combustion*. <http://www.iea-coal.org.uk> (accessed June 2005).
- Kabata-Pendias, A., Pendias, H., 1992. *Trace Elements in Soils and Plants*, second ed. CRC Press, Boca Raton.
- Larco Hoyle, R., 2001. *Los Mochicas, tomo II*, Museo Arqueológico Rafael Larco Herrera, Lima.

- Lechtman, H., 1976. A metallurgical site survey in the Peruvian Andes. *J. Field Archaeology* 3 (1), 1–42.
- Lechtman, H., Moseley, M.E., 1973. The scoria at Chan Chan, non-metallurgical deposits. *Nawpa Pacha* 10 (12), 135–185.
- Lenntech, 1995. Environmental effects of zirconium: Environmental effects of zirconium. <http://www.lenntech.com> (accessed January 2006).
- Manufacturer and Builder, The, 1878. Coalfield in Peru. *The Manufacturer and Builder* 10 (8), 175.
- Mattogno, C., Franco, D., 1993. The crematoria ovens of Auschwitz and Birkenau. <http://www.codoh.com> (accessed June 2005).
- Mays, S., 1998. *The Archaeology of Human Bones*. Routledge, London, 242p.
- McKinley, J.I. 1998. Archaeological manifestations of cremation. *The Archaeologist* 33, 18–20.
- Milton, C., Dwornik, E.J., Finkelman, R.B., Toulmin, P., 1973. Slag from an ancient copper smelter at Timna, Israel. *Bull. Historical Metal. Soc.* 10 (1), 24–32.
- Morris, C., Von Hagen, A., 1993. *The Inka Empire and its Andean Origins*. Abbeville Press, New York, 307p.
- Mucho, R., 1992. Combustión de carbón mineral en el Peru, curso práctico. Informe Interno, Cementos Norte Pacasmayo, Lima, 60p.
- Mujica Gallo, M., 1959. Gold Museum of Peru. Aurel Bongers, Germany, 224p.
- Nakashima, E., 2003. Aid begins to flow into south Asia. *The Washington Post*, December 30, A17.
- Needham, J., 1980. The evolution of iron and steel technology in East and Southeast Asia. In: Wertime, T.A., Muhly, J.D. (Eds.), *The Coming of the Age of Iron*, Yale University Press, New Haven, pp. 507–541.
- Norton, F.H., 1968. *Refractories*. McGraw-Hill, New York, 247p.
- Petersen, C.R., 1983. Coal resources of Peru. In: Kottowski, F.E., Cross, A.T., Meyerhoff, A.A. (Eds.), *Coal Resources of the Americas*, Geological Society of America Special Paper 179, 35–42.
- Petersen, G., 1970. Mining and metallurgy in ancient Perú (a translation by Brooks, W.E., 2010, of *Minería y metalurgia en el Antiguo Perú*, *Arqueológicas* 12, Museo Nacional de Antropología y Arqueología, Pueblo Libre, Lima, Perú): Geological Society of America Special Paper 467, 90p.
- Pfordte, O.F., 1893. Ancient method of silver-lead smelting in Peru. *Trans. Am. Inst. Min. Eng.* 21, 25–30.
- Prothero, S., 2002. *Purified by Fire, a History of Cremation in America*. University of California Press, Berkeley, CA, 266p.
- Raymond, R., 1986. *Out of the Fiery Furnace, the Impact of Metals on the History of Mankind*. Pennsylvania State University Press, University Park, PA, 274p.
- Rowe, J.H., 1991. Behavior and belief in ancient Peruvian mortuary practice. In: Dillehay, T.E. (Ed.), *Tombs for the Living, Andean Mortuary Practices*, *Dumbarton Oaks*, Washington, pp. 27–42.
- Samamé Boggio, M., 1979a. *El Peru minero, tomo I*, Instituto Científico y Tecnológico Minero, Lima.
- Samamé Boggio, M., 1979b. *El Peru minero, tomo IV, tercer volumen*, Instituto Científico y Tecnológico Minero, Lima.
- Shimada, I., Epstein, S., Craig, A.K., 1983. The metallurgical process in ancient north Peru. *Archaeology* 35 (5), 38–45.
- Shimada, I., Merkel, J.F., 1991. Copper-alloy metallurgy in ancient Peru. *Sci. Am.* 265 (1), 80–86.
- Shipman, P., Foster, G., Schoeninger, M., 1982. Burnt bones and teeth, an experimental study of color, morphology, crystal structure and shrinkage. *J. Archaeol. Sci.* 2 (1), 307–325.
- Stracher, G.B., Taylor, T.P., 2004. Coal fires burning out of control around the world: thermodynamic recipe for environmental catastrophe. In: Stracher, G.B. (Ed.), *Coal Fires Burning around the World: a Global Catastrophe*. *Int. J. Coal Geol.* 59 (1–2), 7–17.
- Stillwell, H.D., 1992. Natural hazards and disasters in Latin America. *Nat. Hazard.* 6, 131–159.
- Squier, E.G., 1877. *Incidents of Travel and Exploration in the Land of the Incas*. Harper and Brothers, New York.
- Thery, I., Gril, J., Vernet, J.L., Meignen, L., Maury, J., 1995. First use of coal. *Nature* 373, 480–481.
- Thery, I., Gril, J., Vernet, J.L., Meignen, L., Maury, J., 1996. Coal used for fuel at two prehistoric sites in southern France, Les Canalettes (Mousterian) and Les Uscalades (Mesolithic). *J. Archaeol. Sci.* 23 (4), 509–512.
- Tucker, M.R., 1995. Essential plant nutrients. North Carolina Agronomic Division. <http://www.agr.state.nc.us> (accessed March 2006).
- Tsunami Research Group, 2005. *The 1996 Chimbote tsunami*. University of Southern California. Tsunami Research Group. <http://www.usc.edu> (accessed May 2005).
- Tylecote, R.F., 1962. *Metallurgy in Archaeology*. Edward Arnold, London, 127p.
- Tylecote, R.F., 1980. Furnaces, crucibles, and slags. In: Wertime, T.A., Muhly, J.D. (Eds.), *The Coming of the Age of Iron*, Yale University Press, New Haven, pp. 183–228.
- Ubelaker, D.U., 1978. *Human Skeletal remains*. Aldine Publishing, Chicago, 172p.
- Ubelaker, D.H., Lowenstein, J.M., Hood, D.G., 2004. Use of solid-phase double-antibody radioimmunoassay to identify species from small skeletal fragments. *J. Forensic Sci.* 49 (5), 924–929.

- Universidad Complutense Madrid, 2001. Prehistoric cremations in Spain. Universidad Complutense Madrid. <http://www.ucm.es> (accessed May 2005).
- Verano, J.W., 1991. Where do they rest, the treatment of human offerings and trophies in ancient Peru. In: Dillehay, T.D. (Ed.), *Tombs for the Living, Andean Mortuary Practices*, Dumbarton Oaks, Washington, pp. 189–220.
- Vogel, M., 2001. Heating with wood: Montana State University Extension Service. <http://www.montana.edu> (accessed April 2006).
- Warren, M., Van Rinsvelt, H., 2000. To answer cremation questions, forensics finds unlikely ally in physics. University of Florida News. <http://www.napa.ufl.edu/2000news/cremains.htm> (accessed May 2005).
- Washington Group International, 1982. Venezuelan coal mine, Paso Diablo. Washington Group International Global Project Profiles. <http://www.wgint.com> (accessed November 2005).
- Wax, E., 2000, Succulent success, Peruvian chicken helps immigrants get a foothold. *The Washington Post*, July 27, p. B1.

WWW Addresses: Additional Reading

- (1) **Coal and Cremation in Ancient Peru**
<http://www.agiweb.org/geotimes/feb04/resources.html>
- (2) **Update: World Coal Quality Inventory for Peru**
<http://pubs.usgs.gov/of/2004/1023/index.html>
- (3) **Tschudi Bone Fragment Analysis: MicroAnalytica, LLC**
www.ega.edu/facweb/stracher/TschudiBoneAnalysis.zip

This page intentionally left blank

CHAPTER 5

Geotechnical and Environmental Problems: Coal and Spontaneous Combustion



Opencast extraction of coal ignited by spontaneous combustion, Singrauli coalfield, India.
Photo by International Mining Consultants Limited, 2000.

CHAPTER CONTENTS

5.1 Geotechnical and Environmental Problems

- Introduction
- Origin of Spontaneous Combustion
- Spontaneous Combustion: Life and Human Health
- Coal Seam and Colliery-Spoil Heap Fires
- Control and Prevention of Spontaneous Combustion and Coal Fires
- Examples of Spontaneous Combustion and Coal Fires
- Conclusions
- Acknowledgments
- Important Terms
- References



5.1. Geotechnical and Environmental Problems

Laurance J. Donnelly
Fred G. Bell

Coal fire in an opencast coal mine,
Singrauli coalfield, India.

From Bell and Donnelly (2002; 2006) with modifications, reprinted with permission of Taylor & Francis. Photo by International Mining Consultants Limited, 2000.

Introduction

When coal mixes with air, it may result in the **spontaneous combustion** of the coal and result in a **coal fire** (Anon, 1999) (Figure 5.1.1). Fire is one of the principal hazards during the mining, transportation, storage, and disposal of coal and carbonaceous-waste materials (Walker, 1999). The objectives of this chapter are to (1) provide a general overview and information about coal fires based on the research and work undertaken by other authors and (2) present case studies of coal fires from South Africa, India, Colombia, and England, based on the observations



Figure 5.1.1. The spontaneous combustion of coal, note how flame migration is controlled by the orientation of the bedding and cleats (joints) in the coal, Jayant Opencast coal Mine, Singrauli coalfield, India. Photo by Donnelly 2000.

and experiences of the authors. These studies demonstrate that some of the geotechnical and environmental problems caused by coal fires are as follows:

- Sterilization.
- Lock up of coal reserves and resources.
- Generation of **noxious gas** that may sink to the bottom of an opencast mine because it is denser than air. The noxious gas may have a detrimental effect on mine workers and those living in surrounding communities (Walker, 1999; Stracher, 2004a,b; Finkelman et al., 2002).
- Residual ash or red shale produced from burning coal, observed by the authors to influence the stability of benches and slopes in opencast-mining operations. This has resulted in the failure of open-pit slopes that has delayed mining, damaged mine infrastructure, and has been anecdotally reported to have caused occasional loss of life.
- Ground **fissures** and sinkholes, or localized **subsidence**, especially in association with abandoned **shallow mines**.
- Destruction of flora and fauna habitats.

In addition to coal seams, **colliery spoil heaps (spoil tips)** and carbonaceous shale are susceptible to combustion. This may present problems during reclamation, particularly if **hot spots** are encountered and long-term **smoldering** has occurred. Some of these hot spots have been reported to be at temperatures of 600–900 °C (Bell, 1996). Colliery-spoil heap fires produce **residual deposits** including ash, burnt shale, **red shale**, and **clinker**. These have been observed by the authors to accumulate up to several meters thick. **Subsurface cavities** present in some colliery spoil heaps that have undergone combustion could present a localized subsidence problem, either naturally or by a load exerted onto the pile like heavy-engineering machinery or even a person walking on the pile.

Natural coal fires occur in the geological record. For example, coal fires occurred during the Pliocene in the Power River basin of Wyoming and western North Dakota (Heffern and Coates, 2004) and in the Pleistocene in northwest China (Kroonenberg and Zhang, 1997). These fires were dated by uranium–thorium/helium ratios found in detrital clinker and by sedimentary strata relationships (Stracher, 2007a).

Coal fires, especially when they are **burning underground**, may be difficult to locate and investigate and many cannot be extinguished. The investigation, monitoring, control, and mitigation of coal fires may be very expensive and time consuming. Where the cost to manage and control these fires outweighs the economic benefits of coal mining, this may result in closure of the mine. For example, in China, financial losses of approximately US \$125–250 million were reported and it is expected that US\$651 million is required to control the fires (Stracher, 2004a). Stracher (2004) also documents that in the Jharia coalfield in India, almost 1500 million tons of coal are locked up in about 70 separate coal fires. In addition, a total surface area of around 10 km² in India is estimated to be affected by underground fires (Michalski and Gray, 2001).

Origin of Spontaneous Combustion

There are several factors that may influence the generation of coal fires in mines and colliery spoil heaps (Mohan, 1996). These include the rank of the coal, the surface area of the exposed coal, **moisture content** of the coal, and the presence of volatile gases. According to Mohan (1996), the rate of oxidation increases above 40 °C and may be self-sustaining for bituminous coals at temperatures greater than 70–80 °C and for lignites at temperatures as low as 50 °C. The **pyrite content** of coal is also a significant factor in promoting combustion. Michalski et al. (1990) suggest that if the pyrite content exceeds 2%, an **exothermic reaction** during the oxidation of pyrite may cause the coal to **ignite**. It was also noted by Michalski et al. (1990) that the **volatile content** of the coal is important for promoting coal fires. Once coal fires have started, their perpetuation is influenced by a constant air supply. Van Vuuren (1995) calculated that approximately 6000–7000 m³ of air is required for the combustion of 1 ton of coal. Furthermore, Voracek (1997), noted that an air flow velocity of 0.3–0.4 m/min, with a minimum oxygen content of 7%, will be sufficient to maintain oxidation and burning of the coal.

Spontaneous Combustion: Life and Human Health

Coal fires are destructive because they consume finite coal resources, may destroy floral and floral habitats, and they negatively impact people who live and work near the fires. Potentially harmful gas components may be emitted from coal seam and spoil-heap fires. These include acids, aerosols, toxic-particulate matter, carbon

monoxide, carbon dioxide, sulfur dioxide, benzene, toluene, numerous other toxins, and hydrogen sulfide (Stracher, 2004; Stracher and Taylor, 2004). These gas components may be hazardous to animal and human life if inhaled in certain concentrations (Anon, 1973). The emissions potentially harmful to health may be accelerated by disturbing a burning-spoil heap, for example during an attempt to extinguish a fire.

Carbon monoxide is one of the most dangerous gas components, as it cannot be detected by taste, smell, or irritation and may be present in potentially harmful concentrations. Sulfur-based gas components are more easily detected and may also cause health problems, if inhaled. In Pennsylvania, United States, over 200 coal fires have generated gases that have destroyed large tracts of vegetation while high concentrations of sulfur and other pollutants nucleated on the ground. These contribute to acidic stream and ground water flows (Stracher and Taylor, 2004). Illnesses reported from exposure to coal-fire gas include carbon monoxide poisoning, pulmonary disease, cancer, strokes, arsenosis, and bronchitis (Stracher and Taylor, 2004; Finkelman et al., 2002; Pone et al., 2007).

Coal Seam and Colliery-Spoil Heap Fires

Air flowing into shallow **abandoned mine workings**, via mine entries (shafts and adits), subsidence induced ground fissures, and collapsed workings (**crown holes**), may promote **self-ignition** (South African example, below). In addition, combustion may be influenced by ventilation within the mine. In pillar and stall workings, the sides of support pillars may be fractured and thereby increase the surface area of coal available for oxidation. If exothermic reactions occur, this may cause the coal to self-ignite. Partially burnt-coal pillars may collapse, leading to the development of subsidence troughs and fissuring of the ground surface, thereby further accentuating the problem by permitting additional air to enter the mine workings.

It is often desirable for colliery spoil heaps to become rehabilitated as this type of dereliction can generate urban blight (Barnsley, England example, below). If, however, these have undergone combustion or are susceptible to combustion, this may present a series of challenges that have to be overcome. The rehabilitation of colliery spoil heaps often involves the removal and reinstatement of large volumes of rock and/or soil. Each colliery spoil heap has a different shape, moisture content, coal/carbonaceous shale content, sulfide (pyrite) mineralogy, porosity, permeability, method of tipping, and bulk density particulate type and size, all reflecting the geology of the mine from where it was derived and the method of tipping.

During the placement of the colliery spoil, coarse discard often consists mainly of gravel and cobble-sized materials, but subsequent breakdown on weathering reduces the particle sizes. The extent to which breakdown occurs depends on the type of parent material. For example, mudstones, shales, and seatearth (a layer of sedimentary rock which underlies a coal seam) exhibit rapid disintegration to gravel and some seatearths may disintegrate within a few cycles of wetting and drying. Once buried within a spoil heap, coarse discard undergoes little further reduction in size. Hence, older and surface samples of spoil contain a higher proportion of fines than those at depth.

Spontaneous combustion of colliery spoil may cause long-term smoldering. Fissures in spoil heaps should be avoided during rehabilitation and workers should wear lifelines if they walk over areas deemed unsafe, since the ground may suddenly collapse. Subsurface cavities in spoil heaps may be formed by spontaneous combustion, the roofs of which may be incapable of supporting a person or machine. When steam comes in contact with hot carbonaceous material, **water-gas** is formed. If this is mixed with air, over a wide range of concentrations, it becomes potentially explosive. If a cloud of coal dust is formed near burning spoil when reworking a heap, then this can ignite and explode. Damping with a spray may prove useful in the latter case.

Control and Prevention of Spontaneous Combustion and Coal Fires

Before the options to control, prevent, or mitigate spontaneous combustion can be determined, the factors that control coal fires should first be understood. Spontaneous combustion may be monitored and investigated by a **site investigation**. This may include, for example, temperature measurement monitoring in boreholes, geophysical surveys, and the acquisition of airborne **thermal imagery** (Lamb, 2000) (Nottinghamshire, England example, below) (Figure 5.1.2).

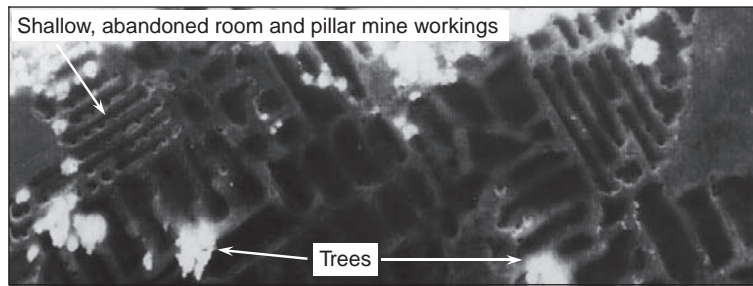


Figure 5.1.2. Airborne, pre-dawn, thermal image at high spatial resolution, showing near-surface room and pillar mining in Southern Africa. The mine is possibly affected by underground coal fires. After Lamb 2000; photo by Anglo American PLC 2000.

Each coal fire will have its own unique characteristics and as far the authors are aware, there seems to be no approved general methodology for investigating and controlling all types of coal fires. However, a number of techniques are recognized. These involve depriving the fire of oxygen, building barriers to isolate the burn front, saturating the coal with water, or dosing the coal with water and grout-slurry mixes. These techniques require significant financial resources which unfortunately are not always available in many countries where these fires occur.

Underground Coal Fires

Gases that are not reactive were used in the nineteenth century to extinguish some underground coal-seam fires. For example, at the Clackmannan Mine in Scotland, a mixture of CO_2 , N_2 , SO_2 , and steam was pumped into a mine for about one month to extinguish a fire (Adamus, 2002; Morris, 1987). In the twentieth century, nitrogen was used to extinguish fires underground (and to control spontaneous combustion in spoil piles) and to protect rescue workers. Adamus (2002) provides an example of the use of nitrogen at the Doubrava Mine, in the Czech Republic. At this mine, a fire was initially exacerbated by a methane and coal dust explosion. It was subsequently controlled by the sealing of both the downcast and upcast shafts with an airtight plug of sand and clay. For 35 days after this, approximately 17000 m^3 of nitrogen was pumped into the mine to extinguish the fire.

Burning-coal seams may be extinguished by the injection of grout, pulverized fuel ash, or foam into boreholes which are drilled to intercept the workings (Bell, 1996). The boreholes need to be drilled on a closely spaced grid around the hot spots. Grout injection begins at the lowest stratigraphic horizon where burning occurs. This process then proceeds toward the higher levels of the mine workings or area of burning. Before the grouting takes place, any abandoned mine shafts, ground fissures, boreholes, or areas of ground collapse (crown holes) would need to be sealed to prevent the flow of air into the mine workings (Bullock and Bell, 1997).

According to Michalski and Gray (2001), in the Jharia coalfield in India, about 30 million tons of fuel ash is produced each year from thermal power stations. They suggested this may be injected into underground mines or dumped into opencast mines for its disposal and to contribute to the control or prevention of coal-mine fires.

Coal fires in shallow abandoned mine workings may be extinguished by flooding (Bullock and Bell, 1997). This requires impoundment with dams or fast pumping rates to prevent re-ignition. It is also necessary to monitor water levels to reduce the chance of re-ignition during a decline in the levels. The force of water flowing through a mine may affect ground water flow and thus contaminate aquifers, streams, and lakes. The stability of mine pillars, and therefore subsidence, may also be influenced by large volumes of water being pumped into mine workings.

Controlled explosions have been used with variable success in China to extinguish coal-mine fires (Bell and Donnelly, 2006). However, this method has to be used carefully because rock fissures and fragmentation may enable the storage or passage of air, promoting combustion (Figure 5.1.3).

Where coal seams are burning at shallow depth, the fire may be contained by excavating a trench into the seam ahead of the fire and then backfilling (South Africa example, below). However, this depends on the ability to accurately monitor and forecast the direction of burning and the depth of the coal seam.



Figure 5.1.3. Controlled-directional blasting used to extinguish an underground coal-mine fire, Beishan coalfield, Qitai County, China. Reproduced with permission of Taylor & Francis. After Bell and Donnelly 2006; photo by Bell 1985.

Opencast Sites

At present, there is no completely reliable and successful method for the control and prevention of spontaneous combustion of coal seams in opencast mines. However, in the Singrauli coalfield, India, the authors observed combustion control using fire-prevention techniques (Bell and Donnelly, 2002, 2006). The techniques consisted of the following procedures. Soon after stripping the overburden, the coal and associated rocks were cleaned using a powerful water-jet hose. This served a dual purpose. The first was to remove any loose rock debris choking areas where air would be trapped and the second was to cool the coal and nearby rocks. The coal and other rocks were then sprayed with a liquid-bitumen-based compound that temporarily seals fissures where air could penetrate and promote combustion. After about one year, the coal seam was extracted. This method has been used in India with varying degrees of success. However, an adverse secondary effect of this technique is the generation of large quantities of steam and ash, observed by one of the authors to present a nuisance to workers within the opencast mine and surrounding areas (Figure 5.1.4).

Colliery Spoil Heaps

The spontaneous combustion of coal in colliery spoil heaps may be reduced if oxygen is prevented from mixing with the waste and if there is an excess of moisture to contain any heating that may occur.

For spontaneous combustion to occur in colliery spoil, three things must be present. These are a substance with sufficient calorific value to support combustion, a continual supply of air (oxygen), and a source of ignition. If one or more of these are absent, then there is no potential for combustion to occur (Bell and Donnelly, 2006).

It was suggested by Cook (1990) that the emplacement of layers of compacted colliery discard on a spoil heap may prevent or smother combustion by preventing air ingress. This blanketing technique, along with trenching, the injection of non-combustible materials (e.g., pulverized fuel ash), and spraying with water potentially reduce the risk of **self-heating** (Anon, 1973; Bell, 1996). Compacting with discard, although potentially effective in reducing air flow into colliery spoil, must be done cautiously since this may induce collapse or subsidence if shallow voids exist in the burnt spoil.

Temperature monitoring in boreholes may be used to verify and monitor the migration of a burning front within a colliery spoil (Nottinghamshire, England example, below). Furthermore, **loss-on-ignition** tests may be undertaken and compared with threshold limits (Richards et al., 1993). These range from 2 MJ/kg (unlikely to burn) to 10 MJ/kg (almost certainly combustible) (Interdepartmental Committee on the Redevelopment of Contaminated Land (ICRCL), 1986).



Figure 5.1.4. Fires extinguished by first spraying with water and then with a bitumen compound at high pressure to seal fissures and prevent air ingress (operated by two specially trained fire fighters). Reproduced with permission of Taylor & Francis. From Bell and Donnelly 2006; photo by Donnelly 2000.

Examples of Spontaneous Combustion and Coal Fires

Case studies of spontaneous combustion are based on observations made by the authors. Some of these are published in more detail in Bell and Donnelly (2002, 2006). They include the following:

- Witbank coalfield, South Africa
- Singrauli coalfield, India
- Cerrejón coalfield, Colombia
- Yorkshire coalfield, Barnsley, England
- Nottinghamshire coalfield, Shirebrook, England.

Spontaneous Combustion in the Witbank Coalfield, South Africa

Coal mining by the pillar and stall method took place at Middelberg Steam Colliery, in the Witbank coalfield, South Africa, in the early 1900s. Mining occurred there until about 1947, when the mine was abandoned, apart from the localized and temporary reopening of the mine in the early 1980s. The coal was extracted at a relatively shallow depth of approximately 20 m and the height of the mine was 2.5 m. Following closure of the mine, coal fires were observed from the mine workings and these continue to the present, burning for at least 65 years over an area of 150–200 ha (Bullock and Bell, 1997) (Figure 5.1.5).

Steam and noxious gases were and are emitted from the mine via ground fissures and crown holes. These were induced by the collapse of support pillars, possibly exacerbated by pillar robbing which took place from the 1930s to 1947 (Bullock and Bell, 1997). Attempts to extinguish the coal fires in the past included the excavation of cut-off trenches backfilled with an inert material ahead of the burn zones, water injection, and controlled explosions to collapse the workings and cut off air flow. However, none of these methods have been completely successful. The ground fissures and crown holes continue to permit the flow of air into the workings and so help promote the **oxidation of coal** and combustion. Collapse of some pillars may have been as caused by pillar robbing which may have took place in the final stages of mine abandonment. The burning and subsequent collapse of the remnant coal pillars leads to the generation of additional fissures, allowing the ingress of air currents in the collapsed workings. A combination of collapsed mine workings, ground fissures and crown holes, and high volatile coal containing pyrite all seem to promote spontaneous combustion (Bell and Donnelly, 2006).



Figure 5.1.5. Steam emitted from a crown hole above workings in the No. 2 coal seam, caused by a burning-coal seam, Witbank coalfield, South Africa. Reproduced with permission of Taylor & Francis. From Bell and Donnelly 2006; photo by Bell 1976.

Slope Failure in the Singrauli Coalfield, India

Coal fires are common throughout India in opencast coal mines, underground mines, and on spoil heaps (Ghosh, 1989; Gupta and Prakash, 1998; Mansor et al., 1994; Prakash et al., 1997; Prakash and Gupta, 1998; Saxena et al., 1991). Coal fires in India have had a dramatic effect on the landscape and have negatively influenced the lives of people who work and live near the burning-coal seams.

In the Singrauli coalfield in India, coal seams were extracted during spontaneous combustion (Bell and Donnelly, 2002, 2006). Gas and dust was observed to sink to the lower part of the open pit, reducing visibility with blue–grey smoke, creating unpleasant and potentially dangerous conditions for the mine workers (Figure 5.1.6).

The spontaneous combustion of coal in opencast mines transforms it into an unconsolidated residual ash. This frequently causes local instability and slope failure, when the residual ash accumulates in moderate thickness. However, since the zone of burning is usually restricted to the outer layers of the coal, penetrating to about 1 m behind the face, small rock falls and topples tend to be a more frequent occurrence than large slope failures.

Many of the large opencast mines in India are worked by draglines. Individual rock faces may reach at least 2 km in length. The reach of the draglines, around 45 m, and the extraction of the coal, along the face known as a **high wall**, creates a working face up to 100 m high in some mines (Bell and Donnelly, 2006). Where the coal seams dip into the high wall, instability problems are less likely. The dragline operations leave behind remnant coal pillars which vary from 2 to 10 m at their base and up to approximately 18–20 m high. These pillars support the spoil tip emplaced by the draglines.

The coal pillars are broken by a network of discontinuities. These include **cleats** (joints in the coal) bedding planes and faults caused by mining operations. Smoldering begins along the discontinuity surfaces about 6 hours to around 15 days following their exposure by large-scale removal of the overburden. Once burning begins, it was described anecdotally by the mine workers to advance at about 1 m/day. Failure of the burnt residual ash may cause collapse of the mine spoils onto the floor of the mine. This may be exacerbated by groundwater flow from the monsoon rains that collects within the spoil tip (Figure 5.1.7). Examples of failures for a one year period in one of the opencast mines are given in Table 5.1.1.

Evening inspections reveal that the coal fires tend to concentrate on and migrate along discontinuities in the coal. This generates small but frequent block failures and topples. The toppled debris accumulates at the toe of mining benches as a **burning debris cone**, sometimes accompanied by explosions, probably associated with the release of gas as it expanded and escaped from the burning coal (Figure 5.1.8).

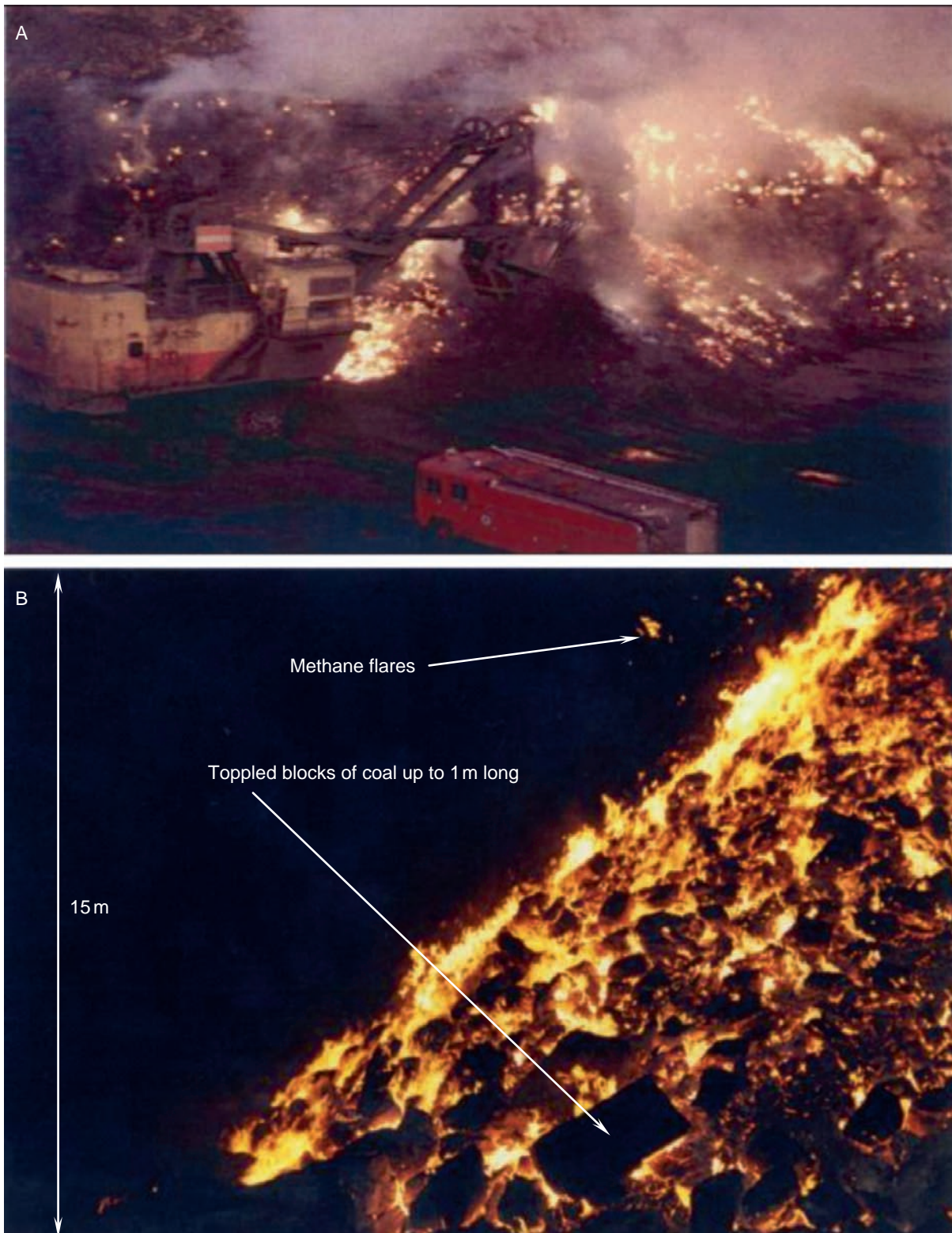


Figure 5.1.6. (A) Open-pit extraction of coal undergoing severe spontaneous combustion. (B) Toe of a failed slope undergoing violent burning, caused by spontaneous combustion, Singrauli coalfield, India. Photo by Donnelly and International Mining Consultants Limited, 2000.

By contrast, there are fewer fires on the high wall of open-pit mines. This is not fully understood but may possibly be attributed to the presence of groundwater that prevents ignition (observed where water seeps through the coal) combined with less dilated discontinuities, reducing air ingress into the coal seams.



Figure 5.1.7. (A) Pillar failure caused by the spontaneous combustion of support pillars in an opencast coal mine. (B) Burning-coal pillars causing the failure of tipped material. (C) Smoldering and burning coal carried by local villagers, Singrauli coalfield, India. Photo A reproduced with permission of Taylor & Francis. Photo by Donnelly 2000.

Table 5.1.1
Examples of slope failures induced by spontaneous combustion, at an Indian Opencast Coal Mine, Singrauli coalfield. Reproduced with permission of Taylor & Francis.

Date of failure	Description of events
October 3, 1997	The total preslide tip height was 106 m and the overall slope was 48° , steepening to 76° in the lower 50 m of the slope. Failure affected the dragline tip 50 m high and 220 m long. The collapsed material accumulated on the floor of the mine where the Turra seam was being extracted. The coal pillar underwent translational shift by 7 m toward the high wall face.
February 10, 1997	A slope failure affected the lower section of the steepest part of the dragline tips, to a height of 48 m. The total height of the tip before failure was 83 m and was inclined at 54° . The rotational slide was 140 m wide and the coal underwent translational shift by 5 m along the floor of the seam, in the dip direction. The collapsed material accumulated up to 15 m in the mined out section of the workings.
May 28, 1997	A slope failure on, affected the lower 52 m of the tipped material. The total height of the tip before failure was 82 m and was inclined at 51° . The width of the slide was 51 m, and the tip material accumulated 18 m into the workings.
September 19, 1998	A slope failure involved the failure of a 94 m high, 47° , dragline tip. This created a scar 75 m high and 250 m long and caused the down-dip translational shift of the coal pillar by 65 m, stopping just short of the high wall.

Source: Bell and Donnelly (2002, 2006).

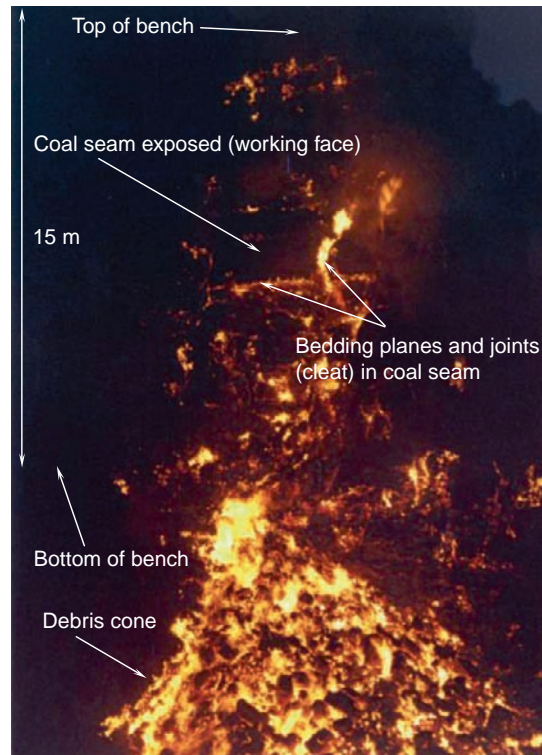


Figure 5.1.8. Coal fire, approximately 20 m high; note how the direction of burning is controlled by the principal joints in the coal seam, Jayant opencast coal mine, Singrauli coalfield, India. Photo by Donnelly 2000.

Slope Failure at El Cerrejón Zona Norte, Colombia

Coal is mined throughout Colombia from artisanal mines located in the Colombian Andes (Donnelly et al., 2001a,b) to large-scale opencast mining operations near the Caribbean coastline. El Cerrejón Zona Norte, an opencast coal mine, is located in the Guajira Peninsula, in northeast Colombia. The Cerrejón coal basin is approximately 50 km long and 5 km wide and it contains a 900 m thick non-marine succession of coal-bearing strata with approximately 55 coal seams; some are 26 m thick (Walker, 2000). In 2000, a field trip to El Cerrejón Zona Norte revealed coal fires in the opencast coal mine. These fires generated plumes of gas, dust and smoke, creating potentially irritant or harmful conditions in parts of the mine. In one instance, a large slope failure was anecdotally reported to have been caused or exacerbated by spontaneous combustion, resulting in the loss of large quantities of coal reserves along one side of the opencast mine (Figure 5.1.9). Similar examples of the failure of opencast slopes and benches caused by coal fires have been observed in China (Figure 5.1.10).

Spontaneous Combustion and Spoil Heap in Barnsley, Yorkshire Coalfield, England

Colliery spoil heaps in Britain are particularly susceptible to burning (Figure 5.1.11). Barnsley is located in the Yorkshire coalfield in northern England. This coalfield has a long and complex mining legacy. Bell and Donnelly (2002, 2006) documented two colliery spoils heaps, covering a total area of approximately 49 ha, requiring rehabilitation so that the sites they were on could be restored for the provision of industrial development and public lands. The total volume of the spoil heaps was around 4 million m³. The moisture content ranged from 6 to 13%, being greater in the finer materials. Most of the spoils materials were sand grade with traces of pyrite.

When the top layers of the spoils were stripped during rehabilitation in 1985, hot spots were encountered with temperatures of approximately 600 °C, and occasionally reaching 900 °C (Bell and Donnelly, 2002). This resulted in a number of operational constraints and logistical challenges, including melted tires on plant machinery, stalled engines on the scrapers, and the rescue of site equipment and operators. To mitigate the colliery-waste fires, the spoil was removed in thin layers around 300 mm thick and subsequently compacted. This method reduced the ground temperature significantly and enabled the work to continue. Hot spot areas were covered with clay which

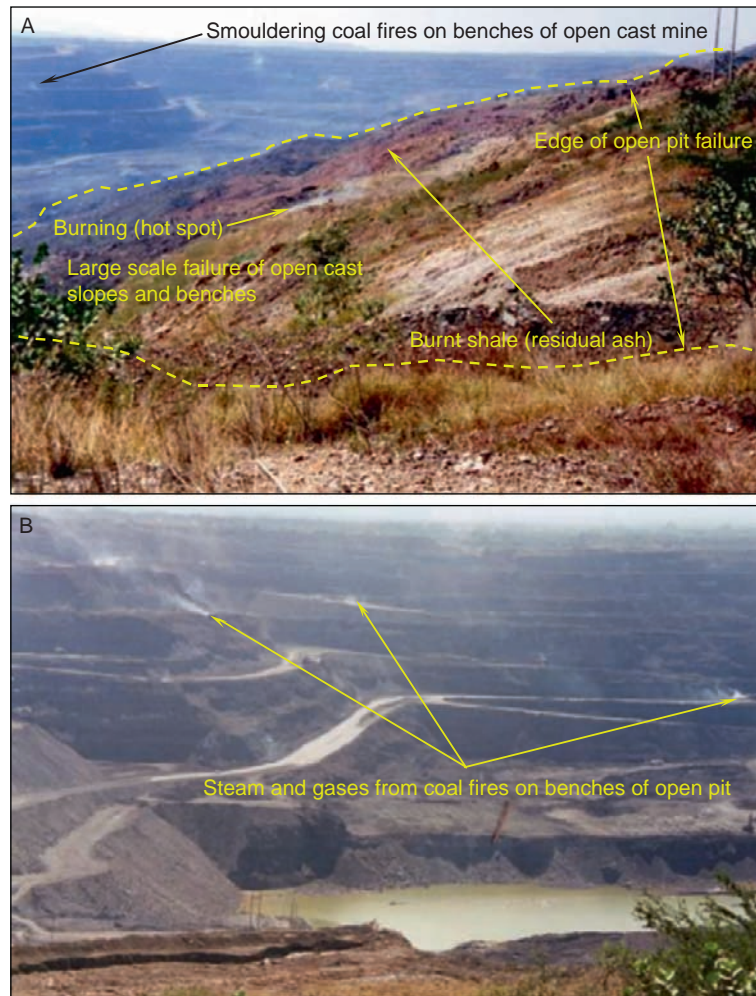


Figure 5.1.9. (A) Large-scale landslide on the flank of the El Cerrejón Zona Norte opencast mine in Colombia. Smouldering-insitu coal fires are indicated by the emissions of carbon monoxide rich smoke rising from the slipped mass and on the walls in the mine. The red-shale residue is visible on the main body of the landslide in the center of the photograph. (B) Gas and steam emanating from vents on the benches of the open pit. Photo by Donnelly 2000.

was compacted into layers about 450 mm thick and then covered with shale. Ground investigation boreholes were drilled about 12 months later and these revealed that the hot spots had not undergone any significant cooling. So, they were extinguished by injecting a pulverized fuel ash curtain around the hot spots. Subsequently the sites were restored (Figure 5.1.12).

Shirebrook Colliery Spoil Tip in Shirebrook, Nottinghamshire Coalfield, England

The former Shirebrook Colliery spoil tip, also known as the “Red Shale Tip” is located southeast of the town of Shirebrook, in north Nottinghamshire, in the English East Midlands. The tip consists of two distinct areas. The northern zone contains dark gray granular spoil covered with vegetation. The southern area is comprised largely of red shale with little vegetation.

A site investigation was carried out from 1999 to 2001 to characterize the colliery spoil and assess its composition. Ground temperatures were monitored via a network of boreholes that recorded maximum temperatures of around 300 °C at 5 m below the surface. These temperatures were associated with steep thermal gradients in contrast to background temperatures that were in the range of 10–30 °C. The thermal conductivity of the colliery spoil was considered to be low and therefore these high ground temperatures were envisaged to be associated with combustion, probably taking place in the vicinity of the boreholes. Alternatively, these high temperatures could



Figure 5.1.10. Coal seams burning in an opencast coal mine in the Beishan coalfield, Qitai County, China, resulting in toppling failure, sliding, and collapse downslope. Reproduced with permission of Taylor & Francis. From Bell and Donnelly 2006. Photo by Bell 1985.

have been associated with heat energy that had not dissipated from previous burning. The tip was reported anecdotally to have undergone combustion for at least the past 50 years.

The high temperatures recorded may have been influenced by the direction and intensity of prevailing winds throughout the part of the year when the measurements were made. Stronger winds may allow more air to penetrate within the spoil heap and so enhance combustion. Depending on the wind direction, odors from burning were detectable on the western flank of the tip.

The dominance of red-shale on the southern part of the tip suggests that combustion may have been completed, whereas burning does not appear to have occurred on the northern part of the tip. However, elevated ground temperatures in the northern areas suggest that some degree of heat conduction and dispersion was occurring. Lime dust was spread over parts of the tip and was successful in temporarily reducing ground temperatures, although combustion and elevated temperatures did eventually resume (Figure 5.1.13).

Infrared thermal imagery had been used to investigate the ground and in particularly shallow, abandoned mine entries and mine workings in other locations with some success (Donnelly and McCann, 2000; Lamb, 2000). Infrared thermal scanning systems were therefore deployed at Shirebrook Tip to detect the direction and rate of migration of the burning front. These techniques were shown to provide a cost-effective method to rapidly assess the effect of burning on large areas of ground, which may otherwise have taken several days or weeks, using conventional ground-based techniques. Pre-dawn airborne thermal data and daytime multispectral thermal mapping are highly dependent upon a range of conditions such as local weather, fluctuations in barometric pressure, time of day, and temperature inversions. However, pre-dawn thermal imagery also provides qualitative data for mapping groundwater springs, entrapped moisture, and/or methane seepages (Figure 5.1.14).

As part of the ground investigation, geophysical surveys were also undertaken and included magnetic, electromagnetic (EM), and resistivity surveys to delineate the areas of spontaneous combustion. The location of geophysical anomalies provided the sites for the installation of temperature monitoring boreholes. The electrical



Figure 5.1.11. (A & B) Earthmoving equipment travelling over a hotspot, at a colliery-waste site, England. Photo by International Mining Consultants 1995.

imaging method successfully identified areas where heating occurred by locating areas where there was an increase in electrical resistivity of the ground that results from it drying out.

An electromagnetic mapping survey was carried out on two scales to investigate whether or not the variations in resistivity seen on the imaging sections could also be detected on the spatial data that the electromagnetic method produced. This method estimated the conductivity (the inverse of resistivity) of the ground by measuring the strength of eddy currents induced there by the instrument (Figure 5.1.15).



Figure 5.1.12. Leveling and reprofiling of a spoil heap undergoing spontaneous combustion, Barnsley, England. Photo by Bell 1985.

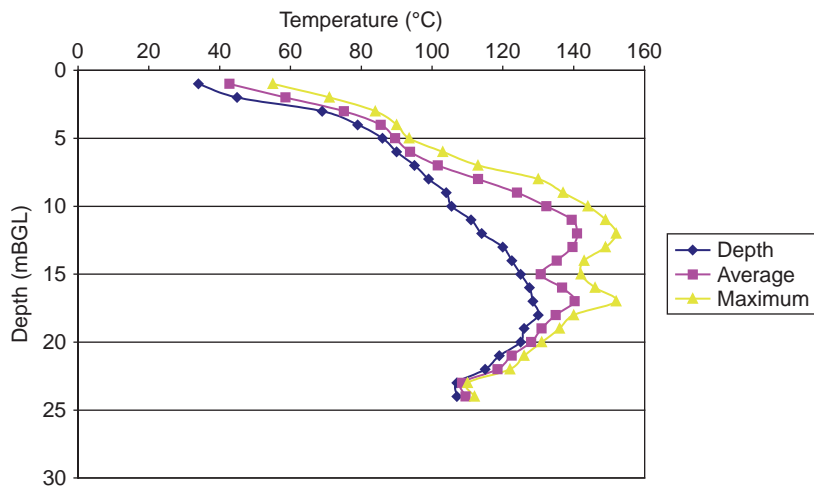


Figure 5.1.13. Ground-temperature increase caused by spontaneous combustion, Shirebrook colliery tip, Nottinghamshire, England. Source: International Mining Consultants.

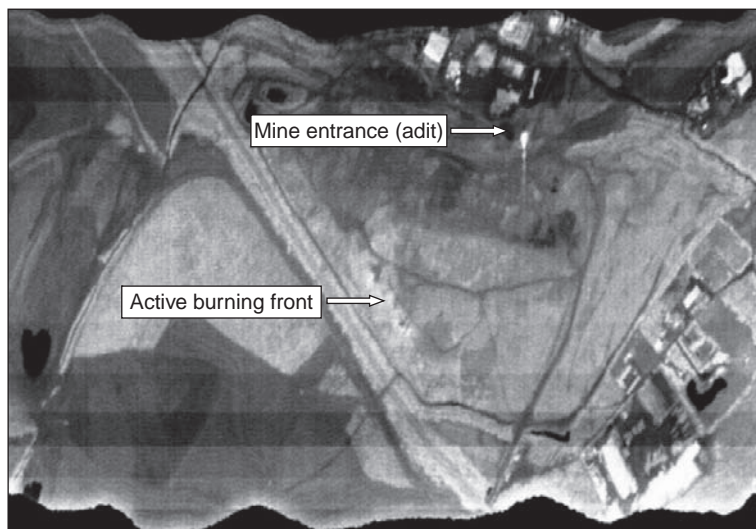


Figure 5.1.14. Pre-dawn infrared thermal image of Shirebrook Colliery Tip. The hotter areas appear (white) in contrast to the burnt and unburnt ground (grey and black). Hot gases escaping from the mine adit can also be seen as a white anomaly. Source: International Mining Consultants; Photo by Infoterra 2002, 2006.

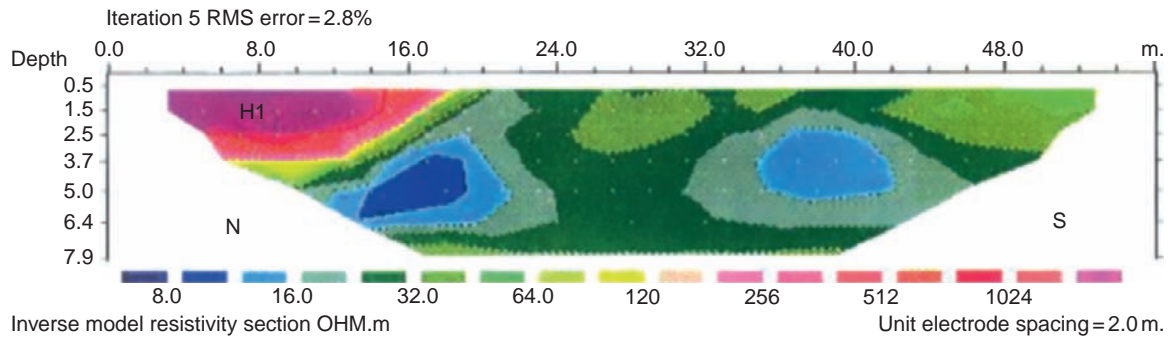


Figure 5.1.15. Resistivity plot for Shirebrook Colliery Tip, Nottinghamshire, UK, showing localized zone of intensely resistive material (anomaly H1), up to 3.7 m below ground level. Blue represents high conductivity, red shows low conductivity or high resistivity, for the resistivity imaging sections. This was subsequently confirmed by drilling and represents a localized heating front. Source: IMC Geophysics Ltd.

A proton precession magnetometer was used to measure the magnetic variability of the ground. Higher magnetic values correlated well with the red shale at the southern end of the site, because of the higher concentrations of iron oxides from baking. Lower magnetic field strengths were found at the northern end of the tip where burning did not occur. Repeated ground investigations of these types using of borehole temperature monitoring, airborne thermal imagery, and geophysical surveys could potentially be useful in monitoring a burning front in a colliery spoil tip, if these are deployed on a routine basis.

📌 Conclusions

The oxidation of coal, when exposed to air during underground or surface mining, can lead to spontaneous combustion. The combustion depends on several interrelated factors that include the coal rank, the surface area of the coal exposed to air, moisture content, temperature, pyrite (sulfide) content of the coal, and ignition source. In addition to coal seams exposed to air in underground workings and opencast sites, colliery spoil heaps are also subject to spontaneous combustion. Such spoil heaps, especially older ones, contain coal and carbonaceous shale that may ignite.

One of the factors contributing to spontaneous combustion in abandoned shallow mines is subsidence. For example, the collapse or partial collapse of pillars may generate fissures that extend to the ground surface, and thus permit air to enter the mine workings. Similarly, crown holes at the surface allow air to penetrate into the workings. This happened at an abandoned colliery in the Witbank coalfield, South Africa. There, pillar robbing prior to closure was responsible for the failure of the pillars, followed by the development of fractures extending to the surface, as well as the formation of crown holes. Spontaneous combustion has continued from when the time the mine was closed until today. Unfortunately, various attempts to extinguish the subsurface fires have proved unsuccessful.

Coal deposits in opencast mines in India and Colombia are susceptible to spontaneous combustion. This generates hazardous working conditions for the mine workers and causes sterilization of the coal reserves. Unfortunately, coal fires in pillars meant to retain spoils weakens the pillars, permitting waste material to collapse into the mine workings, causing loss of production, and anecdotal reports that claim on occasion, the loss of lives.

Some colliery-waste sites in the England have undergone spontaneous combustion for several decades. Hot spots recorded at two colliery tips near Barnsley, England, were mitigated by removing the upper top soil and then compacting with a vibrating roller. Special investigation techniques may enable combustion mechanisms and the migration of burning fronts to be determined. These investigations at Shirebrook Colliery Tip in Nottinghamshire consisted of temperature monitoring in boreholes, geophysical surveys, and thermal imagery which enabled the burning front to be located. Airborne infrared surveys when repeated on a routine basis may potentially allow the migration of the burning front in colliery tips to be monitored.

Acknowledgments

The authors acknowledge the support and assistance provided by Wardell Armstrong LLP; Halcrow Group Ltd; British Geological Survey; International Mining Consultants Ltd; Universidad Nacional de Colombia, Facultad de Minas, Centro del Carbon, Medellin, Colombia; Universidad Popular del Cesar, Valledupar, Colombia; INGEO-MINAS (the Colombian Geological Survey); Central Mine Planning and Design Institute Limited (CMPDIL), India. Parts of this chapter have been reproduced with the kind permission of Taylor & Francis (Bell and Donnelly, 2006).

Important Terms

abandoned mine workings	pyrite content
burning debris cone	red shale
burning underground	residual deposits
cleats	self-heating
clinker	self-ignition
coal fire	shallow mines
colliery spoil heaps (spoil tips)	site investigation
crown holes	smoldering
exothermic reaction	subsurface cavities
fissures	spontaneous combustion
high wall	subsidence
hot spots	thermal imagery
ignite	volatile content
loss-on-ignition	water-gas
moisture content	pyrite content
noxious gas	red shale
oxidation of coal	

References

- Adamus, A., 2002. Review of the use of nitrogen in mine fires, *Trans. Inst. Min. Metall., Sect. A; Number 2: Min. Tech.*, 111, . A89–A98.
- Anon., 1973. *Spoil Heaps and Lagoons*, Technical Handbook. National Coal Board, London, England, 232 p.
- Anon., 1999. *Uncontrolled Fires in Coal and Coal Waste*. IEA Coal Research, London, England, 72 p.
- Bell, F.G., 1996. Dereliction: colliery spoil heaps and their rehabilitation. *Environ. Eng. Geosci.*, 2, 85–96.
- Bell, F.G., Donnelly, L.J., 2002. The problem of spontaneous combustion illustrated by two case histories. Ninth Congress Int. Assoc. Eng. Geol., Durban, South Africa, September 16–20 (CD Rom).
- Bell, F.G., Donnelly, L.J., 2006. *Mining and its Impact on the Environment*. Taylor & Francis, Oxford, England, 547 p.
- Bullock, S.E.T., Bell, F.G., 1997. Some problems associated with past mining in the Witbank Coalfield, South Africa. *Environ. Geol.*, 33, 61–71.
- Cook, B.J., 1990. Coal discard-rehabilitation of a burning heap. In: Rainbow, K. (Ed.), *Reclamation, Treatment and Utilization of Coal Mining Wastes*. Rotterdam, the Netherlands, A.A. Balkema, pp. 223–230.
- Donnelly, L.J., McCann, D.M., 2000. The location of abandoned mine workings using thermal techniques. *Eng. Geol.*, 57, 39–52.
- Donnelly, L.J., Perez J., De La Cruz, H., 2001a. Operation Colombia: The Underground Mining Industry in Colombia Prior to Rationalization in Colombia's Sinifana Coal Basin. *World Coal (April)*, 10 (4), 21–27.
- Donnelly, L.J., De La Cruz, H., Asmar, I., Zapata, O., 2001b. The monitoring and prediction of mining subsidence in the Amaga, Angelopolis, Venecia and Bolombolo Regions, Antioquia, Colombia. *Eng. Geol.*, 59, 103–114.
- Finkelman, R.B., Orem, W., Castanova, V., Tatu, C.A., Belkin, H.E., Zheng, B., Lerch, H.E., Marharaj, S.V., Bates, A.L., 2002. Health impacts of coal and coal use: possible solutions. *Int. J. Coal Geol.*, 50, 425–443.

- Ghosh, R., 1989. Mining in Jharia coalfield, Eastern India: an estimate of its impact index. *J. Geol. Soc. India*, 33, 353–360.
- Gupta, R.P., Prakash, A., 1998. Reflectance aureoles associated with thermal anomalies due to subsurface mine fires in the Jharia coalfield, India. *Int. J. Remote Sens.*, 19 (14), 2619–2622.
- Heffern, E.L., Coates, D.A., 2004. Geologic history of natural coal-bed fires, Powder River Basin, USA. In: Stracher, G.B. (Ed.), *Coal Fires Burning Around the World: A Global Catastrophe*. *Int. J. Coal Geol.*, 59 (1–2), 25–47.
- Interdepartmental Committee on the Redevelopment of Contaminated Land (ICRCL), 1986. *Notes on the Fire Hazards of Contaminated Land, Guidance Note 61/84*, Second edition, London, England, 16 p.
- Kroonenberg, S.B., Zhang, X., 1997. Pleistocene coal fires in northwestern China: energy for early man. In: Van Hinte, J.E. (Ed.), *One million years of anthropogenic global environmental change, Proceedings of the ARA Symposium at the Royal Netherlands Academy of Art & Sciences (KNAW), Project ID: 2-74690*, pp. 39–44.
- Lamb, A., 2000. Earth observation technology applied to mining-related environmental issues. *Trans. Inst. Min. Metall., Sec. A: Min. Tech.*, 109, A153–A156.
- Mansor, S.B., Cracknell, A.P., Shilin, B.V., Gornyi, V.I., 1994. Monitoring of underground coal fires using thermal infrared data. *Int. J. Remote Sens.*, 15, 1675–1685.
- Michalski, S.R. and Gray, R.E., 2001. Ash disposal – mine fires – environment: an Indian dilemma. *Bull. Eng. Geol. Environ.*, 60, 23–29.
- Michalski, S.R., Winschel, L.J., Gray, R.E., 1990. Fires in abandoned mines. *Bull. Assoc. Eng. Geol.*, XXVII, 479–495.
- Mohan, S., 1996. Genesis of mine fires. *J. Mines, Met. Fuels*, 44, 195–198.
- Morris, R.A., 1987. A review of experiences of the use of inert gases in mine fires. *Min.Sci. Tech.*, 6, 37–69.
- Pone, J.D.N., Hein, K.A.A., Stracher, G.B., Annegarn, H.J., Finkelman, R.F., Blake, D.R., McCormack, J.K., Schroeder, P., 2007. The spontaneous combustion of coal and its by-products in the Witbank and Sasolburgh coalfields of South Africa. *Int. J. Coal Geol.*, 72, 124–140.
- Prakash, A., Gupta, R.P., 1998. Land-use mapping and change detection in a coal mining area – a case study in the Jharia coalfield, India. *Int. J. Remote Sens.*, 19 (3), 391–410.
- Prakash, A., Gupta, R.P., Saraf, A.K., 1997. A Landsat-TM based comparative study of surface and subsurface fires in the Jharia coalfield, India. *Int. J. Remote Sens.*, 16, 2105–2109.
- Richards, J.G., Palmer, J.P., Barratt, P.A., 1993. *The Reclamation of Former Coal Mines and Steel Works. Studies in Environmental Science*, v. 56, Elsevier, Amsterdam, the Netherlands, pp. 213–215.
- Saxena, N.C., Malhotra, K.K., Mukhopadhyay, A.K., Prasad, R.M., Chattopadhyay, S., 1991. Conceptual environmental management plan for Jharia Coalfield. In: Eden, M.J., Parry, J.T. (Eds.), *Remote Sensing and Tropical Land Management*. John Wiley and Sons, New York, pp. 237–254.
- Stracher, G.B. (Ed.), 2004. *Coal fires burning around the world: a global catastrophe*. *Int. J. Coal Geol.*, 59 (1–2), 1–151.
- Stracher, G.B., 2007a. Coal fires burning around the world: opportunity for innovative and interdisciplinary research: *GSA Today (Groundwork article)*, 17, 11, 36–37.
- Stracher, G.B. (Ed.) 2007b. *Geology of coal fires: case studies from around the world*. *Rev. Eng. Geol.*, XVIII, 278 p.
- Stracher, G.B., Taylor, T.P., 2004. Coal fires burning out of control around the world: thermodynamic recipe for environmental catastrophe, In: Stracher, G.B. (Ed.), *Coal Fires Burning Around the World: a Global Catastrophe*. *Int. J. Coal Geol.*, 59 (1–2), 7–17.
- Van Vuuren, M.C.J., 1995. *Guidelines for the Prevention of Spontaneous Combustion of Coal During Storage and Transport*, Report No. ES9307. Ministry of Minerals and Energy Affairs, Pretoria, South Africa, 55 p.
- Voracek, V., 1997. Current planning procedures and mine practice in the field of prevention and suppression of spontaneous combustion in deep coal mines in the Czech part of the Upper Silesian Coalfield, New Delhi, India. *Proceedings 27th International Conference Safety in Mines Research Institutes*, pp. 437–441.
- Walker, S., 1999. *Uncontrolled fires in coal wastes*, Report CCC/16, International Energy Agency, Coal Research, London, England, 72 p.
- Walker, S., 2000. *Major Coalfields of the World*, International Energy Agency, Coal Research, London, England, 131 p.

CHAPTER 6

The Effects of Global Coal Fires



Important effects of coal fires include the destruction of a valuable natural resource and the emission of toxic and greenhouse gases. The fire in the exposed coal seam (left) occurred in the Jharia coalfield, India. Jharia is the largest coalfield in India, and the country's primary source of coking coal. The surface and subsurface fires burning there comprise one of the largest coal-mine-fire complexes in the world. The excavated material (right) is backfilled to seal openings, called goafs, left after mining. The smoke is high in particulates in addition to oxides and dioxides of sulfur, carbon, and nitrogen. *Photo by Anupma Prakash, 1994.*

CHAPTER CONTENTS

6.1 The Global Catastrophe

- Introduction
- The Mining Hazard
- Catastrophic Coal Fires
- Discussion
- Acknowledgments
- Important Terms
- References
- WWW Addresses:
Additional Reading



6.1. The Global Catastrophe

Glenn B. Stracher
Tammy P. Taylor

Coal-seam fire emitting toxic and greenhouse gases, Jharia coalfield, India.

From Stracher and Taylor (2004) with modifications, reprinted with permission of Elsevier. Photo by Anupma Prakash, 1994.

Introduction

Fire is a force of nature that often demands human attention and resources; however, few people realize that fire is consuming coal seams and culm banks in major coal-producing countries including China, the United States, India, and Indonesia (Table 6.1.1). Numerous seams have been burning for decades and some in China for several centuries. Geological evidence for Pliocene coal fires includes fission-track dates obtained for zircons extracted from sandstone clinker found southwest of Forsyth, Montana, and west of Colstrip, Montana (Coates and Heffern, 2000). Evidence for Pleistocene coal fires, some with temperatures exceeding 1000°C, includes unconformable relationships among baked and unbaked sedimentary rocks southwest of Urumqi in the Xinjiang autonomous region of northwest China (Figure 6.1.1) (Zhang and Kroonenberg, 1996; Kroonenberg and Zhang, 1997; International Institute for Geo-Information Science and Earth Observation (ITC), 2003). Although this evidence suggests that coal fires are a natural event, coal mining by humans has facilitated the proliferation of these fires and the environment is suffering.

Environmentally catastrophic effects from coal fires include the emission of noxious gases and particulate matter into the atmosphere and condensation products responsible for stream and soil pollution. Coal fires have killed

Table 6.1.1
The major hard coal-producing countries and statistics about coal consumption.

Major coal-producing country*	Coal production (Mt)	Coal consumed	
		Generating electricity (% production)	Steel production (Mt)
China	1294	78	152.3
USA	945	52	90.1
India	312.5	77	27.3
Australia	257	77	ND
South Africa	224.5	88	ND
Russia	168	ND	59.0
Poland	104	96	ND
Indonesia	92.5	ND	ND
Ukraine	82	ND	33.1
Kazakhstan	73	ND	ND

Note: Coal production and electrical data for 2001 (electricity for China and India, 2000). Courtesy of the World Coal Institute (2002). Steel production data for 2001. Courtesy of the World Coal Institute (2003).

* Total world hard coal production in 2001 (including countries not listed) was 3834 Mt. In 2001, Germany was the top producer of brown coal/lignite, with just under 20% of world production (903 Mt) (World Coal Institute, 2002).
Mt, million tons; ND, no data.

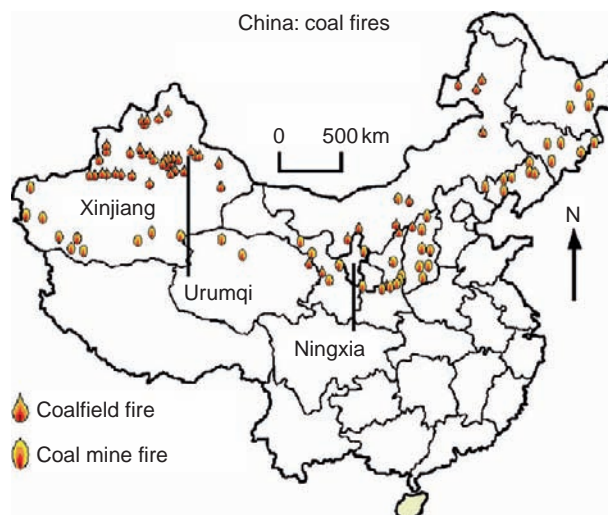


Figure 6.1.1. Coal fires across China: provinces are outlined. Anthracite reserves are concentrated in the Xinjiang and Ningxia Hui provinces (autonomous regions). Urumqi, capital city of Xinjiang, is one of the most polluted cities in the world. Coalfield fires are surface fires in seams, some of which occur in open-pit mines. Coal mine fires include underground and surface fires in government and private mines. Photo by Anupma Prakash, 2003, with modifications.

people, have forced entire communities to abandon their homes and businesses, have destroyed floral and faunal habitats, and are responsible for perilous land subsidence.

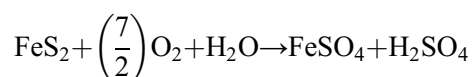
This chapter discloses the severity of the coal fires problem. The objectives of the analyses presented herein are to describe the origin of coal fires and related gases, discuss some of the world's most problematic coal fires and associated environmental hazards, and briefly consider techniques used to combat these fires.

The Mining Hazard

Although coal has been mined for over a thousand years as a heating and cooking fuel, large-scale mining, necessary to support the industrial revolution, did not begin until the nineteenth century (World Coal Institute (WCI), 2000). Since 1995, coal and oil reversed rankings, with oil overtaking coal as the primary resource for energy consumption (US Department of Energy (DOE), 1995, p. 19; WCI, 2000). As long as coal is **strip or deep mined** in order to stoke the electrical and steel fuel-hungry economies of industrialized and developing nations, the potential for uncontrollable fire exists.

Origin of Coal Fires

Most coal mine-related fires are ignited by (1) mine-related activities such as cutting and welding, explosives and electrical work, and smoking, which may ignite gases such as methane and hydrogen (Mine Safety and Health Administration, 1996; Pennsylvania Department of Environmental Protection (PDEP), 2001a); (2) surface fires transmitted to culm banks or coal seams by lightning, forest or bush fires, and burning trash (DeKok, 1986, p. 20; Geissinger, 1990; Discover, 1999); and (3) spontaneous combustion induced either by coal fines, oil-soaked rags, lumber, hay, or manure in culm banks or by **exothermic oxidation reactions** catalyzed by oxygen circulating through coal seam joints (Jones and Scott, 1939; Anthony et al., 1977, p. 29; DOE, 1993; ITC, 2003). One such oxidation reaction is (Limacher, 1963)



This reaction exemplifies the fact that moisture is conducive to spontaneous combustion (DOE, 1993).

According to the DOE (1993), many spontaneous fires start in storage facilities including open-air stockpiles, coal bunkers, and silos. The DOE attributes combustion to numerous factors. These include improperly loaded and compacted storage in facilities, which promotes the diminution of coal into highly combustible fines, and storage for prolonged periods of time, which promotes exothermic oxidation reactions in high-sulfur coals. Spontaneous fires in storage bins have been extinguished by injecting N_2 or CO_2 into the bins. Water has also been used, but with extreme caution, because of the risk of steam explosions. The DOE (1993) has published guidelines for preventing spontaneous combustion in coal storage facilities. These include recommendations for the shape, height, and composition of stockpiles.

The significance of spontaneous coal fires in storage facilities was conveyed in the testimony of John Dilley to the US Senate (1912). Dilley, of Southampton, England, was a survivor and fireman in the engine department on the RMS Titanic that sank about 640 km south of Newfoundland on Monday, April 15, 1912 (US Senate, 1912). According to Dilley, the bottom of a coal bunker containing hundreds of tons of coal was on fire from the time the ship departed Southampton for New York City on April 10, until the iceberg that the Titanic hit on the evening of April 14 tore open this bunker and the incoming water put out the fire.

Although coal fires often start at storage facilities where they can be extinguished relatively easily, larger and more problematic fires frequently start in the excavations of the **abandoned workings** or **workings** of a coal mine (PDEP, 1965). Fires in abandoned underground workings are the most problematic because they are difficult or impossible to locate precisely. According to the latest estimate of the US Department of the Interior, more than \$651 million is needed to control these fires in the United States alone (Office of Surface Mining, 1999).

Coal Gas

Carbon dioxide concentrations exceed those of other gases produced by coal fires; however, CO_2 concentrations are not entirely controlled by the coal itself. The concentrations are also determined by Mitchell (1996, p. 70): (1) **blackdamp (chokedamp)** produced by the respiration of miners and working animals (formerly used in the United States), cellulose-decomposing monerans in wooden supports, and the oxidation of wood, pyrite, or coal; (2) CO_2 associated with coal, gypsum, potash, and salt-bearing strata encountered during mining; and (3) chemical reactions between acidic water and carbonate rocks, rock dust, or inclusions in strata.

Carbon monoxide, hydrogen, and the hydrocarbons ethylene (C_2H_4), propylene (C_3H_6), and acetylene (C_2H_2) are monitored as **coal-fire detector gases** because they are released sequentially as temperature increases during heating. Consecutive temperatures at which release begins in medium-volatile bituminous coal, for example, are about $110^\circ C$ (CO), $170^\circ C$ (H_2), $240^\circ C$ (C_2H_4), and $300^\circ C$ (C_3H_6) (Chamberlain, 1971). Combustion occurs between about 110 and $170^\circ C$, and flames appear at about $200^\circ C$ (Chamberlain and Hall, 1973).

The late D.W. Mitchell (1996, pp. 45–61, 64–97), a leading authority on mine fires, discussed gas collection devices, concentration detectors, and the complexities associated with using coal-fire detector and **wood-fire detector gases** such as formaldehyde (CH_2O), formic (CH_2O_2) and acetic ($C_2H_4O_2$) acid, and glyoxal ($C_2H_2O_2$) for identifying mine fires.

Other gases associated with coal fires include (1) N_2 , Ar, and trace amounts of other noble gases, all mainly from air; (2) O_2 mostly from air, occasionally from coal strata; (3) hydrogen sulfide or **stinkdamp** (H_2S), oxides of sulfur (SO_x) and nitrogen (NO_x) from oxidation and combustion processes; and (4) the hydrocarbons ethane (C_2H_6), propane (C_3H_8), and methane (CH_4) released in increasing amounts during heating and consumed once flames erupt (Mitchell, 1996; Alvarez et al., 1997; WCI, 2000; PDEP, 2001a; ITC, 2003). Methane is the most combustible gas associated with blasting and burning coal, but CO and H_2 also contribute to combustion hazards (PDEP, 2001a). Methane, a component of virgin coal, accumulates in underground mines, especially in poorly ventilated shafts. Oxygen supports combustion and the amount necessary for burning is a function of the proportion of any combination of methane, carbon monoxide, and hydrogen to other gases. Five to fifteen percent methane in air, for example, is highly combustible (PDEP, 2001a).

Condensation products, associated with burning coal, form as gas exhaled from surficial vents, cracks, coal seams, and culm banks first cools and then condenses (Christie, 1926; Rost, 1937; Limacher, 1963; Lapham et al., 1980;

Stracher 1995). The exhalation–condensation process is analogous to the way minerals form in fumarolic environments (Lindgren, 1933; Stoiber and Rose, 1974; Smithsonian Institution, 2003). Using a four-step analytical technique called **thermodynamic loop analysis**, Stracher (1995) derived a **P–T stability diagram** for the condensation of orthorhombic sulfur from anthracite gas associated with the Centralia mine fire, Pennsylvania. The significance of any such stability diagram is that it serves as an environmental indicator of conditions that tend to favor the condensation of gaseous exhalations as opposed to the absorption of those exhalations into the atmosphere. In addition, such diagrams reveal information about gas composition.

Fortunately, thermodynamic data is available for additional condensates associated with the Centralia fires, as well as coal fires in Russia. Consequently, the authors are currently deriving *P–T* stability diagrams for these materials. In addition, samples collected from coal fires in La Plata County, Colorado, and condensates from Indonesia and northern China have the potential to serve as **environmental P–T indicators**.

Catastrophic Coal Fires

Some of the oldest, largest, most prevalent, and environmentally catastrophic coal fires in the world are described below. Environmental hazards associated with these fires and techniques used to control them are briefly discussed.

Northern China

China leads the world in coal production (Table 6.1.1); with one-third of the global output, coal accounts for about three-fourths of China's total energy consumption (Williams, 1999; WCI, 2000). Its reserves are concentrated in the Xinjiang Uygur and Ningxia Hui autonomous regions of northwest and north-central China, respectively. Coal fires burning throughout these regions and across northern China (Figure 6.1.1) started by lightning, spontaneous combustion, and mining operations on all scales. The fires were estimated to consume up to 200 million tons of coal per year (Rosema et al., 1993; Discover, 1999) and may account for as much as 2–3% of the annual world emission of atmospheric CO₂ from burning fossil fuels (Cassells and van Genderen, 1995; Zhang and Kroonenberg, 1996). More recent studies by Voigt et al. (2004) however, claim that 20 million tons of coal are consumed each year in China by uncontrolled fires, while about 200 to 300 million tons of coal in China are inaccessible each year because fires are an obstacle to mining operations.

Xinjiang contains some of the largest untapped coal reserves in the world. Underground coal fires in the Liu Huangou coalfield have been burning for over 20 years and possibly as long as 40 years. Chinese officials suspect the fires started by accidents inside small illegal mineshafts dug by local farmers. Particulates and noxious gases released by combustion are blown by winds over the region's capital city, Urumqi (Figure 6.1.1), one of the 10 worst polluted cities in the world. The estimated cost of extinguishing the fires over a 4-year period is at least \$10 million (the United States) (Wingfield-Hayes, 2000).

In the Rujigou coalfield of Ningxia, underground coal fires are responsible for land subsidence and the release of hydrogen sulfide into the atmosphere (Discover, 1999). The length, width, and depth of surficial cracks induced by subsidence are as much as several kilometers long, tens of meters wide, and hundreds of meters deep. These cracks promote subsurface burning by providing a conduit through which oxygen can circulate to support combustion. Subsidence due to underground fires in northwest China has been identified with thermal, microwave, and optical satellite data (Prakash et al., 2000). Research using synthetic aperture radar (SAR) to identify subsidence has yielded promising results (Prakash, 2003).

Optical and thermal images acquired by the Beijing Remote Sensing Corporation (BRSC) and heat measurements from surface and subsurface detectors have been used to determine coal fire size, depth of greatest intensity, and burning direction (Vekerdy et al., 1999; ITC, 2003, and references therein). Temperatures exceeding 800°C for surface fires have been recorded with ground-based thermal detectors (Prakash and Gupta, 1999). Combining the information acquired for numerous fires with Global Positioning System (GPS) and geologic data, ITC scientists in cooperation with the BRSC, the Netherlands Institute of Applied Geoscience, and the Environmental Analysis and Remote Sensing firm in the Netherlands designed the computer-based geographic information system, **COALMAN** (Vekerdy et al., 1999, 2000). COALMAN is used to assist Chinese firefighters in the field by generating a time series of firefighting maps and subsurface images of the fire. The COALMAN project was funded by the

Dutch and Chinese governments and the computer system can be user updated as new information about a fire becomes available (Vekerdy et al., 1999).

Once the various forms of technology are used to locate the greatest intensity of an underground fire, firefighters either inject a water–mud slurry into cracks created by subsurface burning or drill a series of holes into underground shafts, drifts, and slopes and pump in the slurry to smolder the flames. The surface is then covered with thousands of tons of soil to prevent oxygen from circulating back into the ground and rekindling the fire (Discover, 1999, Wingfield-Hayes, 2000). Surface fires are extinguished by burying burning coal under a 1 m layer of soil (Discover, 1999) or by removing the coal and carrying it away by truck to an area in which it is flooded with water or community sewage (Vekerdy, 1999). Extinguishing all such fires, however, is cost prohibitive, and fires not likely to spread to nearby coal seams are sometimes allowed to burn (Prakash, 2003).

Atmospheric pollution in China, primarily from coal combustion, is among the highest in the world (Johnson et al., 1997). Acid rain from SO₂ and NO is a problem in 88 major Chinese cities and the problem has spilled over into Taiwan, Japan, Korea, and the Philippines (World Resources Institute (WRI), 1999, pp. 63–67; United Nations Development Program, 2000). The economic loss from burning coal resources in China alone is estimated to be as high as \$125–250 million (the United States) (Prakash, 2003). These problems are compounded by a rise in lung cancer, bronchitis, stroke, pulmonary heart disease, and chronic obstructive pulmonary disease in China linked to coal gas and particulate emissions and, in some cases, directly linked to coal emissions from indoor cooking and heating (Johnson et al., 1997, p. 19; WRI, 1999, pp. 63–67). In Guizhou Province alone, over 10 million people have contracted arsenosis and fluorosis from eating foods such as corn and chili peppers dried over coal-burning stoves (Finkelman et al., 1999, 2001, 2002).

Pennsylvania, USA

Coal mining in Pennsylvania began in the mid-1700s in response to colonial America's demand for iron. Since then, Pennsylvania coal has supplied energy to the United States and countries abroad. This includes 60% of the fuel used to generate the state's electricity (PDEP, 2001b). Although Pennsylvania ranks fourth at 6.7% of US coal production after Wyoming, West Virginia, and Kentucky, more than a third of the abandoned mine-related problems in the United States occur in Pennsylvania and coal fires are among the worst such problems (Piposzar and Jones, 2000; PDEP, 2001b). Coal fires in Pennsylvania have been recorded since 1772 (Glover, 1998) but the first major fire occurred in 1869 when a ventilating furnace ignited wooden supports in the Avondale mine in Plymouth (Figure 6.1.2), suffocating 110 men trapped below ground. Fortunately, the fire self-extinguished about a year after attempts to put it out with water failed (Roy, 1876, pp. 134–137). Since the Avondale catastrophe, coal

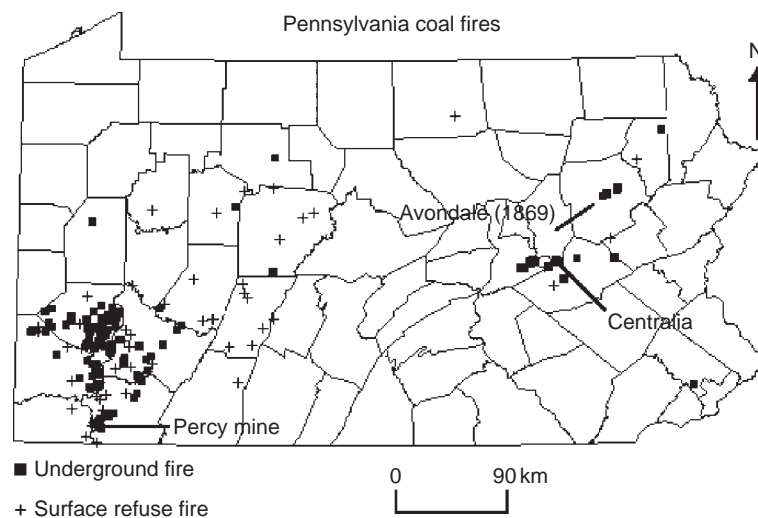


Figure 6.1.2. Coal fires across Pennsylvania: state counties are outlined. Centralia, Percy, and Avondale mine fires of Columbia, Fayette, and Montgomery counties, respectively, are illustrated. Anthracite reserves are concentrated in the east and bituminous reserves in the southwest. Figure courtesy of Michael Klimkos PDEP, 2001c, with modifications.

fires burning across Pennsylvania have destroyed floral and faunal habitats, consumed buildings, emitted toxic fumes into houses, contributed to respiratory illnesses, induced land subsidence over mine tunnels, burned precariously close to natural gas lines, and contributed to making Pennsylvania the leading acid rain producing state in the United States (Glover, 1998; Puposzar and Jones, 2000; Pennsylvania Environmental Network, 2003). According to data from The National Abandoned Land Inventory System of the PDEP (2001c), there are currently 140 underground coal mine fires and 58 burning refuse piles in Pennsylvania (Figure 6.1.2).

In Pennsylvania, coal fires have been fought using the slurry flushing and surface sealing techniques used in China. In some underground fires, mine tunnels have been sealed with brick, tile, cement blocks, or clay barriers to cut off the oxygen supply and reduce the risk of explosion (Glover, 1998; PDEP, 2001a). Aqueous foam firefighting technology is currently under consideration (PDEP 2001b) as well as pneumatic injection of dry fly ash (Magnuson, 2003). Unfortunately, numerous underground coal fires in Pennsylvania are burning unchecked because they are elusive, unpredictable, and cost prohibitive to extinguish. One of the worst underground fires in the United States is the Centralia mine fire (Figure 6.1.2), burning since May 1962 (Geissinger, 1990; Memmi, 2000).

The Centralia fire began when the Centralia Borough Council decided to burn trash to reduce the volume and control rodents in an abandoned strip-mining cut used as an unregulated dump at the edge of town. Burning trash ignited anthracite in the Buck Mountain seam concealed behind the refuse and the fire spread along the seam to tunnels beneath Centralia (DeKok, 1986, p. 20; Geissinger, 1990; Memmi, 2000). Between 1985 and 1991, the US Congress appropriated \$42 million (the United States) for Pennsylvania to relocate the 1100 residents of Centralia and its businesses. About 5 people are left in a town and its environs damaged by toxic gases, subsidence, smoke-filled valleys, polluted streams, scorched woodlands dusted with sulfur, highways cracked by temperatures as high as 455°C, surficial fires induced by heat from subsurface burning, and an underground fire that may burn for another 100 years (Memmi, 2000; Schogol, 2001). Because of deteriorated living conditions and the state's declaration of eminent domain in 1992, these people, now living in a town with an unmanned firehouse, may be forced to relocate (Schogol, 2001).

The Percy mine fire in Youngstown, Pennsylvania (Figure 6.1.2), has been burning underground for over 30 years. Like the Centralia fire, it apparently started when people ignited trash near a coal seam. Although fly ash has been used to plug conduits to the fire, the town also appears to be destined for the same fate as Centralia, with an estimated cost of \$30–40 million (the United States) necessary to extinguish the fire. Neither the state nor the federal government has offered to extinguish the fire or relocate the town's residents, whose homes are worthless (Glover, 1998).

Jharkhand, India

Commercial coal mining in India began in 1774. Production was at first slow, but it increased with the advent of steam locomotives in 1853 (Ministry of Coal and Mines (MCM), 2003a). In order to improve safety standards and develop coal resources judiciously, coal mines were nationalized between 1971 and 1973 (Bharat Coking Coal Limited (BCCL), 2003; MCM, 2003a). Consequently, 90% of Indian coal is currently mined by subsidiaries of Coal India Limited, a holding company headquartered in Calcutta (World Bank, 1997; MCM, 2003b). Singareni Collieries Ltd., co-owned by the state of Andhra Pradesh and the central government of India, in addition to privately owned companies, mines the remaining 10% (World Bank, 1996; MCM, 2003a). Today, India is the third largest coal-producing nation in the world. Two-thirds of its energy requirements are supplied by coal, 68% of which is used to generate electricity (Table 6.1.1). The remainder is used to produce steel and as boiler fuel in industrial plants (World Bank, 1997).

Fires have beset Indian coalfields since the earliest days of mining (Sinha, 1986; BCCL, 2003). Surface and subsurface fires burning throughout the Jharia coalfield (JCF) (Figure 6.1.3) comprise one of the largest coal-mine-fire complexes in the world (Gupta and Prakash, 1998; Western Pennsylvania International Business Newsletter, 1998). The JCF is located in the Dhanbad district, north of the Damodar River, in the state of Jharkhand. It is the largest coalfield in India and the country's primary source of coking coal (Gupta and Prakash, 1998; Prakash and Gupta, 1998). Mining in the JCF began in 1894, and the first coal fire broke out at Bhowrah in 1916. By the 1960s, numerous fires spread throughout the entire coalfield, with flames locally reaching heights of 20 m (BCCL, 2003). Today, about 70 fires are burning in the JCF (PDEP, 2001d; BCCL, 2003; Figure 6.1.4).

Most fires in the JCF were ignited by the spontaneous combustion of coal subsequent to opencast and deep mining. Exploitation without fire prevention codes prior to nationalization was responsible for these fires (BCCL, 2003). In

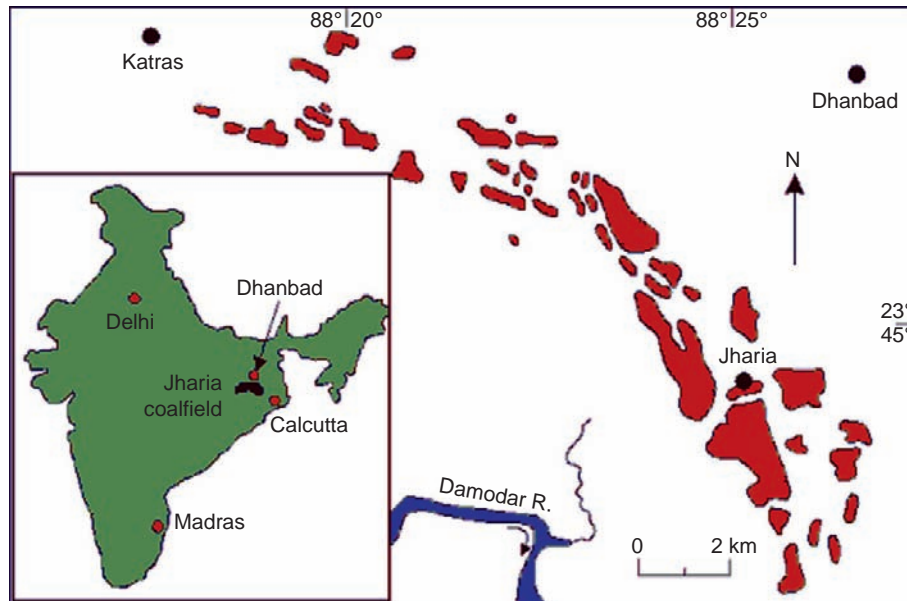


Figure 6.1.3. Location of the Jharia coalfield, India. The figure shows in red the location and extent of coal fires in the eastern part of the coalfield. Figure by Anupma Prakash, 2000.



Figure 6.1.4. Coal fire in an open-pit mine in the Jharia coalfield, India. People who work in such mines are exposed to toxic gases, particulate matter, and the risk of ground subsidence. Photo by Prasun Gangopadhyay, 2006.

addition, the illegal distillation of alcohol in abandoned underground mines is purported to be the origin of some JCF fires (Stracher et al., 2002). At present, approximately 37 million tons of coal has been lost to JCF fires and approximately 1453 million tons are locked up under fire (BCCL, 2003).

As in China and Pennsylvania, JCF fires are responsible for environmental degradation and human suffering (Figure 6.1.5). Noxious vapors and toxic fly ash that pollute air, water, and soil promote human disease including lung and skin as well as asthma and chronic bronchitis. In addition, land subsidence, endangered and inoperable rail lines, displaced communities of people, increased mining hazards, overburden dumps, the destruction of floral and faunal habitats, and the loss of coal as a valuable resource are products of these fires (Saraf, et. al., 1995; Gupta and Prakash, 1998; BCCL, 2003; Sierra Club, 2003). According to the National Center for Atmospheric Research



Figure 6.1.5. Fire in an open cast coal mine located in the Jharia coalfield, India. Miner's slums are visible along the top of the hill, where children play and people live with constant exposure to coal-fire gas. Photo by Prasun Gangopadhyay, 2006.

in Boulder, Colorado, JCF fires contribute to atmospheric sulfate aerosols derived from industrial emissions. These aerosols absorb or scatter solar radiation, thereby reducing the amount of sunlight that reaches earth's surface. This amounts to as much as a 15% reduction for the Indian subcontinent (Collins, 2000; Perkins, 2001).

Several forms of technology have been used to investigate JCF fires. Multispectral and temporal data from the Landsat Thematic Mapper (TM), for example, reveal that subsurface fires are more extensive than surface fires (Prakash et al., 1997). Surface thermal anomalies (25.6–31.6°C) detected with TM-6 thermal infrared data signify subsurface fires at depths of 45–55 m (Saraf et al., 1995; Prakash et al., 1997). Alternatively, subpixel estimates using TM-5 and TM-7 short-wave infrared data reveal surface fires ranging in temperature from 342 °C to 731 °C. IR pointing thermometers and ground-based thermal detectors confirm such surface fire temperatures (Prakash and Gupta, 1999). In addition to remotely acquired TM data, BCCL (2003) has integrated GPS data into a Geographic Information System (GIS) to locate, map, and monitor surface fires, ground subsidence, and borehole temperatures.

In the JCF, the population density is much higher than in the coalfields of northern China (Prakash, 2003), thereby necessitating the relocation of large communities of people from endangered regions to newly constructed townships in noncoal-producing areas. Fortunately, the Ministry of Coal and the Government of India have provided some relocation funds for this purpose (BCCL, 2003).

Once highly problematic coal fires in the JCF are identified with the available technology, a number of techniques are used to contain or extinguish them. For surface fires, these include trenching, analogous to a forest firebreak, and surface sealing with soil or some other noncombustible material to cut off oxygen from the fire. Inert gas injection, sand–bentonite slurry flushing, and surface sealing have been used for subsurface fires. In spite of the success with these techniques, the fires continue to burn in large areas where subsidence and inaccessible underground workings present a high risk and impasse to firefighters (BCCL, 2003).

Discussion

Regardless of origin, coal fires consume a valuable natural resource and constitute a thermodynamic recipe for environmental catastrophe. Fires in China, Pennsylvania, and India exemplify this. Industrial smokestacks and motorized vehicles are usually cited in the news as the primary sources of pollution including acid rain and greenhouse gases. The enormous amount of toxic gases and particulate matter emitted by coal fires burning around the world over many years contributes significantly to the global destruction of the environment and the health of

its inhabitants. However, little media attention has focused on these devastating fires. The overall effects of coal fires on the earth's atmosphere, hydrosphere, biosphere, geosphere, and cryosphere are worthy of intense study because of their sizeable contribution to the myriad of environmental pollutants induced by human activities.

Acknowledgments

The authors thank the following individuals and agencies for providing them with the documents and information necessary to complete the research for this manuscript: Charlotte Griffiths, The World Coal Institute, London, England; Charles Meyers, Office of Surface Mining, US Department of the Interior, Washington, DC; Peggy Wells, Energy Information Administration, US Department of Energy, Washington, DC; Timothy Altares, Michael Klimkos, and Steve Jones, Pennsylvania Department of Environmental Protection (PDEP), Harrisburg, PA; Michael Hill, PDEP, Pottsville, PA; David Zazac, Allegheny County Health Department, Pittsburgh, PA; Terry Rodgers, Tribune-Review, Greensburg, PA; Janet Carleton, Ohio University Libraries, Athens, OH; Anupma Prakash, Geophysical Institute, University of Alaska, Fairbanks; and Zoltan Vekerdy, Geological Survey Division, ITC, Enschede, The Netherlands. We also thank Jay C. Close of the ChevronTexaco Corp. and Jim Hower of the University of Kentucky Center for Applied Energy Research for their careful review of the manuscript.

Important Terms

abandoned workings

blackdamp

chokedamp

COALMAN

coal-fire detector gases

deep mined

environmental P–T indicator

exothermic oxidation reactions

P–T stability diagram

stinkdamp

strip mined

wood-fire detector gases

workings

thermodynamic loop analysis

References

- Alvarez, R., Clemente, C., Gómez-Limón, D., 1997. Reduction of thermal coals, environmental impact by nitric precombustion desulfurization. *Environ. Sci. Technol.* 31 (11), 3148–3153.
- Anthony, J.W., Williams, S.A., Bideaux, R.A., 1977. *Mineralogy of Arizona*. University of Arizona Press, Tuscon, 256 p.
- Bharat Coking Coal Limited (BCCL), 2003. Brief History of BCCL, Koyla Bhavan, Dhanbad, Coal India Limited, <http://bccl.nic.in/About-us.htm>, (accessed November 2003), pp. 1–3.
- Cassells, C.J.S., van Genderen, J.L., 1995. Thermal modeling of underground coal fires in northern China. In: *Remote Sensing in Action, Proceedings of the 21st Annual Conference of the Remote Sensing Society*, University of Southampton, England, pp. 544–551.
- Chamberlain, E.A.C., 1971. *The Ambient Temperature Oxidation of Coal*. National Coal Board, Hobart House, London, England.
- Chamberlain, E.A.C., Hall, D.A., 1973. The ambient temperature oxidation of coal in relation to the early detection of spontaneous heating: Part 2. *Min. Eng.*, 132 (152), 387.
- Christie, W.A.K., 1926. An occurrence of cryptohalite (ammonium fluosilicate). *Rec. Geol. Surv. India* 59, 233–236.
- Coates, D.A., Heffern, E.L., 2000. Origin and geomorphology of clinker in the Powder River Basin, Wyoming and Montana. In: Miller, R., (Ed.), *Coal Bed Methane and Tertiary Geology of the Powder River Basin*. Casper, Wyoming, Wyoming Geological Association 50th Annual Field Conference Guidebook, pp. 211–229.
- Collins, W., 2000. Human-induced climate change: improved knowledge and continuing uncertainties, San Francisco, California, American Geophysical Union Fall 2000 (December 17) Meeting, AGU Press Conference Release No. 00-29A.
- DeKok, D., 1986. *Unseen Danger*. University of Pennsylvania Press, Philadelphia, PA, 299 p.
- Discover, 1999. China's on fire. *R&D News* 20 (10), 20.

- Finkelman, R.B., Belkin, H.E., Zheng, B., 1999. Health impacts of domestic coal use in China. *Proc. Natl. Acad. Sci. U.S.A.* 46, 3427–3431.
- Finkelman, R.B., Orem, W., Castranova, V., Tatu, C.A., Belkin, H.E., Zheng, B., et al., 2002. Health impacts of coal and coal use: possible solutions. *Int. J. Coal Geol.* 50, 435–443.
- Finkelman, R.B., Skinner, H.C., Plumlee, G.S., Bunnell, J.E., 2001. Medical geology. *Geotimes* 46 (11), 21–23.
- Geissinger, J., 1990. Managing underground mine fires: the case of Centralia, PA. *Pa Geogr.* 28 (2), 22–26.
- Glover, L., 1998. Underground mine fires spark residents' fears. *Greensburg Pa Trib. Rev.* (May 3), A-1, –A-10.
- Gupta, R.P., Prakash, A., 1998. Reflectance aureoles associated with thermal anomalies due to subsurface mine fires in the Jharia coalfield, India. *Int. J. Remote Sens.* 19 (14), 2619–2622.
- International Institute for Geo-Information Science and Earth Observation (ITC), 2003. ITC's coal fire home page, <http://www.itc.nl/personal/coalfire/index.html> (accessed November 2003).
- Johnson, T.M., Liu, F., Newfarmer, R., 1997. *Clear Water, Blue Skies. China's Environment in the New Century*, Washington, DC, World Bank, 114 p.
- Jones, G.W., Scott, G.S., 1939. Chemical considerations relating to fires in anthracite refuse. U.S. Bureau of Mines Report of Investigations 3468, 13 p.
- Kroonenberg, S.B., Zhang X., 1997. Pleistocene coal fires in northwestern China, energy for early man. In: van Hinte, J.E. (Ed.), *One Million Years of Anthropogenic Global Environmental Change. Proceedings of the ARA Symposium at the Royal Netherlands Academy of Art and Sciences (KNAW)*, Project ID: 2-74690, pp. 39–44.
- Lapham, D.M., Barnes, J.H., Downey, W.F., Jr., Finkelman, R.B., 1980. *Mineralogy Associated with Burning Anthracite Deposits of Eastern Pennsylvania*, Pennsylvania Geological Survey, Harrisburg, PA, Mineral Resource Report 78, 82 p.
- Limacher, D., 1963. A propos de la formation de minéraux lors de la combustion des Charbons. *Soc. Geol. Nord. Ann.* 83, part 4, 287–288.
- Lindgren, W., 1933. *Mineral Deposits*, fourth ed.; McGraw-Hill, Inc., New York, 930 p.
- Magnuson, M., 2003. Centralia mine fire control failure. In: Shannon, S. (Ed.), *Case Histories of Mine Reclamation and Regulation: Reno, Nevada and Vancouver, British Columbia*, Environmental Technology for Mining, Robertson GeoConsultants Inc., http://technology.infomine.com/enviromine/case_hist/centralia/fire.html, (accessed November 2003), pp. 1–2.
- Memmi, J., 2000. Cooking centralia: a recipe for disaster. *Geotimes* 45 (9), 26–27.
- Mine Safety and Health Administration, 1996. *Underground electrical installation*. US Department of Labor, v. 61, no. 18, Section 75.340, p. 2543.
- Ministry of Coal and Mines (MCM), 2003a. *Coal mining in India: The past*. Department of Coal, Shastri Bhawan, New Delhi, India, <http://coal.nic.in/abtcoal.htm>, (accessed November 2003), pp. 1–2.
- Ministry of Coal and Mines (MCM), 2003b. *Coal India limited and its subsidiaries*. Department of Coal, Shastri Bhawan, New Delhi, India, http://coal.nic.in/coal_india_limited.htm, (accessed November 2003), p. 1.
- Mitchell, D.W., 1996. *Mine Fires, Prevention-Detection-Fighting*. Intertec Publishing, Chicago, IL, 167 p.
- Office of Surface Mining, 1999. *20th anniversary surface mining control and reclamation act, a report on the protection and restoration of the Nation's land and water resources under the surface mining law, part 2: statistical information, June 1*. US Department of the Interior, Washington, DC, 24 p.
- Pennsylvania Department of Environmental Protection (PDEP), 1965. *Anthracite coal mining laws of Pennsylvania for underground mines, "Act 346," Article I, Section 103*. Pottsville District Mining Office, Pottsville, PA.
- Pennsylvania Department of Environmental Protection (PDEP), 2001a. *Questions and answers on mine rescue and recovery operations following coal mine fires and explosions*. Pottsville District Mining Office, Pottsville, PA, <http://www.dep.state.pa.us> (accessed August 2001).
- Pennsylvania Department of Environmental Protection (PDEP), 2001b. *A status report on the environmental legacy of coal mining in Pennsylvania*. Division of Mines, Harrisburg, PA, <http://www.dep.state.pa.us>, (accessed September 2001), pp 1–2.
- Pennsylvania Department of Environmental Protection (PDEP), 2001c. *National Abandoned Land Inventory System (NALIS), Open-File Coal Fires Database (September 25)*. Bureau of Abandoned Mines and Reclamation, Harrisburg, PA.
- Pennsylvania Department of Environmental Protection (PDEP), 2001d. *DEP Geologist helps fight mine fires in India*. Division of Mines, Harrisburg, PA, <http://www.dep.state.pa.us>, (accessed November 2001), p. 1.
- Pennsylvania Environmental Network, 2003. *PEN Mining Leadership Team*, <http://www.penweb.org/issues/mining> (accessed November 2003), pp. 1–6.
- Perkins, S., 2001. *Pollution in India may effect climate*. *Science News* 159 (1), 15.
- Piposzar, D.J., Jones, M., 2000. *Topic: mining. Allegheny County Health Department – Risk Information System, Pittsburgh, PA*, <http://achd@trfn.clpgh.org/Environment/pollution.html> (accessed September 2001), pp. 1–2.

- Prakash, A., 2003. Coal fire web page. Geophysical Institute, University of Alaska-Fairbanks, <http://www.gi.alaska.edu/~prakash> (accessed November, 2003).
- Prakash, A., Fielding, E.J., Gens, R., van Genderen, J.L., Evans, D.L., 2000. Data infusion for investigating land subsidence and coal fire hazards in a coal mining area. *Int. J. Remote Sens.* 22 (6), 921–932.
- Prakash, A., Gupta, R.P., 1998. Land-use mapping and change detection in a coal mining area—a case study in the Jharia coalfield, India. *Int. J. Remote Sens.* 19 (3), 391–410.
- Prakash, A., Gupta, R.P., 1999. Surface fires in Jharia coalfield, India – their distribution and estimation of area and temperature from TM data. *Int. J. Remote Sens.* 20 (10), 1935–1946.
- Prakash, A., Gupta, R.P., Saraf, A.K., 1997. A Landsat TM based comparative study of surface and subsurface fires in the Jharia coalfield, India. *Int. J. Remote Sens.* 18 (11), 2463–2469.
- Rosema, A., Guan, H., van Genderen, J.L., Veld, H., Vekerdy, Z., Ten Katen, A.M., Prakash, A.P., 1999. Manual of coal fire detection and monitoring. Report of the Project ‘Development and implementation of a coal fire monitoring and fighting system in China.’ Netherlands Institute of Applied Geoscience, Utrecht, NITG 99-221-C, ISBN 90-6743-640-2, 245 p.
- Rosema, A., van Genderen, J.L., Schalke, H.J.W.G., 1993. Environmental monitoring of coal fires in north China. Project Identification Mission Report, BCRS 93-29, ISBN 90 5411 1054.
- Rost, R., 1937. The minerals formed on burning heaps in the coal basin of Kladno. *Academy of Sciences Bohemia, Bulletin*, pp. 47–53.
- Roy, A., 1876. *The Coal Mines*: Athens, Ohio, On Microform, Ohio University Libraries, Robison Savage and Company.
- Saraf, A.K., Prakash, A., Sengupta, S., Gupta, R.P., 1995. Landsat-TM data for estimating ground temperature and depth of subsurface coal fire in the Jharia coalfield, India. *Int. J. Remote Sens.*, 16 (12), 2111–2124.
- Schogol, M., 2001. As Centralia’s fires smolder, residents hang on. *The Philadelphia Inquirer*, Philadelphia, PA, March 18, p. 1.
- Sierra Club, 2003. International People’s Organizations Demand Global Fossil Fuel Phaseout, <http://www.sierra-club.ca/national/media/fossil-fuel-india-01-02-03.html>, (accessed November 2003), pp. 1–2.
- Sinha, P.R., 1986. Mine fires in Indian coalfields. *Energy* 11, 1147–1154.
- Smithsonian Institution, 2003. Global volcanism program. <http://www.volcano.si.edu/gvp> (accessed November 2003).
- Stoiber, R.E., Rose, W.I., Jr., 1974. Fumarole incrustations at active Central American volcanoes. *Geochim. Cosmochim. Acta* 38, 495–516.
- Stracher, G.B., 1995. The anthracite smokers of eastern Pennsylvania: Ps₂(g)-T stability diagram by TL Analysis. *Math. Geol.*, 27 (4), 499–511.
- Stracher, G.B., Taylor, T.P., 2004. Coal fires burning out of control around the world: thermodynamic recipe for environmental catastrophe. In: Stracher, G.B. (Ed.), *Coal fires burning around the world: a global catastrophe*. *Int. J. Coal Geol.* 59 (1–2), 7–17.
- Stracher, G.B., Taylor, T.P., Prakash, A., 2002. Coal fires: a synopsis of their origin, remote sensing detection, and thermodynamics of sublimation. In: Shannon, S. (Ed.), *Case Histories of Mine Reclamation and Regulation, Environmental Technology for Mining: Reno, Nevada, and Vancouver*, British Columbia, Robertson Geo-Consultants Inc., http://technology.infomine.com/enviromine/case_hist/coal%20fires/Stracher_et_al.html, (accessed January 2002), pp. 1–7.
- United Nations Development Program, 2000. Urban and rural pollution: urban air pollution. <http://www.unchina.org/undp/press/html/airp.html> (accessed September 2001), pp. 1–5.
- US Department of Energy (DOE), 1993. The fire below: spontaneous combustion in coal: Washington, DC, Environmental Safety and Health Bulletin, No. EH- 93-4, pp. 1–5.
- US Department of Energy (DOE), 1995. International energy outlook 1995. Energy Information Administration E1-84, Office of Integrated Analysis and Forecasting, Washington, DC, <http://tonto.eia.doe.gov/FTPROOT/forecasting/048495.pdf> (accessed November 2003).
- US Senate, 1912. “Titanic Disaster” Senate report No. 806, pursuant to S. Res. 283, 62nd Congress, 2d session. U. S. Government Printing Office, Washington, DC, <http://www.titanicinquiry.org> (accessed August 2001).
- Vekerdy, Z., 1999. Ningxia photo gallery, 1, http://www.itc.nl/personal/vekerdy/NingPhoto_e.htm (accessed November 2003).
- Vekerdy, Z., Prakash, A., Gens, R., 1999. Data integration for the study and visualization of subsurface coal fires: Vancouver, British Columbia, Thirteenth, International Conference on Applied Geologic Remote Sensing, Enschede, the Netherlands, vol. 2, pp. 150–151.
- Vekerdy, Z., ten Katen, A.M., Veld, H., 2000. Handbook of the Coal Fire Monitoring and Management System (CoalMan), software manual: International Institute for Geo-Information Science and Earth Observation, the Netherlands, <http://www.itc.nl/personal/coalfire/index.html> and references therein (accessed November 2003).

- Voigt, S., Tetzlaff, A., Zhang, J., Künzer, C., Zhukov, B., Strunz, G., Oertel, D., Roth, A., van Dijk, P.M., Mehl, H., 2004. Integrating satellite remote sensing techniques for detection and analysis of uncontrolled coal seam fires in North China. In: Stracher, G.B. (Ed.), *Coal Fires Burning Around the World: A Global Catastrophe*. *Int. J. Coal Geol.* 59 (1–2), 121–136.
- Western Pennsylvania International Business Newsletter, 1998 (Fall). Pennsylvania District office, University of Pittsburgh International Business Center and the Western Pennsylvania District Export Council, in cooperation with the U.S. Department of Commerce, Pittsburgh, PA, <http://www.pitt.edu/~ibcmod/newsletter/Fall98/localcomp.html>, pp. 1–3, (accessed November 2003).
- Williams, D.J., 1999. Fugitive emissions from coal mining. The Australian Academy of Technological Sciences and Engineering, <http://www.atse.org.au> (accessed December 2000), pp. 1–8.
- Wingfield-Hayes, R., 2000. China battles coal fires (August 3): BBC News Online and BBC News on FireNet (Electronic Pages for the British Fire Service), <http://news.bbc.co.uk> and <http://wwwfire.org.uk> (accessed August 2001).
- World Bank, 1996. India-coal sector environmental and social mitigation project INPA43310. Public Information Center of the World Bank, Washington, DC, <http://www.worldbank.org> (accessed November 2001), pp. 1–12.
- World Bank, 1997. India-coal sector rehabilitation project INPE9979. Public Information Center of the World Bank, Washington, DC, <http://www.worldbank.org> (accessed November 2001), pp. 1–8.
- World Coal Institute (WCI), 2000. *Coal-power for progress*, fourth ed., World Coal Institute, London, England, <http://www.wci-coal.com> (accessed August 2001).
- World Coal Institute (WCI), 2002. *Coal facts*. Ecoal 44, 8.
- World Coal Institute (WCI), 2003. *Coal and steel facts*. Ecoal 45, 8.
- World Resources Institute (WRI), 1999, 1998–1999 *World Resources: A Guide to the Global Environment, Environmental Change and Human Health*. Oxford University Press, <http://www.wri.org> (accessed September 2001).
- Zhang, X., Kroonenberg, S.B., 1996. Pleistocene coal fires in Xinjiang, northwest China. Abstracts of the 30th International Geologic Congress, Beijing, China, August 4–14, vol. 1, p. 457.

WWW Addresses: Additional Reading

- (1) **Australian Academy of Technological Sciences and Engineering**
<http://www.atse.org.au>
- (2) **Bharat Coking Coal Ltd.**
<http://bccl.cmpdi.co.in>
- (3) **Centralia Mine Fire Control Failure**
http://technology.infomine.com/enviromine/case_hist/centralia/fire.html
- (4) **Coal Fires**
<http://www.gi.alaska.edu/~prakash>
- (5) **Coal Fires: A Synopsis of Their Origin, Remote Sensing Detection, and Thermodynamics of Sublimation**
http://technology.infomine.com/enviromine/case_hist/coal%20fires/Stracher_et_al.html
- (6) **Coal India limited and Its Subsidiaries**
http://coal.nic.in/coal_india_limited.htm
- (7) **Coal Mining in India – The Past**
<http://coal.nic.in/abtcoal.htm>
- (8) **Fire Net International**
<http://www.fire.org.uk>
- (9) **Global Volcanism Program**
<http://www.volcano.si.edu/gvp>
- (10) **International Energy Outlook**
<http://tonto.eia.doe.gov/FTP/ROOT/forecasting/048495.pdf>
- (11) **International Institute for Geo-Information Science and Earth Observation**
<http://www.itc.nl/personal/coalfire/index.html>
- (12) **Pennsylvania Department of Environmental Protection**
<http://www.dep.state.pa.us>
- (13) **Sierra Club**
<http://www.sierraclub.ca/national/media/fossil-fuel-india-01-02-03.html>
- (14) **The World Bank**
<http://www.worldbank.org>

- (15) **Titanic Inquiry Project**
<http://www.titanicinquiry.org>
- (16) **United Nations in China**
<http://www.un.org.cn/index.htm>
- (17) **Western Pennsylvania International Business Newsletter**
<http://www.pitt.edu/~ibcmmod/newsletter/Fall98/localcomp.html>
- (18) **World Coal Institute**
<http://www.worldcoal.org>
- (19) **World Resources Institute**
<http://www.wri.org>

CHAPTER 7

Environmental and Health Impacts of Coal Fires



Destruction of floral and faunal habitat along Big Mine Run Road near the town of Centralia in the Appalachian Mountains of eastern Pennsylvania. The Western Middle Field of anthracite coal has been mined here since the mid-1800s. The Centralia Mine Fire that deforested this hillside started in May 1962 from trash burnt in an abandoned strip-mining cut, to reduce the volume of refuse and control rodents in this unregulated dump. Note the smoke-filled valley in the upper right-hand corner. This area would be too dangerous to venture into for the purpose of collecting gas and mineral samples. One could easily get lost, and not make it out alive. A sink hole (photo center), above an abandoned underground mining tunnel, is coated with sulfur, and a coating of sulfur covers the dead trees and other vegetation on this hillside. Field of view is about 35m. *Photo by Glenn B. Stracher, 1991.*

CHAPTER CONTENTS

7.1 Environmental and Health Impacts of Coal Fires

- Introduction
- Environmental Consequences
- Health-Related Effects
- Discussion
- Important Terms
- References
- WWW Addresses: Additional Reading



7.1. Environmental and Health Impacts of Coal Fires

Robert B. Finkelman
Glenn B. Stracher

Sulfur littering this hillside at the Centralia mine fire reacts with rain and snowmelt to form sulfuric acid that pollutes the hydro-logic system.

Photo by Glenn B. Stracher, 1991.

Introduction

Pollutants released from burning coal beds and waste piles are a potential environmental and human-health hazard. On a global scale, large volumes of **greenhouse** and **toxic gases** released from burning-coal beds and waste piles may contribute to **climate change**, alter ecosystems, and affect patterns of disease occurrence. On regional and local scales, the emissions from burning coal beds and waste piles of acidic gases, particulates, organic compounds, and trace elements may contribute to environmental degradation and a range of respiratory and other human-health problems. Although there are few published reports about health problems caused by these emissions, the potential for such problems is significant. In India, large numbers of people were displaced from their homes because of health problems associated with burning coal beds (Bharat Coking Coal Limited, 2003; Sierra Club, 2003; Stracher and Taylor, 2004). Volatile elements such as arsenic, fluorine, mercury, and selenium are commonly enriched in coal (Table 7.1.1). As the coal burns, these elements may volatilize and eventually be adsorbed on or by food crops, condense on dust particles that are inhaled and ingested by humans and livestock, and bio-accumulated in birds, fish, and other animals (Keefer and Sajwan, 1993). In addition, selenium, arsenic, lead, tin, bismuth, fluorine, and other **toxic elements** are incorporated into compounds that nucleate where hot-gaseous emissions mix with the ambient air, forming mats of concentrated efflorescent minerals on the surface of the ground (Figure 7.1.1; Figure 14 in Lapham et al., 1980). Toxic elements in these mats leached by rainwater may enter the hydrologic system, opening the possibility to other routes of exposure or ingestion by biota. Although there is little available data linking burning-coal beds and waste piles with human-health problems, an example of what can happen exists in rural China, where mineralized-coal burned in residential environments has caused widespread and severe health problems including **fluorosis** (fluorine poisoning, Figure 7.1.2) and **arsenosis (hyperkeratosis or arsenic poisoning, Figure 7.1.3).**

Table 7.1.1
Concentrations (parts per million) of the volatile elements arsenic, fluorine, mercury, and selenium in the earth's crust and in US coal.

Element	Crustal average*	US coal average [†] whole coal basis	US Coal average ash basis [‡]
Arsenic	1.8	24	183
Fluorine	625	98	748
Mercury	0.08	0.17	1.3
Selenium	0.05	2.9	21.4

* Mason (1966).

[†] Orem and Finkelman (2003).

[‡] Based on an ash yield of 13.1 wt% and assuming no volatilization.

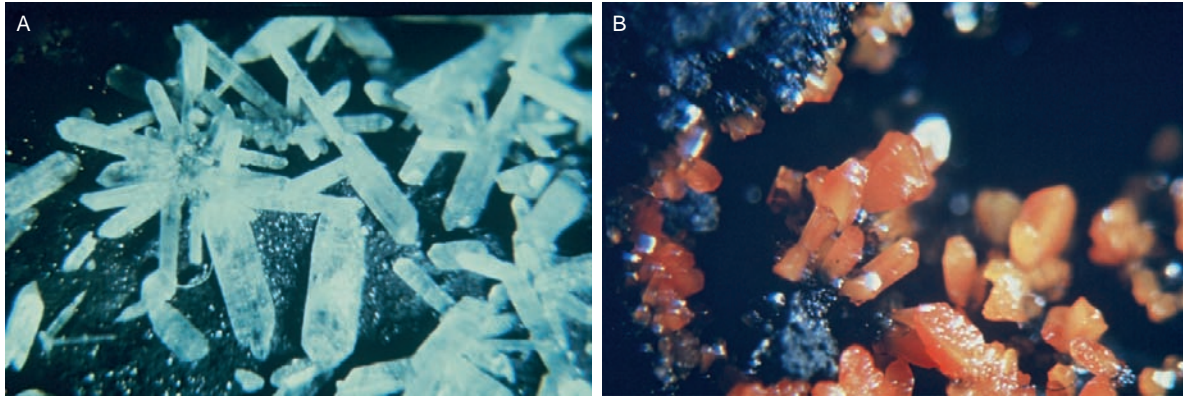


Figure 7.1.1. Crystals from a burning coal-waste pile in Glen Lyon, Pennsylvania: (A) downeyite (SeO₂), Finkelman and Mrose (1977) and (B) realgar (AsS), Lapham et al. (1980) pp 31–32.



Figure 7.1.2. Dental fluorosis in Guizhou Province, China, caused by burning coal briquettes enriched in fluorine Finkelman et al., 1999.



Figure 7.1.3. Arsenosis (hyperkeratosis) in Ghizhou Province, China, caused by burning coal enriched in arsenic Finkelman et al., 1999.

Coal fires are an undesired but ubiquitous consequence of coal exposed to air at or near the earth's surface. These fires start by numerous processes including spontaneous combustion, lightning strikes, forest fires, arson, and mining accidents (Stracher and Taylor, 2004). Although coal is exposed at the surface due to tectonic uplift and erosion, the amount of coal exposed to air has increased dramatically since the industrial revolution in Europe

(Stracher and Taylor, 2004; Stracher, 2007) and as a consequence, so has the number of coal fires. Today these fires occur in every region of the world where coal is mined. Walker (1999) notes that uncontrolled coal fires have been reported in the United States, Canada, China, Australia, India, Indonesia, South Africa, England, Germany, Poland, Czech Republic, Russia, Ukraine, Turkey, and Thailand. Coal fires have also been reported from Columbia, Egypt, France, Portugal, and New Zealand (this atlas, Stracher et al., 2005; Masalehdani et al., 2007a, b).

In this chapter we review and illustrate some common **environmental impacts** of coal fires and briefly discuss the possible health consequences. According to Finkelman (2004), “It is difficult to think of a natural or anthropogenic process that has absolutely no societal benefit.” In addition, he states “Coal fires, both surface and in-ground, represent the rare phenomenon that is totally devoid of societal value.” The more common environmental problems caused by surface and in-ground coal fires are, according to Finkelman (2004):

- Visual blight and the loss of potentially valuable acreage;
- Destruction of the nearby ecosystem;
- Forest fires;
- Windblown dust and siltation of streams;
- Deterioration of cultural infrastructures by acidic gases;
- Destruction of personal and public property;
- Disruption of families and communities;
- Physical hazards from collapse or explosion;
- Health hazards due to respiration of dust and aerosols, exposure to acidic gases, potentially toxic trace elements, and organic compounds;
- Pollution of surface and ground water;
- Loss of valuable energy resources;
- Significant amounts of the major greenhouse gas carbon dioxide (CO₂).

Environmental Consequences

Visual Effects

Although piles of burning coal waste (called **gob piles** in bituminous coal regions and **culm banks** in anthracite coal regions) on the surface are more obvious, underground coal-bed fires have left a long legacy of environmental damage. Deforestation, smoke, **clinker** (rock baked and oxidized by burning coal), ground fissures, gas vents, sinkholes, and solid by-products of combustion including minerals and creosote are the first images visible in an area affected by a coal fire. High temperatures and gas perpetuate the appearance of a scarred landscape by preventing the growth of new vegetation (Figure 7.1.4). Kuenzer et al. (2007) provide a comprehensive description of the environmental and geomorphic impacts of underground coal fires in north-central China. They estimate that toxic gases and heat from the Wuda coalfield fires in Inner Mongolia have destroyed more than 95% of the vegetation in a region scarred by trenches, pits, cracks, and subsidence. These authors note that “Coal fire-induced uncontrolled subsidence poses a great threat to local infrastructure and buildings.” The classic case of this is Centralia, Pennsylvania (Figures 7.1.5 and 7.1.6) where a large portion of this once thriving town was evacuated due to the danger of toxic gases and subsidence associated with the Buck Mountain anthracite seam burning in abandoned coal-mine tunnels beneath the town. In 1962, Centralia had about 1100 residents, but by 2003 the underground coal fires had reduced the population to about 20 people. Today, only a handful of people remain (DeKok, 1986; Stracher et al., 2006).

Heffern and Coates (1997) noted that clinker covers an area of about 1600 mi² (~1442 km²) in the Powder River Basin in Wyoming and Montana. They estimate that this represents about 30–40 billion tons of burned coal and that there may have been about 10 times more clinker than today that has been eroded. Barren turf produced by a coal fire exposes fine particulates to wind and rain, facilitating high levels of particulates in the air and runoff leading to stream siltation.

Coal fires also cause forest and range fires that may promote additional coal fires. These fires also destroy homes and other buildings (Figure 7.1.7), render ranch land useless, and may consume mining equipment (Figure 7.1.8).

Unless extinguished, there is little chance for new vegetation to take root in a landscape altered by a coal fire. However, once a fire is put out or burns out by itself, reclamation can return the area to one of useful purposes. The



Figure 7.1.4. Deforestation and subsidence caused by bituminous coal burning underground in the Late Cretaceous Fruitland Formation on the Southern Ute Indian Reservation in southwestern Colorado. Photo by Glenn B. Stracher, 2002.



Figure 7.1.5. Centralia, Pennsylvania. Barren lots mark the locations where houses once stood. The families were relocated after all attempts failed to extinguish the coal fire raging beneath the town. Note the emission of toxic coal-fire gas in the foreground. From Kubiszewski and Cleveland 2006.

cost of land reclamation after a coal fire can be substantial. According to an Internet article by Stein (2007), the estimated cost of extinguishing just the Centralia Mine Fire in Pennsylvania is in excess of \$600 million dollars (US).

Solid By-Products of Combustion

The combustion process mobilizes many elements that were concentrated in the coal. These elements commonly nucleate as compounds at the surface on rock and soil, dead vegetation, and on all sorts of refuse from masonry blocks and rubber tires to children's toys discarded in waste dumps. The compounds, typically **minerals** and **creosote (coal tar)**, nucleate when coal fire gas cools and on occasion reacts with the depositional substrate. Stracher et al. (2005; Chapter 9, this book) gives detailed explanations of the various processes that lead to the formation of mineral assemblages.



Figure 7.1.6. Route 61 through Centralia, PA. The cracks are due to subsidence of the road into abandoned coal-mine tunnels beneath the road. Subsidence occurs when coal pillars supporting the roof of a tunnel burn and collapse. Note the toxic gas exhaled along the cracks. Photo by Janet L. Stracher, 2003.



Figure 7.1.7. A coal fire of uncertain origin partially destroyed a home in East Kalimantan, Indonesia. The fire started in September 1997 in a coal bed exposed in a stream valley and burned beneath the house shown here, near the Samarinda–Balikpapan road. The house was relocated across the road, repaired, and the fire extinguished by November 1999. Photo by Alfred E. Whitehouse, 1998.

In a comprehensive study of minerals nucleated adjacent to gas vents associated with surface and underground coal fires in the Anthracite Region of Pennsylvania, Lapham and others (1980) described 33 mineral species, many containing potentially toxic compounds. These minerals include native selenium (Se), galena (PbS), realgar (AsS), orpiment (As₂S₃), arsenolite (As₂O₃), downeyite (SeO₂), and unnamed As₂Se₃ (subsequently named laphamite,



Figure 7.1.8. Mining equipment ignited by a coal fire at the Blair Athol Coal Mine, New South Wales, Australia: (A) drag line and (B) coal-hauling truck. Photos courtesy of the Law Offices of Countryman and McDaniel (<http://www.CargoLaw.com>), Los Angeles, California, 2009.

Dunn et al., 1986), several fluorine-bearing minerals including cryptohalite $(\text{NH}_4)_2\text{SiF}_6$, bararite $(\text{NH}_4)_2\text{SiF}_6$, and an unmanned KAlF_4 . Some of the minerals were so abundant, that they formed a carpet of crystals extending about a meter around each vent. Similar minerals were found at other burning coal sites in the former Czechoslovakia (Rost, 1937) and Russia (Chesnokov, 1997). Recently, Pone et al. (2007) reported finding mercury in association with minerals around a gas vent in a burning waste pile in the Witbank coalfield of South Africa.

Health-Related Effects

Despite the abundant literature about the origin of coal fires, their environmental impacts, and the efforts to extinguish them, relatively little has been written about the **human-health impacts** of burning-coal beds and waste piles.

In addition to the respiratory problems and fatalities caused by inhaling carbon monoxide (CO) and other toxic gases (Stracher and Taylor, 2004; Stracher et al., 2006), physical hazards are frequently hidden beneath landscapes altered by coal fires. Commonly, temperatures in excess of 600°C occur just below the surface, capable of severely burning inquisitive but unsuspecting people who venture over these hot spots. There have been several deaths or near misses due to equipment and people falling into sinkholes formed by subsidence of thin crust above abandoned underground mining tunnels, once coal pillars used as roof supports burn and collapse (Stracher et al., 2006).

Stracher and Taylor (2004) note that pollution from the burning coal beds in the Jharia coalfield in India are causing people to suffer from asthma, chronic bronchitis, and skin and lung diseases. They also state that documented illnesses from coal fires include stroke, pulmonary heart disease, and chronic obstructive pulmonary disease. The Indian Government has initiated a large-scale relocation plan so that people can escape the high concentration of toxic gases and particulates generated by the Jharia coal fires (Stracher, 2002; Stracher and Taylor, 2004).

During a study of uncontrolled coal fires in north-central China, Kuenzer et al. (2007) found that people living near these fires suffer from exposure to CO and other toxic gas compounds. They state that people are commonly seen wearing facemasks to protect themselves from gas emissions and particulates. In addition, they note an increased risk for respiratory illness, tuberculosis, and lung cancer because of the immune-system deterioration of people living in the vicinity of these fires.

Finkelman (2004) describes the extensive and commonly severe health problems caused by the release of arsenic, fluorine, selenium, and mercury from domestic coal use in China, the same elements found in a suite of minerals by Lapham et al. (1980) to be forming around coal-fire vents in the Appalachian region of the United States and in other countries. Finkelman (2004) suggests that by analogy, we might expect that the health of people living near coal-bed and waste-pile fires may be at risk from the emission of trace elements, gases, and particulates. Perhaps

exposure to mobilized-trace elements may account for the occurrence of lung and skin disease in people living near the Jharia coalfield fires in India.

Toxic elements in native form or in minerals nucleated at the surface from coal-fire gas exhaled at vents and ground fissures, especially if in a water-soluble phase, may present a threat to ecosystems and to human health (see below). However, not all of the harmful elements precipitate on the surface. Large amounts of potentially toxic gases are emitted into the atmosphere. Kuenzer et al. (2007) note that the gases released from the fires in north-central China are rich in CO, CO₂ and other greenhouse-gases, methane (CH₄), sulfur dioxide, nitrous oxides, and toxic gases H₂S and N₂O.

Estimates of the contribution of CO₂ from the coal fires in China alone range as high as 2–3% of the total world CO₂ production due to fossil fuels (International Institute for Geo-Information Science and Earth Observation, 2009). If true, the fires would be one of the largest sources of this greenhouse gas and a major contributor to global climate change.

According to a study by Pone et al. (2007), gases emitted from burning-waste piles in the Witbank and Sasolburg coalfields of South Africa were found to contain part per million levels of the toxins toluene (5.2–397), benzene (6.6–50), and xylene (0.1–5.9) as well as lesser amounts of many other volatile organic compounds. CO₂ levels ranged from almost 1% to more than 3% by volume of the gases generated by the fires in these coalfields.

In the Eastern Kentucky coalfield near the towns of Hazard and Bulan, gas exhaled from vents and ground fissures in sandstone; associated with an underground coal fire in the Pennsylvanian Hazard No. 7 coal bed, transformed upon cooling into creosote deposits overlain by a dusting of sulfur and salammoniac (NH₄Cl) adjacent to the vents and fissures (Stracher et al., 2008). Gas analyses revealed 47 compounds including the toxins toluene and xylene; greenhouse gases CH₄ and CO₂; and the potential ozone-forming gases ethene, ethane, propene, and propane, all emitted from the vents (165–385°C) into the atmosphere. Analysis of the creosote revealed the presence of pyrogenic **polycyclic aromatic hydrocarbons** (Emsbo-Mattingly et al., 2008). The solid by-products of combustion could present a potential health hazard as soil and water pollutants.

Mercury may be another potential environmental and human-health problem caused by coal fires. Mercury-bearing minerals are uncommon around gas vents and ground fissures but this may be because mercury is so volatile that it does not precipitate from the gas. Assuming a conservative estimate that about 200 million tons of coal are consumed annually by uncontrolled coal fires worldwide, Pirrone et al. (2009) estimate that this would release about 32 tons of mercury into the atmosphere or nearly only about one-third less than the 48 tons of mercury released by the roughly one billion tons of coal burned in the United States every year for generating electricity (U.S. Environmental Protection Agency, 1997).

According to Rosema et al. (1999) 100 to 200 million tons of coal are lost each year due to coal fires in China. However, more recent studies report that 20 million tons of coal are being burnt in uncontrolled coal fires in China each year and about 200 to 300 million tons of coal are lost in China each year, because the fires hinder the accessibility for mining operations in their surroundings (Voigt et al., 2004).

Unfortunately, there is no comprehensive assessment of the amount of coal consumed worldwide per annum by coal-bed, coal-waste, and coal-stockpile fires. The 200 million ton estimate noted above would represent an enormous loss of a valuable energy resource. If this estimate is reasonably accurate, it means that about 3% of all the 6.5 billion tons of coal burned annually each year is lost to uncontrolled coal fires and that these uncontrolled fires are consuming more coal than do all but the five largest coal consuming countries: China, Germany, India, Russia, and the United States (Energy Information Agency, 2009).

Discussion

Uncontrolled fires in underground coal mines and coal waste piles present a range of environmental and human-health hazards. In consuming large quantities of a valuable energy resource, these fires destroy the local ecosystem, pollute air and water, emit large volumes of greenhouse and toxic gases, and put at risk the health of coal miners and people living in nearby communities. Unfortunately, the health problems have been poorly studied. Finkelman (2004) offers several explanations for the lack of epidemiological studies. These include:

- The gross environmental devastation may have deflected attention from the health problems;
- The manifestations of the health problems may be quite subtle;

- Many current fires are in remote areas of developing countries with limited health-care facilities;
- The health problems may be masked by other health issues in these generally poor coal-mining communities;
- The health problems may, indeed, be rare.

Finkelman (2004) recommends that researchers be aware of the potential health problems and clinical symptoms that can be caused by burning coal beds and waste banks. Any indication of health problems should be brought to the attention of the proper health officials.

The only solution to this cycle of environmental devastation and threat to human safety and health is vigorous efforts to extinguish existing fires and concerted efforts to prevent the inevitable coal fires from getting out of hand. Though initially costly, these measures may prove to be cost effective by preserving valuable coal resources, preventing degradation of large swaths of land, avoiding air and water pollution, reducing CO₂ and other greenhouse gas emissions, saving public property and local infrastructure, and reducing health-care costs while increasing worker productivity. All in all, a fair trade for the elimination of a phenomenon totally devoid of societal value.

Important Terms

arsenosis (hyperkeratosis)
climate change
clinker
culm banks
creosote (coal tar)
environmental impacts
fluorosis

gob piles
greenhouse gases
human-health impacts
minerals
polycyclic aromatic hydrocarbons
toxic elements
toxic gases

References

- Bharat Coking Coal Limited, 2003. Brief History of BCCL: Koyla Bhavan, Dhanbad, Coal India Limited, <http://bccl.nic.in/About-us.htm>, pp. 1–3 (accessed November 2003).
- Chesnokov, B.V., 1997. Overview of results on mineralogical investigation of burnt dumps of the Chelyabinsk coal basin during 1982–1995, 10th report, Ural'sky mineralogical sbornik N 7. Miass: Institute of Mineralogy, Ural branch, Russian Academy of Sciences, pp. 5–32 (in Russian).
- DeKok, D., 1986. Unseen Danger. University of Pennsylvania Press, Philadelphia, Pennsylvania, 299 p.
- Dunn, P.J., Peacor, D.R., Criddle, A.J., Finkelman, R.B., 1986. Laphamite, and arsenic selenide analogue of orpiment from burning anthracite deposits in Pennsylvania. *Mineral. Mag.* 50, 279–282.
- Emsbo-Mattingly, S.D., Stout, S.A., Stracher, G.B., Hower, J.C., 2008. Extractable PAHs in Coal: The effects of rank and natural/anthropogenic coking: Society of Environmental Toxicology and Chemistry, North America 29th Annual Meeting, November 16–20, Tampa, Florida, p. 324.
- Energy Information Agency, 2009. <http://www.eia.doe.gov/pub/international/iealf/table14.xls> (accessed February 2009).
- Finkelman, R.B., 2004. Potential human health impacts of burning coal beds and waste piles. In: Stracher, G.B. (Ed.), *Coal Fires Burning Around the World: A Global Catastrophe*. *Int. J. Coal Geol.* 59 (1–2), 19–24.
- Finkelman, R.B., Belkin, H.E., Zheng, B., 1999. Health impacts of domestic coal use in China. *Proc. Natl. Acad. Sci. U.S.A.* 96, 3427–3431.
- Finkelman, R.B., Mrose, M.E., 1977. Downeyite, the first verified natural occurrence of SeO₂. *Am. Mineral.* 62, 316–320.
- Heffern, E.L., Coates, D.A., 1997. Clinker—its occurrence, use, and effects on coal mining in the Powder River Basin. *Wyo. State Geol. Surv. Publ. Inf. Circ.* 38, 151–166.
- International Institute for Geo-Information Science and Earth Observation, 2009. http://www.itc.nl/personal/coal-fire/problem/china_coalfire.html (accessed February, 2009).
- Keefer, R.F., Sajwan, K.S. (Eds.), 1993. *Trace Elements in Coal and Coal Combustion Residues*. Lewis Press, Boca Raton, FL, 308 p.

- Kubiszewski, I., Cleveland, C.J., 2006. Centralia, Pennsylvania: Encyclopedia of the Earth, http://www.eoearth.org/article/Centralia,_Pennsylvania (accessed June, 2009).
- Kuenzer, C., Zhang, J., Terzlaff, A., van Dijk, P., Voigt, S., Mehl, H., Wagner, W., 2007. Uncontrolled fires and their environmental impacts: Investigating two arid mining regions in north-central China. *Appl. Geogr.* 27, 42–62.
- Lapham, D.M., Barnes, J.H., Downey, W.F., Jr., Finkelman, R.B., 1980. Mineralogy associated with burning anthracite deposits of Eastern Pennsylvania. Pennsylvania Geological Survey, Mineral Resource Report 79, 82 p.
- Masalehdani, M.N.-N., Black, P.M., Kobe, H.W., 2007a. Mineralogy and petrography of iron-rich slags and paralavas formed by spontaneous coal combustion, Rotowaro coalfield, North Island, New Zealand. In: Stracher, G.B. (Ed.), *Geology of Coal Fires: Case Studies from Around the World: Reviews in Engineering Geology XVIII*. Geological Society of America, pp. 117–131.
- Masalehdani, M.N.-N., Paquette, Y., Bouchardon, J.-L., Guy, B., Stracher, G.B., Chalier, J., 2007b. Vapor deposition of arsenic-bearing minerals originating from a burning culm bank: St Etienne, the Loire Region, France. *Geol. Soc. Am. Abstr. Programs* 39 (6), 298.
- Mason, B., 1966. *Principles of Geochemistry*, third ed. John Wiley & Sons, New York, 329 p.
- Orem, W.H., Finkelman, R.B., 2003. Coal formation and geochemistry. In: Mackenzie, F.T. (Ed.), *Sediments, Diagenesis, and Sedimentary Rocks*, vol. 7, a series. In: Holland, H.H., Turekian, K.K. (Eds.), *Treatise on Geochemistry*. Elsevier-Pergamon, Oxford, pp. 191–222.
- Pirrone, N., Cinnirella, S., Feng, X., Finkelman, R.B., Friedli, H.R., Leaner, J., et al., 2009. Global mercury emissions to the atmosphere from natural and anthropogenic sources. In: Pirrone, N., Mason R.P. (Eds.), *Mercury Fate and Transport in the Global Atmosphere: Measurements, Models and Policy Implications*, Chapter 1. Springer Publishing (in press).
- Pone, J.D.N., Hein, K.A.A., Stracher, G.B., Annegarn, H.J., Finkelman, R.B., Blake, D.R., et al., 2007. The spontaneous combustion of coal and its by-products in the Witbank and Sasolburg coalfields of South Africa. *Int. J. Coal Geol.* 72, 124–140.
- Rosema, A., Guan, H., van Genderen, J.L., Veld, H., Vekerdy, Z., Ten Katen, A.M., Prakash, A.P., 1999. Manual of coal fire detection and monitoring. Report of the Project 'Development and implementation of a coal fire monitoring and fighting system in China.' Netherlands Institute of Applied Geoscience, Utrecht, NITG 99-221-C, ISBN 90-6743-640-2, 245 p.
- Rost, R., 1937. The minerals formed on burning heaps in the coal basin of Kladno. *Acad. Sci. Bohemia Bull.* 47–53.
- Sierra Club, 2003. International People's Organizations Demand Global Fossil Fuel Phaseout. <http://www.sierra-club.ca/national/media/fossil-fuel-india-01-02-03.html>, pp. 1–2 (accessed November 2003).
- Stein, A., 2007. Nasty little rascals—coal fires responsible for hundreds of millions of tons of CO₂. <http://www.terrapass.com/blog/posts/nasty-little-ra> (accessed February 2009).
- Stracher, G.B., 2002. Coal fires—a burning global recipe for catastrophe. *Geotimes* 47 (10), 36–37, 66.
- Stracher, G.B., 2007. Coal fires burning around the world: opportunity for innovative and interdisciplinary research: GSA Today ("Groundwork" article). *Geol. Soc. Am.* 17 (11), 36–37.
- Stracher, G.B., Hower, J.C., Schroeder, P., Fleisher, C., Kitson, J., Barwick, L., et al., 2008. Environmental Dangers of Coal Fires in Kentucky and Alabama, 2008. Geological Society of America Abstracts with Programs, Paper No. 310-7, 40 (6), p. 493.
- Stracher, G.B., Nolter, M.A., Schroeder, P.A., McCormack, J.K., Blake, D.R., Vice, D.H., 2006. The Great Centralia Mine Fire: A Natural Laboratory for the Study of Coal Fires. In: Pazzaglia, F.J. (Ed.), *Excursions in Geology and History: Field Trips in the Middle Atlantic States*. *Geol. Soc. Am. Field Guide* 8, 33–45.
- Stracher, G.B., Prakash, A., Schroeder, P., McCormack, J., Zhang, X., Van Dijk, P., Blake, D., 2005. New mineral occurrences and mineralization processes: Wuda coal-fire gas vents of Inner Mongolia. *Am. Mineral.* 90, 1729–1739.
- Stracher, G.B., Taylor, T.P., 2004. Coal fires burning out of control around the world: Thermodynamic recipe for environmental catastrophe. In: Stracher, G.B. (Ed.), *Coal Fires Burning Around the World: A Global Catastrophe*. *Int. J. Coal Geol.* 59 (1–2), 7–17.
- U.S. Environmental Protection Agency, 1997. Mercury study report to Congress, vol. 1, Executive summary, Office of Air Quality, Planning, and Standards, and Office of Research and Development, Washington, DC, EPA-452/R-97-003, 95 p.
- Voigt, S., Tetzlaff, A., Jianzhong Zhang, Künzer, C., Zhukov, B., Strunz, G., Oertel, D., Roth, A., Dijk, P.M. van, Mehl, H., 2004. Integrating satellite remote sensing techniques for detection and analysis of uncontrolled coal seam fires in North China. In: Stracher, G.B. (Ed.), *Coal Fires Burning Around the World: A Global Catastrophe*. *Int. J. Coal Geol.* 59 (1–2), 121–136.
- Walker, S., 1999. Uncontrolled fires in coal and coal wastes. International Energy Agency, London. Report CCC/16, p. 72.

WWW Addresses: Additional Reading

- (1) **Coal Fires and Carbon Dioxide**
<http://www.terrapass.com/blog/posts/nasty-little-ra>
- (2) **Environmental Dangers of Coal Fires in Kentucky and Alabama**
http://gsa.confex.com/gsa/2008AM/finalprogram/abstract_142640.htm
- (3) **Global Fossil Fuel Phaseout**
<http://www.sierraclub.ca/national/media/fossil-fuel-india-01-02-03.html>
- (4) **International Institute for Geo-Information Science and Earth Observation, 2009**
http://www.itc.nl/personal/coalfire/problem/china_coalfire.html
- (5) **Mercury Study Report to Congress**
<http://www.epa.gov/mercury/report.htm>
- (6) **New Mineral Occurrences from the Wuda Coalfield of Inner Mongolia**
http://gsa.confex.com/gsa/2004AM/finalprogram/abstract_73402.htm
- (7) **Vapor Deposition of Arsenic-Bearing Minerals**
http://gsa.confex.com/gsa/2007AM/finalprogram/abstract_132667.htm

This page intentionally left blank

CHAPTER 8

Analysis of Coal-Mine-Fire Gas



Gloria Liu in the process of preconcentrating a coal-mine-gas sample preparing for injection it onto the separation columns. *Photo by Timothy R. Blake, 2007.*

CHAPTER CONTENTS

8.1 Trace Gas Analyses

- Introduction
- Gas Collection
- Sample Analyses
- Methane System
- CO/CO₂ System
- VOC System
- Quality Control: Standards
- Modifying
- Important Terms
- References
- WWW Addresses: Additional Reading



Photo by Timothy R. Blake (2007).

8.1. Trace Gas Analyses

Timothy R. Blake
Simone Meinardi
Donald R. Blake

Research group member Gloria Liu trapping a coal gas sample on the five column/detector trace gas analytical system.

Introduction

Gas Chromatography (GC) is the technique used by the Blake/Rowland research group for analyzing components of samples taken in the field. We use chemically treated **columns** to “un-mix” the sample into groups of its individual chemical constituents. This is achieved by the column being coated (for capillary) or filled (for packed) with a bonded phase substrate to which the species in the sample are attracted by varying degrees. As compounds are moved through the column by a carrier gas such as helium, the attraction of the substrate on the column provides resistance to this movement based on chemical attraction. Columns containing various substrates are employed for different separation, based on different chemical affinities. Chemical properties such as molecular weight, size, and polarity of the sample components to be analyzed are considered in determining which type of column to utilize. This affinity can be controlled by temperature, and thus columns are housed in temperature-controlled ovens. The oven that contains the column is heated as the sample passes further through the column providing intraspecies separation but controlling interspecies separation. At the end of the column the properly separated compounds pass through a detector that records the data. Each column in the Blake/Rowland lab is coupled with an **Electron Capture Detector (ECD)**, **Quadrupole Mass Spectrometer Detector (MSD)**, **Flame Ionization Detector (FID)**. These various detectors specialize in quantifying specific groups of compounds, similarly to how a person’s senses respond to different stimuli. Thus, different detectors are employed for different columns. A column that preferentially separates hydrocarbons is coupled with an FID, which essentially counts the carbon atoms that pass through it. As can be seen, the pairing of column and detector is important to data quality and the Blake/Rowland group has five different column detector combinations that analyze each **volatile organic compound (VOC)** sample. The Blake/Rowland group has been analyzing samples and refining system parameters since the 1970s and was recently recognized as the top lab for nonmethane hydrocarbons (NMHCs) in the National Science Foundation NSF-funded **nonmethane hydrocarbon intercomparison experiment (NOMHICE)** study which compared analysis by 30 International groups.

Gas Collection

The Blake/Rowland group has used sampling canisters (currently seventh generation) in the analysis of gases from various regions around the world since the 1970s. Samples are collected in evacuated two-liter (2L) **stainless steel canisters** through a Swagelock valve (Figure 8.1.1). As the valve is opened at the sampling sight, the surrounding air fills the evacuated canister and the valve is closed, sealing the sample until analysis (Figure 8.1.2). Canisters are treated and tested continuously to ensure that they are inert to the quantified gases. The thousands of canisters in the group’s inventory are constantly shipped around the world for sampling and back to the lab for analysis.

For this project samples were collected on site using 2L stainless steel canisters fitted with a 6-foot stainless steel extension tube attached to the Swagelock valve by an ultra-torr union. The extension was inserted into a hole in the coal area and the valve was opened at which point a sample from the coal bed rushed into the evacuated canister. Samples were taken on site and subsequently returned to the lab for analysis.



Figure 8.1.1. Sampling canister.



Figure 8.1.2. Canister evacuation pump-out vacuum line.

Sample Analyses

The Blake/Rowland group's comprehensive systematic analysis of air samples is accomplished by analyzing a portion of the 2L sample contained in each canister through three separate systems (Figure 8.1.3). The first system quantifies methane (CH_4), the second quantifies carbon monoxide and carbon dioxide (CO and CO_2), and the third measures 50–100 VOCs and all the rest of the compounds. The reason for using multiple systems to measure certain gases from each sample is that **background concentrations** of CO , CO_2 , and methane are so much higher than most gases quantified and that analysis of these gases in the same sample would be off the scale at which other compounds need to be measured. The Blake/Rowland group specializes in measuring gases of concentration levels from parts per million to parts per trillion.

Methane System

The most basic system configuration is the **methane system**; samples are run on this system first. For this system about 1.0 cm^3 of the sample is loaded into the 2.0 cm^3 sample loop, then injected into the column for separation.



Figure 8.1.3. Gas-handling manifolds for the three analytical systems.

Methane concentrations are high enough (parts per million level) to measure with a smaller sample size than the other systems require. The FID at the end of the column responds to carbon and outputs the electrical response to **Chromeleon Chromatography software** which generates a **chromatogram**. Because the concentrations of methane are high compared to other hydrocarbon species in the sample, these other compounds are separated on the column but do not show up on the chromatogram [since they are about 1000 times less concentrated (parts per billion)].

CO/CO₂ System

The second system used in the group's chromatographic analysis is the **CO/CO₂ system**. This system is really two systems with samples loaded through a common port. The CO₂ portion of this system works the exact same way as the methane system but with a larger sample size of about 10 cm³ being loaded into a 30 cm³ sample loop. This sample is injected into the column and output to a TCD and the response is sent to Chromeleon software which outputs a chromatogram.

The CO unit of this system uses a 10 cm³ sample size on a 20 cm³ sample loop which is injected into a 5 meter 1/4" molecular sieve column. This system also incorporates a **catalyst** (which O₂ destroys) to change the CO to methane because the FID at the end of the column does not count carbon atoms in the CO form. By converting the carbon from CO to CH₄, the quantity of carbon is maintained. Therefore, the column outlets to a four-port switching valve and after 3.5 minutes of venting to the room (sufficient time to allow O₂ to completely elute from the column) the switching valve redirects the flow to a nickel oxide catalyst maintained at 285°C bathed in ultra high purity (UHP) hydrogen. Upon passing through the catalyst CO is converted to methane which is then directed to the FID. Detector output is sent to Chromeleon software and converted to chromatogram form.

VOC System

The third analytical system is set up in much the same way as the other two. However, because more volatile compounds such as N₂, O₂, Ar, CH₄, and CO are orders of magnitude more concentrated than the compounds that the **VOC system** is designed to measure, these compounds are removed from the sample by implementing preconcentration inside the sample loop (Colman et al., 2001). A 120 cm³ sample is drawn through the sample loop that is submerged in a liquid nitrogen dewar (Figure 8.1.4). The less-volatile compounds adhere to the cold glass beads (which provide surface area for the compounds to adsorb onto), while the volatile compounds do not adhere to the beads (due to their low boiling points) and are subsequently pumped out by a vacuum pump. Once a known volume is trapped, the external liquid N₂ dewar is replaced with hot water and the compounds are volatilized and ready for injection into the columns Figure 8.1.5.

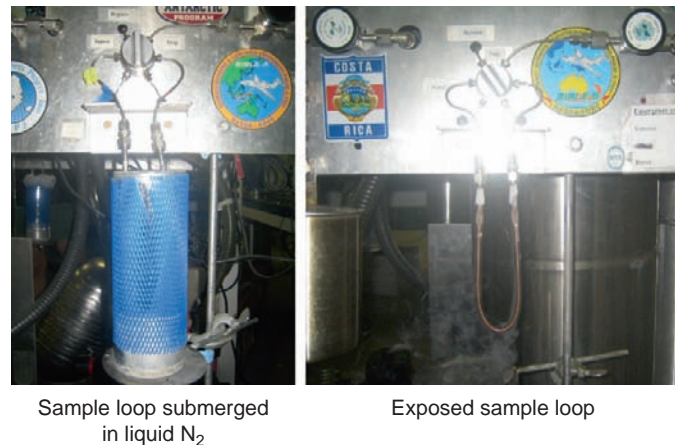


Figure 8.1.4. Sample loop for VOC system.

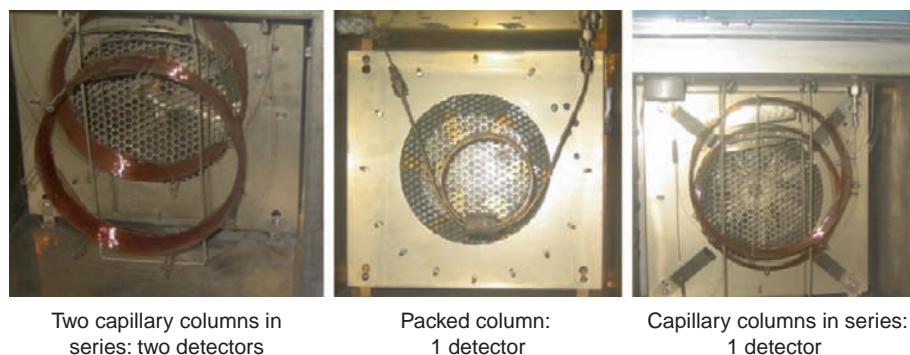


Figure 8.1.5. Columns in various GC ovens.

Once the sample is prepared, it is transported by a helium carrier gas through a junction which reproducibly divides the sample into five streams. Each of these streams is sent through one of the system's five columns. The ratio of sample sent through each column is set to maximize detection of compounds for each of the five detectors.

After being separated within the column, the groups of compounds from the sample are measured by the detector at the end of the respective columns. This response of the detector is then integrated by Chromeleon chromatography software as a chromatogram. In the form of a chromatogram, the compound groups appear as a peak when plotted against time. A typical chromatogram is shown in Figure 8.1.6.

The sample percentage sent to each of the 5 columns is:

GC-1:

Durabond-5 (DB-5)RESTEKECD 6.8%

Durabond-5MS (DB-5MS)MSD 10.1%

GC-2:

RESTEKECD 7.2%

Porous layer open tubularDurabond-1 (DB-1)FID 60.8%

GC-3:

DB-1FID 15.1%

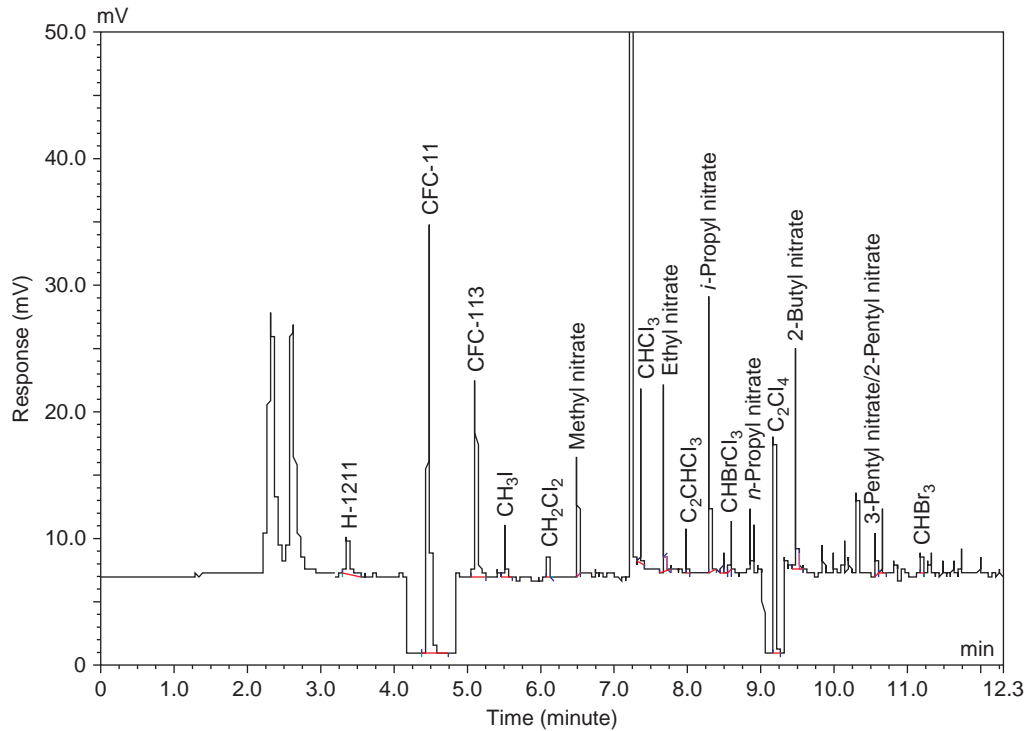


Figure 8.1.6. Chromatogram from an electron capture detector.

DB-5→RESTEK is a 50 m × 0.25 mm id DB-5 column connected to a 5 m × 0.25 mm id RESTEK 1701 column

DB-5MS is a 50 m × 0.25 mm id DB-5MS column

RESTEK is a 50 m × 0.25 mm id RESTEK column

PLOT→DB-1 is a 30 m × 0.52 mm id PLOT column connected to a 3 m × 0.25 id DB-1 column

DB-1 is a 50 m × 0.25 mm id DB-1 column

Quality Control: Standards

As conditions in and around the system change, precision analysis suffers. Because of this the Blake/Rowland group has adopted several methods of monitoring these changes as they happen. One method of quality control used by the group is running standardized samples through the system after every four field samples. The group makes its own working **standards** at White Mountain Research station located in the Sierra Nevada Mountains in California (altitude 10,500 ft). This air is too clean for some cases so selected gases are added to the cylinder in the lab so that concentrations in the cylinder are representative of gas concentrations that are measured. Precalibrated standards are also used for calibrating the systems and are purchased from analytical suppliers. The standards used with the field samples are as representative as possible of what compounds are expected to be measured in the samples. The standardized samples (Figure 8.1.7) contain known amounts of compounds and the systems quantitative analysis can be weighed against these known values to illuminate changes in system sensitivity. Thus, compound retention times (time of elution) in the resulting chromatogram can be compared to previous standards to determine a shift in retention time of the system.



Figure 8.1.7. Whole air standard used for calibration on the VOC system.

Modifying

A second method of quality control is human oversight of the computer software's identification of compounds as peaks on a chromatogram. This technique is called **modifying** and is very labor intensive but necessary for high-quality data. This process involves an individual reviewing every peak quantified. The computer assigns peaks based on known standard retention times and if a systematic retention time shift occurs the peak is usually missed or incorrectly assigned by the computer software. This human oversight is vital to high-quality data and illuminates the intuitive limitations inherent in extremely advanced scientific instruments and computer software.

Important Terms

background concentrations

catalyst

chromatogram

Chromeleon chromatography software

CO/CO₂ system

columns

electron capture detector

flame ionization detector

gas chromatography

methane system

modifying

nonmethane hydrocarbon intercomparison experiment

quadrupole mass spectrometer detector

stainless steel canisters

standards

thermal conductivity detector

VOC system

volatile organic compound

References

Colman, J.J., Swanson, A.L., Meinardi, S., Sive, B.C., Blake, D.R., Rowland, F.S., 2001. Description of the analysis of a wide range of volatile organic compounds in whole air samples collected during PEM-Tropics A and B. *Anal. Chem.* 73 (15), 3723–3731, <http://pubs.acs.org/cgi-bin/abstract.cgi/ancham/2001/73/i15/abs/ac010027g.html>

 **WWW Addresses: Additional Reading**

- (1) **The Rowland–Blake Group: Analytical Atmospheric Chemistry**
<http://www.physsci.uci.edu/~rowlandblake>

CHAPTER 9

Gas Vent Mineralization and Coal Combustion



Acicular sulfur crystals nucleated around a gas vent in a burning-culm bank, Witbank coalfield, South Africa. Crystal growth occurred during a 2-week period. The gas temperature just inside the vent on the day of collection, August 10, 2004, was 37°C. *Photo by Glenn B. Stracher, 2004.*

CHAPTER CONTENTS

9.1 The Origin of Gas Vent Minerals

- Introduction
- Mineral-Forming Processes
- Isochemical Mineralization
- Mass Transfer Mineralization
- Discussion

9.2 Sample Collecting and Field Data

- Introduction
- Safety Precautions
- GPS and Temperature Measurements
- Mineral and Rock-Collecting Techniques
- Gas-Collecting Techniques
- In Situ Chemical Analyses
- Discussion
- Acknowledgments
- Important Terms
- References
- WWW Addresses: Additional Reading



9.1. The Origin of Gas Vent Minerals

Glenn B. Stracher

Acicular Sulfur Crystals, Witbank Coalfield, South Africa.

From Stracher (2007) with modifications, reprinted with permission of the Geological Society of America. Photo by Glenn B. Stracher, 2004.

Introduction

Gas vents associated with coal fires are circular to semicircular conduits in the earth or openings at its surface through which the by-products of coal combustion are transported. **Gas fissures** associated with such fires are elongate cracks in the earth or at its surface through which these by-products pass.

Near or at the surface, these vents and fissures are often encrusted with minerals commonly assumed to form by the condensation of coal-fire gas. As the gas is exhaled at the surface, it cools and subsequently one or more minerals may sublime or a liquid may form which, when further cooled, solidifies to form a mineral assemblage (Lapham et al., 1980; Stracher, 1995; Witzke, 1997a). These same reactions may also occur at volcanic gas vents (Stoiber and Rose, 1974), at times resulting in the formation of mineral assemblages similar to those associated with coal-fire gas. However, other complex thermochemical processes involving multiple reactions may be responsible for the gas-related origin of minerals at either type of vent.

The purpose of this section is to delineate the processes by which mineral assemblages form at or in the vicinity of coal-fire gas vents and ground fissures as a consequence of combustion. For the sake of brevity, reference herein is made to gas vents only, since analogous processes occur at both vents and fissures.

Mineral-Forming Processes

Isochemical and mass transfer processes occur in association with the crystallization of a mineral assemblage at a gas vent. As described below, these processes may proceed along a variety of reaction paths.

An **isochemical mineralization** process herein refers to one in which the bulk composition of a mineral is equivalent to that of the original (primary) gas phase from which it formed at a coal-fire vent. A **mass transfer mineralization** process is one in which the bulk composition of the mineral is different than that of the primary gas phase due to the transfer of mass into or out of this phase or a liquid condensed from the phase, via chemical reactions. The reaction path followed during the crystallization of a mineral assemblage at a coal-fire gas vent depends on one or more combinations of the following variables (Stracher, 1995; Stracher et al., 2005a): gas and substrate chemistry, presence or absence of aqueous solutions, pressure and exhalation temperature of the gas, and temperature of the substrate encountered by the gas during exhalation at the surface.

Isochemical Mineralization

Condensation is the isochemical process whereby a gas undergoes a change in state during cooling and transforms directly into a liquid or a solid (Hawley, 1971, p. 231). Two condensation-related processes,

discussed below, may occur during the crystallization of minerals derived from coal-fire gas. The first, sublimation, is strictly a condensation process. The second involves condensation to a liquid followed by solidification (freezing).

Sublimation occurs when a gas component exhaled from a coal-fire vent rapidly cools below the liquid to solid transformation temperature (supercools) and subsequently condenses to a solid without an intervening liquid state (Hawley, 1971, p. 832). Supercooling occurs in response to a temperature gradient between the gas and the substrate (heat sink) encountered by the gas at the surface. Heat sinks include rock, sediment, vegetation, the atmosphere, etc. (Stracher, 1995). During sublimation, the gas isochemically condenses to a mineral. The process is represented by the exothermic reaction



where X(g) and X(s) designate an element or compound in the gas and solid states, respectively. If a mineral encrusting a vent formed by sublimation, then the chemical composition of the mineral and the substrate on which it sublimated are independent of one another. In other words, no mass transfer occurs between the sublimating gas and the substrate as solidification occurs. Evidence for sublimation includes mineral encrustations whose elements are contained in the gas and euhedral crystals as well as crystal faces that do not touch, suggestive of growth in a nonrestrictive environment (Stracher et al., 2005a).

A variety of minerals are reported as the sublimation products of coal-fire gas including hydrous sulfates (Lausen, 1928), downeyite (SeO₂) (Finkelman and Mrose, 1977), orthorhombic sulfur (Stracher, 1995), coccinite (HgI₂) (Witzke, 1997b), and salammoniac (NH₄Cl) (Stracher et al., 2005a). At first glance, minerals encrusting gas vents may appear to be sublimation products of the gas, especially if the minerals appear powdery and the substrate from which the minerals were collected appears unaltered. This was the case in a recent study by Stracher et al. (2005a) of mineral assemblages collected from the Wuda coalfield, Inner Mongolia. The gas-vent assemblages occurred on quartzofeldspathic sand and sandstone that appeared chemically unaltered in the field (Figure 9.1.1). However, X-ray diffraction, energy dispersive spectrometry, gas chromatography, and micro-Dumas analyses coupled with

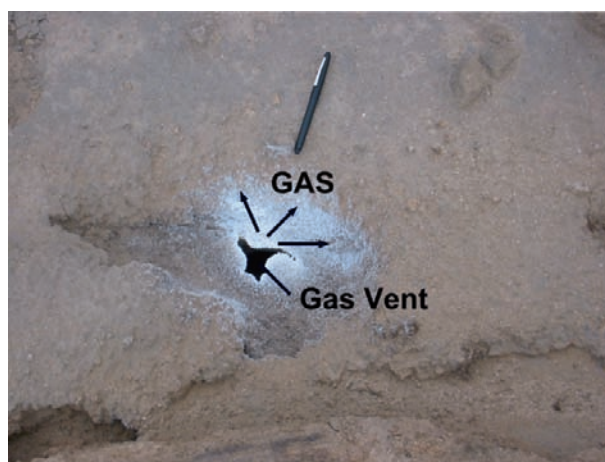


Figure 9.1.1. Alunogen, coquimbite, voltaite, and an unidentified phase comprise the white-colored mineral assemblage at a gas vent in the Wuda coalfield, Inner Mongolia. The underlying substrate is quartzofeldspathic sand and sandstone that appeared chemically unaltered in the field. Sample analyses and SEM imaging suggested otherwise. The distribution of the assemblage suggests mineralization occurred in response to a gas moving toward the upper right in the photo. From Stracher et al., 2005a, with permission of the Mineralogical Society of America.

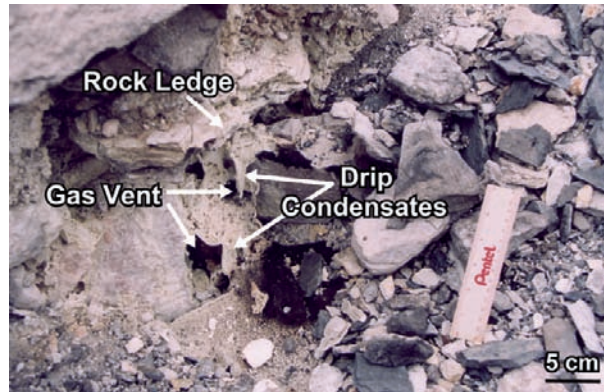
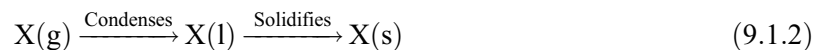


Figure 9.1.2. GLS process suggested by unidentified “drip condensates” on a rock ledge overhanging a gas vent at the Centralia mine fire, Pennsylvania. The drip texture suggests that a gas component exhaled from the vent condensed to a liquid that subsequently solidified. Photo by Glenn B. Stracher, 2005.

textural evidence from scanning electron microscope (SEM) images revealed that a more complex sequence of events occurred. These included condensation, hydrothermal alteration and crystallization from solution, fluctuating vent temperatures, boiling, and dehydration reactions. Consequently, it is possible that minerals originally described as sublimates may have formed by one or more complex thermochemical process.

Gas-Liquid Solidification (GLS) occurs when a gas component first condenses to a liquid and then as cooling continues the liquid solidifies. Drip (stalactite) and flow (ripple) textures observed on rocks overhanging gas vents or on nearby rock facings are evidence for GLS (Figure 9.1.2). Because they resemble dripstones and flowstones found in caves, mineral assemblages with drip and flow textures are aptly called **drip condensates** and **flow condensates**, respectively. An isochemical GLS process is represented by the exothermic reaction

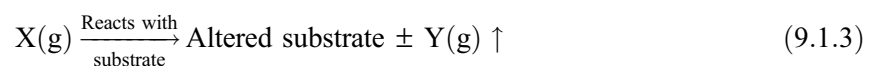


where X(l) designates an element or compound in the liquid state.

Mass Transfer Mineralization

Mineralization processes at coal-fire gas vents that involve mass transfer are more complex than isochemical ones. These include a variety of reactions, likely more common than previously documented, based on field evidence and laboratory observations as discussed next.

Gas-Altered Substrate (GAS) occurs when a hot gas component(s) exhaled at a vent reacts with the substrate and alters it (Figure 9.1.3). This process is analogous to pneumatolytic alteration associated with igneous activity. Consequently,



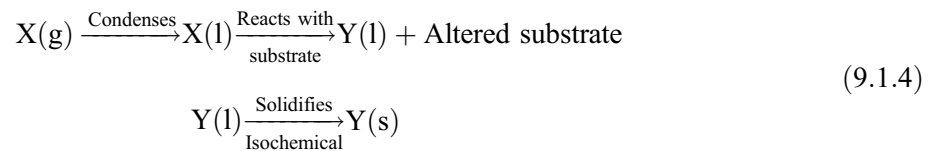
where Y(g) is the composition of the remaining gas. Clinker, rock baked and oxidized by combustion, is suggestive of GAS or other substrate-altering processes, as discussed below.

Gas-Liquid-Altered Substrate (GLAS) occurs when a liquid condensed from the gas reacts with the substrate and chemically alters it, resulting in the crystallization of minerals on the altered substrate. For example, if a liquid



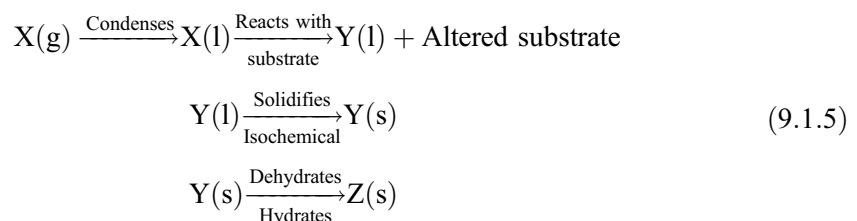
Figure 9.1.3. Possible outcrops of GASs. (A) Red clinker (light color) surrounding an anthracite coal-fire gas vent at the Centralia mine fire, Pennsylvania. Hot gas altered the Pennsylvanian Llewellyn formation (black shale) surrounding the vent. Glenn B. Stracher is measuring the vent temperature with a thermocouple probe. A LaMotte hand pump on the ground was used to collect a gas sample for analysis. (B) Baked Ferron clinker (sandstone) and red-black nonmarine shale within the Ferron Sandstone Member of the Mancos Shale, Emery coalfield, Utah. Note the reverse fault in the Ferron sandstone and its collapse into the area where the I coal bed completely burned, at knee level to G.B. Stracher. From Stracher et al., 2006, photo A; 2005b, photo B with modifications, permission of the Geological Society of America.

condensed from the gas reacts with the substrate, thereby altering the chemical composition of the liquid (and substrate) prior to mineralization, the reaction path may be



where the reaction of $X(l)$, perhaps an acidic solution, with the substrate forms a different liquid $Y(l)$ which then isochemically solidifies to form the mineral $Y(s)$. On the microscopic scale of observation, the former presence of a liquid $Y(l)$ may be revealed by vesicles observed in SEM images (Figure 9.1.4; Stracher et al., 2005a) or mineral chemistry, as discussed below.

If $Y(s)$ is hydrous and it dehydrates or hydrates, perhaps due to a temperature increase or decrease, respectively, at the vent, then expression 9.1.4 becomes



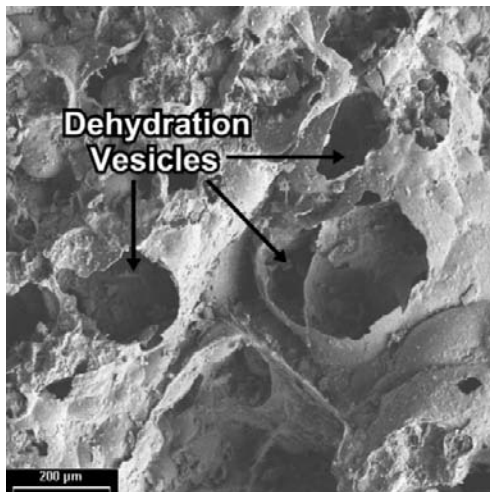
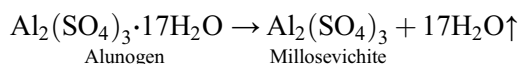


Figure 9.1.4. GLAS process revealed by a cryptocrystalline mass of millosevichite and alunogen from a gas vent in the Wuda coalfield, Inner Mongolia (SEM). Vesicular texture and Al ions in the mineral assemblage, collected from a quartzofeldspathic sandstone substrate, suggest reaction (9.1.5) occurred, as discussed in the text. From Stracher et al., 2005a, with permission of the Mineralogical Society of America.

where the mineral Z(s) is the dehydration or hydration product of Y(s). In the Wuda coalfield of Inner Mongolia, a sample encrusting a gas vent was collected from quartzofeldspathic sandstone. The sample is vesicular (Figure 9.1.4) and contains both alunogen, $\text{Al}_2(\text{SO}_4)_3 \cdot 17\text{H}_2\text{O}$, and millosevichite, $(\text{Al})_2(\text{SO}_4)_3$. The vesicles, Al ions likely acquired from the sandstone substrate, and the simultaneous occurrence of these minerals suggest that process (9.1.5) occurred at the vent (Stracher et al., 2005a). The occurrence of both millosevichite and alunogen and the vesicles suggest the dehydration reaction



The vesicular texture may have developed as liquid water or water vapor escaped from the assemblage. In addition, the incomplete breakdown of alunogen, evident from its occurrence with millosevichite, is the result of a temperature decrease subsequent to the increase that promoted dehydration. As suggested by Stracher et al. (2005a), the fluctuating temperatures and concomitant effects on the assemblage are accounted for by variations in combustion and atmospheric conditions and possibly removal (temperature decrease) of the assemblage from the vent during sample collecting. It is possible that the reaction path involving the vesicular assemblage found at Wuda is more complicated than that presented above. For example, millosevichite may have initially formed at the vent and in the presence of water vapor exhaled at the surface or atmospheric moisture, hydrated to alunogen as the vent temperature fell, followed by the incomplete dehydration of this mineral as described above.

Gas-Liquid Precipitation (GLP) occurs when a gas first condenses to a liquid from which a solid precipitates, followed by solidification of the remaining liquid. Described by Wagner and Ellis (1964), the first and only recorded *natural* occurrence of this process (Figure 9.1.5) was observed by Finkelman et al. (1974) in association with burning anthracite in Forestville, Pennsylvania. According to Finkelman et al. (1974) and Lapham et al. (1980), sulfur droplets condensed from a $\text{S}_2(\text{g})$ component in the anthracite gas. The droplets then acted as a catalyst and absorbed Ge from the gas to form a S-Ge solution. Once the solution was saturated in Ge, germanium sulfide (GeS_2) precipitated. The process resulted in the nucleation of elongate GeS_2 crystals capped by bulb-like amorphous sulfur, solidified from the remaining liquid sulfur, S(l), droplets at the end of the GeS_2 crystals. The process is summarized by the reactions

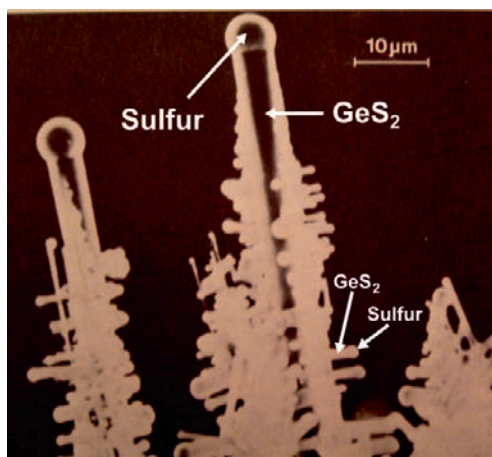
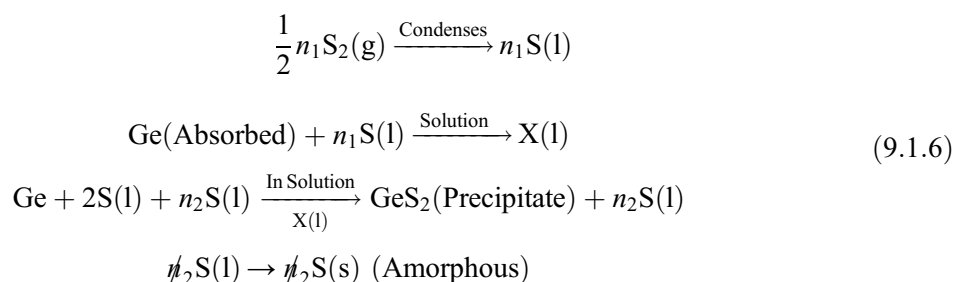


Figure 9.1.5. GLP process observed in an SEM image of elongate GeS₂ crystals capped by a bulb of amorphous sulfur. Note the smaller rods of GeS₂ capped by the small sulfur bulbs. From Mineral Resources Report 78, Lapham et al., 1980 with modifications, permission of the Pennsylvania Geological Survey.

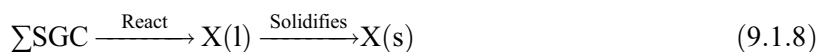


where X(l) designates the liquid phase containing n_1 moles of S(l) and absorbed Ge and the total number of moles of S(l) in X(l) is $n_1 = 2 + n_2$ with 2 being the number of moles of S(l) that react with each mole of absorbed Ge to form GeS₂ and n_2 designating the *remaining* number of moles of S(l) from X(l) that condense to amorphous S(s).

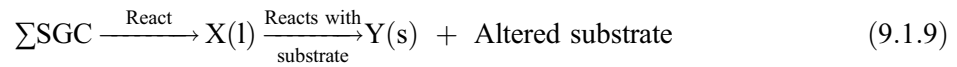
Gas Reaction ± Liquid-Solidification (GRLS) is a hypothetical mineral-forming process initiated by gas reactions during or after exhalation at the vent. Such reactions, however, are undocumented in the literature. GRLS consists of one or more of the steps in reactions (9.1.1) through (9.1.5). Many gas-vent assemblages attributed to sublimation may have actually formed by GRLS. For example, salammoniac (NH₄Cl) occurs globally in association with coal fires as well as volcanic vents and burning oil shale. It is often cited in the literature as a sublimate (Cole, 1975; Gaines et al., 1997; Lapham et al., 1980; West, 2001). Textural evidence offered in support of this includes euhedral crystals that do not share faces (Stracher et al., 2005a). Although salammoniac contains elements commonly found in the components of coal-fire gas, the salammoniac molecule is absent from gas analyses. Consequently, salammoniac may be the solid reaction product of N-, H-, and Cl-bearing gas components. In general, the exothermic reaction for such mineralization processes is



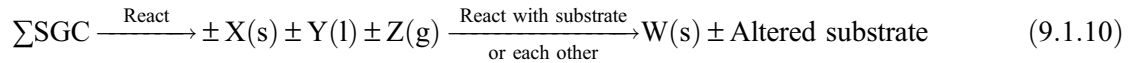
where SGC denotes select gas components that react to produce an element or compound X(s), like salammoniac. This is not sublimation in the strictest sense of the definition; note that the process is not isochemical. Additional plausible, although also undocumented GRLS processes include



where the liquid reaction product X(l) solidifies to X(s);



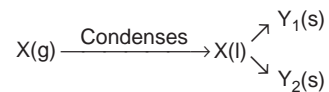
where X(l) reacts with the substrate to form the solid Y(s); and



where the solid, liquid, and gas reaction products X(s), Y(l), and Z(g) react with the substrate or each other to form the solid W(s).

Discussion

The above reactions exemplify mineral-forming processes at gas vents, they are not all inclusive, and additional processes are possible. As a simple example, consider reaction (9.1.2) rewritten as



In this case, subsequent to condensation, two solid phases Y₁(s) and Y₂(s), perhaps in a drip or flow condensate, nucleated simultaneously from a liquid phase at its eutectic temperature.

The absence of a mineral assemblage at or in the vicinity of a coal-fire gas vent does not imply that it never formed. Many assemblages consist of water-soluble powdery materials that are easily dissolved by rainwater or eroded by wind. Consequently, if the mineralized by-products of combustion are eroded, it may be extremely difficult to determine whether an altered substrate formed by GSA, GLAS, or GRLS.

Determining the reactions in the SGC of a coal fire during and after exhalation is a formidable task, yet to be performed. As burning proceeds, gas composition fluctuates in accordance with chemical diversity in the burning coal, as well as in the sediment, rock, and aqueous solutions encountered by the gas *en route* to the surface. Exchange reactions between the gas, sediment, rocks, and solutions continuously change gas chemistry, thereby influencing, along with temperature and SGC partial pressures, the mineral assemblages that crystallize in association with the gas.

The identification of trace elements in minerals formed as a consequence of coal combustion may reveal certain minerals that are vectors for the transmission of toxins to humans by inhaled dust particles or even by food grown in soils that contain these minerals. The proliferation and catastrophic effects of coal fires subsequent to the industrial revolution in Europe include trace elements that promote air, soil, and water pollution (Stracher and Taylor, 2004). These pollutants have destroyed natural habitats; have killed people; have forced communities to relocate; and are accountable for human diseases including hyperkeratosis (arsenic poisoning), dental and skeletal fluorosis (osteosclerosis), thallium poisoning, lung cancer, and pulmonary heart disease (Johnson et al., 1997, p. 19; World Resources Institute, 1999, pp. 63–67; Finkelman et al., 1999, 2001, 2002; Finkelman, 2004).



9.2 Sample Collecting and Field Data

Glenn B. Stracher (left) and Steve Renner, South Cañon Number 1 Coal Mine Fire, Glenwood Springs, Colorado.

From Stracher (2003) with modifications, reprinted with permission of the Center for Applied Energy Research, University of Kentucky, Lexington. Photo by Janet L. Stracher, 2004.

Introduction

Wherever coal is **strip** (open pit) or **deep mined**, the potential for fire exists. Coal fires associated with the **abandoned workings** or **workings** of coal mines are reported from mining areas around the world (Prakash et al., 1999; Stracher and Taylor, 2004). Surface expressions of underground coal fires observable in the field include baked rocks, areas of dead vegetation, land subsidence, and gas vents and fissures (Stracher, 1995; Gupta and Prakash, 1998).

Coal-fire gas exhaled from vents and fissures and minerals derived from cooling gas reveal important information about the chemical composition of burning coal and the possible interaction of the gas with rock and water on its way to the surface prior to exhalation. The chemistry of these minerals and the exhaled gas is reflective of elements and compounds that may be released as pollutants into the atmosphere, soil, streams, or ground water. Such pollutants may be responsible for a variety of environmental and human health problems including the destruction of floral and faunal habitats (Stracher, 2002; Stracher and Taylor, 2004), stroke and pulmonary heart disease (World Resources Institute, 1999, pp. 63–67), and arsenosis and fluorosis (Finkelman, 2001). Consequently, the study of coal-fire gas and associated minerals can be critically useful in understanding environmental pollution problems associated with coal-mine fires.

Safety Precautions

Safety precautions are essential in the field when collecting minerals derived from coal-fire gas or the gas itself. The most dangerous impediments when sampling from active vents and fissures are toxic vapors, heat, and subsidence. Figure 9.2.1 illustrates all three of these at the southern end of Centralia, Pennsylvania. The Centralia mine fire began in and has been burning since 1962, when an abandoned strip-mining cut was ignited to reduce its volume and control rodents. The Buck Mountain anthracite seam in the landfill ignited and the fire spread to abandoned underground coal mine tunnels (DeKok, 1986, p. 20; Geissinger, 1990). For safety, it is best to never collect alone. In addition, a walking stick used to test the ground ahead of oneself while heading toward a vent or fissure is a wise precaution against subsidence. One should never venture, even with a field assistant and gas mask, into an area completely engulfed in smoke like the valley in the upper right-hand corner of Figure 9.2.1. The consequence of becoming disoriented could prove fatal. Once a vent or fissure is found with material worthy of collection, gloves may be necessary to avoid getting burned when working at or near the collection site (Figure 9.2.2). Extreme caution is necessary to avoid breathing as much coal gas as possible, and a gas mask should be worn where fresh air is not immediately nearby or when sampling requires an extended period of time surrounded by toxic vapors. I have recorded temperatures and collected gas and gas-associated minerals from vents and fissures by holding my breath (Figure 9.2.2) and then “coming up for air” after moving to a location several meters away with adequate ventilation. For safety sake, someone was always standing nearby to watch my activities. This is advisable because the temptation to breathe and doing so while collecting data could be dangerous while surrounded by thick smoke and toxic gas. Consequently, I wear a gas mask now when I must work close to a vent.

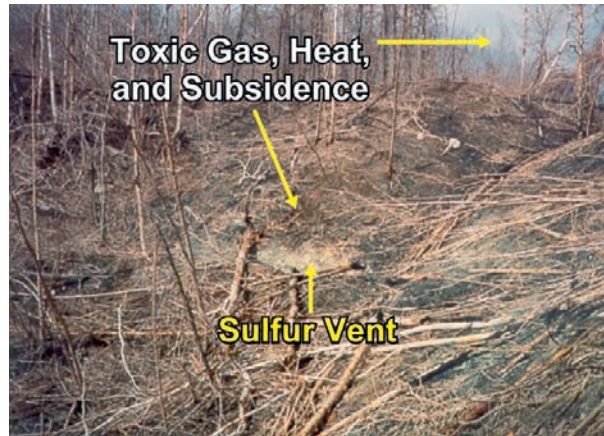


Figure 9.2.1. Hazards of collecting coal-fire minerals (sulfur in this case) and gas observed at the southern end of Centralia, Pennsylvania. Note subsidence around the sulfur vent, extending into the smoke-filled valley in the upper right corner of the photo. Field of view is ~35 m. Photo by Glenn B. Stracher, 1995.



Figure 9.2.2. Hazards associated with collecting coal-fire minerals and gas. Glenn B. Stracher is holding his breath to avoid inhaling toxic fumes. Note the insulated leather glove used to protect his right hand during insertion of a thermocouple temperature probe into a coal-fire vent: adjacent to a closed section of Route 61 on the eastern end of Centralia, Pennsylvania. The white Teflon[®] tube near the bottom of the photo was used to extract gas out of the vent with a hand pump (see text). Gas temperature was 126.2°C. CO and CO₂, measured with Dräger tubes, were highly toxic at 1000 and 2200 ppm, respectively. The nucleation products (probably minerals), associated with coal-fire gas from this vent; have yet to be identified. Photo by Janet L. Stracher, 2003.

GPS and Temperature Measurements

Two necessary instruments used to record field data at a gas vent prior to sampling include a handheld **Global Positioning Satellite (GPS)** unit for documenting sample location and a high-temperature **thermocouple probe** for measuring gas temperature inside the vent. These instruments are easy to learn how to use and are manufactured by a number of companies. A Pasco[®] physics thermocouple probe with a digital temperature display and a Magellan[®] handheld GPS unit are illustrated in Figures 9.2.3 and 9.2.4, respectively. The Pasco[®] instrument consists of a digital gauge to which a high-temperature stainless steel thermocouple probe is attached. The stainless steel probe is inserted into a gas vent or fissure and once the temperature stops increasing on the digital display screen of the gauge, the value of the gas temperature is recorded. Similar probes are offered by other manufacturers.

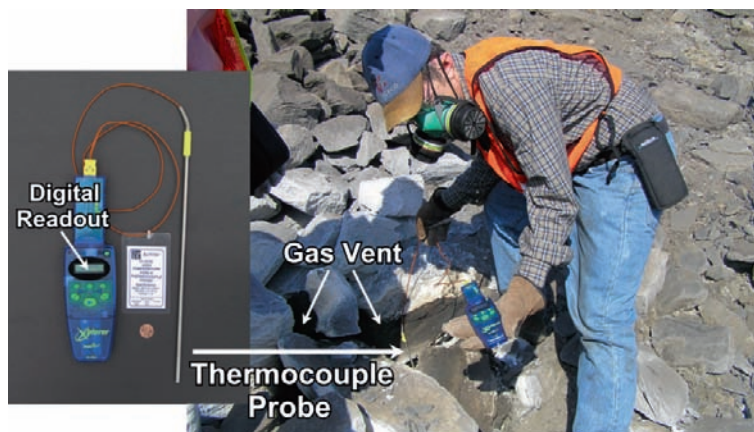


Figure 9.2.3. G.B. Stracher using a Pasco[®] physics (Roseville, California) Explorer data logger and high-temperature type K thermocouple probe at a South African mine fire. Gas temperature at this vent was 320°C and climbing fast when Stracher had to remove his hand, with an insulated leather glove, from the vent to avoid being burned by the intense heat. The heat also partially melted the insulation on the wire connecting the digital readout gauge to the stainless steel probe. Encasing the wire in high-temperature insulation may have prevented this from happening. From Stracher et al., 2005b, with permission of the Geological Society of America.



Figure 9.2.4. Magellan[®] handheld GPS unit. This model is waterproof and includes a backlit screen for readability on a cloudy day or after sunset. Similar units are offered by other manufacturers. Photo by Glenn B. Stracher, 2009.

Mineral and Rock-Collecting Techniques

The most difficult part of collecting the mineral by-products of combustion associated with coal-fire gas for identification and chemical analysis is to avoid contaminating the minerals with the soil or rock substrate they nucleated on. X-ray diffraction and electron probe analysis of the minerals are then easier to interpret. One method for collecting delicate or small amounts of these minerals is to scrape them off of the underlying substrate into a vial using a metal spatula and laboratory scoop (Figure 9.2.5). Some separation of the



Figure 9.2.5. Tammy P. Taylor from the Chemical Division of Los Alamos National Laboratory, using a spatula and scoop to scrape a mineral off of rock and soil and into a plastic vial, while using caution to minimize contamination from these substrates. The sample was identified by X-ray diffraction as orthorhombic sulfur-8. It was collected from the Southern Ute Indian Reservation near Durango, Colorado, where an underground coal fire is thought to have been ignited by a forest fire started by lightning. Photo by Glenn B. Stracher, 2001.

minerals from contaminants may still be necessary, and it is absolutely essential for wet chemical analysis. On one occasion, I was sent several beautiful samples from coal fires in East Kalimantan, Indonesia. Numerous coal fires in Indonesia started when fire was used to clear forested areas for rubber, oil palm plantations, pulpwood, and farming (Whitehouse and Mulyana, 2004). The specimens I received were never separated from the soil they nucleated on. By the time they reached my lab, the minerals from the coal-fire gas were completely pulverized and mixed with the soil, rendering separation and identification impossible. Another useful method for collecting minerals formed from coal-fire gas is to “force” the gas to “condense” onto a substrate placed partially over a vent or fissure. Unglazed ceramic tiles were successfully used in East Kalimantan for this purpose (Figure 9.2.6A), and minerals appeared within 2 weeks on the sides of the tiles



Figure 9.2.6. Collecting coal-fire minerals from unglazed ceramic tiles emplaced over coal-fire gas vents: (A) East Kalimantan, Indonesia and (B) Centralia, Pennsylvania. The minerals on the bottom of the Indonesian tile (not visible in the photo) that were identified by X-ray diffraction are gypsum and sulfur. The tile in Centralia was removed multiple times from the vent and tossed on the ground by visitors to the fire, rendering the collection procedure unsuccessful. Photos by (A) Asep Mulyana, 2002 and (B) Janet L. Stracher, 2003.

exposed to the gas. Several tiles were sent to my lab, where the minerals were removed and identified by X-ray diffraction as gypsum and orthorhombic sulfur-8. In addition, several tiles were emplaced in 2004 and 2005 over gas vents associated with the Centralia fire (Figure 9.2.6B). The results were unsuccessful, as the tiles were removed and tossed on the ground by visitors to the mine fire. Furthermore, the minerals collected from such tile experiments are now questionable in origin. They may not actually be condensates but instead the reaction products of gas with the tile substrate, as was analogously demonstrated by Stracher et. al. (2005a) for coal-fire minerals collected from a quartzofeldspathic sandstone substrate in the Wuda coalfield of Inner Mongolia.

Gas-Collecting Techniques

For complete laboratory analysis of gas exhaled from coal-fire vents and fissures, two collection techniques have been used. The first technique, no longer used, uses a **Tedlar[®] gas bag** made of Dupont[™] Teflon[®] connected to a LaMotte (or other manufacturer) air sampling pump and Teflon[®] intake and exhaust lines (Figure 9.2.7) for pumping gas out of a vent or fissure and into the collection bag. This pump illustrated delivers 50 ml per stroke and the bags hold 600 ml, so 12 strokes fill a bag. The bags have a swage lock used to seal the gas inside. A circular disk 3 mm in diameter on the side of the bag is used to insert a hypodermic needle and extract the gas for analysis. If a vent is hot enough to melt the Teflon[®] tubing, gas may still be obtained by working quickly. Although glass storage vials are available, I initially used Tedlar[®] gas bags because they are compact to store and do not break easily.

The current collection technique for coal-fire gas uses stainless steel gas canisters and a stainless steel intake line (Figure 9.2.8). Laboratory tests have shown the stainless steel canisters to be more reliable than Tedlar[®] bags in that the bags tend to be permeable with respect to coal-fire gas over a storage period of 2 weeks or more.

The stainless steel canisters are evacuated; contain a valve on the top and a fitting into which one end of a stainless steel gas extraction line is inserted. The other end of the line is then inserted into a vent or fissure. When the valve is opened, a “whooshing” sound is heard as the coal-fire gas enters the canister. After the noise ceases, the valve is then closed and the sample collecting procedure is completed. The sample is then sent to a laboratory for gas chromatographic analysis.



Figure 9.2.7. Tedlar[®] bag, gas collection technique, Centralia, Pennsylvania. Glenn B. Stracher (right) pumping coal-fire gas from a vent through a Teflon[®] exhaust line into a Tedlar[®] gas bag, held by Tim Nolter (left). The intake line in Stracher’s left hand (leather glove) extends several centimeters down into the gas vent. The gas temperature measured there with a thermocouple probe was 363°C. From Stracher et al., 2007, with modifications, permission of the Geological Society of America.



Figure 9.2.8. Gas collection technique using a stainless steel canister, South Canyon, Colorado. G.B. Stracher extracting coal-fire gas from a borehole into a fire in an underground coal-mine tunnel at the South Cañon Number 1 Coal Mine fire, Colorado. Photo by Janet L. Stracher, 2004.

In Situ Chemical Analyses

A number of portable gas analyzers are available from scientific-instrument-distributing companies for use in the field, including instruments transportable by hand for quickly obtaining in situ analysis of a coal-fire gas component. One limitation of these analyzers is that only a limited number of gases (typically from one to five) may be analyzed for simultaneously. The accuracy of these instruments is a function of their design, and some are only useful for determining the lower and upper compositional limits of a gas component.

One such instrument is manufactured by the Dräger Company (Figure 9.2.9). The Dräger system consists of a hand-operated **Dräger pump**, **Dräger tubes** for the gases one wishes to analyze for, and a high-temperature gas extraction line made of flexible Teflon[®] or some other material. There is a button and counter on top of the pump. The counter records the number of times the pump has been pressed to extract a gas sample. Before a sample is extracted, the button is pressed to reset the counter to zero. A Dräger glass tube for the gas one wishes to analyze for is broken off at both ends with a small glass cutter on the bottom of the pump. Each tube has an arrow on it. The end of the tube that the arrow points to is then inserted into the pump. The flexible gas extraction line is next inserted over the other end of the Dräger tube. This gas extraction line is then inserted into a gas vent or fissure. Then, the pump is pressed by hand and released. This sucks gas from the opening through the flexible extraction line and into the tube. As the gas goes into the tube, it reacts with a chemical reagent in it. The reagent then changes color from the top to the bottom (end in the pump) of the tube, i.e., if the gas analyzed for is present within detection limits. Graduated scales on the side of the Dräger tube are used to read the gas concentration. If the pump is pressed 1 time, the scale labeled $n = 1$ is read; if the pump is pressed 10 times, the scale labeled $n = 10$ is read; and so on.

Several portable mercury analyzers on the market, including the RA-915+ **mercury analyzer** (Figure 9.2.10), are useful for the measurement of Hg emissions at coal-fire gas vents. This instrument is currently in use for studying

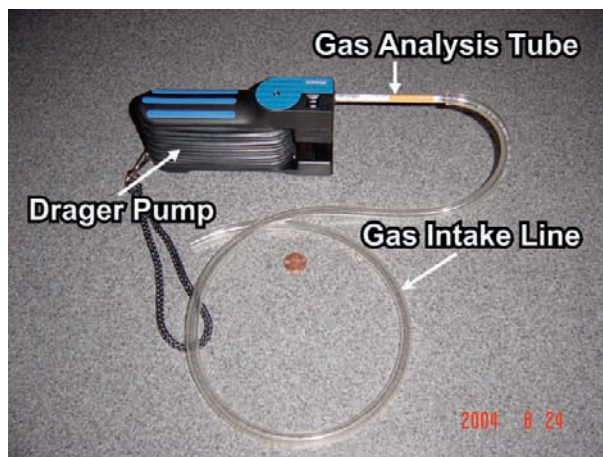


Figure 9.2.9. Dräger hand pump and tube apparatus used to extract coal-fire gas and measure the concentration of a select gas component, depending on the tube used. From Stracher et al., 2007, with modifications, permission of the Geological Society of America.

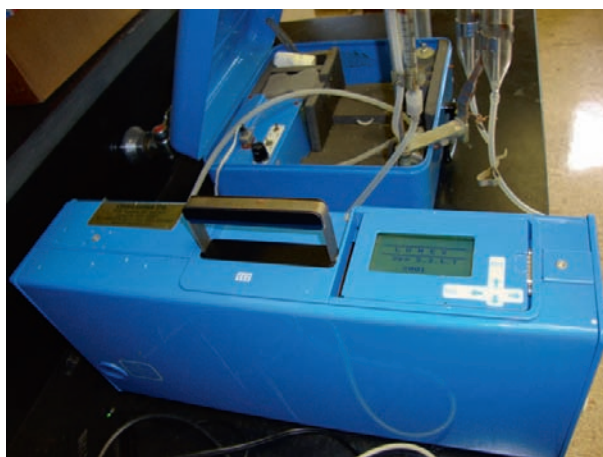


Figure 9.2.10. The RA-915+ mercury analyzer used for measuring Hg emissions at coal-fire gas vents. This instrument is a product of Ohio Lumex Co., Inc., 9263 Ravenna Road, Unit A-3, Twinsburg, Ohio 44087, USA.

Hg emissions from gas vents in the Powder River Basin, Wyoming, and the eastern Kentucky coalfield, USA. According to Kevin Henke of the Center for Applied Energy Research, University of Kentucky, Lexington: “The instrument is a typical mercury cold vapor atomic absorption spectrometer, which uses a magnetic field (the Zeeman Effect) to improve the sensitivity of the instrument. Unlike most atomic absorption units, the RA-915+ is field portable. The RA-915+ has attachments that permit the measurement of mercury in water, air, and solids. Air samples directly enter into the absorption cell. An ultraviolet beam (wavelength of 253.7 nm) passes through the cell. Any mercury vapor in the air will absorb some of the ultraviolet radiation. The amount of absorbed radiation is proportional to the mercury concentration of the air (the Beer–Lambert Law). The instrument has a mercury detection limit in air of about 2 ng/m³. The quantification range is about 10–100 000 ng/m³.”

The **pitot tube** is useful for measuring the flow velocity of coal-fire gas at a vent (Figure 9.2.11; see “WWW Addresses: Additional Reading”). This instrument uses the fluid density and pressure differential between the static and stagnation pressures to determine the velocity of a fluid. Although several types of pitot tubes exist, S-type tubes are ideal for work with coal fires as they are not easily plugged by particulate matter or readily affected by high temperatures. In addition, they work well at a variety of gas velocities. Pitot tubes are typically used in



Figure 9.2.11. Pitot instrumentation (tube and flow meter (red box)) used for measuring the velocity of coal-fire gas exhaled from vents at the surface. This instrument is a product of FlowKinetics LLC, 528 Helena Street, Bryan, Texas 77801, USA. Photo by Jennifer M.K. O’Keefe, 2009.

conjunction with a flow meter, such as the Flow Kinetics FKT 1DP1A-SV, which contains pressure transducers used to measure the pressure differential, as well as absolute pressure, temperature, and relative humidity. By collecting multiple measurements for each of these parameters at a coal-fire gas vent, the mass flow, volume flow, and variability in flow can be quickly assessed. This information is critical for estimating gas flow rates from coal-fires vents.

Discussion

The procedures described above for collecting coal-fire gas and minerals were successfully field tested and a number of analyses obtained for fires in SW Colorado, Indonesia, and the Wuda coal field, Inner Mongolia autonomous region of northern China. Work with samples from Centralia will soon begin. All results will be published in forthcoming chapters along with pressure–temperature stability diagrams. One such diagram (Figure 9.2.12) was derived by Stracher (1995) for the condensation of orthorhombic sulfur from anthracite gas

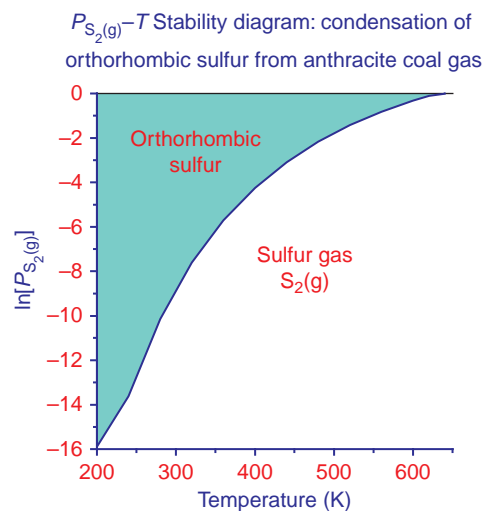


Figure 9.2.12. Pressure–temperature stability diagram for the condensation of orthorhombic sulfur from anthracite gas, Centralia mine fire, Pennsylvania. From Stracher, 1995.

by considering polymorphic transformations in the sulfur during cooling. The diagram illustrates gas-orthorhombic sulfur stability fields below ~600 K.

Acknowledgments

Field work and analyses were funded by National Geographic International; the Weather Channel; Darlow Smithson Productions Ltd., UK; the University System of Georgia; and the East Georgia College Foundation. The author thanks Tammy P. Taylor of Los Alamos National Laboratory, New Mexico; Robert B. Finkelman, Emeritus, US Geological Survey, Reston, Virginia; and Jim Hower, Center for Applied Energy Research, University of Kentucky, Lexington for their review of various sections of this chapter.

Important Terms

abandoned workings

condensation

deep mined

Dräger pump

Dräger tubes

drip condensates

flow condensates

gas-altered substrate (GAS)

gas fissures

gas-liquid altered substrate (GLAS)

gas-liquid precipitation (GLP)

gas-liquid solidification (GLS)

gas reaction ± liquid-solidification (GRLS)

gas vents

Global Positioning Satellite (GPS)

isochemical mineralization

mass transfer mineralization

mercury analyzer

pitot tube

strip mined

sublimation

Tedlar[®] gas bag

thermocouple probe

workings

References

- Cole, D.I., 1975. Observations on a burning cliff. Proceedings of the Dorset Natural History and Archaeological Society for 1974. Dorchester, Dorset, UK, Dorset Natural History and Archaeological Society, vol. 96, pp. 16–19, <http://www.dor-mus.demon.co.uk> (accessed July 2005).
- DeKok, D., 1986. Unseen Danger. University of Pennsylvania Press, Philadelphia, PA, 299 p.
- Finkelman, R.B., 2004. Potential health impacts of burning coal beds and waste banks. In: Stracher, G.B. (Ed.), Coal fires burning around the world: a global catastrophe. *Int. J. Coal Geol.* 59 (1–2), 19–24.
- Finkelman, R.B., Belkin, H.E., Zheng, B., 1999. Health impacts of domestic coal use in China. *Proc. Natl. Acad. Sci. U.S.A.* 46, 3427–3431.
- Finkelman, R.B., Larson, R.R., Dwornik, E.J., 1974. Naturally occurring vapor-liquid-solid (VLS) whisker growth of germanium sulfide. *J. Cryst. Growth* 22, 159–160.
- Finkelman, R.B., Mrose, M.E., 1977. Downeyite, the first verified natural occurrence of SeO₂. *Am. Mineral.* 62, 316–320.
- Finkelman, R.B., Orem, W., Castranova, V., Tatu, C.A., Belkin, H.E., Zheng, B., Lerch, H.E., Marharaj, S.V., Bates, A.L., 2002. Health impacts of coal and coal use: possible solutions. *Int. J. Coal Geol.* 50, 435–443.
- Finkelman, R.B., Skinner, H.C., Plumlee, G.S., Bunnell, J.E., 2001. Medical geology. *Geotimes* 46 (11), 21–23.
- Gaines, R.V., Skinner, H.C., Foord, E.E., Mason, B., Rosenzweig, A., 1997. Dana's New Mineralogy, eighth ed. John Wiley and Sons, Inc., New York, 1819 p., <http://webmineral.com/danaclass.shtml> (accessed July 2005).
- Geissinger, J., 1990. Managing underground mine fires: the case of Centralia, Pennsylvania. *Pa Geogr.* 28 (2), 22–26.
- Gupta, R.P., Prakash, A., 1998. Reflection aureoles associated with thermal anomalies due to subsurface mine fires in the Jharia coalfield, India. *Intl. J. Remote Sens.* 19 (14), 2619–2622.
- Hawley, G.G. (Ed.), 1971. The Condensed Chemical Dictionary, eighth ed. Van Nostrand Reinhold Company, New York, 971 p.
- Johnson, T.M., Liu, F., Newfarmer, R.S., 1997. Clear Water, Blue Skies: China's Environment in the New Century. World Bank, Washington, DC, 114 p.

- Lapham, D.M., Barnes, J.H., Downey, W.F., Jr., Finkelman, R.B., 1980. Mineralogy associated with burning anthracite deposits in eastern Pennsylvania. Pennsylvania Geological Survey, Mineral Resource Report 78, Harrisburg.
- Lausen, C., 1928. Hydrous sulphates formed under fumerolic conditions at the United Verde Mine. *Am. Mineral.* 13 (6), 203–229.
- Prakash, A., Gens, R., Vekerdy Z., 1999. Monitoring coal fires using multi-temporal night-time thermal images in a coalfield in North-west China. *Intl. J. Remote Sens.* 20 (14), 2883–2888.
- Stoiber, R.E., Rose, W.I., Jr., 1974. Fumarole incrustations at active Central American volcanoes. *Geochim. Cosmochim. Acta* 38, 495–516.
- Stracher, G.B., 1995. The anthracite smokers of eastern Pennsylvania: $P_{S_2(g)}-T$ stability diagram by TL analysis. *Math. Geol.* 27 (4), 499–511.
- Stracher, G.B., 2002. Coal fires: a burning global recipe for catastrophe. *Geotimes* 47 (10), 36–37, 66.
- Stracher, G.B., Lindsley-Griffin, N., Griffin, J.R., Renner, S., Schroeder, P., Viellenave, J.H., et al., 2007. Revisiting the south cañon number 1 coal mine fire during a geologic excursion from denver to glenwood springs, Colorado. In: Reynolds, R.G. (Ed.), *Roaming the Rocky Mountains and environs: geological field trips. Geol. Soc. Am. Field Guide* 10, 101–110.
- Stracher, G.B., Nolter, M.A., Schroeder, P., McCormack, J., Blake, D.R., Vice, D.H., 2006. The great centralia mine fire: a natural laboratory for the study of coal fires. In: Pazzaglia, F.J. (Ed.), *Excursions in geology and history: field trips in the Middle Atlantic States. Geol. Soc. Am. Field Guide* 8, 33–45.
- Stracher, G.B., Prakash A., Schroeder, P., McCormack, J., Zhang, X., Van Dijk, P., et al., 2005a. New mineral occurrences and mineralization processes: Wuda coal-fire gas vents of Inner Mongolia. *Am. Mineral.* 90, 1729–1739.
- Stracher, G.B., Tabet, D.E., Anderson, P.B., Pone, J.D.N., 2005b. Utah's state rock and the emery coalfield: geology, mining history, and natural burning coal beds. In: Pederson, J., Dehler, C.M. (Eds.), *Interior Western United States. Geol. Soc. Am. Field Guide* 6, 199–210.
- Stracher, G.B., Taylor, T.P., 2004. Coal fires burning out of control around the world: thermodynamic recipe for environmental catastrophe. In: Stracher, G.B. (Ed.), *Coal fires burning around the world: a global catastrophe. Int. J. Coal Geol.* 59 (1–2), 7–17.
- Wagner, R.S., Ellis, W.C., 1964. Vapor-liquid-solid mechanism of single crystal growth. *Appl. Phys. Lett.* 4 (5), 89–90.
- West, I.M., 2001. Burning beach, burning cliffs and the Lyme volcano: oil-shale fires; geology of the Dorset Coast: United Kingdom, School of Ocean and Earth Sciences, Southampton University, pp. 1–16, <http://www.soton.ac.uk/~imw/kimfire.htm> (accessed July 2005).
- Whitehouse, A.E., Mulyana, A.A.S., 2004. Coal fires in Indonesia. In: Stracher, G.B. (Ed.), *Coal fires burning around the world: a global catastrophe. Int. J. Coal Geol.* 59 (1–2), 19–24.
- Witzke, T., 1997a. A new aluminum chloride mineral from Oelsnitz near Zwickau, Saxony, Germany. *Neues Jahrbuch Für Mineralogie-Monatshefte* (7), 301–308.
- Witzke, T., 1997b. New data on the mercury iodide mineral coccinite, HgI_2 . *Neues Jahrbuch Für Mineralogie-Monatshefte* (11), 505–510.
- World Resources Institute, 1999. 1998–1999 World Resources: A Guide to the Global Environment, Environmental Change and Human Health. New York, Oxford University Press, 369 p. See also <http://www.wri.org> (September 2001).

WWW Addresses: Additional Reading

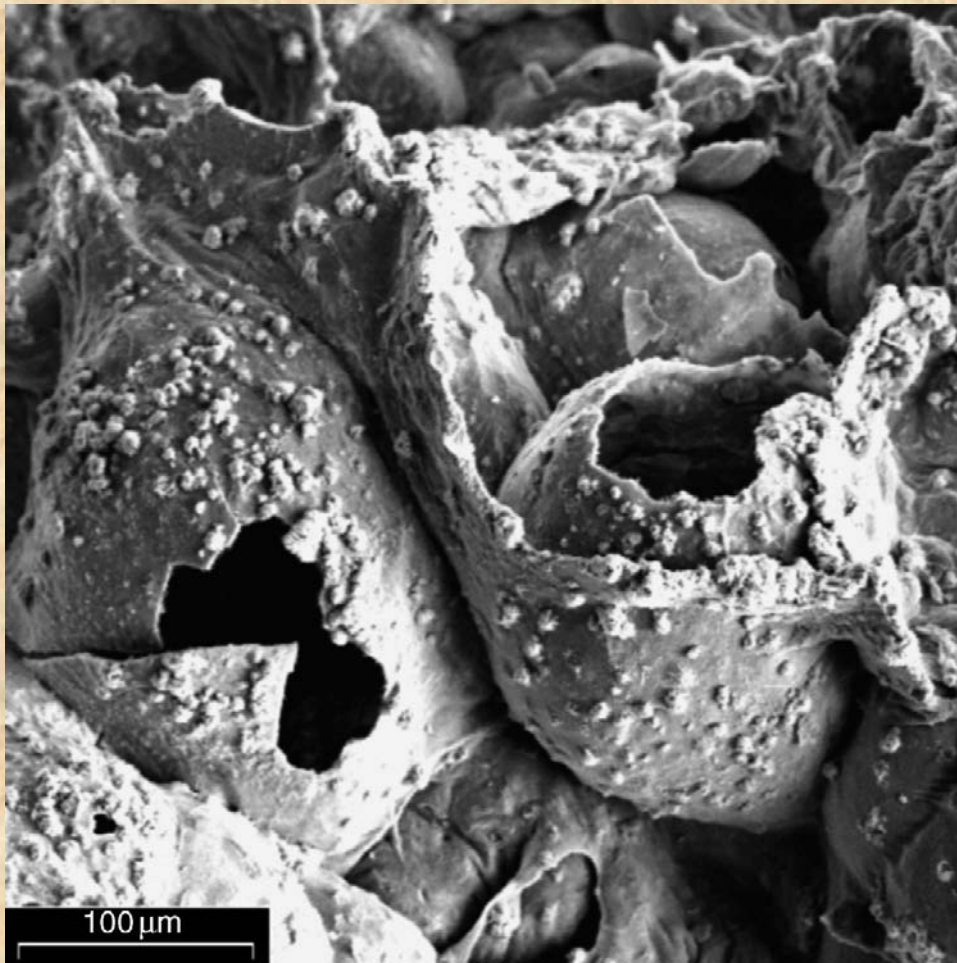
- (1) **Centralia Mine Fire Collecting Extravaganza with National Geographic**
http://gsa.confex.com/gsa/2004AM/finalprogram/abstract_73398.htm
- (2) **Coal Fires: A Burning Global Recipe for Catastrophe**
<http://www.agiweb.org/geotimes/oct02/geophen.html>
- (3) **Coal Fires: A Synopsis of Their Origin, Remote Sensing Detection, and Thermodynamics of Sublimation**
http://technology.infomine.com/enviromine/case_hist/coal%20fires/Stracher_et_al.html
- (4) **Coal Mine Fire-Gas and Condensation Products: Collection Techniques for Laboratory Analysis**
http://www.caer.uky.edu/energeia/PDF/vol14_5.pdf
- (5) **Gas Vent Mineralogy and Geochemistry: The Burning-Culm Banks of South Africa**
http://gsa.confex.com/gsa/2005AM/finalprogram/abstract_91289.htm

- (6) **Gas Vent Mineralogy of Coal Fires Burning around the World**
http://gsa.confex.com/gsa/2007SE/finalprogram/abstract_117338.htm
- (7) **LaMotte Company**
<http://www.lamotte.com/pages/edu/air.html>
- (8) **New Mineral Occurrences and Mineralization Processes: Wuda Coal-Fire Gas Vents of Inner Mongolia**
<http://www.minsocam.org/MSA/AmMin/TOC/2005/ND05.html>
- (9) **Pitot Instrumentation: Flow Kinetics LLC**
<http://www.flowkinetics.com/index.htm>
- (10) **Pitot Tube: From the Wikipedia Encyclopedia**
http://en.wikipedia.org/wiki/Pitot_tube
- (11) **RA 915+ Mercury Analyzer**
<http://ohiolumex.com>
- (12) **Tedlar® Gas Bag**
<http://jenseninertproducts.thomasnet.com/category/all-categories-gas-sampling-bags>
- (13) **The Origin of Gas Vent Minerals: Isochemical and Mass Transfer Processes**
http://gsa.confex.com/gsa/2006AM/finalprogram/abstract_111311.htm

This page intentionally left blank

CHAPTER 10

Sample Identification and Imaging of Gas-Vent Mineral Assemblages



Scanning electron microscope image of coquimbite rosettes (small bumps) that nucleated in the laboratory several weeks after collection on a cryptocrystalline mass consisting of voltaite, alunogen, coquimbite, and an unidentified phase (UP) nucleated from coal-fire gas on sandstone in the Wuda coalfield of Inner Mongolia. The vesicles in the sample may be due to boiling water in a crystallizing solution or dehydration reactions after crystallization was completed. *From Stracher et al. (2005).*

CHAPTER CONTENTS

10.1 Sample Identification and Imaging

- Introduction
- X-Ray Diffraction
- Electron Microprobe
- Short-Wave Infrared Spectroscopy
- Other Analytical Methods
- Comments
- Acknowledgments
- Important Terms
- References
- WWW Addresses: Additional Reading



Photo by Glenn B. Stracher, 2004.

10.1. Sample Identification and Imaging

Paul A. Schroeder
Chris Fleisher
Glenn B. Stracher

Vesicular mineral assemblage nucleated from anthracite gas on thermally altered mudstone at the Centralia mine fire in Pennsylvania. The assemblage consists of alunogen, copiapite, voltaite, quartz, and sulfur.

Introduction

The **gas vents** and **ground fissures** associated with burning waste piles of coal and underground coal beds occur in isolated areas and form on relatively short-lived geologic time scales. As previously noted (Chapter 9; Stracher et al., 2005), the types of minerals that form in and adjacent to these gas vents and fissures are related to the complexities of the (1) burning coal's composition, (2) depth and temperature of burning, (3) chemistry of the adjacent and overburden rocks and any fluids they contain, and (4) atmospheric conditions when the vented gas is exhaled at the surface (Figure 10.1.1A). These factors result in rapidly formed crystals (sometimes within a few days) of unusual chemistry that make the identification of coal-fire minerals a challenging undertaking. Similar mineral-forming environments that occur in equally complex and isolated locations include terrestrial volcanic vents, industrial plants that burn coal, and perhaps volcanic vents and fissures on other planets. Methodologies used to characterize the mineral assemblages at such sites (both remotely and by ground truth) can be employed to study minerals nucleated from coal-fire gas exhaled from vents and fissures.

Coal-fire gas vents are similar to terrestrial volcanic vents because when exhaled at the surface, hot-reduced gases come into contact with the cooler oxidizing atmosphere (Figure 10.1.1B). Volcanic vent mineralization sometimes has a component of biological mediation (Figure 10.1.1B; Kyle et al., 2007), so it is possible that coal-fire mineral assemblages also contain some aspects of biological mediation. Coal-fire **biomineralization** is an area that requires future work. Smokestacks associated with industrial coal burning represent a man-made environment where similar, yet distinctive, vent-like mineral assemblages occur (Figure 10.1.1). The common process in all of these environments is the very rapid time scale of mineral formation (particularly in terms of geologic time).



Figure 10.1.1. Three different environments where similar mineral assemblages are found: (A) Gas vent from the underground Centralia mine fire, Pennsylvania. Minerals nucleated from the gas, on the ground around the vent, at the base of the smoke plume. (B) Vent at a volcanic hot spring in Uzon Caldera, Kamchatka, Russia. Thermophilic bacteria and archaea biologically induce mineralization in the springs (Konhauser and Ferris, 1996). (C) Coal-burning power plant in Emery County, Utah. Smokestacks are sites where fly ash accumulates and rapid sulfate mineralization occurs. Photos by Paul A. Schroeder (A) 2006, (B) 2006, and (C) 2005.

A consequence of rapid formation is that the crystals are tiny ($<10\ \mu\text{m}$), with the possible exception of long acicular growths and therefore are difficult to study using traditional optical microscopes or a hand lens. There are numerous ways to characterize the mineral assemblages comprised of such tiny crystals; however, each approach varies in expense, time, and the need for specialized equipment.

The purpose of this chapter is to introduce common methods (i.e., techniques generally available to most geology departments) that can be used to identify minerals that nucleate from coal-fire gas. A brief overview of the practice and principles of (1) **X-ray powder diffraction (XRD)**, (2) **electron microprobe analysis (EMPA)**, and (3) **short-wave infrared spectroscopy (SWIR)** is introduced. Other techniques can be used to provide added insight about the crystal chemistry of vent minerals and the **micro-Dumas carbon–nitrogen method (MDCN)** is briefly discussed as just one example.

It is important to point out that no single method provides all the information about these gas-vent mineral assemblages. A good analogy for knowing how to accurately characterize a mineral assemblage that is beyond examination by the unaided eye is like trying to identify an elephant using only the feel of your hand (i.e., your eyes, ears, and nose are closed). It is not until you collectively sense enough parts (e.g., the trunk, ears, hide, and tail) that you begin to get the whole picture and realize you are not studying a hippo or giraffe! The more analytical methods one can employ to characterize a mineral assemblage, the more evidence available for understanding the nucleation process. Examples of XRD, EMPA, and SWIR data from gas-vent mineral assemblages that occur around the world will be presented to learn what minerals are common to coal-fire vents, volcanic vents, and smokestacks, and what minerals are unique to coal-fire vents alone.

X-Ray Diffraction

Each analytical method used for the detection and quantification of an unidentified mineral partly relies on the interaction between **electromagnetic radiation** and **atomic planes** in the mineral. XRD is a mineral identification technique based on a particular and essential feature for which all wave-interference phenomena are based. This is the situation where the distances between the atomic planes in a mineral are similar to the wavelength of the waves being scattered. This same principle applies to the constructive and destructive interference of all waves including ocean waves, seismic waves, light waves, and sound waves.

Minerals by definition have a generally uniform composition and a repeating orderly arrangement of atoms, i.e., a **crystal structure**. Repeat distances of basic **crystal motifs (unit cells)** are on the order of **angstroms** ($1\ \text{\AA} = 10^{-10}\ \text{m}$) and **nanometers** ($1\ \text{nm} = 10^{-9}\ \text{m}$). A unit cell is the smallest volume of a mineral that can exist and still retain all the physical and chemical properties of that mineral.

X-rays are part of the **electromagnetic spectrum** and have wavelengths on the order of angstroms. X-rays for diffraction experiments are generated by applying a large potential energy difference called **voltage** (usually around 40 kV) across electrodes in a **vacuum tube**. Electrons in the tube stream from a filament and hit a metal target. When these electrons collide with the electrons of atoms that are in the metal target, the electrons in the target atoms move to higher energy levels. When the displaced electrons fall back to their original energy level, a “monochromatic” source of X-rays is generated. Filtering X-rays of higher and lower energy by using energy-sensitive detectors, curved monochromatic crystals, and/or metal-foil absorption windows results in a single wavelength of X-rays used to analyze the mineral sample of interest.

One commonly used target that is bombarded with electrons to generate X-rays is copper, which generates X-rays with a $1.54059\ \text{\AA}$ wavelength, referred to as **Cu-K α_1** radiation. This single wavelength of radiation then constructively and destructively interferes with a mineral sample ground to a fine powder. The powdered sample is pressed into a disk shape before it is exposed to the beam of X-rays. Once exposed, the X-ray beam is diffracted from the mineral’s atomic planes in all possible crystal orientations in the powder, and it is then detected by positioning an **electronic detector** in the hemisphere surrounding the sample. This is done by either moving a detector through the hemisphere in an arc-like path or having a position-sensitive detector on an arc of the hemisphere. A goniometer is a device that makes it possible to orient something at a specific angle in space while measuring the angle. Therefore, the motorized device that orients the X-ray source, sample, and detector is called an **X-ray goniometer**. Using either a moving detector or a detector that simultaneously senses all angles allows analysts to observe the unique **diffraction pattern** scattered into space by a crystal structure (Figure 10.1.2).

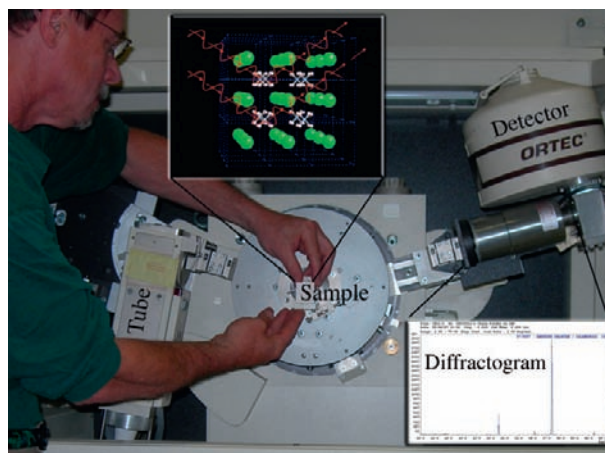


Figure 10.1.2. X-ray diffractometer arrangement. The X-ray source (tube) generates monochromatic radiation that is focused on the sample. Upper inset shows the ideal crystal structure of salammoniac (NH_4Cl , N=light blue, H=pink, and Cl=green) with waves schematically entering and scattering off of atomic planes according to Bragg's law. Blue lines outline the edge (3.89 \AA) of the repeating unit cell. Lower right inset shows the diffraction pattern (diffractogram) obtained by scanning over a wide range of angles and detecting the coherent-constructive interference of the X-rays. The pattern is unique to the types of atoms in the unit cell, shape of the unit cell, and geometry of the X-ray beam path. Photo by Paul A. Schroeder, 2007.

The combination of (1) the diffractometer geometry (goniometer positions) and X-ray wavelength, (2) the location and types of atoms in the unit cell, and (3) the shape of the unit cell results in each mineral producing a unique pattern of diffracted X-rays. These relationships were established by the physicist W.L. Bragg in 1912 and are summarized in **Bragg's law**, $\lambda = 2d\sin\theta$, where λ is the radiation wavelength, d is the spacing between repeating crystal planes, and θ is the angle of X-ray incidence. The detected signal is sometimes referred to as the "reflected beam." It is like reflected light in the sense that the angle of incidence equals the angle of scattering. It is unlike light in that light will reflect at all angles, but diffracted X-rays will only "reflect" under the Bragg condition. Diffraction patterns are therefore plotted using 2θ on the horizontal scale. Searching computer libraries of known diffraction data (i.e., patterns), such as the **Powder Diffraction File** (PDF) available from the International Centre for Diffraction Data (<http://www.icdd.com>) or the American Mineralogist Crystal Structure Data Base (<http://www.minsocam.org>), allow one to closely match an unknown pattern with that of a known mineral (Figure 10.1.3).

The diffraction pattern search and match process, however, is not always simple and complete matches are difficult because of natural variability in a mineral's crystal structure and chemistry. So, do not expect a computer search and identification process to be fool proof if its search algorithms are not designed for complex mixtures. There are many other factors that can lead to a discrepancy between database diffraction patterns and the pattern of an unknown sample of interest (Hurst et al., 1997). It is also possible that there are new minerals to be discovered in association with coal-fire gas vents; not in the current databases. Finally, the sensitivity or detection limit of XRD is dependent upon the crystallinity of the material. If a mineral has a highly disordered crystal structure and is in low abundance, then the XRD method may not uniquely detect the mineral, even in concentrations of up to 5–10% by weight. This is in sharp contrast to the EMPA method (discussed below), which can clearly image and chemically analyze a small mineral grain distinctive in its crystal shape and appearance, yet in very low abundance. Moore and Reynolds (1989) and Hurst et al. (1997) are good sources for learning more about X-Ray diffraction.

Table 10.1.1 contains a list of coal-fire sites around the world where sulfur-bearing mineral assemblages nucleated from the gas. Although the collective mineral assemblages from each site are not exactly the same, there is a commonality of hydrated sulfate minerals. In many cases, the **ammonium cation** (NH_4^+) is a common constituent, likely derived from the volatilization of nitrogen in the coal under anoxic conditions.

When mineral assemblages from coal fires and volcanic hot springs are compared (Table 10.1.1), it is readily seen that similar NH_4^+ and Fe-bearing hydrated sulfate minerals are present. Their differences are **stoichiometric** or seen in the proportions of K, Ca, Fe, Mg, and Al in the hydrated sulfates. These distinctions can be attributed to the difference between the silicate mineralogy of volcanic host rocks (as volcanics are quite variable in composition) and the mineralogy of the sedimentary rocks hosting the coals. For example, clastic sedimentary rocks tend to be

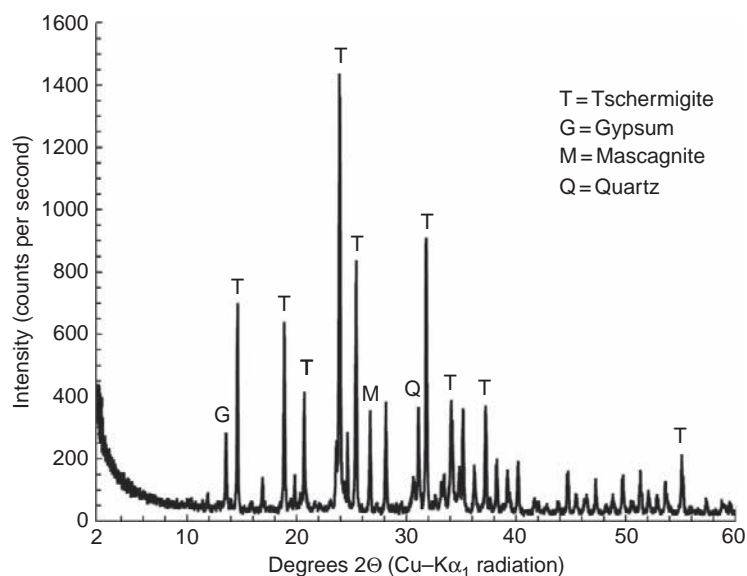


Figure 10.1.3. X-ray diffractogram of minerals encrusting a coal-fire gas vent in sandstone, Williams Fork Formation, Colorado. The temperature ~5 cm (2 in) inside the vent on May 18, 2004 was 89 °C (193 °F). Labeled peaks are strong line reflections for the major minerals in the sample. Peak positions and intensities best match respective phases with the following International Centre for Diffraction Data Powder Diffraction File numbers: tschermigite (7-22), mascagnite (7-2), gypsum (33-311), and quartz (33-1161). The minerals nucleated from coal- fire gas with the exception of quartz, likely picked up from the Williams Fork sandstone during sample collecting. Photo by Paul A. Schroeder, 2008.

more enriched in Si, Fe, and Al and depleted in K, Ca, and Mg when compared to unweathered volcanic rocks. Volcanic rocks associated with subduction zones versus those associated with spreading centers are compositionally differentiated, with the latter generally even more depleted in Si and Al and more enriched in Fe and Mg than the former. Other factors likely influencing these differences include climatic, hydrologic, geomicrobial, and temperature conditions. One example includes the observation that the Fe-rich mineral goethite is commonly found in the Fe-rich hot springs of Iceland, hosted in the volcanic rocks of a spreading center (Konhauser and Ferris, 1996, Geptner et al., 2005).

Sulfate minerals are also found in the fly ash from smoke stacks used to vent gas from burning coal into the atmosphere. However, the mineral assemblages that occur in fly ash appear to be less hydrated and not as diverse in the number and types of sulfate minerals. Ca-bearing sulfates commonly appear with smokestack vents. Also included in Table 10.1.1 are mineral assemblages associated with burning coal heap piles (Dokoupilova et al., 2007). These are dump piles sitting on the earth's surface with more exposure to the atmosphere. It is interesting to note that there are some minerals in common with volcanic and underground coal fire vents such as the Ca-, K-, NH_4 -, and Fe-bearing. The notable difference is that the heap piles often contain Na- and Mg-bearing phases, the volcanic and underground vents do not.

Electron Microprobe

EMPA is one of many analytical techniques based on the principle of sample bombardment with an electron beam in a vacuum and the subsequent detection of scattered electrons, light photons, and X-rays. Other commonly employed analytical and imaging techniques include scanning electron microscopy (SEM), cathode luminescence (CL), and transmission electron microscopy (TEM). The primary mission of EMPA is to generate and measure X-rays from a small volume of a sample and to visualize compositional variations using electrons scattered from the sample. Electrons emitted from a tungsten or lanthanum hexaboride filament in a vacuum column are accelerated through a high potential difference of 10–25 kV, so the energy gained or lost by the charge/electric field system is 10–25 keV. The resulting beam is focused to a spot of ~1 μm in diameter (i.e., ~1/100th the thickness of a human hair). The **electron beam** is then either rastered over the sample at varying magnifications to visualize sample surface morphology and compositional variation or focused on a single spot to generate X-rays within the sample.

Table 10.1.1
Sulfur-bearing mineral assemblages* found in coal-fire vents[†], volcanic vents[‡], coal-burning smoke stacks[§], and burning coal piles^{||}.

Name and location of coal mine or site	Minerals* identified by XRD	Alphabetic list of minerals with idealized formulas
Wuda basin, Inner Mongolia, China [†]	Alunogen, anhydrite, coquimbite, godovikovite, millosevichite, tschermigite, salammoniac, volaite	Aluminite $\text{Al}_2\text{SO}_4(\text{OH})_4 \cdot 7(\text{H}_2\text{O})$ Alunite $\text{KAl}_3(\text{SO}_4)_2(\text{OH})_6$ Alunogen $\text{Al}_2(\text{SO}_4)_3 \cdot 17\text{H}_2\text{O}$
Witbank and Sasolburg coalfields, South Africa [†]	Barite, gypsum, letovicite, mascagnite, sulfur	Anhydrite CaSO_4 Aphthitalite $(\text{K},\text{Na})_3\text{Na}(\text{SO}_4)_2$
Centralia Mine Fire, Pennsylvania, USA [†]	Alunogen, copiapite, hydrobasaluminite, pyrophyllite, volaite, sulfur	Arcanite K_2SO_4 Barite BaSO_4 Blödite $\text{Na}_2\text{Mg}(\text{SO}_4)_2 \cdot 4\text{H}_2\text{O}$
South Cañon No. 1 Coal Mine Fire, Colorado, USA [†]	Gypsum, mascagnite, tschermigite	Copiapite (Fe,Mg) $\text{Fe}_4(\text{SO}_4)_6(\text{OH})_2 \cdot 20\text{H}_2\text{O}$
Ruth Mullins Fire, vent 1, Kentucky, USA [†]	Salammoniac, sulfur	Coquimbite $\text{Fe}_2(\text{SO}_4) \cdot 9\text{H}_2\text{O}$ Epsomite $\text{Mg}(\text{SO}_4) \cdot 7\text{H}_2\text{O}$
East Kalimantan, Indonesia [†]	Gypsum, sulfur	Godovikovite $\text{NH}_4(\text{Al},\text{Fe})_x(\text{SO}_4)_2$
Uzon Caldera, Kamchatka, Russia [‡]	Aluminite, alunite, alunogen, barite, copiapite, coquimbite, gypsum, halotrichite, huangite, jarosite, minamiite, natroalunite, pyrite sulfur, tschermigite	Gypsum $\text{CaSO}_4 \cdot 2\text{H}_2\text{O}$ Glauberite $\text{Na}_2\text{Mg}(\text{SO}_4)_2$ Halotrichite $\text{FeAl}_2(\text{SO}_4)_4 \cdot 22\text{H}_2\text{O}$ Hexahydrite $\text{Mg}(\text{SO}_4) \cdot 6\text{H}_2\text{O}$ Huangite $\text{Ca}_{0.5}\text{Al}_3(\text{SO}_4)_2(\text{OH})_6$
Coal-burning smokestacks and fly ash [§]	Anhydrite, gypsum	Hydrobasaluminite $\text{AlSO}_4(\text{OH})_{10} \cdot 12\text{-}36\text{H}_2\text{O}$
Coal-fire minerals identified on burning coal-waste heaps in the Nord-Pas-De-Calais and Loire region in St. Etienne, France (including bituminous coal and black shale \pm sandstone)	Thenardite, blödite, konyaite, aphthitalite, langbeinite, arcanite, glauberite, gypsum, epsomite, hexahydrite, alunogen, rozenite, godovikovite, kalinite, pickingerite, halotrichite, tschermigite, mascagnite, lecontite, salammoniac, sulfur, realgar, orpiment	Jarosite $\text{KFe}_3(\text{SO}_4)_2(\text{OH})_6$ Kladnoite $\text{KFe}_3(\text{SO}_4)_2(\text{OH})_6$ $(\text{C}_6\text{H}_4)_2(\text{CO})_2\text{NH}$ Kalinite $\text{KAl}(\text{SO}_4)_2 \cdot 11\text{H}_2\text{O}$ Konyaite $\text{NaMg}(\text{SO}_4)_2 \cdot 5\text{H}_2\text{O}$ Kratochvilite $(\text{C}_6\text{H}_4)_2\text{CH}_2$ Langbeinite $\text{K}_2\text{Mg}_2(\text{SO}_4)_3$ Lecontite $(\text{NH}_4,\text{K})\text{Na}(\text{SO}_4) \cdot 2\text{H}_2\text{O}$
Minerals associated with combustion metamorphism in the Czech Republic: coal basins located in the area of the Bohemian Massif (Žáček et al., 2005)	Tschermigite, sulfur, letovicite, kratochvilite, kladnoite, koktaite, rostitite	Letovicite $(\text{NH}_4)_3\text{H}(\text{SO}_4)_2$ Mascagnite $(\text{NH}_4)_2\text{SO}_4$ Millosevichite $(\text{AlFe})_2(\text{SO}_4)_3$ Minamiite $(\text{Na},\text{Ca},\text{K})\text{Al}_3(\text{SO}_4)_2$ Natroalunite $\text{NaAl}_3(\text{SO}_4)_2(\text{OH})_6$ Orpiment As_2S_3 Pickingerite $\text{MgSO}_4\text{Al}_2(\text{SO}_4)_3 \cdot 22\text{H}_2\text{O}$ Pyrite FeS_2 Realgar AsS Rozenite $\text{Fe}(\text{SO}_4) \cdot 4\text{H}_2\text{O}$ Pyrophyllite $\text{Al}_2\text{Si}_4\text{O}_{10}(\text{OH})_2$ Salammoniac NH_4Cl Sulfur S Thenardite Na_2SO_4 Tschermigite $(\text{NH}_4)\text{Al}(\text{SO}_4)_2 \cdot 12\text{H}_2\text{O}$ Volaite $\text{K}_2\text{Fe}_5^{2+}\text{Fe}_3^{3+}\text{Al}(\text{SO}_4)_{12} \cdot 18\text{H}_2\text{O}$

* This list contains only minerals positively identified using methods described herein. Other minerals may be present in these and other vents in minor abundance.

[†] Pone et al. (2007); Stracher et al. (2004, 2005, 2006).

[‡] Kyle et al. (2007).

[§] Vassilev and Vassileva (2007).

^{||} Gomes et al. (1998); Jehlicka et al. (2007).

The affected volume is teardrop shaped. The depth and cross-sectional area of the affected volume varies, depending on the accelerating voltage of the beam and the density of the sample. The affected volume is usually less than $10\ \mu\text{m}^3$, making it one of the smallest analytical volumes that can be quantitatively measured. Generally, the volume affected by the X-rays increases with increased accelerating voltage and decreases with increasing sample density.

The interaction of the electron beam with the sample's **crystal lattice** (internal arrangement of atoms) generates several phenomena that may be used to characterize the sample. **Inelastic scattering** occurs when the electron beam collides with the outer shell electrons in the sample's lattice. Deceleration of the electron beam transfers energy to the sample lattice and knocks some of the inner shell electrons to higher energy levels within the sample. When these electrons cascade back down to the inner shells of the atoms, the sample will emit **characteristic radiation** (i.e., energy) that is unique to each element in the sample. This is similar to the way characteristic radiation is generated by X-ray diffraction, except that the mineral is the target instead of the copper anode used in an X-ray tube. **Secondary electrons** are also scattered out of the sample and have energies on the order of 50 eV, much less than characteristic radiation. A magnetic field can be used to attract them to a secondary electron detector that is usually mounted at the back of the sample chamber. Although secondary electrons are generated throughout the affected volume, only those generated at or near the surface escape the sample. Thus, secondary electrons are employed to visualize the details of surface morphology (Figure 10.1.4).

Elastic scattering occurs when the electron beam is deflected by positively charged atomic nuclei in the sample lattice, with some energy loss through heat dissipation and grounding. The deflections cause relatively minor energy losses to the scattered electrons, but some of the beam can be scattered back out of the sample. These **backscattered electrons** have high kinetic energy and are relatively unaffected by magnetic fields in the electron microprobe. They are usually detected by a solid-state backscattered electron detector mounted coaxially with the electron optical system immediately above the sample. The number of backscattered electrons increases with the increasing average atomic number (analogous to density) of the sample. Backscattered electrons are employed to visualize compositional variations within a sample (backscattered electron image) and zonation within individual phases.

As noted above, a fraction of the electron beam collides with the inner shell electrons in the atoms of the sample lattice with sufficient energy to eject these electrons to higher orbitals and raise the atoms to an excited or ionized state. Electrons from the outer electron shells cascade down to fill the inner shell vacancies, releasing a discrete amount of energy, usually in the form of an X-ray photon, i.e., a packet of X-ray energy. Each element has a unique electron configuration, so the X-rays emitted are characteristic of the atoms in the sample. The amount of energy released and the ability to detect that energy are related to an element's atomic mass. Lighter elements such as H, C, and N are consequently difficult to detect. Most electron microprobes are equipped with two types of X-ray spectrometers and corresponding detectors: (1) **energy dispersive spectrometer** (EDS) and (2) **wavelength dispersive spectrometer** (WDS).

EDS detectors are solid-state detectors that are sensitive to a wide range of X-ray energies. Most microprobes are equipped with SiLi EDS detectors. These are silicon semiconductors with lithium drifted through them to

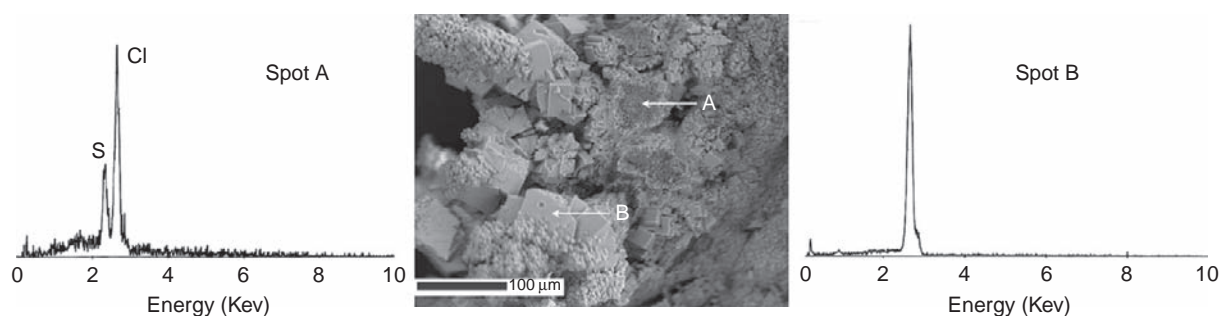


Figure 10.1.4. Secondary backscattered electron image (center) of a mineral nucleated at a coal-fire gas vent in Perry County, eastern Kentucky. The EDS spectra of two different analytical spots reveal a drusy coating of elemental sulfur (spot A). The spectrum on the left (A) reveals previously formed salammoniac beneath the sulfur coating. Note that both spectra do not reveal N in the salammoniac because the EDS detector cannot efficiently gather a signal from this relatively light element. At spot B, only the Cl signal from salammoniac was detectable. Inconsistencies brought about by irregular surface geometry and penetration of the beam beyond the surface made calibration of the intensity (vertical height) difficult for accurate elemental quantification. Photo by Paul A. Schroeder, 2008.

compensate for minor amounts of contaminants in the silicon. These detectors must be cooled with liquid nitrogen to enhance their performance and prevent the migration of the lithium out of the crystal sensor. When an X-ray photon strikes the detector, it generates an output signal that is proportional to the energy of the X-ray photon. A **multichannel analyzer** sorts output signals into different energy ranges and plots a histogram of the X-ray energies detected over time (Figure 10.1.4). Most EDS detectors have a Be (beryllium) window that is strong enough to withstand the pressure change when the vacuum column is vented to the atmosphere. The window protects the detector by maintaining the chamber vacuum, but it also absorbs X-rays from elements lighter than Na so that light elements cannot be detected. Some EDS detectors are equipped with thinner windows or are windowless by continuous chamber evacuation strategies. These detectors can detect X-rays emitted by light elements. EDS spectra provide a rapid way to qualitatively identify the elements present in a sample. An **X-ray spectrum**, i.e., an energy distribution graph, can be acquired in just a few seconds and with a little experience, the analyst can quickly identify the different phases present in a sample. Newer electron probes are equipped with silicon drift detectors (SDDs), which are photodiodes. These are similar to EDS detectors but do not require liquid nitrogen for cooling, but use reverse electronic bias to thermally cool the sensor, thus they can process at much higher count rates, which makes them capable of detecting light elements.

WDS detectors contain an X-ray proportional counter and a diffracting crystal of known d-spacing, i.e., the spacing between atomic planes. The counter and crystal are moved along the circumference of a goniometer-focusing circle to satisfy Bragg's law for the X-ray of interest. Unlike an EDS detector, a WDS detector is only tuned to one element at a time. Most microprobe spectrometers contain two or four diffracting crystals and are configured so that most of the X-ray spectrum can be detected.

Each X-ray detector chosen for a project has strengths and weaknesses that must be considered in order to determine which detector best satisfies the requirements of the project. EDS detectors are fast, relatively inexpensive, and easy to maintain, and can detect and measure X-rays from rough surfaces, but they have several disadvantages. Since the EDS detector looks at a wide range of the X-ray spectrum simultaneously, the background signal is fairly high, and it cannot detect concentrations below about 0.5 wt% (5000 ppm). EDS detectors also have relatively poorer energy resolution than a dedicated wavelength energy detector. Many elements have such similar characteristic X-ray energies that the EDS detector cannot distinguish between them. For example, the emission energy of the S $K\alpha$ peak is 2.308 keV and of the Pb $M\alpha$ peak is 2.346 keV. A peak in this energy range could indicate the presence of elemental sulfur, elemental lead, or PbS, which is the mineral galena. This is a particularly important concern if peaks are misidentified by automated vendor-supplied software. The EDS detectors also generate several artifacts that must be considered when interpreting EDS spectra. Escape peaks occur when the SiLi detector absorbs an X-ray photon and emits a Si photon. The output X-ray will generate a small peak with energy of 1.74 keV lower than the original X-ray photon. This can also result in the presence of a small spurious silicon peak when, in fact, no silicon is present. Overlapping peaks result when two different X-ray photons arrive at the detector so close together that the detector cannot distinguish them. The result is a peak with energy that is the sum of the two contributing photons and can indicate the presence of elements that are not present in the sample.

WDS Spectrometers are large and mechanically complicated. However, they have much better energy resolution than EDS detectors and can usually distinguish most peak overlaps that plague EDS detectors. WDS detectors only sample a narrow portion of the X-ray spectrum at a time, so they have a much lower background signal and in some cases can detect elemental concentrations as low as 100 ppm. Since WDS detectors only look at one element at a time, the analyses of multiple elements must be done sequentially and therefore take longer. An example of mapping a particular element of interest with a WDS detector is shown in Figure 10.1.5. The center figure shows tiny salammoniac crystals covered with sulfur. The adjacent WDS maps (X-ray maps) to the left and right of this figure show the location of Cl and S in the minerals. WDS detectors are also much less forgiving of fragile mineral samples like those found at coal-fire gas vents. Optimum quantitative analyses require samples that are flat and polished. Fragile materials like many coal-fire residues may not survive the rigors necessary to produce a polished section for optimum analytical results.

The capabilities of XRD and the electron microprobe are complimentary. Although an XRD pattern is sensitive to the kinds of atoms in a mineral, some minerals are **isostructural**. Such minerals have the same crystal structure, but they contain some different kinds of atoms. Consequently, their diffractogram patterns may be very similar. EMPA provides a means to quickly determine what elements are present in a sample and to quantitatively measure the sample's composition. Backscattered and secondary electron imaging document compositional and morphologic variations in a sample, and WDS mapping documents the distribution of elements in a sample.

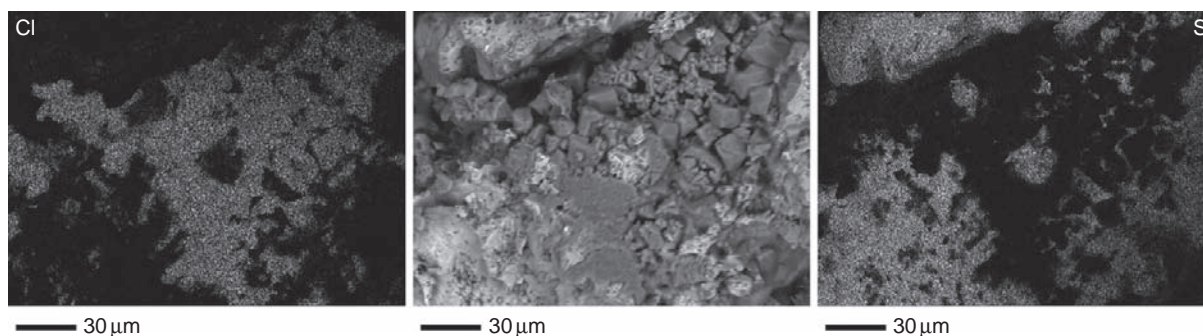


Figure 10.1.5. Secondary backscattered electron image (center) of minerals nucleated at a coal-fire gas vent, Mulga gob fire, Alabama. WDS maps the location of specific elements. The WDS map on the left shows the location of chlorine, found in salammoniac. This map corresponds with the slightly darker gray, euhedral crystals in the center photo. The WDS map on the right shows the location of native sulfur and corresponds to the very tiny, brighter gray crystals in the center photo. Photo by Paul A. Schroeder, 2007.

Short-Wave Infrared Spectroscopy

A popular approach used to assist in the exploration of economic ore deposits is SWIR (Herrmann et al., 2001; Sun et al., 2001). SWIR is useful in the field, where data can be collected with a portable unit that measures reflectance in the spectral range of 1300–2500 nm (Figure 10.1.6). Newer spectrometers accommodate higher frequencies, which occur in the very near infrared range (VNIR), i.e., down to 500 nm (recalling that wavelength and frequency of electromagnetic radiation are related by the speed of light).

Absorption in the SWIR range is attributed to “harmonics” (analogous to musical overtones and combinations of tones) that result from fundamental molecular vibrations in chemical groups such as CO_3^{2-} , NH_4^+ , SO_4^{2-} , Al-O-H , Fe-O-H , Mg-O-H , H_2O , and OH^- (Figure 10.1.7). Crystal vibration theory is extremely complex; therefore, spectra that can be interpreted for phase identification on the first principle theories of vibration spectroscopy are rare (Schroeder, 2002). The interpretation of SWIR spectra and their relationship to mineral composition and structure are accomplished by comparing specific groups of mineral spectra and correlating those spectra with other data about crystal chemistry acquired by XRD, EMPA, etc.

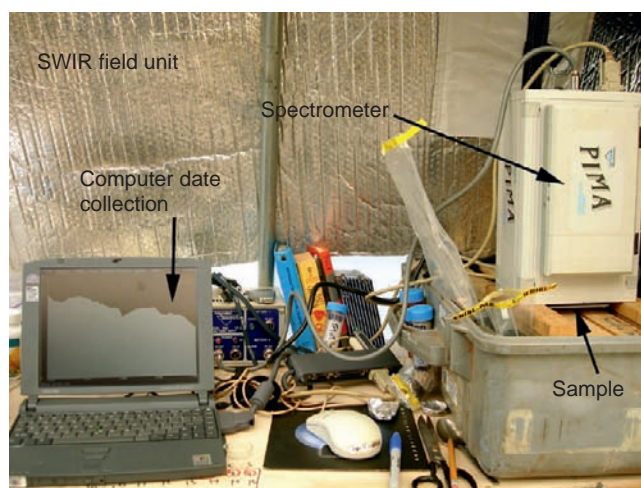


Figure 10.1.6. Portable field-based short-wave infrared spectrometer. The lower end of the spectrometer contains a port that emits an infrared (IR) light source through a window port. The computer controls the experiment by measuring the ratio of an instrument signal blank to the instrument signal with the sample in the window. Wavelengths absorbed by the minerals appear as “valleys” or absorption bands in the IR spectrum. In this example, the bands are seen on the computer screen. The spectrometer is pictured here in a field tent, but it can also be brought directly to an outcrop in the field. Water inside of or on the sample can contribute significantly to the signal and must be carefully interpreted by the analyst. Photo by Paul A. Schroeder, 2006.

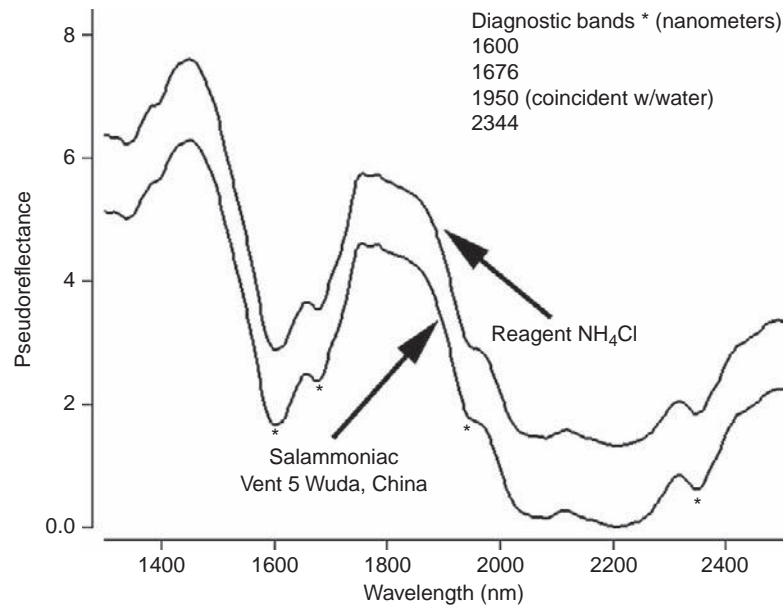


Figure 10.1.7. SWIR spectrum of salammoniac collected from vent 5 in the Wuda coalfield, Inner Mongolia autonomous region of northern China (Stracher et al., 2005). The valleys in the spectra represent wavelengths of infrared absorbed by the molecular vibration of ammonia and water in the sample. Plotted above with a vertical offset is the spectrum for reagent grade NH_4Cl . Both spectra are very similar to the ammonium chloride GDS77 spectrum in the US Geological Survey Spectral Library (<http://speclab.cr.usgs.gov>). The asterisk, *, marks the location of prominent bands that serve as diagnostic spectral features for the identification of salammoniac. The vertical scale represents “pseudoreflectance”, which is similar to “reflectance” in spectroscopy. Reflectance is a measure of the ratio of the total amount of light reflected by a surface to the total amount of light incident to the surface. The SWIR spectrometer uses its own radiation source and hence the reflectance is relative to radiation reflected from a standardized surface. Reflectance is a complex phenomenon that is a function of radiation wavelength, refractive indices of the media through which the light travels, and the angle of incidence of the light. Photo by Paul A. Schroeder, 2008.

In addition to confirming the identification of a phase, SWIR may provide field data that can potentially be correlated with satellite spectral, reflectance studies. This is possible because some satellites are equipped with spectrometers that measure the reflectance of the earth’s surface. Such reflectance studies are effective reconnaissance tools for identifying hydrothermal alteration areas of regional extent. These areas are economic targets for mineral exploration. Some commonly used spectral bands are shown in Figure 10.1.8.

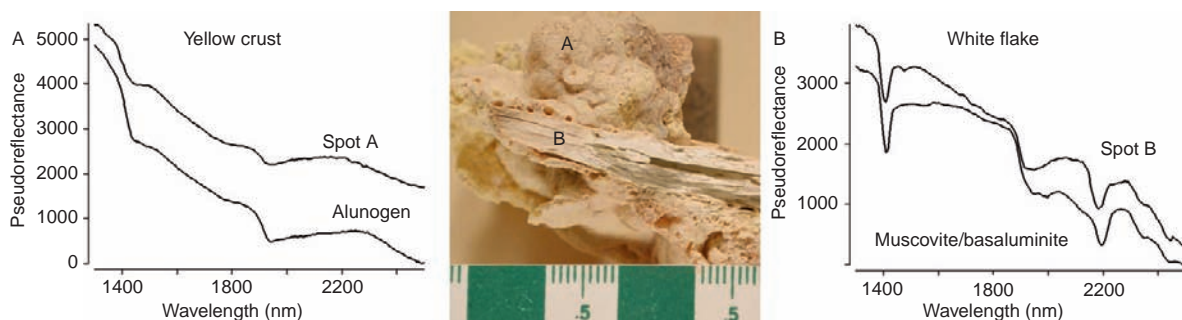


Figure 10.1.8. SWIR spectra of gas-vent minerals from the Centralia mine fire, Pennsylvania (Stracher et al., 2006). The center image is a reflected light photograph (scale bar in centimeters) showing frothy yellow vent mineralization at A and a white flake at B of a rock fragment altered by high temperature. The SWIR spectrum in the upper part of the left photo is from location A and the spectrum beneath this for alunogen, from the US Geological Survey Spectral Library (<http://speclab.cr.usgs.gov>). The SWIR spectrum in the upper part of the right photo is from location B and the spectrum beneath this is for a 50:50 mixture of muscovite and basaluminite, from the US Geological Survey Spectroscopy Lab (<http://speclab.cr.usgs.gov>). See Figure 10.1.7 concerning pseudoreflectance. Photo by Paul A. Schroeder, 2007.

One example of this potential application was demonstrated by Reddy et al. (1993) who used SWIR data for the evaluation of an active volcano (Barren Island volcano), a coal mine fire (Jharia coalfield), and industrial hot spots (Bokaro Steel Plant). Subsequent applications using SWIR and satellite data are found in Chatterjee (2006), Chatterjee et al. (2007), Guha et al. (2008), Gangopadhyay et al. (2005, 2006), and Zhang et al. (2004).

Other Analytical Methods

There are numerous other methods potentially useful for characterizing minerals nucleated from coal-fire gas. Cost, analysis time, and accessibility to specialized equipment are limiting factors. Other methods that might be utilized include (1) **infrared spectroscopy**, (2) **Raman spectroscopy**, (3) **optical spectroscopy**, (4) **nuclear magnetic and electron spin resonance spectroscopy**, (5) **X-ray fluorescence spectroscopy**, and (6) **thermal gravimetric analysis**. Calas and Hawthorne (1988) review the details about these and other spectroscopic methods.

To demonstrate how additional information can be used to characterize coal-fire mineral assemblages, an example of a common method used for analyzing the nitrogen content of a sample is presented. This is the MCDN method that is useful when nitrogen is present in small quantities in a sample (>100 ppm). Recall from above that EDS and WDS have limited use in detecting nitrogen even at percent levels.

Using MCDN, the total nitrogen content of a mineral assemblage from a gas vent is determined by transforming solid matter (minerals and organics) to a gas phase via the rapid flash combustion (with pure O₂) of a powdered sample (~10 mg) encapsulated with tin in a furnace at 1200°C (Schroeder and Ingall, 1994). The method is described in more detail in Figure 10.1.9. The gases are next separated in a **gas chromatograph**, where the amount of nitrogen is measured. Carbon and sulfur can also be detected during the same process because their gaseous oxides also form and the travel times of these combustion products are different in the gas chromatograph. After calibration with known standards, very low limits of detection (ppm) and high precision are possible.

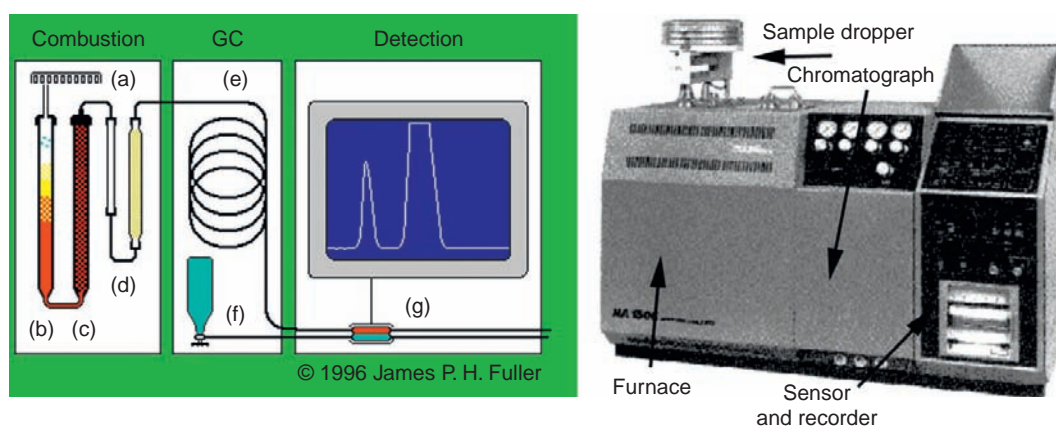


Figure 10.1.9. The rotating multisample dropper (a) delivers one sample at a time into the top of the quartz combustion tube, (b). Each sample is enclosed in an ultrapure tin or silver capsule. The combustion tube contains granulated chromium III oxide, a combustion catalyst, held at 1200°C. Flash combustion products from (b) into (c) occur when a pulse of pure O₂ gas is injected into the quartz tube with the sample, generating a temperature as high as 1700°C. Carbon in the sample is converted to CO₂. The nitrogen-bearing gas products of combustion include N₂ and nitrous oxides, NO_x. The gases are swept out of (c) by a constant stream of nonreactive He carrier gas, which entered at (a). The gases then pass through a reduction column filled with chopped Cu wire (600°C) in which the NO_x release oxygen and N₂ gas. Some oxygen is reacted with the Cu and this spent material must be periodically replaced as new Cu wire. Water vapor is removed by a gas trap at (d) that contains magnesium perchlorate. The clean sample gases then pass through a gas chromatograph column (e), where they are separated into N₂ and CO₂. A stream of the gas sample and a separate reference stream of helium from (f) pass through the detector at (g). Differences in thermal conductivity between the two streams are displayed as visible peaks and recorded as numerically integrated areas. Linear regression applied to the combustion of known standard materials yields a regression line by means of which peak areas from unknowns are converted into total element values for each sample. Figure modified with permission from Tom Maddox, <http://www.uga.edu/~sisbl/udumas.html>.

As an example of how this method has been used to further characterize minerals nucleated from coal-fire gas adjacent to five gas vents, we can look at specimens that were analyzed by XRD (samples from Wuda coalfield in Inner Mongolia analyzed by Stracher et al. (2005)). At vent numbers 1 and 4 in the Wuda coalfield, the minerals godovikovite and tschermigite, respectively, were identified. Each vent sample had several other minerals present and thus consisted of complex mixtures. Godovikovite and tschermigite are nitrogen-bearing phases with the **stoichiometry** of $\text{NH}_4(\text{Al,Fe}^{3+})(\text{SO}_4)_2$ and $\text{NH}_4\text{Al}(\text{SO}_4)_2 \cdot 12\text{H}_2\text{O}$, respectively. The total nitrogen content of the mineral assemblages at vents 1 and 4 were measured to be $0.327 \pm 0.02\%$ and $0.427 \pm 0.03\%$ by weight, respectively. Using the formula weights of godovikovite (251.5 g/mole) and tschermigite (453.0 g/mole), it was determined that godovikovite comprised ~6% by weight of the vent 1 mineral assemblage and tschermigite ~14% by weight of the vent 4 assemblage. Although these numbers are not as spectacular to look at as spectral curves and the **electron micrographs** (images) discussed above, they give more precise quantitative meaning to the characterization of mineral assemblages nucleated at coal-fire gas vents.

Comments

The first question asked when looking at a coal-fire vent sample is “What is it?” The above methods are often the first line of defense in solving the problem. Once the mineral assemblage is identified, the question that follows is “How much of each mineral is present?” The same analytical techniques and other methods can be employed, but an increase in the level of rigor and time is required. Both questions are simple at face value, but not necessarily simple to answer if the constraints on characterization are few. The identification and quantification of coal-fire mineral assemblages is an important step that leads to a better understanding of the role of coal fires in today’s environment and in the geologic past. Using the above specialized methods allows the researcher to establish a more accurate understanding of these complex mineral occurrences.

Acknowledgments

Authors Paul A. Schroeder and Chris Fleisher thank Glenn B. Stracher, East Georgia College, Swainsboro, for the opportunity to participate in coal-fires mineral research and for his insightful editing skills. XRD and EMPA facilities are supported by the Department of Geology, University of Georgia, Athens. Matt Hastings and John McCormack, Department of Geological Sciences and Engineering, University of Nevada, Reno, contributed to data collecting. We also acknowledge the National Science Foundation Program for Collaborative Research: Kamchatka Geothermal Microbial Observatory, MCB-MO-0238407.

Important Terms

Ammonium cation	A positively charged polyatomic structure comprised of a nitrogen atom with four bonded hydrogen atoms in tetrahedral coordination.
Angstrom	A unit of length used to describe the scale of atoms. It is equal to one 10-billionth of a meter or one-tenth of a nanometer, i.e., 10^{-10} m.
Atomic planes	A two-dimensional arrangement of two or more atoms on a flat surface.
Backscattered electrons	Produced by incident electrons deflected by the positive nuclei of atoms in a specimen. The electrons scattered back out of the sample at 180° (nearly parallel to the beam) with no appreciable loss of energy are then detected. The efficiency of scattering is related to the mass of the nucleus such that sample areas with heavier elements appear brighter in a backscattered electron image.
Biom mineralization	The process by which living organisms produce minerals. Controlled mineralization is the case where an organism specifically precipitates a mineral to harden or support tissues (bones or shells). Induced mineralization is the case where a mineral precipitates in,

	<p>on, or near the organism as a result of chemical change caused by the organism's metabolism. The latter may benefit the organism for the purpose of sensing or minimizing poisoning.</p>
Bragg's law	<p>Derived by physicist Sir William Lawrence Bragg in 1912, it defines the relationships between the wavelength of incident radiation (λ), the distance between atomic scattering planes (d), and the angle (θ) of resultant coherently scattered waves.</p>
Characteristic radiation	<p>Electromagnetic radiation or energy unique to the elements in a sample.</p>
Crystal lattice	<p>An orderly arrangement of atoms in a mineral, usually thought of as an infinite series of "cells" forming a "latticework" of atoms in three dimensions.</p>
Crystal motif	<p>The fundamental recurring unit of pattern of atoms in a crystal, which is also known as the unit cell. It is repeated in space by translation, rotation, or inversion to create a pattern.</p>
Crystal structure	<p>The repeating orderly arrangement of atoms within a crystal. The symmetry pattern is defined by crystal axes of lengths a, b, and c and by the angles α, β, and γ between the axes.</p>
Cu-Kα_1	<p>A form of X-ray radiation generated by the energy released when an excited core electron drops back down into the inner most electron shell. It has a wavelength of 1.540 59 Å, similar to the distances between atomic planes in a crystal.</p>
Diffraction pattern	<p>The unique record of high-intensity, coherently scattered electromagnetic waves, usually recorded in terms of the angle away from the incident beam. It is a direct consequence of the types of atoms and their arrangements in a specimen as well as the type of incident radiation.</p>
Electromagnetic radiation	<p>Electromagnetic waves produced by the motion of charged particles. These waves radiate from the electrically charged particles and they travel through a vacuum as well as through air and other substances.</p>
Electromagnetic spectrum	<p>The full range of frequencies from radio waves to gamma rays that characterize electromagnetic radiation.</p>
Electron beam	<p>A stream of electrons that flow in a vacuum from a cathode (positively charge metal) to an anode (negatively grounded metal), also known as a cathode beam.</p>
Electronic detector	<p>Any device that can sense electrons or electromagnetic radiation. Commonly, it is a device that senses changes in current due to the interaction between the source and the sensing medium (e.g., charge-coupled devices or CCDs).</p>
Electron microprobe analysis	<p>A technique that uses an electron beam to bombard a sample in a vacuum. Detectors record the interactions between the beam and the sample, recording primary, secondary, and diffracted electrons.</p>
Electron spin resonance spectroscopy	<p>Also called electron paramagnetic resonance, this is a technique for studying chemical species that have one or more unpaired electrons, such as minerals possessing a transition metal ion (e.g., Fe or Mn). This technique can, for example, distinguish ferrous and ferric iron.</p>
Energy dispersive spectrometers	<p>Devices designed to detect the characteristic energy of core electrons that is released when an electron beam excites a sample. Each element has a unique energy transition, which is recorded by a detector.</p>

Gas chromatograph	A device in which a sample is vaporized and injected into the end of a long chromatographic column. The sample is transported through the column by the flow of an inert gas. Differences in mass and chemical properties result in different arrival times at a detector. Numerous detectors are available to measure different properties of the exiting components.
Gas vents	Any opening in the earth's surface where gas escapes into the atmosphere. Vents transport heat energy from sources that may include underground coal fires or near-surface molten rock.
Ground fissures	A fracture on the earth's surface through which gases and fluids can be exchanged between the atmosphere and the subsurface.
Inelastic scattering	The process by which an electron or a photon interacts with an atom and kinetic energy is not conserved. As a result, the frequency of the resultant scattered particle is shifted.
Infrared spectroscopy	The absorption measurement by a sample of infrared radiation for the purpose of structural studies and compound identification. Infrared radiation has wavelengths ranging from ~ 0.78 to $1000 \mu\text{m}$ (10^{-6} m), between visible light and microwaves.
Isostructural	A term that refers to minerals that have the same crystal structure and some different kinds of atoms.
Micro-Dumas carbon–nitrogen method	A technique where a carbon- and/or nitrogen-bearing phase is combusted at a high temperature and the product gases are analyzed using a chromatographic device.
Multichannel analyzer	A device that takes the very small voltage signal produced by a detector, reshapes it into a Gaussian or trapezoidal shape, and converts that signal into a digital signal.
Nanometer	A unit of length used to describe the scale of atoms. It is equal to a one-billionth of a meter or 10 \AA (10^{-9} m).
Nuclear magnetic resonance spectroscopy	A technique that measures the nearing neighbor environment of atoms by placing a sample in a strong magnetic field. The spin of the atom is tilted by an electromagnetic pulse and the relaxation of the signal is recorded. The technique is applicable to odd integer elements without large amounts of paramagnetic (i.e., Fe) components. It is the same technology used in the medical field for magnetic resonance imaging (MRI).
Optical spectroscopy	A technique that employs the scattering of light as it interacts with a phase. Light can scatter, absorb, or fluoresce and be detected electronically or with the human eye.
Powder Diffraction File	An electron database that holds diffraction patterns for inorganic and organic compounds, including minerals.
Raman spectroscopy	An inelastic scattering technique that detects molecular vibrations. It is useful for identifying bonds and compounds that vibrate in the same range as infrared electromagnetic radiation.
Secondary electrons	Produced by incident electrons colliding with atoms in the specimen, near enough to impart some of their energy to lower energy electrons (usually in the K-shell of the atoms). This causes a slight energy loss and path change in the incident electrons and transition of electrons in the specimen atom. The electrons that leave the surface of the specimen have a very small kinetic energy (in the range of 2–50 eV), which are attracted to a special detector.

Short-wave infrared spectroscopy	One of several types of vibrational spectroscopy (see Raman Spectroscopy) that employs the interaction of infrared (IR) radiation and absorption in a sample. An IR source is either transmitted or reflected off of a sample and a detector records the transmittance or reflectance of the various wavelengths in the IR region of the electromagnetic spectrum.
Stoichiometry	The quantitative assessment of atoms involved in the reactant and products of a chemical reaction.
Thermal gravimetric analysis	An analytical technique based on the weight loss or gain of a sample as a function of temperature. Weight loss may be caused by the release of gas from the sample during heating. Weight gain may be caused by reaction of the sample with the atmosphere in the laboratory.
Unit cell	The smallest volume of atoms or molecules whose repetition at regular intervals in three dimensions using symmetry operations produces a crystal lattice.
Vacuum tube	A glass or ceramic tube that contains a high vacuum for the free movement of electrons.
Voltage	The potential difference in joules per coulomb of electrical charge between two points in an electrical circuit. When divided by the resistance (ohms) between those points, the result is equal to the current flowing between those points in amperes or coulombs per second.
Wavelength dispersive spectrometers	Devices that detect a specific energy or wavelength of characteristic radiations (e.g., Cu-K α_1) by geometrically positioning the detector according to Bragg's Law using a crystal with a known d-spacing. This allows for improved detection limits when compared to EDS.
X-ray fluorescence spectrometry	An analytical technique used to identify and measure the concentration of elements in a sample by measuring the wavelengths of radiation emitted from the sample when irradiated with X-rays.
X-ray goniometer	An motorized instrument used to orient a source of X-rays, a sample, and a detector in X-ray powder diffraction studies.
X-ray powder diffraction	A special form of diffraction that detects all possible crystal orientations by powdering the sample into many small, randomly oriented particles. Moving the X-ray beam and detector through a range of angles produces an X-ray powder diffraction pattern that is unique to each crystal structure.
X-rays	High-energy electromagnetic radiation with wavelengths that range from ~0.05 to 100 Å.
X-ray spectrum	A region of the electromagnetic spectrum that corresponds with the energies needed to excite the core electrons in all the elements. Each energy transition is recorded such that a sample's elemental composition can be determined by measuring the intensity and position of peaks detected and recorded.

References

Bragg, W.L. 1912, The specular reflection of X-rays: Nature. 90, 410 p.

Calas, G., Hawthorne, F.C., 1988. Introduction to spectrographic methods. Rev. Mineral. Geochem. 18, 1–9.

- Chatterjee, R.S., 2006. Coal fire mapping from satellite thermal IR data – a case example in Jharia coalfield, Jharkhand, India. *ISPRS J. Photogramm. Remote Sens.* 60, 113–128.
- Chatterjee, R.S., Wahiduzzaman, M., Shah, A., Raju, E.V.R., Lakhera, R.C., Dadhwal, V.K., 2007. Dynamics of coal fire in Jharia coalfield, Jharkhand, India during the 1990s as observed from space. *Curr. Sci.* 92, 61–68.
- Dokoupilova, P., Sracek, O., Losos, Z., 2007. Geochemical behaviour and mineralogical transformations during spontaneous combustion of a coal waste pile in Oslavany, Czech Republic. *Mineral. Mag.* 71, 443–460.
- Gangopadhyay, P.K., Lahiri-Dutt, K., Saha, K., 2006. Application of remote sensing to identify coalfires in the Raniganj Coalbelt, India. *Int. J. Appl. Earth Obs. Geoinf.* 8, 188–195.
- Gangopadhyay, P.K., Maathuis, B., Van Dijk, P., 2005. ASTER-derived emissivity and coal-fire related surface temperature anomaly: a case study in Wuda, north China. *Int. J. Remote Sens.* 26, 5555–5571.
- Geptner, A.R., Ivanovskaya, T.A., Pokrovskaya, E.V., 2005. Hydrothermal fossilization of microorganisms at the earth's surface in Iceland. *Lithol. Mineral. Res.* 40, 505–520.
- Gomes, S., Francois, M., Pellissier, C., Evrard, O., 1998. Characterization and comparative study of coal combustion residues from a primary and additional flue gas secondary desulfurization process. *Cem. Concr. Res.* 28, 1605–1619.
- Guha, A., Kumar, K.V., Kamaraju, M.V.V., 2008. A satellite-based study of coal fires and open-cast mining activity in Raniganj coalfield, West Bengal. *Curr. Sci.* 95, 1603–1607.
- Herrmann, W., Blake, M., Doyle, M., Huston, D., Kamprard, J., Merry, N., et al., 2001. Short wavelength infrared (SWIR) spectral analysis of hydrothermal alteration zones associated with base metal sulfide deposits at Rosebery and Western Tharsis, Tasmania, and highway-reward, Queensland. *Econ. Geol.* 96, 939–955.
- Hurst, V.J., Schroeder, P.A., Styron, R.W., 1997. Accurate quantification of quartz and other phases by powder X-ray diffractometry. *Anal. Chim. Acta* 337, 233–252.
- Jehlicka, J., Zacek, V., Edwards, H.G.M., Shcherbakova, E., Moroz, T., 2007. Raman spectra of organic compounds kladnoite (C₆H₄(CO)(2)NH) and hoelite (C₁₄H₈O₂) – rare sublimation products crystallizing on self-ignited coal heaps. *Spectrochim. Acta A* 68, 1053–1057.
- Konhauser, K.O., Ferris, F.G., 1996. Diversity of iron and silica precipitation by microbial mats hydrothermal waters, Iceland: implications for precambrian iron formations. *Geology* 24, 323–326.
- Kyle, J.E., Schroeder, P.A., Wiegel, J., 2007. Microbial silicification in sinters from two terrestrial hot springs in the Uzon Caldera, Kamchatka, Russia. *Geomicrobiol. J.* 24, 627–641.
- Moore, D.M., Reynolds, R.C., 1989. *X-ray Diffraction and the Identification and Analysis of Clay Minerals*. Oxford University Press, New York, 378 p.
- Pone, J.D.N., Hein, K.A.A., Stracher, G.B., Annegarn, H.J., Finkelman, R.B., Blake, D.R., et al., 2007. The spontaneous combustion of coal and its by-products in the Witbank and Sasolburg coalfields of South Africa. *Int. J. Coal Geol.* 72, 124–140.
- Reddy, C.S.S., Srivastav, S.K., Bhattacharya, A., 1993. Application of thematic mapper short-wavelength infrared data for the detection and monitoring of high-temperature related geoenvironmental features. *Int. J. Remote Sens.* 14, 3125–3132.
- Schroeder, P.A., 2002. Infrared spectroscopy in clay science, in Steve Guggenheim and Audrey. In: Rule, A.C. (Ed.), *Teaching Clay Science*, Clay Minerals Society Workshop Series. The Clay Minerals Society, Aurora, Colorado, vol. 13, pp. 181–202.
- Schroeder, P.A., Ingall, E.D., 1994. A method for the determination of nitrogen in clays, with application to the burial diagenesis of shales. *J. Sediment. Res. A* 64, 694–697.
- Stracher, G.B., Nolter, M.A., Schroeder, P., McCormack, J., Blake, D.R., Vice, D.H., 2006. The great Centralia mine fire: A natural laboratory for the study of coal fires. In: Pazzaglia F.J. (Ed.), *Excursions in Geology and History: Field Trips in the Middle Atlantic States*. Geological Society of America Field Guide, vol. 8, pp. 33–45.
- Stracher, G.B., Prakash, A., Schroeder, P., McCormack, J., Zhang, X., Van Dijk, P., et al., 2005. New mineral occurrences and mineralization processes: Wuda coal-fire gas vents of Inner Mongolia. *Am. Mineral.* 90, 1729–1739.
- Stracher, G.B., Renner, S., Colaizzi, G., Taylor, T.P., 2004. The South Cañon Number 1 Coal Mine fire: Glenwood Springs, Colorado. In: Nelson, E.P., Erslev E.A. (Eds.), *Field Trips in the Southern Rocky Mountains, USA*. Geological Society of America Field Guide, vol. 5, 143–150.
- Sun, Y., Seccombe, P.K., Yang, K., 2001. Application of short-wave infrared spectroscopy to define alteration zones associated with the Elura zinc-lead-silver deposit, NSW, Australia. *J. Geochem. Explor.* 73, 11–26.
- Vassilev, S.V., Vassileva, C.G., 2007. A new approach for the classification of coal fly ashes based on their origin, composition, properties, and behavior. *Fuel* 86, 1490–1512.

- Zhang, J., Wagner, W., Prakash, A., Mehl, H., Voigt, S., 2004. Detecting coal fires using remote sensing techniques. *Int. J. Remote Sens.* 25, 3193–3220.
- Žáček, V., Skala, R., Chlupacova, M., Dvorak, Z., 2005, Ca-Fe₃₊-rich, Si-undersaturated buchite from Zelenky, North-Bohemian Brown Coal Basin, Czech Republic: *Eur. J. Mineral.*, 17, 622–633.

WWW Addresses: Additional Reading

- (1) **American Mineralogist Crystal Structure Data Base**
<http://www.minsocam.org>
- (2) **Amethyst Galleries**
<http://mineral.galleries.com>
- (3) **EUROMIN**
<http://euromin.w3sites.net>
- (4) **Mindat.org**
<http://www.mindat.org>
- (5) **Mineralogy Database**
<http://webmineral.com>
- (6) **Mineralogy of Russia**
<http://maurice.strahlen.org>
- (7) **Mineraltravel.com**
<http://www.mineraltravel.com>
- (8) **The International Centre for Diffraction Data**
<http://www.icdd.com>
- (9) **US Geological Survey Spectroscopy Lab**
<http://speclab.cr.usgs.gov>

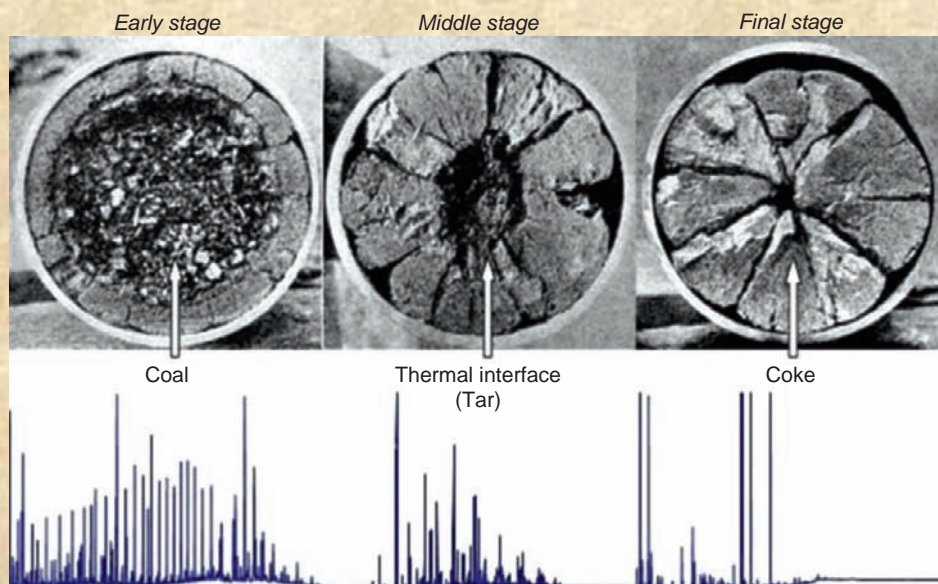
This page intentionally left blank

CHAPTER 11

Semivolatile Hydrocarbon Residues of Coal and Coal Tar

Coal carbonization

Cross section of vertical report oven during the coking cycle



The industrial carbonization of coal, as exemplified in the photographs above, produces by-products including coal tar and coke. Natural coal fires produce comparable by-products with molecular signatures that help characterize the nature of the residues when encountered in the environment. The gas chromatograms of the extractable hydrocarbons present in coal, coal tar, and coke (above) exemplify the thermal transformation of coal described in this chapter. The chemical analysis of semivolatile hydrocarbons in coal and its by-products helps understand the carbonization and combustion processes and environmental impacts of the pyrolytic and pyrosynthetic coal by-products.

CHAPTER CONTENTS

11.1 Source Identification

- Source Signatures
- Fossil Fuels
- Carbonization
- Lines of Evidence

11.2 Sample Preparation

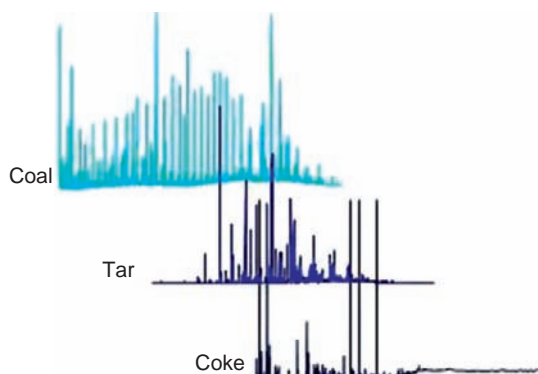
- Collection
- Extraction
- Cleanup

11.3 Sample Analysis

- Introduction
- Total Organic Carbon
- Total Extractable Material
- High-Resolution Hydrocarbon Scan
- Polycyclic Aromatic Hydrocarbons
- Saturated Hydrocarbons
- Geochemical Biomarkers

11.4 Coal-Fire Residues

- Semivolatile Hydrocarbons
- Dominant Hydrocarbons
- PAH Transformations
- Saturated Hydrocarbon Residues
- Biomarker Stability
- Conclusions
- Acknowledgments
- Important Terms
- References



11.1. Source Identification

Stephen D. Emsbo-Mattingly
Scott A. Stout

Thermal transformation of coal to coke.

Photo by Stephen D. Emsbo-Mattingly, 2003.

Source Signatures

Coal contains thousands of organic compounds and macromolecules derived from ancient biomass and reformed by biogeochemical processes over geological time at moderate temperatures (<400°C). Many factors control the specific chemical composition of coal; for example, different **types** of coal are formed depending upon the species of prehistoric terrestrial plants and the conditions in the ancient depositional environment (e.g., mineral content and oxygen concentration) in which the plant debris accumulated. Different **ranks** of coal are formed depending upon the geologic conditions (temperature and pressure) and duration of burial. The collective process of **coalification** imbues the coal bed with physical and chemical features that can differentiate coals and coal by-products from different formations.

Source signatures can be broadly classified by properties that differentiate one material from another. Recognizing source signatures is an important component of any investigation of coal and coal-derived by-products in the environment, including those associated with coal fires. In most cases, different coals exhibit distinct physical or microscopic properties that allow coals of different type and rank to be distinguished by long established (mostly) physical testing methods. However, as modern chemical testing methods improve, the number of source signatures based upon diagnostic molecular features of different coal types and ranks greatly expands. By using multiple lines of physical and chemical evidence, the ability to recognize and define independent source signatures increases and the distinctions among coals of different types and ranks and the distinction of coal from other fossil fuels (e.g., petroleum) becomes more resolved or specific. Similarly, these same multiple lines of evidence help differentiate coal and coal-derived by-products formed during the carbonization of coal via natural (e.g., coal fires) or industrial (e.g., coking) processes. Of particular use in the chemical source signatures of coal and coal-derived by-products are semivolatile **hydrocarbons**, which are the focus of this chapter.

Semivolatile hydrocarbons are solvent-extractable compounds found in coals and coal-derived by-products that include a broad range of compounds. We have functionally defined semivolatile hydrocarbons as solvent-extractable compounds that elute between about *n*-nonane (*n*-C₉) and *n*-tetratetracontane (*n*-C₄₄) on a **gas chromatograph** (GC) equipped with a non-polar silicone capillary column. The semivolatile hydrocarbons include normal alkanes, acyclic isoprenoids, **aromatics**, sesqui-, di-, and triterpanes, regular and rearranged steranes, mono- and triaromatic steranes, and many other compound groups.

The specific nature of these compounds in fossil fuels and other forms of ancient organic matter, including coals, were originally investigated by geochemists in order to identify and locate oil-bearing formations (Peters et al., 2007 and references therein). Numbering in the thousands of individual compounds, the relative abundances or absolute concentrations of diagnostic semivolatile hydrocarbons can differentiate fossil fuels (e.g., coals and crude oils) and various derived products, such as coke, coal tar, kerosene, diesel fuel, heating fuel, heavy fuel oil, lube oil, asphalt, and many others (Stout et al., 2002; Douglas et al., 2007). By contrast, volatile hydrocarbons, which include hydrocarbons and other compounds that elute before approximately *n*-dodecane (*n*-C₁₂), are very useful for

the identification and differentiation of gasoline and light solvents; however, these hydrocarbons are less stable in the environment and less useful for the study of source signatures of coal and coal-derived by-products. Similarly, nonvolatile hydrocarbons eluting after n -C₄₄ comprise a small and poorly characterized portion of the solvent extractable fraction of coal and coal-derived by-products that are less useful for observing the thermal processes associated with coal fires.

The purpose of this chapter is to describe and provide examples of the current analytical methods used for the characterization of the semivolatile hydrocarbon source signatures of coal and coal-derived by-products. A particular focus is given to the thermally derived by-products of coal formed from its thermal decomposition by industrial carbonization (coking), which mirror the by-products formed during natural coal fires. The similarity between these natural and industrial processes is relevant for environmental assessments because many of the environmental impacts derived from coal-derived tars associated with anthropogenic sources (e.g., coke and industrially-manufactured gas), such as elevated carcinogens like benzene and **polycyclic aromatic hydrocarbons** (PAHs), may also exist around natural sources such as coal-fire sites.

Fossil Fuels

Fossil fuels form from prehistoric biomass that accumulated at the bottom of water bodies faster than ambient microbes could remineralize and recycle it. Most coal formed from the residues of terrestrial plants and trees that accumulated in marshes and swamps while most petroleum formed from algae residues that accumulated in marine or lacustrine areas. The biomass mixed with varying amounts of inorganic materials (sediment) before burial over geological time. The weight of the overburden and heat from the earth over long periods of time transformed the terrestrial and marine biomass into fossil fuels. Although sometimes described differently by coal and petroleum scientists, the geochemical transformations that convert biomass into fossil fuels occurred in three general stages, often termed **diagenesis**, **catagenesis**, and **metagenesis** (Tissot and Welte, 1984).

Coal and petroleum theoretically exhibit formation-specific source signatures resulting from the accumulation of characteristics associated with the prehistoric biomass, depositional environment, and formation conditions. Prehistoric biomass generally consisted of the dominant photosynthetic and microbial communities at the time of accumulation. Biological evolution dictated that the biomass sources changed significantly over time. Once in the sediment, some biomass experienced different degrees of microbial alteration before burial. The **suboxic** or **anoxic** nature of the depositional waterbodies significantly influenced the properties of the biomass. Differences also occurred during fossil fuel formation; that is, biomass rarely experienced the same degree or duration of exposure to temperature and pressure regimes. Consequently, the chemical composition and therefore source signatures of fossil fuels varies considerably around the world.

Carbonization

Carbonization is the complex process of concentrating and purifying carbon by denaturing organic matter with heat in the presence of little to no oxygen. In the context of coal, carbonization consists of four coincident and partly competing steps. First, heat distills the mobile and freely moving volatile and semivolatile hydrocarbons into a vapor phase. Second, surplus heat pyrolyzes the hydrocarbon vapors; that is, some to most of the carbon-carbon bonds break or “crack” forming increasingly lighter and smaller hydrocarbon gases. This process is often catalyzed by the presence of metallic surfaces. **Pyrolysis** also cleaves thermally unstable molecules (e.g., hydrocarbons and heteroatomic moieties) off of polymeric coal matrix, which can subsequently crack. Third, surplus heat helps pyrosynthesize ever larger molecules from smaller, cracked reactive molecular fragments, thereby forming increasingly condensed polymeric networks of aromatized carbon (coke). Fourth, the volatile and semivolatile hydrocarbons in the vapor phase condense into stable gases, PAH-rich liquid coal tar, and particulate soot as the vapor phase cools. Collectively, carbonization of coal produces four organic-dominated by-products: coke (thermally stable coal minerals bound by graphitic carbon), coal tar (liquid pyrolytic condensate), soot (solid pyrolytic condensate), and hydrocarbon gases (methane, ethane, acetylene, carbon monoxide, and others).

By contrast, **combustion** is the thermal decomposition of organic matter in the presence of oxygen. The processes of distillation, pyrolysis, **pyrosynthesis**, and condensation (described above) are largely the same during the combustion of coal, except oxygen acts powerfully to transform most of the hydrocarbon vapors into nonhydrocarbon gases

(e.g., carbon dioxide, nitrogen oxides, sulfur oxides, and water) (Swaine, 1990). As a result, little or no liquid coal tar is produced from the combustion of coal. Natural coal fires will predominantly involve carbonization (and thereby the formation of coal tar) although combustion can also occur depending upon the conditions (oxygen availability).

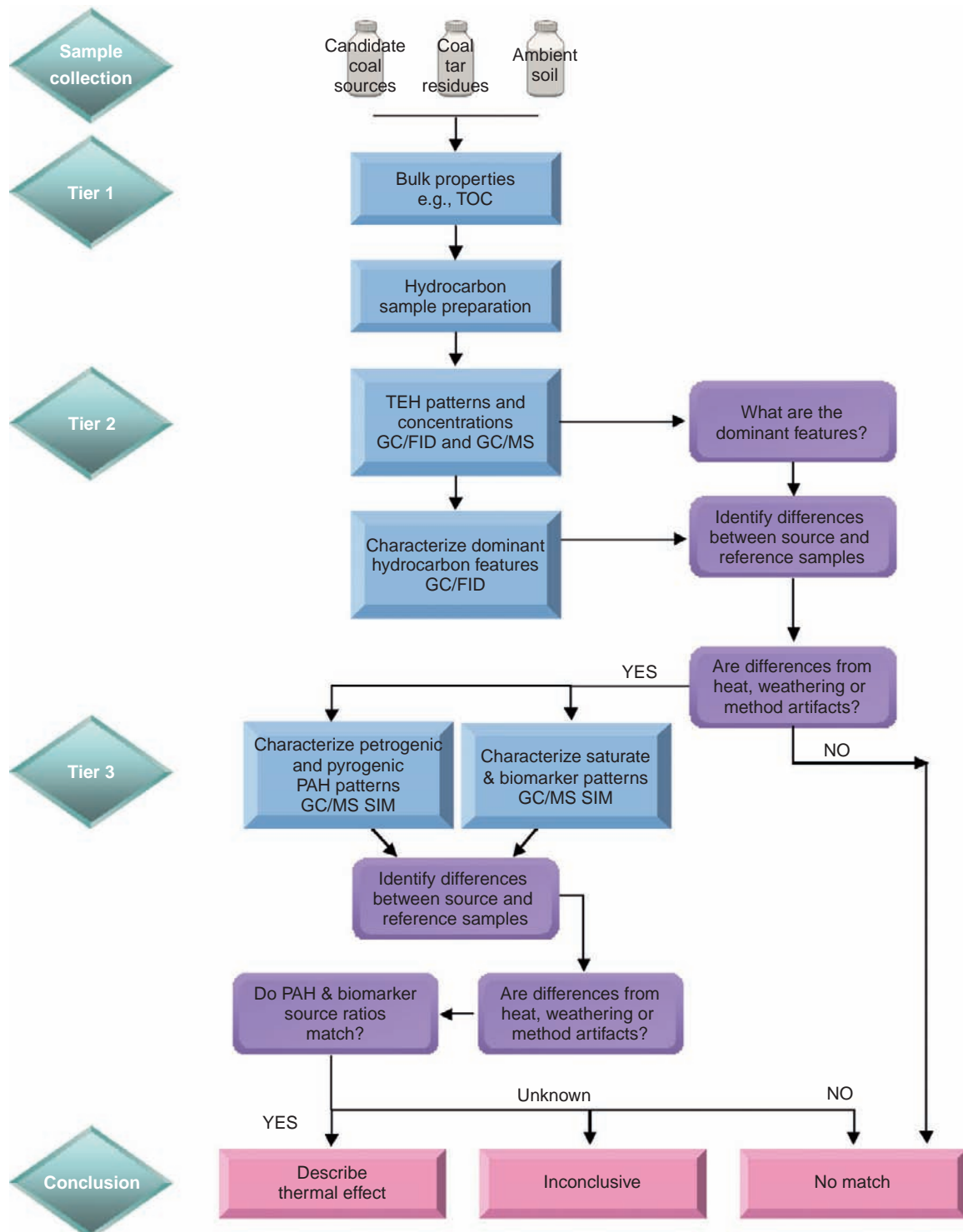


Figure 11.1.1. The multiple lines of evidence approach is a systematic protocol for reviewing hydrocarbon signatures. Tier 1 involves the review of bulk chemical features. Tier 2 incorporates dominant hydrocarbon features from the GC/FID and summation data. Tier 3 folds in the detailed PAH and biomarker results. The conclusions summarize the salient similarities and differences among the laboratory samples compared to each other or reference samples. See subsequent text for acronyms.

Lines of Evidence

The thermal transformation of coal and its by-products can be evaluated on a molecular level using multiple lines of chemical fingerprinting evidence (Figure 11.1.1). Ideally, the chemical results are interpreted in the context of the field, historical, geotechnical, hydrological, and physical (e.g., maceral) data. In keeping with the objective of this chapter, however, the line of evidence of greatest emphasis is the molecular composition of the extractable semivolatile hydrocarbons associated with authentic samples of coal and coal carbonization by-products, particularly liquid coal tar. Coal-tar source investigations benefit greatly from the collection and analysis of uncarbonized (parent) coal and carbonization residues (e.g., coke, coal tar, soot or soils containing mixtures of these).

The lines of chemical evidence are generally evaluated from the major to minor constituents by mass. The measurement of **total organic carbon** (TOC) provides a commonly employed tool for normalizing the concentrations of solvent extractable compounds from coal and coal by-product samples. This normalization minimizes the effect of variable mineral and moisture content. The solvent extractable compounds can include both hydrocarbons and nonhydrocarbons. The measurement of **total extractable material** (TEM) describes the mass of hydrocarbons and nonhydrocarbon extracted from the sample using an organic solvent, such as dichloromethane (DCM). This measurement is primarily used to assure that the optimal hydrocarbon mass is loaded onto the various chromatography columns as described below. The measurement of **total extractable hydrocarbons** (TEHs) is the mass of semivolatile hydrocarbons eluting between $n\text{-C}_9$ and $n\text{-C}_{44}$. The TEH fraction is isolated from the TEM through the chemical adsorption of more polar nonhydrocarbon compounds (see below). The instrument used to measure the concentration of TEH also produces a high-resolution hydrocarbon “fingerprint,” or source signature, that chromatographically depicts the dominant hydrocarbons in the sample. The PAHs comprise a fraction of the TEH that consists of two to six benzene rings with various alkyl side chains. Related to PAHs are numerous condensed aromatic compounds containing various **heteroatomic** (nitrogen, sulfur, and oxygen—NSO) rings or functional groups (side chains). As a class, the PAHs and related heterotomic compounds are dominant features of coal tars but only minor components of coal (see below). The specific PAH patterns for different coals, however, can provide source specific information regarding the thermal maturity or rank of the coal. In addition to PAHs, the TEH of coal and coal by-products also include various saturated hydrocarbons. The concentration and chromatographic “fingerprint” of **saturated hydrocarbons**, such as normal alkanes, acyclic isoprenoid hydrocarbons, and normal alkylcyclohexanes can also help identify coal rank or type as well as distinguish coal distillates in coal tars. Finally, the TEH also includes **geochemical biomarkers** that are always minor constituents of coal and coal by-products; however, these recalcitrant compounds can differentiate coals from different geologic formations and feedstocks from which coal tars originate. Collectively, the multiple lines of chemical evidence derived from the molecular characterization of extractable hydrocarbons in coals and coal by-products help differentiate coals and coal-tar sources while revealing details about the geologic origin and effects of carbonization. The specific analytical methods and interpretative strategies utilized in providing source signatures based upon the semivolatile hydrocarbons extractable from coal and coal by-products, particularly coal tar, comprise the remainder of this chapter.



11.2. Sample Preparation

Organic solvent extraction in the laboratory.

Photo Courtesy of Alpha Analytical Laboratory, Mansfield, Massachusetts, 2009.

Collection

The collection of coal and coal-tar samples for the analysis of semivolatile hydrocarbons is fairly simple. The sample preparation and analysis can be completed with as little as about 5 g of sample; however, a nominal sample size of ~100 g ensures the complete analysis by multiple methods including replicates, if needed. The conventional sample container is a 4 oz (118.25 mL) wide mouth amber jar with Teflon-lined cap that is devoid of organic residues (US Environmental Protection Agency (USEPA), 2003). The samples are labeled with a unique sample identity that often includes a code for the site, location, and depth interval. The samples are wrapped in packing material (e.g., bubble wrap) and shipped to the hydrocarbon laboratory. Coal and coal tar do not require special preservation; however, soil samples are commonly chilled to 2–6°C with ice that is sealed in a plastic bag. A **chain of custody** is commonly completed to assure that the sample collection information (e.g., sample identities, date and time of sampling, field team names, required testing methods, and custodial authority signature) is communicated to the laboratory. Upon receipt, the laboratory inspects the samples for damage during shipment and sample preservation integrity, if applicable.

Extraction

Samples of coal are extracted using a procedure developed for the extraction of semivolatile hydrocarbons from highly sequestered soil and sediment (NOAA, 1993). The sample is initially subjected to particle size reduction with mortar and pestle or equivalent to the approximate consistency of sand. Unless previously determined, approximately 5 g of coal is weighed in an aluminum-weigh boat on an electronic balance (± 0.0001 g). After baking at 105°C for a minimum of 4 hours, the sample is re-weighed and percent moisture determined by difference. A second aliquot of coal (~10 g) is placed in a solvent rinsed glass extraction vessel (8 oz jars with Teflon-lined caps). An equal mass of anhydrous sodium sulfate (Na_2SO_4) is added to remove residual moisture. The sample is spiked with a mixture of **surrogate** compounds that demonstrate the sample extraction efficiency. Thirty to sixty milliliters (mL) of DCM are added on top of the spiked and dried sample. The vessel is sealed and agitated on a shaker table for a minimum of 12 hours. The first extract is decanted through a powder funnel containing anhydrous Na_2SO_4 and collected in an Erlenmeyer flask. The extraction vessel is recharged with DCM (30–60 mL) and extracted a second time on the shaker table for at least 1 hour. After decanting, the extraction vessel is recharged with DCM (30–60 mL) and extracted a third time on the shaker table for at least 1 hour. The combined DCM extract is concentrated by Kuderna Danish apparatus to less than 10 mL. The sample is brought up to exactly 10 mL in a calibrated graduated cylinder. A small aliquot is removed to determine the TEM.

Coal-tar samples are homogenized in the sample collection container with a laboratory spatula. Approximately 2 g are transferred to a dilution vessel (10 mL scintillation vial or equivalent) with Teflon-lined cap. Approximately 4 mL of DCM are added to the vial. The vessel is capped and shaken by hand, vortexed, or sonicated for ~2–5 minutes. The sample is filtered through a powder funnel containing anhydrous Na_2SO_4 that drains into a 10 mL

calibrated volumetric (Class A). The extract is spiked with surrogate and brought up to 10 mL volume. A small aliquot is removed to determine the TEM.

Cleanup

Pure coal and coal-tar samples may not require cleanups due to the relative hydrocarbon purity. If the sample contains high concentrations of interferences, like polar (NSO-bearing) compounds or elemental sulfur, then one or more cleanups are recommended. The isolation of geochemical biomarkers is always recommended for coal-tar samples.

Alumina Solid Phase Cleanup of Polar Organics

Alumina solid phase cleanup is used to remove polar organic compounds from the sample extract. The reference method is EPA Method 3611B (USEPA, 2008). A chromatography column is fitted with a Teflon stop cock. A glass wool plug is placed inside the column, on top of the stop cock. The column is packed with a 10 g bed of alumina (solvent rinsed and oven dried granular aluminum oxide) topped with 1 cm of anhydrous Na_2SO_4 . The column is rinsed with three bore volumes of DCM. A suitable volume of extract containing 10 mg of TEM is transferred to the top of the column and drawn into the solid-phase packing by opening the stop cock. The column is then eluted with 30 mL DCM and collected into a concentrator tube. The extract is evaporated with a stream of high-purity nitrogen gas to less than 1 mL. The extract is quantitatively transferred with rinses to a GC autosampler vial and brought up to 1 mL with DCM.

Copper Solid-Phase Cleanup of Sulfur

Elemental sulfur and sulfide can interfere with the measurement of hydrocarbons. High-sulfur coal and coal-tar samples collected near sulfur crystals benefit from this cleanup step. The reference method is EPA Method 3660B (USEPA, 2008) or NOAA Status and Trends Program methods (NOAA, 1998). The granular copper (99% purity) is activated by suspension in 6N hydrochloric acid. While preventing exposure to air, the copper granules are rinsed with deionized water and stored in DCM. Approximately 2 g of activated copper powder are placed in a 10 mL scintillation vial that contains the sample extract. The Teflon-lined cap is closed and the sample is mixed by hand, vortex, or sonicator. If the copper turns black, the cleanup is repeated with a fresh aliquot of activated copper powder.

Silica Gel Solid Phase Purification of Aliphatic Hydrocarbons

The presence of PAHs interferes with the detection of selected saturated hydrocarbons and geochemical biomarkers. The aromatic interferences are removed by fractionation with silica gel. The reference method is EPA Method 3630C (USEPA, 2008). Silica gel is made from sodium silicate and sulfuric acid (100/200 mesh). The silica gel is purified by extraction with DCM and oven drying overnight at 130°C. A chromatography column fitted with a Teflon stop cock and glass wool plug is loaded with a bed of silica gel (5 g) topped with 1 cm of anhydrous Na_2SO_4 . The column is rinsed with three bore volumes of pentane. A suitable volume of extract containing 25 mg of TEM is solvent exchanged to hexane under a stream of nitrogen. The extract is transferred to the top of the column and drawn into the solid-phase packing by opening the stop cock. The column is then eluted with 20 mL pentane and collected into a concentrator tube. The extract is evaporated in a stream of nitrogen to less than 1 mL. The extract is quantitatively transferred with rinses to a GC autosampler vial and brought up to 1 mL with hexane.



11.3. Sample Analysis

Gas chromatograph/mass spectrometer, Agilent Model 6890.

Photo Courtesy of Alpha Analytical Laboratory, Mansfield, Massachusetts, 2009.

Introduction

Complex hydrocarbon patterns, like those comprising the TEH of coal and coal tars, consist of thousands of compounds in widely varying concentrations. The exploration of these hydrocarbon assemblages benefits greatly by the use of multiple analytical techniques.

Some methods describe the dominant features while others specialize in low concentration constituents with potent source specific information. For example, bulk measurements, like TOC, help relate modern analyses with older datasets whereas highly detailed measurements, like high-resolution gas chromatography in combination with mass spectrometry (GC/MS), help identify dominant semivolatile hydrocarbons with common (e.g., normal alkanes) and highly variable patterns (e.g., terpanes). Diagnostic measurements derived from GC/MS, like the concentrations and distributions of alkylated PAHs and geochemical biomarkers, often reveal source-specific patterns employed by modern geochemists to define formation-specific source signatures of coal and coal by-products. Collectively, multiple methods are used to develop synoptic source signatures across the vast molecular landscape occupied by coal and its by-products.

Total Organic Carbon

The field samples are often tested for TOC for the purpose of normalizing the hydrocarbon concentrations; minimizing the influence of mineral and moisture content; and comparing results with literature values. TOC is commonly measured by EPA Method 9060A (USEPA, 2008). The samples are thoroughly homogenized, and water is removed by evaporation for at least 4 hours in an oven heated to 105°C. The dried sample is ground up with mortar and pestle. Phosphoric acid is added to remove inorganic carbon (e.g., carbonates). Once homogenized and purged of water and carbonates, an aliquot of sample (2–10 mg) is loaded into a tin cup and catalytically combusted at ~1000°C in a stream of oxygen to CO₂. The gas passed through scrubber columns that remove sulfur and halogens. The CO₂ can be measured by several types of detectors including infrared and thermal conductance. The TOC concentration is calculated in mg/kg based on a calibration factor based on multiple calibration standards formulated with carbon source, such as potassium hydrogen phthalate. The initial calibration curve should be verified by accurately measuring the concentration of an independent reference sample with known TOC content. The nominal detection range is 0.01–70% TOC. All samples should be analyzed in duplicate and reported as the average of the replicate runs.

Total Extractable Material

The semivolatile sample extracts are measured for TEM to assure that the proper mass of organic material is injected onto the GC capillary column or silica gel cleanup column. The TEM is measured from the 10 mL sample extract. All gravimetric measurements are performed on an electronic balance capable of measuring ± 0.0001 g.

The procedure involves the transfer of a small aliquot of this extract (nominally 50 μL) into a preweighed aluminum pan resting on a hot plate at about 35°C (5°C below the solvent boiling point). After the solvent evaporates, the aluminum pan containing the extractable material is reweighed and the mass determined by difference. The TEM is calculated as the mass of the residue divided by the 50 μL of solvent. Based on this concentration, 10 mg of the final extract can be diluted in 1 mL DCM for the high-resolution hydrocarbon scan and the alkylated PAH analysis. Similarly, 25 mg can be solvent exchanged to hexane before it is fractionated for the measurement of saturated hydrocarbons and geochemical biomarkers.

High-Resolution Hydrocarbon Scan

The high-resolution hydrocarbon scan depicts the dominant semivolatile hydrocarbons extracted from the field sample. Often this scan yields recognizable hydrocarbon patterns, but it frequently yields novel features that necessitate supplemental testing. Therefore, the high-resolution scan is instrumental in determining the degree to which the sample resembles known hydrocarbon patterns, interesting variations of known patterns, or new patterns for geochemical inquiry.

The reference method for the high-resolution hydrocarbon scan is EPA Method 8015C (USEPA, 2008). This analysis employs the semivolatile TEH extract described previously. The TEM measurement is used to generate a 1 mL extract with no more than 10 mg/mL of extractable material. Based on personal experience, the injection of more than 10 mg/kg into a GC **injection port** degrades the instrument performance over time. **Internal standards** are added to the 1 mL extract to minimize the effects of evaporative loss during the sample analysis. The extract is injected into a GC instrument equipped with **capillary column** and a **flame ionization detector** (GC/FID). Based on personal experience, one of the better GC systems for TEH analysis is the Agilent 6890 using a 95% dimethyl-5% diphenyl polysiloxane, fused silica capillary column with 0.32 mm inner diameter, 30 m length, and 0.25 μm film thickness. The instrument run program begins with the oven temperature set to 60°C for 2 minutes, then increase the temperature by 10°C/minute for 10 minutes, then increase the temperature by 25°C/minute for 2 minutes, then hold the oven temperature at 310°C for 3 minutes. The carrier gas is hydrogen with an isobaric flow rate of 3 mL/minute.

The **initial calibration** involves the analysis of normal alkanes and selected isoprenoid hydrocarbons eluting between $n\text{-C}_9$ and $n\text{-C}_{40}$ run at multiple concentrations between 1 and 200 $\mu\text{g/mL}$ (Table 11.3.1). The **resolution** of the instrument is assured by demonstrating that height of the valley between phytane and $n\text{-C}_{18}$ is less than 40% of the height of phytane using a common baseline in a standard with equal concentrations of both compounds. In addition to developing relative response factors, the initial calibration standards are used to demonstrate the absence of **mass discrimination** by assuring the ratio of $n\text{-C}_{36}$ relative to $n\text{-C}_{20}$ is greater than 0.85. A crude oil **reference sample** is run with every initial calibration to verify comparable pattern resolution and quantitative precision over time. A **continuing calibration** standard is run every day to demonstrate quantitative precision over time.

Once the instrument accuracy, precision, and sensitivity are assured, field sample extracts can be analyzed. The high-resolution hydrocarbon scans demonstrate a variety of hydrocarbon patterns in coals of different rank (Figure 11.3.1). This figure is not intended to be comprehensive of all coals from all ranks; rather, it demonstrates distinctive hydrocarbon patterns from different US formations and geochemical histories. For example, the hydrocarbon pattern in low ranked coal, like the North Dakota lignite (Figure 11.3.1A), contains complex and undulating unresolved complex mixture (UCM) topped by clusters of resolved terpenoid peaks. Moving up the rank scale, the Wyoming subbituminous coal (Figure 11.3.1B) contains long chain n -alkanes ($n\text{-C}_{25}$ to $n\text{-C}_{36}$) with a strong odd-carbon preference attributed to plant waxes from tree leaves. It also shares many lignite features, like the complex clusters of terpenoid peaks and an undulating UCM. More significant compositional changes occur in the high-volatile bituminous coals. For example, alkylated naphthalenes dominate the sample of high-volatile bituminous coal from Colorado (Figure 11.3.1C). In addition to PAHs, the contour of the UCM becomes more broad and homogenous. This loss of features from the native biomass coincides with the onset of more extreme geochemical alterations. However, these alterations fail to completely change the signatures of the original biomass as evident in the continued presence of long chain, odd-carbon dominated n -alkanes. The high-resolution hydrocarbon scan of medium-volatile bituminous coal from Colorado (Figure 11.3.1D) demonstrates the dominant appearance of a homologous series of normal alkanes eluting between $n\text{-C}_8$ to $n\text{-C}_{44+}$ with no odd-carbon preference. The sample also demonstrates the presence of alkylated naphthalenes and more uniform and unimodal

Table 11.3.1
Saturated hydrocarbon compounds, abbreviations, and general classifications.

Analytes	Abbreviation	Carbon number	SHC	Normal Alkanes	Acyclic isoprenoids
<i>n</i> -Nonane	<i>n</i> -C ₉	9	X	X	
<i>n</i> -Decane	<i>n</i> -C ₁₀	10	X	X	
<i>n</i> -Undecane	<i>n</i> -C ₁₁	11	X	X	
<i>n</i> -Dodecane	<i>n</i> -C ₁₂	12	X	X	
<i>n</i> -Tridecane	<i>n</i> -C ₁₃	13	X	X	
<i>n</i> -Tetradecane	<i>n</i> -C ₁₄	14	X	X	
<i>n</i> -Pentadecane	<i>n</i> -C ₁₅	15	X	X	
<i>n</i> -Hexadecane	<i>n</i> -C ₁₆	16	X	X	
<i>n</i> -Heptadecane	<i>n</i> -C ₁₇	17	X	X	
<i>n</i> -Octadecane	<i>n</i> -C ₁₈	18	X	X	
<i>n</i> -Nonadecane	<i>n</i> -C ₁₉	19	X	X	
<i>n</i> -Eicosane	<i>n</i> -C ₂₀	20	X	X	
<i>n</i> -Heneicosane	<i>n</i> -C ₂₁	21	X	X	
<i>n</i> -Docosane	<i>n</i> -C ₂₂	22	X	X	
<i>n</i> -Tricosane	<i>n</i> -C ₂₃	23	X	X	
<i>n</i> -Tetracosane	<i>n</i> -C ₂₄	24	X	X	
<i>n</i> -Pentacosane	<i>n</i> -C ₂₅	25	X	X	
<i>n</i> -Hexacosane	<i>n</i> -C ₂₆	26	X	X	
<i>n</i> -Heptacosane	<i>n</i> -C ₂₇	27	X	X	
<i>n</i> -Octacosane	<i>n</i> -C ₂₈	28	X	X	
<i>n</i> -Nonacosane	<i>n</i> -C ₂₉	29	X	X	
<i>n</i> -Triacontane	<i>n</i> -C ₃₀	30	X	X	
<i>n</i> -Hentriacontane	<i>n</i> -C ₃₁	31	X	X	
<i>n</i> -Dotriacontane	<i>n</i> -C ₃₂	32	X	X	
<i>n</i> -Tritriacontane	<i>n</i> -C ₃₃	33	X	X	
<i>n</i> -Tetratriacontane	<i>n</i> -C ₃₄	34	X	X	
<i>n</i> -Pentatriacontane	<i>n</i> -C ₃₅	35	X	X	
<i>n</i> -Hexatriacontane	<i>n</i> -C ₃₆	36	X	X	
<i>n</i> -Heptatriacontane	<i>n</i> -C ₃₇	37	X	X	
<i>n</i> -Octatriacontane	<i>n</i> -C ₃₈	38	X	X	
<i>n</i> -Nonatriacontane	<i>n</i> -C ₃₉	39	X	X	
<i>n</i> -Tetracontane	<i>n</i> -C ₄₀	40	X	X	
<i>n</i> -Hentetracontane	<i>n</i> -C ₄₁	41	X	X	
<i>n</i> -Dotetracontane	<i>n</i> -C ₄₂	42	X	X	
<i>n</i> -Tritetracontane	<i>n</i> -C ₄₃	43	X	X	
<i>n</i> -Tetratetracontane	<i>n</i> -C ₄₄	44	X	X	
Farnesane (2,6,10-Trimethyldodecane)	<i>i</i> -C ₁₅	15	X		X
2,6,10-Trimethyltridecane	<i>i</i> -C ₁₆	16	X		X
Norpristane (2,6,10-Trimethylpentadecane)	NP	18	X		X
Pristane (2,6,10,14-Tetramethylpentadecane)	Pr	19	X		X
Phytane (2,6,10,14-Tetramethylhexadecane)	Ph	20	X		X
Count	41		41	36	5

Note: Normal alkanes in the semivolatile range elute from *n*-nonane to *n*-tetratetracontane. The dominant acyclic isoprenoid hydrocarbons elute from farnesane to phytane. The nominal detection limits are 1.0 µg/L in water and 100 µg/kg in solid samples using GC/FID or GC/MS instrumentation.

SHC, saturated hydrocarbons.

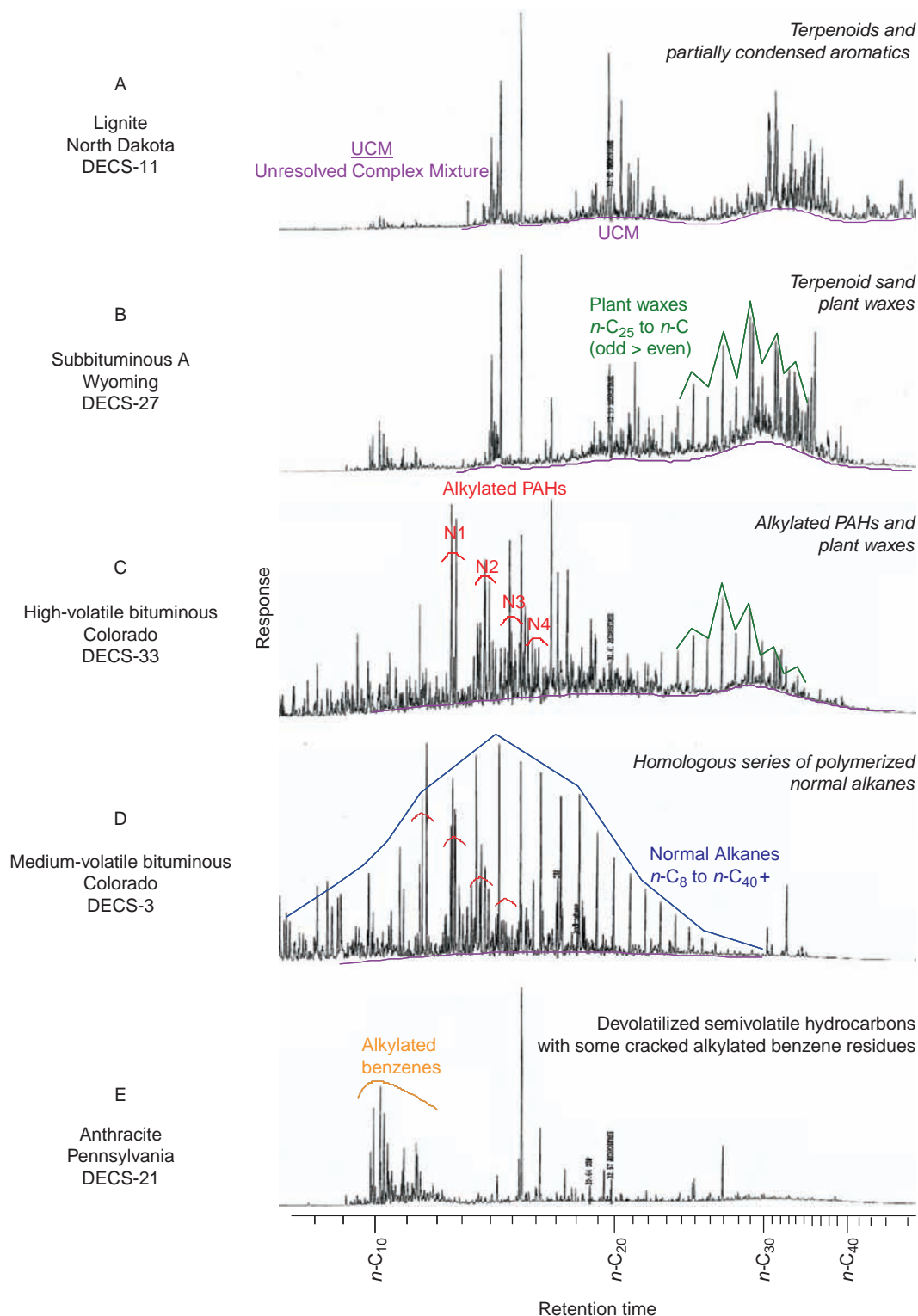


Figure 11.3.1. GC/FID chromatograms of extractable hydrocarbons in selected coals by increasing rank: (A) Lignite (DECS-11) contained terpenoids, partially condensed aromatics and many other compounds, (B) subbituminous coal (DECS-27) contained terpenoids plus plant waxes (normal alkanes eluting between approximately $n\text{-C}_{25}$ and $n\text{-C}_{36}$ with a preference for odd over even number of carbons), (C) high-volatile bituminous coal (DECS-33) contains more aromatic and saturated hydrocarbons from geochemical polymerization, (D) medium-volatile bituminous coal (DESC-3) contains a homologous series of normal alkanes, and (E) anthracite contains relatively simplistic mixture of lighter aromatics. From Stout and Emsbo-Mattingly 2008.

UCM. The semivolatile hydrocarbons in the highest rank coals, like anthracite from Pennsylvania (Figure 11.3.1E), are largely purged out of or condensed into the coal matrix by more extreme geochemical forces. For example, this anthracite contains only low concentrations of alkylated benzenes likely representing pyrolytic residues of the geochemical devolatilization process. Collectively, the hydrocarbon scans of these coal samples demonstrate molecular changes with increasing rank; that is, the early loss of heteroatomic moieties at low rank, the formation of saturated hydrocarbons (e.g., normal alkanes) and PAHs at intermediate rank, and the devolatilization/condensation of semivolatile hydrocarbons at high rank (Van Krevelen, 1993). These general features provide a context for interpreting features observed in other coals and coal tars encountered in the environment.

Polycyclic Aromatic Hydrocarbons

Virtually all fossil fuels and fossil fuel by-products contain PAH patterns with characteristics of hydrocarbon types or specific sources. The high-resolution hydrocarbon scan sometimes depicts the presence of PAHs; however, this method is incapable of comprehensively measuring the majority of PAHs due to the widely varying PAH concentrations and obscuring effects of **coelution** with non-PAH compounds. **Mass spectrometry** solves this problem because PAHs **ionize** with characteristic fragmentation patterns that are accurately measured and differentiated from coeluting compounds. The GC/MS instrument provides the technological means for resolving the concentration of a full range of PAHs and revealing source specific patterns.

Coal predominantly contains variable proportions diagenetic and petrogenic PAHs while coal tar contains high proportions of pyrogenic PAHs. **Diagenetic PAHs** are specific PAH isomers (e.g., retene and perylene) produced by the natural oxidative degradation of vegetative matter. The presence of these compounds in environmental samples indicates the presence of modern or diagenetic residues. **Petrogenic PAHs** contain higher proportions of **alkylated PAHs** relative to **parent PAHs**. This pattern indicates the presence of organic matter that minimally experienced diagenesis and catagenesis (coalification or petroleum formation). The presence of petrogenic PAHs signifies ancient organic matter that became fossil fuel. **Pyrogenic PAHs** contain lower proportions of alkylated PAHs relative to parent PAHs. Thermal exposure preferentially breaks the more reactive bonds of the alkylated side chain before disrupting the more stable PAH ring structure and results in a shift from alkyl-PAH enrichment in fossil fuels to a parent (nonalkyl) PAH enrichment in coal tars and coke.

The reference method for the PAH analysis is EPA Method 8270D (USEPA, 2008). This analysis employs the semivolatile extract described previously. The TEM measurement is used to generate a 1 mL extract with no more than 10 mg/mL of extractable material to maintain consistent instrument performance over time, as discussed previously. Internal standards are added to the 1 mL extract to minimize the effects of evaporative loss during the sample analysis. The extract is injected into a GC instrument equipped with capillary column and a **mass spectrometer** detector operated in the selected ion monitoring mode (GC/MS SIM). Based on personal experience, one of the better GC systems for the characterization of PAHs is the Agilent 6890 using a 95% dimethyl-5% diphenyl polysiloxane, fused silica capillary column with 0.32 mm inner diameter, 30 m length, and 0.25 μm film thickness. The instrument run program begins with the oven temperature set to 60°C for 2 minutes, then increase the temperature by 10°C/minute for 10 minutes, then increase the temperature by 25°C/minute for 2 minutes, then hold the oven temperature at 310°C for 3 minutes. The carrier gas is helium with an isobaric flow rate of 1 mL/minute.

The instrument is initially calibrated with selected PAH isomers containing two to six rings at multiple concentration levels between 1 and 200 $\mu\text{g/mL}$ (Table 11.3.2). The resolution of instrument is assured by demonstrating that height of the valley between benzo[*b*]fluoranthene and benzo[*k*]fluoranthene is less than 40% of the height of benzo[*b*]fluoranthene using a common baseline in a standard with equal concentrations of both compounds. In addition to developing relative response factors, the initial calibration standards are used to demonstrate the absence of mass discrimination by assuring the ratio of benzo[*g,h,i*] perylene relative to phenanthrene is greater than 0.85. A crude oil reference sample is run with every initial calibration to verify comparable pattern resolution and quantitative precision over time. A continuing calibration standard is run every day to demonstrate quantitative precision over time.

Once the instrument accuracy, precision, and sensitivity are assured, field sample extracts can be analyzed. A comparison of the PAH fingerprints demonstrate a variety hydrocarbon patterns in coals of different rank (Figure 11.3.2), recently reviewed by Stout and Emsbo-Mattingly (2008). For example, low rank coal, like the

Table 11.3.2
PAH analytes, abbreviations, and general classifications.

Analytes	Abbreviation	Rings	TPAHs*	EPAPAHs [†]	LPAHs [‡]	HPAHs [§]	SPAHS	Parent PAHs	Alkyl PAHs	Diagenetic PAHs
Naphthalene	N0	2	X	X	X			X		
C1-Naphthalenes	N1	2	X		X				X	
C2-Naphthalenes	N2	2	X		X				X	
C3-Naphthalenes	N3	2	X		X				X	
C4-Naphthalenes	N4	2	X		X				X	
Biphenyl	B	2	X		X			X		
Dibenzofuran	DF	3	X		X			X		
Acenaphthylene	AY	3	X	X	X			X		
Acenaphthene	AE	3	X	X	X			X		
Fluorene	F0	3	X	X	X			X		
C1-Fluorenes	F1	3	X		X				X	
C2-Fluorenes	F2	3	X		X				X	
C3-Fluorenes	F3	3	X		X				X	
Anthracene	A0	3	X	X	X			X		
Phenanthrene	P0	3	X	X	X			X		
C1-Phenanthrenes/Anthracenes	PA1	3	X		X				X	
C2-Phenanthrenes/Anthracenes	PA2	3	X		X				X	
C3-Phenanthrenes/Anthracenes	PA3	3	X		X				X	
C4-Phenanthrenes/Anthracenes	PA4	3	X		X				X	
Dibenzothiophene	DBT0	3	X		X		X	X		
C1-Dibenzothiophenes	DBT1	3	X		X		X		X	
C2-Dibenzothiophenes	DBT2	3	X		X		X		X	
C3-Dibenzothiophenes	DBT3	3	X		X		X		X	
C4-Dibenzothiophenes	DBT4	3	X		X		X		X	
Benzo(<i>b</i>)fluorene	BF	4	X			X		X		
Fluoranthene	FL0	4	X	X		X		X		
Pyrene	PY0	4	X	X		X		X		
C1-Fluoranthenes/pyrenes	FP1	4	X			X			X	
C2-Fluoranthenes/pyrenes	FP2	4	X			X			X	
C3-Fluoranthenes/pyrenes	FP3	4	X			X			X	
Benz[<i>a</i>]anthracene	BA0	4	X	X		X		X		

Table 11.3.2
(continued)

Analytes	Abbreviation	Rings	TPAHs*	EPAPAHs [†]	LPAHs [‡]	HPAHs [§]	SPAHs	Parent PAHs	Alkyl PAHs	Diagenetic PAHs
Chrysene/triphenylene	C0	4	X	X		X		X		
C1-chrysenes	BC1	4	X			X			X	
C2-chrysenes	BC2	4	X			X			X	
C3-chrysenes	BC3	4	X			X			X	
C4-chrysenes	BC4	4	X			X			X	
Benzo[<i>b</i>]fluoranthene	BBF	5	X	X		X		X		
Benzo[<i>k</i>]fluoranthene	BJKF	5	X	X		X		X		
Benzo[<i>a</i>]fluoranthene	BAF	5	X			X		X		
Benzo[<i>e</i>]pyrene	BEP	5	X			X		X		
Benzo[<i>a</i>]pyrene	BAP	5	X	X		X		X		
Perylene	PER	5	X			X		X		X
Indeno[1,2,3- <i>cd</i>]pyrene	IND	6	X	X		X		X		
Dibenz[<i>a,h</i>]anthracene	DA	5	X	X		X		X		
Benzo[<i>g,h,i</i>]perylene	GHI	6	X	X		X		X		
Count	45		45	16	24	21	5	23	22	1

Note: Rings are the number of benzene rings in the PAH molecule. EPAPAHs are the 16 EPA Priority Pollutant PAHs commonly regulated for the protection of environmental health. Light PAHs (LPAHs) contain two or three rings and are prone to environmental weathering (Uhler and Emsbo-Mattingly, 2006). Heavy PAHs (HPAHs) contain four to six rings and are less prone to environmental weathering than LPAHs (Uhler and Emsbo-Mattingly, 2006). Various thiophenes contain sulfur (SPAHs) within the ring structure. Parent PAHs contain no alkylated functional groups attached to the PAH ring structure. The alkylated PAHs (AlkylPAHs) contain one, two, three, or four carbon functional groups attached to the PAH ring structure. Diagenetic PAHs are formed naturally by oxidation of detrital materials generally composed of land plants. The nominal detection limits are 10 ng/L in water and 2 µg/kg in solid samples using GC/MS instrumentation.

* Total 45 PAHs (TPAHs).

[†] EPA Priority pollutant PAHs (EPAPAHs).

[‡] Light two- and three-Ring PAHs (LPAHs) are more prone to environmental weathering.

[§] Heavy four- to six-ring PAHs (HPAHs) are less prone to environmental weathering.

^{||} Sulfur-containing PAHs (SPAHs).

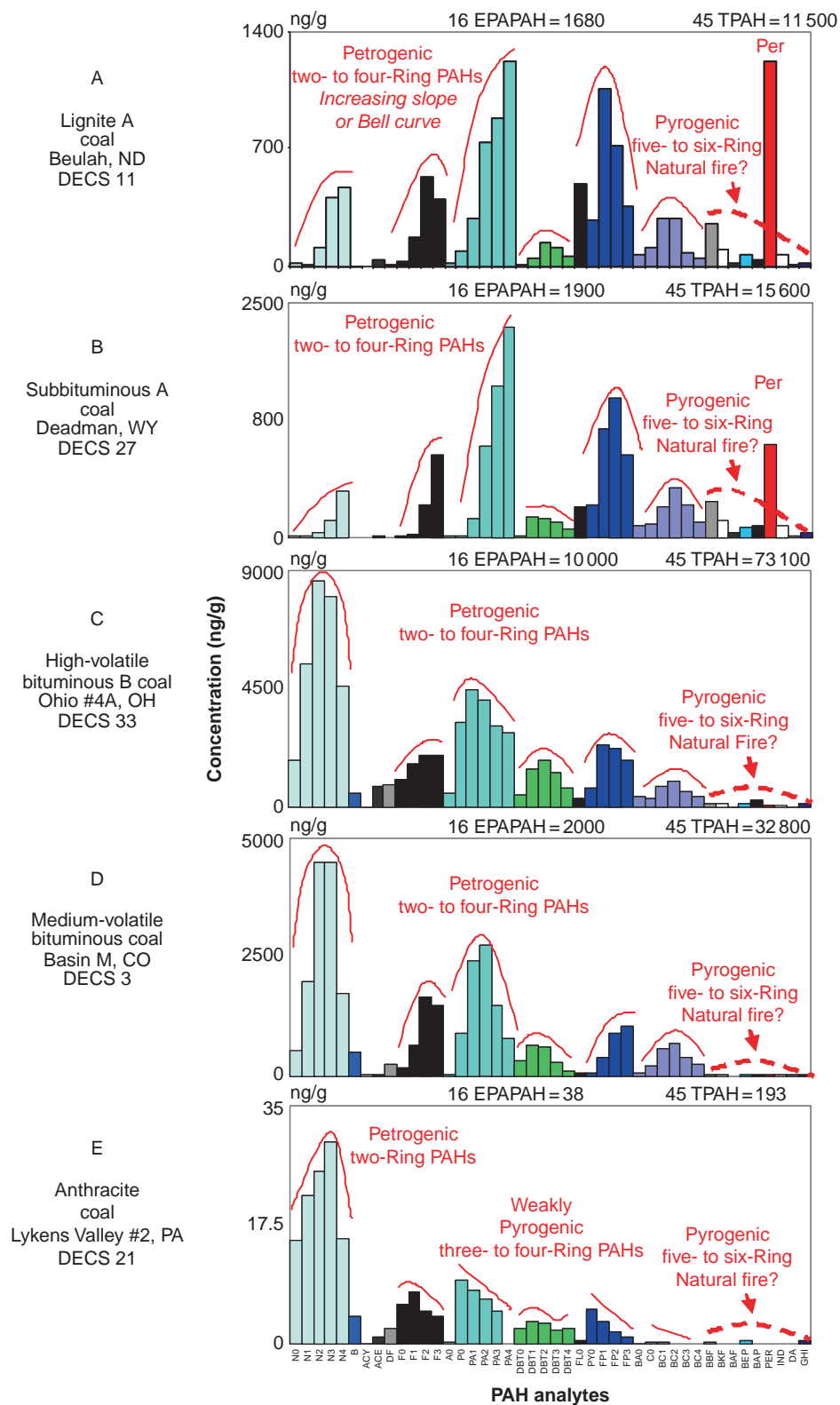


Figure 11.3.2. PAH profiles of extractable hydrocarbons in selected coals by increasing rank. These PAH profiles employ GC/MS to reduce the effects of saturated and polar compounds that obscure these signatures in the GC/FID fingerprints. The purified PAH profile demonstrates some unique features of coal commonly encountered in environmental samples: (A) Lignite (DECS-11) exhibits petrogenic two- to four-ring PAHs with elevated proportions of the diagenetic PAH, perylene, (B) subbituminous coal (DECS-27) resembles the alkylated PAHs in lignite, except the proportions of perylene are lower, (C) high-volatile bituminous coal (DECS-33) exhibits the classic fossil fuel pattern of two- to four-ring PAHs with enriched alkylation, (D) medium-volatile bituminous coal (DESC-3) also exhibits the classic fossil fuel pattern of 2- to 4-ring PAHs with enriched alkylation, and (E) anthracite contains two- to four-ring PAHs with slightly enriched parent PAHs. From Stout and Emsbo-Mattingly 2008.

North Dakota lignite (Figure 11.3.2A), contains low concentrations of PAHs (16 EPAPAHs = 1680 ng/g and 45 TPAHs = 11 500 ng/g) dominated by petrogenic three- and four-ring PAHs (e.g., alkylated phenanthrenes and pyrenes), lower proportions of petrogenic two-ring PAHs and dibenzothiophenes, and a strong perylene peak. The low concentrations of pyrogenic five- and six-ring PAHs are likely attributed to soot derived from prehistoric forest/marsh fires. The Wyoming subbituminous coal (Figure 11.3.2B), also contains low concentrations of PAHs (16 EPAPAHs = 1900 ng/g and 45 TPAHs = 15 600 ng/g) dominated by petrogenic three- and four-ring PAHs, lower proportions of petrogenic two-ring PAHs and dibenzothiophenes, and a strong perylene peak. The low concentrations of pyrogenic five- and six-ring PAHs are likely attributed to soot from prehistoric forest/marsh fires. Some source signature differences between the lignite and subbituminous coals are evident in the different proportions of specific pairs of PAHs, like fluoranthene relative to pyrene, perylene relative to benzo[*a*]pyrene, dialkyl dibenzothiophenes relative to dialkyl phenanthrene, and others. The Wyoming subbituminous coal (Figure 11.3.2B), also contains low concentrations of PAHs (16 EPAPAHs = 1900 ng/g and 45 TPAHs = 15 600 ng/g) dominated by petrogenic three- and four-ring PAHs, lower proportions of petrogenic two-ring PAHs and dibenzothiophenes, and a strong perylene peak. The low concentrations of pyrogenic five- and six-ring PAHs are likely attributed to prehistoric forest fires, coal fires, or volcanic activity. Some source signature differences between the lignite and subbituminous coals are evident in the different proportions of specific pairs of PAHs, like fluoranthene relative to pyrene, perylene relative to benzo[*a*] pyrene, dialkyl dibenzothiophenes relative to dialkyl phenanthrene, and others. The Colorado high-volatile bituminous coal (Figure 11.3.2C), contains higher PAH concentrations compared to the lignite and subbituminous coals (16 EPAPAHs = 10 000 ng/g and 45 TPAHs = 73 100 ng/g). The greater aromatization corresponds with the appearance of high proportions of petrogenic two-ring PAHs and progressively lower proportions of petrogenic three- and four-ring PAHs.

The PAH ratios are unique among the coals in this study (Table 11.3.3). The pyrogenic five- and six-ring PAHs are still present at concentrations comparable with the lignite and subbituminous coals suggesting a preindustrial flux of combustion by-products into prehistoric North American watersheds. The Colorado medium-volatile bituminous coal (Figure 11.3.2D), contains intermediate PAH concentrations compared to the subbituminous and high-volatile bituminous coals (16 EPAPAHs = 2000 ng/g and 45 TPAHs = 32 800 ng/g). The medium- and high-volatile bituminous coals share general features, such as the high proportions of petrogenic two-ring PAHs and progressively lower proportions of petrogenic three- and four-ring PAHs. However, the source specific PAH ratios demonstrate many unique features as well (Table 11.3.2). The pyrogenic five- and six-ring PAHs are present at low concentrations compared to the lower rank coals suggesting the possible importance of watershed size and proximity to combustion sources, or more likely the increasing role that condensation plays on reducing the complexity and molecular size of the extractable hydrocarbons occurring at higher ranks. The Pennsylvania anthracite coal (Figure 11.3.2E), contains trace PAH concentrations compared to lower ranked coals (16 EPAPAHs = 38 ng/g and 45 TPAHs = 193 ng/g). The devolatilized and highly condensed nature of this coal likely resulted from higher temperatures and pressures during formation as indicated by the enrichment of parent relative to alkylated two- to four-ring PAHs. The higher proportion of sulfur in eastern coals is evident in the high proportions of dialkyl dibenzothiophenes relative to dialkyl phenanthrenes, which likely reflects the greater marine influences in the Carboniferous eastern coal basins.

The PAH results from the analyses of coals from different ranks highlight several trends in the semivolatile hydrocarbon signatures. First, lignite and bituminous coals primarily contain petrogenic two- to three-ring PAHs. The PAH concentrations increase by about one order of magnitude from lignite to high-volatile bituminous coal with a commensurate enrichment of petrogenic two-ring PAHs. The PAH content declines by more than an order of magnitude with increasing rank between high-volatile bituminous to anthracite coal. This loss in the amount of extractable semivolatile hydrocarbons throughout the two- to six-ring PAH range and corresponds with an increase in the abundance of nonalkylated, pyrogenic PAHs (e.g., the parent PAHs are higher than the alkylated PAHs in lower rank coals). In short, the character of the PAHs extractable from coal reflects the nature of the initial organic matter and the stage of geochemical maturation.

Saturated Hydrocarbons

The effect of coal type and rank are also reflected in the saturated hydrocarbon signature (Figure 11.3.3). The plant wax patterns and relative abundances vary considerably in coal due to the variable organic matter from which they formed and geochemical maturity. A considerable degree of transformation occurs during the formation of bituminous coals. As rank increases, the declining proportion of plant wax coincides with

Table 11.3.3
Geochemical biomarker analytes, abbreviations, and general classifications.

Analytes	Abbreviation	Saturated rings	Total hopanes	Total steranes
C23 tricyclic terpane	t23	3	X	
C24 tricyclic terpane	t24	3	X	
C25 tricyclic terpane	t25	3	X	
C24 tetracyclic terpane	te24	4	X	
C26 tricyclic terpane-22 <i>S</i>	t26 <i>S</i>	3	X	
C26 tricyclic terpane-22 <i>R</i>	t26 <i>R</i>	3	X	
C28 tricyclic terpane-22 <i>S</i>	t28 <i>S</i>	3	X	
C28 tricyclic terpane-22 <i>R</i>	t28 <i>R</i>	3	X	
C29 tricyclic terpane-22 <i>S</i>	t29 <i>S</i>	3	X	
C29 tricyclic terpane-22 <i>R</i>	t29 <i>R</i>	3	X	
18a-22,29,30-Trisnorneohopane	Ts	5	X	
C30 tricyclic terpane-22 <i>S</i>	t30 <i>S</i>	5	X	
C30 tricyclic terpane-22 <i>R</i>	t30 <i>R</i>	5	X	
17a(<i>H</i>)-22,29,30-Trisnorhopane	Tm	5	X	
17a/b,21b/a 28,30-Bisnorhopane	BNH	5	X	
17a(<i>H</i>),21b(<i>H</i>)-25-Norhopane	25N	5	X	
30-Norhopane	NH	5	X	
18a(<i>H</i>)-30-Norneohopane-C29Ts	C29Ts	5	X	
17a(<i>H</i>)-Diahopane	X	5	X	
30-Normoretane	M29	5	X	
18a(<i>H</i>) and 18b(<i>H</i>)-Oleananes	OL	5	X	
Hopane	HOP	5	X	
Moretane	M	5	X	
30-Homohopane-22 <i>S</i>	H31 <i>S</i>	5	X	
30-Homohopane-22 <i>R</i>	H31 <i>R</i>	5	X	
30,31-Bishomohopane-22 <i>S</i>	H32 <i>S</i>	5	X	
30,31-Bishomohopane-22 <i>R</i>	H32 <i>R</i>	5	X	
30,31-Trishomohopane-22 <i>S</i>	H33 <i>S</i>	5	X	
30,31-Trishomohopane-22 <i>R</i>	H33 <i>S</i>	5	X	
Tetrakishomohopane-22 <i>S</i>	H34 <i>R</i>	5	X	
Tetrakishomohopane-22 <i>R</i>	H34 <i>S</i>	5	X	
Pentakishomohopane-22 <i>S</i>	H35 <i>S</i>	5	X	
Pentakishomohopane-22 <i>R</i>	H35 <i>R</i>	5	X	
13b(<i>H</i>),17a(<i>H</i>)-20 <i>S</i> -Diacholestane	d27 <i>S</i>	4		X
13b(<i>H</i>),17a(<i>H</i>)-20 <i>R</i> -Diacholestane	d27 <i>R</i>	4		X
13b,17a-20 <i>S</i> -Methyldiacholestane	d28 <i>S</i>	4		X
14a(<i>H</i>),17a(<i>H</i>)-20 <i>S</i> -Cholestane	aa27 <i>S</i>	4		X
14a(<i>H</i>),17a(<i>H</i>)-20 <i>R</i> -Cholestane	aa27 <i>R</i>	4		X
13b,17a-20 <i>R</i> -Ethylidiacholestane	d29 <i>R</i>	4		X
13a,17b-20 <i>S</i> -Ethylidiacholestane	d29 <i>S</i>	4		X
14a,17a-20 <i>S</i> -Methylcholestane	aa28 <i>S</i>	4		X
14a,17a-20 <i>R</i> -Methylcholestane	aa28 <i>R</i>	4		X
14a(<i>H</i>),17a(<i>H</i>)-20 <i>S</i> -Ethylcholestane	aa29 <i>S</i>	4		X
14a(<i>H</i>),17a(<i>H</i>)-20 <i>R</i> -Ethylcholestane	aa29 <i>R</i>	4		X
14b(<i>H</i>),17b(<i>H</i>)-20 <i>R</i> -Cholestane	bb27 <i>R</i>	4		X
14b(<i>H</i>),17b(<i>H</i>)-20 <i>S</i> -Cholestane	bb27 <i>S</i>	4		X
14b,17b-20 <i>R</i> -Methylcholestane	bb28 <i>R</i>	4		X
14b,17b-20 <i>S</i> -Methylcholestane	bb28 <i>S</i>	4		X
14b(<i>H</i>),17b(<i>H</i>)-20 <i>R</i> -Ethylcholestane	bb29 <i>R</i>	4		X
14b(<i>H</i>),17b(<i>H</i>)-20 <i>S</i> -Ethylcholestane	bb29 <i>S</i>	4		X
Count	50		33	17

Note: The geochemical biomarkers fall into many classes including the triterpanes and steranes. The nominal detection limits are 10 ng/L in water and 2 µg/kg in solid samples using GC/MS instrumentation.

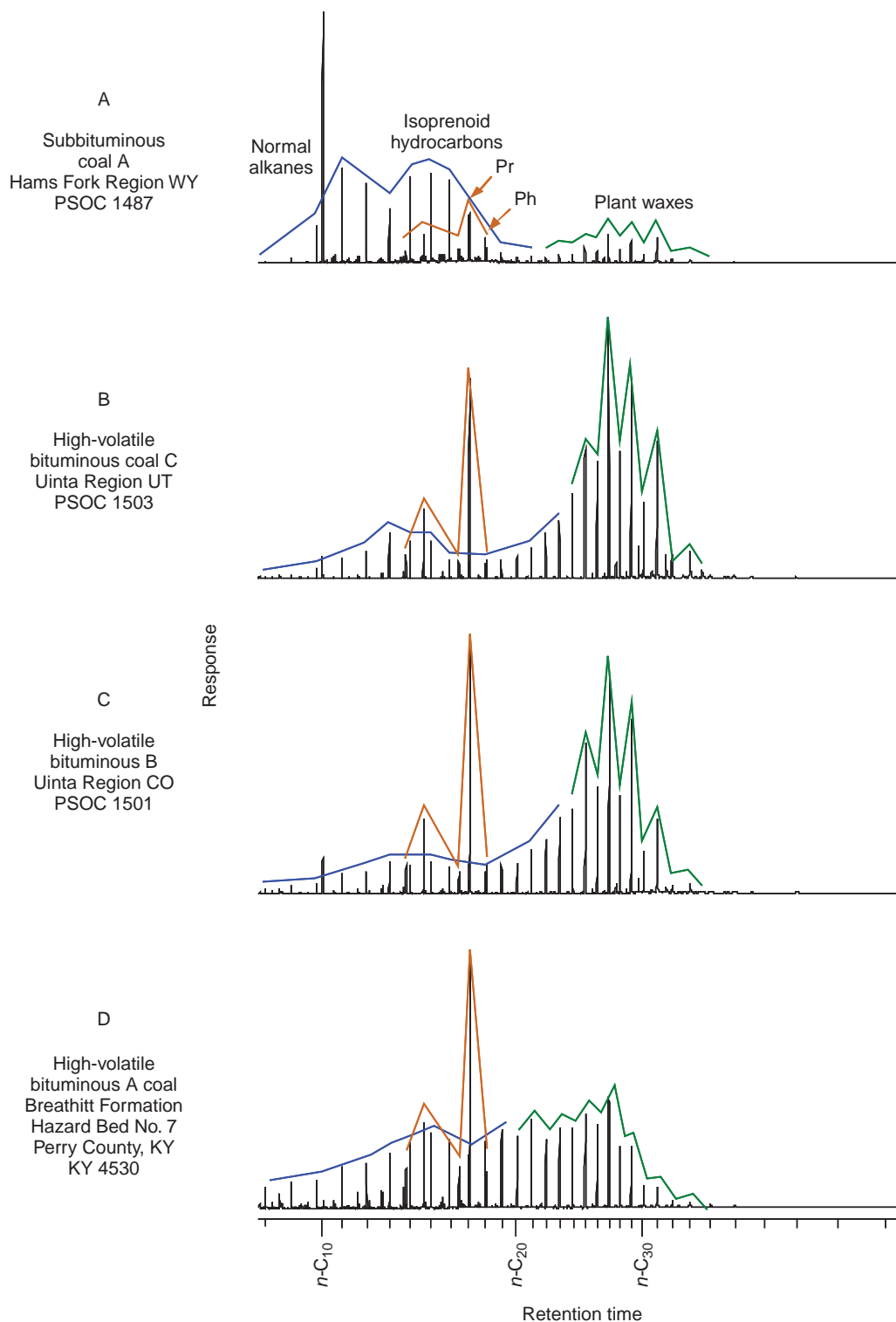


Figure 11.3.3. Saturated hydrocarbon fingerprints (m/z 85) of selected coals by increasing rank. These fingerprints employ GC/MS to reduce the effects of aromatic and heteroatomic compounds that obscure these signatures in the GC/FID fingerprints. The purified saturated hydrocarbon signature demonstrates some unique features of coal commonly encountered in environmental samples: (A) subbituminous coal exhibits the early stages of normal alkane and isoprenoid formation, (B) high-volatile bituminous C coal continues this process while demonstrating a pronounced enrichment of pristane relative to phytane ($>3 \times$), (C) high-volatile bituminous B coal also from the Uinta Formation retains the high ratio of pristane to phytane while demonstrating a slight reduction in the plant wax signature, and (D) high-volatile bituminous A coal from the Breathitt Formation share the high proportion of pristane relative to phytane and the continued geochemical reduction of the plant wax signature.

the increasing abundance of normal alkanes eluting between *n*-octane (*n*-C₈) and *n*-hexatricosane (*n*-C₃₆). Other features reflect the nature of the organic matter from which the coal formed. For example, many coals exhibit different ratios of normal alkanes (e.g., *n*-heptadecane; a.k.a., *n*-C₁₇) relative to acyclic isoprenoid hydrocarbons (e.g., pristane; a.k.a., Pr). Coal frequently contains low proportions of normal alkanes relative to isoprenoid hydrocarbons ($n\text{-C}_{17}/\text{Pr} < 0.5$), largely due to the oxidizing conditions of formation that tend to favor formation of pristane from the phytol side chain of chlorophyll. In petroleum, that is largely derived from marine organic matter under more reducing condition, higher ratios of *n*-C₁₇/Pr are common. In coal that is largely derived from terrigenous organic matter, the ratio of *n*-C₁₇/Pr often reflects the genetic composition of the coal; that is, dominant isoprenoid hydrocarbons formed from chlorophyll mixed with heavy normal alkanes (*n*-C₂₅ to *n*-C₃₇) from leaf waxes. The isoprenoid enrichment is particularly evident in ratios such as *n*-C₁₇/Pr and Pr/Ph that frequently differ by a factor of 4 over broad geographic ranges (Figure 11.3.3B–D).

Geochemical Biomarkers

Geochemical biomarkers include many families of related compounds derived from ancient biomolecules. The triterpane biomarkers are one family of geochemical biomarkers that exhibits a high degree of formation fidelity; that is, the pattern of triterpane biomarkers is frequently specific to a particular contiguous coal bed or petroleum reservoir. The unique triterpane patterns reflect the specific mixture of organic biomass deposited in a region and, for some thermally sensitive stereoisomers, the thermal history of the organic matter after deposition. The triterpane biomarkers are detectable in virtually all fossil fuels, but they are particularly abundant in high and medium volatile bituminous coals (Stout and Emsbo-Mattingly, 2008). Interesting differences appear among many subbituminous and high-volatile bituminous coals reflecting differences in the original biomass and thermal histories of these coals. For example, stereoisomers, like H31-R is more abundant than H31-S (Figure 11.3.4A), which reflects a prominence of the less stable biologically produced H31-R stereoisomer over the more stable, thermally produced H31-S stereoisomer, indicating a lower rank coal that has not yet experienced the thermal stress necessary to form high-volatile bituminous coal with a thermally stable (equilibrated) ratio of H31-S/H31-R greater than 1 typical of higher rank coals (Figure 11.3.4B).

As the coal rank increases, signs of increasing maturity are often evident. For example, the ratio of H32-S/H32-R shifts from less than 1 to greater than 1 as the coal in the Uinta Region matures from high-volatile bituminous C to B (compare Figure 11.3.4B, C). Coals from different formations often exhibit very distinct triterpane patterns that can reflect distinct microbial inputs. For example, norhopane (NH) is less abundant than Tm or hopane in the Uinta Region coals (Figure 11.3.4B, C), but it is the dominant triterpane biomarker in the Breathitt Formation of Kentucky (Figure 11.3.4D). In summary, triterpane biomarkers exhibit features with a high degree of sensitivity reflective of the genetic properties (e.g., types of organic matter and thermal history) that can help distinguish coal by both type and rank.

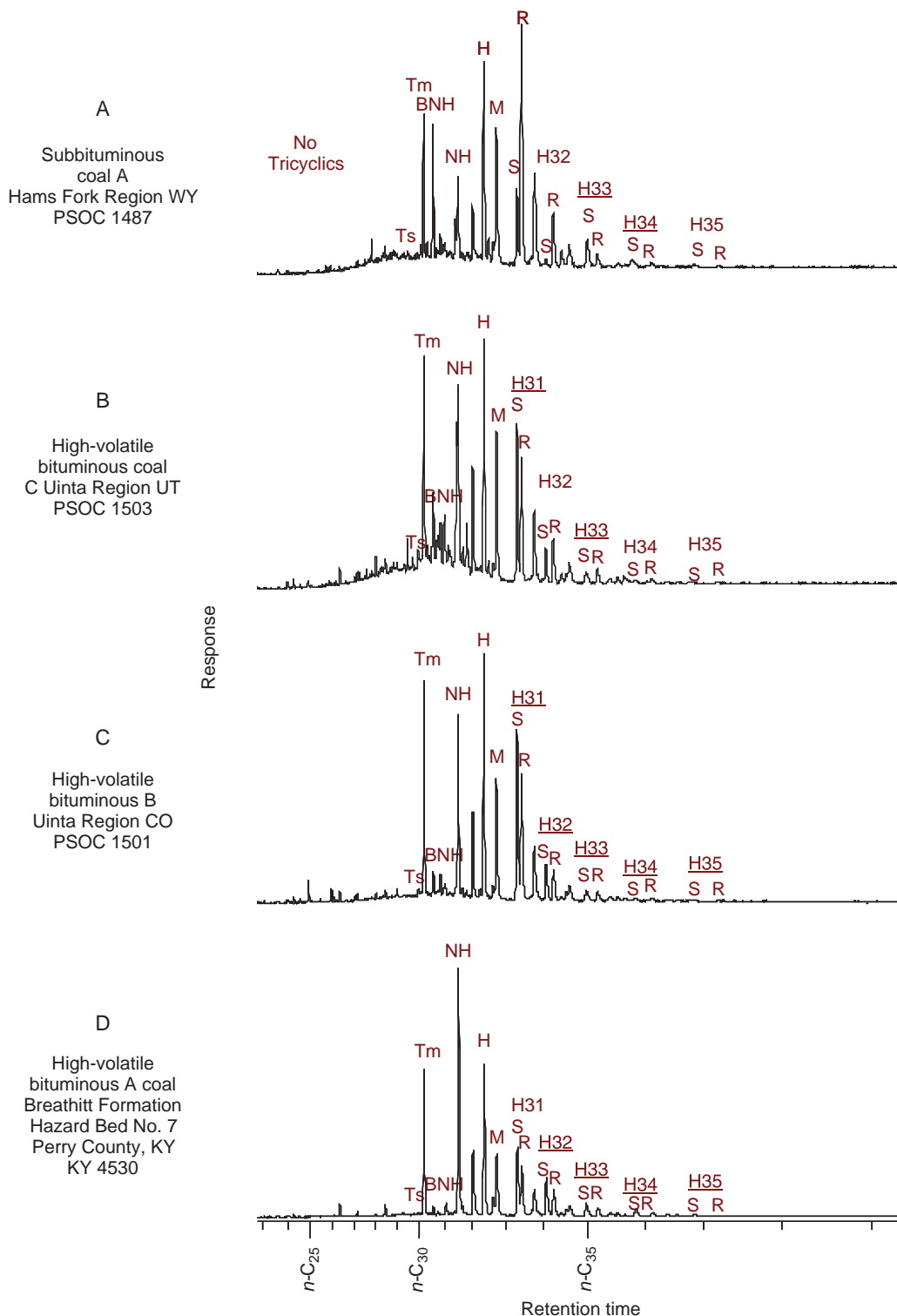


Figure 11.3.4. Triterpane biomarker patterns (m/z 191) in selected coals by increasing rank. These geochemical signatures constitute one of the more unique signatures for differentiating fossil fuel sources: (A) subbituminous A coal contains pentacyclic hopanes and NHs and no significant tricyclic triterpanes frequently observed in petroleum, (B) high-volatile bituminous C coal contains less BNH relative to NH when compared to the subbituminous coal and distinct $R:S$ ratios among the homohopanes stereoisomers, and (C) high-volatile bituminous B coal also from the Uinta Formation retains the triterpane signature of the lower rank coal from the same formation, and (D) high-volatile bituminous A coal from the Breathitt Formation exhibits high proportions of NH relative to hopane (H).



11.4. Coal-Fire Residues

Medium volatile bituminous coal (left) and coke collected from a burning spoils pile at the Mulga, Alabama Gob Fire.

Photos by Stephen Emsbo-Mattingly, 2009.

Semivolatile Hydrocarbons

This section presents source signatures for various groups of extractable semivolatile hydrocarbons from unheated native bituminous coals, carbonized coal residues, and coal by-products. These residues (semicoke or coke) and by-products (tar) were produced naturally and industrially, which are compared and contrasted in the following discussion. The first set of samples represents the transformation of native coal beds associated with the Ruth Mullins coal fire in Perry County, Kentucky (Volume 3). The Ruth Mullins fire occurs in the Hazard No. 7 coal bed in the Pennsylvanian Breathitt Formation. These samples include the unburned native coal, the carbonized coal residues from burned areas of the seam, and liquid coal tars expelled from surface seeps near the fire. The second set of samples represent the transformation of coal in a coke oven and coal distillation apparatus under controlled conditions typical of historic manufactured gas production and modern metallurgical coke production (Emsbo-Mattingly et al., 2003b). Comparing various hydrocarbon signatures from natural and industrial processes is useful in identifying the possible thermal and environmental effects at coal-fire sites.

Dominant Hydrocarbons

The thermal transformations affecting coal and its by-products at coal-fire sites result from the complex interaction of the coal matrix and various factors including temperature, oxygen levels, residence time, and catalytic surfaces. Despite the large number of contributing factors, the character of the semivolatile hydrocarbons produced by these transformations is fairly consistent within a contiguous coal-fire area and around coal carbonization plants. For example, the Ruth Mullins coal fire involves high-volatile bituminous coal in the Breathitt Formation (Volume 3). The primary extractable semivolatile hydrocarbons in this raw, uncombusted coal from the Hazard No. 7 coal bed include alkylated naphthalenes, plant waxes, and a wide, late eluting UCM (Figure 11.4.1A). The effect of thermal exposure on the extractable hydrocarbons is evident in samples of carbonized coal within the coal-fire area and coal tars collected from surface vents. The first sample of partially carbonized coal (site 1) contains three- to six-ring pyrogenic PAHs and a late eluting UCM (Figure 11.4.1B). The second sample of carbonized coal (site 2) contains predominantly four- to six-ring PAHs and a late eluting UCM (Figure 11.4.1C). The greater depletion of two- and three-ring PAHs in the site 2 compared to the site 1 sample indicates that the coal from site 2 experienced a greater degree of thermal stress than the coal from site 1. The relative abundance of four- to six-ring PAHs in the carbonized coal from site 2 may reflect hotter temperature, longer residence time, or more exposure to catalytic surfaces leading to a greater degree of carbonization.

The coal-tar residues from surficial vents also exhibit variable hydrocarbon signatures. The coal-tar sample from vent 1 contains predominantly four- to six-ring PAHs and a late eluting UCM (Figure 11.4.1D). The vent 1 tar sample resembles the carbonized coal from site 2, which indicates that the dominant hydrocarbons in the carbonized coal from site 2 consist of coal-tar residues that were not expelled from the carbonized coal. A second coal-tar sample from vent 5 consists of two- to six-ring pyrogenic PAHs and a late eluting UCM (Figure 11.4.1E). The pattern of PAHs in this tar sample indicates two distinct features. First, the four- to six-ring pyrogenic PAHs and late eluting UCM resemble the vent 1 tar sample. Second, the two- to three-ring pyrogenic PAHs represent a relatively unweathered coal-tar fraction that likely formed due to condensation of volatile vapors produced from the coal fire. Collectively, the source signatures of the extractable hydrocarbons in both carbonized subsurface coals and coal tars found at surface vents from the Perry County coal fire, indicate the widespread

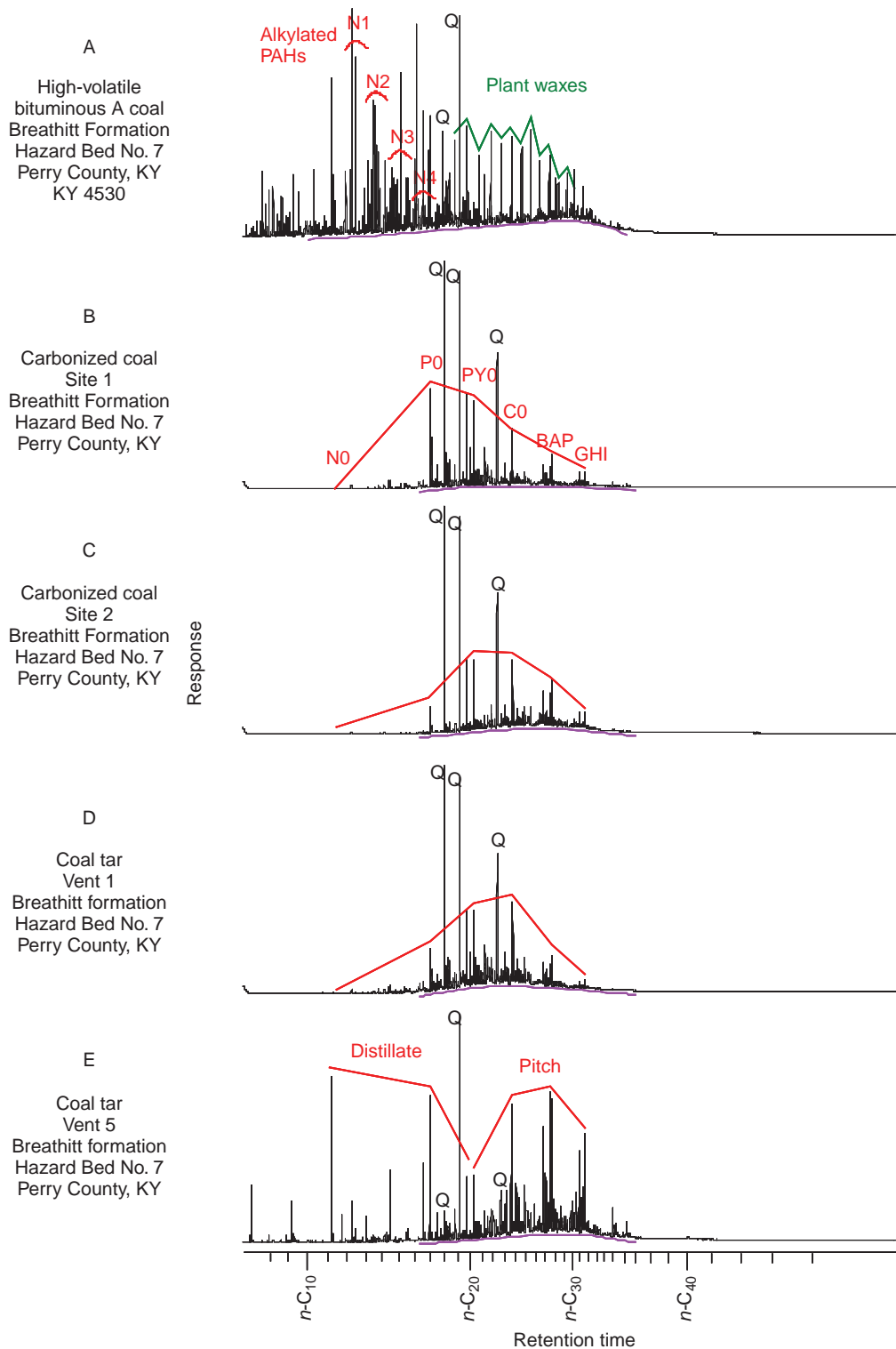


Figure 11.4.1. GC/FID fingerprints of coal and natural coal tars associated with coal fires in the Breathitt Formation, Kentucky: (A) high-volatile bituminous coal from the Breathitt Formation consists of alkylated PAHs, partially reformed plant waxes, and complex mixtures of other hydrocarbons, (B) and (C) coal samples from the fire zone predominantly contain heavy three- to six-ring PAHs, (D) a coal-tar residue collected around surface vent 1 contains heavy PAHs similar to the coal at depth, and (E) a coal-tar residue collected around surface vent 5 contains the heavy PAHs plus lighter two- to three-ring PAHs representing the distillate fraction of coal tar.

presence of PAH-rich residues consistent with variably weathered coal tar. The variability in the coal-tar signatures observed at the vents likely reflect the sequential layering of less weathered and more weathered coal-tar residues. Alternatively, the existence of variously weathered coal tars may represent different mixtures of coal tar and condensates from older (cooked) and newer (leading edge) zones within the coal-fire area.

Unlike an uncontrolled coal fire, the industrial coal carbonization process used for the production of metallurgical coke, manufactured gas, and coal-tar chemical feed stocks occurs in a carefully controlled fashion to assure the quality and quantity of the by-products (Morgan, 1926; Rhodes, 1945). Modern studies of this process demonstrate the molecular changes that occur during the destructive distillation of coal (Emsbo-Mattingly et al., 2003a, b). For example, the extractable hydrocarbon in a “typical” high-volatile bituminous coal feedstock predominantly contains normal alkanes, acyclic isoprenoid hydrocarbons, and a wide UCM (Figure 11.4.2A). The hydrocarbons comprising a carbonized coal distillate produced at 500°C in a glass-lined container with no catalytic surfaces or oxygen predominantly contains alkylated naphthalenes, a homologous series of normal alkane polymers (n -C₉ to n -C₃₆) with no odd-carbon preference, and a broad-boiling UCM (n -C₁₂ to n -C₃₆) (Figure 11.4.2B). The hydrocarbons comprising a carbonized coal distillate produced at 1000°C exhibits nearly identical features as were produced at 500°C (Figure 11.4.2C). Thus, the temperature of formation for a distillate (500°C vs. 1000°C) does not appear to alter the relative distribution of alkylated naphthalenes and prominence of the UCM in the distillate. It is also notable that this distribution of alkyl naphthalene and prominence of a UCM is not atypical for hydrocarbons extracted from uncombusted bituminous coal samples (Figure 11.3.1C, D), perhaps indicating that the longer heating at lower temperatures typical of geological processes can generate the same hydrocarbon distributions produced at higher temperatures over shorter times during controlled carbonization conditions in which catalytic reactions were inhibited. By contrast, pyrogenic PAHs with an absence of any prominent UCM form readily when the same coal is heated to 500°C in an industrial coke oven (Figure 11.4.2D). In this case, a thick coal bed was efficiently heated in an oven lined with refractory brick and metal tubing that collectively provided numerous catalytic surfaces in the form of mineral matter and purified metals. Under these heating conditions, the molecular signature of crude coal tar consists of two- to six-ring pyrogenic PAHs with relative abundances that decline as molecular weight increases (Figure 11.4.2D). Little to no UCM is evident. The coal tar produced in a coke oven at 1000°C resembles the coal tar produced at 500°C (Figure 11.4.2E). Thus, the hydrocarbons comprising distillates or tars produced during the carbonization of coal under controlled conditions are more greatly affected by the potential for reactivity with catalytic surfaces than by the carbonization temperature. The critical difference between the formation of coal distillates and tars appears to be the presence of catalytic surfaces. These results indicate that the variable proportions of pyrogenic PAH and petrogenic UCM among the coal-fire samples (Figure 11.4.1) likely reflect the variable production or mixing of coal tars and coal distillates.

PAH Transformations

Although the dominant hydrocarbons provide significant insight to the hydrocarbons produced during coal fires (see above), the PAH analytical data help specifically reflect the dominant aromatic hydrocarbon signatures in carbonized coals and coal tars. The uncombusted high-volatile bituminous coal from the Breathitt Formation is rather typical of many high-volatile bituminous coals (Stout and Emsbo-Mattingly, 2008). It contains only weakly pyrogenic two- to three-ring PAHs, petrogenic four-ring PAHs, and diagenetic retene (Figure 11.4.3A). However, the carbonized equivalent of this coal from site 1 at the Ruth Mullins coal fire contains a greater abundance of three- to six-ring PAHs that exhibit a strongly pyrogenic distribution (Figure 11.4.3B). The low proportion of two-ring PAHs relative to three- and four-ring PAHs in the carbonized coal is attributable to devolatilization of most two- and some three-ring PAHs associated with a long thermal exposure period. Compared to site 1, the carbonized coal from site 2 contains even lower proportions of two- and three-ring PAHs relative to four-ring PAHs (Figure 11.4.3C), which is likely attributable to even more extreme or longer thermal exposure. Interestingly, the more devolatilized carbonized coal from site 2 exhibits some petrogenic characteristics (e.g., PA0 < PA1 < PA2 > PA3 > PA4) due to the preferential loss of less alkylated homologs (e.g., PA0 and PA1) with higher vapor pressures versus more alkylated homologs (e.g., PA2, PA3, PA4) with lower vapor pressures. These data also demonstrate that retene (RET), a C4-alkylated phenanthrene isomer, is less thermally stable than other PA4 isomers (see change in RET/PA4 ratio among Figure 11.4.3A–C). This thermal instability is a feature shared by many immature coal constituents (e.g., terpenoids, partially condensed aromatics, and, to a lesser degree, plant waxes). The PAHs found in the coal-tar sample from vent 1 (Figure 11.4.3D) resembles the carbonized coal from site 2 with respect to the degree of devolatilization (dashed line). However, the coal tar exhibits lower proportions of fluoranthene and pyrene relative to the alkylated fluoranthenes and pyrenes indicating more extreme devolatilization than in the carbonized coal samples. The coal tar

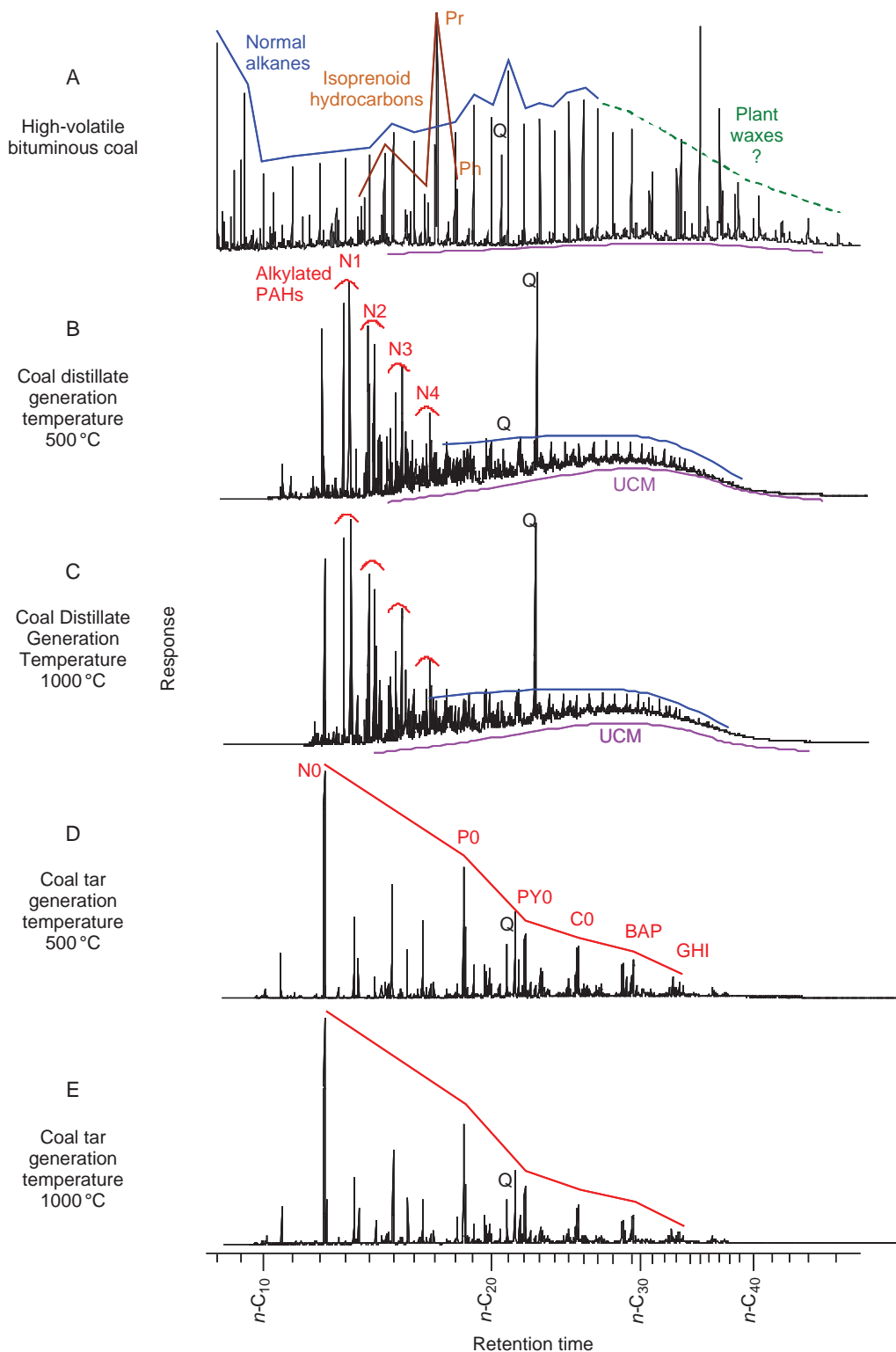


Figure 11.4.2. GC/FID fingerprints of high-volatile bituminous coal under various states of thermal exposure: (A) the high-volatile bituminous coal source material contains a homologous series of normal alkanes, isoprenoids with $Pr/Ph > 3$, and a broad UCM, (B) and (C) coal distillates formed at 500 and 1000°C, respectively, contain nearly identical mixtures of alkylated PAHs, an homologous series of normal alkanes, and a broad UCM, (D) and (E) coal tars formed at 500 and 1000°C, respectively, in a coke oven contained nearly identical mixtures of two- to six-ring PAHs. The passage of the gaseous coal distillate through a hot-coke bed and contact with oven walls are thought to catalyze the transformation of saturated to aromatic hydrocarbons with little sensitivity to temperature in the range of 500–1000°C.

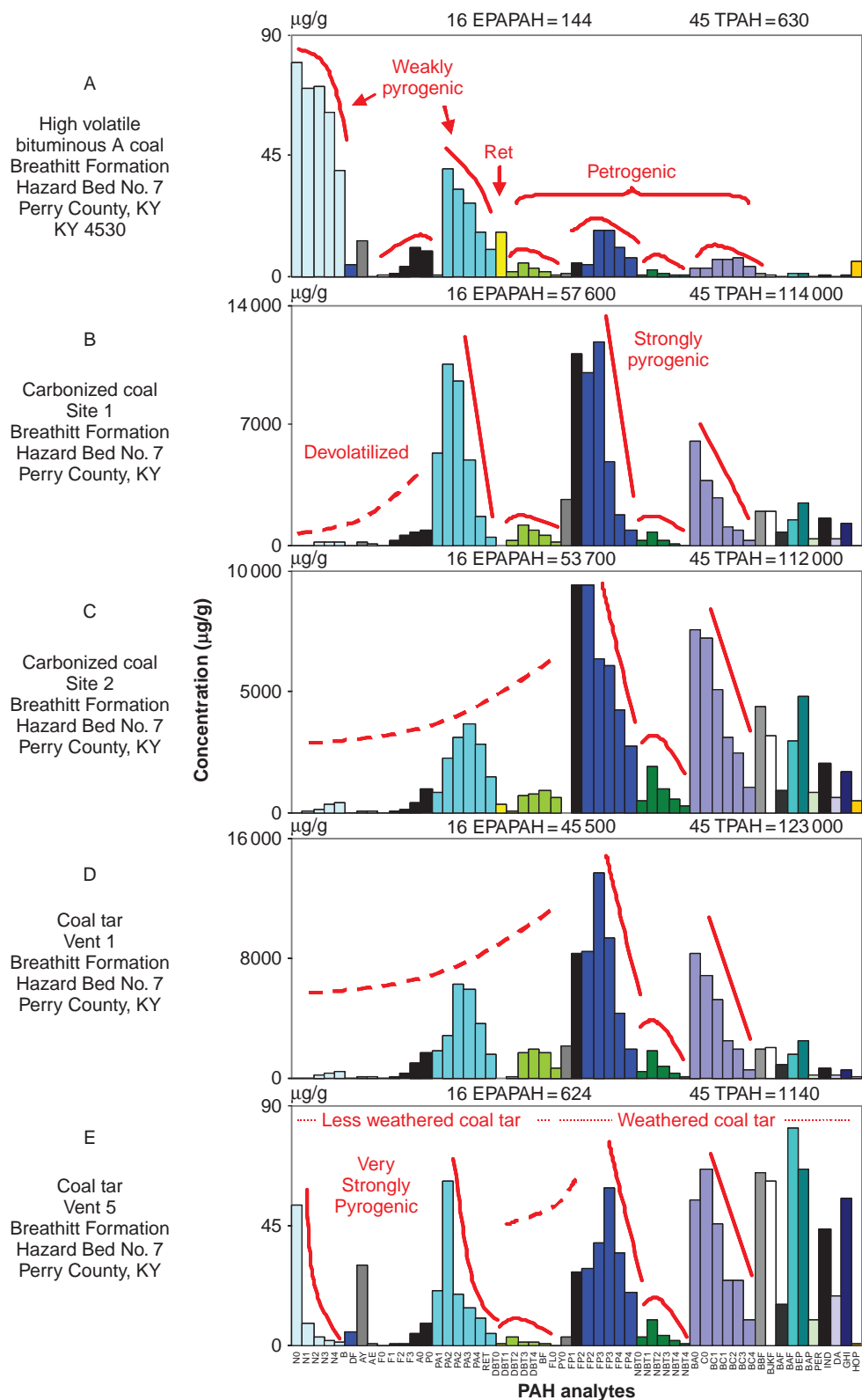


Figure 11.4.3. PAH profiles of coal and natural coal tars associated with coal fires in the Breathitt Formation, Kentucky: (A) high-volatile bituminous coal from the Breathitt Formation contains a mixture of weakly pyrogenic to petrogenic PAHs with retene and hopane, (B) partially carbonized coal beds from the fire zone contain heavy three- to six-ring pyrogenic PAHs consistent with coal-tar pitch (evaporated coal tar), (C) some local coal beds exhibit greater loss of two- to three-ring PAHs due to more extreme devolatilization, (D) a coal-tar residue collected around surface vent 1 contains heavy PAHs similar to the coal at depth, (E) a coal-tar residue collected around surface vent 5 contains heavy pyrogenic PAHs with approximately equal concentrations of fluoranthenes/pyrenes and benz(a)anthracenes/chrysenes due to severe thermal or environmental exposure. It also contains lighter two- to three-ring pyrogenic PAHs representing the distillate fraction of coal tar.

from vent 5 (Figure 11.4.3E) exhibits an even greater degree of devolatilization (e.g., notice the reduced proportion of four-ring PAHs compared to the coal tar from vent 1 and also exhibits lower proportions of (FL0+PY0)/(FP2+FP3)). Despite the apparently high degree of devolatilization in the vent 5 tar, the distillate range two- and three-ring PAHs are enriched in naphthalene (N0) and phenanthrene (P0) and exhibit a strong pyrogenic pattern, which argues for the presence of a relatively unweathered tar. Collectively, this mixture of weathered pyrogenic HPAHs and unweathered pyrogenic LPAH in the vent 5 coal-tar sample demonstrates the presence of a heavily weathered coal tar mixed (giving rise to the prominent four- to six-ring PAHs) with a less weathered coal tar (giving rise to the prominent two- and three-ring PAHs with strong pyrogenic distributions; Figure 11.4.3E).

The PAH patterns for the carbonization products of coal produced under controlled heating conditions (Figure 11.4.4) allows for further interpretation of the naturally produced coal-fire residues shown in Figure 11.4.3. The original coal feedstock consists of weakly pyrogenic two- and three-ring PAHs with lower proportions of petrogenic four-ring PAHs (Figure 11.4.4A), which is typical of high-volatile bituminous coals (Stout and Emsbo-Mattingly, 2008). The coal distillate generated at 500°C contains a nearly identical petrogenic two- to four-ring PAHs as the parent coal (not shown). Similarly, the PAHs in the coal distillate generated at 1000°C also resembled the parent coal (Figure 11.4.4B). However, the coal-tar samples generated at 500°C (Figure 11.4.4C) and 1000°C (Figure 11.4.4D) contain nearly identical pyrogenic two- to six-ring PAHs, which are markedly different from the parent coal and the coal distillates. The relative abundance of the PAH homologs decreases with increasing ring number in the coal-tar samples. Also, the ratio of RET/PA4 decreases slightly during distillation (Figure 11.4.4B) and decreases dramatically during carbonization (Figure 11.4.4C, D) indicating the thermal instability of RET. Importantly, the extractable PAHs from the resulting coke residue predominantly contains two-ring pyrogenic PAHs dominated by naphthalene (Figure 11.4.4E). This naphthalene enrichment is likely attributable to the sequestered vestiges of the coal cracking process that occur when the final coal vapors fail to completely migrate out of the carbonized coal bed. The more highly volatile two-ring PAHs that successfully migrate to the surface frequently condense upon contact with cooler surficial soils and air; for example, the vent 5 coal-tar sample from the coal-fire site (Figure 11.4.3E).

On a quantitative level, the Breathitt high-volatile bituminous coal contained 144 mg/kg EPAPAHs or 630 mg/kg 45PAHs (Figure 11.4.3A). The PAH concentrations of the carbonized coals from sites 1 and 2 and the coal tar at vent 1 increased by more than 2 orders of magnitude (Figure 11.4.3B–D). The coal-tar residue from vent 5 contained only double the PAH concentration measured in the source coal (Figure 11.4.3E). The difference between the vent 1 and vent 5 samples likely reflected mixing/dilution with ambient soil.

The high-volatile bituminous reference coal contained 19 700 mg/kg EPAPAHs or 83 700 mg/kg 45PAHs (Figure 11.4.4A). The coal distillates generated at 500°C (same as Figure 11.4.4B) and 1000°C (Figure 11.4.4B) contained about half of the PAHs of the original coal sample. However, the coal tars generated at 500°C (Figure 11.4.4C) and 1000°C (Figure 11.4.4D) contained 5–10 times more PAHs than the original coal. These data suggest that the concentration PAHs associated with coal distillates are significantly lower than the concentration of PAHs derived from coal tar. Essentially, these disparate PAH production rates demonstrate that the PAH composition of carbonization residues is principally attributed to the coal-tar fraction and not to the coal distillate fraction. The amount of coal tar remaining in (or extractable from) the coke residue is relatively low (EPAPAHs = 8100 mg/kg and 45 PAHs = 12 000 mg/kg) because the minerals and graphitic carbon effectively dilute or inhibit the extraction of the coal-tar residue.

Saturated Hydrocarbon Residues

The transformation of saturated hydrocarbons in coal and its by-products provides another line of evidence demonstrating the effects of thermal exposure and subsequent volatilization experienced during coal fires. Unlike the high-resolution hydrocarbon fingerprints (GC/FID) that primarily resolve the dominant hydrocarbon features (e.g., plant waxes and UCM profiles), the saturated hydrocarbon fingerprints reflected in the *m/z* 85 extracted ion chromatograms obtained using GC/MS reveal more clearly the full spectrum of normal alkanes and acyclic isoprenoid hydrocarbons (Figure 11.4.5). In addition to plant waxes, the Breathitt high-volatile bituminous coal contains abundant pristane and a homologous series of lighter alkanes (*n*-C₈ to *n*-C₂₀) (Figure 11.4.5A). The distribution of these compounds was not as clearly evident in the high-resolution fingerprint for this coal (Figure 11.4.1A). Upon heating in the Ruth Mullins coal fire, the odd-carbon preference among the plant waxes evident in the parent coal disappears (Figure 11.4.5B–E). In addition, the lighter alkanes are depleted in the carbonized coal by-products due to devolatilization. The progressively more extreme degree of devolatilization that was evident in the PAH profiles (Figure 11.4.3) is

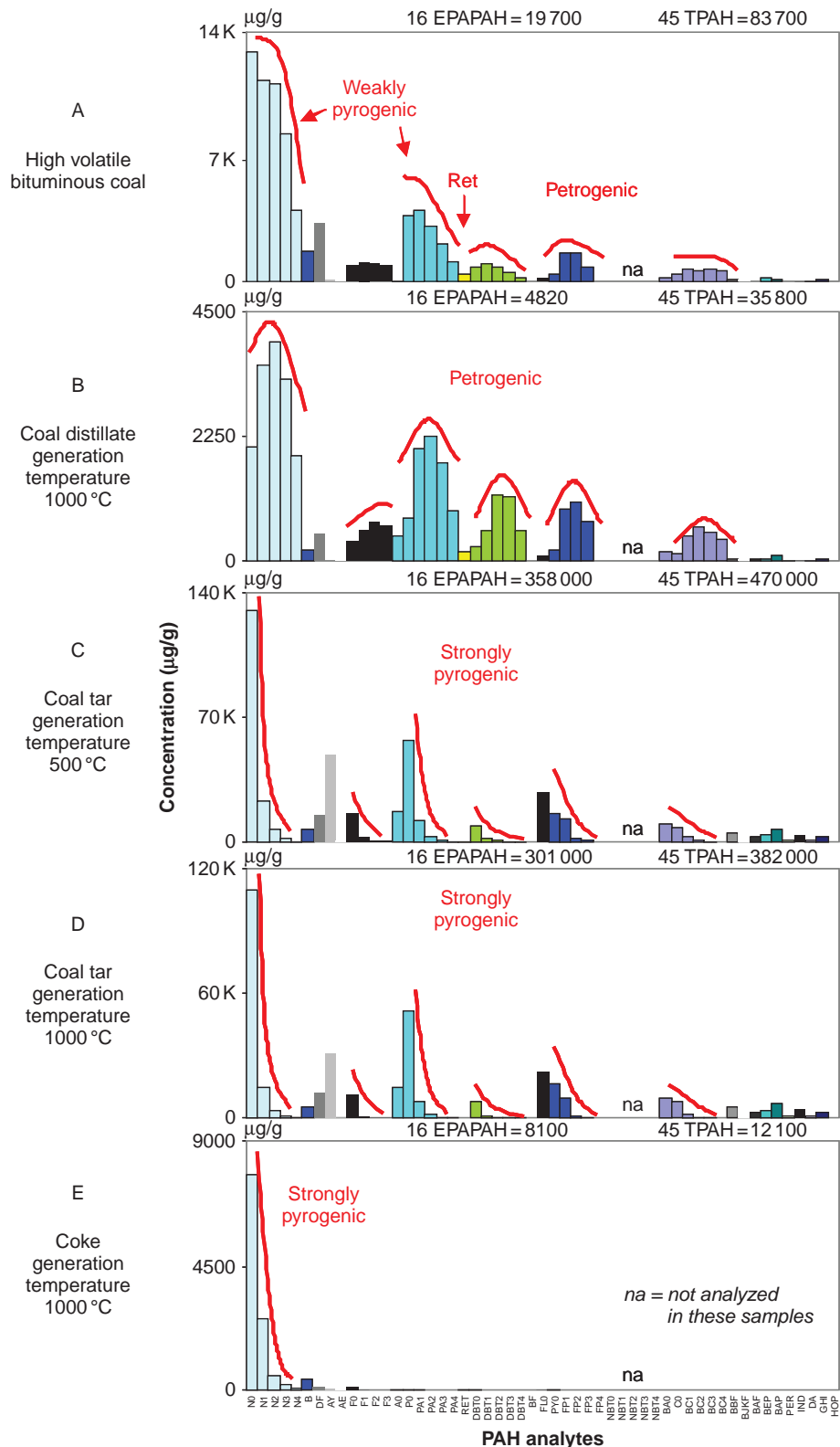


Figure 11.4.4. PAH profiles of high-volatile bituminous coal under various states of thermal exposure: (A) the high-volatile bituminous coal contains weakly pyrogenic and petrogenic PAHs plus retene and hopane, (B) coal distillates formed at 500°C (not shown) and 1000°C, respectively, contain nearly identical mixtures of alkylated two- to four-ring PAHs, (C) and (D) coal tars formed at 500 and 1000°C, respectively, in a coke oven contained nearly identical mixtures of two- to six-ring pyrogenic PAHs. The passage of the gaseous coal distillate through a hot-coke bed and contact with oven walls are thought to catalyze the transformation of saturated to aromatic hydrocarbons with little sensitivity to temperature in the range of 500–1000°C, and (E) coke generated at 1000°C.

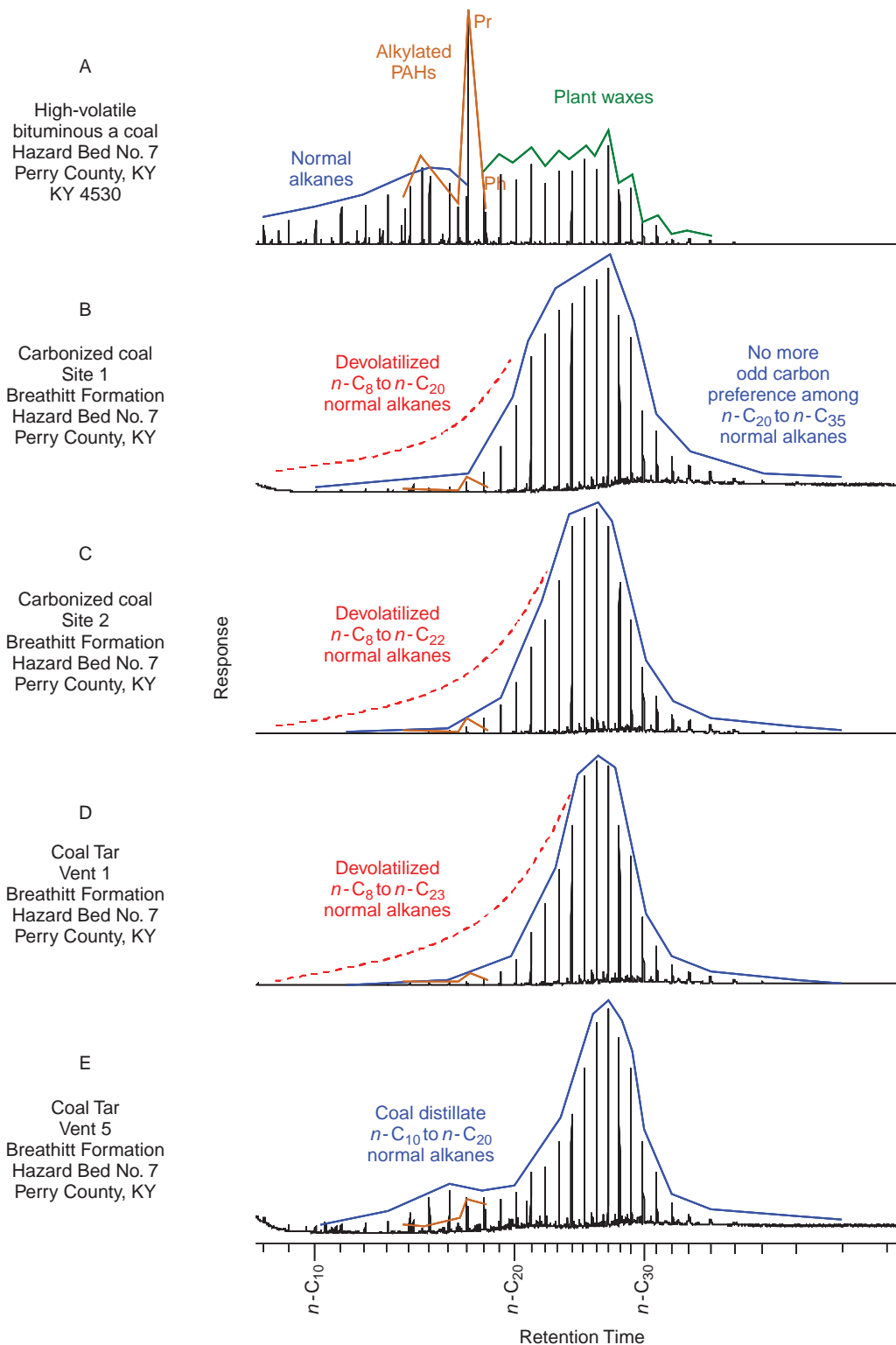


Figure 11.4.5. Saturated hydrocarbon fingerprints (GC/MS m/z 85) of coal and natural coal tars associated with coal fires in the Breathitt Formation, Kentucky: (A) high-volatile bituminous coal from the Breathitt Formation contains a homologous series of normal alkanes eluting between $n\text{-C}_8$ and $n\text{-C}_{36}$. The late eluting normal alkanes exhibited a subtle odd-carbon preference indicative of geologically reformed plant waxes. The ratio of Pr/Ph exceeded 3, (B) the partially carbonized coal bed at site 1 contains a homologous series of normal alkanes eluting from approximately $n\text{-C}_{10}$ and $n\text{-C}_{38}$ with a devolatilized $n\text{-C}_{10}$ and $n\text{-C}_{20}$ and no odd-carbon preference among late eluting normal alkanes, (C) the coal bed at site 2 exhibits greater loss of $n\text{-C}_{10}$ and $n\text{-C}_{22}$ due to more extreme devolatilization, (D) vent 1 coal tar exhibits greater loss of $n\text{-C}_{10}$ and $n\text{-C}_{23}$ due to more extreme devolatilization or evaporation at the ground surface, and (E) vent 5 resembles vent 1, except it also contains $n\text{-C}_{10}$ and $n\text{-C}_{20}$ attributed to a coal-tar distillate.

also evident in the saturated hydrocarbon fingerprints of the carbonized coal (Figure 11.4.5B, C) and coal-tar samples (Figure 11.4.5D, E). The coal-tar residue from vent 5 alone exhibits a distinctive n -C₁₀ to n -C₂₀ normal alkane profile that is analogous to a middle range petroleum distillate, like diesel fuel oil (Figure 11.4.5.E).

The high-volatile bituminous coal reference sample exhibits normal hydrocarbons in the n -C₉ to n -C₃₆ range with a slight odd-carbon preference (Figure 11.4.6A) that is typical of bituminous coals of this rank (Stout and Emsbo-Mattingly, 2008). As evident in many other bituminous coals, the proportion of pristane is significantly more abundant than n -C₁₇ and phytane. The coal distillates generated under controlled heating conditions at 500 and 1000°C contain a more complete homologous series of n -C₉ to n -C₃₆ normal alkanes with no odd-carbon preference or pristane dominance (Figure 11.4.6B). Interestingly, the coal tar generated at 500°C exhibits a bimodal normal alkane profile with a depression in the n -C₂₂ and n -C₂₃ range (Figure 11.4.6C). The heavier hydrocarbons (n -C₂₃ to n -C₃₆) exhibit no odd-carbon preference and likely represent the residual coal-tar distillate that remains after the lighter hydrocarbons cracked into gas-phase fragments.

The distillate range hydrocarbons (n -C₉ to n -C₂₃) likely represent more recently formed normal alkanes distilled from the carbonized coal bed. The coal tar generated at 1000°C also exhibits middle distillate and residual range normal alkanes (Figure 11.4.6D). However, the former is strongly skewed toward an abundance of lower molecular weight hydrocarbons (approximately n -C₉ to n -C₁₁). These lower molecular weight hydrocarbons may form due to the cracking and hydrogenation of higher molecular weight alkanes or liberation from the increasingly carbonized coal matrix.

Coke is an extreme example of devolatilized coal. In addition to pyrogenic two-ring PAHs (Figure 11.4.4E), it contains light molecular weight normal alkanes (Figure 11.4.6E). The presence of lighter normal alkanes in the absence of acyclic isoprenoid hydrocarbons suggests that these light hydrocarbons have been cleaved from larger molecular weight hydrocarbons or from the coal matrix. Despite relatively higher vapor pressures, these light hydrocarbons are often the last semivolatile compounds to volatilize out of heavily carbonized coal or coke. This apparent contradiction makes sense if these light hydrocarbons continuously crack off larger, more thermally stable coal constituents after the initial assemblage of semivolatile hydrocarbons are devolatilized out of the coal matrix. The coke residue also contains long-chain normal alkanes that exhibit a very strong to exclusive even-carbon preference. The origin of these hydrocarbons is suspicious (contamination or misidentification) and under investigation.

Biomarker Stability

Geochemical biomarkers maintain source-specific molecular signatures over geological time and resist environmental weathering very well. Does this recalcitrance extend to thermal exposure over relatively short time frames, that is, coal fires? Inspection of the distributions of pentacyclic triterpanes in unburned coal versus those in its carbonized equivalent and coal-tar residues in this section (Figure 11.4.7) argue that biomarkers are mostly stable with subtle difference under the heating conditions of coal fires; however, complete destruction is theoretically possible under extreme conditions.

The Breathitt high-volatile bituminous coal (Figure 11.4.7A) is dominated by NH followed by Tm and H and exhibits a distribution of triterpanes typical of most bituminous coals (Stout and Emsbo-Mattingly, 2008). The higher proportion of geologically stable *S* versus biologically active *R* stereoisomers among the homohopanes is consistent with the bituminous coals, but not less mature lignite or subbituminous coals that have yet to reach equilibrium conditions (Figure 11.3.4). As noted above, there are several subtle, but significant differences between the Breathitt coal and the carbonized coal residues (Figure 11.4.7B, C). The proportions of bisnorhopane (BNH)/Tm, M/H31-S, Tm/NH, and H/NH are all slightly lower in the native coal compared to the carbonized coal residues. These triterpane pattern differences apparently reflect subtle changes attributable to thermal exposure. Importantly, the triterpane pattern among carbonized coals (Figure 11.4.7B, C) and coal tars (Figure 11.4.7D, E) is virtually identical. This compositional similarity demonstrates a high degree of source signature stability imparted to both the carbonized coal residues and to the coal tars produced during the coal-fire process.

The pattern of triterpane biomarkers in the high volatile bituminous reference coal is dominated by H with lower concentrations of NH and H31-S, with still lower concentrations of Tm, M, and the rest of the homohopanes (Figure 11.4.8A). This pattern is quite different from the Breathitt coal, but it shares the absence of tricyclic triterpanes and very low concentrations of Ts (compare Figures 11.4.7A and 11.4.8A). The absence of tricyclic triterpanes in coals is not unexpected since these compounds are typically derived from marine algal precursors, not

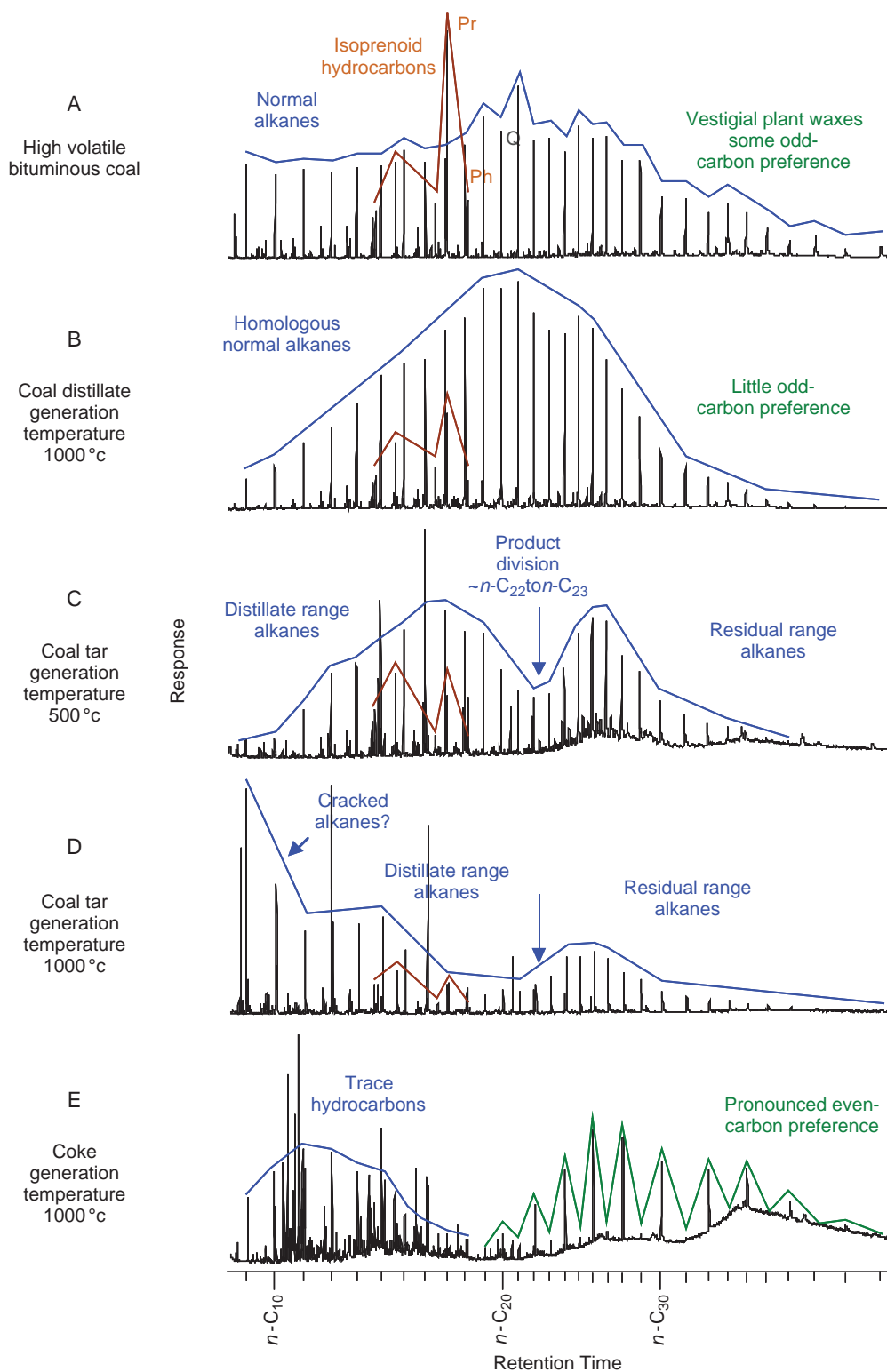


Figure 11.4.6. Saturated hydrocarbon fingerprints (GC/MS m/z 85) of high-volatile bituminous coal under various states of thermal exposure: (A) the high-volatile bituminous coal contains a homologous series of normal alkanes eluting between n -C₈ and n -C₃₉₊. The late eluting normal alkanes exhibited a subtle odd-carbon preference indicative of geologically reformed plant waxes. The ratio of Pr/Ph exceeded 3, (B) coal distillates formed at 500°C (not shown) and 1000°C, respectively, contain nearly identical mixtures of n -C₈ and n -C₃₉₊ with no odd-carbon preference, (C) coal tar generated at 500°C contains a trough in the normal alkane series between n -C₂₂ or n -C₂₃ that separates distillate range and residual range normal alkanes, (D) coal tar generated at 1000°C contains multiple troughs or inflection points in the normal alkane profile demarking light alkanes, distillate range alkanes, and residual range alkanes, and (E) coke formed at 1000°C contained n -C₉ to n -C₁₈ that coeluted with other complex hydrocarbons plus heavy even alkanes eluting between n -C₁₈ and n -C₃₈.

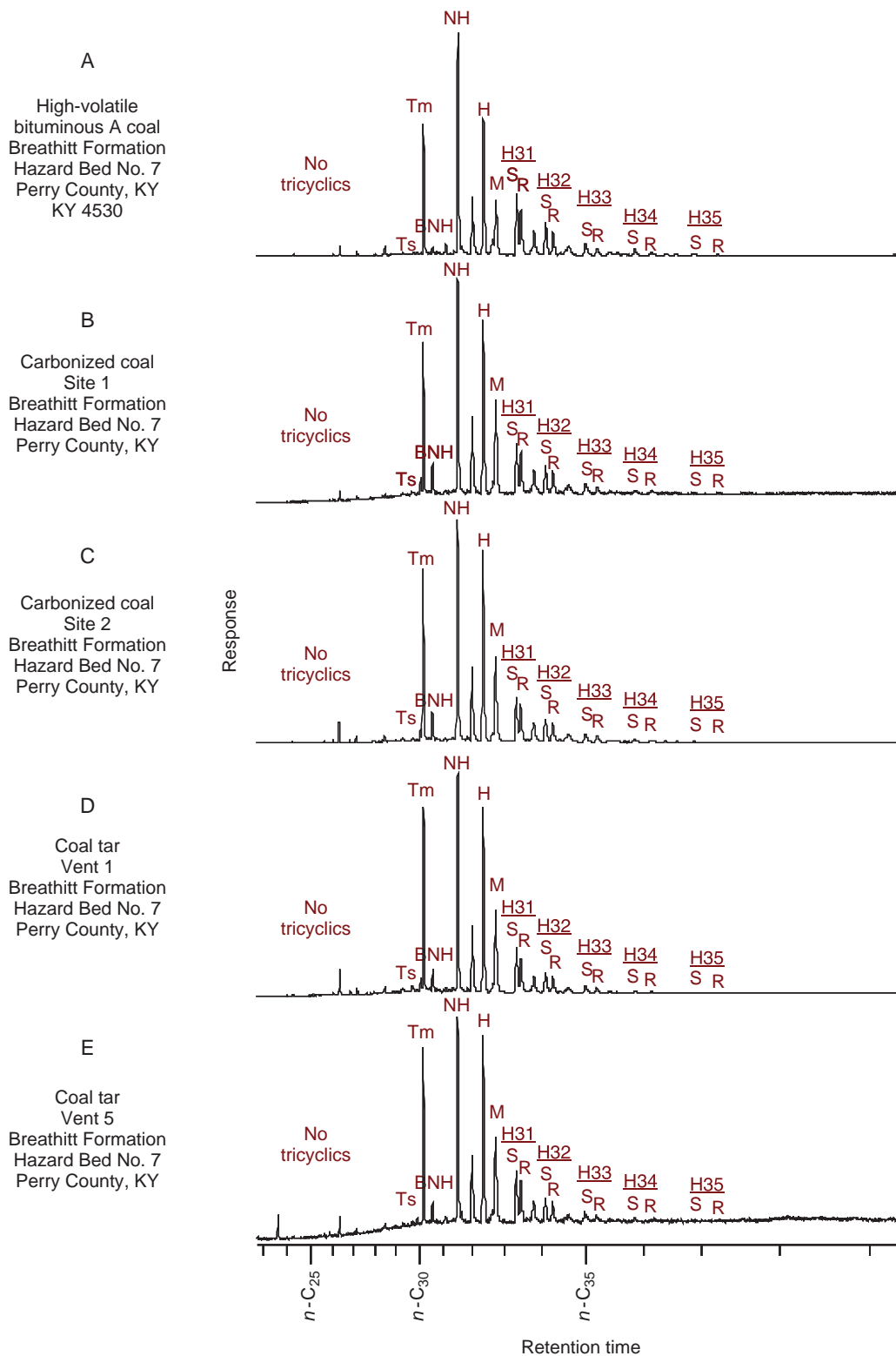


Figure 11.4.7. Triterpane fingerprints (GC/MS m/z 191) of coal and natural coal tars associated with coal fires in the Breathitt Formation, Kentucky: (A) high-volatile bituminous coal from the Breathitt Formation contains triterpanes with high proportions of NH, Tm, H, M, and homohopanes with higher proportions of *S* relative to *R*, (B) and (C) carbonized coal resembles the coal with lower proportions of NH relative to H and higher proportions of BNH and M relative to H, and (D) and (E) coal tars collected at vents 1 and 5 closely resembled the proximal carbonized coals.

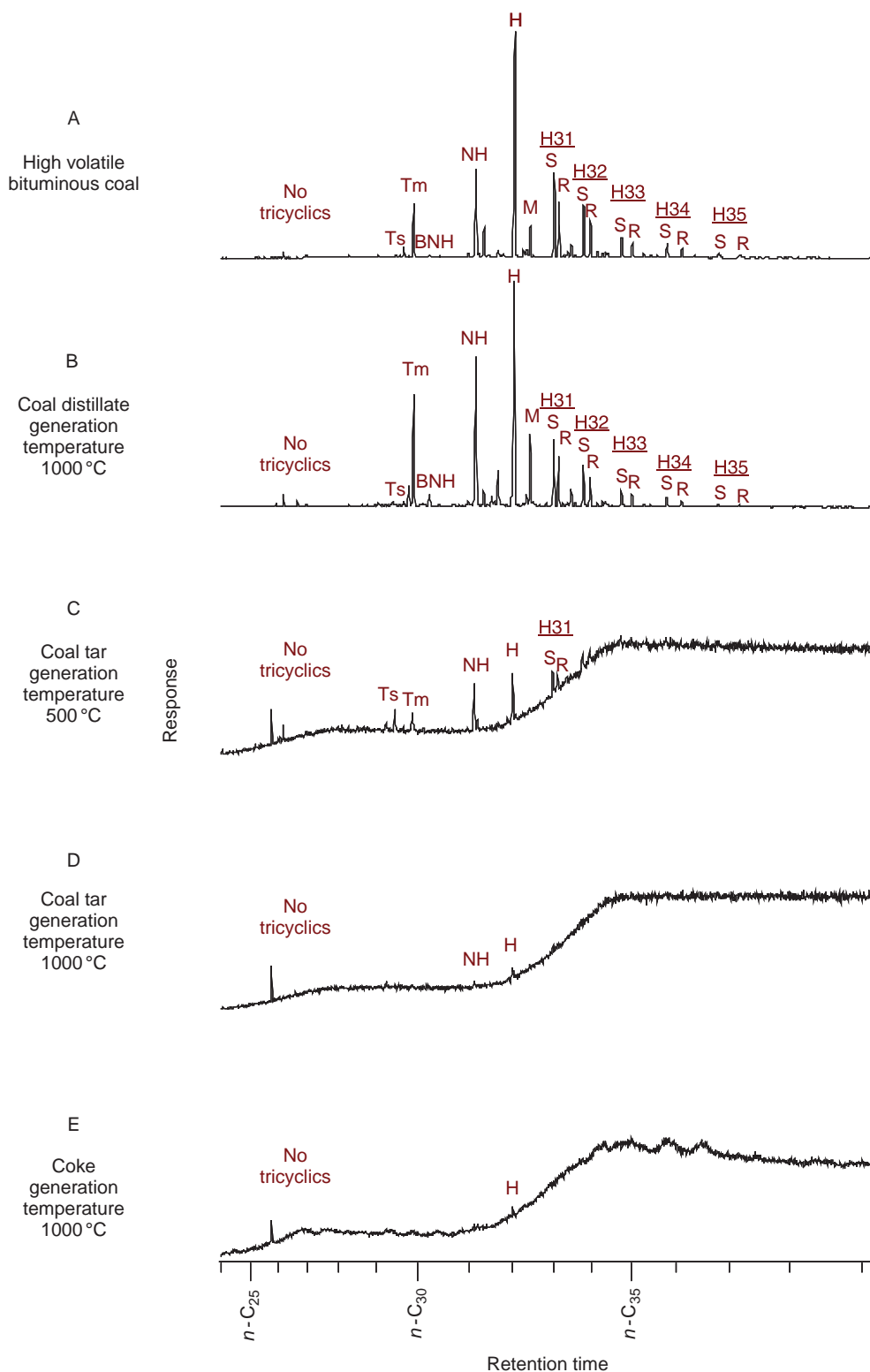


Figure 11.4.8. Triterpane fingerprints (GC/MS m/z 191) of high-volatile bituminous coal under various states of thermal exposure: (A) the high-volatile bituminous coal contains triterpanes with high proportions of H and lesser amounts of NH, Tm, M, and homohopanes with higher proportions of S relative to R, (B) coal distillates formed at 500°C (not shown) and 1000°C resemble the coal, but with higher abundances of Tm, NH, and M relative to H, (C) coal tar generated at 500°C demonstrates triterpane destruction, (D) coal tar generated at 1000°C demonstrates even greater triterpane destruction, and (E) coke demonstrates the near complete destruction of triterpanes.

land plants or microorganisms (Peters et al., 2007). The triterpane pattern of the coal distillate (Figure 11.4.8B) resembles the parent coal, although again several subtle differences attributable to thermal exposure are evident. These differences include the relative abundances of BNH/Tm, M/H31-S, Tm/H, and NH/H that are all slightly lower in the native coal compared to the coal distillate. These same changes were evident in the coal-fire sample set described above. When carbonized efficiently at 500°C (Figure 11.4.8C) many of the biomarkers degrade leading to markedly lower overall abundances and changes in the relative abundances of individual triterpanes; for example, the ratio of Ts/Tm and NH/H increase while M/H31-S decreases. Triterpane biomarkers experience additional losses at higher temperature (1000°C) (Figure 11.4.8D) before reaching almost complete destruction in the coke sample (Figure 11.4.8E). Based on personal experience, the complete destruction of triterpane biomarkers is rarely observed in either coal fire or industrial coal carbonization plants. The retention of triterpane signatures in the course of coal fires (Figure 11.4.7) and industrial coal tars is the norm, not the exception, which is likely due to the fact that it is very difficult to carbonize coal and prevent the commingling of coal distillate and coal-tar vapors. Nevertheless, it is important to know that it is possible to destroy triterpane biomarkers under extreme heating conditions typical of industrial coal carbonization between 500 and 1000°C.

Conclusions

Sophisticated analytical methods exist for the chemical characterization of the extractable, semivolatile hydrocarbons that occur in the nonvolatile by-products produced in the course of coal fires, namely, carbonized coal residues and coal tars. The composition of extractable hydrocarbons in these coal fire by-products resemble those found in the products produced in the course of the industrial carbonization of coal (e.g., coal tar and coke).

Both, coal fires and industrial coal carbonization plants produce by-products with hydrocarbon signatures imbued with information about the native (unburned) parent coal, the conditions of carbonization, and the weathering of the by-products in the environment (particularly volatilization). This information can prove useful in environmental investigations that involve coal carbonization by-products. Both coal fires and industrial coal carbonization involve incomplete and variably efficient carbonization that yields high concentrations of semivolatile hydrocarbons that are readily isolated and measured in modern chemistry laboratories. Of particular utility in the characterization of carbonization by-products are (1) the high-resolution hydrocarbon fingerprints that identify the dominant semivolatile compounds, (2) the distributions and concentrations of PAHs and related sulfur-containing aromatics (S-PAHs) that gauge the degree of pyrogenicity (the severity of heating) and the extent of weathering in the environment, (3) the saturated hydrocarbons that reflect the character of the condensed-distillate fraction produced during carbonization, and (4) the triterpane biomarkers that help associate a parent coal with its carbonization by-products. The growing collection of reference samples from both coal fires and industrial carbonization processes helps recognize and interpret hydrocarbon signatures when evaluating the fate, transport, and potential adverse effects of coal carbonization by-products in the environment.

Acknowledgments

The analytical chemistry discussed in this chapter was produced by the dedicated chemists of the Alpha Woods Hole Laboratory in Raynham, Massachusetts. The authors offer special thanks to Mr. Nicholas Corso (general manager), Elizabeth Porta (director), Norman Lauriano (GC/FID chemist), and Andrew Cram (GC/MS chemist).

Important Terms

Alkylated PAHs	PAHs with hydrocarbon side chains; e.g., 1-methylnaphthalene, 2-ethylphenanthrene, 3-propylpyrene, and 4-butylchrysene.
Anoxic	An environment with little to no oxygen.
Aromatics	Compounds with a conjugated system of fused carbon rings exhibiting high stability from very stable π -bonds (pi-bonds).
Capillary column	A narrow bore column made of fused silica.

Carbonization	The destructive distillation of organic matter with heat in the presence of little to no oxygen.
Catagenesis	The chemical and physical alteration of organic matter at elevated temperature and pressure typically associated with the formation of natural gas.
Chain of custody	The conventional legal format for recording sample collection information; for example, sample identity, collection location, date, personnel, and ownership transfer.
Coalification	The geochemical process of coal formation (Chapter 1).
Coelution	The commingling of chromatographic peaks using a GC instrument.
Combustion	The thermal decomposition of organic matter in the presence of oxygen.
Continuing calibration	GC instrument stability is monitored by running a mid concentration calibration standard every 20 samples.
Diagenesis	The chemical, physical, or biological alteration of organic matter in sediment at ambient temperature.
Diagenetic PAHs	PAHs formed during diagenesis; for example, retene and perylene.
Flame ionization detector	A device that measures the increase in electron emission when a compound is combusted in a hydrogen flame.
Gas chromatograph	This instrument vaporizes a range of compounds ($P_0 > 10\text{--}12$ atm) before separation, typically on a capillary column.
Geochemical biomarkers	Saturated and heteroatomic hydrocarbons consisting of geochemically altered, but stable biomolecules.
Heteroatomic	Containing different atoms, such as hydrocarbons bonded to nitrogen, sulfur and oxygen.
Hydrocarbons	Compounds composed of hydrogen and carbon.
Initial calibration	GC instruments measure target analyte concentrations against a series of calibration standards run at known concentrations.
Injection port	A component of the GC instrument that rapidly increases the temperature to vaporize the target analytes prior to separation on a capillary column.
Internal standard	A quality control compound added by the laboratory to accurately measure target analytes.
Ionize	The destabilization of molecules after electron bombardment.
Mass discrimination	A loss of sensitivity for a molecular weight range.
Mass spectrometer	A device that bombards compounds with electrons and detects the abundances of the resulting fragments.
Mass spectrometry	The science of measuring analyte concentrations and interpreting ion fragment patterns.
Metagenesis	The chemical and physical alteration of organic matter at warm temperature and moderate pressure typically associated with the formation of coal and petroleum.
Parent PAHs	PAHs with no hydrocarbon or heteroatomic side chains; for example, naphthalene, phenanthrene, pyrene, and chrysene.
Petrogenic PAH	PAHs formed during metagenesis exhibit high proportions of alkylated relative to parent PAHs.
Polycyclic aromatic hydrocarbons	Compounds consisting of hydrogen and carbon in fused rings.

Pyrogenic PAHs	PAHs formed during exposure to high heat in the presence (combustion) or absence (carbonization) of oxygen exhibit high parent relative to alkylated PAHs.
Pyrolysis	The cleaving of molecular bonds caused by excess heat energy.
Pyrosynthesis	The condensation of polymeric aromatic carbon networks facilitated by excess heat energy.
Rank	The coal rank is the degree to which geochemical processes alter prehistoric organic matter.
Reference sample	A field sample with known concentrations of target analytes measured repeatedly to demonstrate measurement precision over time.
Resolution	The separation of chromatographic peaks using a GC instrument.
Saturated hydrocarbons	Compounds consisting of hydrogen and carbon connected by single bonds in linear (normal), branched, or cyclic configurations.
Semivolatile hydrocarbons	Compounds that are (1) solids or liquids at room temperature, (2) extractable in organic solvents, and (3) elute on a GC capillary column between <i>n</i> -C ₉ and <i>n</i> -C ₄₄ .
Source Signatures	The properties of a material capable of differentiating one source from another.
Suboxic	An environment with low oxygen concentrations.
Surrogate	A quality control compound added by the laboratory to demonstrate the extraction and analytical efficiency.
Total extractable hydrocarbons	The mass of all hydrocarbons that can be extracted in an organic solvent.
Total extractable material	The mass of all material that can be extracted using an organic solvent.
Total organic carbon	The concentration of all carbons in all organic compounds.
Type	The coal type refers to the biological origin of the prehistoric organic matter and its depositional environment.

References

- Douglas, D.S., Emsbo-Mattingly, S.D., Sout, S.A., Uhler, A.D., McCarthy, K.J., 2007. Chemical fingerprinting methods. In: Murphy, B., Morrison, R. (Eds.), *Introduction to Environmental Forensics*, second ed. Academic Press, Burlington, MA, pp. 311–454.
- Emsbo-Mattingly, S.D., Boehm, P.D., Coleman, A., 2003a. Identifying PAHs from manufactured gas plant sites. Electric Power Research Institute (EPRI) Technical Report 1005289, Palo Alto, California.
- Emsbo-Mattingly, S.D., Uhler, A.D., Stout, S.A., Douglas, G.S., Coleman, A., 2006. Determining the source of PAHs in sediments. *Land Contam. Reclam.* 14 (2), 403–411.
- Emsbo-Mattingly, S.D., Stout, S.A., Uhler, A.D., McCarthy, K.J., 2003b. Identifying coal and ash derived PAHs in soil and sediment. In *Int'l Conf. Contaminated Soils, Sediments and Water*. 19th Annual Meeting, Amherst, MA.
- Emsbo-Mattingly, S.D., 2009. Photo micrographs of medium volatile bituminous coal and coke collected from a burning spoils pile at the Mulga, Alabama Gob Fire.
- Morgan, J.J., 1926. *Manufactured Gas: A Textbook of American Practice*, first ed. Corrected. Jerome J. Morgan: New York, NY, 518 p.
- National Oceanic and Atmospheric Administration, 1993. Trace organic analytical procedures. In: Lauenstein, G. G., Cantillo, A.Y. (Eds.), *Sampling and Analytical Methods for the National Status and Trends Program Mussel Watch Project: 1984–1992*. NOAA Technical Memorandum NOS/ORCA 71: Silver Spring, MD, 201 p.
- National Oceanic and Atmospheric Administration, 1998. Trace organic analytical procedures. In: Lauenstein, G. G., Cantillo, A.Y. (Eds.), *Sampling and Analytical Methods for the National Status and Trends Program Mussel Watch Project: 1993–1996*. NOAA Technical Memorandum NOS/ORCA/CMBAD 130: Silver Spring, MD, 256 p.

- Peters, K.E., Moldowan, J.M., Walters, C.C., 2007. *The Biomarker Guide: Biomarkers and Isotopes in the Environment and Human History*. vol. 1. Cambridge University Press: New York, NY, 489 p.
- Porter, H.C., 1924. *Coal Carbonization*. American Chemical Society, The Chemical Catalog Company: New York, NY, 442 p.
- Rhodes, E.O., 1945. The chemical nature of coal tar. In: Lowry, H.H. (Ed.), *National Research Council Committee, Chemistry of Coal Utilization*, vol. II. John Wiley & Sons, Inc., London, England, pp. 1287–1370.
- Stout, S.A., Emsbo-Mattingly, S.D., 2008. Concentration and character of PAHs and other hydrocarbons in coals of varying rank—implications for environmental studies of soils and sediments containing particulate coal. *Org. Geochem.* 39, 801–819.
- Stout, S.A., Uhler, A.D., McCarthy, K.J., Emsbo-Mattingly, S.D., 2002. Chemical fingerprinting of hydrocarbons. In: Murphy B., Morrison, R. (Eds.), *Introduction to Environmental Forensics*. Academic Press: New York, NY, pp. 135–260.
- Swaine, D.J., 1990. *Trace Elements in Coal*. Butterworth & Company Publishers: London, 278 p.
- Tissot, B.P., Welte, D.H., 1982. *Petroleum Formation and Occurrence: A New Approach to Oil and Gas Exploration*. Springer-Verlag: New York, NY, 538 p.
- Uhler, A.D., Emsbo-Mattingly, S.D., 2006. Environmental stability of PAH source indices in pyrogenic tars. *Bull. Environ. Contam. Toxicol.* 76 (4), 689–696.
- United States Environmental Protection Agency, 2003. Organic chemicals sampling and analytical requirements, 40CFR 141.24, pp. 370-381, http://edocket.access.gpo.gov/cfr_2003/julqtr/pdf/40cfr141.24.pdf (accessed May 2009).
- United States Environmental Protection Agency, 2008. Test Methods for Evaluating Solid Waste, Physical/Chemical Methods, Update IV of the Third Edition, January 3, 2008: <http://www.epa.gov/epawaste/hazard/testmethods/index.htm> (accessed May 2009).
- Van Krevelen, D.W., 1993. *Coal: Typology, Physics, Chemistry, Constitution*, third ed. Elsevier, Amsterdam, The Netherlands, 890 p.

CHAPTER 12

Magnetic Signatures of Rocks and Soils Affected by Burning Coal Seams



Andrew Sparks measuring the strength of the geomagnetic field with a cesium vapor magnetometer at the location of the Roedeske 4 burning coal seam in western North Dakota, USA. *Photo by Rob Sternberg.*

CHAPTER CONTENTS

12.1 Magnetic Signatures

- Introduction
- Field Work
- Magnetic Anomalies
- Magnetic Properties
- Discussion
- Acknowledgments
- Important Terms
- References
- WWW Addresses:
Additional Reading



Photo by Robert S. Sternberg, 2003.

12.1. Magnetic Signatures

Robert S. Sternberg

Scoria Point Overlook, South Unit, Theodore Roosevelt National Park, North Dakota. Scoria is the local name of the red clinker that formed when Paleocene lithostratigraphic units were exposed and burned during the Quaternary.

Introduction

For coal fires that burn near the Earth's surface, geophysics can be used to make inferences about the extent of the burn. For smaller active burns, the conversion of magnetic minerals in the overlying soil can enhance **magnetic susceptibility** (the ability of a material to become temporarily magnetized in the presence of an applied magnetic field). *In situ* measurements of the susceptibility or detection of the resulting **magnetic anomalies** (magnetic field readings that deviate from the generally smooth magnetic field on the Earth's surface) will both reflect this mineralogical conversion.

The formation of pyrometamorphic rocks, i.e., clinkers, by larger fires is accompanied by the acquisition of a significant **thermoremanent magnetization** (TRM), a permanent magnetization acquired when ferromagnetic minerals are heated to several hundred degrees centigrade, which will generate larger magnetic anomalies. These clinker anomalies allow the geophysical delineation of older coal burns and can locate the transition from coal seams, used as an energy resource, to the less valuable clinker, used as an aggregate. Because the magnetic signatures are generated under unusual geologic conditions of low pressure, high temperature, and high oxygen fugacity, these soils and rocks might also be used to understand magnetization acquired under these conditions.

This chapter will provide a brief overview on the use of magnetometry, although different techniques of geophysics and remote sensing have been applied to the study of coal fires. Zhang et al. (2004) present an excellent discussion of the general nature of coal fires and the use of remote sensing methods to detect them. Other ground-based geophysical techniques include seismic refraction (Sontag, 1984), ground penetrating radar (Lindner and Rüter, 2007), and electromagnetics (Schaumann et al., 2008).

Creation of clinker by burning coal seams (Heffern and Coates, 2004) is a special case of combustion metamorphism (CM), when organic-rich sediments burn. Combustion metamorphism is also found in the bitumen-rich Upper Cretaceous–Lower Tertiary Hatrurim Formation in Israel (Matthews and Gross, 1980). Cisowski and Fuller (1987) looked at combustion metamorphism due to oxidation of fine pyrite in oil-bearing marine carbonaceous rocks in the Monterey and Sisquoc Formations in southern California and the Marcelina Formation in Venezuela. These diagenetic sources of magnetic anomalies over sedimentary rocks contrast with syngenetic magnetic anomaly sources as discussed by Gay and Hawley (1991). According to these authors, both anomaly types were found to coexist in the Kaiparowits Plateau, Utah, in the southwestern United States.

Field Work

The surveys described here all use standard procedures for magnetic surveying (Milsom, 2003; Burger et al., 2006). Studies of the Hatrurim Formation, Israel, show how the airborne and ground results are complementary (Khesin and Itkis, 2002; Khesin et al., 2007). Aeromagnetic surveys flown at elevations of 1000 m showed anomalies with amplitudes of 20 nanoteslas (nT are an SI unit for measuring the strength of the magnetic field), whereas ground-based surveys showed anomalies up to 4000 nT. The amplitude decreases because of the greater height of the airborne sensor above the magnetized rocks causing the anomalies. The anomalies in the ground surveys also show shorter wavelengths due to the highly variable magnetization of the near-surface rocks.

Schaumann et al. (2008) carried out airborne magnetics over coal fires in China with a cesium vapor **magnetometer** (an instrument used to measure the Earth's magnetic field). An area over 100 km² was covered, with line spacings varying from 50 to 250 m and along-profile sampling intervals of about 2 m. This was supplemented by ground surveys using an optically pumped magnetometer, at measurement spacings of 10 m, over an area of about 1300 m by 600 km. Ground surveys, carried out closer to the source, are capable of providing higher resolution of the anomalies if the data are collected at close spacings.

In perhaps the first published reports of ground magnetic surveys over clinkers, Hasbrouck and Hadsell (1976, 1978) reported on ground magnetic profiles at clinker locations in Wyoming and Montana, USA. Station spacings were on the order of 10 m, and profile lengths were 250–750 m long. Anomalies up to 2500 nT were observed.

Sontag (1984) collected ground magnetic data over clinkers in Wyoming, USA, situated in the Tertiary Fort Union Formation. Readings were taken along three profiles with lengths of 300–800 m at station spacings of 7.65 m. A proton precession magnetometer was used, which only had a resolution of 10 nT, although this is adequate to characterize the large anomalies that were observed. A base station was used so that the temporal **diurnal variation**, occurring over the course of the day because of ionospheric effects, could be separately recorded. Removal of this pattern from the data set isolated the actual spatial variation in the magnetic signal. Anomalies were as high as 1500 nT.

Lindqvist et al. (1985) made six ground magnetic traverses over clinkers at three localities in New Zealand. They used a proton precession magnetometer, making measurements every 5–20 m along east–west profiles 200–400 m in length. Anomalies of 1500 nT were observed.

Sternberg and Lippincott (2004) reported on magnetic surveys in the vicinity of two recently extinguished coal-seam fires in western North Dakota. Sixteen profiles were run at these two sites, using a cesium vapor magnetometer and GPS positioning. Measurements were made every 0.5 seconds at walking speeds, with profiles at variable spacings. Anomalies over 1000 nT were typically observed when clinker outcrops were crossed, with a peak anomaly over 2800 nT.

Sternberg et al. (2008) reported on magnetic surveys over active and recently extinguished Tertiary lignite coal-seam fires in western North Dakota, USA. Five sites were surveyed with a cesium vapor magnetometer. Anomalies over 1000 nT were observed.

Lindner and Rüter (2007, 2008) described magnetic surveys over burning coal as part of the Sino-German Coal Fire Research Initiative. In the Xinjiang Autonomous Region, two fire zones were surveyed, with measurements made every 1–2 seconds at walking speed with an Overhauser survey magnetometer, along with a proton precession magnetometer base station. Sub-centimeter positioning by differential GPS allowed measurements to be made in “random walk-mode,” which was advantageous in the rugged terrain. Grids were 200–300 m long by 40–80 m wide. Anomalies over the burning Jurassic strata exceeded 500 nT (Lindner and Rüter, 2007).

Lindner and Rüter (2007) also cite a study by Logačev and Zacharov (1973) of magnetic measurements over steeply dipping burning coal seams in Siberia, with anomalies over 800 nT.

Thus, magnetic surveys have been reported over ancient as well as current coal fires in North America, Europe, Asia, and Oceania, and over similar combustion metamorphic rocks in South America. The general amplitudes of the strongest anomalies seem quite similar, so the next section will graphically present some of the profiles.

Magnetic Anomalies

Magnetic measurements taken along a profile can be represented as simple x - y plots. A few examples will suffice to show the results that typify measurements over clinkers and burning coal seams.

Figure 12.1.1, taken from Hasbrouck and Hadsell (1978), is a magnetic profile across a clinker area near Decker, Montana, USA, with a peak-to-peak change of 1500 nT. There was a surface indication of the burn from red-colored ground to the left on the profile, from 0 to 25 m. Although the ground color beyond 25 m was not indicative of further burning, the magnetic anomaly suggests a clinker edge more than 100 m further, past 150 m, as indicated. The dramatic change of about 1200 nT at 160 m is an edge effect as the magnetic clinker butts up against the nonmagnetic coal seam. The location of the edge of the clinker, as interpreted on the profile from the magnetics, was corroborated by rocks recovered from subsequent drill holes. Furthermore, once the clinker has been passed and the subsurface coal seam continues underground, the profile is very subdued. Over the clinker, the smaller magnetic anomalies are probably reflective of the variable magnetization of the clinker. Interestingly, one such anomaly coincides with the soil color change. This and other examples in Hasbrouck and Hadsell (1976, 1978) show that the magnetic survey can integrate the subsurface magnetic nature of the clinker and reveal its presence where otherwise not visibly indicated on the ground surface.

In a profile over clinkers from the area of the Coal Vein Trail, Theodore Roosevelt National Park, North Dakota, USA, Sternberg and Lippincott (2004) traversed 850 m (Figure 12.1.2). Very quiet zones indicate the normal stratigraphy of sedimentary rocks, consistent with control profiles run over areas that had no coal fires or clinker. Two zones where clinker was shown on the geologic map of the Park (Gonzalez and Biek, 2003) are marked on the profile. The magnetics suggests that the northern border of the southern clinker zone is actually about 50 m south of where it was mapped. On the other hand, for the northern clinker zone, the southern border of the clinker zone from the magnetics is about 70 m further south than what is shown on the geologic map. The northern and southern edges of both zones show layer of high magnetization clinker juxtaposed against a layer of low magnetization unbaked sediments.

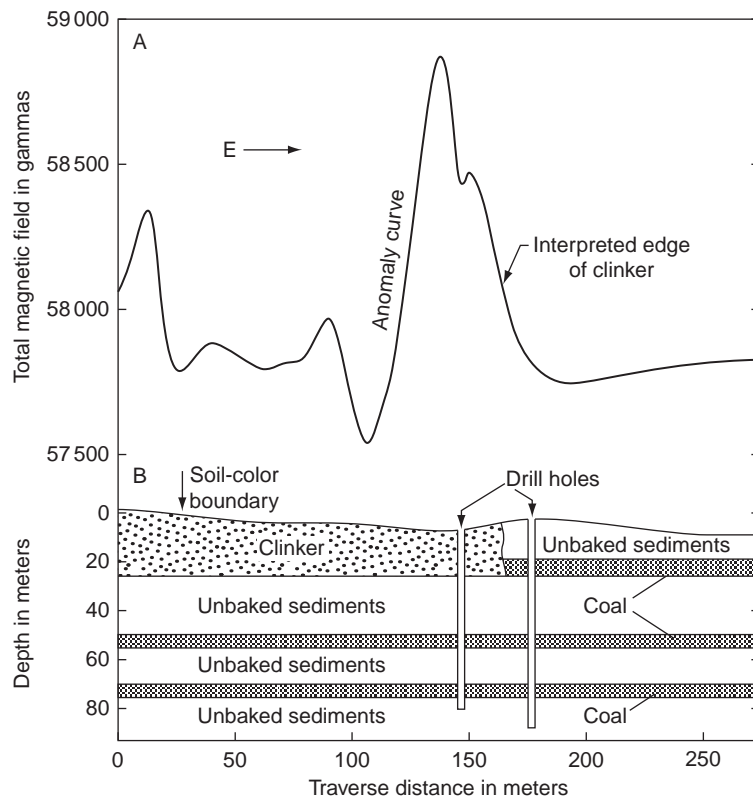


Figure 12.1.1. Magnetic field readings over several coal seams and clinker near Decker, Montana, USA. Magnetic units are in gammas, the cgs (centimeter–gram–second) numerical equivalent of the SI unit of nanoteslas (nT). From Hasbrouck and Hadsell 1978, with permission of the Colorado Geological Survey.

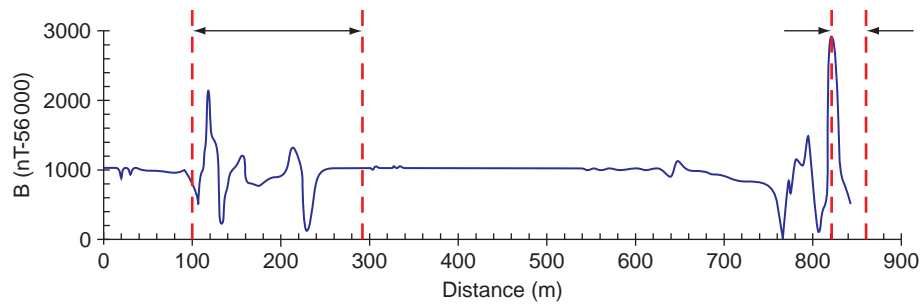


Figure 12.1.2. Magnetic field readings recorded over clinker in Theodore Roosevelt National Park, North Dakota, USA. The red-dashed lines designate the extent of two bodies of clinker mapped by Gonzalez and Biek 2003.

A third magnetic profile over clinker in New Zealand is shown in Figure 12.1.3 (Lindqvist et al., 1985). The strong anomaly at mid-profile was recorded over areas of exposed clinker. The anomaly at the western edge of the profile was thought to correspond to an unexposed lignite bed which had been logged elsewhere on the site.

The examples above all highlight surveys over paleoclinkers. Sternberg and Lippincott (2004) and Sternberg et al. (2008) also report magnetic survey results over areas of recent coal-seam fires in western North Dakota. About 30 coal-seam-outcrop fires over an area of 30 000 hectares were ignited in 1999 as a result of the so-called Gap grassland wildfires, which were set by weed burning on the Montana border. In some cases, these fires have continued to burn underground, and grass fires occasionally are reignited (Beechie, 2004). Four profiles over the Cummings A burn showed anomalies up to 1000 nT (Figure 12.1.4; Sternberg and Lippincott, 2004). Anomalies to the south end of the profiles are attributed to paleoclinkers. The extent of the zone marked as “surface burn” was based on observations of slumped and discolored soil material. The four profiles show anomalies within this zone and not beyond, although without much correlation from profile to profile. This suggests the possibility of anomalies due to mineralogical changes in the burned soil.

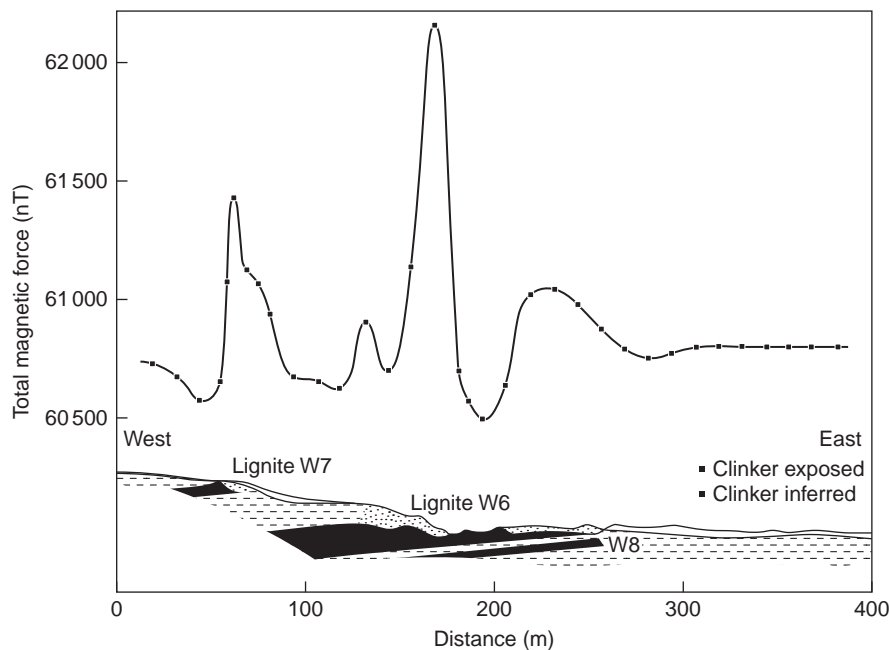


Figure 12.1.3. Magnetic field readings at the southern end of the Waimumu deposit, the New Vale Coal Company, eastern Southland, New Zealand. From Lindqvist et al. 1985 with permission of the Royal Society of New Zealand.

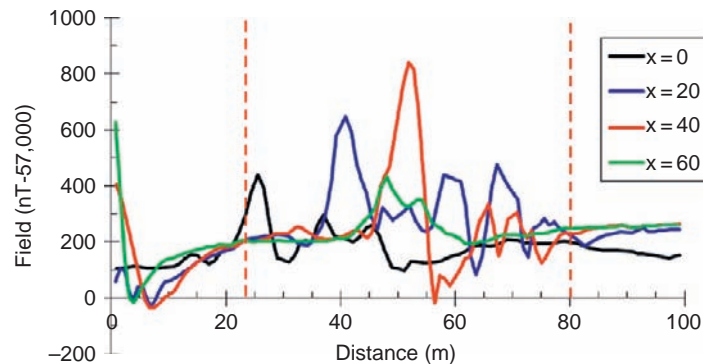


Figure 12.1.4. Four parallel profiles at 20 m intervals over an active coal-seam fire at the Cummings A, North Dakota, area after Sternberg and Lippincott, 2004. The red-dashed lines designate the zone of active burning.

Magnetic Properties

High-temperature, low-pressure, pyrometamorphic rocks develop unusual mineral assemblages and lithologies (Foit et al., 1987; Cosca et al., 1989; Clark and Peacor, 1992; Stracher et al., 2005; Masalehdani et al., 2007; Sokol and Volkova, 2007; Vapnik et al., 2007). These rocks acquire a TRM in much the same way as igneous rocks, although the nature of the magnetic minerals may be somewhat different. In addition, the alterations tend to enhance the magnetic susceptibility of these minerals. Either the TRM or the enhanced susceptibility can cause magnetic anomalies. These magnetic properties can be measured in paleomagnetism laboratories. The field of paleomagnetism is concerned with the history of the Earth's magnetic field, the application of these changes to geologic problems, and the magnetic properties of geologic materials (Butler, 1992).

Cisowski and Fuller (1987) note that the **natural remanent magnetization** (NRM; the resultant of all naturally acquired permanent magnetization) of CM samples from Southern California can be increased up to 4 orders of magnitude by thermal metamorphism, far above the normal for sedimentary rocks and comparable to extrusive igneous rocks. Glassy samples are weak due to iron residing in **paramagnetic** (grains that have magnetic susceptibility but do not acquire a permanent magnetization) or **superparamagnetic** (grains that are effectively paramagnetic by virtue of being very fine grained) phases rather than ferromagnetic (a special case of **ferromagnetism**, characteristic of minerals that can acquire a permanent magnetization).

Rock magnetic analyses suggest that white-to-pink pyrometamorphic rocks are magnetite-rich and red samples are hematite-rich. Susceptibilities of these rocks also tend to increase 1 or 2 orders of magnitude. Ron and Kolodny (1992) also find that samples of chalks and marls in the Mottle Zone of Israel increase their NRM intensity due to oxidation of iron sulfides into maghemite and hematite (and some magnesioferrite). Khesin and Itkis (2002) find that altered rocks in the Hatrurim Basin of Israel have susceptibilities about an order of magnitude higher on the average than slightly altered rocks, although for particular samples this correlation does not always hold. Further magnetic studies of rocks from this region (Khesin et al., 2005) reveal the complexity of their magnetization, including heterogeneity over distances of millimeters to centimeters. Some of the highest susceptibilities in the Hatrurim basin were for brick-like rocks and porcellanites (Khesin et al., 2005). There is also a general correlation between NRM and susceptibility. Magnetite, hematite, and goethite seem to be important in different samples.

De Boer et al. (2001) explicitly looked at the TRM properties of pyrometamorphic rocks from CM of coal seams in China, using a variety of techniques of **rock magnetism**. The mineralogical change caused by the heating enhanced susceptibilities and remanences 2–3 orders of magnitude above characteristic values for the parent sedimentary rocks. Magnetite, maghemite, and hematite were all involved in bearing the remanence, mainly as fine-grained **pseudo-single domain** grains (with just a few domain walls, nearly as small as **single domain** grains). Some samples even contained pure metallic iron, a rare occurrence in terrestrial rocks. Thorpe et al. (1998) also found a highly magnetic coked zone containing native iron due to the intrusion of magmatic fluids into a coal seam and the consequent reduction of pyrite. As noted by Cosca et al. (1989) and reiterated by de Boer et al (2001), the magnetic minerals found in pyrometamorphic rocks depend in a complex way on chemical and physical variables

such as the composition of the parent rock, the temperature and degree of melting, and the atmosphere of the firing. The pyrometamorphism does not just change the oxidation state of preexisting iron oxides, but utilizes iron from clay minerals, ferromagnesian silicates, and/or pyrite.

Only one other study has focused on the magnetic susceptibility properties of pyrometamorphic rocks. Hooper (1987) complemented magnetic studies of more than 60 samples with chemical analyses using X-ray fluorescence and mineralogical examination using X-ray diffraction and optical mineralogy. Comparison of the mineralogy with unbaked samples was used to infer the temperature of heating using temperatures of known phase changes. Unbaked sediments had low susceptibilities, while those of the baked rocks were variable and generally proportional to the titanomagnetite content. Hooper (1987) also finds that most of the magnetite and the hematite were derived from thermal decomposition of iron-rich clays. The mineralogy and magnetic susceptibility depend on bulk iron content and the hematite–magnetite equilibria governed by both temperature and oxygen fugacity. Temperature increases alone do not necessarily increase susceptibility. Over 40% of the baked rocks have low susceptibilities, suggesting that they were subject to conditions favoring hematite formation. Parent lithology is a factor, with baked siltstones having higher susceptibilities than sandstones and shales. Volatiles escaping through vents favored magnetite formation. Siltstones showed surface oxidation to hematite, with magnetite-rich interiors.

Hooper (1987) did not investigate remanence. Jones et al. (1984) carried out a paleomagnetic study of nearby clinkers from the Powder River Basin, Wyoming and Montana. Their analyses included **isothermal remanent magnetization** (IRM) acquisition (within strong laboratory fields) and **thermal demagnetization** by heating the samples to increasingly higher temperatures and cooling in field-free space. They infer that clinker magnetization is a TRM residing in a titanomagnetite phase, with hematite and goethite possibly contributing a thermochemical magnetization as grains grew through a critical volume and became magnetized.

Sternberg and Lippincott (2004) noted a general correlation between susceptibility and remanence in clinkers from North Dakota, interpreted as representing magnetite concentration. In accordance with Hooper (1987), samples near chimney vents had the highest susceptibilities and remanences, with nearly similar contributions from induced and remanent magnetization. On the other hand, darkened soil samples from areas of currently burning coal seams showed no remanence but an enhanced susceptibility and high IRMs (Sternberg and Lippincott, 2004; Sternberg et al., 2008), suggesting reduction to magnetite. Similar processes occur on occupation surfaces at archaeological sites (Crowther, 2003).

Lindqvist et al. (1985) suggest that pyrrhotite and an assemblage of titanomagnetites could be carrying some of the remanence in their clinker samples from New Zealand. Limestones from the Kuar Keng fire zone in China baked by coal-seam fires are reddened and also have susceptibilities that are increased by 1–2 orders of magnitude (Lindner and Rüter, 2007). Because these susceptibilities are not high enough to account for the magnetic anomalies, a TRM is also inferred. Susceptibilities of baked sandstones in Wuda, Inner Mongolia, are little changed, although clinker susceptibilities from Rujigou, Ningxia, are enhanced by 2 orders of magnitude (Lindner and Rüter, 2008).

In summary, the general picture for pyrometamorphic rocks is that magnetization is complex and heterogeneous. For many samples the susceptibility is enhanced and a remanence is also acquired as a result of pyrometamorphism.

Discussion

The profiles shown above suggest that magnetics can be very useful to locate the edge of a clinker burn and the boundary with the unburned portion of the coal seam. This would be helpful for better outlining the hazard of a burning coal seam, as well as estimating unburned coal resources. The high resolution of ground magnetics could allow tracking of hot spots over time to delineate and monitor the path of underground fires (Gielisch, 2007).

The magnetic anomaly over a layer of clinker can be modeled (Telford et al., 1976, equation 3.38b). Figure 12.1.5 shows the result from one such model, using median values of the susceptibility and remanence for North Dakota samples, a depth to the top of the clinker layer of 5 m, and a thickness for the clinker layer of 5 m. The transition from negative to positive anomaly is quite sharp for this shallow source and centered on the edge of the magnetic half-space. This anomaly is similar to those observed in Figures 12.1.1, 12.1.2, and 12.1.3. The magnetic anomaly is intrinsically associated with the burned and altered material in the near subsurface, whereas thermal and aromatic anomalies might be at least partially controlled by fractures that affect diffusion of hot gases. Modeling of anomalies, using

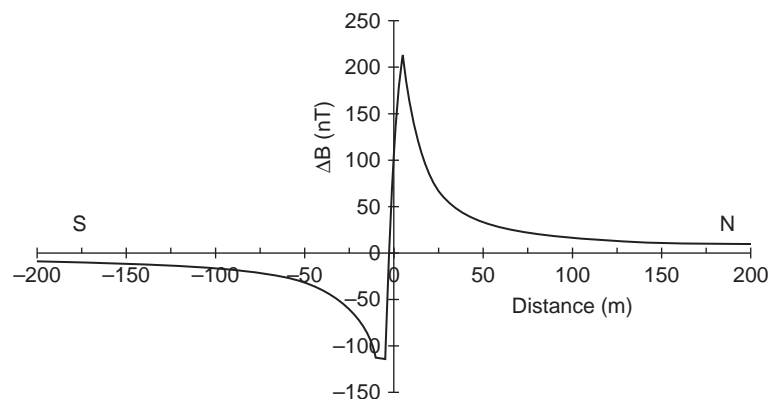


Figure 12.1.5. Magnetic edge effect of a clinker layer, assuming magnetization typical for North Dakota samples (Sternberg and Lippincott (2004)). The depth to the top of the clinker is 5 m, and the thickness of the clinker layer is also 5 m. The clinker occupies the half-plane to the south of zero on the horizontal axis, adjoining unbaked sediments to the north of zero.

known magnetizations, could also allow the separation of different magnetic sources (Khesin and Itkis, 2002), such as older clinkers and younger surface burns.

Although not stressed here, the ability of pyrometamorphic rocks to acquire a remanent magnetization makes them potentially useful for paleomagnetic studies of field direction (Jones et al, 1984; Lindqvist et al., 1985; Parse and Sternberg, 1989; Radan and Radan, 1998; de Boer et al., 2001) and field strength, or **paleointensity** (Krs, 1968; Krsová et al., 1989; Liu and Sternberg, 1993). Accurate recording of the paleomagnetic field would require rocks that have not mechanically rotated since becoming magnetized (Jones et al., 1984; de Boer et al, 2001).

Acknowledgments

I thank the National Park Service (Theodore Roosevelt National Park) for accommodations, and the NPS and the US Forest Service for permissions to work on federal lands. Oscar Knudtson of the US Forest Service was a knowledgeable guide to localities of recently burning coal seams. Caitlin Lippincott assisted with sample measurements and Andy Sparks with field work and compilation of data. Franklin & Marshall College provided various types of financial assistance.

Important Terms

diurnal variation
ferromagnetism
isothermal remanent magnetization
magnetic anomalies
magnetic susceptibility
magnetometer
nanoteslas
natural remanent magnetization
paleointensity

paleomagnetism
paramagnetic
pseudo-single domain
rock magnetism
single domain
superparamagnetic
thermal demagnetization
thermoremanent magnetization

References

- Beechie, B., 2004, Coal outcrop fire suppression in the North Dakota Badlands; North Dakota Public Service Commission, <http://psc.nd.gov/> (accessed 10 June 2010).
Burger, H.R., Sheehan, A.F., Jones, C.H., 2006. Introduction to Applied Geophysics, second ed. W.W. Norton and Co., New York, 554 p.

- Butler, R.F., 1992. Paleomagnetism. Blackwell Scientific, Boston, MA, 319 p.
- Cisowski, S.M., Fuller, M., 1987. The generation of magnetic anomalies by combustion metamorphism of sedimentary rock, and its significance to hydrocarbon exploration. *Geol. Soc. Am. Bull.* 99, 21–29.
- Clark, B.H., Peacor, D.R., 1992. Pyrometamorphism and partial melting of shales during combustion metamorphism: mineralogical, textural, and chemical effects. *Contrib. Mineral. Petrol.* 112, 558–568.
- Cosca, M.A., Essene, E.J., Geissman, J.W., Simmons, W.B., Coates, D.A., 1989. Pyrometamorphic rocks associated with naturally burned coal beds, Powder River Basin, Wyoming. *Am. Mineral.* 74, 85–100.
- Crowther, J., 2003. Potential magnetic susceptibility and fractional conversion studies of archaeological soils and sediments. *Archaeometry* 45 (4), 685–701.
- de Boer, C.B., Dekkers, M.J., van Hoof, T.A.M., 2001. Rock-magnetic properties of TRM carrying baked and molten rocks straddling burnt coal seams. *Phys. Earth Planet. Inter.* 126, 93–108.
- Foit, F.F., Jr., Hooper, R.L., Rosenberg, P.E., 1987. An unusual pyroxene, melilite, and iron oxide mineral assemblage in a coal-fire buchite from buffalo, Wyoming. *Am. Mineral.* 72, 137–147.
- Gay, S.P.J., Hawley, B.W., 1991. Syngenetic magnetic anomaly sources: three examples. *Geophysics* 56 (7), 902–913.
- Gielisch, H., 2007. Detecting concealed coal fires. In: Stracher, G.B. (Ed.), *Geology of Coal Fires: Case Studies from Around the World. Reviews in Engineering Geology XVIII*. Geological Society of America, Boulder, pp. 199–210.
- Gonzalez, M.A., Biek, R.F., 2003. Geology of the Fryburg NW, North Dakota Quadrangle. North Dakota Geological Survey (geologic map), Bismarck.
- Hasbrouck, W.P., Hadsell, F.A., 1976. Geophysical exploration techniques applied to Western United States coal deposits. In: Muir, W.L.G. (Ed.), *Coal Exploration. Proceedings of the First International Coal Exploration Symposium*. Miller Freeman, San Francisco, CA, pp. 256–287.
- Hasbrouck, W.P., Hadsell, F.A., 1978. Geophysical techniques for coal exploration and development. In: Hodgson, H.E. (Ed.), *Proceedings of the Second Symposium on the Geology of Rocky Mountain Coal–1977*. Colorado Geological Survey, Denver, CO, pp. 187–218.
- Heffern, E.L., Coates, D.A., 2004. Geologic history of natural coal-bed fires, Powder River Basin, USA. In: Stracher, G.B. (Ed.), *Coal fires burning around the world: a global catastrophe*. *Int. J. Coal Geol.*, 59 (1–2), 25–47.
- Hooper, R.L., 1987. Factors affecting the magnetic susceptibility of baked rocks above a burned coal seam. *Int. J. Coal Geol.* 9, 157–169.
- Jones, A.H., Geissman, J.W., Coates, D.A., 1984. Clinker deposits, Powder River Basin, Wyoming and Montana: A new source of high fidelity paleomagnetic data for the Quaternary. *Geophys. Res. Letters*, 11, 1231–1234.
- Khesin, B., Feinstein, S., Itkis, S., 2007. Possible sources of magnetic anomalies over thermally metamorphosed carbonate rocks of the mottled zone in Israel. In: Stracher, G.B. (Ed.), *Geology of Coal Fires: Case Studies from around the World: Reviews in Engineering Geology XVIII*. Geological Society of America, Boulder, pp 177–196.
- Khesin, B., Feinstein, S., Vapnik, Y., Itkis, S., Leonhardt, R., 2005. Magnetic study of metamorphosed rocks of the Hatrurim formation, Israel. *Geophys. J. Int.* 162, 49–63.
- Khesin, B., Itkis, S., 2002. Revision of aeromagnetic data: ground magnetic investigations of altered sedimentary rocks (Hatrurim Basin, Israel). *Proc. Est. Acad. Sci. Geol.* 51 (1), 16–32.
- Krs, M., 1968. Geomagnetic field intensity during the plio-pleistocene derived from the thermo-remanence of porcellanites and palaeo-slugs. *Pure Appl. Geophys. (PAGEOPH)* 69, 158–167.
- Krsová, M., Krs, M., Pruner, P., Chvojka, R., 1989. Palaeointensity of the geomagnetic field during upper caenozoic derived from palaeo-slugs and porcellanites in North Bohemia. *Stud. Geophys. Geod.* 33, 338–361.
- Lindner, H., Rüter, H., 2007. Results of geomagnetic surveys on the coal seam fire Kuar Keng, Xinjiang Autonomous Region, China: unpublished report, 23 p.; personal communication with the authors, Sino-German Coal Fire Research, http://www.coalfire.caf.dlr.de/intro_en.html (accessed March 2009).
- Lindner, H., Rüter, H., 2008. Results of geomagnetic surveys on fire zone 18 and a TEM- array in Wuda, Inner Mongolia Autonomous Region, P.R. China and Rujigou, Ningxia Autonomous Region, China: unpublished report, 36 p., personal communication with the authors, Sino-German Coal Fire Research, http://www.coalfire.caf.dlr.de/intro_en.html (accessed March 2009).
- Lindqvist, J.K., Hatherton, T., Mumme, T.C., 1985. Magnetic anomalies resulting from baked sediments over burnt coal seams in southern New Zealand. *N.Z. J. Geol. Geophys.* 28, 405–412.
- Liu, X.G., Sternberg, R., 1993. Paleointensities and petrochemistry of clinkers from southeastern Montana: EOS, transactions, American Geophysical Union. Spring Meet. Suppl. 74 (16), S113.
- Logačev, A.A., Zacharov, V.P., 1973. *Magnitozazvedka*. Nedra Press, Leningrad, Russia, 347 p. (in Russian).
- Masalehdani, M.N.-N., Black, P.M., Kobe, H.W., 2007. Mineralogy and petrography of iron-rich slags and paralavas formed by spontaneous coal combustion, Rotowaro coalfield, North Island, New Zealand. In:

- Stracher, G.B. (Ed.), *Geology of Coal Fires: Case Studies from around the World: Reviews in Engineering Geology XVIII*. Geological Society of America, Boulder, pp 117–131.
- Matthews, A., Gross, S., 1980. Petrologic evolution of the mottled zone (Hatrurim) metamorphic complex of Israel. *Isr. J. Earth Sci.* 29, 93–106.
- Milsom, J., 2003. *Field Geophysics*, third ed. Wiley, Chichester, England, 232 p.
- Parse, D.F., Jr., Sternberg, R.S., 1989. A paleomagnetic study of clinkers from the Powder River Basin, south-eastern Montana: EOS, transactions. *Am. Geophys. Union* 70, 341.
- Ron, H., Kolodny, Y., 1992. Paleomagnetic and rock magnetic study of combustion metamorphic rocks in Israel. *J. Geophys. Res.* 97 (B5), 6927–6939.
- Radan, S.C., Radan, M., 1998. Rock magnetism and paleomagnetism of porcellanites/clinkers from the western Dacic Basin (Romania). *Geol. Carpath.* 49 (3), 209–211.
- Schaumann, G., Siemon, B., Chun, Y.C., 2008. Geophysical investigation of Wuda coal mining area, Inner Mongolia: electromagnetics and magnetics for coal fire detection. In: Voigt, S., Rüter, H., Jiahong, L., Jing, L., and Jayakumar, R. (Eds.), (Eds.), *Spontaneous Coal Seam Fires: Mitigating a Global Disaster*, ERSEC Ecological Book Series. Tsinghua University Press, Beijing, China, vol. 4, pp. 336–350.
- Sokol, E.V., Volkova, N.I., 2007. Combustion metamorphic events resulting from natural coal fires. In: Stracher, G. B. (Ed.), *Geology of Coal Fires: Case Studies from around the World: Reviews in Engineering Geology XVIII*. Geological Society of America, Boulder, pp 97–115.
- Sontag, K.D., 1984. Delineation of a Coal Burn Edge with Seismic Refraction and Magnetism. M.S. thesis, Wright State University, Dayton, OH, 55 p.
- Sternberg, R., Lippincott, C., 2004. Magnetic surveys over clinkers and coal seam fires in western North Dakota: Geological Society of America Abstracts with Programs, paper no. 15-9, vol. 36, no. 5, p. 43.
- Sternberg, R., Sparks, A., Knutson, O., 2008. Magnetic surveys over burning and remediated coal seam fires in western North Dakota. *Proceedings of the 21st Symposium on the Application of Geophysics to Engineering and Environmental Problems*. Environmental and Engineering Geophysical Society Annual Meeting, Denver, CO, pp. 389–398 (on CD).
- Stracher, G.B., Prakash, A., Schroeder, P., McCormack, J., Zhang, X., van Dijk, P., et al., , 2005. New mineral occurrences and mineralization processes: Wuda coal-fire gas vents of Inner Mongolia. *Am. Mineral.* 90 (11–12), 1729–1739.
- Telford, W.M., Geldart, L.P., Sheriff, R.E., Keys, D.A., 1976. *Applied Geophysics*, first ed. Cambridge University Press, Cambridge, England, 860 p.
- Thorpe, A.N., Senftle, F.E., Finkelman, R.B., Dulong, F.T., Bostick, N.H., 1998. Change in the magnetic properties of bituminous coal intruded by an igneous dike, Dutch Creek Mine, Pitkin County, Colorado. *Int. J. Coal Geol.* 36, 243–258.
- Vapnik, Y., Sharygin, V.V., Sokol, E.V., Shagam, R., 2007. Paralavas in a combustion metamorphic complex: Hatrurim Basin, Israel. In: Stracher, G.B. (Ed.), *Geology of Coal Fires: Case Studies from around the World: Reviews in Engineering geology XVIII*. Geological Society of America, Boulder, pp 133–153.
- Zhang, J., Wagner, W., Prakash, A., Mehl, H., Voigt, S., 2004. Detecting coal fires using remote sensing techniques. *Int. J. Remote Sens.* 25 (16), 3193–3220.

WWW Addresses: Additional Reading

(1) Geomagnetism

<http://www.ngdc.noaa.gov/geomag/geomag.shtml>

(2) Paleomagnetism

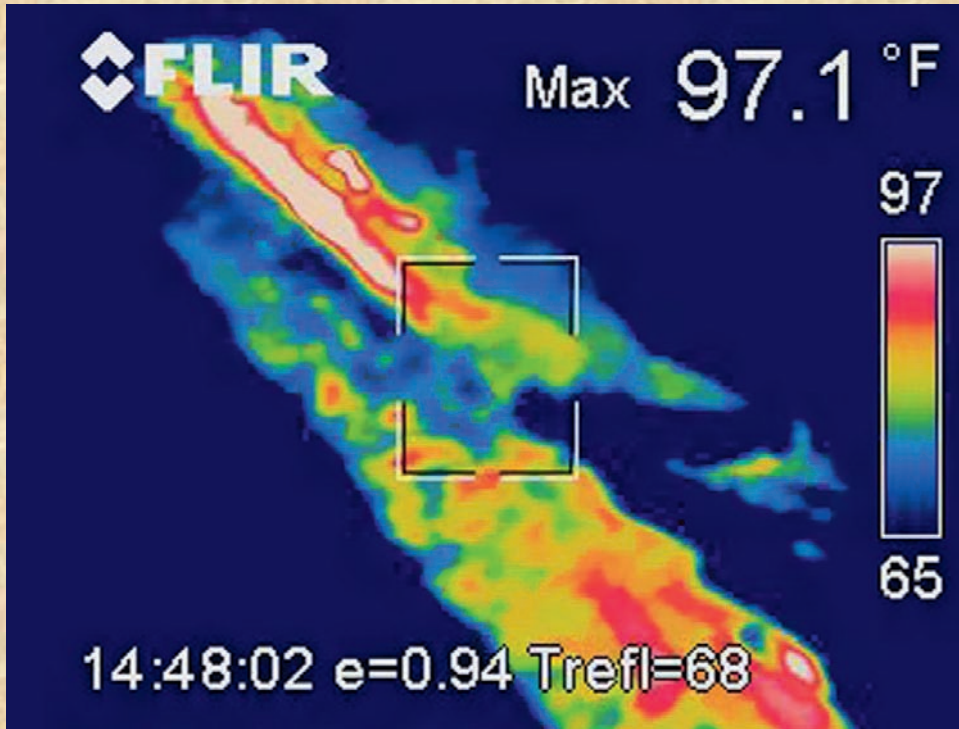
<http://www.geo.arizona.edu/Paleomag/book>

(3) North Dakota's Clinker (North Dakota Notes No. 13, North Dakota Geological Survey)

http://www.dmr.nd.gov/ndgs/ndnotes/ndn13_h.htm

CHAPTER 13

Historical Use of Airborne Thermal Infrared Imaging for Detecting and Studying Coal Fires



Forward looking infrared (FLIR) camera image of the Elk Creek Coal Mine Fire, Garfield County, Colorado (September 30, 2002). The camera detects infrared radiation associated with thermal energy to create a picture such as the one shown here. The aerial view is toward the northwest (upper left), along strike of the Grand Hogback monocline. The scale to the right represents relative heat energy flow and is misleading in that ground surface temperatures greatly exceed the scale values. This anomaly is because of the distance between the model camera used in flight and the fire on the ground. The image roughly corresponds to the position of the aircraft that took the gray-scale thermal infrared image on the next page. The numbers at the bottom of the image from left to right are military time, emissivity (a measure of the radiation emitted from an object when compared to a perfectly black body), and the reflected ambient temperature (used to compensate for radiation emitted from the atmosphere). *Photo courtesy of Steven Renner; Colorado Division of Reclamation, Mining and Safety.*

CHAPTER CONTENTS

13.1 Airborne Thermal Infrared Imaging

- Introduction
- Thermal Infrared Imaging
- Color Infrared Imaging
- Early Use
- Later Use
- Depth Estimation
- Discussion
- Acknowledgments
- Important Terms
- References
- WWW Addresses:
Additional Reading



13.1. Airborne Thermal Infrared Imaging

Daniel H. Vice

Airborne image of the Elk Creek Coal Mine Fire, Garfield County, Colorado (September 30, 2002). The view toward the northwest (upper left) is along strike of the Grand Hogback monocline. The red areas are clinker, due to subsurface burning.

Photo courtesy of Steven Renner, Colorado Division of Reclamation, Mining and Safety.

Introduction

A continuing problem in trying to control **coal fires** is determining their extent and direction of movement. The extent of underground coal fires has been difficult to determine because of a number of surface factors, including the amount of vegetative cover, the thickness of the rock and soil cover over the coal bed, and the varying intensity of the coal fire over time can mask the location of the fire.

Thermal infrared (TIR) is a remote sensing method that detects variations of heat (i.e., radiant flux) on the Earth's surface. This method has been used to map and study fires associated with coal beds and/or coal mining culm banks since the 1960s.

The purpose of this chapter is to review the use of **airborne TIR** for mapping and studying coal fires over the past 40 years. One reason for restricting the study to airborne TIR is that historically more use has been made of this method due to its greater resolution and availability than of satellite TIR.

Thermal Infrared Imaging

Thermal infrared imaging is a remote sensing method that detects differences in the radiant flux on the Earth's surface (Sabins, 1997). Since everything above absolute zero (-273°C) emits energy (i.e., radiant flux) in the thermal infrared range of the electromagnetic spectrum (Gangopadhyay, 2007), the problem becomes how to measure the differences. Variations in radiant flux from the ground surface are caused by differences in the ability of rocks and other surface materials to absorb solar radiation and store this energy as heat (thermal capacity) and then to emit this energy back into the atmosphere in the TIR range (Kahle, 1980; Sabins, 1997). Surface factors, such as the amount of moisture in a soil, the presence of a stream or wetland, height differences of adjacent blocks of trees in a forest, and/or active transpiration of trees in a forest, can affect the radiant flux and thus change the tone of the TIR imagery. Topography can also create anomalies in TIR imagery, e.g., deep valleys may show as warm areas because of transpiration of trees or being sheltered from the wind. Large animals, e.g., cattle or buffalo, can also show up in the TIR imagery as hot spots and thus give false anomalies.

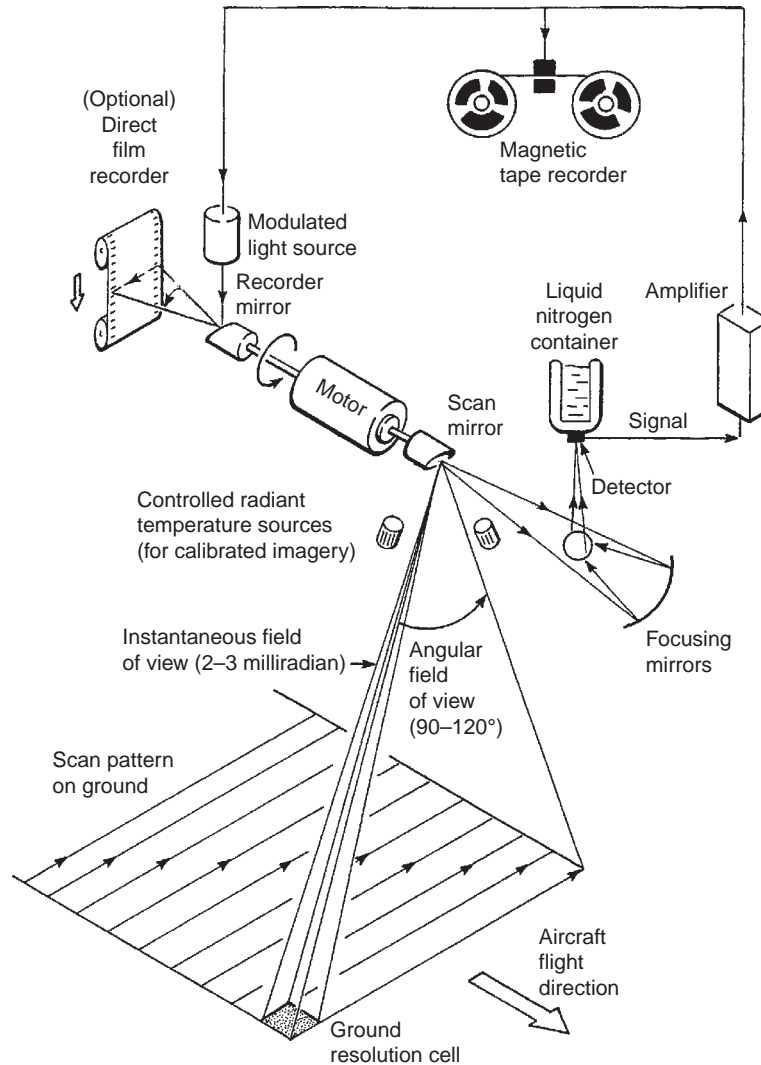


Figure 13.1.1. Diagram of the TIR scanner and its operation Sabins, 1997.

The TIR instrumentation (Figure 13.1.1) is mounted in an airplane, which flies over the study area at a predetermined altitude (e.g., 1525 m (~5000 ft)) above average ground level. The TIR sensor makes a series of rapid, side-to-side sweeps to cover the land surface in a swath on either side of the airplane (Sabins, 1997). Although the instrumentation shown in Figure 13.1.1 has a magnetic tape recorder, essentially all the data are now recorded in digital format and then transferred to strips of film for use.

The differences in radiant flux occurring on the land surface are shown as variations in the brightness of the TIR imagery (on a gray scale) and are a good approximation of the temperature of the ground surface at the time of the TIR survey (Loughlin, 1991). Warm areas appear as shades of white or light gray in the TIR imagery while cool areas appear as shades of dark gray.

The **instantaneous field of view (IFOV)** is the amount of area on the ground that is viewed by the scanner at any one instant. The IFOV of the TIR scanner affects the resolution of the imagery because a smaller IFOV can detect smaller and subtler anomalies than can an instrument with a larger IFOV. For example, an instrument with an IFOV of 1 milliradian will have a better resolution than an instrument with an IFOV of 3 milliradian. The temperature sensitivity of an instrument is also important in whether it can detect subtle anomalies in ground temperature. Airborne TIR has been used more for studying coal fires because the smaller IFOV provides much better resolution.

The author Vice (2007) found that both the time of day and the time of year are important in conducting TIR surveys for geothermal energy in the Pacific Northwest. Predawn surveys were needed to reduce the number of

anomalies caused by differential solar heating. TIR surveys conducted during the fall (e.g., during November) also helped to reduce anomalies created by solar heating and/or by the transpiration of vegetation.

A recent development in the use of airborne TIR imaging for detecting coal fires is the development of **forward looking infrared** (FLIR) imaging. This is a digital TIR system that looks forward from the platform rather than vertically downward and from side-to-side as do the older scanners (Figure 13.1.1; Wikipedia, 2009). FLIR offers a number of operational and logistical advantages, including the acquisition of oblique images of a coal fire, not available with the older TIR scanners. Andrup-Henriksen et al. (2007) discuss the use of FLIR in studying coal fires in the Jharia coalfield in India, although the scanner was not mounted in an aircraft. Another advantage of FLIR is being able to mount the scanner in a helicopter, permitting much closer coordination with ground-based units. Technical Innovation and Professional Services (2005) describes a survey of coal fires in North Dakota where the scanner was mounted in a Cobra AH-1 helicopter. Detection of coal fires using a FLIR systems Star SAFIRE III camera was good, but it was weather dependent. The primary problem was solar heating during sunny days because this created numerous false anomalies. The number of anomalies can be reduced by conducting FLIR surveys before sunrise (Ellyett and Fleming, 1974; Rathmore and Wright, 1993; Vice 2007). The anomalies may also be reduced and corrected by conducting field surveys.

Color Infrared Imaging

Color infrared (CIR) imaging involves the use of color photo film that been changed so that the spectral sensitivities of the film can record energy in the 0.7–0.9 μm range of the electromagnetic spectrum (Sabins, 1997). One advantage of CIR film is that it shows the health of vegetation, often before any stress in the vegetation is visible to the person on the ground (i.e., the previsual stage). Thus, healthy vegetation in a broadleaf forest will show as various shades of red to magenta color while stressed vegetation will exhibit shades of pink to blue in the previsual stage (Sabins, 1997). Broadleaf forest vegetation can be stressed by drought, disease, insect infestation, or other factors that will prevent the leaves from getting water (Sabins, 1997).

The ability to detect stress in vegetation before it is visible to the naked eye has led to attempts to use CIR for detecting the location and extent of a coal fire. Shallenberger (1993) suggested that heat from a burning coal fire would reduce the available capillary moisture in the soil (i.e., water held in the pore spaces between soil particles by surface tension) and thus move the plant toward the wilting stage more quickly than nearby plants that are unaffected by the coal fire. In addition, continuously heating deep-rooted plants like broadleaf trees, in the area around Centralia, killed them. An area where this occurs produces a geobotanical anomaly, a change in the health of the plants and/or barren ground where the plants were killed. This appears in CIR imagery in colors other than red.

Early Use

Although TIR imaging has been used to study coal fires since 1964, which was shortly after the technology was declassified by the Defense Department, the literature seems to suggest an early rush of studies in the 1960s and 1970s followed by only limited use in the 1980s. However, starting in the 1990s the use of TIR increased again and has gone beyond detecting coal fires to get additional information from the imagery. Much of the published work in the past 10–15 years has been by researchers in Europe and/or China. This study makes an arbitrary division of the TIR studies in the literature into an early group from 1964 to 1993 and a later group, which extends from 1990 to the present. There is some overlap in time between the two groups.

Slavecki (1964) published the results of the first study of coal fires using TIR imagery. A Reconofax IV, Mark 2, instrument was used to look for fires in culm banks at the Huber Colliery near Wilkes-Barre and the Richmond Colliery at Scranton. This study demonstrated that the TIR scanner could be used to detect fires in coal beds and in refuse piles (or culm banks) and was the first to test the effectiveness of TIR for detecting coal fires after the technology had been declassified by the Defense Department.

Fisher and Knuth (1968) briefly describe a TIR study of several coal fires by the Pennsylvania Department of Mines and Mineral Industries. The authors noted that the TIR imagery detected the coal fires and suggested that the extent of the fires could be determined. An HRB-Singer instrument was used for the study (Fisher and Knuth, 1968).

Another early study of coal fires by the US Geological Survey (Greene et al., 1969) investigated 22 fires in the anthracite fields of Northeastern Pennsylvania and in the bituminous coal fields near Pittsburgh in Western Pennsylvania. A Reconofax IV instrument was used for these surveys and imagery was acquired just before dawn and during the daytime. The predawn TIR imagery proved to be more effective because of greater contrast (Greene et al., 1969).

Greene et al. (1969) suggested that TIR could detect coal fires at shallow and intermediate depths (i.e., those less than 30 m below the surface). They suggest that TIR was effective for detecting deeper coal fires only if they had been burning for more than 10 years. The authors suggested that this amount of time was necessary for the heat from the deeper fire to be conducted to the surface. However, based on anecdotal information, most coal fires have been burning for extended periods and so the 10-year requirement should not be a problem. For example, the Centralia coal fire has been burning for 40+ years, the Laurel Run coal fire has been burning for 90+ years, and the Burning Mountain coal fire in Australia (Ellyett and Fleming, 1974, see below) has been burning for at least 180 years.

The US Bureau of Mines reported a study of coal fire control projects (Dierks et al., 1971) where TIR imaging was used to survey the Cedar Avenue coal mine fire on the southeastern edge of Scranton, Pennsylvania. The authors noted that thermal anomalies were detected in a landfill and in nearby burning banks; however, these were only part of the area affected by the coal fire. Dierks et al. (1971) suggested that the lack of detection was due to the depth of the coal fire and that TIR was ineffective for detecting coal fires deeper than 30 m. However, the authors gave no indication of the type of TIR instrument used for the survey, the time of day the survey was flown, or the time of year the survey was flown, which are all factors that can affect whether the TIR instrument would detect deeper areas of the coal fire.

Ellyett and Fleming (1974) describe a TIR study conducted over The Burning Mountain coal fire in New South Wales, Australia. This coal fire has been known since at least 1829, and evidence (e.g., slag and baked sediments) suggested that the fire had burned over a distance of 6 km and so may have been burning for several thousand years. Hot gases were escaping to the atmosphere from a moving chimney at this site, which is similar to the moving fronts at Centralia (Nolter and Vice, 2004). The authors conducted three separate TIR surveys (during mid-day, evening, and dawn) using a Daedalus scanner over the Burning Mountain and were able to delineate some of the features of the coal fire but not others. They did not give an IFOV or temperature sensitivity for the instrument they used.

The authors Ellyett and Fleming (1974) concluded that the solar heating made detection of any anomaly associated with the coal fire difficult in the mid-day TIR survey. Ground measurements by the authors indicated that there was little lateral conduction of heat from the chimney. The limited aerial extent of the TIR anomaly associated with the coal fire meant that it could easily be overpowered by any solar anomaly. The evening TIR survey also had extensive anomalies created by solar heating (Ellyett and Fleming, 1974), which tended to mask the anomaly associated with the chimney. Only the dawn TIR survey had an easily detected anomaly associated with the chimney (Ellyett and Fleming, 1974, p. 83). This is comparable to the author's experience in conducting TIR surveys for geothermal surface manifestations in the Washington Cascades and in Western Montana (Vice, 2007). The TIR surveys needed to be conducted in the early morning hours in order to avoid solar anomalies (Vice, 2007). Greene et al. (1969) and Hong et al. (1996) also noted that predawn airborne thermal IR surveys were best for detecting coal fires.

Bakker et al. (1978) reviewed some uses of a custom-built TIR scanner with a temperature sensitivity of 0.15°C and note that imagery obtained during the African dry season was better for most uses because the vegetative cover was less during this time. As part of this review, the authors described a coal fire at Witbank in the Republic of South Africa. Most of the warm areas in the TIR imagery are associated with subsidence areas on the land surface (the coal bed is at a depth of 30 m and was mined using room and pillar). The authors suggest that the general area of the fire is visible in the imagery but the fire's extent cannot be determined.

Miller and Watson (1980) described the use of TIR imaging to detect coal fires in the Sheridan area of Northeastern Wyoming. This area is part of the Powder River basin, which contains large deposits of subbituminous coal. The study was based on surveys in July of 1975 and October of 1978 using a Texas Instruments RS14A scanner with an IFOV of 3 milliradian. The authors noted that a number of surface factors including (1) meteorological conditions, (2) physical property differences (e.g., such as differences in the composition of soil and rocks), (3) topographic differences, and (4) near-surface geothermal effects (which probably refers to the movement of groundwater) could

affect the interpretation of the TIR imagery. Vice (2007) observed many of these same effects while using TIR scanners for geothermal exploration. For example, a light fog can obscure the radiant flux of an area. A wet, marshy area could give a dark (i.e., cool) signal while a bare, south-facing rock that stands up above the surrounding rock or loose soil could give a very light (i.e., warm) signal. A taller stand of trees within a forest might give a light (warm) signal compared to the surrounding forest.

Vice (1980) detected a coal fire as an “accidental outcome” during a TIR survey of the Black Diamond area of King County, Washington, as part of the Burlington Northern geothermal exploration program. A Daedalus model 1230 scanner was used for this survey, which had an IFOV of less than 1 milliradian and a temperature sensitivity of 1°C. The TIR survey was flown at night during November 1977. The high resolution of the 1230 model Daedalus scanner helped to separate the coal fire from a vegetation anomaly on some nearby hills (Figure 13.1.2).

This “Burning Field” coal fire (Figure 13.1.2) occurs on state parks and recreation land near the Green River in King County, Washington, and is a shallow coal fire on the number 12 seam in the Puget Group (Eocene) (William Kobol, Manager, Palmer Coking Coal Co., personal communication). Disturbed vegetation and warm soil temperatures characterize the “Burning Field” coal fire. For example, the author observed some ground subsidence, 26.6°C ground temperatures, and numerous blackberry bushes, which normally occur on open or disturbed ground, while doing some field work in the area about 25 years ago. At the present time, the soil temperatures are 21.1°F (William Kobol, Manager, Palmer Coking Coal Co., personal communication).

A review by Rathmore and Wright (1993) on the monitoring of the environmental impacts of coal mining briefly discusses the use of TIR. They note that a sensor altitude of less than 3 km (~9000 ft) and a spatial resolution of less than 3 m work best for detecting coal fires. Rathmore and Wright (1993) also note that imagery acquired during the night or early morning works best for detecting the coal fires because of the greater thermal contrast.

A report by Kim and Chaiken (1993) on coal fires in abandoned mines and culm banks suggests that attempts to use TIR for locating the fires had not been successful, although they did not cite any reports. However, Bureau of Mines personnel were involved in some of the earlier studies (Greene et al., 1969; Dierks et al., 1971). Therefore, this suggestion may be based on the earlier studies.

The above literature suggests that TIR imagery works best for locating shallow or medium depth coal fires (Greene et al., 1969; Dierks et al., 1971). Studies by Ellyett and Fleming (1974), Miller and Watson (1980), and Rathmore and Wright (1993) note that a number of operational factors, i.e., time of day, surface metrological conditions, physical properties of the ground materials, and topographic conditions, can affect the interpretation of the TIR imagery. The

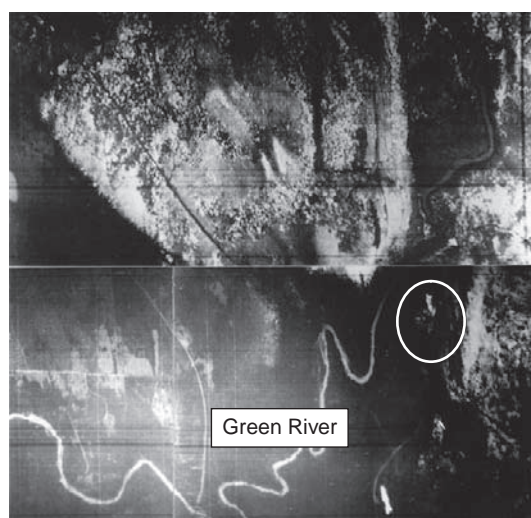


Figure 13.1.2. TIR image of the “Burning Field” coal fire, King County, Washington (white oval). The image was part of a Burlington Northern Railroad survey flown in the fall of 1976 by Intera, a consulting firm in Calgary, Alberta, Canada. The instrument used for the image was a Daedalus 1210 model thermal line scanner, with an 8–14 μm detector, mounted in a light aircraft and flown at an altitude of ~1524–1829 m (5000–6000 ft) above ground level. Scale is 1:16 000.

review by Rathmore and Wright (1993) suggests that the TIR sensor works best below an altitude of 3 km (~9000 ft) above average ground level. Rathmore and Wright (1993) also suggest that a spatial resolution of less than 3 m works best for detecting coal fires. However, part of the problem with these early surveys is that the TIR scanners used in many of the studies did not have the resolution and temperature sensitivity needed to detect small or subtle anomalies. It is also possible that many of the early TIR surveys were not conducted at the right time of day or during the right season to reduce the effects of solar heating and other surface factors that can create false anomalies.

Later Use

One of the characteristics of the later remote sensing studies of coal fires has been the use of several different remote sensing methods in combination. This has given the researcher(s) different ways to look at the coal fires and thus provided more information. One of the first studies to combine remote sensing methods was by Yong-fang et al. (1990) to study coal fires in areas along the “Silk Road.” In this area of Western China, some coal fires had apparently been burning for more than 1000 years (Yong-fang et al. 1990). These researchers used a Daedalus 1230 model infrared scanner, which would have had an IFOV of 1 milliradian in combination with CIR aerial photos to locate and determine the direction of movement of coal fires (Yong-fang et al., 1990).

Another early study to use TIR to go beyond the location and delineation of coal fires was a remote sensing study by Shallenberger (1993) at the Centralia coal fire in northeastern Pennsylvania. He looked at imagery from Landsat, Skylab, U2 aircraft, C-130 aircraft, and other aircraft mounted thermal infrared imagery. Shallenberger (1993) used TIR imagery from surveys conducted in 1971, 1980, and 1982 to determine the progression of coal fire at Centralia and found that the repeated use of airborne TIR surveys were the most useful remote sensing method for determining the advance of the coal fire.

Shallenberger (1993) found geobotanical anomalies present in CIR imagery at Centralia (i.e., areas where the vegetation did not show the normal healthy red color). He used National Aerial Photographic Program CIR photos (1:24 000 scale) that had been taken in August of 1987 for his Centralia study. He noted that the distinctive thermal and geobotanical anomalies were evident only where the burning coal bed was at relatively shallow depths. This observation was supported by a thermal model, which suggested that no detectable surface anomalies would occur below a depth of ~30.5 m (100 ft) (Shallenberger, 1993).

Hong et al. (1996) briefly described using airborne TIR and Landsat TM band 6 to detect coal fires. They noted that the time of day the data were acquired, the type of TIR sensor, the surface morphology of area, and the extent and temperature of any surface anomalies could all affect the ability to detect coal fires. The authors noted that predawn TIR surveys were best for detecting coal fires.

Peng et al. (1997) used both airborne TIR imagery and color infrared photographs to depict the fire front and outcrop of coal seams. Then the location of the fire front and its direction of movement were combined with topographic data using geographic information systems (GIS) to estimate the depth of the coal fire. Using these techniques, they estimated the depth of several coal fires to range between 54 and 125 m. Note that this depth is greater than the 30 m depth that had been considered the lower limit for detection.

Zhang et al. (1999) used a combination of satellite and airborne remote sensing methods including TIR to detect coal fires in northern China. These authors used high-resolution optical satellite imagery, satellite TIR data, and satellite-based microwave data with airborne TIR imagery and aerial photography using computer programs to obtain better results than could be obtained from one system alone. In addition, they were able to obtain a wider coverage using the satellite imagery than would have been possible using airborne imagery alone. This was important because they were working in a large area of northern China that was often remote and lacked ground access.

Kick et al. (2004) describe an experiment combining a TIR scanner and a Fourier transform spectrometer to detect and analyze coal fires. As part of their approach, they fuse (i.e., combine the data from the two instruments together).

Gielisch (2007) described the effort by the People’s Republic of China to control coal fires and noted that infrared photography has been very important in that effort. He indicated that TIR surveys were necessary for locating and defining the limits of coal fires.

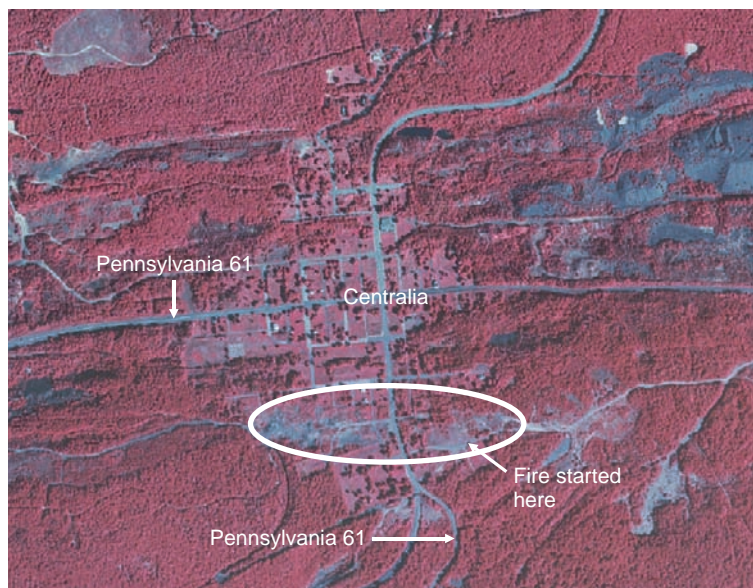


Figure 13.1.3. Color infrared photo of Centralia, Pennsylvania, showing stressed vegetation (white oval) at the “cemetery front.” Resolution is ~1 m; scale is 1:9600. Photo courtesy of the National Agricultural Imagery Program (NAIP) administered by the US Department of Agriculture.

Gangopadhyay (2007) conducted a brief review of the coal fires in the world and whether thermal infrared imaging had been used on them. He notes that coal fires are a common occurrence in coal-producing countries and that aerial TIR has been used on coal fires in Australia, China, India, the United States, and possibly Germany.

The author is aware of two current research projects using TIR and/or CIR imagery to study coal fires. Vice and Madigan are working on a project using CIR photography to help delineate the “cemetery” front at Centralia and determine if the fire is advancing to the west beyond the limits of the available drill hole data (Figure 13.1.3).

The second project is using TIR imagery obtained during the summer of 2007 and comparing it with TIR imagery from previous surveys (1972, 1980, 1981, 1982, and 1983) (J.M. Elick, 2007, personal communication). TIR imagery is being integrated with data from aerial photographs taken in 1993 and 1997 and also from some CIR photographs to track the movement of the “cemetery front” at Centralia.

Depth Estimation

In addition to attempts to more accurately detect and outline coal fires, some workers have attempted to find ways to determine the depth of the coal fire. Prakash et al. (1995) proposed using a half-anomaly width function for estimating the depth of burial of hot features using TIR data. The method is not limited to coal fires but the authors suggested that it could be used on coal fires to estimate their depth. The method uses two separate sets of TIR data to create a set of characteristic curves showing the relationship between a ratio of temperature and time between surveys. Prakash and Berthelote (2007) refined the method of estimating the depth of an underground fires by proposing that a linear anomaly surface transect (LAST) function be used instead of the half-anomaly width function. Zhang et al. (2007) used ground-based TIR measurements to estimate temperature anomalies and then used a point-source inversion model to determine the depth of coal fires.

Discussion

Several studies using TIR imagery to study coal fires were published in the 1960s and 1970s. As with any new technology, there was an initial “learning curve.” The purpose of the early surveys was mainly to determine if TIR scanner could be used to detect coal fires and under what conditions. Slavecki (1964), Fisher and Knuth (1968), Greene et al. (1969), and Dierks et al. (1971) demonstrated that TIR imagery could be used to detect shallow and

moderate depth coal fires. Several of these studies indicated that to be used effectively, the TIR surveys needed to be conducted in the early morning hours (i.e., predawn) and the imagery needed to be carefully interpreted because a number of surface conditions could affect the imagery.

Early studies by Greene et al. (1969), Dierks et al. (1971), and Kim and Chaiken (1993) suggested that TIR surveys were not useful if the fire was deeper than 30 m. This seems to have discouraged the use of TIR imaging for studying coal fires because fewer studies on the use of TIR were published from the early 1970s until about 1993. Poorer resolution and temperature sensitivity of many early instruments may be part of the reason for the lack of detection of deeper coal fires. However, both Shallenberger and Elick had access to TIR surveys conducted in the early 1980s over Centralia, so the lack of papers may be due to little interest in publishing rather than a lack of the use of TIR.

Much of the more recent work has continued to use TIR for locating and delineating coal fires (e.g., Gielisch, 2007). However, other studies (e. g., Shallenberger, 1993; Hong et al., 1996; Peng et al., 1997; and Zhang et al., 1999) have shown that TIR imaging can be used to go beyond detection of coal fires and attempted to determine the depth and/or rate of advance of the coal fire. These later studies usually used a combination of remote sensing methods rather than just TIR alone.

Interesting new developments are the studies by Prakash et al. (1995) and Prakash and Berthelote (2007) demonstrating a method that takes data from two separate TIR surveys to estimate the depth of a coal fire. Zhang et al. (2007) described a second method for determining the depth of a coal fire by using ground-based TIR surveys and a point-source inversion model.

Acknowledgments

The author thanks Dave Miller of Pennsylvania State University, Hazleton, for his review of this chapter and Glenn Stracher of East Georgia College for his help and direction in preparing this work. Lee Miller at Pennsylvania State University, Schuylkill, assisted with illustrations. The library staff at Pennsylvania State University, Hazleton, Schuylkill, and the Earth and Mineral Sciences Library at Pennsylvania State University, University Park, assisted in the acquisition of numerous references. Peter Linehan of Pennsylvania State University, Mount Alto, provided the Centralia CIR photo. I also thank Dr. Shelton Alexander (emeritus) of Pennsylvania State University, University Park, for our discussion about the Shallenberger senior thesis and my wife, Beth, for her patience while I worked on this project.

Important Terms

**airborne thermal infrared
coal fires
color infrared imaging
forward looking infrared**

**instantaneous field of view
thermal infrared
thermal infrared imaging**

References

- Andrup-Henriksen, G., Prakash, A., Blake, D.R., 2007. Estimation of gas emissions from shallow subsurface coal fires in Jharia coalfield, India, using FLIR data and coal fire gas analysis. Geological Society of America Abstracts with Programs, vol. 39, no. 6, p. 298, http://gsa.confex.com/gsa/2007AM/finalprogram/abstract_132434.htm (accessed September, 2009).
- Bakker, P., Church, D.J., Feuchtwanger, T.F., Grootenboer, J., Lee, C.A., Longshaw, T.G., et al., 1978. Some practical applications of thermal infrared linescanning. Min. Mag. October, 398–399, 401, 403, 405, 407, 409, 411, and 413.
- Dierks, H.A., Whaite, R.H., Harvey, A.H., 1971. Three mine fire control projects in Northeastern Pennsylvania. U. S. Bureau of Mines Information Circular 8524, Washington, D. C.

- Ellyett, C.D., Fleming, A.D., 1974. Thermal infrared imagery of the burning mountain coal fire. *Remote Sens. Environ.* 3, 79–86.
- Fisher, W., Knuth, W.K., Jr., 1968. Detection and delineation of subsurface coal fires by aerial infrared scanning. *Geol. Soc. Am. Bull.* 115, 67–68.
- Gangopadhyay, P.K., 2007. Application of remote sensing in coal-fire studies and coal-fire-related emissions. In: Stracher, G.B. (Ed.), *Geology of Coal Fires: Case Studies from around the world Reviews in Engineering Geology XVIII*. Geological Society of America, Boulder, CO, pp. 239–248.
- Gielisch, H., 2007. Detecting concealed coal fires. In: Stracher, G.B. (Ed.), *Geology of Coal Fires: Case Studies from around the World, Reviews in Engineering Geology XVIII*. Geological Society of America, Boulder, CO, pp. 199–210.
- Greene, G.W., Moxham, R.M., Harvey, A.H., 1969. Aerial infrared surveys and borehole temperature measurements of coal mine fires in Pennsylvania. *International Symposium on remote sensing, 6th proceedings*, Environmental Research Institute, University of Michigan, Ann Arbor, Michigan, pp. 517–525.
- Hong, Y., Koopmans, B.N., Yaobao, M., Gaofeng, K., 1996. Detectability of coal fire areas from the airborne thermal data and Landsat TM data in Xinjiang, China. *30th International Geological Congress, Abstract*, p. 455.
- Kahle, A.B., 1980. Surface thermal properties. In: Siegal, B.S., Gilliespie, A.R. (Eds.), *Remote Sensing in Geology*. John Wiley & Sons, New York, pp. 257–273.
- Kick, H., Beier, K., Lindermeir, E., 2004. Combined spectral and imaging IR sensor system for analysis of fires and retrieval of fire parameters. In: Ehlers, M., Posa, F., Kaufmann, H.J., Michel, U., De Carolis, G. (Eds.), *Remote sensing for environmental monitoring, GIS applications and geology IV. Proc. SPIE*, 5574, 137–148.
- Kim, A.G., Chaiken, R.F., 1993. Fires in abandoned coal mines and waste banks. U. S. Bureau of Mines Information Circular 9352, Washington, D. C.
- Loughlin, W.P., 1991. Geological exploration in the Western United States by use of airborne scanner imagery. In: *Remote Sensing: An Operational Technology for the Mining and Petroleum Industries. The Institution of Mining and Metallurgy, 1990 Conference*, London, England, pp. 223–241.
- Miller, S.H., and Watson, K., 1980. Thermal infrared aircraft scanner data of the area of underground coal fires, Sheridan, Wyoming, July 1975 and October 1978. U. S. Geological Survey, Washington, D. C., Open-file report OF 80-2021, 5 p.
- Nolter, M.A., Vice, D.H., 2004. Looking back at the Centralia coal fire with a synopsis of its present status. In: Stracher, G.B. (Ed.), *Coal fires burning around the world: a global catastrophe. Int. J. Coal Geol.*, 59 (1–2), 99–106.
- Peng, W.X., van Genderen, J.L., Kang, G.F., 1997. Estimating the depths of underground coal fires using data interpretation techniques. *Terra Nova* 9, 180–183.
- Prakash, A., Berthelote, A.R., 2007. Subsurface coal-mine fires: laboratory simulation, numerical modeling, and depth estimation. In: Stracher, G.B. (Ed.), *Geology of Coal Fires: Case Studies from around the World, Reviews in Engineering Geology XVIII*. Geological Society of America, Boulder, CO, pp. 211–218.
- Prakash, A., Sastry, R.G.S., Saraf, A.K., 1995. Estimating the depth of buried hot features from thermal IR remote sensing data, a conceptual approach. *Int. J. Remote Sens.* 16 (13), 2503–2510.
- Rathmore, C.S., Wright, R., 1993. Monitoring environmental impacts of coal mining. *Int. J. Remote Sens.* 14 (6), 1021–1042.
- Sabins, F.F., Jr., 1997. *Remote Sensing Principles and Interpretation*. third ed. W. H. Freeman, New York, 494 p.
- Shallenberger, J.P., 1993. The use of remote sensing to track the progression of the underground coal mine fire at Centralia, PA. The Pennsylvania State University, unpublished senior thesis, State College, Pennsylvania. 77 p.
- Slavecki, R.J., 1964. Detection and location of subsurface coal fires. *Proceedings of the Third Symposium on Remote Sensing of the Environment*. Michigan Institute of Science and Technology, University of Michigan, Ann Arbor, Michigan, vol. 3, pp. 537–547.
- Technical Innovation and Professional Services, 2005 (June). *Tips takes flight!* vol. 2, no. 1, pp. 3–4. U.S. Department of the Interior, <http://www.tips.osmre.gov> (accessed September, 2009).
- Vice, D.H., 1980. Unpublished letter to Ellis Von Header, Washington Division of Geology and Earth Resources, 2 p., plus thermal infrared imagery.
- Vice, D.H., 2007. Application of airborne thermal infrared imagery to geothermal exploration. *Geotherm. Resour. Council Trans.* 31, 369–372.
- Wikipedia 2009. Forward looking infrared, 2009, http://en.wikipedia.org/wiki/Forward_lookin_infrared (accessed September, 2009).
- Yong-fang, H., Zhao-ming, Z., Fu-zhen, Z., 1990. Detection and investigation of underground coal fire in coal field using airborne infrared scanning technology. *Proc. Int. Symp. Remote Sens. Environ.* 23 (1), 623.

- Zhang, X.M., Cassells, C.J.S., van Genderen, J.L., 1999. Multi-sensor data fusion for the detection of underground coal fires. *Geol. Mijnbouw* 77, 117–127.
- Zhang, J., Huan, Z., Sun, Y., Tian, Y., Voight, S., Zhao, X., 2007. Three-dimensional thermal-imaging methodology for detecting underground coal fires. In: Stracher, G.B. (Ed.), *Geology of Coal Fires: Case Studies from around the World, Reviews in Engineering Geology XVIII*. Geological Society of America, Boulder, CO, pp. 249–259.

WWW Addresses: Additional Reading

- (1) **Coal Fires: Origin, Remote Sensing Detection, and Sublimation**
http://technology.infomine.com/enviromine/case_hist/coal%20fires/Stracher_et_al.html
- (2) **FLIR Infrared Camera Systems**
<http://www.flirthermography.com>
- (3) **Geology of Coal Fires: Case Studies from Around the World, 2008.** In: Stracher, G.B. (Ed.), *Reviews in Engineering Geology XVIII*, Geological Society of America, 283 p.
- (4) **Thermal Analysis in the Field**
http://www.coalfire.caf.dlr.de/results/result_rs_thermalanalysis_en.html
- (5) **Thermal Infrared Technology and Coal fires**
<http://www.gisdevelopment.net/aars/acrs/1990/12/GD003.asp>
- (6) **Thermography**
http://en.wikipedia.org/wiki/Thermal_imaging

This page intentionally left blank

CHAPTER 14

Remote Sensing of Coal Fires

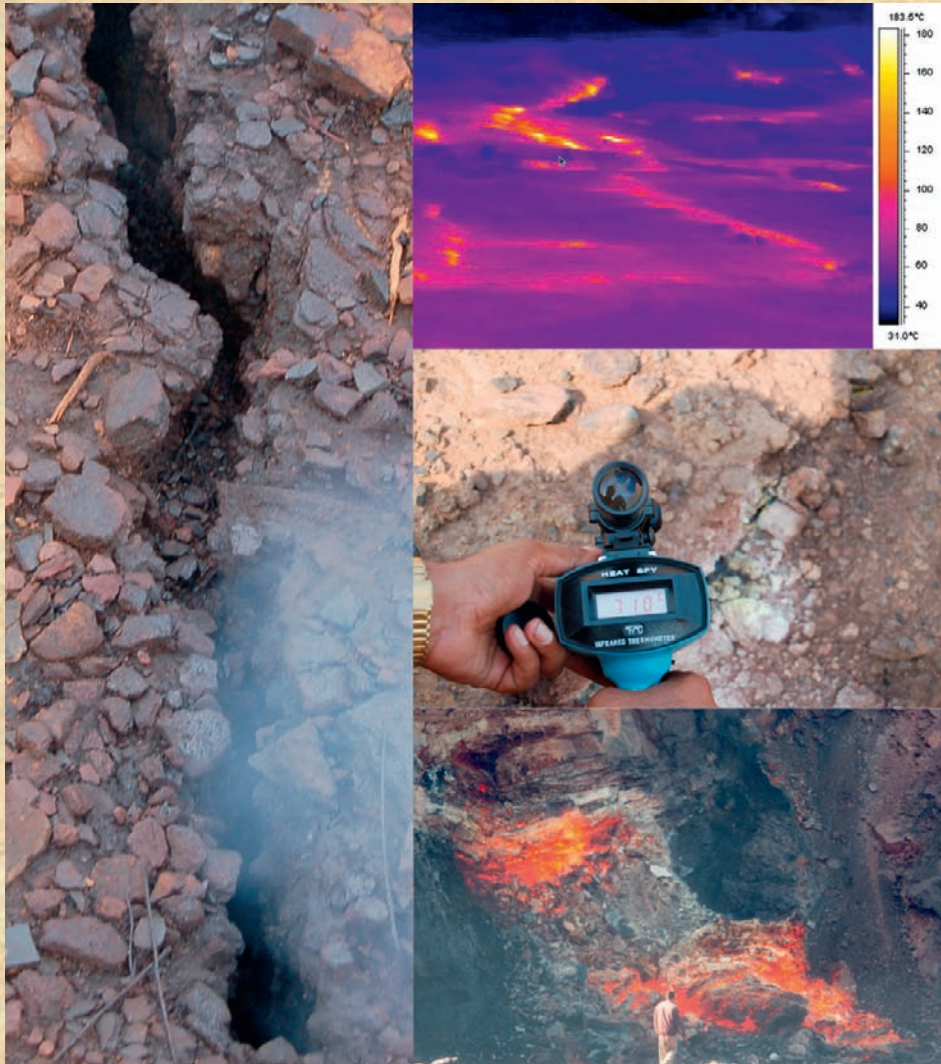


Photo mosaic showing that coal fires are high temperature phenomena that can be mapped, monitored, and quantitatively characterized by using remote sensing and field techniques. The ground fissure on the left, in the Jharia coalfield, India, is 2 m long and 15 cm wide. The thermal image on the upper right is an oblique perspective of a 12 m wide area underlain by an active coal fire in the Jharia coalfield. It was acquired in the 7.5–13 μm wavelength range with a forward looking infrared (FLIR) camera. The yellow to white areas represent relatively higher surface temperatures over ground fissures. The radiometer in the middle-right photo records a temperature of 710°C several millimeters above a fissure in the Jharia coalfield where an active, possibly shallow, underground fire occurs. Note the white by-product of combustion, on the right side of the fissure, nucleated from coal-fire gas. The photo on the bottom right is of a coal fire in an opencast mine in the Ruqigou coalfield, China. *All photos by Anupma Prakash.*

CHAPTER CONTENTS

14.1 Remote Sensing

- Introduction

14.2 Principles of Remote Sensing

- Electromagnetic Energy and Spectrum
- Visible and Near-Infrared Regions
- Shortwave and Thermal Infrared Regions
- Microwave Region

14.3 Remote Sensing Platforms and Sensors

- Overview and Significance

14.4 Coal-Fire Parameter Extraction from Remote Sensing Images

- Introduction
- Crack-Density Mapping
- Reflection-Aureole Mapping
- Land-Cover (Coal Area) Mapping
- Fire-Area Estimation
- Fire-Depth Estimation
- Subsidence Mapping
- Greenhouse-Gas Emissions

14.5 Time Series Analysis and Integrated Interpretation in a GIS

- Introduction
- Important Terms
- References
- WWW Addresses: Additional Reading



14.1. Remote Sensing

Anupma Prakash
Rudiger Gens

Advances in remote sensing and computational science together have changed the way people perceive and study the Earth. This cartoon depicts how satellite images are now routinely visualized on personal computers.

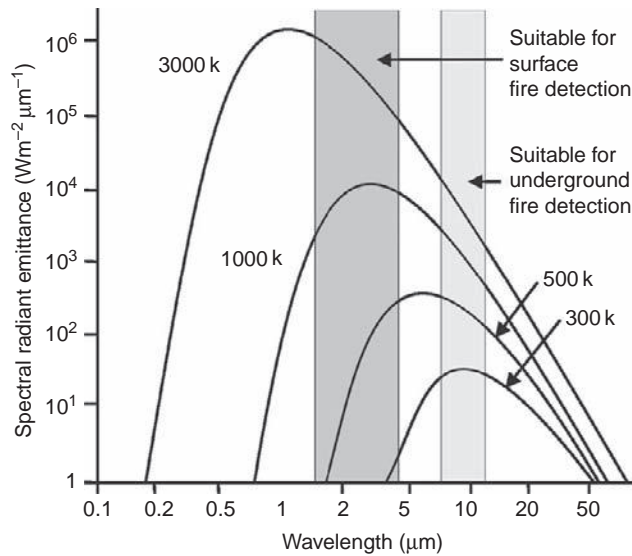
Figure by Anupma Prakash and Rudiger Gens, this work; Source image: NASA Blue Marble.

Introduction

Remote sensing, a noncontact method of acquiring data or information about an object, area, or phenomena, is now a well-established technique applied extensively in mapping, monitoring, environmental research, and in decision and policy making at local, regional, and global scales. The noncontact nature of this technique has unique advantages. For one, the same target can be observed from different distances, providing information at different scales. In general, the further away the observing system (sensor) is placed from the target, the larger is the area it observes, providing a more generalized and synoptic view of the target and its setting. The same target can also be observed several times offering the possibility of using the data for easy monitoring and change detection. The other big advantage is that remote sensing provides spatially continuous data whose accuracy is well understood and documented. These data serve as a permanent and reliable archive available for use in the present and in future to address a variety of application needs.

Though technically any noncontact method of data acquisition falls in the realm of remote sensing, practically the perception is that remote sensing data is acquired from great distances above the Earth's surface, such as by sensors that are mounted on aircraft (airborne remote sensing) or on satellites (satellite remote sensing). These sensors "look down" at the Earth's surface, providing a bird's-eye view of the Earth surface, which is different from the "horizontal view" the human eye takes. Fortunately, programs such as Google Earth™, NASA World Wind™, and Microsoft Virtual Earth™, and extensive use of satellite images in weather reports and travel maps have brought familiarity with this top-down view of the Earth to a stage of cognitive comfort of the general public.

Extensive and excellent introductory material about remote sensing is available in published literature (Rencz and Ryerson, 1999; Gupta, 2003; Janssen et al., 2004; Elachi and van Zyl, 2006; Lillesand et al., 2007; Campell, 2008; Li et al., 2009). The aim of this chapter is not to replicate this available background material on the physical principles of remote sensing, but to focus on the principles, applications, status, and future of remote sensing technology as applicable to the field of coal-fire research – especially detection, mapping, monitoring, characterization, and modeling of coal mining, coal fires, and their associated impacts.



14.2. Principles of Remote Sensing

Illustrated here are the emission spectra of blackbodies at different temperatures. Planck's law is the physical principle guiding how energy is emitted by high-temperature objects.

Figure by Anupma Prakash and Rudiger Gens, this work; adapted from Lillesand et al., 2007.

Electromagnetic Energy and Spectrum

In the most fundamental form, remote sensing relies on measuring the amount of energy reaching the sensor after interacting with the target on the ground and the atmosphere intervening between the target and the sensor¹.

When this energy, also known as the **electromagnetic energy**, is in motion it is referred to as electromagnetic radiation. Electromagnetic radiation can travel in a wavelike form (Figure 14.2.1), even through vacuum, at a constant speed c (the speed of light).

As it follows a wavelike form, it can be characterized simply by measures such as wavelength λ and frequency f . Wavelength and frequency are inversely related according to

$$c = f\lambda \quad (14.2.1)$$

All possible wavelengths and frequencies of the electromagnetic radiation constitute the electromagnetic spectrum (Figure 14.2.2). The **electromagnetic spectrum** ranges from very short wavelength cosmic rays to the long wavelength of standard radio waves. The remote sensing sensors record data only in selected discrete wavelength ranges of the electromagnetic spectrum. These wavelength ranges are often referred to as bands or spectral bands.

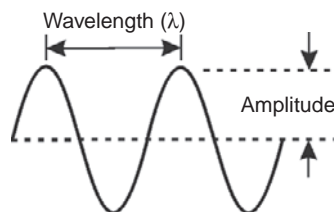


Figure 14.2.1. Wavelike form of electromagnetic radiation.

¹ For additional information about the interaction of matter and energy (i.e., reflection, scattering, transmission, absorption, and emission), see Gens (2009) and Lillesand et al. (2007).

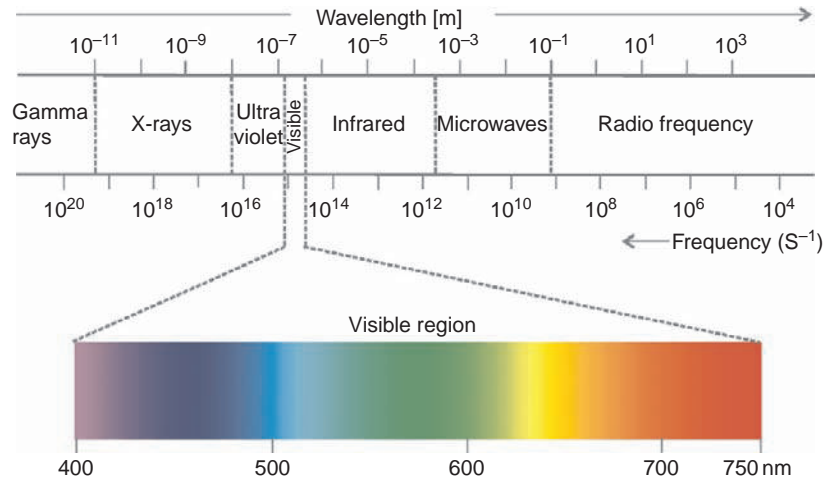


Figure 14.2.2. The electromagnetic spectrum from short wavelength and high frequency gamma rays to long wavelength and low frequency radio waves. Visible light constitutes a very small portion of the electromagnetic spectrum. From Quattrochi et al. 2009.

Visible and Near-Infrared Regions

Visible light, to which the human eye is sensitive, constitutes only a tiny part of the electromagnetic spectrum. Though traditional remote sensing (historic-aerial photography) relied on acquiring data only in this visible part of the spectrum, modern-day sensors acquire data in several different wavelength ranges well beyond the sensitivity of the human eye. This capability of current remote sensing sensors helps us to retrieve new information about the target, which is not possible by simple observations in the field and just a few decades ago was not even conceivable to achieve.

Another important concept to understand is that remote sensing sensors can operate in very small wavelength ranges (narrow bands) or can acquire data integrated over a large span of wavelengths (broad band). When data is available in a few narrow spectral bands, we refer to this as **multispectral remote sensing**. As the bands become narrower, more numerous and nearly continuous across a portion of the spectrum, we transition from the realm of multispectral remote sensing to **hyperspectral remote sensing**. As different Earth surface material's respond rather uniquely in different spectral regions, when remote sensing is carried out in narrow and near-contiguous spectral bands, this spectral information, also known as **spectral response curve** or reflection spectra or spectral signature, becomes diagnostic of the target material. Extensive libraries of reflection spectra of man-made materials and natural materials (minerals, soils, rocks, vegetation, etc.) are now available. Spectral libraries from the US Geological Survey and Jet Propulsion Laboratory (WWW Addresses: Additional Reading at the end of this chapter) are among the best ones known, and these have even been integrated in some commercially available digital image processing software packages. From these libraries, one can extract reflection spectra of tar, bricks, coal, and a variety of typical overburden materials typically seen in a coal-mining area, as well as create synthetic spectra by combining the spectra of individual materials. Figure 14.2.3 shows typical-spectral signatures of clear water, turbid water, coal, healthy green vegetation, stressed vegetation with reduced water content, and dry, brownish-sandy soil.

Examining Figure 14.2.3, it is clear that whereas calm-clear water and clean-coal outcrops have relatively low reflectance across several wavelengths, the reflectance spectra of healthy green vegetation shows quite a dramatic change in reflectance across wavelengths. For green vegetation, the sudden jump in reflectance, from low in the red region to very high in the near-infrared region, is very characteristic. The spectral position of this sudden jump (known as the **red edge**) and the continuous high reflectance in the **near-infrared plateau** are diagnostic for detecting the type and health of the vegetation. In a coal-mining area, it is a common observation that vegetation near the polluted mining areas are stressed, showing a shift in the red edge. Drier vegetation shows a shift in elevation of the infrared plateau and a decrease in the strengths of the absorption peaks in the shortwave infrared regions compared with greener healthier vegetation from the same plant outside the areas affected by mining and fire.

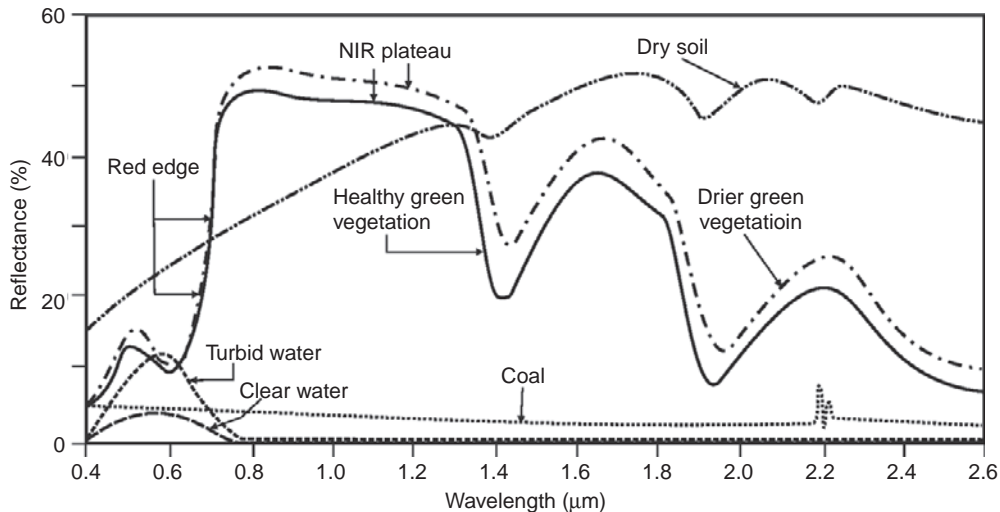


Figure 14.2.3. Reflection spectra of select-surface materials typically seen in a coal-mining area. For a description, see section 14.2. Figure by Prakash and Gens, this work, derived by combing experimentally-acquired spectra with original spectra generalized from the US Geological Survey and Jet Propulsion Lab spectral libraries (see “WWW Addresses: Additional Reading – (2) Resources for Reflectance Spectra”).

Shortwave and Thermal Infrared Regions

Coal fires are high-temperature phenomena, and high-temperature studies require a deep understanding of the interaction of matter and energy in the shortwave infrared and thermal infrared (TIR) regions. All substances (targets), by virtue of their thermal state, emit energy at all wavelengths. The amount of energy emitted by a target varies across the electromagnetic spectrum, as can be seen from its **emission spectra**. The emission spectra also change considerably as the temperature of the target changes. This complex relationship between the target temperature, target type, and the amount of energy it emits at different wavelengths is governed by **Planck’s law**. In the late 1800s, Max Planck developed the concept of **blackbody**, a hypothetical ideal body that would absorb all radiations incident upon it and later would emit all radiations it absorbed to be in perfect thermal equilibrium with its surrounding. For such a blackbody, Planck derived the following relationship:

$$B_{\lambda T} = \frac{2hc^2}{\lambda^5 (e^{hc/\lambda K_B T} - 1)} \quad (14.2.2)$$

where

$B_{\lambda T}$ is the spectral radiance for a blackbody at temperature T ,

λ is the wavelength in meters,

h is Planck’s constant = 6.62×10^{-34} Js,

K_B is the Boltzmann’s constant = 1.38×10^{-23} JK⁻¹,

T is temperature in K, and

c is the speed of light $\approx 3 \times 10^8$ ms⁻¹.

A plot of Planck’s law (equation 14.2.2) is shown in Figure 14.2.4.

What Planck’s law and the plot reveal is that as temperature increases (1) the blackbody emits a greater amount of energy (total energy is represented by the area under the spectral emission curve) and (2) the peak of the emitted radiation shifts toward shorter wavelengths.

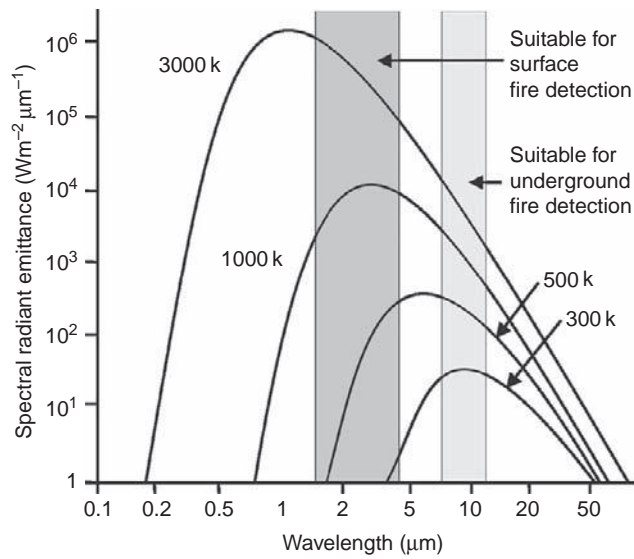


Figure 14.2.4. Planck's emission-spectral curves for black bodies at 300, 500, 1000 and 3000 K. Note that as the temperature of the blackbody rises, the peak of the emitted radiation shifts to shorter wavelengths. The grey zones are spectral regions suitable for temperature-estimation studies of coal fires. Figure by Anupma Prakash; adapted from Lillesand et al. 2007.

This relationship is very important in thermal remote sensing. From the plot of Planck's law, it is clear that to study targets close to about 300 K (ambient temperature of the Earth), the TIR region of the spectrum centered on 10 μm is well suited. However, as the target temperature rises and reaches about 1000 K, the shortwave infrared region (centered on approximately 2 μm) is better suited. This implies that to study underground coal fires that tend to raise the temperature of the overlying land surface only subtly (less than a degree to about 15°), the 8–14 μm spectral region is ideal. For fires in surface coal seams and coal dumps that reach much higher temperatures, the shortwave infrared region is better suited (Prakash et al., 1997; Prakash and Gupta, 1999; Zhang et al., 2004). In large, intense-blazing coal fires, the burn-area temperatures can reach well over 1000 K, and such fires can also be investigated by remote sensing in the visible and near-infrared regions.

The discussion so far has been limited to spectral emissions from a hypothetical blackbody. Natural substances are, however, not blackbodies. Natural targets tend not to absorb all energy that is incident on their surface and subsequently, do not emit all of the energy they absorb. The ratio of energy emitted by a material at a given wavelength and temperature to the energy emitted by a blackbody at the same wavelength and temperature is referred to as its **spectral emissivity**, ϵ_λ . Being a ratio, spectral emissivity has no unit and its value can theoretically range from 0 to 1. Most natural substances show an emissivity value ranging from 0.7 to 0.97. Table 14.2.1 gives the emissivity values of some natural materials encountered in a typical coal-mining area.

For quantitative analysis in thermal remote sensing, emissivity plays a role in two places: (1) In estimating the spectral radiance of a natural substance, the Planck's law needs to be adapted to include spectral emissivity. Planck's law then takes the form

$$B_{\lambda T} = \left(\frac{2hc^2}{\lambda^5 (e^{hc/\lambda K_B T} - 1)} \right) \epsilon_\lambda \quad (14.2.3)$$

where ϵ_λ is the spectral emissivity of the target material and all other factors are the same as defined in equation 14.2.2 and (2) Satellite images record the amount of energy reaching the sensor in the form of quantized **digital numbers** (DNs), which is directly related to the **spectral radiance**, $B_{\lambda T}$, of the target. This relationship between the DN value and the spectral radiance is well defined for all spectral bands of an individual satellite and often provided in either the satellite-image metadata or the data-user handbook for a particular satellite. Once the spectral radiance value is known and an emissivity value is assigned for the target, inverting Planck's law, it is easy to

Table 14.2.1
Generalized emissivity values of some common materials at ambient earth temperature.

Material	Emissivity value
Asphalt	0.95
Brick (red)	0.93
Brick (lime clay)	0.43
Coal	0.95
Grass	0.98
Limestone	0.95–1.00
Soil, dry	0.92
Soil, wet	0.95
Sand	0.90
Sandstone	0.67
Snow	0.80–0.90
Water	0.90–0.95
Wood	0.80–0.95

Note: Emissivity values are compiled from the following sources – <http://www.instrumart.com>, <http://www.infrared-thermography.com>, <http://www.omega.com>, and <http://www.optotherm.com>

compute the **radiant temperature** T , as this is the only remaining unknown in equation 14.2.3. It is important to note that this radiant temperature (also denoted as T_R), derived from remotely sensed data, is almost always lower than the actual *in situ* temperature, or the **kinetic temperature**, T_K , of the target that we can measure directly in the field. Ignoring the contribution from the atmosphere between the target and the sensor, this difference is due to the target's spectral emissivity and is governed by the equation

$$T_R = \varepsilon_\lambda^{1/4} T_K \quad (14.2.4)$$

Quattrochi et al. (2009) provide additional information about TIR remote sensing.

Microwave Region

One of the more popular ways of data acquisition in the microwave region (0.75 cm to 1 m) of the electromagnetic spectrum is by **active remote sensing**, a technique of remote sensing where the sensor itself sends out a pulse of energy at a discrete wavelength instead of relying on the sun, or the thermal state of the target as the source of energy. This pulse comes from the sensor to the target at a fixed angle, rather than straight down and is backscattered (bounced back) from the target. The sensor then measures the time delay between sending the signal and receiving a backscatter response from the target to compute sensor-target distance, which is used to recreate the geometry of the target (Earth's surface). There are several factors that control backscatter: type, sizes, shapes, and orientations of the scatterers in the target area; dielectric properties of the target area; frequency and polarization of the pulses; and the incidence angle of the pulse. The data acquired by the sensor in the microwave region therefore provides information about the target (such as surface roughness, soil moisture content) that is complimentary to the information extracted from data in the visible and infrared regions.

The information about target geometry is particularly useful as it helps to extract digital elevation information about the area. If more than one set of ideally located and timed microwave data pairs over the study area are available, advanced processing techniques (such as differential **Interferometric Synthetic Aperture Radar (InSAR)**) can be used to find subtle deformations and map mining-induced subsidence or elevation increases caused by heaping of coal dumps.

Reviewing the principles, concepts, and advanced developments in the field of microwave, remote sensing data acquisition and processing are well beyond the scope of this chapter. For additional information about this topic, see Ketelaar (2009) and Gens and van Genderen (1996). Specific applications of the techniques discussed above, in the context of coal-fire research, are discussed in section 14.4.4 of this chapter.

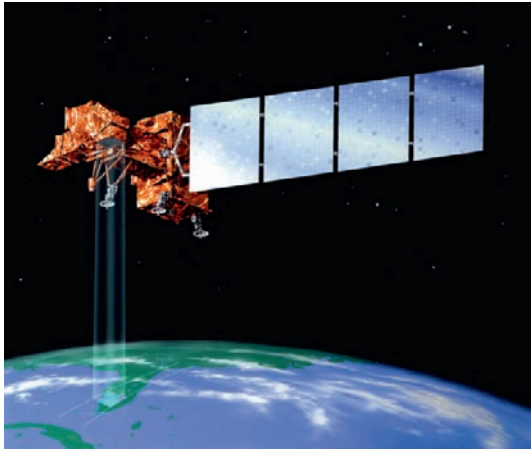
Table 14.2.2
Regions of the electromagnetic spectrum and their significance in coal-mining and coal-fire studies.

Region of spectrum	Wavelength range	Significance in coal-mining and coal-fire studies
Blue (B)	0.4–0.5 μm	Well suited for mapping atmospheric haze, smoke from fires, and pollution in water. It is also helpful in differentiating soil and water. Together with G, R, and NIR, it is used for differentiating, e.g., deciduous from coniferous vegetation.
Green (G)	0.5–0.6 μm	Green vegetation shows a small reflection peak in this region. Together with other spectral bands, it is used for vegetation differentiation and general land cover and land use mapping.
Red (R)	0.6–0.7 μm	Green vegetation shows strong absorption in the red band. Together with the NIR region, this band is ideally suited to map vegetation density, health, stress, biomass, leaf area index, etc. Together with B and SWIR, this region is also useful for alteration-mineral mapping.
Near infrared (NIR)	0.7–1.3 μm	NIR is also known as the vegetation band. Vegetation reflects very strongly in the NIR region. The edge between the R and NIR region where the vegetation shows a sudden jump in reflection is known as the “red edge” and is characteristic of vegetation type. In the NIR region, vegetation also shows a constant high reflection. This high flat reflection region, known as “NIR plateau,” is indicative of vegetation health. In the NIR, water and coal show strong absorption. NIR is therefore also used to delineate bodies of coal and water and to categorize soil by its moisture content.
Shortwave infrared (SWIR)	1.3–3.0 μm	In combination with the NIR and G bands, SWIR is used for differentiating coal from water. SWIR is also used to map variations in soil and vegetation moisture. In combination with the R or NIR regions, it helps accentuate the signal from urban areas and differentiation of soil types. Based on Planck’s law, high temperature bodies such as surface fires that have temperatures around 1000 K show peak emittance in the SWIR region. SWIR is therefore used for detection and quantitative characterization of surface coal fires.
Mid infrared (MIR)	3.0–8.0 μm	Recent research is focused on using the CO ₂ absorption peak in this region to characterize and quantify the locally anomalous CO ₂ concentration near coal fires. The region, in principle, is also suitable for moderately high-temperature mapping.
Thermal infrared (TIR)	8.0–14 μm	TIR region is most important for mapping subtle surface temperature increases associated with underground fires. It is extensively used in underground coal-fire detection, mapping, monitoring and depth estimation. Land surface temperature and emissivity variations estimated from TIR images also provide information about land cover that is complimentary to the information from other spectral regions.
Microwave	55.7 cm – 1 m	Primarily used for mapping surface texture, soil moisture, surface manifestation of faults, elevation estimations, and for mapping and monitoring land subsidence due to coal mining and coal fires.

Note: In the literature, there is little consensus on the nomenclature for different parts of the spectrum and on the specific wavelengths associated with these parts. The nomenclature and range shown in this table is the one that is most commonly followed by the coal-fire remote sensing community.

Source: Table by Anupma Prakash and Rudiger Gens, this work.

Table 14.2.2 summarizes the important wavelength regions of the electromagnetic spectrum in which remote sensing data is acquired, and the significance of each of these regions to coal mining and coal-fire remote sensing.



14.3. Remote Sensing Platforms and Sensors

An artist's rendition of the Landsat 7 satellite orbiting the Earth and acquiring image data.

Image courtesy: NASA.

Overview and Significance

The number of past, present, and planned satellite and airborne remote sensing missions is voluminous. The discussion here is limited to past and present imaging systems (those that acquire images in continuous scan mode) that provide data at a spatial resolution of 1.1 km or less; that have been used or have a strong potential to be used for investigating coal-mining areas and coal fires.

Major technological developments in aerial photography took place between 1914 and 1945, commensurate with World War I and II. In 1960, the first meteorological satellite (TIROS-1) was launched. However, it was only in 1972 with the launch of Landsat-1, the first US-based Earth observing satellite, that remote sensing of the Earth's surface received the required impetus. The US military also recognized the potential of imaging in the **thermal infrared (TIR)** in the 1950s and invested in developing this technology. In 1978, the National Aeronautics and Space Administration (NASA) launched the Heat Capacity Mapping Mission (HCMM), where TIR data was collected day and night at 600 m spatial resolution, thereby opening the pathway for the use of TIR technology for a wide variety of geologic applications.

What followed Landsat was a suite of Earth-observing satellite missions that provided data, with higher spatial resolution, higher spectral resolution, or both. Table 14.3.1 is a list of selected remote sensing platforms and sensors, data characteristics, and comments on their significance for the coal-mining community.

Table 14.3.1
Remote sensing platforms used in coal-mining and coal-fire studies.

Satellite category	Satellite/ sensor	Characteristics	Significance in coal-mining and coal-fire studies
Operational; coarse resolution	AVHRR MODIS	Acquire data in visible through TIR; spatial resolution varies from 250 m in visible to 1.1 km in TIR.	Limited application as spatial resolution is too coarse. Can detect broad regions of intense burning and for mapping smoke and haze over large study areas.
Operational; medium resolution	ASTER Landsat	Acquire data in visible through TIR; spatial resolution varies from 15 m in panchromatic mode to 120 m in TIR. Landsat has a broad TIR band, while ASTER has multispectral TIR bands	Most extensively used image source for land cover and land use mapping, surface and underground fire detection, fire temperature estimation, and change detection and mining-impact assessment. Multispectral TIR bands in ASTER allows emissivity estimations. ASTER band 3 is also used for generating digital elevation models.
Operational; medium to fine resolution	ALOS SPOT IRS	Acquire data in visible and near infrared. Spatial resolution varies from 2.5 m in panchromatic mode to 20 m in multispectral mode.	Good for mapping general land cover including vegetation, soils, rocks, coal outcrops, coal dumps, urban areas, water bodies. etc. Lack SWIR and TIR bands and so not suitable for coal-fire studies.
Commercial; operational high resolution	IKONOS Quickbird	Acquire data in visible and near infrared. Spatial resolution varies from 60 cm in panchromatic mode to 4 m in multispectral mode	Useful as base image for mapping purposes and for geo-referencing other image data sets (such as airborne images). Derived land- cover maps have greater spatial accuracy. Cracks and fractures can be mapped.
Past and present SARsatellites	ERS 1 ERS 2 Radarsat	Acquire data in the microwave region; Spatial resolution varies from about 8 m (pixel size 6.25 m), to generally 30 m. Coarsest resolution is for ScanSAR data (100 m).	Provides information complimentary to the optical and thermal sensors. Good for studying surface roughness, soil moisture, vegetation distribution, and geologic structures. Used extensively for generating digital-elevation models and subsidence studies.
Hyperspectral satellites with limited data acquisition	Hyperion ALI DAIS	Hyperspectral data acquired in several narrow spectral regions from visible through TIR. Spatial resolution variable.	Excellent for mapping land-cover composition. Capable of more accurately discriminating soil, rock, and vegetation types, picking up subtle variations. Potential in coal-mining studies not fully exploited.
Experimental satellite with MIR and TIR bands	BIRD	Acquire data in MIR and TIR channel at 290 m spatial resolution.	A high temperature event detection satellite of the German Space Agency. Ideally suited for forest- fire studies but also very useful for coal-fire detection.

Table 14.3.1
(continued)

Satellite category	Satellite/ sensor	Characteristics	Significance in coal-mining and coal-fire studies
Airborne missions and airborne sensors	Optical cameras U2 Daedalus FLIR	Some of the platforms were precursors to satellite missions. Spectral regions vary from visible to TIR. Spatial resolution depends on flying height and sensor.	Source of legacy data for mining areas. High spatial resolution is particularly well suited for mapping, monitoring, planning, assessing, and decision making. Where accessibility and safety is an issue, this is a good means for reconnaissance study.

Note: Only data sets used most extensively in coal-mining and coal-fire research are listed. Detailed information about these satellites and sensors can be found on their respective web sites listed at the end of this chapter in the subsection WWW Addresses.

Source: Table by Anupma Prakash and Rudiger Gens, this work.

ALL, Advanced Land Imager; ALOS, Advanced Land Observing Satellite; ASTER, Advanced Spaceborne Thermal Emission and Reflection Radiometer; AVHRR, Advanced Very High Resolution Radiometer; BIRD, Bispectral InfraRed Detection; DAIS, Digital Airborne Imaging Spectrometer; ERS, European Remote Sensing Satellite; FLIR, Forward Looking Infrared Radiometer; IRS, Indian Remote Sensing Satellite; MIR, Mid Infrared; MODIS, Moderate Resolution Imaging Spectroradiometer; SAR, Synthetic Aperture Radar; SPOT, Satellite Pour l'Observation de la Terre; SWIR, Shortwave Infrared; TIR: Thermal Infrared



Photo by Anupma Prakash, 2006.

14.4. Coal-Fire Parameter Extraction from Remote Sensing Images

Photo illustrating an active, shallow sub-surface coal fire with several active vents in the Jharia coalfield, India. Remote sensing technology for coal-fire parameter extraction is especially particularly suitable in areas that are large, remote, inaccessible, or hazardous.

Introduction

Coal-fire areas are characterized by several typical surface features, also referred to as **geoenvironmental indicators** of coal fires, that can be recognized, mapped, and quantified using remote sensing techniques. Some other coal-fire parameters, such as fire depth, cannot be directly mapped but can be indirectly inferred. The following is a brief discussion about the extraction of important coal-fire parameters that can be observed or inferred from remote sensing images.

Crack-Density Mapping

Local heating due to the presence of underground coal fires results in thermal cracking of the rock and soil layers overlying the burn area. The dimensions and density of these cracks are variable; ranging from narrow, short, and nearly vertical to massive cracks that are several meters wide and stretch for thousands of meters in length (Figure 14.4.1). The intensity, depth, and longevity of burning in the subsurface will control the dimensions and crack density (cracks per unit area) visible on the surface. In general, the intensity of the **heat source** and the crack density are directly related, with the more intense burning causing greater thermal cracking. In addition, the more shallow fires cause more surface cracking, whereas the deeper fires result in more massive cracks.

High spatial resolution remote sensing images are an excellent source for generating comprehensive maps of surface cracks. Though traditionally these maps were created by manual tracing of cracks inferred from visual interpretation (Chen, 1997), now crack-density mapping can be carried out using digital image processing techniques. In particular, high pass digital filters can be applied to digital images to highlight linear and curvilinear features potentially representing surface cracks. Crack densities can then be computed per unit area using geospatial statistical analyses available with commercial software packages such as ArcGISTM. Although the digital technique is fast and efficient, it has the potential of overestimating cracks as lineaments not associated with cracks may also be inferred as cracks by the system.

Reflection-Aureole Mapping

As mentioned above, underground coal fires locally heat overlying rock and soil layers. The heating removes moisture from the soil. The dryer soil and high temperatures are detrimental to the growth of vegetation, which first becomes stressed and eventually dies. It is, therefore, common to see small halos of locally dry and highly reflective barren areas in an otherwise relatively greener patch of land. These halos, called **reflection aureoles** or **barrenness aureoles** (Gupta and Prakash, 1998), can be well detected on visible and infrared images as well as TIR images (Figure 14.4.2).



Figure 14.4.1. Photograph from the Jharia coalfield, India, showing a typical landscape associated with an area affected by underground fire. The land over the subsurface fire shows several fissures and cracks, some of which may extend for hundreds of meters in length. Photo by Anupma Prakash, 2006.

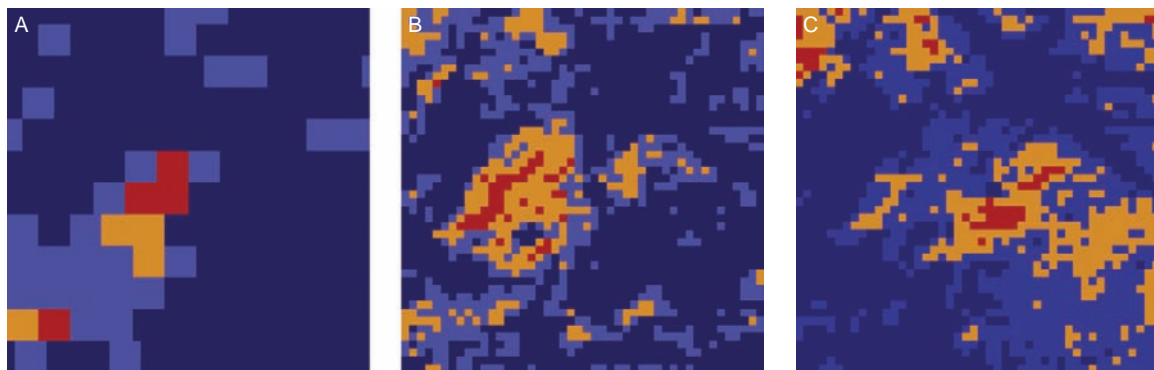


Figure 14.4.2. (A) Thermal infrared image, (B) red band image, and (C) near-infrared image subset of an area above an underground fire. Each subset represents 1.4 km by 1.4 km block. Red represents the highest range of DN values; yellow and light blue represent successively lower DN value range; and blue represents lowest background DN values in each band. It is interpreted that heating due to subsurface fires has raised surface temperature, caused drying of the soil, increased reflectance in red and near-infrared bands and also rendered the soil locally unfit to support vegetation. Image reprocessed; based on Gupta and Prakash 1998.

Land-Cover (Coal Area) Mapping

One of the popular applications of remote sensing in a mining area is for creating classified land-cover and land-use maps. Extensive discussion on various classification schemes for **land-cover mapping** and the detection of land-cover change is available in the published literature (Lambin and Ehrlich, 1996; Lu et al., 2004; Xie et al., 2008). Two issues complicate land-cover mapping in a coal-mining area. The first is the spectral similarity of exposed bodies of coal and water and the second is the presence of fires.

To differentiate between exposed coal and water on Landsat images, Prakash and Gupta (1998) used a false color composite comprising Landsat bands 5, 4, and 2 coded in red, green, and blue, respectively. For this specific combination, the coal outcrops appeared in shades of brownish-black, whereas water bodies appeared in shades of bluish-black.

📊 Fire-Area Estimation

Remote sensing-based fire-area estimates are close approximations of the actual fire area. The reason why they are only approximations is because the term fire area is not rigorously defined. In the field, the fire area may mean the actual area showing visible flames and excessively high temperatures. In remote sensing, however, the fire area implies the area showing a **surface thermal anomaly**. Thermally anomalous areas have pixels that exhibit temperatures higher than a preselected **background temperature**. The remote sensing based area estimates are therefore a function of the pixel size (related to spatial resolution of the images) and the user-defined threshold of the background temperature value.

Where and how to set a threshold to differentiate background areas and fire areas is a subject of debate and continued research. Threshold selection has evolved from using a general value based on trial and error (Prakash et al., 1997), to taking a statistical threshold set at a standard deviation of two (Prakash et al., 1999), to site specific threshold using the shape of the slope of the histogram of the image subset for that site (Rosema et al., 1999), to taking the first local minimum after the main maximum digital value during several iterations of a moving window kernel (Kuenzer et al., 2007a; Figure 14.4.3). However, given the complex nature and differences among fire sites, no one technique is known to work well in all situations to delineate fire areas from remote sensing images.

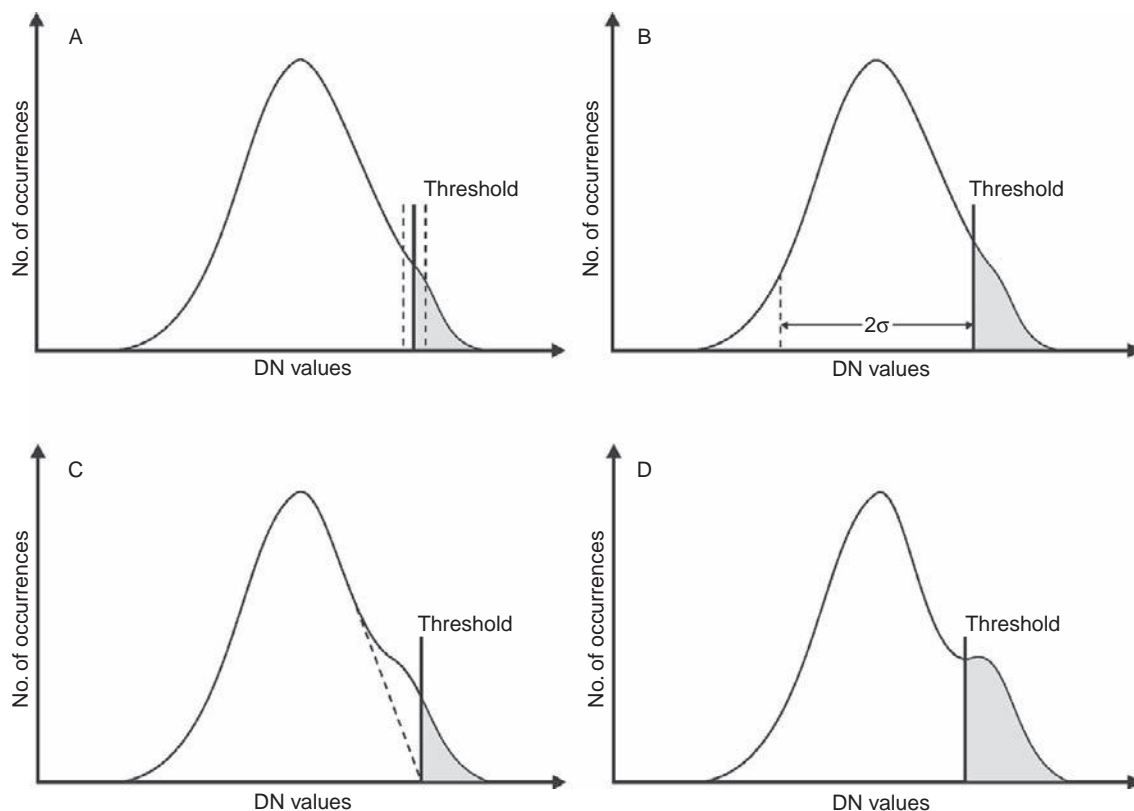


Figure 14.4.3. A conceptual figure showing histograms of a thermal infrared image or an image subset. The Digital Number (DN) value range is shown on the x axis. On the y axis is the frequency or number of occurrences of a specific DN value. Different criteria for selecting a threshold to delineate thermal anomalies from background temperatures are depicted: (A) threshold is selected by trial-and-error and guided by field data; (B) threshold is determined using a statistical parameter, in this case a standard deviation of 2; (C) the location of the change in slope of the histogram is identified and projected on to the x-axis to determine threshold; (D) the first minimum-value dip after a major DN value maxima is selected as the threshold. Figure by Anupma Prakash and Rudiger Gens, this work.

Fire-Depth Estimation

Estimating **fire depth** using remote sensing is and will remain a complex problem, as the intent is to quantify a parameter that is not directly measurable by remote sensing. To model the subsurface condition based on what is observed on the surface requires simplifications and assumptions of naturally occurring processes. Most fire-depth estimation models are based on investigating the location of a surface thermal anomaly and its unique sectional profile.

The simplest and crudest method for fire-depth estimation is a geometric method (Saraf et al., 1995). According to this method, if the location of the surface thermal anomaly associated with an underground fire, and the dip of the proximally outcropping coal seam are known, then a simple geometric construction can help to give an approximate estimate of fire depth (Figure 14.4.4).

The two inaccurate assumptions made in this model are that the proximally outcropping seam is the one on fire, and the surface thermal anomaly is vertically above the underground heat source. Peng et al. (1997) expanded the geometric model to include more geologic (stratigraphic and structural) information of the site under consideration. In the absence of any other sophisticated equipment and data, this technique is still very useful to give a first-order estimate of fire depth.

Other depth-estimation techniques are based on numerical methods that rely on the physical principles of **heat-energy transfer**. Numerical models can be broadly divided into two categories: (1) **conduction** as the sole means of heat transfer from the subsurface to the surface and (2) a combination of conduction and **convection** processes for heat transfer. In both categories, the heat source is modeled as either a point source or a linear/cylindrical source; and the overlying material as one constituting a semi-infinite medium. Most efforts to understand the transfer of heat energy along the surface are supported by finite element analysis. Both types of models have their limitations as discussed below.

Most conduction-based models (Mukherjee et al., 1991; Cassells, 1998; Prakash and Berthelote, 2007; Berthelote et al., 2008) are based on the assumption that the heat transfer from the subsurface to the surface is linear in nature and after a certain time, the system reaches a steady state. The shape of the surface thermal anomaly at this point holds clues to the depth of the heat source. Shallow fires quickly increase the surface temperature, whereas deeper fires cause the surface thermal anomaly to be widespread and very subtle (Figure 14.4.5). A profile of the surface thermal anomaly from a shallow-heat source is therefore considerably different than from a deeper source.

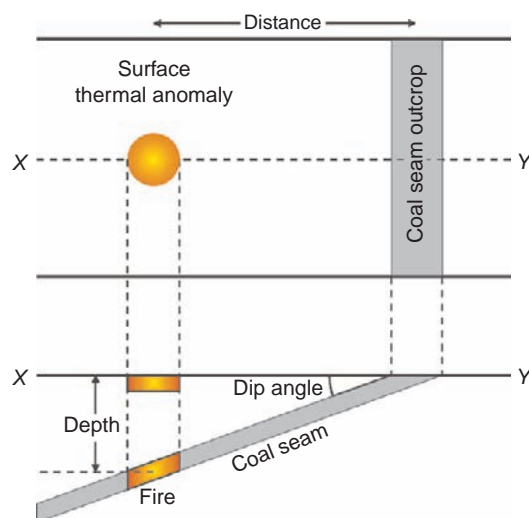


Figure 14.4.4. Diagram illustrating a simple-geometric construction for estimating fire depth. The top portion of the diagram shows a plan view and the bottom a cross-sectional view through the line X – Y . The distance between the coal seam and surface thermal anomaly can be measured *in situ* or from remote sensing images. In addition, by knowing the dip direction of the coal seam below the anomaly, the normal distance from the surface thermal anomaly to the coal seam, is a quick approximation of fire depth. Adapted from Saraf et al. 1995.

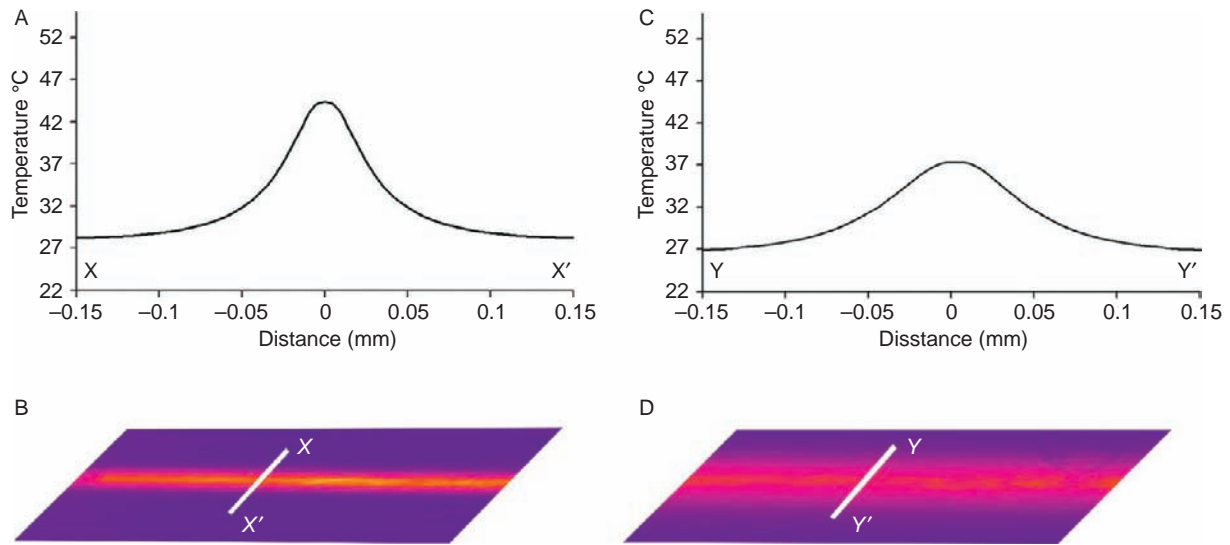


Figure 14.4.5. A conceptual diagram showing the relationship of the depth of a coal fire to its surface thermal anomaly. (A) and (B) are cross-sectional and plan views, respectively, of a thermal anomaly from a laboratory simulation of a shallow fire. (C) and (D) are the cross-sectional and plan views, respectively, of a thermal anomaly from a laboratory simulation of a relatively deeper coal fire. Shallow buried heat sources generate narrower and taller thermal anomaly profiles compared to deeper buried heat sources. From Prakash and Berthelote 2007.

Panigrahi et al. (1995) proposed a mathematical relationship between the thermal profile and fire depth, stating that the full width of the profile at half its maximum intensity (also referred to as **Full Width Half Max**) approximately equates to one-third of the fire depth. Berthelote et al. (2008) carried out laboratory simulations of coal fires and established a more complex empirical relationship between the surface thermal profile and the fire depth, which marginally outperformed the depth estimates of Panigrahi et al. (1995). For the actual empirical relationship and comparative performance evaluation of these models, the readers are referred to Prakash and Berthelote (2007).

In real life, both conduction and convection play a role in heat transfer from depth, with convection arguably playing a more important role. However, modeling the convective component is far more challenging. The interstitial pore spaces in overlying rock units, cracks, fractures, and faults all constitute convective pathways for the heat energy to disseminate. Among other factors, the amount of heat energy actually dissipated is a complex interplay of the intensity of the heat source and the nature, density, and interconnectivity of the convective pathways. The convective pathways differ spatially and temporally over individual fires, making it difficult to model heat transfer in the field as well as from remote sensing images.

Prakash et al. (1995b) accounted for the convective component of heat transfer by a very crude assumption that the convection component of the heat transfer from the subsurface to surface was three to five times greater than heat transfer by conduction alone. Rosema et al. (1999) modeled the convective component as a single chimney system. They made the assumption that the integrated effect of all convection pathways was effectively the same as one single large vent of a certain dimension. Wessling et al. (2008) further analyzed the mechanisms of conduction and convection pathways that cause thermal anomalies on the surface and numerically modeled the effect of these processes.

Refining these existing models with the intent to estimate depth of the buried-heat source is an area that merits further research. It is important to note that these models make an effort to mimic natural processes by replacing them with mathematical representations that are only as accurate as knowledge permits.

Subsidence Mapping

Subsidence of the surface, a phenomenon where the ground surface caves in, is not uncommon in coal-mining areas. If coal is extracted from the subsurface without completely filling the void that the extraction process leaves behind, or without reinforcing the overlying rock strata in some other manner (e.g., by roof bolts), the mined area

becomes prone to the danger of the overlying material collapsing. If a fire starts at a previously mined area that has coal pillars left as support structures for the overlying material, the pillars may burn causing a bigger void and subsidence of the overlying material. Coal fires can therefore contribute to the problem of land subsidence in a coal-mining area.

The dangers of land subsidence are many. Infrastructures above and near the subsidence area can get damaged, the surface can become inhabitable from massive cracking, coal reserves can get blocked for further exploration, subsidence can open new pathways for oxygen to get into the subsurface and thus flare-up old fires or start new ones, and land subsidence may injure or kill mine workers during mining operations.

Traditional and advanced remote sensing techniques can be used to detect and regularly monitor existing subsidence areas, as well as those areas that are likely to be affected in the future. The traditional techniques are based on visual interpretation of aerial photos where areas of subsidence are identified based on photo-interpretation elements such as tone, texture, shape, size, pattern, association, and user knowledge of the field area. Subsidence areas appear as small sinkholes or larger troughs with massive cracks associated with the trough edges.

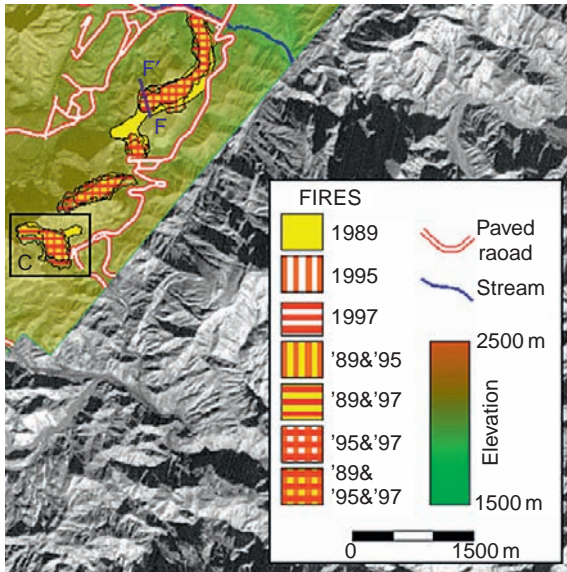
Digital remote sensing methods for land-subsidence detection and monitoring involve the use of InSAR. For a good overview of the principles, techniques, and applications of InSAR, readers are referred to the paper by Gens and van Genderen (1996) and the book by Ketelaar (2009). A good list of references for subsidence mapping using InSAR is also available at http://www.gi.alaska.edu/~rgens/teaching/literature/insar_subsidence.html. The use of InSAR techniques for identifying potential coal-fire related subsidence was first described by Prakash et al. (2001). A report entitled *Coal Fire Interferometry* (Genderen et al., 2000) also discusses this topic. More recently, Voigt et al. (2004) used InSAR techniques in a coalfield in China to map subsidence.

Greenhouse-Gas Emissions

Estimating the **greenhouse-gas** emissions from an individual fire and projecting global estimates is one of the key research questions that is now being actively pursued by coal-fire researchers. Research lead by the US Geological Survey (Kolker et al., 2009) and other institutions carried out a field-based emission estimate at the Mulga fire in Alabama followed by a field-based and airborne-temperature and flux estimate of coal fires in the Powder River basin of Wyoming. Their results showed that an approximate (not definite) correlation exists between land-surface temperatures of areas affected by coal-fire and the emanating CO₂ flux. Similar efforts were made for emission estimates in select coalfields in China (Voigt et al., 2004), Australia (Carras et al., 2009), and India (Prakash et al., 2010).

Gangopadhyay et al. (2005) attempted to use imaging spectroscopy to quantify CO₂ emissions based on spectral absorption by CO₂ molecules in the infrared regions. Though the theoretical concept that this research was based on is powerful, the authors could not convincingly quantify the increase in spectral absorption due to increased CO₂ emissions.

Extrapolating emission estimates from the observations from one fire to another fire in its proximity, or even for the same fire at different times, is challenging due to the spatiotemporal dynamics of burning. Therefore, extrapolating the limited results that are available for greenhouse-gas emissions from individual fires, to project a global estimate has inherent flaws and dangers. This explains why the greenhouse-gas-emission estimates for coal fires in China, which reportedly range from 10 Mt/yr to 200 Mt/year (Rosema et al., 1999; Kuenzer et al., 2007b), have such large variability.



14.5. Time Series Analysis and Integrated Interpretation in a GIS

Figure showing surface extent of coal fires extracted from a time series of satellite images. Images were integrated in a GIS along with ancillary information such as terrain elevation, roads, and water bodies for querying and decision making.

Image adapted from Prakash et al., 1999.

Introduction

A **Geographic Information System (GIS)** is a framework for integrating diverse data sets associated with a specific area. GIS allows a user to efficiently acquire, integrate, manage, analyze, and visualize geospatial data, i.e., data associated with a geographic location. For coal mining, a GIS is most often used as a central database to efficiently store all data related to the mining site and its operation. A more specialized GIS system for a coal-mining region can also include a coal-fire database with very detailed fire-specific information (Rosema et al., 1999; Prakash and Vekerdy, 2004; Zamaraev et al., 2008; Seda et al., 2009). The beauty of such a GIS is that it is dynamic and can be constantly upgraded with new information, making it ideal to serve as an operational-monitoring system. For example, the GIS system could be automated to a certain degree, so that with every new satellite pass over a coal-mining area, the remote sensing image could be added to the database, processed to cut out a subset of just the mining or known fire site, processed using specialized user defined algorithms to compute fire parameters, and compared with previous images to highlight any change in fire parameters. Such critical information, extracted in an efficient and timely manner and displayed in meaningful ways using the GIS, can serve as an excellent decision-making tool in a coal-mining operation and for planning firefighting operations. Some typical examples of information and map outputs from temporal GIS are maps showing changes in fire location, fire depths, intensity of burning, land-surface characteristic, etc. Fire risk, fire hazard, and fire fighting priority maps are other examples of potential outputs from a coal-fire GIS.

Important Terms

- Active remote sensing** A form of remote sensing where the remote sensor provides its own source of electromagnetic radiation. Radar is one example.
- Background temperature** Average temperature of an area representative of the general surrounding (in this case nonfire area).
- Barrenness aureoles** Small halos of locally dry and highly reflective barren areas in an otherwise vegetated patch of land. Also known as reflection aureoles.
- Blackbody** A hypothetical ideal body that absorbs all radiations incident upon it and later emits radiations at the maximum possible rate per unit area at each wavelength for any given temperature, to be in perfect thermal equilibrium with its surrounding. No natural substance is a true blackbody. A large, deep, calm water body is considered a close proxy to an ideal blackbody.

Conduction	(or heat conduction, as implied here) The transfer of internal energy from a medium or region of higher temperature to a medium or region of lower temperature from particle to particle.
Convection	The transfer of heat through a fluid (liquid or gas) caused by molecular motion.
Digital number	Abbreviated as DN, refers to the digital value assigned to a pixel (smallest element) in a digital image. The DN value often represents a physical property, for example, in an optical image it represents the brightness value (related to amount of energy reflected).
Electromagnetic energy	A dynamic form of energy that is caused by the oscillation or acceleration of a charged particle. All substances above absolute zero (0 K or -273.16°C) emit a range of electromagnetic energy.
Electromagnetic spectrum	The entire range of electromagnetic energy. It stretches from short-wavelength gamma rays to long-wavelength radio waves.
Emission spectra	The amount of energy emitted by an object at a given temperature as a function of wavelength. Emission spectra are often shown for an ideal blackbody and are governed by Planck's law.
Fire depth	The vertical distance between the land surface and the center of the underground burning source (coal fire in this case).
Full Width Half Max	The total width of a temperature profile (or a modeled curve fit, e.g., Lorenzian fit) at half the difference between maximum and minimum recorded temperatures.
Geoenvironmental indicators	Qualitative or quantitative records of features, areas, or phenomena of significance on the Earth's surface or its surrounding environment.
Geographic Information System	Science and technology involved in acquiring, integrating, analyzing, managing, and visualizing geospatial data and information.
Greenhouse gas	A gas in the atmosphere that significantly absorbs and emits radiations in the thermal infrared region of the electromagnetic spectrum.
Heat source	In the current context, the subsurface coal fires that are causing ground heating and surface cracking.
Hyperspectral remote sensing	Also increasingly referred to as imaging spectroscopy. It is a form of remote sensing where data is acquired in several narrow, and often near contiguous, spectral channels or spectral bands.
Interferometric Synthetic Aperture Radar (InSAR)	InSAR is a technique for extracting three-dimensional information of the Earth's surface by using the phase content of the radar signal as an additional information source derived from the complex radar data.
Kinetic temperature	The actual temperature of a body as measured with a contact thermometer.
Land-cover mapping	In the current context it implies the use of remote sensing data to map the spatial distribution of the varied physical material on the surface of the Earth.
Multispectral remote sensing	Remote sensing in several discrete spectral wavelengths. For example, data from the Landsat satellite is considered multispectral.
Near infrared	Region of the electromagnetic spectrum where the radiations have wavelengths from just longer than the visible (about $0.7\ \mu\text{m}$) to about $1.3\ \mu\text{m}$.
Near-infrared plateau	The continuous high reflectance from green vegetation in the near-infrared region. This plateau helps to discriminate vegetation type and vegetation health.

Planck's law	Planck's law determines the emission pattern/spectra of the energy radiated from a blackbody as a function of its wavelength and temperature.
Radiant temperature	The temperature of the body/target as recorded by the remote thermal sensor. Ignoring the role of the atmospheric interactions between the target and the sensor, the radiant temperature is dependent on the kinetic temperature of the body and its emissivity.
Red edge	The abrupt reflectance change of the vegetation spectra in the 6.8–7.4 μm region that is caused mainly due to the combined influence of chlorophyll concentration, developmental stage, leaf layering, and leaf water content.
Reflection aureoles	See description of Barrenness aureoles.
Remote sensing	In the simplest form, it is acquiring information about an object or a phenomenon without being in direct contact with it.
Spectral emissivity	Emissivity is the emitting ability of a real material compared to that of a blackbody. Emissivity of a material at a specific wavelength is referred to as spectral emissivity.
Spectral radiance	The total amount of radiant energy measured for a unit solid angle, at a given wavelength.
Spectral response curve	The percent reflectance of a material across a range of wavelengths.
Subsidence	In the current context, the caving-in of the ground surface due to the underground coal/material extraction, or due to underground coal fires.
Surface thermal anomaly	Area with elevated temperature compared to the background.
Thermal infrared (TIR)	In the context of coal fire studies and this chapter, thermal infrared refers to the 8–14 μm spectral range. However, for terrestrial remote sensing, the 3–35 μm region is broadly referred to as thermal infrared.

References

- Berthelote, A.R., Prakash, A., Dehn, J., 2008. An empirical function to estimate the depths of linear hot sources: applied to the Kuhio lava tube, Hawaii. *Bull. Volcanol.* 70 (7), 813–824.
- Campbell, J.B., 2008. *Introduction to Remote Sensing*, fourth ed. The Guilford Press, New York, 626 p.
- Carras, J.N., Day, S.J., Saghafi, A., Williams, D.J., 2009. Greenhouse gas emissions from low-temperature oxidation and spontaneous combustion at open-cut coal mines in Australia. *Int. J. Coal Geol.* 78 (2), 161–168.
- Cassells, C.J.S., 1998, *Thermal Modeling of Underground Coal Fires in Northwest China*: University of Dundee, Scotland, Thesis: The Netherlands, International Institute for Geo-Information Science and Earth Observation (ITC) publication 51 (CD-ROM, ITC library).
- Chen, L.D., 1997, *Subsidence assessment in the Rujigou Coalfield, Ningxia, China*, M.Sc. Thesis. The Netherlands, International Institute for Geo-Information Science and Earth Observation (ITC), 130 p.
- Elachi, C., van Zyl, J.J., 2006. *Introduction to the Physics and Techniques of Remote Sensing*, second ed. John Wiley & Sons, Inc., Hoboken, New Jersey, 672 p.
- Gangopadhyay, P.K., Meer, F., van der Dijk, P.M. van, 2005. Atmospheric modeling using high resolution radiative transfer codes and identification of CO₂ absorption bands to estimate coal fire related emissions. Warsaw, Poland, 4th Workshop on Imaging Spectroscopy, European Association of Remote Sensing Laboratories (EARSeL), April 27–29, p. 92.
- Genderen, J.L. van, Prakash, A., Gens, R., Veen, B.S. van, Liding, C., Tao, T.X., et al., 2000, *Coal fire interferometry*. Netherlands Remote Sensing Board, USP-2-99-32, 63 p.
- Gens, R., 2009. Spectral information content of remote sensing imagery. In: Li, D., Shan, J., Gong, J., eds., *Geospatial Technology for Earth Observation*, first ed. Springer Science + Business Media, LLC., New York, pp. 177–202.
- Gens, R., Genderen, J.L. van, 1996. SAR interferometry – issues, techniques, applications. *Int. J. Remote Sens.* 17 (10), 1803–1835.

- Gupta, R.P., 2003. *Remote Sensing Geology*, second ed. Springer-Verlag Berlin Heidelberg, 656 p.
- Gupta, R.P., Prakash, A., 1998. Reflection aureoles associated with thermal anomalies due to subsurface mine fires in the Jharia coalfield, India. *Int. J. Remote Sens.* 19 (14), 2619–2622.
- Janssen, L.L.F., Huurneman, G.C., Bakker, W.H., Janssen, L.L.F., Reeves, C.V., Gorte, B.G.H., et al., 2004. *Principles of remote sensing. An Introductory Textbook*. The Netherlands, International Institute for Geo-Information Science and Earth Observation (ITC) Educational Textbook Series, 180 p.
- Ketelaar, V.B.H., 2009. *Satellite Radar Interferometry: Subsidence Monitoring Techniques*, first ed. Springer, 270 p.
- Kolker, A., Engle, M., Stracher, G., Hower, J., Prakash, A., Radke, L., et al., 2009. Emissions from coal fires and their impact on the environment. U.S. Geological Survey Fact Sheet, 2009–3084, 4 p.
- Kuenzer, C., Zhang, J., Li, J., Voigt, S., Mehl, H., Wagner, W., 2007a. Detecting unknown coal fires: synergy of automated coal fire risk area delineation and improved thermal anomaly extraction. *Int. J. Remote Sens.* 28 (20), 4561–4585.
- Kuenzer, C., Zhang, J., Tetzlaff, A., Dijk, P. van, Voigt, S., Mehl, H., et al., 2007b. Uncontrolled coal fires and their environmental impacts: investigating two arid mining regions in north-central China. *Appl. Geogr.* 27, 42–62.
- Lambin, E.F., Ehrlich, D., 1996. The surface temperature-vegetation index space for land cover and land-cover change analysis. *Int. J. Remote Sens.* 17 (3), 463–487.
- Li, D., Shan, J., Gong, J., 2009. *Geospatial Technology for Earth Observation*, first ed. Springer Science + Business Media, LLC., New York, 558 p.
- Lillesand, T.M., Kiefer, R.W., Chipman, J.W., 2007. *Remote Sensing and Image Interpretation*, sixth ed. John Wiley & Sons, Inc., Hoboken, New Jersey, 1164 p.
- Lu, D., Mausel, P., Brondi'zio, E., Moran, E., 2004. Change detection techniques. *Int. J. Remote Sens.* 25 (12), 2365–2407.
- Mukherjee, T.K., Bandhopadhyay, T.K., Pande, S.K., 1991. Detection and delineation of depth of subsurface coalmine fires based on an airborne multispectral-scanner survey in part of Jharia coalfield, India. *Photogramm. Eng. Remote Sens.* 57, 1203–1207.
- Panigrahi, D.C., Singh, M.K., Singh, C., 1995. Predictions of depth of mine fire from the surface by using thermal infrared measurement. *Proceedings of the National Seminar on Mine Fires, Varanasi, India, February 24–25, Banaras Hindu University, Varanasi*, pp. 122–134.
- Peng, W.X., Genderen, J.L. van, Kang, G.F., Guan, H.Y., Tan, Y., 1997. Estimating the depth of underground coal fires using data integration techniques. *Terra Nova.* 9 (4), 180–183.
- Prakash, A., Berthelote, A.R., 2007. Subsurface coal mine fires: laboratory simulation, numerical modeling, and depth estimation. In: Stracher, G.B. (Ed.), *Geology of Coal Fires: Case Studies from around the World, Reviews in Engineering Geology XVIII*. Geological Society of America, Boulder, Colorado. pp. 211–218.
- Prakash, A., Fielding, E.J., Gens, R., Genderen, J.L. van, Evans, D.L., 2001. Data fusion for investigating land subsidence and coalfire hazards in a coal mining area. *Int. J. Remote Sens.* 22 (6), 921–932.
- Prakash, A., Gens, R., Vekerdy, Z., 1999. Monitoring coal fires using multi-temporal night-time thermal images in a coalfield in north-west China. *Int. J. Remote Sens.* 20 (14), 2883–2888.
- Prakash, A., Gupta, R.P., 1998. Land-use mapping and change detection in a coal mining area – a case study of the Jharia coalfield, India. *Int. J. Remote Sens.* 19 (3), 391–410.
- Prakash, A., Gupta, R.P., 1999. Surface fires in Jharia coalfield, India – their distribution and estimation of area and temperature from TM data. *Int. J. Remote Sens.* 20 (10), 1935–1946.
- Prakash, A., Gupta, R.P., Saraf, A.K., 1997. A landsat TM based comparative study of surface and subsurface fires in the Jharia coalfield, India. *Int. J. Remote Sens.* 18 (11), 2463–2469.
- Prakash, A., Hendricksen, G.A., Stracher, G., Blake, D.R., 2010. Estimation of gas emissions from shallow subsurface coal fires in Jharia coalfield, India, using FLIR data and coal fire gas analysis. *Int. J. Coal Geol.* (in preparation).
- Prakash, A., Saraf, A.K., Gupta, R.P., Dutta, M., Sundaram, R.M., 1995a. Surface thermal anomalies associated with underground fires in Jharia coal mine, India. *Int. J. Remote Sens.* 16 (12), 2105–2109.
- Prakash, A., Sastry, R.G.S., Gupta, R.P., Saraf, A.K., 1995b. Estimating the depth of buried hot feature from thermal IR remote sensing data, a conceptual approach. *Int. J. Remote Sens.* 16 (13), 2503–2510.
- Prakash, A., Vekerdy, Z., 2004. Design and implementation of a dedicated prototype GIS for coal fire investigations in north China. In: Stracher, G.B. (Ed.), *Coal fires burning around the world: a global catastrophe*. *Int. J. Coal Geol.*, 59(1–2), pp. 107–119.
- Quattrochi, D.A., Prakash, A., Eneva, M., Wright, R., Hall, D.K., Anderson, M., Kustas, W.P., Allen, R.G., Pagano, T., and Coolbaugh, M.F. 2009, *Thermal Remote Sensing: Theory, Sensors, and Applications*, Chapter 3 (81 p.). In *Manual of Remote Sensing 1.1: Earth Observing Platforms & Sensors*, volume ed. Mark Jackson, ASPRS, Bethesda, Maryland, 550 p. ISBN: 1-57083-086-X

- Rencz, A.N., Ryerson, R.A., 1999. *Manual of Remote Sensing, Remote Sensing for the Earth Sciences*, third ed. John Wiley & Sons, Inc., Hoboken, New Jersey in cooperation with the American Society for Photogrammetry and Remote Sensing, 728 p.
- Rosema, A., Guan, H., van Genderen, J.L., Veld, H., Vekerdy, Z., Ten Katen, A.M., et al., 1999, *Manual of coal fire detection and monitoring: Utrecht, The Netherlands Report of the Project Development and implementation of a coal fire monitoring and fighting system in China*. Netherlands Institute of Applied Geoscience, NITG 99-221-C, ISBN 90-6743-640-2, 245 p.
- Saraf, A.K., Prakash, A., Sengupta, S., Gupta, R.P., 1995. Landsat TM data for estimating ground temperature and depth of subsurface coal fire in Jharia coal field, India. *Int. J. Remote Sens.* 16 (12), 2111–2124.
- Seda, S., Mahmut, O.K., Nuray, D., 2009. Development of a GIS-based monitoring and management system for underground coal mining safety. *Int. J. Coal Geol.* 80, 105–112.
- Voigt, S., Tetzlaff, A., Zhang, J., Künzer, C., Zhukov, B., Strunz, G., et al. van, Mehl, H., 2004, Integrating satellite remote sensing techniques for detection and analysis of uncontrolled coal seam fires in North China. In: Stracher, G.B. (Ed.), *Coal fires burning around the world: a global catastrophe*. *Int. J. coal Geol.* 59(1–2), 121–136.
- Wessling, S., Kuenzer, C., Kessels, W., Wuttke, M.W., 2008. Numerical modeling for analyzing thermal surface anomalies induced by underground coal fires. *Int. J. Coal Geol.* 74, 175–184.
- Xie, Y.C., Sha, Z.Y., Yu, M., 2008. Remote sensing imagery in vegetation mapping: a review. *J. Plant Ecol.* 1 (1), 9–23.
- Zamaraev, R.Y., Oparin, V.N., Popov, S.E., Potapov, V.P., Pyastunovich, O.L., 2008. GIS-technologies for integrated assessment of the productive mining areas. *J. Min. Sci.* 44 (3), 302–311.
- Zhang, J., Wagner, W., Prakash, A., Mehl, H., Voigt, S., 2004. Detecting coal fires using remote sensing techniques. *Int. J. Remote Sens.* 25 (16), 3193–3220.

WWW Addresses: Additional Reading

(1) Resources for Emissivity Values.

- <http://www.instrumart.com>
- <http://www.infrared-thermography.com>
- <http://www.omega.com>
- <http://www.optotherm.com>
- <http://emissivity.jpl.nasa.gov>

(2) Resources for Reflectance Spectra.

- <http://speclib.jpl.nasa.gov>
- <http://speclab.cr.usgs.gov/spectral-lib.html>

(3) Resource for InSAR Subsidence Literature.

- http://www.gi.alaska.edu/~rgens/teaching/literature/insar_subsidence.html

(4) Resources for Remote Sensing Satellite and Sensors

- (a) ALI: Advanced Land Imager.
<http://eo1.gsfc.nasa.gov/technology/alihome1.htm>
- (b) ALOS: Advanced Land Observing Satellite.
http://www.alos-restec.jp/index_e.html
<http://www.asf.alaska.edu/aadn>
- (c) ASTER: Advanced Spaceborne Thermal Emission and Reflection Radiometer.
<http://asterweb.jpl.nasa.gov>
- (d) AVHRR: Advanced Very High Resolution Radiometer.
<http://noaasis.noaa.gov/NOAASIS/ml/avhrr.html>
- (e) BIRD: Bi-spectral InfraRed Detection.
<http://www.dlr.de/os/en/desktopdefault.aspx/tabid-3493>
- (f) DAIS: Digital Airborne Imaging Spectrometer.
<http://www.op.dlr.de/DAIS>
- (g) ERS: European Remote Sensing Satellite.
<http://earth.esa.int/ers>
- (h) FLIR: Forward Looking Infrared Radiometer.
<http://www.flir.com>
- (i) Google Earth™.
<http://earth.google.com/>

- (j) Heat Capacity Mapping Mission.
http://rst.gsfc.nasa.gov/Sect9/Sect9_8.html
- (k) Hyperion.
<http://eo1.usgs.gov/hyperion.php>
- (l) IKONOS.
<http://www.geoeye.com>
- (m) IRS: Indian Remote Sensing Satellite.
<http://www.nrsc.gov.in/satellites.html>
- (n) Landsat.
<http://landsat.usgs.gov>
- (o) Microsoft Virtual Earth™.
<http://www.microsoft.com/maps/>
- (p) MODIS: Moderate Resolution Imaging Spectroradiometer.
<http://modis.gsfc.nasa.gov>
- (q) NASA World Wind™.
worldwind.arc.nasa.gov
- (r) Quickbird.
<http://www.digitalglobe.com>
- (s) Radarsat.
<http://gs.mdacorporation.com>
- (t) SPOT: Satellite Pour l'Observation de la Terre.
<http://www.spot.com>

This page intentionally left blank

CHAPTER 15

The Policy Setting for Coal Fires: Indicators for Government Action



East Front of the United States Capitol. The House of Representatives chamber is located to the left and south of the Rotunda, and the Senate chamber to the north. In the background to the west stretches the lawn of the Mall, with the Washington Monument and the Lincoln Memorial in the far distance. *Photo courtesy of the Office of the Architect of the Capitol.*

CHAPTER CONTENTS

15.1 The Policy Setting for Coal Fires

- Introduction
- Phases in the Policy Cycle
- Policy Innovation in the Nineteenth Century
- Lessons for Coal Fires
- Acknowledgments
- Important Terms
- References



15.1. The Policy Setting for Coal Fires

Karen M. McCurdy

Major John Wesley Powell, second director of the United States Geological Society, architect of scientific management of the public lands in the arid region. Portrait painted in 1885 by Henry Ulke.

Courtesy of the Smithsonian American Art Museum, gift of Mary Powell.

Introduction

Coal fires are common natural phenomena that increase in frequency and intensity as a result of mining and other human actions, both intentional and inadvertent. Further, coal fires are a nontrivial producer of greenhouse gases that negatively affect air quality and positively contribute to the global warming phenomenon. Scientists have called for over a decade for government action. Why does not government respond?

In the United States in the nineteenth century, coal developed as a private industry, and coal fires were thus private problems, unless they occurred on public lands. This response to why government is not responsive is overly simplistic, and implies that policy making is static, when instead it is a dynamic process (Baumgartner and Jones, 2002). Aspects of coal mining were subsumed into the public sphere at different times beginning in the 1960s following different policy templates¹. This simple private–public distinction from the early twentieth century was overridden in government action concerning coal producers when the issues were mining safety, air and watershed pollution, surface-mine reclamation, or hazardous-waste mitigation, but not fires. Why are coal fires different? The answer rests in political science not the geosciences and is related to when the policy issue, coal fires in our instance, arose in the policy cycle, and the political setting in which the decision was made, or the balance of power between the majority and minority parties within Congress as well as the power balance between the legislature and the executive branch. These power balances are defined primarily by election results, but also by interest group strength and influence, and public opinion.

The understanding that coal fires are a significant contributor to greenhouse gases emerged in the coal-geosciences community in the late 1990s at about the same time as the broader scientific community was reaching consensus on the contributing factors to global warming (Stracher et al. 2002; Broecker and Kuzig, 2008). This technical information from the coal-research community indicating the importance of mitigating coal fires to assist in reducing global warming was largely ignored by government officials, and even impugned by congressional leaders such as Senator James Inhofe (Republican, Oklahoma)². The reasons that both specific and general scientific advice was unwelcome in the political system at the beginning of the twenty-first century were related to the dynamic nature of the policy cycle. Demographic changes in Congress and the bureaucracy that resulted

¹ Mining health and safety was subject to federal government oversight beginning in 1969 and reinforced by amendments in 1977. Coal mining was further regulated beginning in 1970 under provisions of the Clean Air Act. The Surface Mining and Reclamation Act of 1977 extended the public sphere into postmining activities, and mining runoff problems were subject to mitigation under the Superfund legislation, the Comprehensive Environmental Response, Compensation, and Liability Act of 1980 (CERCLA), and the Superfund Amendments and Reauthorization Act of 1986 (SARA). See McCurdy (2007a) for further explanation of these policy templates.

² Senator Inhofe, chairman of the Senate Committee on Environment and Public Works for the 108th and 109th Congresses (2003–2007) used his leadership position to reject the basis for public discussion or action on global warming based on science. For example, speaking from the Senate floor on September 25, 2006, Inhofe (2006, p. S10056) said: “Mr. President, I rise to speak today about the most media-hyped environmental issue of all time, global warming.”

from increases in the proportion of movement conservatives elected to Congress and appointed in the Executive Branch between 1980 and 2004 produced leaders on the Hill and in the White House that rejected scientific advice and evidence as relevant to decision making (Mooney, 2005; Krugman, 2007; Bartels, 2008—especially Chapter 6).

The 1994 United States congressional elections produced a change in government control that went beyond a mere shift in party control in the House of Representatives for the first time in 48 years. Each subsequent election through 2006 increased the influence of movement conservatism, and the presidential elections of 2000 produced unified Republican control of the United States government for the first time since 1954. The core of this majority was formed around a movement conservatism ideology. Movement conservatives rejected the consensus position in effect for the prior generation of politicians that expert advice based on peer-reviewed science was good for the country, and therefore worthy of a special position in the policy process that remained outside of politics. Elevating scientists above politics had been the position of progressive republicans and democrats at the beginning of the twentieth century (Harrison, 2004). By mid-century, this consensus position was nearly universal, and was reflected in the landmark regulatory environmental protection legislation passed in the late 1960s and 1970s.

This model of government response to policy problems had been developed between the wars, perfected during World War II, and continued afterward. A series of successful government sponsored engineering projects demonstrated and then reinforced the utility of this approach for a generation of legislators and their constituents. Examples of the government consensus that scientific and technical advice should be set above politics and would benefit the nation were seen in a wide variety of projects such as construction of the Boulder dam (1931–1935)³ and the Tennessee Valley Authority begun in 1933 (Barry, 1998); the secret wartime efforts that led to development of RADAR and the atomic bomb (Rhodes, 1986; Conant, 2002), discovery of an effective polio vaccine in 1955 (Oshinsky, 2006), and the mission to put a man on the moon within a decade (Murray and Cox, 1989). Congressional action to promote clean air, water, and environmental reclamation in the early 1970s was the final expression of a phase in the policy cycle when politicians believed that government could fix problems, and that technical expertise was rightly kept above politics. A different consensus developed following the 1980 presidential elections, one that stemmed from the belief that government was part of the problem in society, and that government science was one of the bigger components of the problem. An examination of the phases in the policy cycle and their characteristics is useful at this point.

Phases in the Policy Cycle

Recently the examination of policy in 50-year time periods has generated a better understanding of the policy cycle (Baumgartner and Jones, 1993). Examination of 50–100 years in a policy cycle is most instructive in understanding the public disposition of coal fires. There are five phases in the policy process that are useful when examining a policy cycle greater than 50 years. They are Policy Innovation, Consolidation, Monopoly, Collapse, and Replacement.

Policy Monopoly

Policy monopoly is the most well understood of these five phases of the policy cycle. During this phase, there is electoral consensus on what the public policy problem is, its extent, and the best approach to how it should be addressed (Baumgartner and Jones, 1993). The policy monopoly phase is typically characterized by low conflict in the legislature, incremental budgeting, and a large role in decision making for the bureaucracy (Ripley and Franklin, 1990). In effect, political controversy is eliminated from policy decisions by mutual agreement from both majority and minority politicians. Policy outcomes benefiting constituents can be produced in a policy monopoly with regularity as well as low expenditure of time and political capital on the part of politicians.

³ The dam was renamed in honor of former President Herbert Hoover by a congressional resolution signed by President Harry Truman in 1947. Hoover had been a mining engineer working in China and Europe where he engaged in humanitarian relief efforts during wartime before returning to the United States to serve as Commerce Secretary for Presidents Harding and Coolidge and run for president himself in 1928.

In policy monopoly, the bureaucratic agency is responsible for bringing proposals to the legislature that are based on sound peer-evaluated science. The policies brought forward for legislative action are those perceived as needed and desired by the agency's clients and legislators' constituents, who often overlap considerably if not perfectly. Proposals will gain strong support from those constituents who will benefit directly from the change in the policy status quo. In the smoothest functioning form, policy monopoly will produce the classic textbook iron triangle where there is universal agreement among the political actors, and competing policy proposals and ideas are effectively blocked from consideration in the decision space (Berry, 1989). This nonpermeable subgovernment is short lived because those constituents and clients blocked from meaningful participation can always change the visibility of the issue by appealing to the public. Policy monopoly breaks down as competing alternatives are able to change the political agenda and receive serious consideration in the discussions and negotiations involved in shaping the final form of legislation in the subgovernment decision space.

During policy monopoly, scientists are free to "do their science" without concern for politics, because the overlapping and interlocking clients and constituents will provide the requisite demand for the policy change. There is also a stable consensus in all aspects of the subgovernment: the legislature, the constituency, and both civil service and political appointees in the executive. In effect, the policy making in monopoly phase can proceed without concern for politics, that is, determining who will benefit from the change to the status quo and who will pay the costs for the change, because of the shared belief that these policies are the best options for the country. Policy monopoly does not guarantee success for every proposal. It does however guarantee winning most of the time in a given Congress, and living to return for the next and future Congresses as a serious contender in the deliberations that produce policy decisions.

Predictability in policy making is a valuable political commodity. Constituents can receive the programs they want and politicians can spend minimal time and effort to produce maximum constituency benefits, which should pay off for politicians at re-election time. While a policy monopoly is functioning, science has the luxury to specialize. A stable electoral consensus that produces a policy monopoly allows scientists to be confident about what research is considered relevant for policy makers, to plan according to predictable levels of funding for their work, and enables them to choose what are likely to be fruitful lines of research in the policy process (Stokes, 1997).

Policy Phases Other than Monopoly

Policy monopolies are easily upset. The collapse is not immediate and neatly defined, but instead is marked by diminished predictability in the policy process. Controversies arise in appropriations decisions, conflict, and visibility in the policy arena increases. The phase of collapsing monopoly is fraught with unpleasant surprises as bureaucratic proposals are rejected, new interest groups are able to demand significant compromises or concessions in policy negotiations, and policy decisions become political footballs kicked around during subsequent election campaigns. Legislative defeats initially increase in frequency for bureaucrats, then ultimately the nature of the decision space changes.

Policy replacement occurs when a new policy consensus coalesces around a basic policy approach that is outside the boundaries of the previous consensus. In essence, this is the beginning of a new policy cycle. As such, replacement may be considered either as a separate policy phase, or it may be treated as a transition between policy monopoly collapse and policy innovation, thereby completing the policy cycle. Policy replacement can last for 20–30 years, and in comparison to the typical 5–15-year time frames in which policy studies are conducted, this is a significant time unit. As such, I believe it deserves consideration as a separate but transitional phase.

Two phases in the policy cycle exist prior to the monopoly phase. Policy innovation occurs with a good idea for a pressing policy problem being proposed to the legislature by a trusted agent with a prior record of success with these particular legislators and who has a significant store of political capital to be spent on this issue at this time. This good idea is proposed outside of existing policy structures and is made possible through personal contacts. Politicians are educated about the good idea, as are their constituents. Policy innovation occurs when the economic and demographic conditions have evolved such that the policy status quo is no longer tenable. The form that innovation takes is dependent on the political conditions that produce it. This emerging policy does not necessarily lead to monopoly. It can however develop into a monopoly if conditions are suitable. Monopoly formation would require decades of electoral replacement and evolution in the legislature and bureaucracy. Much like policy replacement, policy consolidation can be seen as a separate phase or a transition from innovation to a successful monopoly. Again like the replacement phase, consolidation can last for 20–50 years, and also deserves to be considered separately.

Policy innovation, policy consolidation, policy monopoly, policy collapse, and policy replacement are five unique phases in the policy cycle. These five phases can be traced in any policy arena through a set of issues. Each issue and its policy arena have unique time sequences and political events which mark the transition zones between the phases. For example, agricultural land can be in policy replacement while mining lands are firmly entrenched in policy monopoly, that is, homesteading on agricultural land can be discontinued by executive order 60 years before mining lands were removed from location.

Where do coal fires fit in the environmental protection policy monopoly? The scientific understanding that coal fires contribute to greenhouse gases came too late to be incorporated into the clean air and clean water templates developed in monopoly condition in the 1970s (Kraft, 2007). This particular policy monopoly was being dismantled by election results in the 1980s, and was moribund by the 1990s. Coal fires did not match in the particulars of the hazards template that emerged during the policy collapse of command and control environmental protection legislation. Nor do coal fires match the market-based solution template that gained favor in Congress at the beginning of the twenty-first century.

During other policy phases and templates, coal-fires research could have led to the public policy outcomes anticipated by many coal-fire researchers, that government will regulate business to encourage best practices, and provide financial support and dampen political controversy in order to extinguish long burning coal fires. Instead during the early years of the twenty-first century, coal fires were not even on the government agenda.

Coal fires in the twenty-first century present a policy problem in search of a policy solution. There is no accepted template in the legislature which can accommodate the problem with coal fires. To understand the implications of this status, it is instructive to examine an analogous policy concern which geoscientists first introduced in the late nineteenth century, but which required the greater part of one hundred years to move through the five policy phases discussed here.

Policy Innovation in the Nineteenth Century

Disposition of the public lands is a public policy that was debated in the federal government in each generation following independence (Clawson, 1983). The predated the Constitution, but did not settle the issue for even one generation. The question of public lands continued to emerge on the federal agenda because the problem experienced in the country continued to evolve. What was first a problem of finance, how to use lands to raise revenues, soon transformed into what to do with illegal settlers who moved into territories in advance of the land sales. Later the problem of how to raise revenues and encourage settlement in the trans-Appalachian region was subsumed in the debate about abolition. Following the civil war, the public lands policy issue was transformed again. This time science joined the policy discussion, and we can see an example of policy innovation.

J.W. Powell: Public Lands

Major John Wesley Powell's *Report on the Lands of the Arid Region of the United States, with a Detailed Account of the Lands of Utah* was presented to Secretary of the Interior Carl Schurz on April 1, 1878, who passed it on to the House of Representatives two days later on April 3, 1878 (Stegner, 1954, pp. 211–231). The scientific document was based on four field seasons of research from 1869 to 1872 by Powell's Geographical and Geological Survey of the Rocky Mountain Region and its predecessor. Powell's report arrived in Washington, DC, at a time when the image of "the great American desert" that had described the Great Plains in scientific reports in the early decades of the nineteenth century and in popular accounts by pioneers crossing to Oregon and Utah in the 1840s was being reshaped. Among the boosters who publicized the findings that settlement was beneficial to the plains was the territorial governor of Colorado, William Gilpin. Reports that soil was rich and deep, and that the "rain would follow the plow" were enthusiastically distributed by the politically well connected Gilpin, and others (Stegner, 1954, pp. 1–8). The policy decision space in the 45th Congress elected in 1876 was defined by these competing views of what farmers would encounter in the arid lands as they sought to establish economically successful agricultural operations on the prairies and high plains.

Policy Setting: 1876–1904

The national political environment in which Powell began his career in 1867 was chaotic. The rift in the nation torn by the civil war was fresh. Reconstruction did not eliminate tensions after the surrender at Appomattox courthouse, but instead sent them underground to fester. The unpredictability of the electorate produced unclear party control of Congress, with a nearly constant divided legislature with one chamber controlled by a Republican majority while the other was controlled by a majority of Democrats. Even when the Congress was controlled by a single party, there was divided government with the opposite party controlling the White House (Table 15.1.1). Presidential elections were also inconclusive between 1876 and 1888 when no party held the White House for more than a single term.

The presidency was wracked by contentious election results or assassinations in the final decades of the nineteenth century. In 1877 after months of uncertainty following the fall election, Republican Rutherford B. Hayes, a reform candidate was selected by a single vote cast along party lines by the 15-man electoral commission. Congress had appointed the commission to sort through the disputed electoral results from three states following the 1876 elections (Rehnquist, 2004). At the beginning of his administration in the hope of gaining some legitimacy with which to govern, Hayes announced that we would not seek re-election. The 1880 election was decided by fewer than 10,000 popular votes, and went to Republican James Garfield who was assassinated four months after his inauguration. Creation of a merit based career bureaucracy was passed during Chester Arthur's completion of Garfield's term, following what had been a decade long effort pressing for civil service reform. The Democratic party held the White House briefly when Grover Cleveland was elected to nonconcurrent terms in 1884, and again in 1892. Benjamin Harrison reclaimed the White House for the Republicans by a 100,000 popular vote margin in the 1888 elections. The 1900 elections gave President McKinley a second term, of which he would serve only six months before his death by assassination in September 1901.

Congressional elections were similarly inconsistent, alternating between divided party government within the legislature and between the Congress and Executive. From March 1877 when the 45th Congress was being sworn in, until Republican control of government resumed in 1897, there were only two instances of unified government. Each party held majority control for two years, Republicans during the 51st Congress (1889–1891) for the first 2 years of President Harrison's administration, and the Democrats for the first 2 years of President Cleveland's

Table 15.1.1
US presidential and congressional election results: 1876–1904.

Congress (years)	House majority party (percent seats)	Senate majority party (percent seats)	President (party)
45th (1877–1879)*	Democrat (52.90)	Republican (52.63)	Hayes (Republican)
46th (1879–1881)†	Democrat (48.12)	Democrat (55.26)	Hayes (Republican)
47th (1881–1883)*	Republican (51.54)	Democrat (48.68)	Garfield (Republican) died September 19,
48th (1883–1885)*	Democrat (60.31)	Republican (50.00)	1881; succeeded by Arthur
49th (1885–1887)*	Democrat (56.00)	Republican (55.26)	Cleveland (Democrat)
50th (1887–1889)*	Democrat (51.38)	Republican (51.32)	Cleveland (Democrat)
51st (1889–1891)	Republican (53.92)	Republican (57.95)	Harrison (Republican)
52nd (1891–1893)*	Democrat (71.69)	Republican (53.41)	Harrison (Republican)
53rd (1893–1895)	Democrat (61.24)	Democrat (50.00)	Harrison (Republican)
54th (1895–1897)†	Republican (71.15)	Republican (48.89)	Harrison (Republican)
55th (1897–1899)	Republican (57.70)	Republican (48.89)	McKinley (Republican)
56th (1899–1901)	Republican (52.38)	Republican (58.89)	McKinley (Republican)
57th (1901–1903)	Republican (56.02)	Republican (62.22)	McKinley (Republican) Died September 14,
58th (1903–1905)	Republican (53.63)	Republican (63.33)	1901; succeeded by T. Roosevelt

Source: Data Sources are Party Divisions, Clerk of the United States House of Representatives, <http://www.clerk.house.gov>; Party Divisions, <http://www.senate.gov>; Presidents <http://www.whitehouse.gov>.

* Divided legislature.

† Divided government.

administration in the 53rd Congress (Table 15.1.1). Electoral results in these decades did not provide the means of producing a stable policy consensus. Instead, institutional arrangements were developed to manage short term working coalitions that could produce policy outputs to satisfy constituents. While neither party could maintain a majority of seats beyond a single election, individual members of Congress were re-elected and did find the means of consolidating power in order to govern and share power with the continually changing Presidents and bureaucrats.

Institutional arrangements within the legislature that could override the stalemate election results arose in the late nineteenth century. Party hierarchies developed, including leadership tracts, lengthened careers, and subject matter standing committees (Polsby, 1968). For a member, retaining your seat produced influence in the chamber, regardless of whether your party maintained the majority. A separate policy making structure developed which centered on the committees, not the political parties. The Republican Speaker of the House in the 51st, 53rd, and 54th congresses Thomas Brackett Reed of Maine, consolidated power in his constitutional office as a counter-balance to the swing in power from the political party leaders to the long serving members of Congress.

Into this politically volatile setting, Powell's policy recommendations challenged the status quo, in the minds, hearts, and experiences of legislators, and in the common law. The report on the arid lands (Powell, reprint 1962) contained two policy recommendations for the orderly settlement of lands west of the 100th meridian (where annual rainfall dipped below that necessary to support economic agriculture). While some years would have adequate rain to bring a crop to harvest and produce a profit for the farmer, this would not be the case on average. The public lands status quo in 1878 presumed that public ownership of land was a temporary and undesirable condition compared to private ownership. Further, land and water rights were inseparable in the common law and the experience of generations who farmed the eastern lands. Powell's data convinced him and his colleagues that a different model was necessary for the practical agricultural development of the arid lands.

Powell's survey was mineralogical and ethnographic. His observations were filled with successful models for farming economically even when rainfall was seasonal and water was scarce and intermittent. Collective water usage had been practiced by the Mormon settlers in the Salt Lake Valley, and in numerous Native American populations who also used collective water practices. Powell based his policy recommendations on the sound scientific evidence available at the time. Congress was incredulous. The life experiences of the representatives could not comprehend the state of aridity Powell's words described. They saw no reason to abandon a policy consensus reached only 16 years earlier when the Homestead Act had passed a legislature diminished by resignations and expulsions precipitated by the state secessions. Further, members of Congress had competing reports from the territories that highlighted the opportunities available for emigrants should policy remain unchanged.

Powell recommended that the cadastral survey be abandoned in the arid lands (Powell, reprint 1962). Instead, he recommended that location of land should proceed by groups of more than nine farmers organized in irrigation districts within watersheds. Powell argued that the irrigation infrastructure necessary for viable farms should be collectivized for the economic benefit of all. Dams and reservoirs would be needed to allow irrigation techniques to supplement crop growth in dry years. Powell's second policy recommendation regarded pasturage districts that he argued should also be collective ventures. As an ancillary proposal in the report, Powell recommended that the four surveys operating in the west be centralized for greater efficiency and cost savings. The 45th Congress acted almost immediately to pass the legislative authority for the United States Geological Survey (USGS) to be founded in 1879 (Rabbit, 1979, 1980). The substantive recommendations in Powell's report did not reach the consensus threshold then, or in the next generation. Successive Congresses failed to build a consensus until a new electoral coalition was produced in the 57th Congress seated in March 1901.

Policy Consolidation: 1902–1934

The twelve elections between 1878 and 1902 added to the proportion of progressives in government (Figure 15.1.1). The possibility for a legislatively effective progressive coalition existed by 1901, with elected officials and civil servants, and in the number of progressively minded constituents and clients served by these government officials. Those "modern men" were found in both political parties. They believed in science and efficiency, and in eliminating government waste, corruption, and graft. These beliefs unified the coalition that passed the 1902 Newlands Act which created the Bureau of Reclamation. The coalition did not hold across a broad array of policy issues, but a majority consensus was able to form around good government issues that created new

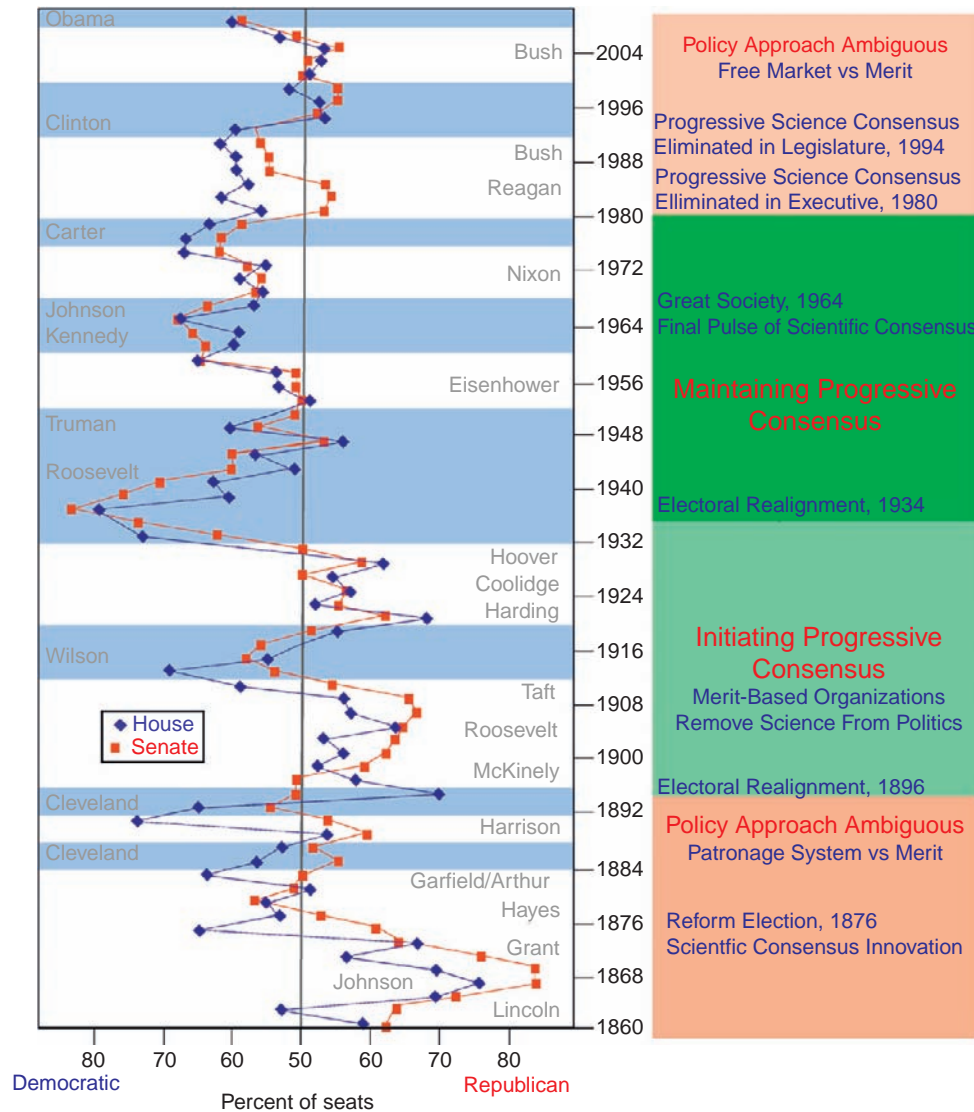


Figure 15.1.1. US election results from 1860–2008 and policy phases.

agencies and bureaus. This consensus produced protective regulatory authority for food and drugs, restricted child labor, allowed labor union greater latitude to organize, as well as passing Prohibition over the subsequent 20 years.

The first of Powell's suggested bills in the *Report on the Arid Lands* was to create irrigation districts. Before Congress was willing to act on this proposal based on scientific evidence, a generation of dry land farmers met ruin, with close to 66% of homesteaders in the last decades of the nineteenth century failing (Stegner, 1954, pp. 202–242). Powell's scientific predictions became all too real and unpleasant experiences for hundreds of thousands of homesteaders on the plains. Either the railway barons, or the ranching kings, or God, or the failure of the rains, or the personal foibles and failures of individuals were blamed for the financial ruin and human misery that resulted (Limerick, 1987). Rarely was the true culprit blamed: a failed public policy decision template. Slowly, the sensibility of Powell's recommendations for community financed irrigation infrastructure became apparent to a majority of elected officials. Additionally, by this point, the USGS had a 20-year track record of producing quality information for Congress. Their recommendations were accepted as more trustworthy for the generation of "modern legislators" elected since Powell's time, and the authority of the Survey could be added to the arguments used to persuade wavering legislators to join a majority to forge a new consensus position.

The core of Powell's second suggested bill, to organize pasturage districts, was taken up by members of the 73rd Congress and resulted in passage of the Taylor Grazing Act in 1934. This legislation marked the end of the old

public policy template that included private ownership as its central theme. Instead, the notion that scientific management of the public lands would produce better long term results for the country was part of this new legislation. During the policy innovation and consolidation phases, bureaucratic agencies were created to provide civil service employees to scientifically manage a wide range of resource issues: minerals by the US Geologic Survey beginning in 1879; irrigation projects by the Bureau of Reclamation beginning in 1902; forests by the US Forest Service beginning in 1905.

The end of homesteading, or the conveyance of public lands into private ownership came in two stages. Executive Order 6910 signed by Franklin Roosevelt on November 26, 1934 removed agricultural lands from location (Woolley and Peters, 1999). This action eliminated the ability of the bureaucracy to register agricultural homestead claims for the duration of Roosevelt's presidency and until a subsequent president would overturn the order, even though the Homestead Act of 1862 was still the law of the land. There was not a majority in Congress willing to change the law until 1976 with passage of the National Land Policy and Management Act. Old policy consensus positions erode slowly in a legislature, and in most instances the erosion comes only with replacement of legislators and not by their conversion to new ideas. Members maintain intense connections with the issues that initially attracted them to political service and the constituents who initially brought them to Washington, DC. Two recent House committee chairmen defeated for re-election provide examples of this connection to a policy position that is no longer held by a majority, either in the nation or the legislature. Wayne Aspinall (Democrat, Colorado) who served from 1949 to 1973 and was the chairman of the House Interior and Insular Affairs Committee, believed his role was to bring water to farmers who would let the desert bloom, even after irrigation projects had become unpopular in the west, even among a majority of his own constituents (Sturgeon, 2002). Similarly, Richard Pombo (Republican, California) who was defeated for re-election in 2006 while the sitting chairman of the House Resources Committee was an outspoken proponent of developing petroleum resources in the Alaska National Wildlife Refuge in spite of strong national opposition to that policy (McCurdy, 2007b).

Policy Collapse: 1980–2008

The collapse of a policy monopoly is difficult to detect while it is happening. The normal give and take of legislative activity can mask the gradual slide into ineffectiveness that is part of the collapse. The policy of pragmatic agriculture supported by scientific evidence that was introduced by J.W. Powell in 1878 as an innovation, moved through consolidation from 1902 to 1934. The monopoly phase that lasted through 1976 was marked by consensus in the legislature, the bureaucracy, and the citizenry that pragmatic resource exploitation was desirable for the public lands. This monopoly was broken by a confluence of competing ideas about the public lands from opposite ideological positions. The environmental protection attack on the pragmatic exploitation consensus began with the Dinosaur National Monument dam authorization battle in the early 1950s (McPhee, 1980, pp. 164–165), and the efforts to preserve portions of the public lands as wilderness (Stegner, 1973). These citizen groups did not believe that the public managers were going far enough to protect resources for future generations. The second attack on public lands management came from the citizen groups who believed that the public managers were doing too much protecting, and that government regulation was producing outcomes that were inferior to those that were made by private enterprise based on market forces. The sagebrush rebellion against federal environmental protection regulations on the western lands swept Ronald Reagan into the presidency in the 1980 elections (Culhane, 1984).

The innovation and replacement phases look very similar from the standpoint of policy making. Both phases produce ambiguous policy approaches (Figure 15.1.1). Predictability increases in the consolidation phase, reaches a pinnacle during policy monopoly, and decreases during the policy collapse phase. Elections which produce sustained periods of unified government where the majority party in the House of Representatives, the Senate, and the party of the president are the same are indicative of policy consolidation or policy monopoly. Divided government, or cycling of party control of Congress or the Presidency, is more typical of policy collapse, replacement, and innovation. Steady policy decisions are difficult to maintain with ambiguous directives from constituents delivered through the blunt instrument of elections. The key difference between innovation and collapse may be one of outlook among participants in the policy process. Outsiders attempting to change the status quo recognize that they must have a strategy for success, while insiders may continue using strategies that have been successful historically, even when they no longer produce desired effects.

Lessons for Coal Fires

J.W. Powell's vision of a scientific bureaucracy submitting policy proposals to a legislature cognizant of the political neutrality represented in those proposals was achieved in the policy monopoly era following World War II that did not end until sometime after 1980. Geoscientists coming of age professionally during the monopoly years had the luxury of doing their science outside of politics. The discipline could specialize and devote a very small proportion of its members to tending policy. Most could engage in good science being confident that there would be incremental increases in budgets and an orderly development for worthy new projects. A collapse of an iron triangle means that a much greater effort needs to be placed on policy than had been the case during the monopoly phase. A new generation of politicians and constituents who were not part of the old monopoly consensus must be educated to the advantages of policy proposals based on scientific evidence.

Coal-fires policy making will only occur within the policy phase in place after 2002. In the United States in 2009 that means that a wide variety of political actors are aware that the progressive era agreement to move science out of politics is no longer in place. There is evidence that a new administration is returning some of the privileged positions once held by scientific evidence in the policy process. But only future election results will determine whether the neutrality of science in the policy process will be promoted or rejected.

The United States case is explained here, but much of the trace of policy making is true for parliamentary structures as well. Changing a policy requires overwhelming evidence that the previous policy is failing. That typically means that a generation of failure must pass before it is obvious to the legislative body as a whole that a new approach is needed. While some elected to the body may see the problem in the current light, others have grown accustomed to believing this problem is fixed and that their favored problems are more pressing.

Coal-fires scientists might look to J.W. Powell for a strategic plan and for an understanding of the time scale required for success. As seen in Figure 15.1.1, policy change is easier when there are large majorities in the legislature. Consensus is easier to reach when large numbers of like minded politicians are elected, and when subsequent elections bring additional like minded public servants to the institution. In the absence of a policy consensus, personal appeals are likely to be more effective in attracting members to a coalition than a scientific report. Taking the time to explain why coal fires are a serious problem for a particular representative's constituents is more effective than describing the magnitude of the problem for the nation or the world. While empirically the latter may be true, only the voters in a particular district can retain a particular representative in office, or throw the bum out and give someone else a chance to fix the problem. A representative must ensure his or her own ability to continue in public service by showing responsiveness to constituents before being able to do good things for the planet.

Another aspect of the policy process outside of the monopoly phase is that a proposal based on sound science will not be accepted by legislators and passed into law as a whole. Instead, fragments of the proposal will pass as a majority coalition is custom built for each piece of legislation. Political conditions will change daily. The political process has shown a stubborn tendency to accept tremendous policy failures for decades in segments of the economy. Opponents to change in the status quo will use every political tactic to undercut support, including lying. Even George Washington and the other founders were not immune to attack by opponents who employed these tactics. Laying the groundwork for a change in public policy can take 20 or 30 years, so a long-range strategy to influence all aspects of the policy process is needed, as well as patience, and the belief that one's efforts spent influencing the policy process will not be wasted in the long run.

Acknowledgments

I am grateful for the support of members of the faculty of Geology and Geography at Georgia Southern University through invitations to Thursday afternoon seminars, as well as the faculty of my home department, Political Science. The probing questions and encouragement I received at meetings of the Geological Society of America, and the American Geophysical Union over the past 5 years allowed me to continue this line of inquiry. Dallas D. Rhodes provided critical advice through discussions of how to translate the words and tables that are common in political science into the figures needed for geologists to grasp concepts comfortably. His tips and emergency assistance in drafting were invaluable. My department chairman, Richard Pacelle, also deserves special thanks for never questioning why it is important for me to communicate political concepts to geoscientists.

Important Terms

policy monopoly

policy cycle

political capital

institutional arrangements

References

- Barry, J.M., 1998. *Rising Tide: The Great Mississippi Flood of 1927 and How it Changed America*. Simon & Schuster, New York, 528 p.
- Bartels, L.M., 2008. *Unequal Democracy: The Political Economy of the New Gilded Age*. Princeton University Press, Princeton, NJ, 325 p.
- Baumgartner, F.R., Jones, B.D., 1993. *Agendas and Instability in American Politics*. University of Chicago Press, Chicago, IL, 298 p.
- Baumgartner, F.R., Jones, B.D., 2002. Positive and negative feedback in politics In: Baumgartner, F.R., Jones, B.D. (Eds.), *Policy Dynamics*. University of Chicago Press, Chicago, IL, pp. 3–28.
- Berry, J.M., 1989. *The Interest Group Society*, second ed. Scott, Foresman and Company, Glenview, IL, 260 p.
- Broecker, W.S., Kuzig, R., 2008. *Fixing Climate: What Past Climate Changes Reveal about the Current Threat—and How to Counter it*. Hill and Wang, New York, 253 p.
- Clawson, M., 1983. *The Public Lands Revisited*. The Johns Hopkins University Press for Resources for the Future, Baltimore, MD, 324 p.
- Conant, J., 2002. *Tuxedo Park: A Wall Street Tycoon and the Secret Palace of Science that Changed the Course of World War II*. Simon & Schuster, Inc., New York, 330 p.
- Culhane, P.J., 1984. Sagebrush rebels in office: Jim Watt's land and water politics. In: Vig, N.J., and Kraft, M.E. (Eds.), *Environmental Policy in the 1980s*. CQ Press, Washington, DC, pp. 293–317.
- Harrison, R., 2004. *Congress, Progressive Reform, and the New American State*. Cambridge University Press, Cambridge, 293 p.
- Inhofe, J.M., 2006. Hot and cold media spin cycle: a challenge to journalists who cover global warming: *Congressional Record* 109th Congress, 2nd session, pp. S10056–S10062.
- Kraft, M.E., 2007. *Environmental Policy and Politics*, fourth ed. Pearson-Longman Press, New York, 308 p.
- Krugman, P., 2007. *The Conscience of a Liberal*. W.W. Norton & Co., New York, 352 p.
- Limerick, P.N., 1987. *The Legacy of Conquest: The Unbroken Past of the American West*. W.W. Norton & Company, New York, 396 p.
- McCurdy, K.M., 2007a, Congressional response to coal fires: illustrating transitions in the policy process. In: Stracher, G.B. (Ed.), *Geology of Coal Fires: Case Studies from Around the World*. Geological Society of America Reviews in Engineering Geology, Geological Society of America, Boulder, CO, vol. XVIII, pp. 271–278.
- McCurdy, K.M., 2007b. Are changes in coal policy on the horizon? An examination of committee changes in the 110th congress. *Geol. Soc. Am. Abstr. Programs* 39 (6) 380.
- McPhee, J., 1980. *Encounters with the Archdruid*. Farrar, Straus and Giroux, New York, 243 p.
- Mooney, C., 2005. *The Republican War on Science*. Basic Books, New York, 352 p.
- Murray, C.A., Cox, C.B., 1989. *Apollo: The Race to the Moon*. Simon & Schuster, New York, 506 p.
- Oshinsky, D.M., 2006. *Polio, An American Story*. Oxford University Press, Oxford, 368 p.
- Polsby, N.W., 1968. The institutionalization of the U.S. House of Representatives. *Am. Polit. Sci. Rev.* 62, 144–168.
- Powell, J.W., 1962 reprint. *The Arid Lands*. In: Stegner, W. (Ed.), foreword by Vernon, J. University of Nebraska Press, Lincoln, 202 p.
- Rabbit, M.C., 1979, *Minerals, Lands, and Geology for the Common Defence and General Welfare*, vol. 1, before 1879. U.S. Government Printing Office, Washington, DC, 331 p.
- Rabbit, M.C., 1980, *Minerals, Lands, and Geology for the Common Defence and General Welfare*, vol. 2, 1879–1904. U.S. Government Printing Office, Washington, DC, 407 p.
- Rehnquist, W.H., 2004. *Centennial Crisis: The Disputed Election of 1876*. Knopf, New York, 288 p.
- Rhodes, R., 1986. *The Making of the Atomic Bomb*. Simon & Schuster, Inc, New York, 886 p.
- Ripley, R.B., Franklin, G.A., 1990. *Congress, the Bureaucracy and Public Policy*, fifth ed. Houghton Mifflin Harcourt Publishers, Boston, MA, 224 p.
- Stegner, W., 1954. *Beyond the Hundredth Meridian: John Wesley Powell and the Second Opening of the West*. Penguin Books, New York, 438 p.

- Stegner, W., 1973. *The Uneasy Chair: A Biography of Bernard DeVoto*. University of Nebraska Press, Lincoln, 464 p.
- Stokes, D.E., 1997. *Pasteur's Quadrant: Basic Science and Technological Innovation*. Brookings Institution Press, Washington, DC, 180 p.
- Stracher, G.B., Taylor, T.P., Prakash, A., 2002. Coal fires: a synopsis of their origin, remote sensing detection, and thermodynamics of sublimation. In: Shannon, S. (Ed.), *Case Histories of Mine Reclamation and Regulation, Environmental Technology for Mining*. Robertson GeoConsultants Inc., Reno, NV, Vancouver, BC, pp. 1–8, http://technology.infomine.com/enviromine/case_hist/coal%20fires/Stracher_et_al.html (accessed September 2009)
- Sturgeon, S.C., 2002. *The Politics of Western Water: The Congressional Career of Wayne Aspinall*. University of Arizona Press, Tuscon, 243 p.
- Woolley, J.T., Peters, G., 1999. *The American Presidency Project* [online]. University of California, Santa Barbara, (hosted), Gerhard Peters (database), <http://www.presidency.ucsb.edu/ucsb.edu/ws/?pid=14786> (accessed May, 2009).

CHAPTER 16

United States Bureau of Mines—Study and Control of Fires in Abandoned Mines and Waste Banks



Emblem of the US Department of Interior, Bureau of Mines (1910–1996).

CHAPTER CONTENTS

16.1 United States Bureau of Mines

- Introduction
- Mine-Fire Control

16.2 Fire-Control Projects in Abandoned Mines and Waste Banks

- Introduction
- Eastern Bituminous Region
- Western United States and Alaska
- Anthracite Coalfields

16.3 Characteristics of Fires in Abandoned Coal Mines and Waste Banks

- Introduction
- Initiation of Coal-Mine Fires
- Geologic and Mining Factors
- Natural Barriers
- Discontinuous Fire Propagation

16.4 Locating Abandoned Mine Fires

- Introduction
- Mine-Fire Diagnostics
- Geophysical Methods
- Temperature Monitoring

16.5 Controlling Abandoned Mine Fires

- Introduction
- Burnout Control
- Water Injection
- Foam Injection
- Cryogenic Slurry Injection
- Summary
- Acknowledgments
- Important Terms
- References
- WWW Addresses:
Additional Reading



16.1. United States Bureau of Mines

Ann G. Kim

Emblem of the US Department of Interior, Bureau of Mines (1910–1996).

Introduction

The United States (US) Bureau of Mines was created by Act of Congress in 1910 as a part of the Department of Interior. Its primary mission was to reduce the number of fatalities due to coal mining accidents, particularly fires and explosions. In 1913, its roll was expanded to the collection, analysis and dissemination of economic data related to mining. The Coal Mine Inspection Act of 1941 gave the Bureau the right to inspect mines for safety conditions and to recommend corrective actions. Enforcement power was limited until the Federal Coal Mine Health and Safety Act of 1969 established mandatory standards.

Since its inception, the Bureau was a research organization developing solutions to a variety of mining related problems, including safer explosives, ignition suppression devices, subsidence control, methane drainage, and mined land reclamation. The Bureau of Mines was recognized nationally and internationally as a source of mining and mineral information and for its mining and environmental research. Over the 86 years of its existence, the Bureau had a significant impact on reducing the number of mining related fatalities (Figure 16.1.1). In 1996, the Bureau of Mines was closed by Congress. Although some of its programs were transferred to other federal agencies, most of its research programs ended. According to Rhea Graham, the last Director of the Bureau of Mines, the accomplishments of this agency had made a difference. Its legacy remains in the hundreds of Reports of Investigations, Information Circulars, Bulletins, and other publications that documented its work.

Mine-Fire Control

Although the Bureau had an extensive program on suppressing and controlling fires in active mines, this report focuses on their work on coal fires in **inactive** or **abandoned mines** and waste banks. When the Bureau of Mines was established, its role in inactive coal-mine fires was limited to investigation and providing advice on controlling them. In 1948, Congress expanded the Bureau's function to controlling fires on Federal land and providing technical and financial assistance for the control of fires on non-Federal lands. Research on the causes and control or extinguishment of fires in outcrops and underground coal formations was also authorized (Griffith et al., 1960). In 1964, the Appalachian Regional Development Act allowed the Bureau to actively participate in controlling fires in abandoned mines in the Appalachian region.

Under the Surface Mining Control and Reclamation Act (SMCRA) of 1977, the **Abandoned Mined Land (AML)** Program was transferred to the Office of Surface Mining, Reclamation, and Enforcement (OSM). Surface and underground fires were categories in OSM's Inventory of AML problems. Fire-control projects were handled by OSM or by states with approved mining reclamation programs. The law also provided for research on mining

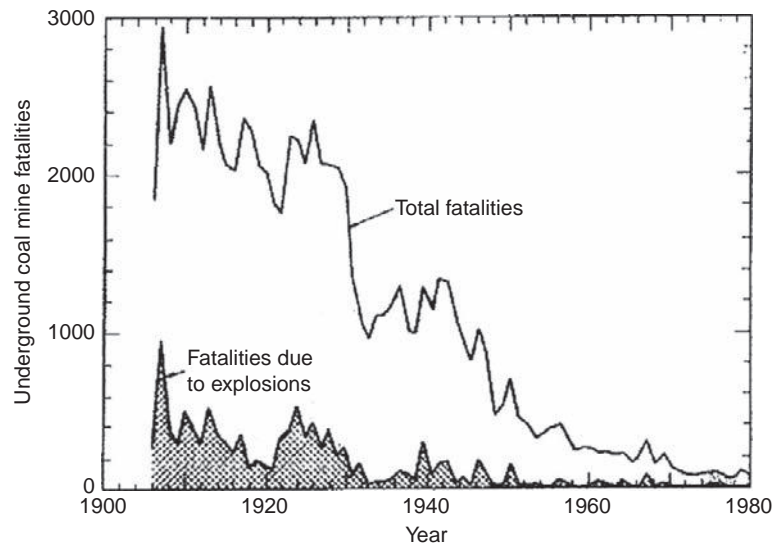


Figure 16.1.1. The number of total underground fatalities and fatalities due to ignition and explosions in US coal mines between 1910 and 1980. From Deul and Kim 1988, p. 3.

reclamation problems which OSM funded through state Mineral Institutes, through contracts or through cooperative projects with other state and federal agencies.

Although fire-control projects were transferred to OSM, the Bureau of Mines continued fire-control research. Several field projects were executed under interagency agreements with OSM or as contracts with state environmental agencies. The OSM research program was transferred to the Bureau in 1987. Under this program, the Bureau evaluated proposals and monitored research contracts in addition to performing in-house work. The Bureau also had a long-standing research program on the control of fires and explosions in active mines. Both the AML work and the in-house program for active mines ended when the Bureau of Mines was closed.

The following sections briefly describe the Bureau's fire-control research and field work performed over a period of more than 60 years. For the most part, the descriptions of the work are taken from the original peer reviewed reports published by the Bureau between 1930 and 1995. Over that period of time, the usual units of measurement changed from the English customary units to the metric system. To avoid confusion, the units given are those in the original publication. Conversion factors are given in Table 16.1.1.

Table 16.1.1
Conversion factors.

English Units		Metric Units	
Unit	Abbreviation	Unit	Abbreviation
1 Acre	ac or A	0.40 Hectare	ha
1 British Thermal Unit	BTU	252 Calories	Cal
		1054 Joules	J
1 Cubic yard	Yd ³	Cubic meter	m ³
1 Degree Fahrenheit	°F	$5/9(°F - 32)$	°C
1 Foot	ft	0.305 Meter	m
1 Gallon	gal	3.8 Liter	l
1 Gallon per minute	gpm	3.8 Liter per minute	lpm
1 Kilowatt-hour	kwh	3.6×10^6 Joules	J
1 Megawatt	MW	1×10^6 Joules/second	J/sec
1 Mile	mi	1.6 Kilometer	km
1 Square foot	ft ²	0.093 Square meter	m ²
1 Cubic foot	ft ³	0.028 Cubic meter	m ³
1 Ton	t	0.91 Metric ton	mt



16.2. Fire-Control Projects in Abandoned Mines and Waste Banks

Fire in abandoned mine in Large, Pennsylvania, 1976, prior to installation of an outcrop seal. Opening is approximately 0.6 m by 0.1 m (2 ft by 1 ft).

Photo Courtesy of Dominion Resources.

Introduction

Prior to 1949 in the United States, no Federal or State agency collected information on the prevalence of fires in inactive or abandoned mines and waste banks. After 1949, in conjunction with its work on the control of fires in abandoned underground mines and in outcrops, the Bureau of Mines published reports listing fire-control projects, extinguishment methods and costs. For the work done by the Bureau of Mines, the country was divided into three regions: the Eastern bituminous region, the Anthracite region and the Western region including Alaska (Figure 16.2.1.).

Eastern Bituminous Region

Between 1949 and 1960, there were 23 fire-control projects in the Eastern bituminous region (Griffith et al., 1960). In the next 12 years, the Bureau participated in an additional 47 fire-control projects (Magnuson, 1974). Three of these projects were located in West Virginia, one in Kentucky, one in Maryland and the remaining 65 were in western Pennsylvania. In 1979, the Bureau listed 52 mine fires in the Eastern bituminous region (Johnson and Miller, 1979). **Surface sealing**, alone or in combination with other methods was used on 45% of the fire-control projects. Ten percent of the fires were excavated, and fire barriers were used at 27. At 15% of the fire-control projects, either dry fly ash or fly ash slurry was injected to control the fire.

Surface sealing was popular because it was considered the only economically feasible method for attacking an established fire under deep cover. The purpose of the seal was to limit ventilation of the fire zone and smother the fire with accumulated CO₂ generated by the fire. Surface seals, if well maintained while the fire area cooled, were considered a successful fire-control method. **Excavation** (or loading out) involved removal and cooling of all burning material before the area was backfilled with incombustible material. It was considered appropriate for recent fires under shallow cover. Economics and equipment limited its use in deep, widespread fires. A **fire barrier** was an incombustible dam placed between the fire zone and adjacent coal. Its purpose was to limit the fire by breaking the continuity of the coal and overlying carbonaceous shale. It had to be wide enough to prevent heat transfer across the barrier. It was assumed that the fire would be extinguished when all the coal on the hot side was consumed. The installation of a **flushed barrier** was intended to fill voids in a fire zone with incombustible material in order to decrease the flow of air. It was considered effective for small fires in flat coal beds (Griffith et al., 1960; Magnuson, 1974). Overall, excavation was the most expensive control method, but it was also the most effective. Surface seals were the least costly, but were only moderately effective (Table 16.2.1.).

Three experiments were conducted on **water injection** at an abandoned mine fire in the Pittsburgh coal bed to develop more effective and efficient fire-control methods. In the first experiment, water was injected through uncased boreholes into the hot area of the mine. Although the fire seemed to be extinguished in the central area of the fire

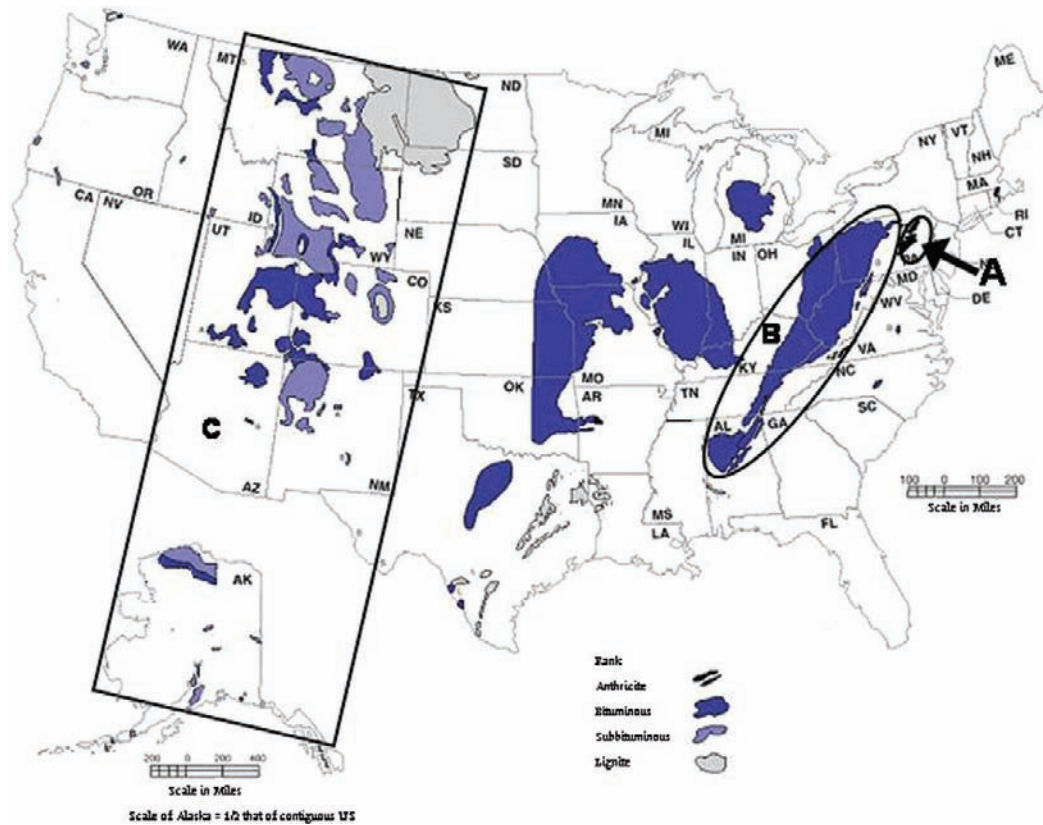


Figure 16.2.1. Coalfields of the United States showing the US Bureau of Mines fire-control regions: A—Anthracite, B—Eastern bituminous, and C—Western.

zone, borehole temperatures around the perimeter indicated that spraying had failed to cool all of the hot material. In the second experiment, water was introduced as a stream through the boreholes at an estimated rate of 378.5 L (100 gallons) per minute. Although some cooling was noted during water injection, temperatures would again rise when the injection stopped. During the third experiment, water was sprinkled continuously over the surface area above the fire. The results indicated that migration of the surface water through the permeable overburden cooled some areas, but increased temperatures were noted in other areas of the mine. And when water sprinkling was discontinued, for 2 weeks, almost half of the boreholes had increased temperatures (Griffeth et al., 1960).

Western United States and Alaska

In the western region, more than 400 coal fires in Alaska and 12 other states west of the Mississippi were reported to the Bureau of Mines between 1949 and 1979. Of 158 fire-control projects during this period, 17 used excavation,

Table 16.2.1
Number of projects, approximate average cost (US\$1000), and estimated effectiveness (%) for US Bureau of Mines fire-control projects in the eastern bituminous region between 1949 and 1978 by method.

Method	Number of projects	Estimated effectiveness (%)	Average cost (US\$1000)
Excavation	57	70	685
Flushing	16	27	533
Surface Seal	86	42	28
Trench Barrier	4	25	119

Source: Data from Kim and Chaiken (1993).

4 were isolation projects and 137 utilized some form of surface sealing (Jolley and Russell, 1959; Shellenberger and Donner, 1979).

In the Western United States, 85% of fire-abatement projects were surface seals, due to the relatively low cost, the topography of the area, and the lack of water needed to implement other methods (Shellenberger and Donner, 1979). Surface sealing or smothering was considered the most effective method, even though tests made several years after the completion of a project indicated that the fire had not been completely extinguished (Jolley and Russell, 1959).

Two surface seal methods were used. In the Missouri River drainage region, the fire sites were generally located on accessible, flat to rolling terrain with a maximum slope of 25°, and the strata over the fire area contained 0.61–3.1 m (~2–10 ft) of relatively thin, friable rocks that could be easily worked by bulldozer. The area was sloped with a bulldozer to fill in large cracks and to grade uneven terrain. Then a seal was emplaced when, a bulldozer starting at the lower perimeter of the fire area, made a cut along the contour. In succeeding upslope cuts, the material was cast onto the previous downslope cut, producing a seal between 1.2 and 2.4 m (~4–8 ft) thick. A diversion ditch around the seal area controlled erosion due to surface runoff (Shellenberger and Donner, 1979).

In the Colorado River basin, slopes were steep and surface strata were massive. In addition to bulldozer cut and cover methods, blasting was often needed to produce material suitable for sealing the fire area. Surface sealing under these conditions was more labor intensive, more time consuming, and more costly. However, it was considered the most practical and cost-effective method of controlling fires in this area (Shellenberger and Donner, 1979).

Anthracite Coalfields

The Bureau of Mines gathered data on 103 major fires and 71 minor fires that occurred in active mines in the anthracite coalfields (Figure 16.2.2) between 1850 and 1936 (McElroy, 1938). Twenty-two of the fires were recurrences of older fires. Complete control of fires in anthracite mines was especially difficult due to chemical, physical, geological, and mining factors. Some fires apparently continued to burn undetected for 15–25 years.

Between 1945 and 1988, more than 50 fires were detected in abandoned mines of the anthracite fields of Pennsylvania (Philbin and Holbrook, 1988). Between 1950 and 1978, the Bureau of Mines was involved in 26 fire-control projects at 17 abandoned mine sites. Five of these fires required 14 separate attempts to control the fire. There were 10 excavation projects, which may have involved complete excavation of the fire zone or excavation of a **trench barrier**, 14 flushing or injection projects, and 2 surface seal projects. In the anthracite region, excavation was estimated to be 80% effective in controlling fires. While flushing projects were on average only 25% as expensive as excavation, they were less than 50% effective (Table 16.2.2). Surface seals were apparently 400 times less expensive than the average cost of excavation, but there was insufficient data to reliably estimate their effectiveness (Chaiken et al., 1983).

Centralia Mine Fire

Probably the most well known of the anthracite-mine fires is that at Centralia, Pennsylvania. In 1962, burning refuse material was discovered in an abandoned strip pit (Figure 16.2.3). Pouring water on the fire and blanketing it with clay failed to extinguish the fire, which spread to the outcrop of the Buck Mountain coal bed. Since it appeared that the fire was spreading rapidly, it was decided to excavate the burning seam until the limits of the fire were reached. After 2 months, the money allocated for the project had been spent, and the fire had advanced beyond the excavation (Chaiken et al., 1983).

The next project involved drilling 80 boreholes and flushing fine **coal refuse** to surround the fire. The breaker refuse was supposed to fill voids and minimize the flow of oxygen to the fire. When funds were depleted, no effective control of the fire had been achieved. In 1963, the Commonwealth of Pennsylvania attempted to excavate an isolation trench around the fire. After 4 months, fire was detected on both sides of the incomplete trench.

In 1965, a two-phase project estimated to cost US\$2.5 million funded by the Bureau of Mines, the Commonwealth of Pennsylvania, and Columbia County, was approved. Phase I would include backfilling and sealing abandoned

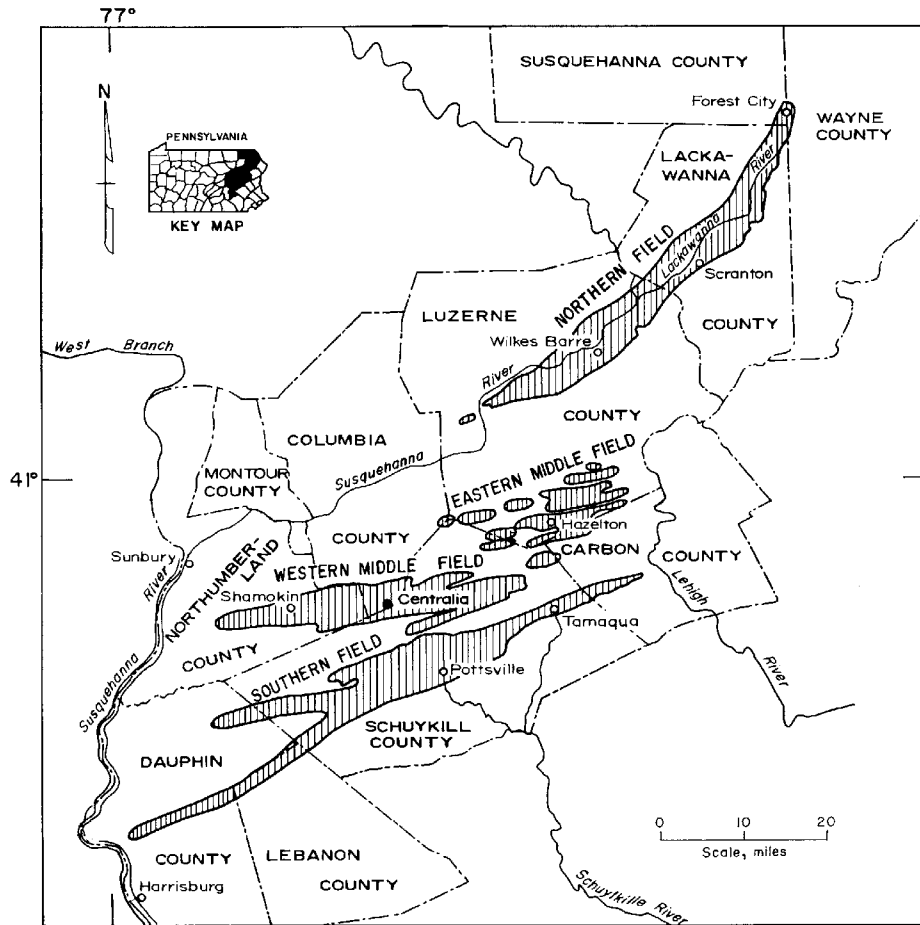


Figure 16.2.2. Map of anthracite coalfields in Pennsylvania. From Chaiken et al. (1983, p.3)

strip pits on the southern edge of the fire to reduce the amount of oxygen entering the mine. It would also include exploratory drilling on the northern, eastern, and western edges to delineate the boundary of the fire. A temporary flushed noncombustible barrier would be emplaced to constrain the fire while the second phase of the control project was completed. Phase II consisted of excavating a permanent isolation trench on the cold side of the **flushed barrier**. The depth of the trench was estimated at between 30.1 and 61.0 m (100–200 ft). Phase I was completed, but exploratory drilling indicated that the *fire had advanced further* than anticipated. Phase II would now require an isolation *trench more than 19.4 m (300 ft) deep*. As the first part of Phase II, an underground barrier west of the fire would be constructed from the outcrop to the mine pool by injecting fly ash into the mine voids. In 1973, an underground flushed barrier was installed, but due to the depth, cost, and the amount of surface disruption

Table 16.2.2
Number, average cost (US\$1000), and estimated success rate (%) of US bureau of mines fire-control projects in the anthracite fields between 1949 and 1978.

Method	Number of projects	Estimated effectiveness (%)	Average cost (US\$1000)
Excavation	10	80	26 581
Flushing	14	43	5306
Surface Seal	2	50	41

Source: Data from Chaiken et al. (1983).

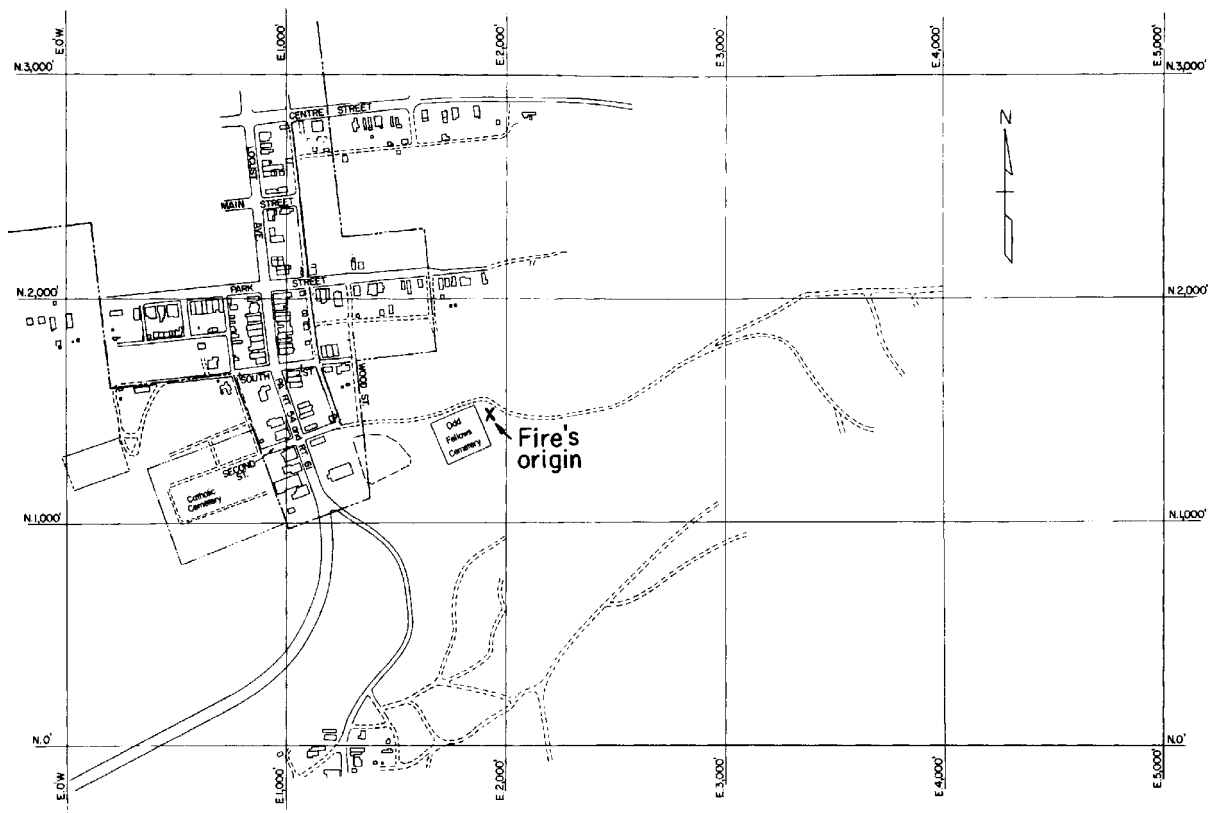


Figure 16.2.3. Map of Centralia Borough, Pennsylvania illustrating the location of the origin of the Centralia mine fire. From Chaiken et al. 1983, p. 24. For ease of determining locations at the Centralia site, a grid was added to the maps (Figures 16.2.3 to 16.2.5). The location of the origin (N0,E0W) outside the fire zone was arbitrary. Grid lines were added at 1000 ft intervals to the east and north of the origin.

it would cause, the isolation trench was replaced with a flushed barrier (Chaiken et al., 1983). Attempts to control the fire between 1962 and 1978 (Figure 16.2.4.) cost over US\$3 million and were unsuccessful.

In 1977, the SMCRA was passed. Under SMCRA, the Bureau's anthracite office was transferred to the OSM, which now had responsibility for safety and environmental problems related to past mining. In 1979, OSM and the Bureau entered into an interagency agreement in which the Bureau would gather data on the Centralia fire and evaluate possible alternatives for extinguishing it. In a report submitted to OSM in 1980 (Chaiken et al., 1980), the Bureau evaluated options including excavation, **inundation** methods, such as **flooding** and hydraulic flushing. It also considered a **water curtain** barrier, underground mining, Burnout Control, and relocation of the community. The four excavation options were considered the technically most feasible. Although complete excavation of the fire zone had the greatest probability of success, it had a high estimated cost (US\$84 million) and would require the destruction of a significant portion of the town (Figure 16.2.5.). While lower in cost, the partial excavation options would leave a fire zone in close proximity to residences and would also involve the destruction of most of the town. The Bureau was concerned primarily with technical factors in various control options, but it emphasized in its report that socioeconomic factors must also be considered (Chaiken et al., 1983).

In 1984, Congress allocated US\$42 million for the relocation of the residents of Centralia. Most of the residents accepted the buyout offers, but some refused to move. (Dekok, 1986). The Pennsylvania Bureau of Abandoned Mine Reclamation now considers the site extremely dangerous due to the presence of toxic gases and the potential for sudden ground collapse. Burning for almost 50 years, the fire continues to spread, and as yet, no viable plan has been developed to extinguish it.

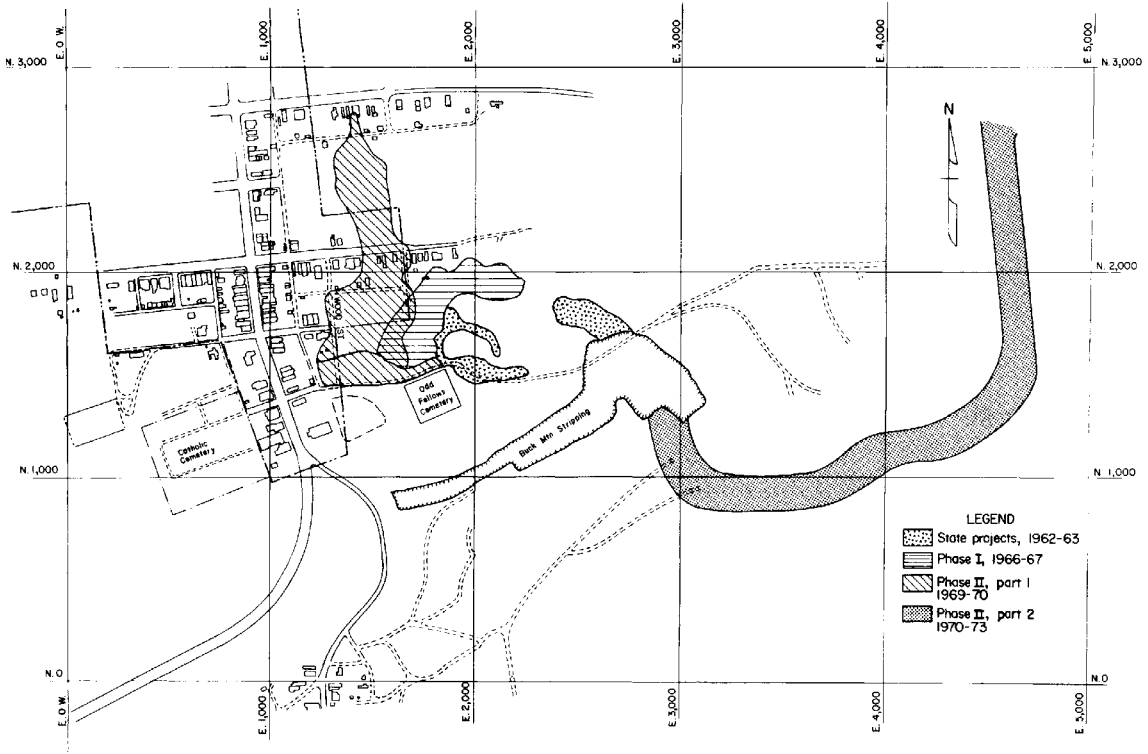


Figure 16.2.4. Composite map of Centralia Borough showing the location of fire-control projects between 1962 and 1978. From Chaiken et al. 1983, p. 33.

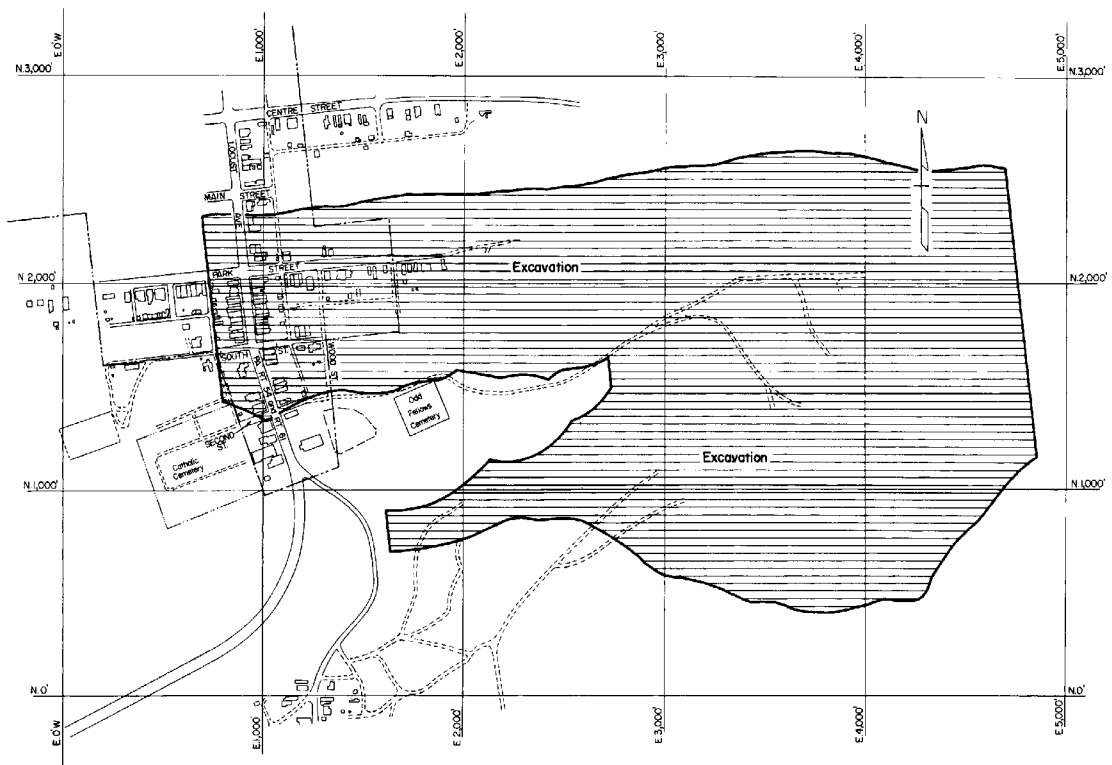


Figure 16.2.5. Map of Centralia Borough, Pennsylvania showing the suggested area for complete excavation of the Centralia mine fire. From Chaiken et al. 1983, p. 46.



16.3. Characteristics of Fires in Abandoned Coal Mines and Waste Banks

This sinkhole formed above an underground coal-mine fire in an abandoned mine located in Renton, Pennsylvania. The sinkhole formed when pillars of coal supporting the roof of an underground mine burned. Subsequently, the roof collapsed, forming the sinkhole.

Photo: US Bureau of Mines, 1985.

Introduction

In the years that the Bureau of Mines worked to control fires in abandoned mines and coal waste banks, they accumulated a significant amount of data on how such fires are started and how they spread. Evaluating the characteristics of such fires enabled Bureau personnel to develop innovative solutions to fire-control problems.

Initiation of Coal-Mine Fires

Any fire requires three elements: fuel, oxygen, and an ignition source. In coal combustion, the fuel is the carbon in the coal, and oxidation of coal occurs constantly. The temperature of the coal is a function of the rate of heat generation versus the rate of heat loss. When these processes occur at the same rate, the temperature of the coal remains constant. When the heat energy generated exceeds the rate of heat loss, the temperature of the reacting system increases. Since the rate of heat generation is an exponential function of temperature and the rate of heat loss is a linear function of temperature (Figure 16.3.1.), as the temperature increases, the reaction rate increases faster than the heat loss. Ignition is a function of the amount of energy released by a reaction and the rate at which it is released, as well as the rate at which energy is transferred from the reacting mass to the surroundings. The reaction rate is a function of the concentration of reactants, carbon and oxygen, the surface area, particle size, temperature, and **activation energy**.

Forced Ignition

There are two types of ignition, forced and spontaneous. In forced ignition, energy is added to the system to increase the rate of reaction to the self-sustaining point. In spontaneous ignition, there is no external heat source; natural reactions supply sufficient energy to sustain combustion. For AML fires, forced-ignition sources include lightning, brush and forest fires, improperly controlled man-made fires, and spontaneous combustion in adjacent materials. Although there are no data on how most AML fires actually start, lightning and other surface fires are

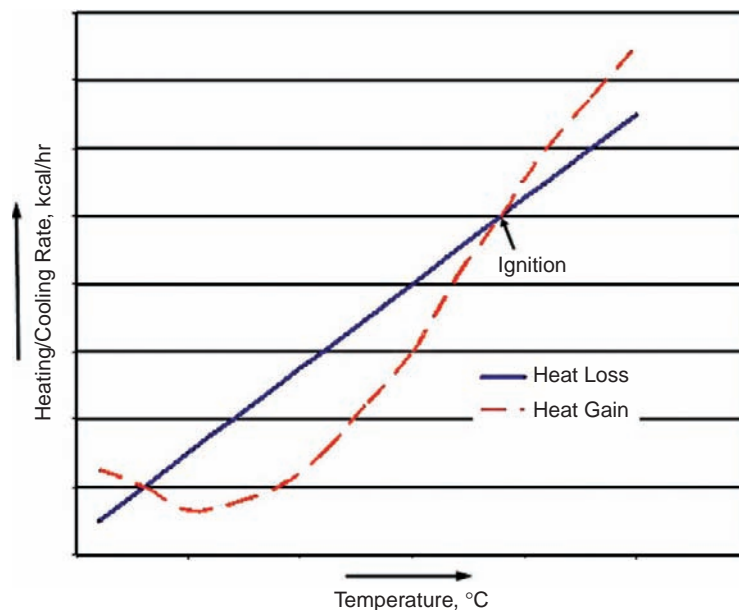


Figure 16.3.1. An example illustrating the rate of heat gain versus the rate of heat loss as a function of increasing temperature. Spontaneous combustion occurs at the ignition point. From Kim and Chaiken 1993, p. 7.

probably more prevalent in the Western outcrop fires. Spontaneous combustion in adjacent materials is also a significant cause of AML fires, since abandoned strip mines and areas where the coal outcrop has been stripped are frequently used as local trash dumps. Spontaneous combustion in the trash will ignite the coal refuse or the outcrop. Such fires may have no visible indications until the fire is well established.

Spontaneous Combustion

Spontaneous combustion in the coal or coal refuse is related to the oxidation of the coal to form CO_2 , CO , and H_2O . The oxidation of pyrite and the **adsorption** of water on the coal surface also are **exothermic** or heat-generating reactions that increase the probability of spontaneous combustion (Kim, 1977). Thermophilic bacteria may also contribute to raising the temperature of the coal. In waste banks, most of the oxygen diffusing from the surface is consumed by bacterial activity within a meter. However, enough oxygen is available at depth to support combustion.

To estimate the spontaneous combustion when coal is stored underground in mines, 46 samples of various ranks were tested in an adiabatic calorimeter (Elder et al., 1945). The rank of the coal, the temperature at which it was stored, the particle size, moisture and ash content, and the availability of oxygen were the primary factors influencing the probability of spontaneous combustion during storage.

The self-heating temperatures of 29 coals were determined in an **adiabatic**-type calorimeter (Kuchta et al., 1980). The data in this experiment indicated that lignite and subbituminous coals can self heat at temperatures as low as 30°C , but bituminous coals require a temperature of 60°C or more. The self-heating tendency of a coal mass can vary with its porosity, moisture content, ventilation rate, and with the humidity of the ventilating air.

In sealed flask experiments, the **CO index**, CO emission, and **O_2 absorption** were found to decrease with increased **coal rank**. Although these are sensitive to increased temperature, the results of sealed flask experiments were not considered directly transferable to the open environment of a coal mine. In another test, the relative self-heating tendencies of six coals, from high-volatile C to low-volatile bituminous in rank, the minimum self-heating temperatures varied from 35°C for the lower rank coals to 105°C for the high-rank coal (Miron et al., 1990). The minimum self-heating temperature was correlated to the amount of O_2 adsorbed by the undried coal samples.

The ignition temperature for coal, which depends on several factors such as coal rank, volatile matter content and particle size, varies between 160 and 685 °C for most coals. Under adiabatic conditions, the minimum temperature at which a coal will self-heat is 35–140°C (Smith and Lazarra, 1987). In a large-scale study, 13 tons of high-volatile C bituminous coal was placed in a packed bed to simulate conditions in a mine **gob** area (Smith et al., 1991). The temperature in the bed increased from 35 to 340°C. At airflow rates between 50 and 200 L/minute, the O₂ concentration in the bed was less than 4%. In addition to the reactivity of the coal, spontaneous combustion was also dependent on particle size, freshness of the coal surface, heat of wetting, and availability of oxygen.

Using a **crossing point method** to determine the maximum temperature by which a sample exceeded the reference temperature under controlled conditions, the relative self-heating tendencies of coal, carbonaceous shales, and coal refuse were determined (Kim, 1995). Data from this study indicated that self-heating involves chemical factors, such as oxygen adsorption, and physical factors that control the rate of heat gain and heat loss. In this group of samples, the concentration of mineral matter was the compositional variable most strongly correlated to self-heating behavior. In another study of self-heating in carbonaceous shale (Miron et al., 1992), pyrite was believed to be responsible for self-heating, even though adiabatic tests did not indicate a correlation between the minimum self-heating temperature and pyrite concentration.

In most abandoned mines and waste piles, conditions favor the retention of heat. Heat is lost by convection or conduction. Since abandoned mines and waste piles have an essentially stagnant atmosphere, convection accounts for very little heat loss. Most heat transfer is probably by conduction to surrounding strata, but rocks tend to be good insulators, keeping heat within the mine or waste bank.

Geologic and Mining Factors

In addition to a physical environment that favors the accumulation of heat energy, other factors influence the propagation of coal fires. The geologic setting, previous mining, the rank of the coal, and environmental conditions also affect the propagation of AML fires. The geologic factors that affect the propagation of mine fires vary depending upon the geologic setting. In bituminous coalfields, the depth of overburden, the degree of fracturing, and the nature of the overlying strata are the primary geologic factors. Mines under shallow cover are usually under more permeable strata and above the water table; shallow strata tend to be more highly fractured. Fires propagate toward the source of oxygen. In shallow beds and in areas near the outcrop, the concentration of oxygen tends to be higher. However, coal fires can smolder in atmospheres with less than 3% oxygen (Leitch, 1940; Justin and Kim, 1987; Dalverny and Chaiken, 1988). Where the overburden is fractured, barometric pressure changes cause the mine to “breathe,” exhausting combustion products and bringing in fresh air. Under these conditions, fires spread very slowly but can continue to burn for very long periods of time.

In anthracite mines and in some western mines, the **dip** or pitch of the beds also influences the propagation of fires. In anthracite areas, the intense folding and faulting (Figure 16.3.2.) have contributed to subsidence fractures extending from the coal bed to the surface. On steep pitches, differences in temperature and elevation are sufficient to control the circulation of oxygen and fumes. A fire near the outcrop of a steeply dipping bed can draw air from within the mine, propagating the fire down dip. The movement of hot gases can transfer heat to other areas. The distance between coalbeds determines the transfer of heat between beds and the possibility of propagation of a fire from the source bed to adjacent beds.

In abandoned mines, the extent of previous mining is a factor in the spread of fires. The amount and condition of carbonaceous material left underground determines the extent of the fuel supply. Rider coals and roof slates that eventually collapse into the mine are capable of initiating and sustaining combustion (Kim and Chaiken, 1993). Coal that **spalls** from ribs and pillars and carbonaceous material in gob areas adds to the volume of fuel. Because the rubbleized coal has a larger surface area than solid coal, it is more combustible. Main entries may be high-oxygen areas along which a fire may propagate. A fire can establish a natural ventilation pattern in which combustion gases are exhausted at one point and fresh air drawn in at another. The number of openings in the outcrop, the number of ventilation shafts, the competence of the overlying strata, and the prevalence of subsidence-induced fractures are other factors that contribute to the prolonged propagation of abandoned mine fires. The condition of the mine determines the amount and surface area of fuel; the availability of oxygen determines the direction, and rate of propagation of the fire.

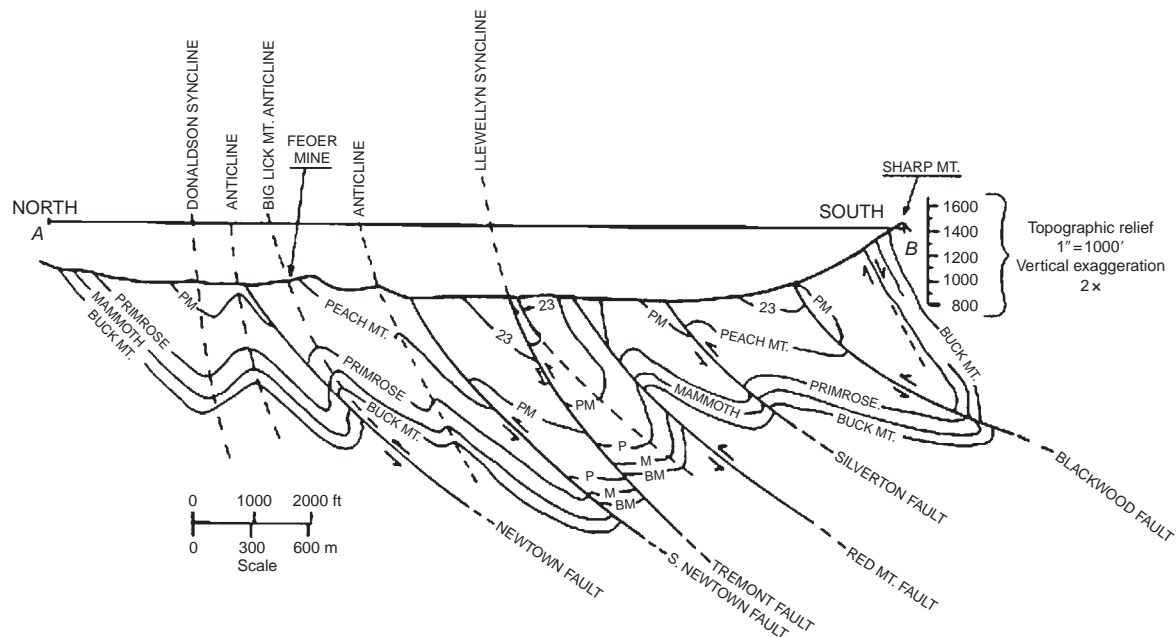


Figure 16.3.2. Generalized cross section of coal beds in the anthracite region. From Deul and Kim 1988, p. 121.

In a discussion of factors influencing the initiation and propagation of coal fires, it is apparent that all factors are related to the three elements: fuel, oxygen, and energy. The amount of combustible material, its particle size, surface area, and tendency to spontaneous combustion are fuel-related factors. The presence of fractures through which air can be drawn into the fire zone, circulation caused by the fire, and changes in barometric pressure control the amount of available oxygen. The rate of heat generation versus the rate of heat loss, the heat-generating reactions (oxidation of coal, oxidation of pyrite, surface adsorption of water vapor, bacterial activity) and the insulation provided by adjacent strata control the amount of energy within the system.

Natural Barriers

Natural barriers to subsurface fire propagation basically affect the availability of fuel and the generation and retention of heat energy. Faults with vertical displacement disrupt the continuity of the coal bed and limit the amount of fuel. Boundary pillars are regarded as natural barriers to fire propagation because solid unfractured coal seams are believed to be less likely to burn. However, the surface of the pillar and any fractured or faulted areas can be combustion zones. The water table serves as a barrier by limiting the amount of oxygen on the coal and by absorbing energy released by the fire. In the absence of these natural barriers, a subsurface fire can, in an extended time period, burn from outcrop to outcrop.

The mass of surrounding rock, because of its low heat conductivity, serves as an insulator, but it is not a barrier to increased combustion. Normal heat transfer occurs by conduction or radiation to the overburden. Overlying **roof coal** and **carbonaceous shale** with carbon contents as low as 25% can conduct or adsorb heat and serve as a pathway for the spread of the fire. Even if no combustion occurs in the roof, heat transfer by conduction through the overburden is an extremely slow cooling mechanism. For example, the combustion of 1 ton of medium-volatile bituminous coal releases 7565 thermochemical calories (30 million BTU). If this energy is simply adsorbed by the roof rock, it would raise the temperature of 75 tons of rock, $\sim 25.5 \text{ m}^3$ (900 ft^3), to 500°C . Depending on the rock, the extent of combustion, and the length of time the fire has been burning, the amount of heat stored in the coal and adjacent strata can be in excess of a 252 trillion thermochemical calories (approximately a billion BTU). If all combustion ceases, it would take 10–20 years for this amount of heat to dissipate by conduction through the overburden. Long-term cooling rates, measured in mines have been found to be as low as 0.1°C per year (Hansen et al., 1990).

Discontinuous Fire Propagation

A typical mine fire generates a higher pressure area which forces heated fumes deeper into the mine while drawing cooler air from the outcrop, through fractures or from other areas of the mine. This type of internal convection cell may account for the discontinuous propagation of mine fires. Even when the supply of oxygen is relatively low, continuous heating at low temperatures may drive off inherent water from the coal and allow for increased absorption of oxygen. Experimental data (Scott, 1944) has shown that accelerated oxidation begins at temperatures between 80 and 120°C for anthracites, depending to some extent upon the amount of prior oxidation. Accelerated reactions begin for bituminous coals at temperatures as low as 50–70°C (Kuchta et al., 1980).

If coal fires were propagated by a flame spread mechanism, coal adjacent to the burning mass would be heated by conduction or radiation to its ignition temperature (Chaiken et al., 1979). Propagation of the fire would follow a continuous pathway. However, in many AML fires, combustion zones are discontinuous, with no apparent propagation pathway (Chaiken et al., 1983; Michalski et al., 1988; Rushworth et al., 1989; Dalverny et al., 1990; Kim et al., 1992; Kim and Dalverny, 1994). In these fires, the movement of hot gases is believed to be a factor in propagation. The fire induces circulating air currents, which carry fumes and heat into nonadjacent areas (Figure 16.3.3.). The effective ambient temperature of a large area of the mine is slowly increased. At temperatures approaching 100°C, the coal is conditioned by drying, leading to accelerated oxidation reactions. If the heat is not dissipated, the temperature of the coal continues to rise until spontaneous ignition occurs.

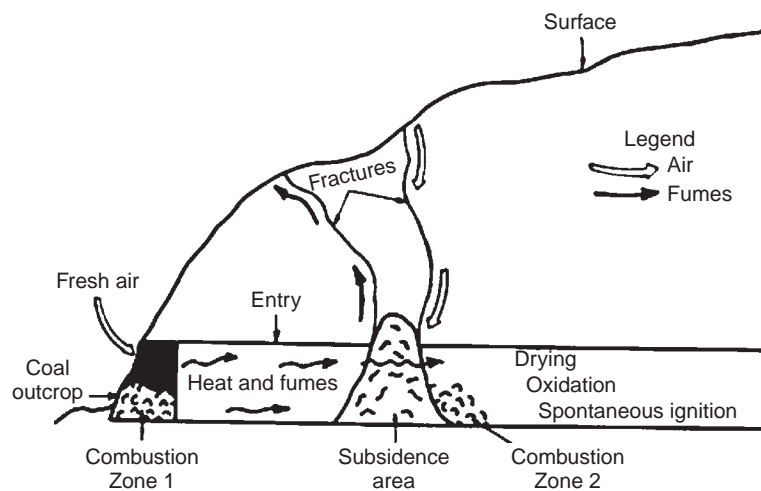


Figure 16.3.3. Postulated mechanism for discontinuous-fire propagation in abandoned coal mines: migration of hot gases, surface drying, increased oxidation rate, and spontaneous ignition. From Kim and Chaiken 1993, p. 25.



16.4. Locating Abandoned Mine Fires

Smoke emitted from a surface fracture (film for scale) at an abandoned mine in Large, Pennsylvania. Surface expressions are usually not good indicators of subsurface combustion.

Photo: US Bureau of Mines, 1985.

Introduction

The emission of smoke and fumes at surface fractures and vents usually indicates a fire in an abandoned mine or waste bank. Because hot gases follow the path of least resistance, the surface evidence of fires may not be related by straight line paths to the source of combustion. The heated combustion source can be distant, laterally and vertically, from the surface expression. Also, coal fires are usually confined to relatively small discontinuous areas of smoldering combustion surrounded by large masses of insulating coal and rock.

A factor in the failure of many abandoned mine-fire-control projects is that the extent of the subsurface fire zone is unknown when the project is planned. A corollary factor is that there is no adequate provision for monitoring the propagation of the fire during and/or after the fire-control project. Conditions in the subsurface, which may be unknown, also affect the application of an extinguishment method and the probability of success for most fire-control projects. The Bureau of Mines developed a method to locate subsurface combustion zones and tested several methods to determine subsurface conditions.

Mine-Fire Diagnostics

In order to locate a remote fire zone, it is necessary that (1) the fire have measurable characteristics, (2) the characteristic be detectable, and (3) the data be interpreted correctly. The Bureau of Mines developed a mine-fire diagnostic (MFD) methodology in which the measurable characteristics are the temperature, pressure, and hydrocarbon concentration at the base of an array of boreholes. The sampling method uses an exhaust fan to impose a pressure gradient to control the direction of flow of the mine atmosphere. The data are compared to an empirical scale based on the laboratory determination of fire signatures.

The combustion signature used in the Bureau's MFD methodology is a ratio based on hydrocarbon desorption from coal. The low-molecular-weight hydrocarbons, methane through pentane, are adsorbed on the internal surface of coal. At normal temperatures methane and a small percentage of higher hydrocarbons are desorbed. As the temperature of the coal increases, the rate of desorption increases and the concentration of higher hydrocarbons

also increases (Kim and Douglas, 1973). In a laboratory study of temperature-dependent desorption from coals and coal wastes (Kim, 1991), a ratio ($R1$) of higher molecular weight hydrocarbon gases (C_2 to C_5), determined as total hydrocarbon gases minus methane, to total hydrocarbons was defined as

$$R1 = \frac{1.01[\text{THC}] - [\text{CH}_4]}{[\text{THC}]} \times 1000 + c \quad (16.4.1)$$

where $[\text{THC}]$ is the concentration of total hydrocarbons in parts per million (**ppm**), $[\text{CH}_4]$ is the concentration of methane in ppm, and c is a constant, 0.01 ppm. The ratio was found to increase with increasing temperature and decrease with decreasing temperature. The concentration of desorbed gas and the ratio were related to the rank of the coal. For bituminous samples, the value of $R1$ is interpreted according to the empirical scale (Table 16.4.1.). The hydrocarbon ratio is sensitive, unaffected by dilution, and requires relatively simple analytical methods (Kim, 1988).

The MFD methodology, in addition to the hydrocarbon ratio, uses communication testing to define hot and cold subsurface zones (Dalverny et al., 1990). An exhaust fan is used to impose a pressure gradient which controls the direction of airflow. This assumes that sufficiently large negative pressure (vacuum) applied to underground regions will cause the gases in the mine atmosphere to flow from some distance toward the point of suction (Figure 16.4.1.). Pressure and temperature measurements are taken at the base of boreholes under both baseline (no suction) and communication (suction) conditions; in-mine gas samples are obtained under the same conditions (Figure 16.4.2.). Repeated sampling at all points in the borehole array provides data to determine the presence or absence of fire along pathways between sampling points.

For each test, a quadrant indicating heating, cooling, or no change is placed on a straight line drawn through the borehole and the suction point. Reiteration of the tests using various boreholes as suction points produces a composite map of heated and cold zones. The tests can be repeated, sometimes with the drilling of additional boreholes, until a cold boundary can be defined.

Four field studies supported the use of the Bureau's MFD methodology to define remote combustion zones. Each of the trials presented different challenges, but each indicated the value of the methodology.

Carbondale

The Carbondale mine-fire site in Pennsylvania's Northern Anthracite Field was located adjacent to an apartment complex (Justin and Kim, 1987). The complex had been built on an area excavated and backfilled during a previous fire-control project. Anomalous snow melt (Figure 16.4.3.) indicated that combustion was occurring in the unreclaimed portion of the mine. According to drillers' logs, there were two anthracite seams in the area. Thirty-four cased boreholes had been installed at the 3.4 ha site. They extended 16–30.5 m beneath the surface through both coal seams. The objective of the MFD project was to determine the proximity of heated zones to the apartment complex (Kim et al., 1992).

Since anthracite has a lower concentration of higher hydrocarbons adsorbed on the coal surface, methane emission was found to be sufficiently temperature dependent to allow its use as a combustion indicator for anthracite. The

Table 16.4.1
Values of diagnostic ratio ($R1$) for bituminous coal.

$R1$ value	Estimated coal temperature	Interpretation
0–50	<30°C	Normal
50–100	30–100°C	Possible heated coal
>100	>100°C	Heated coal

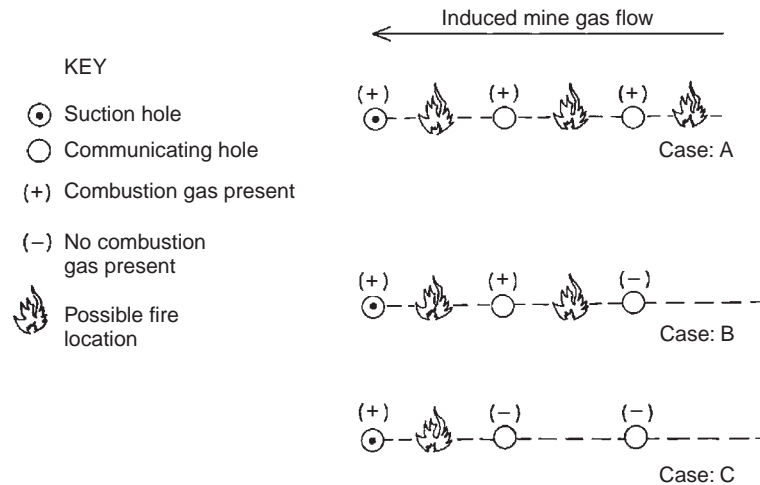


Figure 16.4.1. Schematic of US Bureau of Mines communication testing for MFD. From Kim and Chaiken 1993, p. 43.

use of MFD at Carbondale was considered a test under nonideal conditions because (1) the emission rate of C_2 to C_5 hydrocarbon gases from anthracite is low and does not exhibit strong temperature dependence, (2) many of the boreholes were cased through the coal seams, (3) the borehole diameters and depths were such that half of the rated pressure drop of the suction fan would be used to overcome pipe resistance, and (4) a large rock fracture that bisected the region could limit the effectiveness of the communication tests. To overcome these conditions, the change in the absolute concentration of CH_4 in baseline and communication samples was used as the index of combustion. Two suction fans were connected in series to offset casing resistance and improve communication between boreholes. Pressure and gas composition data indicated that the casing length and the fault did not affect the diagnostic results.

The tests conducted at Carbondale located two large and five small heated zones (Figure 16.4.4.). The noncontiguous combustion zones included one region lying adjacent to an apartment building that had not been detected using temperature and CO concentration measurements. The presence of hydrocarbon gas indicated that coal was heated above the normal underground temperature; time-dependent temperature monitoring indicated that the areas of combustion were moving uphill away from the apartment complex.



Figure 16.4.2. Photos of the US Bureau of Mines MFD system. A—Carbondale Pennsylvania: suction fan with connection to suction borehole, B—Renton, Pennsylvania: instrumented borehole for temperature, pressure, and gas measurements, with suction fan in the background. From US Bureau of Mines project photos, 1986.



Figure 16.4.3. Anomalous snowmelt at the Carbondale mine-fire site. From Kim and Chaiken 1993, p. 23.

Large

The mine fire near Large in Allegheny County, Pennsylvania is in the Pittsburgh coal seam, which, at this location, outcrops at the base of a hill. Approximate depth of overburden ranges from 6 to 55 m. Small vents were visible on the hillside above the buried outcrop. The surface area affected by the mine fire is ~1 ha, and the slope averages 20°. Five natural gas pipelines and three sets of high-voltage power lines cross the property. Areas of venting were confined to a relatively small surface area and indicated propagation along the buried outcrop. Temperature monitoring indicated that large areas of the mine were heated but did not define a combustion zone (Kim and Dalverny, 1994).

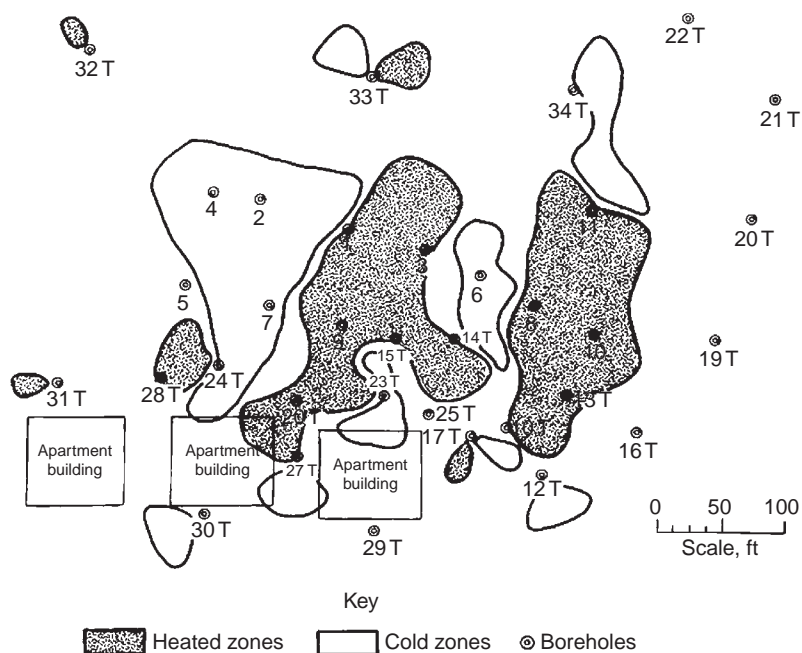


Figure 16.4.4. Map of the Carbondale mine-fire site, showing the location of two large and five small heated areas. From Kim et al. 1992, p. 15.

MFD testing, utilizing almost 60 cased boreholes indicated an L-shaped combustion zone (Figure 16.4.5.). The base of the L (150 m) was near the outcrop; the leg of the L extended 180 m into the mine, probably along a set of main entries. Several small isolated combustion zones were located 300–1000 m from the primary combustion area. Noncontiguous heated areas were detected in the southwest quadrant of the project area.

The direction of propagation into the mine appeared to coincide with the location of a set of main entries. Heated areas were detected to the north and south of this area. Subsurface fires generally move toward a source of air, which could have been either a portal that old mine maps indicated existed in the valley ~1.6 km from the site or permeable zones in the outcrop. The heated areas apparently extended beyond the site boundary, and a cold boundary for the fire area was not located.

Several areas where hydrocarbon concentrations were below 20 ppm CH₄ coincided with areas where water was observed in the boreholes. Water vapor condensed on the surface of the coal could block desorption of hydrocarbons. However, if the temperature of the coal is cool enough to allow water condensation, it can be assumed to be below the combustion point.

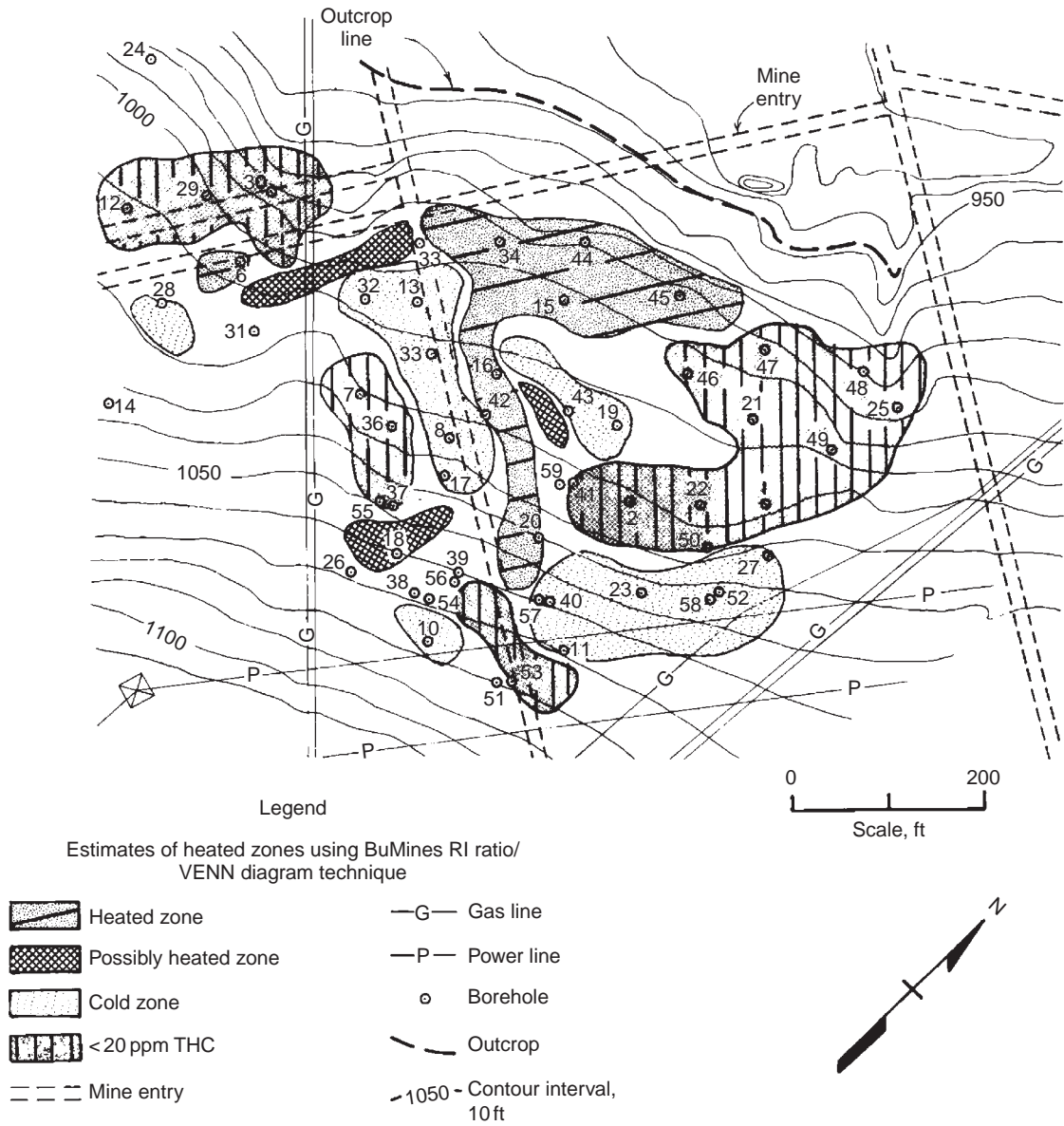


Figure 16.4.5. Map of the Large, Pennsylvania mine-fire site showing heated and cold zones, topographic contours, and estimated position of mine entries. From Kim and Dalverny 1994.

The Large mine fire was typical of problems associated with determining underground fire locations from surface evidence. The observed venting above the buried outcrop gave no indication of the combustion areas in the interior portions of the mine. Also, borehole temperature data, when taken alone, would yield misleading results with regard to the location of the combustion zones.

Renton

The Renton abandoned mine-fire site was a 24 ha region in Allegheny County, southwestern Pennsylvania (Dalverny and Chaiken, 1991). The mine was located in the Pittsburgh coal seam beneath a hill topped by a 4 mL municipal water tank; the overburden ranged between 3 and 30 m. The site was characterized by several large subsidence holes and venting areas.

The MFD located three noncontiguous combustion zones, totaling ~4 ha near the perimeter of the site. These coincided with three heated areas of indefinite extent that had been indicated by visual and historical evidence. Although combustion products had been detected in the central part of the mine, diagnostic tests indicated that heating was occurring only in areas closer to the buried outcrop.

The diagnostic method was also used to monitor progress during and after the water injection extinguishment effort of the project. Over a period of 195 days, ~27mL of water were injected into the three mine-fire areas. Combustion activity decreased in one area (Borehole 14), became static in another area (Borehole 57), and increased in the third area (Borehole 33) (Figure 16.4.6.).

Percy

Approximately 15 years before the MFD project, OSM had attempted to extinguish a fire in the Percy mine by excavation. The abandoned mine was in the Pittsburgh seam on the flank of the Chestnut Ridge anticline in Fayette County, Pennsylvania. The approximate depth of excavation was 30.5 m and the remaining coal had a 10% dip away from the excavation boundary. A double line of temperature monitoring boreholes on 7.5 m centers had been installed around the mine side of the excavated area. Increasing borehole temperatures and the emission of smoke from surface fractures indicated increased combustion in the unreclaimed portion of the mine.

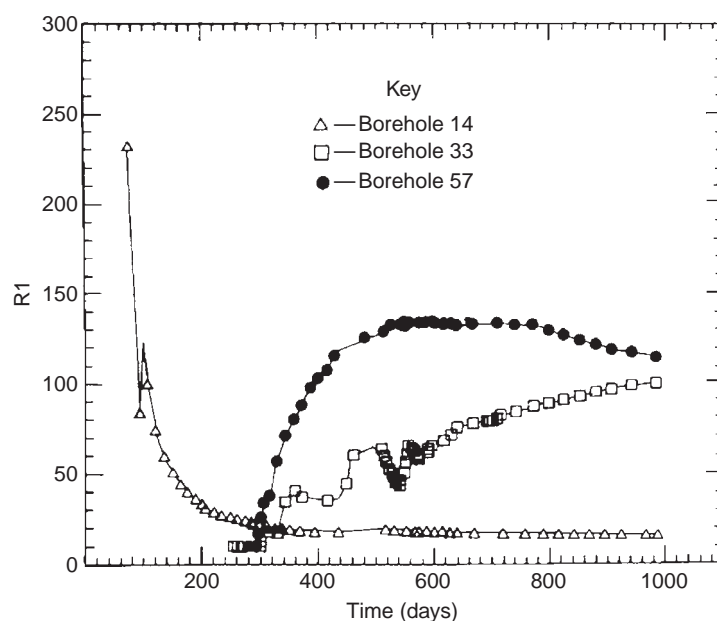


Figure 16.4.6. Long-term changes in MFD ratio at the Renton mine-fire site indicating that one area had cooled (Borehole 14), one area was heated but stable (Borehole 57), and one area continued to heat (Borehole 33). From Kim and Chaiken 1993, p. 45.

To develop an extinguishment plan, it was necessary to determine if combustion was occurring near a group of houses to the south of the reclaimed site. Boreholes were drilled and cased on 30.5 m centers in a narrow area bounded by the houses (south), a water pipeline (west), and a local road (north).

Based on previous experience, the atmosphere in underground mines is assumed to be in a steady state. Although this baseline condition will vary locally due to combustion, proximity to fresh air, microbial activity, etc., the composition of air within a given area is generally constant. Applied suction, as in the Bureau's MFD method, is usually a temporary perturbation. In the Percy mine, there were significant changes in baseline gas composition over periods between 1 day and 3 weeks. The lack of a consistent baseline made the interpretation of the diagnostic results more difficult. However, the results of the diagnostic tests indicated that the primary combustion zone was located near the road. Combustion signatures were detected at two boreholes at the southern end of the site. An area of combustion was apparently located beyond the boreholes between the reclaimed area and the houses.

Geophysical Methods

During the planning stages of a field test of cryogenic-injection-fire control (section 16.5) at a waste bank in Ohio, the Bureau of Mines tested several geophysical techniques (magnetometry, terrain conductivity, seismic refraction, and ground-penetrating radar) to characterize the subsurface conditions.

The burning waste bank was elongated east–west from a remnant strip mine highwall to the concrete foundation for an old tippie. The bank extended southward to a slope and covered an area of about 5000 m² (Figure 16.4.7.). The top of the bank was flat, indicating that it had served as a ramp to the tippie. Drilling 3.0–10.7 m indicated that the subsurface consisted of mine waste (coal, shale, local ceramic, and clay material) 0.3–3.7 m thick, and a clay core up to 7 m thick, with pieces of coal, shale, and ceramic brick and pipe. Weathered sandstone bedrock was detected at a depth of 4.6–8.2 m.

A surface grid (Figure 16.4.7.) measuring 65 m (east–west; lines L1, L2, L3) by 10 m (north–south) with intersections at 5 m intervals, was used for data points for several temperature and geophysical surveys. Developing a model of the structure and estimating its physical properties improved the implementation of fire-control procedures.

Magnetometry

It has been suggested that the measurement of small subsurface magnetic anomalies can be used to delineate fire areas, particularly in coal refuse (Dalverny, 1994). The effect is assumed to be due to the acquisition of remnant

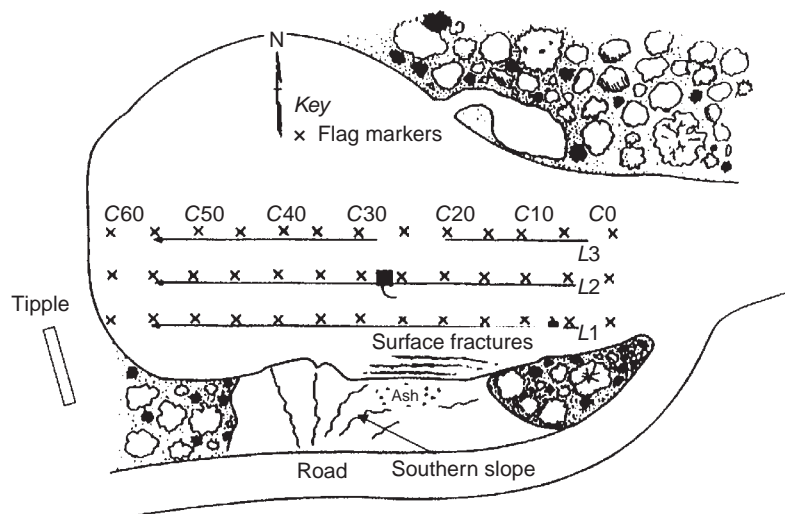


Figure 16.4.7. Sketch of the Midvale waste bank with eroded southern slope and fractures in the eastern fire zone. From Mowrey 1995, p. 100.

magnetism by the exposure of magnetic minerals to high temperatures. Elevated subsurface temperatures due to combustion can alter the mineralogy of iron-bearing rocks and their magnetic properties, for example, **remnant magnetization** and **magnetic susceptibility**.

Three magnetic surveys were conducted over a 4-month period (Dalverny and Kim, 1995). For **proton precession magnetometer** surveys, contour maps were constructed from field gradient and total field intensity values determined at each grid point. The total field intensity at two depths and the magnetic field gradient calculated from the field intensity were used to construct contour maps for each survey. The reinforcing metal in the old tipple foundation created one magnetic anomaly (Figure 16.4.8.). Magnetic anomalies not associated with known metal objects were identified in four areas within the grid (L1, 30, 35, 41 m and L2, 30 m). Two of the magnetic anomalies correlated to areas of subsurface heating.

Terrain Conductivity

In **terrain conductivity**, an electrical field is induced in the ground. The total electrical field that results from the interaction of the induced field and materials in the ground is measured. With the instrument used in this test, penetration depths were 3 and 6 m (Dalverny and Kim, 1995).

The terrain conductivity data indicated anomalies at the approximate midpoint of the bank at the 3 and 6 m depths. The anomalies at 3 m were believed to coincide with heated areas. Those at 6 m depth were believed to indicate the probable flow path of subsurface water.

Seismic Characterization

Seismic techniques were used to obtain subsurface data, such as waste thickness, waste heterogeneity, and nature of the bedrock. **Seismic refraction survey** and **tomographic imaging** were the techniques used (Cohen and Dalverny, 1995).

A seismic refraction survey produced a two-velocity model for the area including the uppermost low velocity layer of waste rock and the higher velocity bedrock layer. Velocities in the upper layer probably represented an average or bulk velocity through varying percentages of waste rock, combustible material, and clay.

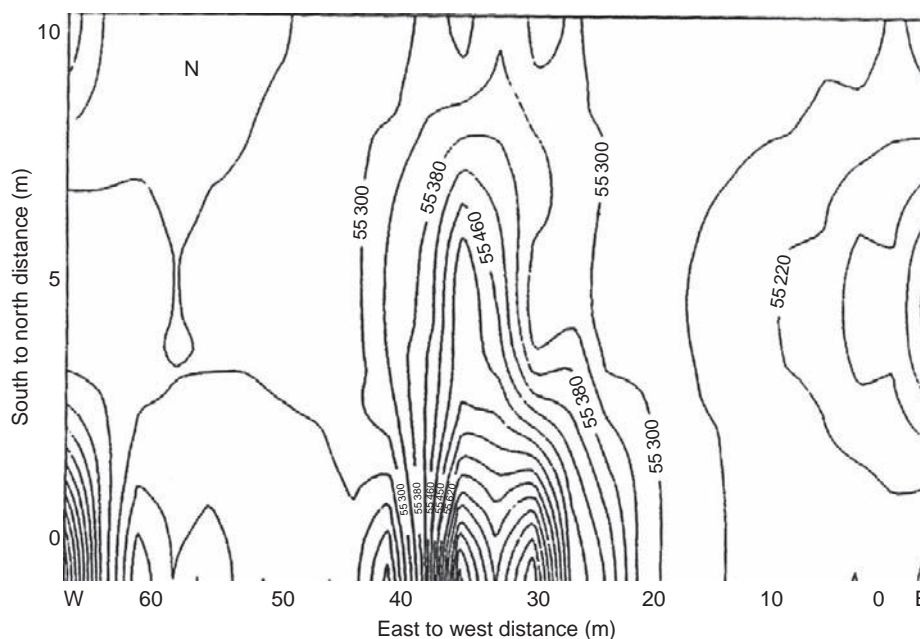


Figure 16.4.8. Results of magnetometer survey at Midvale Waste Bank: Contour plot of total field intensity (gammas) indicates magnetic anomalies between 0 and 5 m north at the west end of the site from remains of abandoned tipple. Other anomalies occur at 30 m and at 40 m at the southern (0) end of the site. From Dalverny and Kim 1995, p. 64.

Near the west combustion zone, seismic tomography was used between two 7.3 m parallel spreads. It represented a plane that dipped about 18° to the south and cut below the heated zone. A curved ray trace tomographic program was used to generate a velocity tomogram containing velocities of 582–683 m/s; these confirmed values determined from the surface surveys. The velocity tomogram did not detect the high-velocity bedrock layer. Velocities determined may represent a larger percent of clay; borehole logs substantiated this interpretation and indicated a thin waste rock layer (<0.61 m) in this area.

Ground-Penetrating Radar

Ground-penetrating radar techniques were used to identify buried objects, material interfaces, voids, and moisture in the waste bank (Mowery, 1995).

A commercial pulse-based radar system displayed continuous profile radar scan records on the lines spaced at 5 m. Surveys used both 300 and 500 antennas for four longitudinal east–west scans and six north–south scans. The 300 MHz antenna detected boundaries to depths of 3 m; the 500 MHz antenna signal penetrated to 2.1 m. The clay boundary data (depth 2.1 m; two-way travel time 44 ns) were used to compute an average speed of 0.0955 m/ns and a dielectric constant of 9.87. Shallow boundaries were also identified at 0.8 and 1.3 m.

Information about the internal structure of the waste bank obtained with geophysical methods identified subsurface features and was very helpful in planning the cryogenic injection test. However, in this and other tests where geophysical methods were used, it had limited utility in defining the subsurface combustion zone.

Temperature Monitoring

Borehole temperature monitoring provides point source data that is of limited utility in locating combustion zones in inactive underground mines. If data are obtained in the mine void, temperatures are essentially taken in a horizontal plane. Temperatures in the rubble on the mine floor cannot be distinguished from temperatures in the roof coal and overlying carbonaceous shale. Such data may be more useful in burning waste banks which are more homogeneous with respect to heat transfer. Also in a waste bank, temperatures may be determined in both horizontal and vertical planes. Although subsurface temperature data was obtained for most of the Bureau's research projects, extensive data sets were available for Centralia and for the Midvale waste bank.

Centralia Mine Fire

To locate combustion in an inactive mine, boreholes are drilled from the surface and thermocouples are lowered to the mine void. An attempt is made to site the holes in areas of mine voids, since holes that terminate in solid coal give inaccurate temperature data due to the low heat conductivity of solid coal. In the mine void, the thermocouple measures the highest temperature within a volume of ~0.28 m³ (10 ft³). Normal underground temperatures are ~12.8–15.6°C (55–60°F). Elevated borehole temperatures may be related to the movement of hot combustion products, rather than to the proximity to burning material. In an inactive mine, elevated temperatures indicate that combustion is occurring, but give limited information about the extent of the combustion zone.

At Centralia, temperature data were collected from 1800 boreholes drilled into three coalbeds over a period of 14 years (Chaiken et al., 1983). The temperature data were used to plot high-temperature zones on a surface (Figure 16.4.9.) or a mine map. Boundaries for temperature zones were extrapolated from the point source temperature data. Areas that are outside the marked temperature zones do not necessarily represent cold zones; they may represent areas in which data was not available. Although there were limitations of temperature maps constructed directly from temperature data, they did indicate the general location of combustion zones and the direction in which the fire was moving.

Midvale Waste Bank

At this site, the waste bank fire was characterized by temperature measurements taken at an array of thermocouple wells placed at regular points along a grid and at injection points over a 30-month period before, during and after injection of cryogenic slurry (Chaiken et al., 1996). A surface grid (Figure 16.4.10.), measuring 65 m (east–west;

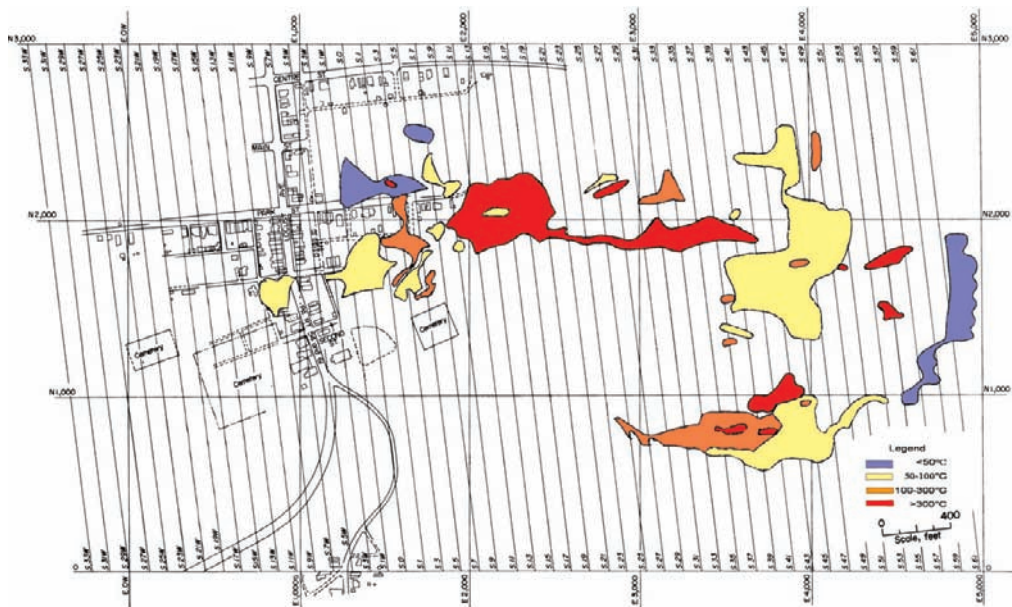


Figure 16.4.9. Temperature zones as inferred from subsurface temperature measurements in Centralia, Pennsylvania. The east to west distance is 5000 ft (1525 m) or ~1 mile (1.6 km). The south to north distance is ~3000 ft (915 m). The maximum temperature (darkest area) is $>600^{\circ}\text{F}$ ($>315^{\circ}\text{C}$). From Chaiken et al. 1983, p. 76.

lines L1, L2, L3) by 10 m (north–south) with intersections at 5 m intervals, was used for data points. The long side of a measurement grid was placed more or less parallel to the southern slope of the waste pile. Temperature data were obtained at 43 vertical thermocouple (TC) wells placed at 5 m spacing over the northern area. The wells extended from the surface to between 3 and 6 m depths. Temperatures were taken every 0.3 m in the wells. Additional TC wells were inserted into the pile from the slope. The initial temperature surveys indicated that there were two areas of combustion. The fire zone in the western portion of the site was smaller and was apparently cooling. A more extensive combustion zone was located in the eastern portion of the site. Hot spots, marked by the emission of water vapor and sulfurous fumes, were located on the southern slope and extended into the bank.

The maximum temperatures in the heated areas were detected at the depths between 2.7 and 2.8 m, indicating that combustion was occurring near the waste/clay interface. A temperature surface for the eastern zone indicates the

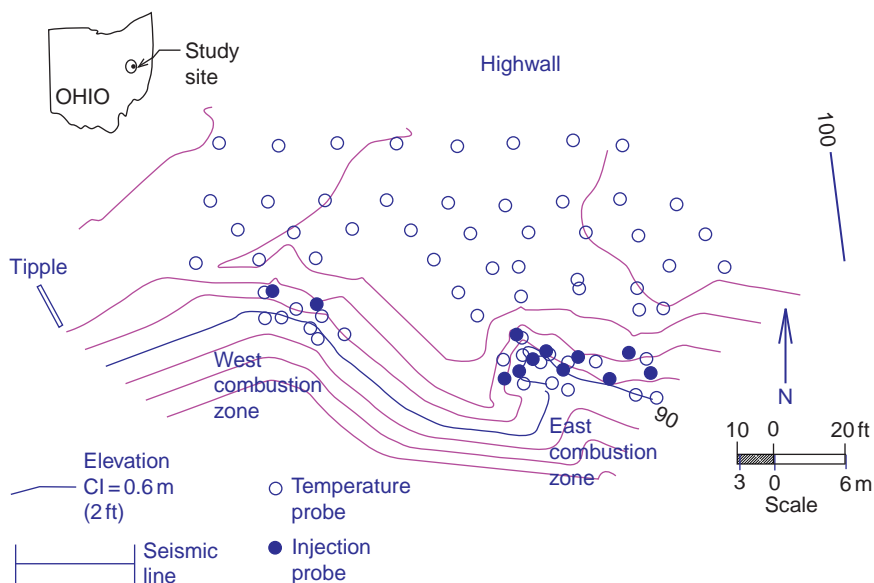


Figure 16.4.10. Map of Midvale waste bank with topographic contours, location of remains of old tipple, temperature wells, and injection probes. From Cohen and Dalverny 1995, p. 71.

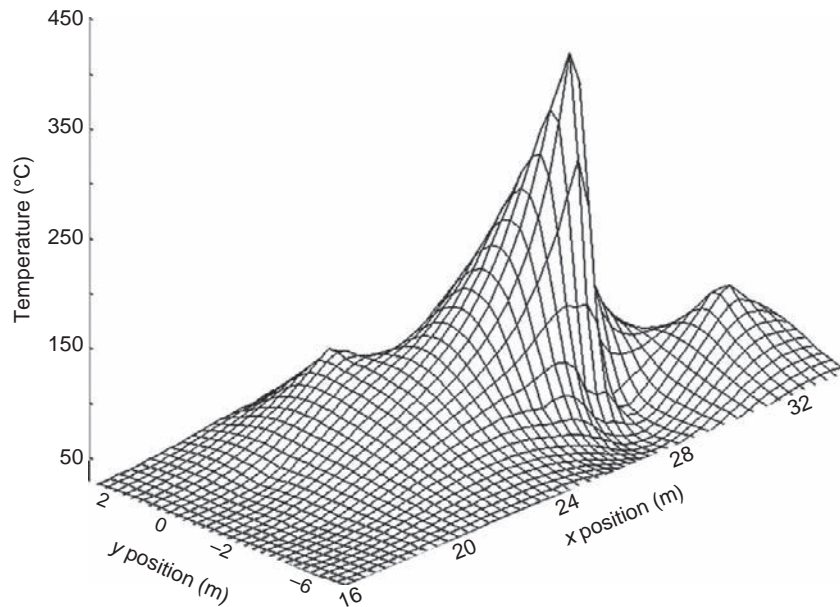


Figure 16.4.11. Temperature surface generated from temperature data obtained at 43 thermocouple temperature wells at a spacing of 5 m. Temperatures were taken at 0.3-m-depth increments. Surface represents highest temperature at any one location. From Chaiken et al. 1996.

localized nature of subsurface combustion (Figure 16.4.11.). It shows a primary combustion zone adjacent to the southern slope and additional heated areas to the northwest and to the east of the primary zone. Temperatures were obtained by inserting a TC probe into the TC well to the appropriate depth, allowing the probe to reach equilibrium, recording the temperature, and then lowering the probe to the next predetermined point. Even for a relatively small site, with computer processing of the data, this was a labor intensive process. However, it had the advantage of providing a three-dimensional view of the heated areas and also showed visual evidence of the effect of the cryogenic injection (Figure 16.4.12.).

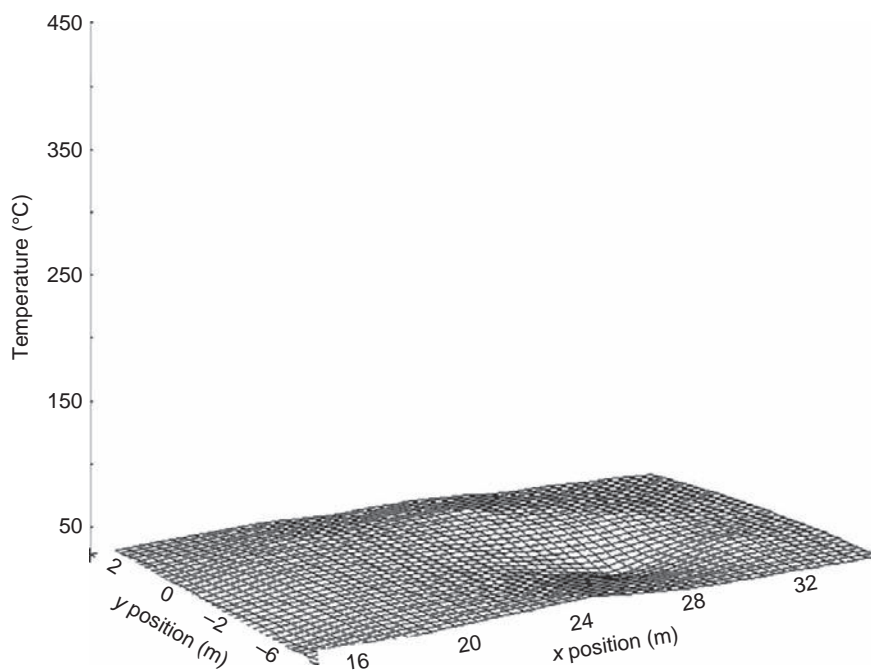


Figure 16.4.12. Temperature surface generated from temperature data obtained at Midvale waste bank after injection of cryogenic slurry. From Chaiken et al. 1996.



16.5. Controlling Abandoned Mine Fires

Excavation of the fire zone at the Calamity Hollow Fire in Pennsylvania.

Photo: US Bureau of Mines, 1982.

Introduction

A fire requires three elements, fuel, oxygen, and energy. To extinguish a fire at least one of these elements must be removed (Figure 16.5.1.). Fuel is removed when it is consumed or when it is physically separated from the burning mass. Oxygen removal depends on either the introduction of an inert atmosphere or on the isolation of the fire zone from sources of fresh air. Heat removal, the cooling of all fuel below the reignition point, can be accomplished by moving a heat-absorbing agent (usually an inert gas or water) through the mine. Given the limitations of conventional fire-control methods, the Bureau of Mines developed and tested several new extinguishment methods.

Burnout Control

The Bureau of Mines developed and patented (Chaiken, 1983) Burnout Control, a technique that can control fires in abandoned coal mines and waste banks, and also extract the thermal energy represented by such coal fires (Chaiken, 1980). The technique involves complete combustion of the coal in place while maintaining control of the resulting heat and fumes. The thermal energy produced and brought to the surface as high temperature flue gas (up to 1000°C) can be 20 times the equivalent thermal energy required to operate the Burnout Control system.

During Burnout Control (Figure 16.5.2.), the burning waste bank or coal mine is placed under negative pressure relative to the atmosphere. Air flows into the underground combustion zones through natural fractures, crevices, pores in the ground, and/or through specially drilled air inlet boreholes. An exhaust ventilation system consists of a large borehole, which acts as a combustion manifold, and a fan which draws hot gases from the fire zone, pulling them out at a single point. In Burnout Control, the affected mine or refuse bank will be at negative pressure, relative to ambient; hence, fumes will be emitted to the atmosphere only at the fan exhaust point. The accumulation of all the fumes allows postburn incineration of the exhaust to insure complete combustion to carbon dioxide and water. If needed, flue gas scrubber treatment can also be applied to remove air pollutants such as sulfur dioxide and particulates.

The heat of combustion of the burning coal will appear as sensible heat in the exhaust at temperatures as high as 1000°C. This heat is recoverable for producing steam and/or electricity. The complete burnout of carbonaceous material and pyrites in a mine or waste bank will permanently solve the environmental problems of an active fire.

Calamity Hollow

Burnout Control had two limited field trials during its development. The first was a 4-month controlled burn of a shallow, abandoned coal-mine fire in a confined area of the Pittsburgh seam, the Calamity Hollow Mine Fire Project (Irani et al., 1983; Chaiken et al., 1984; Dalverny et al., 1984; Soroka et al., 1986; Chaiken et al., 1989).

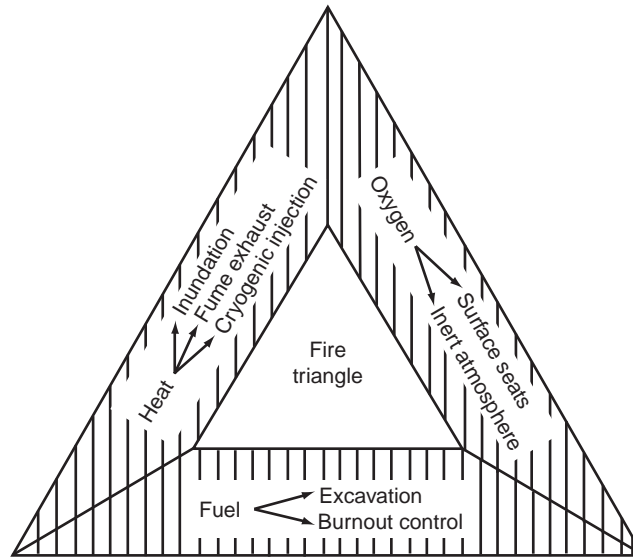


Figure 16.5.1. Fire triangle with fuel removal, oxygen exclusion, and heat reduction fire-control methods. From Kim and Chaiken 1993, p. 24.

At Calamity Hollow, exhaust control was maintained over an underground area of about 2 acres which encompassed the fire zones. Over 102 days of fan operation, an estimated 1100 tons of coal were burned, producing exhaust gases at an average temperature of 600°C and thermal power level of 3.2 MW. The total thermal energy, if converted to electricity through a small mobile steam turbine/generator system, could have produced 14–18 million kwh of electricity, about 20 times more energy than that required to operate the Burnout Control system.

During the course of the mine-fire field trial, slow subsidence and ground fracture did occur, but did not affect the burnout process itself. Surface disturbances were handled by constructing additional footings for equipment

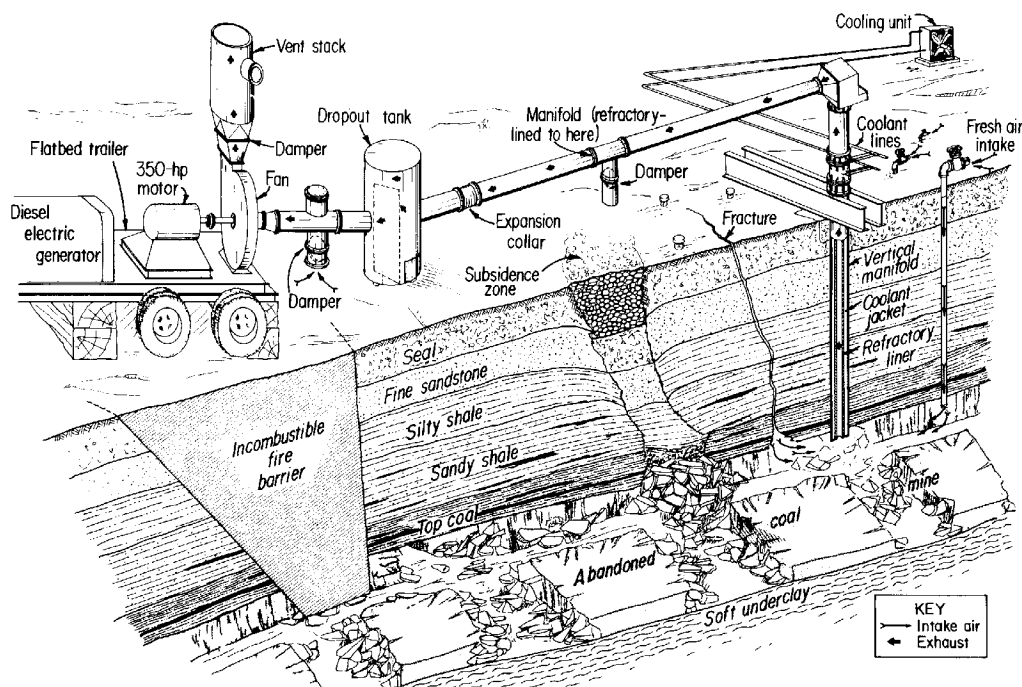


Figure 16.5.2. Burnout Control system as designed for the Calamity Hollow mine-fire project. From Irani et al. 1983, p. 13.

support and by sealing fissures in the ground surface. In terms of air pollution, test data indicated that all the fuel-sulfur appeared as SO_x in the exhaust, but only 5% of the fuel-nitrogen appeared as NO_x . From an environmental viewpoint, removal of SO_x and NO_x from the exhaust will be required if Burnout Control is developed to a commercial system.

Albright Waste Bank

The second trial of Burnout Control was a 1-year test of the process as applied to a 0.9-acre section of a 6.5-acre abandoned coal waste-pile fire, the Albright Waste Bank Fire Project in West Virginia (Chaiken and Bayles, 1988). The field trial of Burnout Control at the Albright waste pile was designed to operate at a 5 MW (thermal), 900°C exhaust output. At Albright, a 0.9 m (3 ft) diameter, 42.7-m (140 ft)-long stainless-steel combustion manifold was set horizontally at the bottom of the pile along its base (Figure 16.5.3.). A 15.2-m (50 ft)-long perforated section of the manifold served to draw heat and fumes from a volume of waste estimated at over 10 000 tons, which at the design output would have taken 0.75 year to burn producing 28 494 billion thermochemical calories (113 billion BTU) of thermal energy. Engineering design problems and the need to control air pollution during the trial prevented long-term continuous burnout operations at the site. However, during 1600 hours of fan operations, an estimated 700 tons of waste were burned producing 2048 billion thermochemical calories (8.12 billion BTU) of exhaust thermal energy. Burnout operations were terminated when excessive temperatures and vacuum combined to collapse the combustion manifold.

A key finding at the Albright field trial was that, as the fire was spread under Burnout Control, the pile acted as a large gasifier that required the after burn of the exhaust gases in the combustion manifold. Only 30% of the fuel-sulfur appeared in the exhaust, but without full stoichiometric burning, reduced sulfur gases (e.g., H_2S , COS , and CS_2) in the exhaust caused odor problems for nearby residents. Subsidence occurred on top of the waste pile over the fire zones, but the holes were readily filled. With improved engineering designs with regard to maintaining the structural integrity of the combustion manifold and improving its operation as an afterburner, Burnout Control could be applied to controlling coal waste-pile fires.

Water Injection

Removing heat, one of the three essential elements, from an underground fire requires the introduction of a heat-absorbing medium, its controlled movement through the mine, and the removal of the heated substance (Dalverny,



Figure 16.5.3. Photograph of a combustion manifold and a steel liner inserted into the Albright waste bank. From Chaiken and Bayles 1991, p. 10.

1988). Where it is plentiful and inexpensive, water is a desirable heat exchange medium because of its high **heat capacity** and its latent **heat of vaporization**.

The Bureau used **water injection** with the suction-induced removal of heated gases in two projects. In theory, when the water is injected into heated subterranean areas, it is converted to steam. Under the influence of an exhaust fan, the steam is moved through the mine, absorbing more heat from the heated coal and roof strata. The heated steam can be exhausted to the atmosphere or to a heat exchanger where its thermal energy can be used.

Calamity Hollow

During the cooldown phase of the Calamity Hollow Mine Fire Project (Chaiken et al., 1984), water was injected by gravity flow through an array of 1-in hose and 2-in pipes. Prior to quenching, the average temperature of the exhaust gas was 600°C. The system was operated at an injection rate of 7.6–11.4 L (2–3 gallons) per minute per borehole for 8 hours per day for 21 days. For an additional 10 days, the water was injected continuously. Over the 31 days, 10.6 mL (2.8 million gallons) of water was injected. The temperature of the exhaust was lowered to 162°C (Figure 16.5.4.), and 75 648 million thermochemical calories (300 million BTU) of heat energy was released from the mine. The estimated heat-removal efficiency was not high, 7 cal/g compared to the heat of vaporization of 540 cal/g. During the operation of the system, much of the water was flowing out of the mine and was not reaching the burning material. When the water injection rate was increased, the seepage rate also increased. However, the system achieved its objective of cooling the combustion zone prior to excavation in a relatively short period of time.

Renton Mine Fire

Based on the Calamity Hollow project, an attempt was made to extinguish a fire in an abandoned mine at Renton, Pennsylvania (Dalverny and Chaiken, 1988, 1991). Water was supplied by gravity to spray nozzles located at the casing bottom in each borehole. In this configuration, the fan was operated for about 6 hours per day, 5 days per week, at a water injection rate of ~3.8 L (1 gallon) per minute per borehole. After 4 months, the injection tubes were reinstalled on the outside of the borehole casings, 0.3–0.6 m (1–2 ft) below the surface. In this arrangement, water flowed down the casing and through the strata above the mine void. However, this modification did not improve the cooling efficiency.

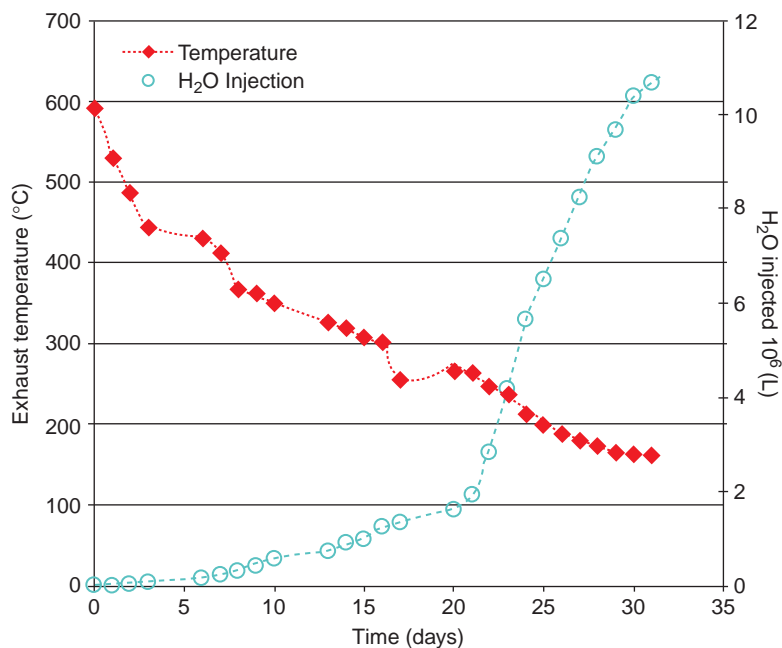


Figure 16.5.4. Average exhaust temperature (°C) and cumulative water injection (10⁶ L) versus time during a quenching experiment at Calamity Hollow. From Chaiken et al. 1984, (Table 2).

Analysis of the data led to the conclusion that combustion was occurring in the roof coal and carbonaceous shales. It was unlikely that the water reached these areas and no significant conversion to steam occurred. Temperature and gas concentration changes did indicate that local cooling occurred. But not enough heat was removed to slow or stop the combustion process. A better delivery system for placing the water in contact with the heated material was required.

Foam Injection

In the Renton fire, it was determined that unless the injected water is rapidly converted to steam, the movement of the water through heated areas of the mine cannot be controlled. The use of foam as a water transport agent had two advantages: it would keep the water in place long enough for it to be entrained in the air stream, and in voids the foam could build upon itself to reach the mine roof where combustion may be seated. Foam is a dispersion of gas in water; it is made of water, a suitable gas, either air or nitrogen, and a surfactant. Depending on its purpose, it may also contain fire-inhibiting chemicals (Gross, 1991). Through its contract research program, the Bureau funded two tests of foam injection to control subsurface fires.

A small-scale test of medium-expansion foam, which is stable and capable of filling voids, was conducted at the Bureau's Lake Lynn facility (Maustellar and Gross, 1996). The test was intended to determine the distribution of injected foam in a 1.8 m³ (64 ft³) block of mine refuse. A 1-in pipe was used to inject the foam into the center of the block. The foam followed the path of least resistance and flowed back through the interstitial space along the injection tube. Dispersion through the refuse was limited, and it appeared that a better injection system would be required before foam could be tested as a heat transfer medium at a waste bank. Subsequent laboratory tests in a simulated waste bank indicated that the use of a polyurethane foam barrier to control foam dispersion and foam injection beneath the fire zone could increase heat transfer from the coal waste to the heat-absorbing foam (Jones et al., 1994).

In cooperation with the Colorado Division of Minerals and Geology (CDMG), the Bureau funded a demonstration of foamed grout technology at the IHI Mine fire in Rifle, CO (Feiler and Colaizzi, 1996). The injected medium was a cement and fly ash grout mixed with foam. The heat resistant material was injected through boreholes; it could penetrate small cracks and fill large voids. The primary fire-containment mechanisms were oxygen exclusion and heat removal.

During 42 calendar days, 1911 m³ (2500 yd³) of foamed grout was injected into the fire zone. At the end of the injection period, the fire was estimated to be 75% controlled. Injection in the area of the old mine portal, believed to be the primary air source for the fire, did not completely terminate the influx of oxygen. At the end of the injection project, the majority of borehole temperatures were above 93.3°C (200°F) and as high as 704.4°C (1300°F). The project was initially considered to have controlled some portion of the fire, but, as of 2005, CDMG lists the fire as active (Renner, 2005).

Cryogenic Slurry Injection

The use of **cryogenic** liquids as a heat-removal medium in coal fires has the potential advantages of uniform distribution of the fluid and isotropic expansion of a cold gas. If water is injected into a waste bank, gravity causes it to flow down dip, and erosion causes the size of the drainage channel to increase. The distribution of the water affects a relatively small area, and cannot be controlled. If a cryogenic liquid is injected, moisture in the material freezes, displacing the injected liquid to another area. This increases the size of the area affected by the injected fluid. Also, as the temperature of the gas increases, the gas expands, creating a cold pressure front which should move uniformly from the point of injection to the surface of the bank.

In small-scale tests of cryogenic injection, liquid CO₂ was used as the heat transfer liquid. The injected CO₂ formed a solid, and in a relatively short period of time, blocked the flow of liquid. In medium-scale tests with liquid nitrogen as the heat transfer medium, the nitrogen acted like a liquid and flowed to the bottom of the box.

In order to overcome the flow constraints, the Bureau developed and patented (Chaiken et al., 1994) an apparatus to produce a pumpable slurry of liquid nitrogen and granular CO₂ at a temperature of ~-180°C. The change in state from the solid or liquid to the gas phase produces a cold pressure wave that moves isotropically away from the

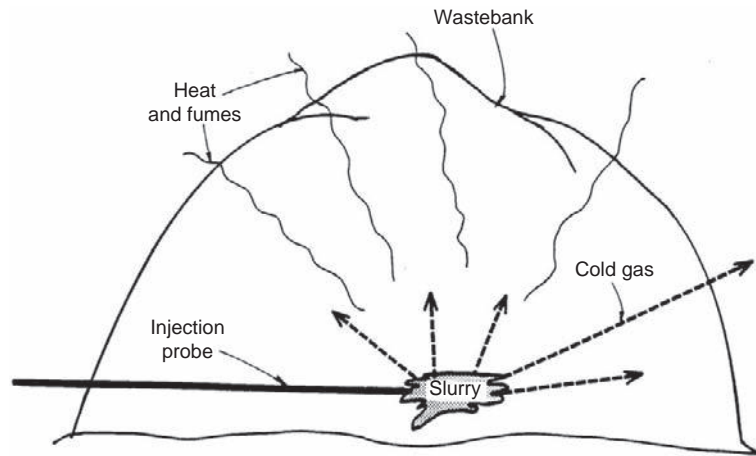


Figure 16.5.5. Sketch of cryogenic slurry injection into a waste bank. Change in state from liquid/solid to gas forces heat adsorbing cold front through the bank to the surface. From Kim 1994, Figure 1.

injection point, adsorbing heat and producing an inert atmosphere. It forces heat, smoke, and fumes from the combustion zone to the surface (Figure 16.5.5.). The movement of the inert gas is controlled by pressure and buoyancy.

To produce a slurry of CO_2 and N_2 , liquid or gaseous CO_2 pumped through a bell-shaped nozzle forms finely powdered particles due to the rapid expansion of the gas. If at the same time, liquid N_2 is injected into the nozzle, it cools the solid particles of CO_2 , and the liquid nitrogen and solid CO_2 form a slurry. The slurry was entrained through a jet pump into another stream of liquid N_2 at a delivery pressure of 80 psi. A stainless-steel injection line carried the slurry to the injection point. When the slurry is pumped into a bed of coal or coal waste, the temperature near the probe drops to -180°C , and the expanding cold gas lowers the temperature in the surrounding material.

A test of the cryogenic method to extinguish subsurface coal fires was conducted at a coal waste bank in Ohio (Kim, 2004). The bank was adjacent to a high wall, and extended east to west along the eroded southern slope to a concrete foundation, believed to be the remains of a tippie. The flat top of the waste bank was ~ 29.7 m above the base (see Geophysical Methods in Section 16.4 for a more complete description of the waste bank).

Temperature surveys indicated that there were two areas of combustion. A small fire zone in the western portion of the site was apparently cooling. The more extensive combustion zone was located in the eastern portion of the site. For logistical and economic reasons, the cryogenic injections were concentrated in the eastern zone. During the first injection, the jet pump designed to inject the slurry failed. Only liquid nitrogen (about 12 600 kg) was injected. Post-injection temperature surveys indicated that the average temperature in the bank had decreased by 6°C , and there was a decrease of 296°C in the maximum temperature. During the second injection, a slurry of 4600 kg of N_2 and 1140 kg of CO_2 was injected at relatively low injection pressures into the eastern portion of the site (Figure 16.5.6.). For the duration of the trial, subsurface temperatures ranged from 19 to 450°C .

Temperatures near the injection point, showed a decrease followed by a return to the pre-injection temperature over a 4-month period. Varying degrees of initial cooling followed by a long-term decline in temperature was indicated in several areas, while there was initial cooling followed by a temperature increase in other areas. The variable nature of the results indicates that combustion was reduced at hot spots near the injection point, but displacement of hot gases could cause an increase in temperature in adjacent areas.

Temperatures measured more than 1 year after the injection of the slurry indicated lower temperatures throughout the site, but a continuing low level of combustion in the interior of the bank. In a detailed analysis of the temperature data, Chaiken et al. (1996) concluded that the second cryogenic injection apparently controlled or eliminated hot spots in the East fire zone reducing heat generation within the waste pile. This allowed environmental cooling rates to exceed heat generation rates. This implied that cryogenic slurry injections quenching localized hot spots might be sufficient to extinguish a waste bank fire.



Figure 16.5.6. Photo of injection of cryogenic slurry at Midvale waste bank showing CO₂ truck, slurry mixing tank, emission of smoke from the bank, and condensation above the bank.

The project at the Midvale site demonstrated that it was possible to produce and inject a cryogenic slurry of liquid nitrogen and solid CO₂. The amount injected was dictated by the economics of the project and was insufficient to completely extinguish the fire. However, it was encouraging that there was a significant reduction in the heat content of the bank for 3–6 months after injection.

Summary

The Bureau of Mines program in the control of fires in inactive or abandoned coal mines and waste banks was relatively small in terms of manpower and budget. Although its original function was to extinguish such fires, Bureau personnel accumulated knowledge on how mine fires were initiated, what conditions fostered their propagation, and what factors improved the probability of extinguishing or controlling them. They also researched methods to locate subsurface fires and improved control technologies.

At its inception in 1910, the US Bureau of Mines' primary focus was on improving mine safety and reducing the loss of life due to fires and explosions in coal mines. Over the years, its role expanded to mine inspection, mineral economics, and reducing the environmental impact of mining. It was always viewed as a source of innovative science and technology in the minerals field. The demise of the Bureau left a void in mining research, and a large collection of mining related literature is no longer readily available.

Acknowledgments

It was my privilege and pleasure to work at the US Bureau of Mines in Pittsburgh from 1967 until it was closed in 1996. For the most part, I found my colleagues there to be intelligent, insightful, and dedicated. Both Mal Magnuson and Don Donner worked diligently to control fires in abandoned mines and waste banks. Maurice Deul provided his effective brand of leadership to the environmental program at the Pittsburgh Research Center. His knowledge of combustion made Bob Chaiken an invaluable resource; and without Gene Dalverny, Tom Justin,

Joe Slivon, Andy Kociban, and Debbie Burse very little real work would have been accomplished. My thanks to Bob Chaiken who reviewed this manuscript for accuracy and completeness.

Important Terms

Abandoned mine	A coal mine where the mine operator has ceased operations without reclaiming the site and the owner/operator cannot be located.
Abandoned Mined Land	Land and water resources adversely affected by past coal mining and left abandoned or inadequately restored.
Absorption	The incorporation a gas, liquid, or solid within another substance, the process by which one phase permeates or is dissolved in another.
Activation energy	The minimum amount of energy needed for a chemical reaction to take place, the energy required to initiate a chemical reaction.
Adiabatic	A process which takes place without any exchange of heat between a system and its surroundings, a chemical or mechanical process which takes place without heat entering or leaving the system.
Adsorption	The adherence of gaseous or liquid molecules to the surface of solids with which they are in contact.
BTU (British Thermal Unit)	The amount of heat required to raise the temperature of one pound of water 1 degree Fahrenheit at 1 atmosphere pressure.
Carbonaceous shale	A coal-like material containing too much mineral matter to be considered coal, may overlies coal seams, frequently formed by an influx of inorganic sediment into the coal swamp.
Coal rank	Describes the stage of coalification attained by a given coal; the place occupied by a coal in a classification of coals according to the degree of metamorphism, or progressive alteration, in the order: <ol style="list-style-type: none"> (1) Lignite or brown coal—less than 8300 moist BTU. (2) Subbituminous—a coal with a heating value greater than that of lignite and less than that of bituminous, between 8300 and 13 000 moist BTU. (3) Bituminous—a coal with a heating value and dry fixed carbon concentration less than that of anthracite: <ol style="list-style-type: none"> (a) High-volatile bituminous c (hvc)—heating value between 11 000 and 13 000 moist BTU. (b) High-volatile bituminous b (hvb)—heating value between 13 000 and 14 000 moist BTU. (c) High-volatile bituminous a (hva)—heating value greater than 14 000 moist BTU and dry fixed carbon concentration less than 69%. (d) Medium-volatile bituminous (mv)—dry fixed carbon concentration between 69 and 78%. (e) Low-volatile bituminous (lv)—dry fixed carbon concentration between 78 and 86%. (4) Anthracite—dry fixed carbon concentration between 86 and 98%
Coal refuse	Waste material in the raw coal that has been removed, usually in a cleaning or preparation plant, frequently disposed of in surface piles, also called tailings.
CO index	$(CO/\Delta O_2)$, the ratio of CO emitted to oxygen adsorbed; the adsorbed oxygen (ΔO_2) is the difference between the measured concentration and the concentration in normal air.

Crossing point method	A method in which the rates at which the temperatures of a sample and a reference increase are compared. The point at which the temperature of the sample equals that of the reference, the crossing point, is considered an indicator of the sample's tendency to self-heat.
Cryogenic	Extremely cold freezing process, using liquid nitrogen or carbon dioxide, any process carried out at very low temperature, such as -50°C .
Dip	The angle at which a stratum or any horizontal feature is inclined to the horizontal.
Excavation	(loading out, daylighting, dig and quench, stripping) A fuel-removal method, involves physically removing the burning material and cooling it to extinguish the fire.
Exothermic	A chemical reaction producing heat.
Fire barrier	A natural feature or excavated structure which breaks the continuity of the coal and carbonaceous shales intended to limit the spread of a subsurface fire.
Flooding	A method of fire control in which a constructed dam is used to raise the natural water level above the fire zone. Rarely used because of the difficulties in remote installation of a dam, the necessity that the surrounding down dip rock must be unfractured, and the risk of catastrophic failure.
Flushed barrier	Designed to fill the voids in an underground fires zone with fine, noncombustible solids which cover the burning material and fill the interstices in adjacent rock, limiting the amount of oxygen in the system and adsorbing heat.
Gob	The space left by the extraction of a coal seam into which waste is packed or the immediate roof caves.
Ground-penetrating radar	A method that uses radar pulses to image the subsurface; detects objects, changes in material, voids and cracks in rock, soil, ice, fresh water, pavements, and structures.
Heat capacity	The amount of heat it takes to raise the temperature of one gram of a material 1°Celsius , a property of a material denoting its ability to adsorb heat.
Heat of vaporization	The heat required per unit mass to change a unit mass of the substance at its boiling point from liquid to gas or vapor.
Inactive mine	Under SMCRA, a coal mining and reclamation operation for which reclamation has been completed or the reclamation bonds have been forfeited.
Inundation	Methods that involve the underground use of water to lower the temperature of the burning material (heat removal) and stop the combustion reaction by oxygen exclusion.
Magnetic susceptibility	A measure of the degree to which a substance is attracted to a magnet; the ratio of the intensity of magnetization to the magnetic field strength.
ppm	Parts per million, a unit of concentration, mg/kg for solids or mg/L for liquids and gases.
Proton precession magnetometer	An instrument used to measure the strength and/or direction of the magnetic field in the vicinity of the instrument. A direct current creates a strong magnetic field around a hydrogen-rich fluid, causing protons to align themselves with the magnetic field. The current is then interrupted, and as protons are realigned with earth's magnetic field the direction of axial rotation changes at a specific frequency. This produces a weak alternating magnetic field. The precession frequency depends only on atomic constants and the strength of the external magnetic field.
Remnant magnetization	Part of the magnetization of a body that does not disappear when the external magnetic field disappears.

Roof coal	The layer immediately over the main coal seam. It may be coal of poor quality or carbonaceous shale, and is frequently left in place during mining.
Seismic refraction survey	A method in which the detecting instruments are placed at a distance from the seismic energy source that is large compared with the depth of the subsurface layers. The seismic waves travel horizontal distances along distinct interfaces; the travel time from source to receiver is related to the depth of subsurface layers.
Spall	A relatively thin, commonly curved, and sharp-edged piece of rock produced by exfoliation, pieces of rock, or coal that break off parallel to a surface.
Surface sealing	A relatively inexpensive method of controlling abandoned mine fires by inhibiting ventilation of the fire zone. The exclusion of air and the accumulation of combustion products suppress the rate of fire propagation.
Terrain conductivity	Electromagnetic conductivity of subsurface soil, groundwater, rock, and objects buried in the ground.
Tomographic imaging	A seismic method to image a particular plane while leaving out undesired detail in other planes.
Trench barrier	Constructed by excavating an open trench between the fire and the threatened area and then backfilled with incombustible material, the trench extends vertically from the surface to the bottom of the coal bed.
Water curtain	Continuous underground spraying of water through nozzles placed at the bottom of a borehole; the borehole array is extensive enough to saturate a designated portion of the mine.
Water injection	Placement of water within a fire zone, so that water saturated air will cool the fire zone.

References

- Chaiken, R.F., 1980. Controlled Burnout of Wasted Coal on Abandoned Coal Mine Lands. US Bureau of Mines RI 8478, 23 p.
- Chaiken, R.F., 1983. Method for Controlled Burnout of Abandoned Coal Mines and Waste Banks. US Patent No. 4,387,655, June 14, 1983.
- Chaiken R.F., Bayles, L.G., 1988. Burnout Control at the Albright Coal Waste Bank Fire. US Bureau of Mines RI 9345, 29.
- Chaiken, R.F., Brennan, R., Heisey, B., Kim, A.G., Malenka, W., Schimmel, J., 1980. Problems in the Control of the Centralia Mine fire. Washington, DC, Report to OSMRE, Interagency Agreement J5101026, 110 p.
- Chaiken, R.F., Brennan, R., Heisey, B., Kim, A.G., Malenka, W., Schimmel, J., 1983. Problems in the Control of Anthracite Mine Fires: A Case Study of the Centralia Mine Fire. US Bureau of Mines RI 8799, 93 p.
- Chaiken, R.F., Dalverny, L.E., Kim, A.G. 1989. Calamity Hollow Mine Fire Project (in five parts), part 2, Operation of the Burnout Control System. US Bureau of Mines RI 9421, 35 p.
- Chaiken, R.F., Dalverny, L.E., Kim, A.G., 1996. Cryogenic slurry for extinguishing a coal waste bank fire. Proceedings 18th Annual Conference of the National Association of Abandoned Mine Land Programs. Kalispell, Montana, September 15–18, pp. 303–313.
- Chaiken, R.F., Divers, E.F., Kim, A.G., Soroka, K.E., 1984. Calamity Hollow Mine Fire Project (in five parts), part 4, Quenching the Fire Zone. US Bureau of Mines RI 8863, 18 p.
- Chaiken, R.F., Kim, A.G., Kociban, A.M., Slivon, J.P., 1994. Cryogenic Slurry for Extinguishing Underground Fires. US Patent No. 5,368,105, November 29, 1994.
- Chaiken, R.F., Singer, J.M., Lee, C.K., 1979. Model Coal Tunnel Fires in Ventilation Flow. US Bureau of Mines RI 8355, 32 p.
- Cohen, K.K., Dalverny, L.E., 1995. Seismic characterization of a coal waste bank fire in Eastern Ohio as a tool to aid reclamation. Proceedings 17th Annual Conference of the National Association of Abandoned Mine Land Programs, French Lick, Indiana, October 15–18, pp. 70–86.

- Dalverny, L.E., 1988. Heat Removal Methods for Control of Underground Abandoned Coal Mine Fires. US Bureau of Mines IC 9184, pp. 343–347.
- Dalverny, L.E., 1994. Temperature induced changes in magnetic susceptibility of Pittsburgh coal seam strata. International Land Reclamation and Mine Drainage Conference, US Bureau of Mines Special Publication SP 06D-94, Pittsburgh, Pennsylvania, vol. 4, pp. 148–152.
- Dalverny, L.E., Chaiken, R.F., 1988. Technical Services to Extinguish the Mine Fire in the Abandoned Renton No 1 Mine in Plum Borough, Allegheny County, Pennsylvania. Report to OSMRE, Interagency Agreement No. HQ-51-CT-6-01492, Pittsburgh, Pennsylvania, 62 p.
- Dalverny, L.E., Chaiken, R.F., 1991. Mine Fire Diagnostics and Implementation of Water Injection with Fume Exhaustion at Renton, PA. US Bureau of Mines RI 9363, 42 p.
- Dalverny, L.E., Chaiken, R.F., Kim, A.G., 1990. Mine fire diagnostics in abandoned bituminous coal mines. Proceedings 1990 Mining and Reclamation Conference, Charleston, West Virginia, West Virginia University Publication Services, April 23–25, pp. 527–534.
- Dalverny, L.E., Chaiken, R.F., Soroka, K.E., 1984. Calamity Hollow Mine Fire Project (in five parts), part 3, Instrumentation for Combustion Monitoring, Process Control and Data Recording. US Bureau of Mines RI 8862, 23 p.
- Dalverny, L.E., Kim, A.G., 1995. Magnetometer and terrain conductivity at a burning coal waste pile. Proceedings 17th Annual of the National Association of Abandoned Mine Land Programs, French Lick, Indiana, October 15–18, pp. 49–69.
- DeKok, D., 1986. Unseen Danger. University of Pennsylvania Press, Philadelphia, 299 p.
- Deul, M., Kim, A.G., 1988. Methane Control Research: Summary of Results, 1964–1980. US Bureau of Mines Bulletin 687, 174 p.
- Elder, J.L., Schmidt, L.D., Steiner, W.A., Davis, J.D., 1945. Relative Spontaneous Heating Tendencies of Coals. US Bureau of Mines Technical Paper 681, 26 p.
- Feiler, J.J., Colaizzi, G.J., 1996. IHI Mine fire control project utilizing foamed grout technology. US Bureau of Mines Research Contract Report 14320395H0002, Rifle, Colorado, 111 p.
- Gross, S.S., 1991. Improved Method for Extinguishing Coal Refuse Fires. US Bureau of Mines AML Research Contract Report JO398007, 100 p.
- Griffith, F.E., Magnuson, M.O., Toothman, G.J.R., 1960. Control of Fires in Inactive Coal Formations in the United States. US Bureau of Mines B 590, 105 p.
- Hansen, L.C., Hodges, J.E., Redmond, K.M., 1990. Determining the Effectiveness of Past Mine Fire Surface Seal Abatement Methods. US Bureau of Mines Research Contract Report J0278004, 235 p.
- Irani, M.C., Chaiken, R.F., Dalverny, L.E., Molinda, G.M., Soroka, K.E., 1983. Calamity Hollow Mine Fire Project (in five parts), part 1, Development and Construction of the Burnout Control System. US Bureau of Mines RI 8762, 29 p.
- Johnson, W., Miller, G.C., 1979. Abandoned Coal-Mined Lands: Nature, Extent and Cost of Reclamation. Bureau of Mines Special Publication, 6–79, 29 p.
- Jolley, T.R. Russell, A.W., 1959. Control of Fires in Inactive Land Deposits in Western United States Including Alaska, 1948–58. US Bureau of Mines IC 7932, 22 p.
- Jones, J.R., Kim, A.G., Kociban, A.M., 1994. The Use of Containment Barriers and Fire Fighting Foams for the Extinguishment of Coal Waste Bank Fires. A Laboratory Study: Pittsburgh, Pennsylvania, International Land Reclamation and Mine Drainage Conference, US Bureau of Mines Special Publication SP 06D-94, vol. 4, pp. 121–128.
- Justin, T.R., Kim, A.G., 1987. Mine Fire Diagnostics: Carbondale, Pennsylvania, Report to OSMRE. Interagency Agreement No. CT745011, Wilkes Barre, Pennsylvania, 52 p.
- Kim, A.G., 1977. Laboratory Studies on Spontaneous Heating of Coal: A Summary of Information on the Literature. US Bureau of Mines IC 8756, 13 p.
- Kim, A.G., 1988. Laboratory Determination of Signature Criteria for Locating and Monitoring Abandoned Mined Land Fires, Report to OSMRE. Interagency Agreement No. HQ-51-CT-6-01535, Pittsburgh, Pennsylvania, 45 p.
- Kim, A.G., 1991. Laboratory Determination of Signature Criteria for Locating and Monitoring Abandoned Mined Land Fires. US Bureau of Mines RI 9348, 19 p.
- Kim, A.G., 1995. Relative Self-heating Tendencies of Coal, Carbonaceous Shales and Coal Refuse. US Bureau of Mines RI 9537, 21 p.
- Kim, A.G., 2004. Cryogenic injection to control a coal waste bank fire. In: Stracher, G.B. (Ed.), Coal Fires Burning Around The World: A Global Catastrophe. *Int. J. Coal Geol.* 59 (1–2), 63–73.
- Kim, A.G., Chaiken, R.F., 1993. Fires in Abandoned Coal Mines and Waste Banks. US Bureau of Mines IC 9352, 58 p.

- Kim, A.G., Dalverny, L.E., 1994. Mine fire diagnostics at the large mine site. International Land Reclamation and Mine Drainage Conference, Pittsburgh, Pennsylvania, US Bureau of Mines Special Publication SP 06D-94, vol. 4, pp. 139–147.
- Kim, A.G., Douglas, L.J., 1973. Gases Desorbed from Five Coals of Low Gas Content. US Bureau of Mines RI 7768, 9 p.
- Kim, A.G., Justin, T.R., Miller, J.F., 1992. Mine Fire Diagnostics Applied to the Carbondale Mine Fire. US Bureau of Mines RI 9421, 16p.
- Kuchta, J.M., Rowe, V.R., Burgess, D.S., 1980. Spontaneous Combustion Susceptibility of U.S. Coals. US Bureau of Mines RI 8474, 42 p.
- Leitch, R.D., 1940. Some Information on Extinguishing Refuse-Bank Fires Near Mahonoy City, Pennsylvania. US Bureau of Mines IC 7104, 16 p.
- Magnuson, M.O., 1974. Control of Fires in Abandoned Mines in the Eastern Bituminous Region of the United States. US Bureau of Mines IC 8620, 53 p.
- Maustellar, J.W., Gross, S.S., 1996. Aqueous Foams for Refuse Pile Fire Control. US Bureau of Mines Research Contract Report 1432 HO349015, 15 p.
- McElroy, G.E., 1938. Some Observations on the Causes, Behavior, and Control of Fires in Steep Pitch Anthracite Mines. US Bureau of Mines IC 7025, 36 p.
- Michalski, S.R., Winshel, L.J., Gray, R.E., 1988. Underground Mine Fires on Abandoned Mine Lands. Proceedings 10th Annual Conference of the National Association of Abandoned Mine Land Programs, Wilkes Barre, Pennsylvania, October 10–14, 29 p.
- Miron, Y., Lazzara, C.P., Smith, A.C., 1992. Cause of Floor Self-Heatings in an Underground Coal Mine. US Bureau of Mines RI 9415, 24 p.
- Miron, Y., Smith, A.C., Lazzara, C.P., 1990. Sealed Flask Test for Evaluating the Self-Heating Tendencies of Coals. US Bureau of Mines RI 9330, 18 p.
- Mowery, G., 1995. Ground penetrating radar and infrared thermography tests at a burning coal waste bank. Proceedings 17th Annual Conference of the National Association of Abandoned Mine Land Programs, French Lick, Indiana, October 15–18, pp. 87–105.
- Philbin, D.R., Holbrook II, J.A., 1988. Progress Toward Abatement of Mine Fires in the Anthracite Coal Fields. US Bureau of Mines IC 9184, pp. 330–336.
- Renner, S., 2005. Report on the Status of fires at abandoned underground coal mines in Colorado, Colorado Division of Minerals and Geology, 80 p., http://mining.state.co.us/final_report_1-27_ab-low.pdf (accessed August 2008).
- Rushworth, P., Haefner, B.D., Hynes, J.L., Streufert, R.K., 1989. Reconnaissance Study of Coal Fires in Inactive Colorado Coal Mines. Colorado Geological Survey, Denver, Colorado, IS26, 60 p.
- Scott, G.S., 1944. Anthracite Mine Fires: Their Behavior and Control. US Bureau of Mines Bulletin 455, 206 p.
- Shellenberger, F.H., Donner, D.L., 1979. Controlling Fires in Unmined Coal Deposits and Abandoned Coal Mines in the Western United States and Alaska. US Bureau of Mines Progress Report 10047, 150 p.
- Smith, A.F., Lazzara, C.P., 1987. Spontaneous Combustion Studies of U.S. Coals: US Bureau of Mines RI 9079, 28 p.
- Smith, A.C., Miron, M., Lazzara, C.P., 1991. Large-Scale Studies of Spontaneous Combustion of Coal. US Bureau of Mines RI 9346, 30 p.
- Soroka, K.E., Chaiken, R.F., Dalverny, L.E., Divers, E.F., 1986. Calamity Hollow Mine Fire Project (in five parts), part 5, Excavation and Evaluation of the Fire Zone. US Bureau of Mines RI 9001, 25 p.

WWW Addresses: Additional Reading

All of the work by the US Bureau of Mines was documented in reports of investigation (RI), information circulars (IC), and bulletins (B) published by the Bureau of Mines and distributed without cost to those who were interested. The discussion of the Bureau's work in this chapter is a relatively brief excerpt of the information in these reports. A more detailed discussion of fires in abandoned or inactive mines and waste banks is contained in the Centralia report (Chaiken et al., 1983) and in an IC on fires in abandoned coal mines and waste banks (Kim and Chaiken, 1993).

I acquired a collection of reports on various fire topics during my tenure as a researcher with the Bureau. Unfortunately, these publications are not as easily obtained now. The National Technical Information Service (<http://www.ntis.gov>) sells copies of items in its collection. Try the advanced search with DIBM as the source agency and one of the words in the title as a keyword. Some publications can be obtained from Amazon.com (<http://www.Amazon.com>) or used book sellers. As successor agencies to the Bureau of Mines, the National

Institute for Occupational Safety and Health (NIOSH) at <http://www.cdc.gov/NIOSH>, the Mine Safety and Health Administration (MSHA) at <http://www.msha.gov/TRAINING/LIBRARY/BureauofMines.htm>, and the US Office of Surface Mining (OSM) at <http://www.wrcc.osmre.gov/glas> may have some publications available through their digital libraries. The USGS also lists some sources for Bureau publications at http://www.usgs.gov/faq/list_faq_by_category/get_answer.asp?id=324.

This page intentionally left blank

CHAPTER 17

Smoldering Combustion Phenomena and Coal Fires



Smoldering charcoal briquettes. The glowing surface of the particles is where the combustion reaction is taking place and the resulting gray ash accumulates. *Photo by J.B. Nielsen, Public Domain, Wikimedia Commons, 2009.*

CHAPTER CONTENTS

17.1 Smoldering and Coal Combustion

- Introduction
- Overall Characteristics
- Structure of a Smoldering Front
- Smoldering-Coal Fires
- Smoldering Wildfires
- Acknowledgments
- Important Terms
- References
- WWW Addresses:
Additional Reading



17.1. Smoldering and Coal Combustion

Guillermo Rein

Smoldering charcoal briquettes.

Photo by J.B. Nielsen, Public Domain, Wikimedia Commons, 2009.

Introduction

Smoldering fires are rare events at the local scale but occur regularly at a global scale. Once ignited, they are particularly difficult to extinguish despite extensive rains or firefighting attempts and persist for long periods of time, spreading over extensive areas and deep into the ground. Smoldering subsurface fires in coal deposits are the longest continuously burning fires on Earth and pose significant economic, social, and environmental threats (Stracher and Taylor, 2004). A hypothetical smoldering-coal fire and suppression attempts are shown in Figure 17.1.1. Geologists are not alone in their study of smoldering fires; these are a hazard of importance to several other scientific disciplines (Rein, 2009). Ecologists and forest scientists study smoldering wildfires because they destroy large amounts of biomass and cause greater damage to the soil ecosystem than flaming fires (Frandsen, 1997). Atmospheric scientists have studied acute pollution episodes caused by the Indonesian **peat** fires in 1997 and the destruction of vast amounts of stored carbon in the soil (Page et al., 2002). In the realm of **fire safety engineering**, smoldering is an important threat because it is the leading cause of deaths in residential fires and causes economics losses of the order of \$350 million per year in property damage in the United States alone (Hall, 2007).

Smoldering is a slow, low-temperature, flameless form of combustion of a solid fuel (Ohlemiller, 2002). Whereas flaming combustion has been widely studied and is the aim of hundreds of papers per year, smoldering combustion has received very little attention. Combustion and fire scientists were the first to research the topic in the 1950s. The first widely available scientific work of merit on the topic was published in 1957 (Palmer, 1957). Palmer's seminal work consisted of a collection of observations from simple experiments involving burning piles of dust. This pioneering work was followed by research on dust, fibrous materials, polymeric foams, cigarettes, polyurethane foam, and cellulose. It is only in the last decade that smoldering phenomena has been studied significantly by other scientific fields such as geology, ecology, and atmospheric sciences.

This chapter attempts to synthesize a comprehensive view of smoldering combustion bringing together contributions from other scientific disciplines. For an in-depth review, the reader is referred to the work of Ohlemiller (1985), which today still stands as the only review of the fundamental scientific concepts behind smoldering combustion. A more recent and general review on smoldering phenomena was carried out by Rein (2009), upon which this chapter is based.

Overall Characteristics

Smoldering is a fundamental combustion problem involving **heterogeneous chemical reactions** and the transport of heat, mass, and momentum in the gas and solid phases. The cover of this chapter shows a most familiar example smoldering-charcoal briquettes.

The fundamental difference between smoldering and **flaming combustion** is that, in the former, the **oxidation reaction** and the heat released occur on the solid surface of the fuel or porous matrix and, in the latter, these occur

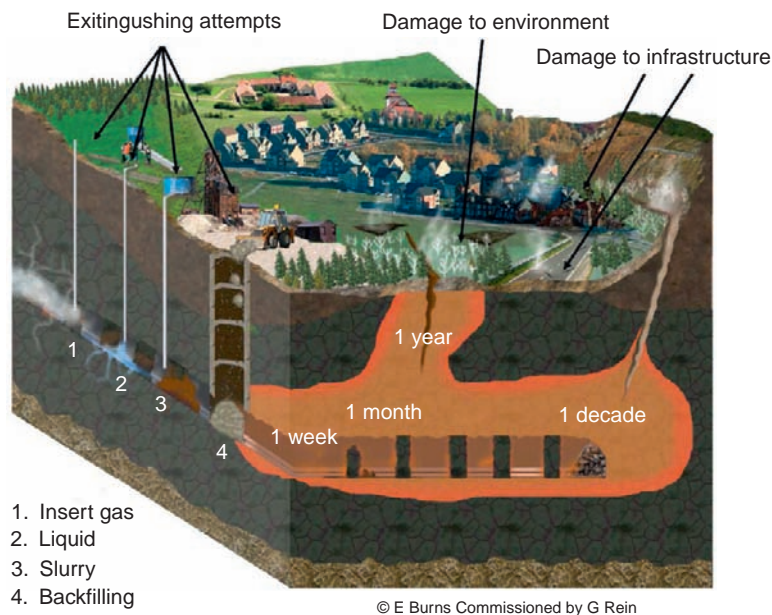


Figure 17.1.1. Artistic rendition of a smoldering fire that began in an abandoned coal mine and subsequently spread. Fire-fighting efforts (left) are ineffective because the fire was not accurately located. The vertical mine shaft is being backfilled to prevent the ingress of oxygen. Hypothetical damage to the forest and buildings is shown. Illustration by Emma Burns, 2008; commissioned by Guillermo Rein, 2008, University of Edinburgh (Rein, 2009).

in the gas phase surrounding the fuel (i.e., the flame). Figure 17.1.2 shows the two burning regimes for forest fuels. The characteristic temperature, spread rate, and heat released during smoldering are low compared to those in the flaming combustion of a solid. Typical values in smoldering at ambient conditions are around 500–1000°C for the peak temperature and 6–12 kJ/g for the average heat of combustion; whereas typical values during flaming are around 1500–1800°C and 16–30 kJ/g, respectively. Because of these characteristics, smoldering propagates at creeping velocities, typically around 10–30 mm/hour, approximately two orders of magnitude lower than the velocity of typical flame-spread.

Because of its low temperature, smoldering is characteristically an incomplete oxidation reaction and thus emits a mixture of unburned fuel, toxic, asphyxiant, and irritant gases and particulates at a higher yield than flaming fires. It favors CO₂ to CO ratios around 1 (as opposed to ratios around 10 in flaming combustion), so CO is an important toxic factor in smoldering fires (Purser, 2002; Rein et al., 2009).

Porous material as in coal piles or fractured coal seams are susceptible to smoldering combustion. The porous nature of coal pile allows air to feed the exothermic reaction while protecting the reaction zone from **heat losses** to the surroundings. But many other solid materials can sustain a smoldering reaction, including cotton, tobacco, dust, paper, peat, duff and humus, wood, board of organic fibers, synthetic foams, and charring polymers including foams. Smoldering fuels are characterized by having a significantly greater characteristic **thermal time** than fine fuels but allow oxygen transport to the surface. These characteristics lead to the slow but persistent burning typical of smoldering combustion. In general terms, a smoldering fuel consists of an aggregate and permeable medium formed by particulates, grains, fibers, or a porous matrix. These aggregate fuel elements facilitate the surface reaction with oxygen by providing a large surface area per unit volume.

It is well established that the two limiting factors in smoldering propagation are the oxidizer flow to, and the heat losses from, the reaction zone. Thus, porous organic materials foster propagation because they act as thermal insulation that reduce heat loss but, at the same time, permit oxygen transport to the reaction sites by **convection** and **diffusion**. Smoldering ignition requires the supply of heat flux to the solid fuel. The subsequent temperature increase of the solid first sets off the thermal degradation reactions (mainly **pyrolysis**) and then oxidations, until the net heat released by oxidation is high enough to balance the heat required for propagation. This net heat released by the reactions is partially transferred by **conduction**, convection, and **radiation** ahead of the



Figure 17.1.2. Photo of the two regimes of combustion of solid fuels: flaming grass on top of peat and smouldering peat. The flame is about 10 mm high. Photo by Guillermo Rein, 2006 (Rein et al., 2008).

reaction and partially lost to the environment. The oxidizer is transported to the reaction zone by diffusion and convection, in turn feeding the oxidation reactions. Once ignition occurs, the reaction advances gradually through the material.

The transition from smouldering to flaming fires is of concern in coal mines and when subsurface fires reach the free surface. This transition is a spontaneous gas-phase ignition supported by the smolder reaction which acts both as the source of gaseous fuel (pyrolysate, CO, etc.) and of heat to carry the reaction. The transition occurs when critical conditions inside the pores of the solid are met, triggering the onset of gas-phase reactions (flaming). These conditions include the flammability of the gas mixture inside the pores and a net excess of heat released by strong solid-phase oxidation reactions. Increased levels of oxygen and airflow (e.g., caused by wind) can strongly influence transition. But currently understanding of the process is rather limited.

When studying smouldering propagation through the interior of combustible materials, it is common to consider the simpler one-dimensional process and to classify it in two main configurations: opposed and forward propagation. These are defined according to the direction in which the smolder reaction propagates relative to the oxidizer flow. Figure 17.1.3 shows the two one-dimensional configurations. In opposed smolder, the reaction front

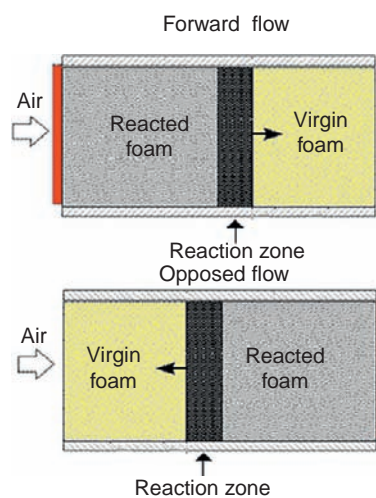


Figure 17.1.3. Configurations in one-dimensional smoldering; forward, and opposed. Illustration by Guillermo Rein, 2005 (Rein et al., 2006).

propagates in the direction opposite to the oxidizer flow, and in forward smolder, the front propagates in the same direction.

These two configurations are distinguished by the roles played by heat and mass transport mechanisms and chemical reactions. In forward propagation, the oxygen flows through the **char**, reacts at the smolder zone and then the oxygen-depleted gas flow continues through the virgin fuel. Convective heat transport is towards the virgin fuel ahead and results in preheating. In opposed propagation, the oxygen flows through the virgin fuel and reacts at the smolder zone. Then the oxygen-depleted gas flow travels through the burned region where char is. Convective transport is toward the burned fuel left behind the front, reducing the preheating of the fuel.

Structure of a Smoldering Front

When a smoldering front has been initiated and is propagating laterally, generally speaking, there are four discernable regions propagating. As one moves toward the front from unburned fuel, these are:

1. Preheating of the undisturbed fuel: heat from the reacting front is transported ahead preheating the fuel up to temperatures where water evaporation takes place. This front does not emit gases in any significant quantity.
2. Evaporation: this endothermic reaction occurs at a significant rate within the range of temperatures from ~80 to 100°C, emitting water vapor. In this front the mass loss depends on the moisture content.
3. Burning region: this front is where the pyrolysis and oxidation reactions take place and net heat is released. Pyrolysis reaction absorbs heat and converts the fuel into volatile gases, polyaromatic hydrocarbons, CO, CO₂, and water vapor. It leaves behind a solid carbonaceous **char** or **coke**. Pyrolysis starts approximately at temperatures above 200–250°C. Subsequent heating above this temperature increases the pyrolysis rate if fuel is available. Pyrolysis is stronger at deeper layers of the fuel where oxygen transport is reduced and thus oxidation rate is lower. The oxidation involves the exothermic reaction of the fuel left by the pyrolysis front. The peak temperature is found in this region and is where most of the fuel mass is lost. This reaction overlaps with the pyrolysis depending on the propagation mode and oxygen availability. The oxidation reaction occurs at temperatures over 300°C and is the main source of CO and CO₂. More CO₂ is formed where the oxygen supply is large (e.g., closer to the oxygen supply or free surface) and more CO where it is limited (e.g., further from the oxygen supply or deeper into the fuel layers).
4. Char and ash region: this is where the smoldering has ceased and the remaining matter cools to ambient temperature. The ash left is the mineral content present in the original fuel and the char or coke is the result of incomplete burning.

The propagation rate of self-sustained smoldering is typically controlled by oxygen transport and net heat losses. Yet, heterogeneous chemical kinetics governs the front structure and dictates the effective value of the global heat released. The degradation of a solid fuel involves multiple pathways to chemical changes (pyrolysis and oxidation), and these pathways are not yet fully understood. In spite of the complex kinetic behavior, experimental evidence suggests that mechanisms consisting of only a few global reactions capture the most important characteristics of the decomposition process. The polymers for which smoldering kinetics are best known are cellulose (Kashiwagi and Nambu, 1992) and polyurethane foam (Rein et al., 2006).

In forward smoldering propagation, the oxidation and the pyrolysis reactions form two distinct propagating fronts. The pyrolysis front arrives first to the virgin foam and then followed by the oxidation front. This is in agreement with experimental measurements of forward propagation where two distinct fronts are observed in the temperature profiles. In opposed smoldering, the oxidation and the pyrolysis reactions overlap to form a single propagating front. This is also in agreement with experimental observations in opposed propagation where a single front is observed in the temperature profiles.

Figure 17.1.4 shows the one-dimensional representation of a smoldering front in a fuel rod and the approximate correspondence with a burning cigarette (one of the most common examples of smoldering). As shown by the results in Figure 17.1.4 for forward smoldering, the pyrolysis front is located at the leading edge of the cigarette burning front since it does not need oxygen to permeate into the solid. The oxidation reaction takes place at the

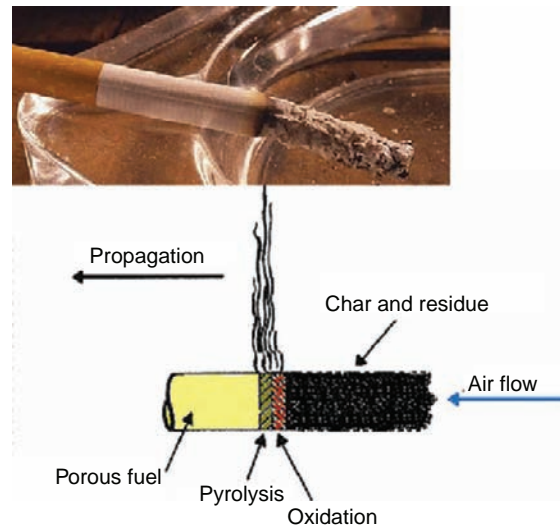


Figure 17.1.4. Structure of a one-dimensional reaction front in forward smoldering, correlated with a burning cigarette. Photo and illustration by Guillermo Rein, 2006 (Rein, 2009).

trailing edge of the burning cigarette, where the oxygen supply is available from the surrounding environment, and the heat released is transferred ahead of the front into the virgin fuel and pyrolysis front to drive the propagation.

Smoldering-Coal Fires

Smoldering fires of coal can burn in shallow or deep fronts. Each has different dynamics. A shallow front burns near the free surface and is open to the atmosphere, thus having large supplies of oxygen available but exposed to convective heat losses. A deep subsurface fire burns many meters below the ground, and thus has a limited supply of oxygen but is insulated from heat losses to the atmosphere.

The primary three controlling mechanisms of subsurface smoldering fires are the net fuel load, the flow of oxygen, and the heat losses. The net fuel load is dictated by the amount of carbon content per unit volume and enhances ignition and spread. Thus the water and inert contents hinder spread. Porosity affects the bulk density and this in turn affects the process. In general, the larger the bulk density the lower is the spread rate and the higher the temperature. The oxygen transport enhances the spread. In porous coal beds, it is predominantly by diffusion and dictated by the distance to a free surface and the permeability of the medium. Porous beds of lower flow permeability offer larger transport rates of oxygen. The presence of cracks or channels increases the transport of oxygen to feed the smoldering front and thus results in higher spread rates and temperatures. Coal fires are fed by small quantities of air flowing through fractured strata, cracks, natural networks, openings, or mines shafts and galleries, which permit oxygen to circulate to the subsurface. The heat losses hinder the spread. These are predominantly by water evaporation and heat conduction.

The reduced heat losses of underground coal deposits, together with the high fuel availability and the small oxidizer flows, promote long-term smoldering combustion and allow for creeping but extensive propagation both in depth and in area. These fires prove difficult to be detected and frustrate most efforts to be extinguished. Little technical research has been undertaken on the subject and as a result, the understanding of how to tackle these fires is very limited (Hadden and Rein, 2010).

The effects of smoldering fires on the landscape can range from small areas (pockets of burning in superficial layers), to large areas (burning of a hilltop). The changes to the soil and rocks produced by smoldering fires are driven by two factors: the loss of mass and the enhanced heating. Mass loss at surface layers leads to enhanced

erosion, and loss at deeper layers leads to potential structural collapse. Overhangs, holes in the ground, and pan-shaped voids are commonly produced and can lead to local subsidence. Smoldering fires lead to enhanced heat transfer to the soil for much longer durations, that is, temperatures above 400°C for residence times longer than one hour (Rein et al., 2008). This induces sterilization and chemical changes in the surrounding materials.

Smoldering Wildfires

Smoldering fires of the forest floor are in general better documented than coal fires, and much can be learnt from reviewing this information. Forest fuels prone to smolder during wildfires can be divided in two categories, thick fuels and organic soils. Natural thick fuels are stumps, snags, downed logs, large branches, and roots. Organic soils are humus, duff, and **peat**. Smoldering does not have the visual impact of the forest flaming fires but is nonetheless an important factor in wildfires and in the subsequent damage to the forest. By propagating below the surface, smoldering fires offer the means for flaming combustion to reestablish during wildfires in unexpected locations (e.g., across a fire break) and at unexpected times (e.g., long after burn out of the flaming front). These fires represent a large contributor to biomass consumption and a significant source of combustion emissions to the atmosphere.

The largest peat fires registered to date took place in Indonesia during the El Niño dry season of 1997 and lasted for several months, destroying over 2.44 million ha of peat (Page et al., 2002). The smoky haze covered large parts of Southeast Asia for weeks, disrupting shipping and aviation and causing large economic losses, long-term damage to the environment, and health-care problems. It has been estimated that the 1997 Indonesia fires alone released between 0.8 and 2.6 Gton of carbon emissions into the atmosphere, equivalent to 13–40% of the global fossil fuel emissions for that year (Page et al., 2002).

A recent case of a smoldering fire causing damage to the landscape and the ecosystem is a wildfire that occurred in a 40-year-old, 15 ha plantation of lodge pole pines at Rothiemurchus, near Aviemore, Scotland, during July 2006 (Rein et al., 2008). The flaming fire was extinguished by the fire service within 3 days, but the peat underneath the forest continued to burn for more than 40 days despite the occasional rains (Figure 17.1.5). To stop the spread, the fire service dug a firebreak trench 5 m wide and 0.5–2 m deep at the perimeter of the burning areas to remove the peat and expose the mineral soil. Figure 17.1.5 shows photographs of adjacent forest stands after the fire. While the flaming fire scorched the trees up to 1 m from the floor and consumed some of the grass, the smoldering fire burned the peat up to depths of 0.5–1 m removing large quantities of the soil.



Figure 17.1.5. Photographs illustrating adjacent forest stands in the July 2006 Rothiemurchus peat fire, Scotland, UK (Rein et al., 2008). In this forest, the peat is 0.5–2 m deep. Burning involved flames for 3 days and smoldering for 6 weeks. Stand (left) not affected by the fire, showing trees growing in a peat layer covered with grass. Stand (right) of tree trunks charred by flames. After the grass burned off, smoldering fire burned off about 0.5 m of peat, leaving roots exposed. The roots might extend into a soil horizon beneath the peat. Regardless, the entire stand fell over about three weeks later, when winds picked up. The horizontal field of view in each photo is about 6 m. Photos by Guillermo Rein, 2006.

Acknowledgments

I am grateful to Carlos Fernandez-Pello (University of California, Berkeley) and Jose Torero (University of Edinburgh) for our important discussions about smoldering combustion. Thanks also to Rory Hadden (University of Edinburgh) for providing so much insight about smoldering coal. In addition, I thank Albert Simeoni (University of Corsica) and Ali Rangwala (Worcester Polytechnic Institute) for their review of this chapter.

Important Terms

Char	Carbon-rich porous solid material that remains after volatile gases, pyrolysis gas, and tar are released from an organic material.
Coke	Carbon-rich solid residue that forms from the heating of coal.
Conduction	Transfer of thermal energy in a mass or between masses at different temperatures.
Convection	Transport of heat and mass by motion of currents in a fluid (gas or liquid).
Diffusion	Transport of heat and mass from a region of higher concentration to one of lower concentration by random molecular motion.
Fire safety engineering	The application of science and engineering principles to protect people and artificial as well as natural environments from the destructive effects of fire and smoke.
Flaming combustion	An exothermic oxidation reaction that takes place in the gas phase, resulting in high-temperature gases. These gases could be hot enough to radiate their own light and thus the flame would be visible to the naked eye.
Heat loss	Energy transferred away from a system via conduction, convection, and radiation.
Heterogeneous chemical reactions	Reactions taking place at the interface between two or more phases, that is, between a solid and a gas, a liquid and a gas, or a solid and a liquid.
Oxidation reaction	A reaction in which an element loses electrons; an example is the combustion reaction of carbon with oxygen to form carbon dioxide and the subsequent release of energy.
Peat	The accumulation in the soil of partially decayed vegetation, especially in wetlands. Under proper conditions, peat will turn into lignite coal over geologic of time.
Pyrolysis	Chemical decomposition of a solid- or liquid-organic substance by heating that occurs spontaneously at high temperatures. The process produces gases and liquids and leaves a carbonaceous solid residue.
Radiation	Transport of heat by electromagnetic waves emitted by one body; that travel through space until absorbed by another body.
Smoldering	The slow, low-temperature, flameless combustion of a solid fuel.
Thermal time	Characteristic time that it takes for a thermal effect to travel from the surface to the core of a fuel particle.

References

- Frandsen, W.H., 1997. Ignition probability of organic soils. *Can. J. Forest. Res.* 27, 1471–1477.
- Hadden, R., Rein, G., 2010, Burning and suppression of smoldering coal fires, coal and peat fires, a global perspective, Vol 1, Chapter 18, pp. 319–327.
- Hall, J.R., 2007, The smoking-material fire problem. Fire Analysis and Research Division, National Fire Protection Association, Quincy, MA, [http://www.nfpa.org/assets/files// PDF/OS.SmokingMaterials.pdf](http://www.nfpa.org/assets/files//PDF/OS.SmokingMaterials.pdf) (accessed October, 2009).

- Kashiwagi, T., Nambu, H., 1992. Global kinetic constants for thermal oxidative degradation of a cellulosic paper. *Combust. Flame* 88, 345–368.
- Ohlemiller, T.J., 1985. Modeling of smoldering combustion propagation. *Prog. Energy Combust. Sci.* 11, 277–310.
- Ohlemiller, T.J., 2002. Smoldering combustion. In: Beyler, C.L., Custer, R.L.P., Walton, W.D., Watts, J.M., Drysdale, D., Hall, J.R., Jr., Dinunno, P.J. (Eds.), *SFPE Handbook of Fire Protection Engineering*, third ed. National Fire Protection Association, Quincy, MA, pp. 2.200–2.210.
- Page, S.E., Siegert, F., Rieley, J.O., Boehm, H.-D.V., Jaya, A., Limin, S., 2002. The amount of carbon released from peat and forest fires in Indonesia during 1997. *Nature* 420, 61–65.
- Palmer, K.N., 1957. Smoldering combustion in dusts and fibrous materials. *Combust. Flame* 1, 129–154.
- Purser, D.A., 2002. Toxicity assessment of combustion products. In: Beyler, C.L., Custer, R.L.P., Walton, W.D., Watts, J.M., Drysdale, D., Hall, J.R., Jr., Dinunno, P.J. (Eds.), *SFPE Handbook of Fire Protection Engineering*, third ed. National Fire Protection Association, Quincy, MA, pp. 2.83–2.171.
- Rein, G., 2009. Smoldering combustion phenomena in science and technology. *Int. Rev. Chem. Eng.* 1 (1), 3–18, <http://hdl.handle.net/1842/2678> (accessed October 2009).
- Rein, G., Cleaver, N., Ashton, C., Pironi, P., Torero, J.L., 2008. The severity of smoldering peat fires and damage to the forest soil. *Catena* 74, 304–309.
- Rein, G., Cohen, S., Simeoni, A., 2009. Carbon emissions from smoldering peat in shallow and strong fronts. *Proc. Combust. Inst.* 32, 2489–2496.
- Rein, G., Lautenberger, C., Fernandez-Pello, A.C., Torero, J.L., Urban, D.L., 2006. Application of genetic algorithms and thermogravimetry to determine the kinetics of polyurethane foam in smoldering combustion. *Combust. Flame* 146, 95–108.
- Stracher, G.B., Taylor, T.P., 2004. Coal fires burning out of control around the world: thermodynamic recipe for environmental catastrophe. In Stracher, G.B. (Ed.), *Coal Fires Burning around the World: a Global Catastrophe*. *Int. J. Coal Geol.* 59 (1–2), 7–17.

WWW Addresses: Additional Reading

- (1) **BRE Centre for Fire Safety Engineering, University of Edinburgh**
<http://www.see.ed.ac.uk/fire>

This page intentionally left blank

CHAPTER 18

Burning and Water Suppression of Smoldering Coal Fires in Small-Scale Laboratory Experiments



Small scale apparatus developed to study the burning characteristics and suppression of smoldering coal. *Photo by Rory Hadden, 2009.*

CHAPTER CONTENTS

18.1 Burning and Suppression Experiments

- Introduction
- Suppression of Smoldering Coal Fires
- Small-Scale Experimental Work
- Conclusions
- Acknowledgments
- Important Terms
- References
- WWW Addresses: Additional Reading



18.1. Burning and Suppression Experiments

Rory Hadden
Guillermo Rein

Small-scale apparatus developed to study the burning characteristics and suppression of smoldering coal

Photo by Rory Hadden, BRE Centre for Fire Safety Engineering, University of Edinburgh, 2009.

Introduction

Understanding the burning and suppression behavior of subsurface coal fires is essential if these fires are going to be monitored and extinguished in a scientific and cost effective manner. In this chapter, small-scale experiments are presented in which the burning and suppression behavior of **smoldering** coal is studied.

The laboratory experiments presented here are undertaken at a small scale (0.1 m). Some in-situ large scale experiments are reported in detail in Chapter 16 (Kim, 2010). The advantage of reducing the scale and the scope of the problem by studying suppression in the laboratory is that most of the complexities of in-situ experiments such as locating and mapping the fire, and the delivery of the **suppression agent** to the fire seat are eliminated. Meanwhile, the important variables (fire size, particle size, thermal and flow conditions, etc) can be controlled. The results presented here are only a first step in understanding the suppression of coal fires once they have been detected and located, and the liquid water used as suppression agent has been delivered to the fire seat. Application of the results to larger scales requires field trials.

Subsurface coal fires are driven by smoldering combustion which is defined as a slow, low temperature flameless form of combustion sustained by the heat evolved when oxygen directly attacks the surface of a condensed phase fuel (Ohlemiller, 2002). Therefore, a subsurface coal fire propagates at a low speed governed primarily by the rate at which oxygen can diffuse through the ground to the reaction zone as well as the heat losses from the system and the thermal properties of the coal (Ohlemiller, 2002; Rein, 2009). Material properties such as moisture content, carbon content, heat transfer properties and flow **permeability** are important parameters dictating the ignition and spread of subsurface fires. Typical smoldering temperatures of coal are in the range 700-1000°C and the propagation speed is on the order of 0.1 mm·min⁻¹ (Rein et al., 2008).

However, although the general behavior is known, little experimental work on the combustion behavior of smoldering coal is present in the literature. This knowledge is essential to aid understanding of the phenomena and to prevent future events occurring. This chapter presents research which, for the first time, studies the burning and suppression behavior of smoldering coal in small-scale laboratory experiments.

Suppression of Smoldering Coal Fires

In the United States alone, it is estimated that subsurface coal fires affect over 400 ha and estimated reclamation costs exceed \$42 million (Kim, 2004). Kim (2004) and Colaizzi (2004) show that extinguishing coal fires is a costly, resource intensive procedure which often fails to produce the desired results. Common techniques of suppression often include sealing of the affected area or injection of foams to prevent oxygen ingress thereby **smothering** the fire, injection of inert gas to displace oxygen and water injection to cool the coal. Additional methods such as injection of a cryogenic liquid have been investigated (Kim, 2004) however, the advantages may be outweighed by high cost. All of these methods require long timescales and large quantities of materials. Alternatively, the most successful method to suppress a smoldering fire is the removal of the fuel, though this is

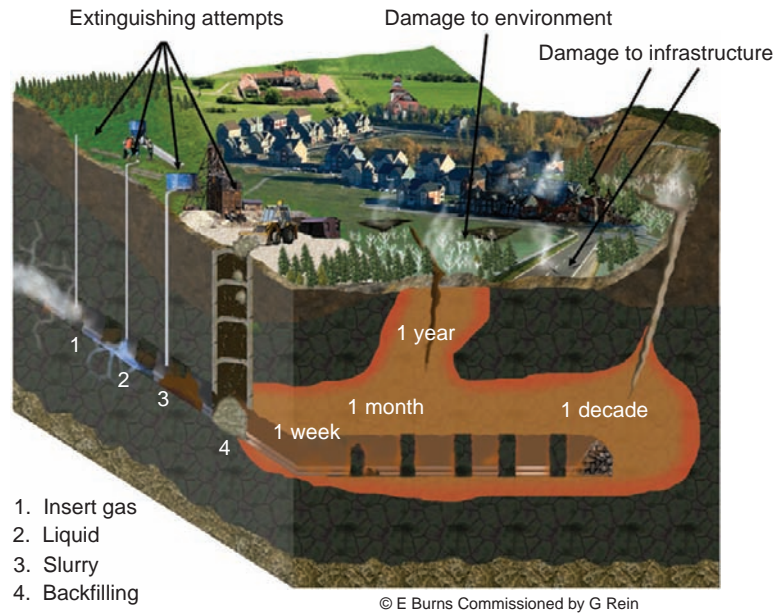


Figure 18.1.1. Artistic impression of a smoldering fire in an abandoned coal mine and illustration of possible fire damage and suppression attempts. Illustration by E. Burns, 2008 (commissioned by G. Rein, University of Edinburgh).

rarely practical because of the large amount of fuel involved in subsurface coal fires. All these methods are reviewed in detail in Chapter 16 (Kim, 2010) and are shown in Figure 18.1.1 which is an artistic representation of a subsurface coal fire including typical damage to the environment and infrastructure. Hypothetical growth of the fire with time is indicated as well as suppression attempts that are: (1) injection of inert gas, (2) injection of liquid, (3) injection of slurry or foam, and (4) sealing of the mine shaft.

In order to understand suppression, it is important to consider the processes that govern the spread of smoldering fires (Chapter 17, Rein (2010)) and how these are disrupted by different suppression methods.

For a smoldering reaction to propagate, a feedback mechanism must be established where the heat released from the reacting fuel is greater than the sum of the heat losses from the reaction zone and the energy required to preheat the surrounding fuel. If the heat balance is altered by increasing heat loss to the surroundings, the rate of spread will decrease and if the losses are increased sufficiently, the smoldering combustion may be quenched.

Increasing the heat losses from the reaction zone can be achieved by introducing a suppression agent to the reaction zone to cool the coal. The thermal properties of the suppression agent such as heat capacity and heat of vaporization play an important role in determining its efficiency. This **forced cooling** is employed in suppression of subsurface coal fires by injecting a suppression agent below the surface and allowing it to penetrate through the ground to the seat of the fire. In order for **forced cooling** to be effective, it is necessary to ensure that the temperature of the coal everywhere in the reaction zone is reduced below the **re-ignition temperature**. The re-ignition temperature is dependent on the coal properties and the geometry and geology of the coal seam but is on the order of 50°C (Kuenzer et al., 2007; Zhang et al., 2007). Given the size of coal seams, this method requires large quantities of the suppression agent and it is challenging to ensure that sufficient quantities reach the seat of the fire as the suppression agent disperses through the subsurface layers. More invasive cooling methods include total or partial flooding of the affected area.

Smothering of the fire exploits the experimental observations by Ohlemiller (2002), Walther et al. (2000), and Palmer (1957), which show that if the concentration of oxygen is reduced below a critical level, the exothermic oxidation reaction will stop and insufficient heat will be released to overcome losses, quenching the reaction. The critical concentration below which a smoldering reaction in coal will not propagate is currently unknown but research indicates it would be around 16% as measured by Belcher et al. (2010) for peat. Smothering can be attempted by covering the area of the fire with a seal or cap (surface sealing) to prevent oxygen ingress from the free surface or displacement of the oxygen surrounding the fire with an inert fluid.

Because oxygen supply has a strong effect on the smoldering spread rate (Belcher et al., 2010; Rein, 2009; Ohlemiller, 2002) and some methods of smothering are cheap compared to other techniques (Kim, 2010), it might be assumed that smothering by oxygen displacement is the most efficient method to suppress the fire. However, the size and thermal properties of coal seams indicates that the short term efficiency of this method is low as detailed below.

Coal seams can be on the order of 100 m in length and 1-10 m thick. Coal has a low thermal conductivity (e.g., $k = 0.13 \text{ W}\cdot\text{m}^{-1}\cdot\text{K}^{-1}$), high density (e.g., $\rho = 1300\text{-}1500 \text{ kg}\cdot\text{m}^{-3}$) and high specific heat capacity (e.g., $C_p = 0.8\text{-}1.6 \text{ kJ}\cdot\text{kg}^{-1}\cdot\text{K}^{-1}$) (Babrauskas, 2003). This results in a system with a high **thermal inertia** which means it has the ability to retain heat for long periods of time. Simple calculations show that a 1 m diameter sphere of coal (equivalent to approximately 5000 kg) will take on the order of one year to cool to from 900°C, a typical peak value for smoldering, to 50°C with an ambient ground temperature of 10°C. For larger coal masses (and taking into account surrounding rock which will also have been heated by the coal combustion), natural cooling will take longer. Therefore in order for smothering to be effective, oxygen must be excluded from the reaction zone for extended periods of time. It is thought that poorly maintained exclusion methods will fail within 1-3 years (Kim, 2004). For these reasons, smothering is a long-term, secondary approach to suppress subsurface fires.

Suppression by forced cooling, the objective of this paper, could offer results in shorter time scales and with potentially higher efficiency. As this is the first time that experiments of this nature with smoldering coal have been conducted in the laboratory, the findings are intended to be a first step into the topic. Extrapolation of these results to larger field scale requires further research and a larger effort especially in understanding the subsurface distribution of the suppression agent. However, results at the small scale are required before understanding at the large scale is possible.

Small-Scale Experimental Work

Apparatus

The tests were conducted in a $100 \times 100 \times 100 \text{ mm}^3$ box constructed from insulating board and open at the top. Coal samples occupy all the free volume of the box. A U-shaped electrical heater of length 290 mm is introduced on one side of the sample as an ignition source. The setup is based on that of (Rein et al., 2008) for studying peat fires. Opposite the heater, a window measuring $95 \times 30 \text{ mm}^2$ is created on the wall while the bottom has 25 holes of diameter 6 mm. The purpose of these was to allow air flow through the coal sample to assist combustion. K-type **thermocouples** were placed at 7 locations in the sample: one on the heater and six spaced in three rows of two thermocouples at distances 20, 50, and 80 mm from the igniter at a depth of 50 mm. Figure 18.1.2 shows the

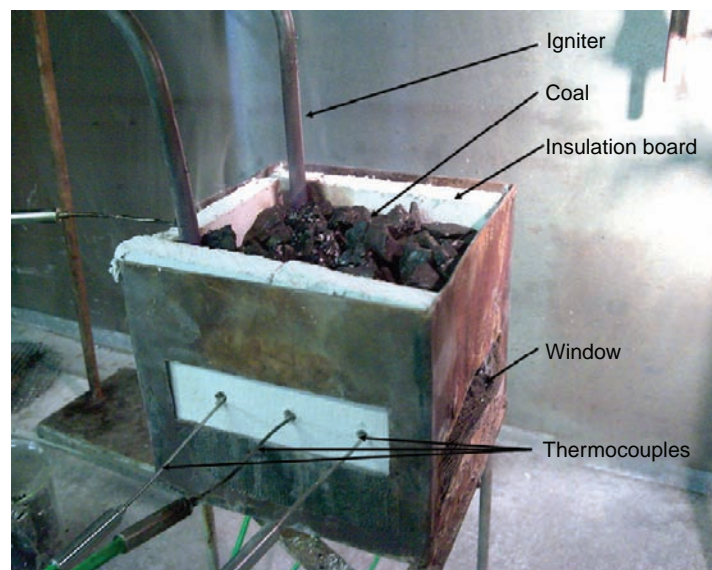


Figure 18.1.2. Image of the experimental apparatus.

experimental set-up. The temperature traces were used to infer ignition, propagation rate, smoldering temperature, oxygen dependence, and extinguishing characteristics.

The coal used in these experiments was Premium House Coal an anthracitic coal sourced from CPL Distribution, UK. The true density was measured to be $1200 \pm 3\% \text{ kg}\cdot\text{m}^{-3}$.

The ignition protocol consisted of supplying the heater with a power of approximately 80 W for 150 minutes. This protocol was chosen as a strong ignition source minimizes sensitivity of the results to the ignition protocol and allows ignition across a wide range of particle sizes.

The ignition and suppression experiments were undertaken as a function of the particle size of the coal. The original coal particles were broken and sorted by measuring the longest side of the pieces. The particle size ranges studied were $7 \pm 3 \text{ mm}$, $10 \pm 5 \text{ mm}$, $15 \pm 5 \text{ mm}$, $20 \pm 5 \text{ mm}$, $30 \pm 5 \text{ mm}$, $30 \pm 10 \text{ mm}$, $35 \pm 5 \text{ mm}$, and $45 \pm 5 \text{ mm}$. Void fraction was measured as the “free volume” i.e. the volume not occupied by coal divided by the total volume of the box, by filling a known volume with coal then using water to fill the voids to the same level. The volume of water required is the void fraction. The void fractions for the samples studied ranged from 54% to 61%.

Base Experiment

Before the experimental series is conducted, it is necessary to define an experimental protocol capable of providing a repeatable smoldering fire. This led to the definition of the ignition protocol presented above. In order to ensure the suppression results were independent of the ignition protocol used, the smoldering fire was allowed to develop for a further 150 minutes after ignition before extinction was attempted. In this time, the fire was observed to have spread throughout the entire sample mass prior to commencing the suppression.

Figure 18.1.3 shows the thermocouple traces and mass loss for a smoldering reaction carried out in the apparatus using 30 mm particles. The ignition, steady burning and suppression regimes can be seen.

The temperature profile near the igniter is seen to be governed by the heat applied by the igniter until approximately 120 minutes into the experiment where the sudden change in gradient indicates ignition in this region. The reaction is then seen to propagate away from the igniter and the front reaches the thermocouple at 20 mm at 150 minutes, 50 mm at 200 minutes, and 80 mm at 250 minutes. The spread of a strong smoldering front to 80 mm away from the igniter after it has been switched off indicates that the fire is self-sustaining. The maximum temperature observed was 840°C at 290 minutes into the experiment. The spread rate can be calculated using the average temperatures in each location and the distance between them. The average spread rate for 30 mm particles is $0.11 \pm 0.3 \text{ mm}\cdot\text{min}^{-1}$. At 300 minutes, the suppression is started and the temperatures decrease rapidly.

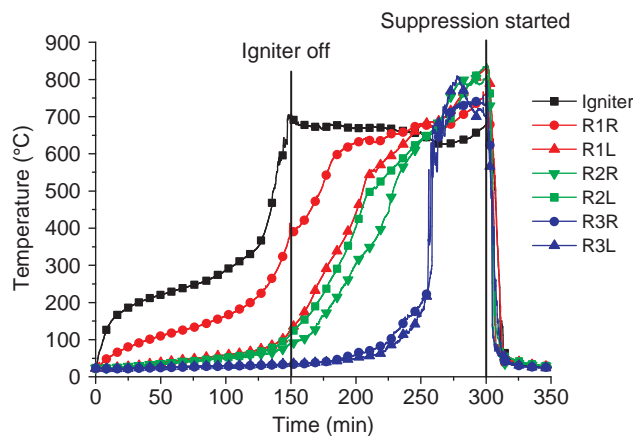


Figure 18.1.3. Temperature measurements vs. time for different locations in the sample. Base experiment for coal particles of mean diameter 30 mm and suppression with a water spray. Black line is the igniter temperature, the red, green and blue lines are temperatures 20, 50 and 80 mm from the igniter respectively.

Ignition and Propagation Experiments

The effect of particle size on the ignition and propagation dynamics was investigated. Particle size affects the porosity of the coal bed, the bed flow permeability, the effective thermal conductivity and the surface area available for the heterogeneous reactions. Figure 18.1.4 shows the time to ignition for samples of different particle size. Ignition is deemed to occur when temperatures measured 50 mm from the igniter exceed those at 20 mm from the igniter. This criterion was chosen as it is independent of heat transfer effects from to the igniter and infers a chemical reaction with net heat release has been established. It can be seen in Figure 18.1.4 that the ignition time decreases from 180 minutes for particles of 15 mm to 140 minutes for particles of 30 mm in size, but then begins to increase as heat transfer to the larger coal becomes more significant up to 220 minutes for particles of 45 mm. It was not possible to ignite particles smaller than 7 mm in the time scale of these experiments (150 minutes) due to the low flow permeability of the bed which prevents sufficient oxygen flow. Particles larger than 45 mm had a very high thermal inertia and poor contact with the heater, which prevented ignition in this time scale. This suggests that for small particles, the reaction is limited by oxygen flow through the bed and for larger particles, heat transfer to the coal plays an important role in the ignition.

The maximum smoldering temperature was observed to be constant for particles larger than 15 mm with temperatures in the range 720 - 930°C. Lower temperatures observed for smaller particles suggest that the lower flow permeability for fine particles significantly hinders the intensity of the fire.

Suppression Experiments

Three suppression mechanisms were considered to study their effectiveness: single point injection, shower, and spray. Water was used as the extinguishing agent. The single point injection was a pipe buried 10 mm below the surface of the sample. Water was allowed to flow freely through the pipe into the coal. The shower was generated by allowing water to flow through holes of 4 mm diameter in the bottom of a liquid reservoir and the spray was generated using a hand operated atomizer. The water flow rates of each method are $75 \text{ ml}\cdot\text{s}^{-1}$, $10 \text{ ml}\cdot\text{s}^{-1}$, and $2 \text{ ml}\cdot\text{s}^{-1}$, respectively.

The fire was deemed extinguished when all the temperature measurements in the box were below 50°C , since this is below the self ignition temperature found by Kuenzer et al. (2007) and Zhang et al. (2007). Measurements of the amount of water required for suppression were made by measuring the time for the application of each and multiplying by the flowrate. The run-off generated was collected and measured immediately after extinguishing. Run-off gives an indication of efficiency as large values mean that more water has to be applied to achieve the same extinguishing effect. A method which results in low run-off will therefore be more efficient.

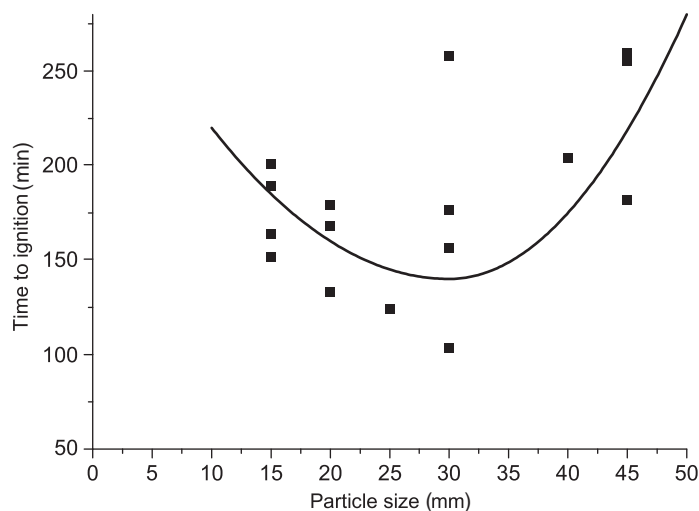


Figure 18.1.4. Experimentally observed relationship between time to ignition and particle size.

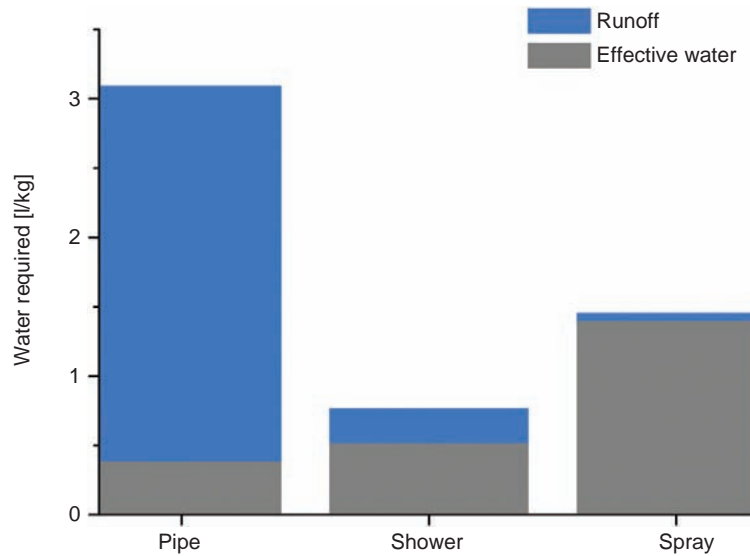


Figure 18.1.5. Comparison of suppression methods showing effective or absorbed water (grey) and run-off (blue) for coal particles with a 30 mm diameter.

The results of water required and run-off for each suppression method can be seen in Figure 18.1.5. The most efficient method with respect to total water required is the shower however, using a spray results in less water run-off and better control of the flow. The injection pipe is significantly less efficient requiring three times more water than a spray of which more than 80% is lost as run-off.

The reason for the poor performance of the injection pipe is due to channeling of the liquid through the coal bed, which was observed in the experiments. The channeling arises when the majority of the water takes the same flow path through the bed. The result of this is that there is little global evaporation as the contact surface area between the water and the coal is small; resulting in poor heat transfer. This coupled with a low residence time of water results in large quantities of water being required.

The shower reduces this problem by applying the water over a larger area. This results in the coal being cooled more uniformly and the generation of steam occurs throughout the bed to displace oxygen. However, the large volumetric flow rate results in high liquid velocities through the bed, which again results in channeling, larger run-off, and poor control of the flow. Using the spray allows greater control of the water application and more uniform application across the free surface of the coal. It is believed that it is the good distribution of water over the coal surface and subsequent slow flow through the bed that leads to the enhanced suppression properties of the spray and not the droplet form of the water which plays a smaller role.

Effect of Particle Size on Suppression

Figure 18.1.6 shows the amount of water required using a spray to extinguish the small-scale smoldering fires. The water required is expressed per unit mass of burning coal, assuming that the entire bed is burning at the time suppression is attempted. This is a good assumption confirmed by visual observation and temperature measurements in all experiments. The trend suggests that the amount of water per mass of coal decreases with particle size and levels off for larger particles.

The volume of water per unit mass of burning coal required to extinguish a smoldering fire is in the range from 1 to 2 l·kg⁻¹. A figure larger than this could be required in field-scale fires to account for the water lost due to the complex flow path through the subsurface and cooling of surrounding rock.

Using the thermal properties of coal and water and the average temperature at the time of suppression, the theoretical quantity of water required per mass of burning coal can be estimated by equation 18.1.1, where m_w is the mass of water required, m_c is the mass of coal undergoing combustion, $C_{p,c}$ is the specific heat capacity of coal, ΔT_c is the temperature difference between the average coal temperature at the time of suppression and the

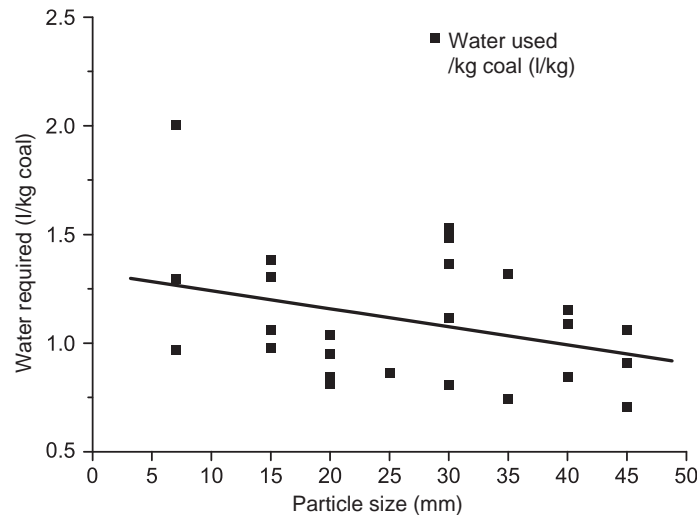


Figure 18.1.6. Experimentally observed relationship between water required for suppression per burning coal mass vs. particle size using a spray.

extinguished coal, T_w is the initial temperature of the water, and $C_{p,w}$ and λ are the specific and latent heats of water, respectively.

$$m_w = \frac{m_c C_{p,c} \Delta T_c}{C_{p,w}(100 - T_w) + \lambda} \quad (18.1.1)$$

The amount of water required is found to be approximately $0.5 \text{ l}\cdot\text{kg}^{-1}$. This is the same order of magnitude as the experimental results. The difference can be attributed to the effect of heterogeneous heat transfer, fluid flow and adsorption of water by the coal.

Conclusions

The small-scale combustion and suppression behavior of smoldering coal has been studied in the laboratory. The smolder reaction was characterized by maximum temperatures of $700\text{--}1000^\circ\text{C}$, which were seen to be independent of particle size for particle larger than 15 mm . Time to ignition showed a minimum for particles around 30 mm in diameter, with larger particles requiring longer times due to limited heat transfer from the igniter to the fuel. Smaller particles were limited by oxygen transport through the coal.

Water was identified as an effective extinguishing agent and was used in small-scale tests. The extinguishing of subsurface fires is dictated by the ability of the delivery method to reach the source of the fire. It was shown that in small-scale tests, significant differences in extinguishing efficiency can arise due to the nature of the extinguishing-agent application. Water was used because, as shown, the overall quantity of extinguishing agent required is large and therefore cost must be kept low. The amount of water required was measured to be on the order of 1 to 2 liters of water per kg of burning coal.

Additional work is required to determine the effects of scale on the reaction. Especially important is determining a relationship which will allow the extrapolation of data from small-scale experiments to applications involving subsurface coal fires in the field.

Acknowledgments

The assistance of José Garcia, Freddy Jarvis, and Wolfram Jahn in undertaking the experiments is appreciated. Conversations with José Torero were enlightening and added to the depth of this chapter. The Engineering and Physical Sciences Research Council, International Fire Investigators and Consultants, and the Small Grants scheme

at the University of Edinburgh are acknowledged for providing financial support for this project. A preliminary version of this work was presented at the Second International Conference on Coal Fire Research organized by the Sino-German Coal Fire Research Initiative, Berlin, 2010.

Important Terms

Forced cooling	The application of a suppression agent to cool smoldering coal.
Permeability	The ability of a porous material to allow a fluid to flow through it.
Re-ignition temperature	The temperature below which coal must be cooled in order to suppress a fire. It depends on the composition and thermal properties of the coal as well as the surrounding rock.
Smoldering	A slow and low temperature form of combustion where oxygen directly attacks the surface of a solid fuel.
Smothering	The suppression of a fire by preventing the flow of oxygen.
Suppression agent	A material used in suppressing a fire.
Thermal inertia	A measure of the responsiveness of a material to changes in temperature.
Thermocouples	Electronic devices used to measure temperature.

References

- Babrauskas, V. (2003), *Ignition Handbook*, first edition: Issaquah, Washington, Fire Science Publishers, Fire Science and Technology, Inc.
- Belcher, C.M., Hadden, R., McElwain, J.C. and Rein, G., 2010, Fuelling the palaeoatmospheric oxygen debate: how much atmospheric oxygen is required for ignition and propagation of smoldering fires?: *Geophysical Research Abstracts*, v. 12, EGU2010-6334.
- Colaizzi, G.J., 2004. Prevention, control and/or extinguishment of coal seam fires using cellular Grout, *in* Stracher, G. B., ed., *Coal Fires Burning around the World: a Global Catastrophe: Int. J. Coal Geol.*, v. 59, issues 1–2, p. 75–81.
- Kim, A.G., 2004. Cryogenic injection to control a coal waste bank fire, *in* Stracher, G.B., ed., *Coal Fires Burning around the World: a Global Catastrophe: Int. J. Coal Geol.*, v. 59, issues 1–2, p. 63–73.
- Kim, A.G., 2010, United States Bureau of Mines—Study and Control of Fires in Abandoned Mines and Waste Banks, *in* Stracher, G.B., Prakash, A., and Sokol, E.V., eds., *Coal and Peat Fires: A Global Perspective: Elsevier, the Netherlands, Chapter 16, Volume 1.*
- Kuenzer, C., Zhang, J., Tetzlaff, A., van Dijk, P., Voigt, S., Mehl, H., and Wagner, W., 2007, Uncontrolled coal fires and their environmental impacts: Investigating two arid mining regions in north-central china: *Applied Geography*, v. 27, no. 1, p. 42–62.
- Ohlemiller, T.J., 2002, Smoldering combustion *in* Beyler, C.L., Custer, R.L.P., Walton, W.D., Watts, J.M., Drysdale, D., Hall, J.R. Jr., and Dinunno, P.J., eds., *SFPE Handbook of Fire Protection Engineering*, 3rd ed.: Quincy, Massachusetts, National Fire Protection Association, p. 2.200–2.210
- Palmer, K.N., 1957, Smoldering combustion in dusts and fibrous materials: *Combustion and Flame* 1, p. 129–154.
- Rein, G., 2009. Smoldering combustion phenomena in science and technology: *International Review of Chemical Engineering*, v. 1, p. 3-18, <http://www.era.lib.ed.ac.uk/handle/1842/2678> (accessed November, 2009).
- Rein, G., 2010, Combustion Phenomena and Coal Fires, *in* Stracher, G.B., Prakash, A., and Sokol, E.V., eds., *Coal and Peat Fires: A Global Perspective: the Netherlands, Elsevier, Chapter 17, Volume 1.*
- Rein, G., Cleaver, N., Ashton, C., Pironi, P., and Torero, J.L., 2008, The severity of smoldering peat fires and damage to the forest soil: *Catena*, v. 74, p. 304-309.
- Walther, D.C., Anthenien, R.A., and Fernandez-Pello, A.C., 2000, Smolder ignition of polyurethane foam: effect of oxygen concentration: *Fire Safety Journal*, v. 34, no. 4, p. 343–359.
- Zhang, J., Kuenzer, C., Tetzlaff, A., Oertel, D., Zhukov, B., and Wagner, W., 2007, Thermal characteristics of coal fires 2: Results of measurements on simulated coal fires: *Journal of Applied Geophysics*, v. 63, issues 3-4, p. 135–147.

WWW Addresses: Additional Reading

- (1) **BRE Center for Fire Safety Engineering, University of Edinburgh**
<http://www.eng.ed.ac.uk/fire>

CHAPTER 19

Modern-Foam-Injection Technology for Extinguishing Coal Fires



Compressed-nitrogen foam used to extinguish an underground coal fire at the Buchanan No. 1 Mine, Clay Pool Hill, Virginia. A pressure-relief bore hole in the photo is releasing compressed-nitrogen foam from a foam-filled mine cavity (gob and entries). This bore hole was located ~914 m horizontally from the original injection bore hole, at a depth of ~884 m. *Photo by Mark Cummins, 2007.*

CHAPTER CONTENTS

19.1 Modern-Foam-Injection Technology

- Introduction
- New Method of Foam Generation
- Experimental Fires
- Fire Science
- Compressed Foam
- Quality Control
- New Developments
- What the Future Holds
- The Grand Finale
- Important Terms
- References
- WWW Addresses: Additional Reading



Photo by Mark Cummins, 2007.

19.1. Modern-Foam-Injection Technology

Lisa LaFosse'
Mark Cummins

Brown 79 493 L (21 000 gallon) frac (fracturing tanks) installed at the Buchanan No. 1 Mine; used for mixing water with firefighting foam to extinguishing this underground coal-mine fire.

Introduction

In the past, there have been several traditional methods for extinguishing coal mine fires. Two of these methods used, digging out the refuse and quenching with water until cooled, or drilling bore holes in the fire zone and injecting a foamed grout, or mud slurry have not been very successful. The method of drilling bore holes to inject a mud like slurry is not entirely successful because the slurry is heavy and peaks out, not fully reaching the 'ceiling' or all areas of the void where the combustion has burned. Then the slurry dries and cools, it shrinks and cracks allowing new air to come into the combustion zone to reignite the fire. The method of digging out and soaking has left many sub-surface fires out of the reach because for every cubic foot of burning material dug out, there is a hole that is generated that needs to be filled with clean material and a pile that needs to be extinguished, which makes digging out a fire that lay several hundred to several thousand feet below the surface, impractical.

The federal Surface Mining Control and Reclamation Act (SMCRA) started regulating all coal mining August 3, 1977, and designated coal fires that were burning before 1977 were considered 'historical'.

In the 1980s there were several experiments using a new foam-generating method that enabled a much safer and more effective way to fight the **subterranean** fires by use of bore holes from the surface, drilled into the area of the mine cavities and areas of combustion.

This new foam technique was different from earlier attempts to use highly **aerated foam**, which was called "high-expansion foam." The high-expansion foam was generated by a fan blowing air into a device with a foaming agent mixed with water, similar to dish washing soap, sprayed onto a screen, which created massive amounts of bubbles that were supposed to absorb the heat and block **ventilation** of fresh air coming into the mine.

This high-expansion foam (developed in the early 1900's) had several faults. One of the faults of this type of foam system was that it had to be brought into the burning mine and set up as close to the fire as possible. In most cases this is impossible, due to the heat and toxic gases that fill the burning mine. High-expansion foam or blown foam, as it is sometimes called, cannot be pushed through a hose, pipe or bore holes because of **back pressures** causing the foam to back up into the fan. Another problem was that high-expansion foam contained a lot of air and oxygen and the bubbles were very large and fragile. These fragile bubbles burst immediately when they came in contact with smoke and heat, releasing the oxygen in the bubble into the combustion area. This generally fed the fire, instead of extinguishing it.

An interesting fact about water-based foam is that the water in the thin film of the bubbles is composed of hydrogen and oxygen molecules (H_2O). When the thin film of the large bubbles comes in contact with extreme heat, the hydrogen and oxygen can be separated back into their elemental forms, where hydrogen is a fuel and oxygen in the presence of heat completes the old fire triangle. This is a reason the compressed-foam method of generating very small, and very durable bubbles (more like shaving cream), has proven to be far more effective than the high expansion foam generators in extinguishing super heated fires.

New Method of Foam Generation

The new method of generating compressed foam, developed by Mark Cummins, in the early 1970's is very simple and reliable. The reason this method of foam generation is superior to other standard techniques and other fire suppressant materials, cooling materials, swelling clays; sand grout mixtures, water slurry mixtures; liquid nitrogen fluxion; alternate pumping of water and sand, **inert** gas, injection, simple backfilling is for the simple reason, that generating compressed foam has many variables that can be changed. Compressing the foam gives us the ability to change its properties to be a heavy, solid and dense, material to a light and fragile bubble. It was discovered that pumping a foamable solution of dishwashing detergent mixed with water into a common "T" fitting, where the second inlet of the "T" was connected to an air compressor, where the soapy water and compressed air mixed in the "T." This mixture was then discharged into a fire hose that lead to a bore hole that was drilled from the surface down into the burning coal mine. It was discovered that the friction inside of the fire hose and pipe caused intense mixing and compression of the foam.

An interesting phenomenon of the compressed-foam technique was that the soapy bubbles that cling to the inside of the hose, act like little ball bearings and caused a **laminar flow** of fast moving foam in the core of the hose. This fast moving stream in the center of the hose has practically no friction loss and is able to be pumped through extremely long hose lays or long pipelines, without deterioration. In fact, the further the foam goes, the better it becomes.

Experimental Fires

One of our early firefighting experiments occurred in the early 1980s in cooperation with the US Bureau of Mines, Kentucky. This taught us a valuable lesson. We drilled a single bore hole into an old historical coal-mine fire. We began pumping compressed foam in the bore hole and shortly after the first volume of wet foam went into the combustion area; we saw a great steam column exploding from around the bore hole. Mark thought he could see the ground bulging and several trees leaning away from the bore hole. We immediately reduced the water content which produced very dry foam that looked like shaving cream. This insulated the bore hole, and the steam was reduced to a manageable release. Additional bore holes were drilled to ventilate the confined, poorly ventilated area in the mine to relieve the steam buildup. There were several other experiments conducted in cooperation with the US Bureau of Mines, until the agency was terminated. Some of the experiments were published, but sadly, much of the knowledge gained by those valuable experiments was shelved, or lost.

We used the compressed-foam-injection method to extinguish a hidden source of ignition in an active coal mine, the Pinnacle Mine near Pineville, West Virginia (Hookham, 2004). Between August 31 and September 7, 2003 a series of explosions occurred in the active longwall district of the Pinnacle Mine. Carbon monoxide readings in the bleeder entries of the active longwall district indicated that there was a small but active fire at an unknown location. From the surface, the operator began drilling holes into the longwall to detect the heat source. **National Institute for Occupational Safety and Health (NIOSH)** used **transducers** lowered into the mine to detect pressure changes. These transducers were able to locate with pin point accuracy the position of an explosion as it happened. This was the perfect opportunity to use compressed foam in this area.

We used nitrogen to inflate the foam in order to prevent any oxygen from being injected into the area of the ignition source, and began pumping operations to fill the areas with nitrogen foam. We had two complete nitrogen membrane systems and pumped two bore holes simultaneously. At each site, the foam was batch mixed at 1 or 2% in four 79 493 L (21 000 gallon) frac (fracturing) tanks (Figure 19.1.1) and pumped into the mine using a 21.2 m³ (750 ft³) per minute **nitrogen membrane separation unit**. The foam was pumped at an average rate of about 18 927 L (5000 gallons of expanded nitrogen foam) per minute for 9 days. In total, ~68 million liters (18 million gallons) of nitrogen foam was pumped into the mine. After the foam injection, the monitoring systems indicated the mine was safe to reestablish complete coal production.

At another very large coal-mine fire in Virginia, we used the same compressed-nitrogen method to inject over 2650 million liters (700 million gallons) of compressed-air foam and compressed-nitrogen foam to displace carbon monoxide and toxic gasses out of the mine and into a **gas recovery system** which had the capability of separating



Figure 19.1.1. Extinguishing coal-mine fires: (A) truck transporter used to carry frac (fracturing) tanks to the job site; (B) typical 79 493 L (21 000 gallon) frac tanks (brown tanks, left side of photo) installed at the Buchanan No. 1 Mine in Clay Pool Hill near Oakwood, Virginia. About 275 gallons of foam concentrate was first pumped into each tank before the tanks were filled with mine or creek water. The foam thoroughly mixes with the water as the tank is filled. The mixing produces a foam head at the top of the tank, but there is little waste—see the photo just before the introduction to this chapter. Photos by Mark Cummins, 2007. Figure B by Lisa LaFosse.

the methane from the toxic gasses, and used the methane for commercial applications. Quoting from Chemguard and Specialty Chemicals (2007): “Mansfield, Texas, September 17, 2007—Chemguard chemists developed specialized Class A foam for use in a Virginia mine shut down by high carbon monoxide (CO) levels. Formulated for compressed air foam systems (CAFS), the Class A foam concentrate can shorten recovery time and cut costs in toxic gases dissipation and fire-fighting operations in subsurface environments.

Chemguard produced the **gas-displacement** foam at the request of CAFSCO, a Joshua, Texas, firm that specializes in the use of **compressed air foam systems (CAFS)** for fire protection and control and for management of chemical, medical, and industrial pollution. CAFSCO had been engaged by the mine owners in July after a roof fall had released CO into the working area of the mine, closing the mine and entombing millions of dollars of equipment.

Rather than inject massive amounts of nitrogen into the mine to dilute the CO, an effective but time-consuming and expensive undertaking, CAFSCO developed a nitrogen-foam-injection plan that would reduce the volume of costly nitrogen and improve the dissipation rate. Because it is a semi-solid, Chemguard’s nitrogen-enhanced foam would displace the toxic gasses while slowly releasing conservative amounts of nitrogen, maintaining dilution in the foamed areas of the mine. Because of its penetrating and wetting characteristics, the foam would saturate the interior of the mine from floor to ceiling, entering all cracks and crevices, effectively soaking out all sources of ignition.”

Today, there are new reasons to reactivate and further develop the subterranean firefighting technology. The concern about global warming and the prediction of fossil-fuel depletion has brought about new applications for the compressed-foam technology.

Mark Cummins, the pioneer of the CAFS that was used by the US Bureau of Mines, in the early 1980s, has partnered with Lisa LaFosse’. Together, they have created a Texas based coal-mine firefighting company, called CAFSCO.

The Foam Engineers at CAFSCO use the earlier method of generating compressed foam and is developing new methods to apply the foam for coal-mine fire fighting, environmental protection, and other applications. Experience has taught us that the quality of the foam has a direct effect on its ability to accomplish multiple objectives. We can change the chemical composition of the foaming agents to cause the foam to soak and saturate into the water repellant coal dust and coal formations. Another type of chemical will cause the foam to soak into the water-repellant ash created by the combustion of coal. With the use of compressed foam, and the ability to change the chemical composition we have leaned the importance of studying the fire behavior of coal-mine fires, closer. The combustion of coal leaves an ash blanket which covers much of the raw coal that is involved in the combustion process. This ash blanket insulates the combustion area from the open environment of the mine, and reduces the

ability of ventilation with inert gasses to extinguish the fire. This is why nitrogen or CO₂ gas **inertization** techniques require extremely long and expensive application time to cause any reduction to the deep seated combustion. The wetting ability of the compressed foam is essential to soak and saturate the ash, in order to reach and cool the combustion area.

Fire Science

Fire science teaches us that any surface that is wet with water cannot be hotter than the boiling temperature of the water, which is roughly 212 °F. This temperature is very important in coal-mine firefighting, because coal must be hotter than 212 °F to **pyrolyze** or degrade by heat into volatile gasses, which burn. In other words, if it is wet, it will not burn.

Compressed Foam

Inert gasses cannot wet the coal, like compressed foam does. When we use an inert gas to inflate the compressed foam, we create an inert foam. When the water drains out of the foam and the bubbles burst, the inert gas is released into the surrounding atmosphere. This helps to smother the fire by diluting the oxygen. The water that drains out of the foam wets the coal and cools the fuel below the fire gas distillation temperature of 212 °F.

The compressed foam can be modified with the chemical stabilizers which will cause the foam to become even more durable. This allows the foam to build upon itself, as the stream from the bore hole continues to inject more foam. The pressure in the bore hole will begin to rise as it fills the mine from floor to ceiling. This is also known as “**roofing out**.” As the pressure rises from the foam pushing against the foam filled cavity, this pressure forces the foam into cracks, crevices, and fissures that can lead off in all directions. These cracks, crevices, and fissures are very hard to extinguish and can be hidden ignition sources that can come to life weeks or months after extinguishing efforts have ceased. Additional bore holes are drilled to provide pressure relief and we often see foam coming out of nearby bore holes, which gives us the ability to monitor the direction and progress of the foam in the mine. We then extend the discharge hose to the relief holes that become the “new” injection sites.

Quality Control

We have developed an essential quality control program for the foam. This quality control program assures we produce the right foam for the right purpose. Our quality control program is designed to test every batch of chemical to be certain there have been no mistakes in the chemical compositions or mixing ratios. Mistakes can produce weak or inferior foam. Weak or inferior foam cannot accomplish the planned results. For additional quality control, we add a simple connection to our well head adaptor with a valve that can be opened at any time to see the quality of the foam being injected into the mine (Figure 19.1.1). This sometimes presents a new problem of how to dispose of all the test foam we have accumulated on the surface. The problem is not generally a serious one, but involves our employees playing in the foam on their break time.

New Developments

CAFSCO is developing new ways to use encapsulated CO₂. The CO₂ will be captured from the source of combustion which causes global warming such as electric power generators and other fossil-fuel combustion processes. The CO₂ foam can then be used to extinguish deep seated coal-mine fires. The carbon encapsulated foam can be permanently stored in the subterranean cavities. The CO₂ gas is heavier than air and will gravitate to the lowest part of the cavity. The water and foamable agent that drains from the CO₂ foam will also gravitate to the lowest part of the subterranean cavity where it will be pumped back to the surface where it will be recycled to continue the creation of the new CO₂ foam.

The simplicity of the compressed-foam system allows us to use other chemicals and products such as waste fly ash, and bottom ash created by the electric power companies that burn coal. This fly ash and bottom ash can be mixed with water to produce a foamable slurry that can be turned into compressed foam and injected into the burned out areas, thereby creating structurally sound, solid blocks of waste material to prevent **subsidence** and damage to homes and

businesses that have been undermined. The fly ash and bottom ash will be treated with the pH balancing chemicals, when the slurry is turned into foam, to help neutralize acid water drainage caused by the previous coal-mine fire.

What the Future Holds

Looking forward, we designed a method to capture the CO₂ created by all coal-mine fires and prevent this global-warming gas from entering the atmosphere. With this method, we will use the compressed foam as a transport medium to inject the CO₂ back into the burning coal mine. After the coal-mine fire has been extinguished, we will capture CO₂ from other sources and continue to use CO₂ foam to displace methane gasses that will accumulate in the upper areas near the roof of the coal mine. The methane gas is 20 times more global warming than CO₂. We will drill bore holes into the areas where the methane collects and use the methane gas to power local electric generators to produce renewable energy. We will capture the CO₂ produced by the electric generators, and recycle this CO₂ to produce CO₂ foam, and inject it back into the mine from which it came from. This then gives us a way to generate power and prevent coal-mine CO₂ and methane from being released into the earth's atmosphere. We have acquired a patent pending for this process.

Our plans are to use the advanced methods of CO₂ capture and to use the CO₂ as a fire extinguishing gas encapsulated in the foam to be injected into the coal-mine fires in China, which are emitting CO₂ greenhouse gasses, equal to 50–100% of the total volume of all car and truck emissions released in the United States (Furchtgott-Roth, 2008).

In short, we will use the CO₂ being produced by China burning coal mines, to generate the foam, and extinguish the fire. The cavities created by the fire will be used to permanently sequester the CO₂ foam.

The Grand Finale

After we have extinguished all of the world's coal-mine fires, and gasoline has reached \$10.00 dollars a liter, we will add methane generating microbes to our foamable solution and continue injecting a special formula of foam into the coal mines to create a microbial biosphere that produces an endless source of inexpensive methane gas to power the world Mother Natures way!

Important Terms

aerated foam

back pressure

compressed air foam systems (CAFS)

gas recovery system

gas-displacement

inert

inertization

laminar flow

National Institute for Occupational Safety and Health (NIOSH)

nitrogen

nitrogen membrane separation unit

pyrolyze

roofing out

subsidence

subterranean

transducers

ventilation

References

Chemguard and Specialty Chemicals, 2007. Chemguard Gas-Displacement Foam Dilutes CO in Virginia Mine, Mansfield, Texas: Chemguard, <http://www.chemguard.com/about-us/news/2007/chemguard-gas-displacement-foam.htm> (accessed September 24, 2008).

Cummins Industries Corporation Texas based company 1990–2009.

Furchtgott-Roth, D., 2008, The wrong fire. *New York Sun* (July 13).

Hookham, M., 2004. New multi-class foam suppresses fire. *International Longwall News* (March 1), Leederville, Western Australia http://www.cafsc.com/Longwall_News_Article.pdf (accessed September 23, 2008).

WWW Addresses: Additional Reading

- (1) **CAFSCO Nitrogen Foam and Compressed Air Foam**
<http://www.CAFSCO.com>
- (2) **U.S. Patent 4457375**
http://www.cafSCO.com/US4457375_Cummins.pdf
- (3) **U.S. Patent 4318443**
http://www.cafSCO.com/US4318443_Cummins.pdf
- (4) **Chemguard Specialty Chemicals and Equipment**
<http://www.chemguard.com/about-us/news/2007/chemguard-gas-displacement-foam.htm>
- (5) **Nitrogen Foam at the Pinnacle Mine Fire**
<http://www.cdc.gov/niosh/mining/pubs/pdfs/tuone.pdf>
- (6) **The New York Sun: The Wrong Fire**
<http://www.nysun.com/opinion/wrong-fire/58374>
- (7) **The Post-Gazette: Underground Coal Fires**
<http://www.post-gazette.com/healthscience/20030215coalenviro4p4.asp>

This page intentionally left blank

Author Index

A

Adamus, A. 87, 99
Affölter, R.H. 24
Agarwal, P.K. 60–61
Agramonte, J. 65, 78
Agricola, G. 64, 78
Akgün, F. 48, 61
Allardice, D.J. 60–61
Allen, R.G. 251
Altaner, S.P. 25
Alvarado, B. 64, 78
Alvarez, R. 104, 110
Ames, M.R. 27
Anderson, M. 251
Anderson, P.B. 152
Andrup-Henriksen, G. 222, 227
Annegam, H.J. 100, 124, 170
Anthenien, R.A. 325
Anthony, J.W. 103, 110
Arana, P.P. 65, 78
Arisoy, A. 60–61
Ashley, G.H. 5, 24
Ashton, C. 315, 325
Asmar, I. 99
Atkinson, T. 60, 62

B

Babrauskas, V. 320, 325
Bakker, P. 223, 227
Bakker, W.H. 251
Bandhopadhyay, T.K. 251
Banerjee, D.D. 56, 61
Banerjee, S.C. 17, 24, 56, 61
Barakat, M.A. 79
Barghoorn, E.S. 2, 24
Barnes, J.H. 124, 152, 228
Baroffio, J.R. 28
Barratt, P.A. 100
Barry, J.M. 257, 265
Bartels, L.M. 256–257, 265
Barwick, L. 124
Bates, A.L. 99, 151
Baumgartner, F.R. 256–257, 265
Bayles, L.G. 295, 295*f*, 302
Beamish, B.B. 60–61
Beccq, G. 25
Beier, K. 228
Belcher, C.M. 319–320, 325
Belkin, H.E. 99, 111, 123, 151
Bell, F.G. 85, 87–88, 88*f*, 89, 89*f*, 90, 90*f*, 93–94, 95*f*, 97*f*, 99
Bench, B.M. 26
Bennett, A.J.R. 5, 24
Berry, J.M. 258, 265
Berthelote, A.R. 226–228, 245–246, 246*f*, 250–251
Bhat, S. 60–62
Bhattacharya, A. 170
Bhattacharya, K.K. 60–61
Bialecki, R. 62
Bideaux, R.A. 110
Biek, R.F. 212, 213*f*, 217
Black, P.M. 26, 124, 217
Blake, D.R. 100, 124, 152, 170, 227, 251
Blake, M. 170

Blazak, D.G. 60–61
Blazek, C. 39, 44
Bloomquist, R. 76
Blumenthal, W.B. 73, 79
Boehm, H.-D.V. 315
Boehm, P.D. 207
Bostick, N.H. 218
Bouchardon, J.-L. 124
Boussafir, M. 25
Bowen, S. 65, 79
Bowler, J.M. 75, 79
Bragg, W.L. 170–171, 169
Brennan, R. 25, 302
Broecker, W.S. 256–257, 265
Brondi'zio, E. 251
Brooks, W.E. 64–65, 65*f*, 67–69, 70*t*, 72*t*, 74–75, 74*f*, 76*f*, 79–80
Brownfield, I.K. 12, 24
Brownfield, M.E. 12, 24
Bruhn, R.W. 21, 24, 37, 42, 44
Buch, J.W. 36, 44
Bullock, S.E.T. 87, 89, 99
Bunnell, J.E. 111, 151
Burger, H.R. 216
Burger, R.L. 65, 79
Burgess, D.S. 304
Burnham, A.K. 10, 25
Bustin, R.M. 55, 61
Butler, R.F. 214, 217

C

Calas, G. 165, 169
Caley, E.R. 66, 79
Cameron, A.R. 27, 61
Campell, J.B. 232, 250
Cao, Y. 9, 25
Carras, J.N. 247, 250
Carrascal, R. 64–65, 74, 79
Caslavsky, M. 27
Cassells, C.J.S. 105, 110, 229, 245, 250
Cassidy, S.M. 2, 25, 28, 64, 75, 79
Castanova, V. 99
Cathcart, J.D. 24
Cavaroc, V.V. 6, 25
Chaiken, R.F. 8*f*, 16*f*, 17–20, 18*f*, 21*f*, 22, 22*f*, 25–26, 40–41, 45, 224, 227–228, 272*t*, 273–275, 274*f*, 274*t*, 275*f*, 276*f*, 276*f*, 278*f*, 279, 281, 281*f*, 284*f*, 285*f*, 287, 287*f*, 290–291, 291*f*, 292*f*, 292*f*, 293, 294*f*, 295, 295*f*, 296, 296*f*, 297–298, 302–304
Chakrabarty, G. 17, 24
Chakravorty, R.N. 60–61
Chalier, J. 124
Chamberlain, E.A.C. 104, 110
Chandra, D. 60–62
Chatterjee, R.S. 165, 170
Chattopadhyay, S. 100
Che, J. 27
Chen, L.D. 242, 250
Chesnokov, B.V. 120–121, 123
Chipman, J.W. 251
Chlupacova, M. 171
Christanis, K. 62
Christie, W.A.K. 104–105, 110
Chun, Y.C. 218

- Church, D.J. 227
 Chvojka, R. 217
 Cinnirella, S. 124
 Cisowski, S.M. 210, 214, 217
 Clark, B.H. 214, 217
 Clawson, M. 259, 265
 Cleaver, N. 315, 325
 Clemente, C. 110
 Cleveland, C.J. 119*f*, 124
 Clifford, D.J. 6–7, 25
 Coates, D. 26
 Coates, D.A. 85, 100, 102, 110, 118, 123, 210, 217
 Cohen, K.K. 289, 291*f*, 302
 Cohen, S. 315
 Colaizzi, G.J. 21, 25, 297, 303, 325
 Colbert, E.H. 5, 26
 Cole, D.I. 141–142, 151
 Coleman, A. 207
 Collins, W. 108–110
 Colman, J.J. 130
 Conant, J. 257, 265
 Connor, J.J. 73, 79
 Conrad, G.W. 65, 79
 Cook, A. 9, 25
 Cook, B.J. 88, 99
 Coolbaugh, M.F. 251
 Cooper, G. 10, 25
 Copard, Y. 8, 25
 Corgan, J.A. 36, 44
 Cosca, M.A. 214–215, 217
 Cox, C.B. 257, 265
 Cracknell, A.P. 100
 Craddock, P.T. 68, 79
 Craig, A.K. 80
 Craig, J.R. 66–67, 73, 79
 Criddle, A.J. 123
 Crowley, S.S. 28
 Crowther, J. 215, 217
 Culhane, P.J. 263, 265
 Custer, E.S., Jr. 45
- D**
 Dadhwal, V.K. 170
 Dalla T. M. 10, 25
 Dalverny, L.E. 17, 25, 279, 281, 283, 285, 286*f*, 287–289, 289*f*,
 291*f*, 293, 295–296, 302–304
 Damberger, H.H. 9, 25
 Daniels, E.J. 9, 25
 Daulay, B. 9, 25
 Davis, A. 25, 62
 Davis, J.D. 303
 Day, S.J. 250
 de Boer, C.B. 214–217
 De La Cruz, H. 99
 Dehn, J. 250
 Dekkers, M.J. 217
 DeKok, D. 42, 44, 103, 107, 110, 118, 123, 143, 151, 275, 303
 Demir, I. 25
 Deul, M. 269*f*, 280*f*, 303
 Diamond, W.P. 26
 Diaz, A. 65, 78
 Didari, V. 60, 62
 Dierks, H.A. 223–227
 Diessel, C.F.K. 55, 58*t*, 59*t*, 61–62
 Dinunno, P.J. 315, 325
 Disnar, J.R. 25
 Divers, E.F. 302, 304
 Dokoupilova, P. 159, 170
 Dolbear, G.E. 44
 Donnelly, L.J. 84*f*, 87–90, 88*f*, 89*f*, 90*f*, 91*f*, 92*f*, 92*t*, 93–95, 93*f*,
 94*f*, 95*f*, 99
 Donner, D.L. 15, 22, 27, 272–273, 304
 Douglas, D.S. 174–175, 207
 Downey, W.F., Jr. 111, 124, 152
 Doyle, M. 170
 Doyle, W.S. 18, 25, 45
 Drysdale, D. 315, 325
 Dulong, F.T. 218
 Dunin-Borkowski, E. 64–65, 79
 Dunkl, I. 27
 Dunn, P.J. 120–121, 123
 Dutta, M. 251
 Dvorak, Z. 171
 Dwornik, E.J. 80, 151
- E**
 Easby, D.T. 66, 79
 Eavenson, H.H. 15, 25, 45
 Edmunds, W.E. 4, 4*f*, 25
 Edwards, H.G.M. 170
 Ehrlich, D. 243, 251
 Elachi, C. 232, 250
 Elder, J.L. 278, 303
 Ellis, W.C. 140–141, 152
 Ellyett, C.D. 222–225, 228
 Emsbo-Mattingly, S.D. 122–123, 173–208, 183*f*, 185*t*, 187*f*
 Engle, M. 251
 Ephraim G. Squier. 79
 Epstein, S. 80
 Ernst, W.G. 25
 Escudero, J. 64, 79
 Essene, E.J. 217
 Esterle, J.S. 62
 Evans, D.G. 60–61
 Evans, D.L. 112, 251
 Eneva, M. 251
 Evrard, O. 170
- F**
 Falcon, R.M. 60–61
 Feiler, J.J. 297, 303
 Feinstein, S. 217
 Feng, X. 124
 Fern, J.C. 6, 25
 Fernandez-Pello, A.C. 315, 325
 Ferris, F.G. 156*f*, 158–159, 170
 Feuchtwanger, T.F. 227
 Fielding, E.J. 112, 251
 Finkelman, R.B. 27
 Finkelman, R.B. 16, 25, 68–69, 73, 79–80, 85, 87, 99–100, 106,
 111, 116*t*, 117*f*, 118, 121–124, 137–138, 140–143, 151–152,
 218
 Finkelman, R.B. 100
 Fisher, W. 222, 226–228
 Fleisher, C. 124
 Fleming, A.D. 222–225, 228
 Fletcher, J.D. 69, 79
 Flores, D. 62
 Foit, F.F., Jr. 214, 217
 Foord, E.E. 151
 Foster, G. 80
 Fowler, P. 9, 25
 Francis, W. 7*t*, 8, 25
 Franco, D. 80
 Francois, M. 170
 Frandsen, W.H. 308, 314
 Franklin, G.A. 257, 263, 265
 Freese, B. 45, 75, 79

- Friedli, H.R. 124
 Fuller, M. 210, 214, 217
 Furchtgott-Roth, D. 332
 Fu-zhen, Z. 228
- G**
- Gaines, R.V. 141–142, 151
 Gangopadhyay, P.K. 108*f*, 109*f*, 165, 170, 220, 226, 228, 247, 250
 Gaofeng, K. 228
 Gay, S.P.J. 210, 217
 Gayer, R.A. 9, 25–26, 56, 62
 Geissinger, J. 103, 107, 111, 143, 151
 Geissman, J.W. 217
 Geldart, L.P. 218
 Genderen, J.L. van. 27, 105, 110, 112, 124, 228–229, 237, 247, 250–252
 Gens, R. 237, 247, 250–251
 Gentzis, T. 56, 62
 Geptner, A.R. 158–159, 170
 Ghosh, R. 90, 100
 Ghosh, S.K. 61
 Gielisch, H. 215, 217, 225, 227–228
 Giraudon, J.F. 25
 Glover, L. 106–107, 111
 Goldhaber, M.B. 26
 Golding, S.D. 27
 Gomes, S. 160*t*, 170
 Gómez-Limón, D. 110
 Gong, J. 250–251
 Gonzalez, M.A. 212, 213*f*, 217
 Goodarzi, F. 56, 62
 Gornyi, V.I. 100
 Gorte, B.G.H. 251
 Gouws, M.J. 62
 Grandy, D.W. 14, 27
 Gray, R.E. 85, 87, 100, 304
 Greene, G.W. 223–228
 Grieve, D.A. 61
 Griffin, J.R. 152
 Griffith, F.E. 268, 271, 303
 Gril, J. 80
 Grootenboer, J. 227
 Gross, S. 210, 218
 Gross, S.S. 297, 303–304
 Guan, H.Y. 27, 112, 124, 251–252
 Guha, A. 165, 170
 Güney, M. 60, 62
 Gunn, R.D. 62
 Gunn, R.G. 62
 Gupta, R.P. 15, 25, 27, 90, 100, 105–109, 111–112, 143, 151, 232, 236, 242–243, 243*f*, 251–252
 Gurmendi, A.C. 79
 Guy, B. 124
- H**
- Hack, J.T. 64, 79
 Hackley, P.C. 64, 79
 Hadden, R. 312, 314, 318, 325
 Hadsell, F.A. 211–212, 212*f*, 217
 Haefner, B.D. 304
 Hagemann, H.W. 55, 57*t*, 62
 Hall, D.A. 104, 111
 Hall, D.K. 251
 Hall, J.R. Jr. 308, 314–315, 325
 Hamilton, G.R. 60–61
 Han, Z. 10, 25
 Hansen, L.C. 280, 303
 Hansen, M.C. 31
 Hardoy, J.E. 65, 79
- Harrison, M.J. 56, 62
 Harrison, R. 257, 265
 Harvey, A.H. 227–228
 Hasbrouck, W.P. 211–212, 212*f*, 217
 Hasenhuettl, C. 27
 Hatch, J.R. 26
 Hatcher, P.G. 6–7, 25
 Hatherton, T. 217
 Hawley, B.W. 210, 217
 Hawley, G.G. 136–137, 151
 Hawthorne, F.C. 165, 169
 Heffern, E.L. 85, 100, 102, 110, 118, 123, 210, 217
 Hein, K.A.A. 100, 124, 170
 Heisey, B. 25, 302
 Hendricks, T.A. 2, 26
 Hendricksen, G.A. 251
 Herrmann, W. 163, 170
 Hertle, M. 8, 26
 Hessley, R.K. 2, 6, 11–13, 26
 Hilt, C. 56, 62
 Hodge, F.W. 64, 79
 Hodges, J.E. 303
 Holbrook II, J.A. 273, 304
 Hollowell, J.L. 66, 79
 Hong, Y. 223, 225, 227–228
 Hood, D.G. 64, 80
 Hookham, M. 329, 332
 Hooper, R.L. 215, 217
 Hower, J. 251
 Hower, J.C. 9, 24, 26, 48, 55, 58*t*, 62, 123–124
 Huan, Z. 229
 Huffman, G.P. 27
 Huggins, F.E. 27
 Hurst, V.J. 158, 170
 Huston, D. 170
 Huurneman, G.C. 251
 Hyams, E. 65, 79
 Hynes, J.L. 304
- I**
- Ingall, E.D. 165, 170
 Inhofe, J.M. 256–257, 265
 Irani, M.C. 293, 294*f*, 303
 Itkis, S. 211, 214–217
 Ivanovskaya, T.A. 170
- J**
- Janssen, L.L.F. 232, 251
 Janssen, R.E. 4, 26
 Jaya, A. 315
 Jehlicka, J. 160*t*, 170
 Jelen, B. 27
 Jianzhong Zhang, Künzer, C. 27, 124
 Jirasek, J. 27
 Johnson, T.M. 106, 111, 142–143, 151
 Johnson, W. 16, 26, 303
 Johnston, H. 79
 Jolley, T.R. 272–273, 303
 Jones, A.H. 215–216
 Jones, B.D. 257, 265
 Jones, C.H. 216
 Jones, G.W. 103, 111
 Jones, J.R. 297, 303
 Jones, M. 106–107, 111
 Justin, T.R. 15, 279, 283, 303–304
- K**
- Kabata-Pendias, A. 68–69, 72*t*, 73, 79
 Kahle, A.B. 220, 228

- Kalkreuth, W.D. 61
 Kamaraju, M.V.V. 170
 Kamprard, J. 170
 Kang, G.F. 228, 251
 Kanury, A.M. 17, 26
 Kashiwagi, T. 321, 325
 Kay, G.M. 5, 26
 Kaymakçi, E. 60, 62
 Keefer, R.F. 116, 123
 Kent, J.D. 79
 Kessels, W. 252
 Ketelaar, V.B.H. 237, 247, 251
 Keys, D.A. 218
 Khesin, B. 211, 214–217
 Kick, H. 225, 228
 Kiefer, R.W. 251
 Kim, A.G. 3*f*, 8*f*, 11*f*, 12, 16*f*, 17–20, 18*f*, 22, 21*f*, 22*f*, 25–26, 40–41, 41*f*, 42*f*, 45, 217–218, 224, 227–228, 269*f*, 272*t*, 278–279, 278*f*, 280*f*, 281, 281*f*, 282–283, 284*f*, 285, 285*f*, 286*f*, 287*f*, 289, 289*f*, 294*f*, 298, 298*f*, 318–320, 325
 Kissell, F.N. 3*f*, 11*f*, 26
 Kitson, J. 124
 Knuth, W.K., Jr. 222, 226–228
 Knutson, O. 218
 Kobe, H.W. 26, 124, 217
 Kociban, A.M. 302–303
 Koeppen, R.P. 26
 Kolada, R.J. 60–61
 Kolker, A. 9, 26–27, 247, 251
 Kolodny, Y. 214, 218
 Konhauser, K.O. 156*f*, 158–159, 170
 Koopmans, B.N. 228
 Kosanke, R.M. 5–6, 26
 Kraft, M.E. 259, 265
 Krajick, K. 42, 45
 Krishnaswamy, S. 60
 Kroonenberg, S.B. 85, 100, 102, 105, 111, 113
 Krs, M. 216–217
 Krsová, M. 216–217
 Krugman, P. 256–257, 265
 Krumbein, W.W. 5–6, 26
 Kubiszewski, I. 119*f*, 124
 Kuchta, J.M. 278, 281, 304
 Kuenzer, C. 118, 121–122, 124, 244, 247, 251, 319, 322, 325
 Kumar, K.V. 170
 Kummel, B. 4, 26
 Künzer, C. 27, 113, 124, 252
 Kustas, W.P. 251
 Kuzig, R. 256–257, 265
 Kyle, J.E. 156–157, 160*t*, 170
- L**
 Lahiri-Dutt, K. 170
 Lakhera, R.C. 170
 Lamb, A. 86, 87*f*, 95, 100
 Lambin, E.F. 243, 251
 Lapham, D.M. 104–105, 111, 116, 117*f*, 120–122, 124, 136, 140–142, 141*f*, 152
 Larco Hoyle, R. 65, 79
 Larson, R.R. 151
 Lausen, C. 137–138, 152
 Lautenberger, C. 315
 Lavender, D. 15, 26
 Lazarra, C.P. 279, 304
 Leaner, J. 124
 Lechtman, H. 66–68, 80
 Lee, C.A. 227
 Lee, C.K. 302
 Leitch, R.D. 17, 26, 279, 304
 Leonhardt, R. 217
- Lerch, H.E. 99, 151
 Li, D. 232, 250
 Li, J. 251
 Liding, C. 250
 Lillesand, T.M. 232–233, 236*f*, 251
 Limacher, D. 103–105, 111
 Limerick, P.N. 262, 265
 Limin, S. 315
 Lindbergh, K. 30, 34, 45
 Lindermeir, E. 228
 Lindgren, W. 104–105, 111
 Lindner, H. 210–211, 215, 217
 Lindqvist, J.K. 211, 213, 213*f*, 215–217
 Lindsley-Griffin, N. 152
 Lippincott, C. 211–213, 214*f*, 215, 216*f*, 218
 Littke, R. 8, 26
 Liu, F. 111, 151
 Liu, X.G. 218
 Logačev, A.A. 211, 217
 Longshaw, T.G. 227
 Losos, Z. 170
 Loughlin, W.P. 221, 228
 Lowenstein, J.M. 80
 Lu, D. 243, 251
- M**
 Maathuis, B. 170
 Mackowsky, M.-Th. 25
 Mackowsky, M.W. 12, 26
 Magnuson, M.O. 107, 111, 271, 303–304
 Mahlmann, R.F. 25
 Mahmut, O.K. 252
 Malenka, W. 25, 302
 Malhotra, K.K. 100
 Mansor, S.B. 90, 100
 Marharaj, S.V. 99, 151
 Marshak, S. 25, 62
 Martínez, M. 64, 79
 Masalehdani, M.N.-N. 16, 26, 117–118, 124, 214, 217
 Mason, B. 116*t*, 124, 151
 Matos, C. 79
 Matthews, A. 210, 218
 Mattoño, C. 75, 80
 Maury, J. 80
 Mausel, P. 251
 Maustellar, J.W. 297, 304
 Mays, S. 76, 80
 McCabe, P.J. 5, 26–27
 McCann, D.M. 95, 99
 McCarthy, K.J. 207–208
 McCormack, J.K. 100, 123–124, 152, 170, 218
 McCulloch, C.M. 5, 26
 McCurdy, K.M. 263, 265
 McElroy, G.E. 273, 304
 McElwain, J.C. 325
 McKinley, J.I. 76, 80
 McNay, L.M. 18–19, 26
 McPhee, J. 263
 McQuaid, J. 38, 45
 Meeker, G.P. 26
 Meer, F. 250
 Mehl, H. 27, 113, 124, 27
 Meier, L. 80
 Meignen, L. 80
 Meinardi, S. 0
 Memmi, J. 107, 111
 Merkel, J.F. 68, 80
 Merry, N. 170
 Michalski, S.R. 16, 21, 24, 26, 30, 33, 35*f*, 39, 41–42, 44–45, 85–87, 100, 281, 304

- Miller, E.W. 45
 Miller, G. 16, 26
 Miller, G.C. 271, 303
 Miller, J.F. 26, 304
 Miller, S.H. 223–225, 228
 Milsom, J. 211, 218
 Milton, C. 66, 80
 Miron, M. 304
 Miron, Y. 278–279, 304
 Misra, B.K. 60, 62
 Mitchell, D.W. 104, 111
 Mitchell, G.D. 25
 Mohan, S. 85–86, 100
 Moldowan, J.M. 208
 Molinda, G.M. 303
 Mooney, C. 256–257, 265
 Moore, D.M. 158, 170
 Moran, E. 251
 Morgan, J.J. 195, 207
 Moroz, T. 170
 Morris, C. 65, 80
 Morris, R. 60, 62
 Morris, R.A. 87, 100
 Moseley, M.E. 66–68, 79–80
 Mott, R. 13*t*, 26
 Mowery, G. 290, 304
 Moxham, R.M. 228
 Mroczkowski, S. 27
 Mrose, M.E. 117*f*, 123, 137–138, 151
 Mucho, R. 65, 79–80
 Muhly, J.D. 80
 Mujica Gallo, M. 65, 80
 Mukherjee, T.K. 245, 251
 Mukhopadhyay, A.K. 100
 Mulyana, A.A.S. 16, 28, 145–147, 146*f*, 152
 Mumme, T.C. 217
 Munshi, P.L. 45
- N**
- Naesner, C.W. 26
 Nakashima, E. 75, 80
 Nambu, H. 311, 315
 Nandy, D.K. 61
 Needham, J. 68, 80
 Newfarmer, R. 111
 Newfarmer, R.S. 151
 Nicholls, G. 12*t*, 27
 Nolter, M.A. 124, 152, 170, 223, 228
 Norton, F.H. 69, 80
 Novak, A. 62
 Nuray, D. 252
- O**
- Oertel, D. 27, 113, 124, 325
 Ohlemiller, T.J. 308, 315, 318–320, 325
 Olley, J.M. 79
 Olmez, I. 27
 Onasch, C.M. 62
 Oosthoek, K.J.W. 30, 45
 Oparin, V.N. 252
 Ordish, G. 65, 79
 Orem, W. 99–100, 151
 Orem, W.H. 116*t*, 124
 Oshinsky, D.M. 257, 265
 Otto, H.H. 36, 45
- P**
- Pagano, T. 251
 Page, S.E. 314–315
 Palmer, C. 27
 Palmer, J.P. 100
 Palmer, K.N. 308, 315, 319, 325
 Pande, S.K. 251
 Pang, Z. 25
 Panigrahi, D.C. 246, 251
 Paquette, Y. 124
 Parrish, J.T. 85
 Parse, D.F., Jr. 216, 218
 Peacor, D.R. 123, 214, 217
 Pellissier, C. 170
 Pendias, H. 68–69, 72*t*, 73, 79
 Peng, W.X. 225, 227–228, 245, 251
 Perez, J. 99
 Perkins, S. 108–109, 111
 Peters, G. 263, 266
 Peters, K.E. 201–206
 Petersen, C.R. 64–65, 80
 Petersen, G. 65–66, 80
 Petmecky, S. 8, 27
 Petrakis, L. 14, 27
 Pfordte, O.F. 65, 80
 Philbin, D.R. 273, 304
 Pickel, W. 62
 Pierce, B.S. 79
 Pine, J. 25
 Pipozar, D.J. 106–107, 111
 Pironi, P. 315, 325
 Pirrone, N. 122, 124
 Plumlee, G.S. 111, 151
 Plunkett, E.R. 19, 27
 Pokrovskaya, E.V. 170
 Pollock, J.D. 62
 Polsby, N.W. 261, 265
 Pone, J.D.N. 87, 100, 120–122, 124, 152, 160*t*, 170
 Popov, S.E. 252
 Porter, H.C. 173–208
 Postrzednik, S. 56, 62
 Potapov, V.P. 252
 Powell, J.W. 259–265
 Prakash A. 15, 25, 27, 90, 100, 102, 103*f*, 105–109, 108*f*, 111–112, 124, 143, 151–152, 170–171, 218, 226–228, 232–233, 235*f*, 236, 236*f*, 238*t*, 240*t*, 242–248, 243*f*, 243*f*, 244*f*, 246*f*, 250–252, 266, 325
 Prakash, A. 27, 124
 Prasad, R.M. 100
 Prasad, Y.V.S. 60–61
 Prescott, J.R. 79
 Prothero, S. 75, 80
 Provorse, B.L. 30, 34, 45
 Pruner, P. 217
 Purser, D.A. 309, 315
 Pyastunovich, O.L. 252
- Q**
- Quattrochi, D.A. 234*f*, 237, 251
- R**
- Rabbit, M.C. 261, 265
 Radan, M. 216, 218
 Radan, S.C. 216, 218
 Radke, L. 251
 Raju, E.V.R. 170
 Rantitsch, G. 9, 27
 Rathmore, C.S. 222, 224–225, 228
 Raymond, R. 64, 80
 Reasoner, J.W. 26
 Reddy, C.S.S. 165, 170
 Redmond, K.M. 303
 Reeves, C.V. 251
 Rehnquist, W.H. 260, 265

- Rein, G. 308–309, 309*f*; 310*f*; 310*f*; 311–315, 312*f*, 313*f*, 318–321, 319*f*, 325
- Reiners, P.W. 26
- Reiser, H. 27
- Rencz, A.N. 232, 252
- Renner, S. 143, 152, 170, 297, 304
- Reynolds, R.C. 158, 170
- Rhodes, E.O. 195, 208
- Rhodes, R. 257, 265
- Rhone, R.D. 36, 45–46
- Richards, J.G. 88, 100
- Rieley, J.O. 315
- Riley, J.T. 26
- Ripley, R.B. 257, 265
- Robert, P. 62
- Roberts, R.G. 79
- Ron, H. 214, 218
- Rose, W.I., Jr. 104–105, 112, 136, 152
- Rosema, A. 16, 27, 105, 112, 122, 124, 244, 246–248, 252
- Rosenberg, P.E. 217
- Rosenzweig, A. 151
- Rost, R. 104–105, 112, 120–121, 124
- Roth, A. 27, 113, 124
- Rowe, J.H. 75, 80
- Rowe, V.R. 304
- Rowland, F.S. 0
- Roy, A. 106–107, 112
- Rushworth, P. 281, 304
- Russell, A.W. 273, 303
- Rüter, H. 210–211, 215, 217–218
- Ryerson, R.A. 232, 252
- S**
- Sabins, F.F., Jr. 220, 221*f*, 221–222, 228
- Sachsenhofer, R.F. 9
- Saghafi, A. 250
- Saha, K. 170
- Sajwan, K.S. 116, 123
- Samamé Boggio, M. 64–66, 80
- San Filipino, J.R. 28
- Saraf, A.K. 100, 108–109, 112, 228, 245*f*; 251–252
- Sarofim, A.F. 27
- Sastry, R.G.S. 228, 251
- Saward, S.A. 5, 27
- Saxena, N.C. 90, 100
- Schalke, H.J.W.G. 112
- Schaumann, G. 210–211, 218
- Schimmel, J. 25, 302
- Schmidt, L.D. 303
- Schmidt, R.A. 33–34, 36, 38, 45
- Schoeninger, M. 80
- Schogol, M. 107, 112
- Scholz, R. 62
- Schopf, J.M. 2, 27
- Schroeder, P.A. 100, 124, 152, 156*f*; 158*f*; 159*f*; 161*f*; 163, 163*f*; 164*f*; 165, 170, 218
- Scott, G.S. 17, 27, 103, 111, 281
- Seccombe, P.K. 170
- Seda, S. 248, 252
- Sen, S.K. 61
- Senftle, F.E. 218
- Sengupta, S. 112, 252
- Senior, C.L. 13*t*, 27
- Sha, Z.Y. 252
- Shacklette, H.T. 73, 79
- Shagam, R. 218
- Shah, A. 170
- Shah, N. 27
- Shallenberger, J.P. 222, 225, 227–228
- Shan, J. 250–251
- Sharygin, V.V. 218
- Shawcross, W. 79
- Shcherbakova, E. 170
- Sheehan, A.F. 216
- Shellenberger, F.H. 15, 22, 27, 272–273, 304
- Sheriff, R.E. 218
- Shilin, B.V. 100
- Shimada, I. 68, 80
- Shipman, P. 77, 78*f*; 80
- Siegert, F. 315
- Siemon, B. 218
- Silva, O. 79
- Simeoni, A. 315
- Simmons, W.B. 217
- Simon, J.A. 26
- Singer, J.M. 302
- Singh, B. 61
- Singh, B.D. 60, 62
- Singh, C. 251
- Singh, M.K. 106
- Sinha, P.R. 107, 112
- Sive, B.C. 0
- Sivek, M. 8, 27
- Skala, R. 171
- Skeen, C.J. 69, 79
- Skinner, B.J. 79
- Skinner, H.C. 111, 151
- Slavecki, R.J. 222, 226–228
- Slivon, J.P. 302
- Sloss, L.L. 5–6, 26
- Smith, A.C. 45, 279, 304
- Smith, A.F. 304
- Smith, G.G. 5, 7*t*, 10*t*
- Sokol, E.V. 16, 27, 214, 218, 325
- Sontag, K.D. 210–211, 218
- Soroka, K.E. 293, 302–304
- Sout, S.A. 207
- Sparks, A. 218
- Specht, E. 62
- Spooner, N.A. 79
- Squier, E.G. 66–67, 79–80
- Sracek, O. 170
- Srivastav, S.K. 170
- St. George, J.D. 61
- Stach, E. 50, 54*t*, 55*t*, 59*t*, 62
- Stegner, W. 259, 262–263, 265–266
- Stein, A. 118–119, 124
- Steiner, W.A. 303
- Sternberg, R.S. 210–213, 214*f*; 215–216, 216*f*; 217–218
- Stillwell, H.D. 75, 80
- Stoiber, R.E. 104–105, 112, 136, 140–141
- Stokes, D.E. 258, 266
- Stopes, M.C. 13–14, 27, 58*t*, 62
- Stout, S.A. 123, 174–175, 184–188, 187*f*; 191, 195–198, 201, 207–208
- Stracher, G.B. 15–16, 25–28, 64, 80, 85–87, 100, 102, 104–105, 107–108, 112–113, 116–119, 119*f*; 121–124, 136–143, 137*f*; 138*f*; 139*f*; 140*f*; 144*f*; 145–147, 145*f*; 146*f*; 148*f*; 149*f*; 150–151, 150*f*; 152, 156, 164*f*; 166, 170, 214, 217–218, 228–229, 251–252, 256–257, 265–266, 303, 308, 315, 325
- Streufert, R.K. 304
- Stricker, G.D. 24
- Strunz, G. 27, 113, 124
- Sturgeon, S.C. 263, 266
- Styron, R.W. 170
- Sun, Y. 163, 170–171
- Sundaram, R.M. 251
- Swaine, D.J. 175–176, 208

Swanson, A.L. 0
 Sweeney, J.J. 10, 25
 Sykorova, I. 48, 62

T

Tabet, D.E. 152
 Tan, Y. 251
 Tao, T.X. 250
 Tatsch, J.H. 4, 13*t*, 27
 Tatu, C.A. 99, 111, 151
 Taylor, G.H. 50, 55*t*, 56, 62
 Taylor, T.P. 15–16, 27, 64, 80, 85–87, 88*f*, 89*f*, 100, 102, 112, 116–118, 121, 124, 142–143, 146*f*, 152, 170, 266, 308, 315
 Teichmuller, M. 6–8, 27, 59*t*, 62
 Teichmuller, R. 6–8, 27, 59*t*, 62
 Telford, W.M. 215–216, 218
 Ten Katen, A.M. 27, 112, 124, 252
 Terry, R.C. 21, 27
 Terzlaff, A. 124
 Tetzlaff, A. 251
 Thery, I. 64, 80
 Thiede, D.S. 27
 Thiessen, R. 28
 Thorpe, A.N. 214–215, 218
 Tian, Y. 229
 Tietz, J. 42, 45
 Tissot, B.P. 175, 208
 Toothman, G.J.R. 303
 Torero, J.L. 315, 325
 Toulmin, P. 80
 Trescott, P.C. 28
 Tucker, M.R. 69–73, 80
 Tylecote, R.F. 68, 69*t*, 69–73, 80

U

Ubelaker, D.U. 75–77, 80
 Uhler, A.D. 185*t*, 207–208
 Urban, D.L. 315
 Uysal, T. 9, 27

V

van Dijk, P.M. 27, 113, 124, 152, 170, 218, 250–251, 325
 van Genderen, J.L. 27, 105, 110, 112, 124, 228–229, 237, 247, 252
 van Hoof, T.A.M. 217
 van Krevelen, D.W. 3, 27, 181–184, 208
 van Rinsvelt, H. 68, 81
 van Vuuren, M.C.J. 85–86, 100
 van Zyl, J.J. 232, 250
 Vapnik, Y. 214, 217–218
 Vassilev, S.V. 160*t*, 170
 Vassileva, C.G. 160*t*, 170
 Vaughan, D.J. 79
 Veen, B.S. van. 250
 Vekerdy, Z. 27, 105–106, 112, 124, 152, 248, 251–252
 Veld, H. 27, 112, 124, 252
 Verano, J.W. 75, 81
 Vernet, J.L. 80
 Vice, D.H. 124, 152, 170, 221–224, 228
 Viellenave, J.H. 152
 Vogel, M. 67, 81
 Voigt, S. 16, 27, 105, 113, 122, 124, 171, 218, 229, 247, 251–252, 325
 Volkova, N.I. 16, 27, 214, 218
 Von Hagen, A. 65, 80
 Voracek, V. 85–86, 100

W

Wade, L. 62
 Wagner, R.S. 140–141, 152, 171, 218, 251–252, 325
 Wagner, W. 124
 Wahiduzzaman, M. 170
 Walker, S. 84–85, 93, 100, 117–118, 124
 Walters, C.C. 208
 Walther, D.C. 319, 325
 Wang, D. 25
 Wanless, H.R. 5, 26, 28
 Warren, M. 68, 81
 Warwick, P.D. 12, 28, 79
 Watson, K. 223–224, 228
 Watts, J.M. 315, 325
 Weast, R.C. 40, 45
 Weller, J.M. 5–6, 28
 Welte, D.H. 175, 208
 Wessling, S. 246, 252
 West, I.M. 141–142, 152
 Whaite, R.H. 227
 White, D. 3, 11*t*, 28
 White, E.M. 18, 28
 White, L. 7*t*, 10*t*, 11*t*, 28
 Whitehouse, A.E. 16, 28, 120*f*, 145–147, 152
 Wiegel, J. 170
 Wild, G.D. 62
 Willett, J.C. 68–69, 79
 Williams, D.J. 105, 113, 250
 Williams, S.A. 110
 Wilman, H.B. 26
 Wingfield-Hayes, R. 105–106, 113
 Winschel, L.J. 44, 100
 Winshel, L.J. 304
 Witzke, T. 136–138, 152
 Wolf, M. 62
 Woolley, J.T. 266
 Wright, R. 222, 224–225, 228, 251
 Wuttke, M.W. 252

X

Xie, Y.C. 243, 252

Y

Yager, T.R. 79
 Yang, K. 170
 Yang, Q. 25
 Yaobao, M. 228
 Yeasted, J.G. 44
 Yong-fang, H. 225, 228
 Yu, M. 252

Z

Žáček, V. 160*t*, 170–171
 Zacharov, V.P. 211, 217
 Zamaraev, R.Y. 248, 252
 Zapata, O. 99
 Zeng, T. 27
 Zhang, X. 85, 100, 102, 105, 111, 113, 124, 152, 170, 218
 Zhang, J. 113, 124, 165, 171, 210, 218, 226–227, 229, 236, 251–252, 319, 322, 325
 Zhang, X.M. 225, 227, 229
 Zhao, X. 229
 Zhao-ming, Z. 228
 Zheng, B. 99, 111, 123, 151
 Zhukov, B. 27, 113, 124, 252, 325

This page intentionally left blank

Subject Index

A

Abandoned mine lands (AMLs) 16, 39–40, 42, 268–269
Abandoned mine workings 87, 98, 104, 143
Absorption 104–105, 157, 163, 234, 247
Acid mine drainage (AMD) 2, 38
Acid rain 106
Activation energy 17, 277
Active remote sensing 5–6, 12, 39–40, 237, 319–320
Acyclic isoprenoid hydrocarbons 190*f*
Adiabatic conditions 60, 278–279
Adsorption 17, 40, 56, 60, 177, 278–281, 322
Airborne thermal infrared imaging 39, 98, **219–229**, 309
 color infrared imaging 222
 depth estimation 226
 early use 222
 “Burning Field” coal fire 224*f*
 custom-built TIR scanner, uses of 223
 environmental impacts of coal mining 224
 first study of coal fires 222
 geothermal surface manifestations 223
 study of coal fires (US Geological Survey) 223
 subbituminous coal 223–224
 surface factors 223–224
 TIR surveys, three separate 223
 later use 225
 aerial photography using computer programs 225
 depth of coal fire, estimation of 225
 Fourier transform spectrometer 225
 infrared photography 225
 National Aerial Photographic Program CIR photos 225
 remote sensing methods 225
 stressed vegetation at “cemetery front” 226*f*
 TIR and CIR imagery 226
 thermal infrared imaging (TIR) 220
Alaska National Wildlife Refuge 263
Albright waste bank 295*f*, 295
Alginite 14
Algorobo charcoal 77
Alkylated PAHs 178, 180, 184, 188
Allochthonous or drift coals 13
American Mineralogist Crystal Structure Data Base 158
Ammonium cation (NH₄⁺) 158
Ancient Greeks 64
Ancient man
 calcium in soil 67
 ¹⁴C date 74
 Chan Chan 65
 coal in Peru 64
 modern brick from Trujillo 65*f*
 cremation at Tschudi burn 76
 cremation in society 74
 fuel ash chemistry 68
 fuel for cremation 75
 metallurgical furnace or crematorium 66
 oxide and trace element data 69
 sulfur in soil 68
 temperature of Tschudi burn 66
Angiosperms 5
Angstrom 157
Anhydrous sodium sulfate (Na₂SO₄) 178
Ankerite 50, 54
Anoxic condition 12, 158, 175

Anthracite 187*f*, 188
 coalfields 273
 Centralia mine fire, *See* Centralia mine fire
 fire zone or excavation of trench barrier 273
 map of anthracite coalfields in Pennsylvania 274*f*
 US bureau of mines fire-control projects 274*t*
 mining 36
 chute-and-pillar mining 36
 gangways 36
Aromatics 174, 195–198
Arsenosis 116
Asphyxian 309
Atomic planes 157, 162
Auger mining 38
Autochthonous coals 13

B

Background concentrations 129
Background temperature 244
Backscattered electrons 161
Bacteria theory 85
Barrenness aureoles 242
Barrier pillar operation 17, 36
Beer–Lambert law 148–149
Beijing Remote Sensing Corporation (BRSC) 105–106
Bell pit 30, 33
Benzo[*b*]fluoranthene and benzo[*k*]fluoranthene 184
Benzo[*g*, *h*, *i*]perylene 184
Bharat Coking Coal Limited (BCCL) 107
“Big Muskie” 32
Biomarker stability 201
 high volatile bituminous reference coal 201–205
 mature lignite 201
 pentacyclic triterpanes 201
 saturated hydrocarbon fingerprints 202*f*
 sulfur-containing aromatics (S-PAHs) 205
 tricyclic triterpanes 201–205
 triterpane biomarkers 204*f*
 triterpane fingerprints
 coal fires in Breathitt 203*f*
 thermal exposure 204*f*
 triterpane signatures 204*f*
Biomineralization 156–157
Bisnorhopane (BNH) 201
Bitumen-rich Upper Cretaceous–Lower Tertiary Hatrum
 Formation 210
Bituminite 48–49, 49*t*
Bituminous
 chemical properties 9
 coalfields 17, 223
 coal seams 33
 eastern fires 16
 high-volatile 6, 94, 181–184, 188, 193, 198, 201
 Breathitt Formation 193, 198–201
 uncombusted 195–198
 low-volatile 6, 14, 278
 medium-volatile 6, 104, 181–184, 188, 280
 rank 7, 9
 subbituminous 6, 18–19, 55, 188, 223–224
Blackbody 235–236
Blackdamp (chokedamp) 104
Black Death, *See* Cremation in society
Blake/Rowland group 132

- "Bord-and-pillar" mining 33
 Boulder dam (1931–1935) 257
 Boundary pillars 19, 280
 Bragg's law 158, 162
 British thermal unit (BTU) 66–67
 Bucket-wheel excavators 32
 Buck Mountain coal seam 42
 Bulldozers 31
 Burial patterns, *See* Cremation in society
 Burlington Northern geothermal exploration program 223–224
 Daedalus model 1230 scanner 224
 Burning and water suppression of smoldering-coal fires **317–326**,
 apparatus 318, 320
 domestic anthracitic coal 319
 thermocouples 319
 base experiment 321
 experimental setup of coal sample 319, 320^f
 thermocouple traces and mass loss 320, 321^f
 effect of particle size on suppression 323
 adsorption of water 322
 experimental setup of coal sample 319, 320^f
 fluid flow 322
 hand operated atomizer 321
 heterogeneous heat transfer 322
 thermal properties of coal and water 322
 extinguishing mechanisms 318
 back filling 318
 coal seams 318
 critical reignition temperature 318
 displacement of oxygen 318
 E Burns commissioned by G Rein 319^f
 oxygen availability, effect on smoldering 319
 permeability 318–319
 porosity 318–319
 subsurface smoldering fire 318, 319^f
 suppression by cooling 319
 thermal inertia 318–319
 ignition and propagation experiments 322
 burning coal mass versus particle size 324^f
 ignition and particle size 320, 322^f
 ignition/propagation dynamics 320
 maximum smoldering temperature and particle size 320–321, 323^f
 suppression experiments
 global evaporation 321
 hand operated atomizer 321
 poor heat transfer 321
 shower 321
 single point injection 321
 spray 321
 suppression mechanisms 321
 water application method 324^f
 Burning colliery spoil 84–85
 "Burning Field" coal fire 224
 Burning Mountain coal fire in Australia 85, 223
 Burning underground 64, 85, 107
 Burnout control 41, 293
 Albright waste bank 295
 calamity hollow 293
 exhaust ventilation system 293
 heat of combustion of burning coal 293
 system 294^f
 Burnt ashes 84–85, 88
- C**
 CAFSCO 330
 CO₂ gas inertization techniques 330–331
 compressed air foam systems (CAFS) 330
 Calamity Hollow mine fire project 296
 Calcite 50
 Calorific value 89
 Capillary column 131–132, 174, 180–181, 184
 Carbominerites 54
 Carbonaceous shale 12, 17–18, 84–85, 271, 279–280, 290, 297
 Carbonates 12, 50, 54, 180
 Carbon cycle 3^f
 Carboniferous coals 3
 coal-forming plants 4^f
 Carbonization 175
 combustion 175–176
 PAH-rich liquid coal tar 175
 pyrolysis 175
 pyrosynthesis 175–176
 temperature 195
 Carbonized coal
 bed 198, 201
 residues 193, 201, 205
 sites 194^f, 197^f, 200^f, 203^f
 Catagenesis 175, 184, 178
 Catalyst 40–41, 130, 140–141
 Catastrophic coal fires
 Jharkhand, India 107
 Bharat Coking Coal Limited (BCCL) 107
 Jharia coalfield 108^f, 108^f, 109^f
 commercial coal mining 107
 geographic information system (GIS) 109
 landsat thematic mapper (TM) 109
 Ministry of Coal and Mines (MCM) 107
 noxious vapors and toxic fly ash 108–109
 subsurface fires 109
 Northern China 105
 acid rain 106
 Beijing Remote Sensing Corporation (BRSC) 105–106
 COALMAN project 105–106
 coal production 105
 fires across Pennsylvania 106^f
 Global Positioning System (GPS) 105–106
 Rujigou coalfield of Ningxia 105
 surface fires 106
 synthetic aperture radar (SAR) 105
 underground coal fires, Xinjiang 105
 World Resources Institute (WRI) 106
 Pennsylvania, USA 106
 aqueous foam fire fighting technology 107
 Avondale catastrophe 106–107
 Centralia Borough Council, burning of trash 107
 fly ash 107
 generating electricity 106–107
 slurry flushing and surface sealing techniques 107
¹⁴C date 74
 carbonized plant material (*Tillandsia latifolia*) 74, 74^f, 75^t
 Peruvian coal 74
 sulfur content of coal 74
 Cedar Avenue coal mine fire 223
 Cellulose 48, 55–56, 104, 308, 311
 Centralia mine fire 42, 273, 290
 burning refuse material 273
 coal refuse 273
 flushed barrier 273–275
 inundation methods 275
 burnout control 275
 flooding and hydraulic flushing 275
 relocation of community 275
 underground mining 275
 water curtain barrier 275
 map of Centralia Borough 276^f,
 excavation 276^f
 location of fire-control projects 276^f
 origin of 275^f

- temperature zones 291*f*
 two-phase project 273–275
 backfilling and sealing abandoned strip pits 273–275
 excavating permanent isolation 273–275
- Chan Chan 65
 Chimu Empire 65
 Inca Empire 65
 location 65
- Channel sands 5
- Char 311
- Characteristic radiation 161
- Chemical fingerprinting evidence, lines of 175
 dichloromethane (DCM) 177
 protocol for reviewing hydrocarbon 176*f*
 saturated hydrocarbons 177
 thermal transformation 177
 total extractable hydrocarbons (TEHs) 177
 total extractable material (TEM) 177
 total organic carbon (TOC) 177
- Chokedamp 104
- Chromatogram 129–133, 198–201
- Chromleon chromatography software 129–131
- Clarite 54
- Clarodurite 54
- Clastic sedimentary rocks 158–159
- Clays 50, 215
- Cleanup, coal and coal tar samples 179
 alumina solid phase cleanup 179
 EPA Method 3611B 179
 See also US Environmental Protection Agency (USEPA)
 GC autosampler vial 179
 NSO-bearing 179
 polar organics 179
- Climactic theories 6
- Climate change 116, 122
- Clinker
 age of zircons 15
 baked ferron 139*f*
 creation of 210, 260, 331
 location 211
 magnetic 212
 northern clinker zone 212
 out crops 211
 paleoclinkers 213
 pyrometamorphic rocks 210
 red 139*f*
 sandstone 102
 southern clinker zone 1 212
- Coal
 -bed fires 15
 definition 2
 distillate 198
 field 31
 matrix 201
 metamorphism 9
 “molecule” 17
 –oxygen complex theory 85
 preparation plant 16, 32, 37
 -producing countries 64
 refuse 17, 19, 273, 278–279, 288–289
- Coal fires
 across China 103*f*
 across Pennsylvania 106*f*
 in an open-pit mine in Jharia coalfield 108*f*
 biomineralization 156–157
 burn across Jharia coalfield 108*f*
 catastrophic, *See* Catastrophic coal fires
 detector gases 104
 gas vents 136, 156–157
 lessons for 264
 in open cast coal mine 109*f*
 origin of 103
 policy setting for 255–266
 residues 193
 biomarker stability 201
 dominant hydrocarbons 193
 metallurgical coke 193
 PAH transformations 195
 Ruth Mullins coal fire 193
 saturated hydrocarbon residues 198
 semivolatile hydrocarbons 193
- Coalification 6–8, 11–12, 48–50, 55–56, 174, 184
 cretaceous/tertiary coalfields 8*f*
 experimental studies
 vitrinite reflectance 10*t*
 hydrothermal fluids 9
 igneous activity and tectonism 9
 increased coal due to heat/pressure/time 7*f*
 mechanisms for increasing coal rank
 depth of burial 8
 metamorphism in normal coal series 7*t*
 removal of H₂O 6
 transition from peat to hard coal 6*f*
- COALMAN project 105–106
- Coal Mine Inspection Act of 1941 268
- Coal mines
 Goyllarisquizga 64–65
 in Peru’s Santa Valley 64–65
- Coal mining
 evolution of 30
 fires
 abatement 41
 discovery and investigation 39
 mine atmosphere 40
 monitoring 39
 machines 32
 methods of 34
 layout of a modern coal mine 35*f*
 longwall coal mining 34
 room-and-pillar coal mining 34
 surface coal mining
 area mining 38
 auger mining 38
 contour mining 37
 mountain top removal 38
 surface mining 37
 techniques 31
 underground
 methods of coal mining 34
 special case of anthracite mining 36
 underground mining 33
 ventilation 36
 use/risk factors 2
- Coal rank 31, 55
 bituminous coals 55
 coalification 55–56
 fire clay coal bed 56*f*
 humification 55–56
 maximum value of rank parameters 59*t*
 physicochemical coalification 56
 vitrinite reflectance 55
- Coal seams
 colliery spoil heap fires 86
 abandoned mine workings 87
 long-term smoldering 88
 moisture content of spoil 87
 restoration of spoil heap 87

- Coal seams (*Continued*)
 self-ignition 87
 spoil heaps 87
 geologic distribution of 3
 carboniferous coals 3
 cretaceous/tertiary coals 5
- Coal swamps 5
 epeirogenic sinking of land 5
 epigenetic minerals 5
 eustatic rise 5
 syngenetic minerals 5
- Coelution 184
- CO₂ gas inertization techniques 330–331
- Coke
 anthropogenic sources 175
 aromatized carbon 175
 carbonaceous 311
 industrial coke oven 195
 organic by-products 175
 PAH enrichment 184
 thermal transformation 174
- Collective water usage 261
- Colliery spoil heaps 84–85, 87, 94–95
- Colliery waste 88
 calorific value 89
 loss-on-ignition tests 89
 self heating, factors for 89
 shrouding of burning spoil heap 89
- Colorado Division of Minerals and Geology (CDMG) 297
- Color infrared imaging (CIR) 222
 advantages 222
 broadleaf forest vegetation 222
 healthy vegetation 222
 capillary moisture 222
 color photo film 222
- Columns 128, 130, 131–132, 177, 180
- Combustion 40
- Combustion metamorphism (CM) 210
- Composition 10
 macroscopic and microscopic 13
 proximate composition 11*t*,
 coal from peat to anthracite, heating values of 11*f*
 elements in coal ash, distribution of 12*t*
 minerals identified in coal 13*t*
 ultimate composition 13*t*
- Compound retention times (time of elution) 132
- Compressed air foam systems (CAFS) 329–330
- Condensation
 coal-fire gas 136
 degree of 49
 devolatilization 183*f*
 exhalation 104–105
 heat of 90
 of moisture 60
 processes 136–137
 products 102–103, 104–105
 pyrolytic 7*f*
 reactions 6–7
 role 188
 solid phases 142
 volatile vapors 174, 193–195
 water 286
- Condensed phase fuel 318
- Conduction 17, 98, 223, 245–246, 279–281, 283–284,
 309–310, 312
- Conifers 5
- Conservatism ideology 257
- Continuing calibration 181, 184
- Continuous miner 32, 34
- Contour mining 37
- Convection 17, 245–246, 279, 281, 308–310
- Convective heat transport 311
- Conventional and continuous mining systems 33
- Conventional construction procedures 41
- Copper solid-phase cleanup of sulfur 179
 EPA method 3660B 179
 See also US Environmental Protection Agency (USEPA)
- GC autosampler 179
 granular copper 179
 high-sulfur coal 179
 NOAA Status and Trends Program methods 179
 silica gel 179
 sodium silicate 179
- CO₂ toxic factor 309
- Crack-density mapping 242
 ArcGIS™ 242
 digital image processing techniques 242
 geospatial statistical analyses 242
 heat source 242
 high spatial resolution remote sensing images 242
 massive cracks 242
 surface cracking 242
 thermal cracking 242
- Cremation in society 74
 Chimu burials 75
 description (La Rosa) 74–75
 global mortuary practice 75
 secondary cremations 75
- Creosote (coal tar) 119
- Cretaceous/tertiary coals 5
- Critical reignition temperature 318
- Crossing point method 279
- Cryogenic slurry injection 297, 298*f*, 299*f*
 inert gas movement 297–298
 injection test 290
 liquid or gaseous CO₂ 297–298
 postinjection temperature surveys 298
 preinjection temperature 298
 second cryogenic injection 298
 subsurface coal fires 298
 use of cryogenic liquids 297
- Crystal
 lattice 161
 motif 157
 structure 157–158, 162
- Culm banks 102–103, 104–105, 118, 220, 222, 224
- Custom-built TIR scanner 223
- Cyclothem 5
 definition 5–6
 “ideal” cyclothem 5–6
 Southern Appalachian or Piedmont-type 5–6
- D**
- Daedalus scanner 223
- Dehydroxylation 6–7
- Demethylation 6–7
- Department of Energy (DOE) 2, 64
- Detrovitrite 48
- Devolatilization 198–201
- Diagenesis 9, 50, 175, 184
- Diagenetic PAHs 184
- Diastrophic theories 6
- Dibenzothiophenes 187*f*
- Dichloromethane (DCM) 177
- Diffraction pattern 77, 157–158
- Diffusion 215–216, 309–310, 312
 characteristics 309–310
 conduction 309–310
 pyrolysis 309–310

- Dinosaur National Monument dam authorization battle 263
Dip 18, 21, 245, 279, 287, 297
Discontinuous fire propagation 281, 281*f*
mine fire 281
wasted-coal fires 281
Displacement of oxygen 318
Distillate range hydrocarbons (*n*-C₉ to *n*-C₂₃) 201
Diurnal variation 211
Dolomite 50
Dominant hydrocarbons 193
alkyl naphthalene 195
carbonization temperature 195
destructive distillation of coal 195
GC/FID fingerprints of coal and natural coal tars 194*f*
semivolatile hydrocarbons 193
UCM, *See* Unresolved complex mixture (UCM)
Dräger pump/tubes 148
Drift coals 13
Drift mine 30, 33
Drilling and blasting 38
Drip condensates 138
Dry ash-free (daf) basis 11
Durabond (DB) 131–132
Durite 54
Duroclarite 54
- E**
Eastern bituminous region 271
coalfields of United States 272*f*
excavation 271
fire barrier 271
flushed barrier 271
surface sealing 271
US bureau of mines fire-control projects 272*t*
water injection 271–272
Eastern fires 16
E Burns commissioned by G Rein 319*f*
Electromagnetic energy and spectrum
cosmic rays 233
reflection spectra 234, 235*f*
spectral bands 233
standard radio waves 233
wavelike form of electromagnetic radiation 233, 233*f*
Electromagnetic radiation 157
Electromagnetic spectrum 220, 222, 233–234
Electron beam 157, 159–161, 163
Electron capture detector (ECD) 128
Electron microprobe 159
backscattered electrons 161
cathode luminescence (CL) 159–161
characteristic radiation 161
crystal lattice 161
electron beam 159–161
energy dispersive spectrometer (EDS) 161–162
multichannel analyzer 161–162
silicon drift detectors (SDDs) 161–162
X-ray spectrum 161–162
inelastic scattering 161
scanning electron microscopy (SEM) 159–161
secondary backscattered electron image 161*f*, 163*f*
transmission electron microscopy (TEM) 159–161
wavelength dispersive spectrometer (WDS) 161–162
maps (X-ray maps) 162
XRD pattern
isostructural 162
Electron microprobe analysis (EMPA) 157
Electron spin resonance spectroscopy 165
El Niño dry season 313
Energy consumption (1635–2006) 4*f*
Energy dispersive spectrometers 161–162, 165
Energy Information Administration 34
Environmental and health impacts 31, 118, 121, 175, 224
arsenosis (hyperkeratosis) 117*f*
concentrations of volatile elements 116*t*
crystals on burning coal-waste pile 117*f*
dental fluorosis 117*f*
environmental consequences 118
solid by-products of combustion 119
visual effects 118
health-related effects 121
See also Health-related effects
Environmental P–T indicator 105
Epirogenic 5
Epigenetic 5, 9, 12
Equilibrium moisture 55
Erlenmeyer flask 178
Ether cleavage 2, 6–7
Eustatic rise 5
Excavation
abandoned workings 104
burning seam 41
cost of 273
fire zone 273, 275
surface mining 36
trench barrier 273
Exothermic reactions 16–17, 56, 84–86, 103–104, 137–138, 141–142, 278, 309, 311
Extraction 178
anhydrous sodium sulfate (Na₂SO₄) 178
calibrated volumetric 178–179
Erlenmeyer flask 178
Kuderna Danish apparatus 178
surrogate compounds 178
- F**
Federal Coal Mine Health and Safety Act of 1969 268
Ferromagnetism 214
Field strength, or paleointensity 216
Fingerprints, saturated hydrocarbon 189*t*, 190*f*
acyclic isoprenoid hydrocarbons 190*f*
high-volatile bituminous 190*f*
plant wax signature 190*f*
subbituminous coal 190*f*
Fire abatement measures 41–42
Fire-area estimation 244
background temperature 244
fire area 244
statistical threshold 244
surface thermal anomaly 244
TIR images 242, 243*f*, 244, 244*f*
Fire barrier 271
Fire-depth estimation 245
conduction 245
convection 245
Full Width Half Max 246
geometric method 245
heat energy transfer 245
interstitial pore spaces 246
simple-geometric construction 245, 245*f*
single chimney system 246
surface thermal anomaly 245, 246*f*
Fire safety engineering 308
Fire science
pyrolyze 333
Fire triangle 42*f*, 294*f*,
conventional mine fire control techniques 41
unconventional or unproven mine fire control techniques 41
Fissures
gas 140*f*
ground 118

- Flame ionization detector (FID) 128, 181
 Flaming combustion 40, 308–309, 313
 Flooding 30–31, 41–42, 78, 88, 278, 318
 Flow condensate reaction 138
 Fluorosis 87, 106, 116, 142–143
 Flushed barrier 271
 Flushing 21
 Foam
 aqueous foam fire fighting technology 107
 compressed 331
 high-expansion 328
 injection 297
 water-based 328
 weak or inferior 331
 See also Modern-foam-injection technology
 Formation-specific source signatures 180
 Forward looking infrared (FLIR) imaging 222
 advantages 222
 FLIR systems Star SAFIRE III camera 222
 solar heating, risk factors 222
 Fossil fuels 175
 ambient microbes 178
 catagenesis 178
 diagenesis 178
 geochemical transformations 178
 metagenesis 175
 suboxic 179
 Fourier transform spectrometer 225
 Fuel
 ash chemistry 68
 charcoal 68
 coal quality inventory 68–69
 compositions 69*t*
 destructive process 68
 olive oil 68
 for cremation 75
 coal / wood 75
 natural hazards 75
 wood-fueled pyres 75
 removal method 19–20
 Fusinite 14, 49, 60
- G**
 Galena 50, 120–121, 162
 Gangway 36
 Gas-altered substrate (GAS) 138
 igneous activity 138
 possible outcrops 139*f*
 Gas and solid phases 308
 Gas chromatography (GC) 128, 137–138, 147, 165, 174, 180
 CO/CO₂ system 130
 gas collection 128
 methane system 129
 modifying 133
 Nomhice 133
 quality control standards 132
 whole air standard used for calibration 133*f*
 sample analysis 129
 VOC system 130
 Gas-collecting techniques 128, 147
 canister evacuation pump-out vacuum line 129*f*
 sampling canister 128, 129*f*
 Teflon[®] tubing 147
 using stainless steel canister 148*f*
 using Tedlar[®] bag 147
 Gas composition
 day-to-day variations 40–41
 hole-to-hole variations 40–41
 Gas fissures 136, 140*f*
 Gas-liquid-altered substrate (GLAS) 136, 138–139
 alunogen and millosevichite 140
 dehydration reaction 139–140
 mineral chemistry 138–139–140
 process by cryptocrystalline mass 140*f*
 quartzofeldspathic sandstone 139–140
 reaction path 138–139
 Gas-liquid precipitation (GLP) 140–141
 GeS₂ crystals 140–141
 Pennsylvania Geological Survey 140–141
 process in SEM image 141*f*
 S-Ge solution 140–141
 Gas-liquid solidification (GLS) 138
 “drip condensates” 138*f*
 drip (stalactite) and flow (ripple) textures 138
 flow condensates 138
 Gas-phase reactions 310
 Gas reaction+liquid-solidification (GRLS) 141–142
 salmoniac (NH₄Cl) 141–142
 select gas components (SGC) 141–142
 solid/liquid/gas reaction products 141–142
 Gas vent(s) 15, 87, 118, 120–121–122, 136, 137–138, 143, 148–149, 156–157–158, 162, 166
 Gas-vent mineral assemblages **155–171**,
 analytical methods 165
 with different environments 156*f*
 electron microprobe 159
 short-wave infrared spectroscopy 163
 X-ray diffraction 157
 Gas vent mineralization and coal combustion
 origin of gas vent minerals
 isochemical mineralization 136
 mass transfer mineralization 138
 mineral-forming processes 136
 pressure–temperature stability 150*f*
 sample collecting and field data 143
 gas-collecting techniques 147
 GPS and temperature measurements 144
 in situ chemical analyses 148
 mineral- and rock-collecting techniques 145
 safety precautions 143
 GC, *See* Gas chromatography (GC)
 Gelovitrinite 48
 Geochemical biomarkers 189*t*,
 hopane 191
 norhopane (NH) 191
 stereoisomers 191
 triterpane biomarker patterns 191, 192*f*
 Geochemical devolatilization process 183*f*
 Geographical and Geological Survey of the Rocky Mountain Region (Powell) 259
 Geographic information system (GIS) 109
 decision-making tool 248
 time series analysis and integrated interpretation 248
 Geologic and mining factors 279
 anthracite mines and western mines 279
 bituminous coalfields 279
 cross section of coal beds in anthracite region 280*f*
 natural ventilation pattern 279
 rider coals and roof slates 279
 Geomorphology 31
 Geophysical methods 288
 ground-penetrating radar 290
 magnetometry 288
 seismic characterization 289
 terrain conductivity 289
 Geosciences community 256–258

- Global catastrophe
catastrophic coal fires
 Jharkhand, India 107
 Northern China 105
 Pennsylvania, USA 106
coal fires across China 103*f*
coal-producing countries and statistics 102*t*
mining hazard
 coal gas 104
 origin of coal fires 103
- Global Positioning System (GPS) 105–106, 144
 temperature measurements 144
 Magellan® handheld GPS unit 145*f*
 Pasco® physics explorer data logger 145*f*
- Gob piles 118, 279
- Godovikovite 87, 166
- Grass fires 15
- Gravity flow method 21
- Greenhouse gas 122, 256–257, 259
 emissions 247
 emanating CO₂ flux 247
 greenhouse-gas emissions 247
 spatiotemporal dynamics 247
 US Geological Survey 247
 toxic gases 116
- Ground-based geophysical techniques 210
 ground penetrating radar and electromagnetics 210
 seismic refraction 210
- Ground fissures 118, 122, 136, 156
- Ground-penetrating radar 288, 290
- Grout slurries 21
- H**
- Hazards, mining. *See* Mining hazards
- Health-related effects 121
 burning-waste piles, gases 122
 causes of severe health problems 121–122
 epidemiological studies 122–123
 human-health impacts 121
 International Institute for Geo-Information Science and Earth
 Observation 122
 large-scale relocation plan 121
 mercury-bearing minerals 122
 Pennsylvanian Hazard No. 7 coal bed 122
 physical hazards 121
 pollution from burning coal beds 121
 pyrogenic PAHs 122
 study of uncontrolled coal fires 121
 toxic elements 122
- Heat capacity 239, 295–296, 318–319, 322
- Heating value 11, 55, 94
- Heat loss 17, 40, 277, 279–280, 309–313, 318
- Heat of combustion 309*f*
- Heat of reaction 85
- Heat of vaporization 295–296, 322
- Hemicellulose 55–56
- Heterogeneous chemical reactions 308, 311
- High-expansion foam 328
- High-resolution hydrocarbon fingerprint (GC/FID) 198–201
- High-resolution hydrocarbon scan 181
 agilent 6890 181
 capillary column 181
 EPA method 8015C 181
 GC/FID chromatograms of extractable hydrocarbons 183*f*
 geochemical devolatilization process 183*f*
 high-volatile bituminous coal 181–184
 medium-volatile bituminous coal 181–184
 saturated hydrocarbon compounds 182*t*
 unresolved complex mixture (UCM) 181–184
- High-sulfur coal 179
- High-volatile bituminous coal 181–184, 187*f*, 188,
 201–205
- Hilt's Rule 7–8
- Homestead Act of 1862 263
- Hopane 191
- Horizontal boring machine 38
- Hot spots 39–40, 84–85–86, 88, 90, 95, 121, 165, 220, 298
- HRB-Singer instrument 222
- Human-health impacts 121
- Humification 55–56
- Hydrocarbon patterns 180
- Hyperkeratosis or arsenic poisoning. *See* Arsenosis
- I**
- Ignition
 forced and spontaneous 17
 and particle size, relationship between 322*f*, 320
 points 85
 propagation dynamics 320
 and propagation experiments 322
 protocol 320
 thermophilic bacteria 17
- Illite 50
- Inactive mine 290
- Industrial carbonization 175
- Industrial coal burning 156–157
- Inelastic scattering 161
- Inert gas 318, 331
- Inertinite 14, 48–49, 54
- Inertization 330–331
- Infrared photography 225
- Infrared regions, visible and near 234
 calm-clear water 234
 clean-coal outcrops 234
 hyperspectral remote sensing 234
 Jet Propulsion Laboratory 234
 multispectral remote sensing 234
 near-contiguous spectral bands 234
 near-infrared plateau 234
 red edge 234
 spectral response curve 234
 US Geological Survey 234
- Infrared spectroscopy 157, 165
- Initial calibration 179, 180–181, 184, 201, 191
- Injection port 181
- Inorganic matter in coal 51*f*, 52*f*, 53*f*,
 carbonates 50
 clays 50
 mineral matter 50–52
 minerals found in coal 54*t*
 oxides 50
 silicates 50
 sulfides 50
- In situ chemical analyses 148
 Beer-Lambert Law 148–149
 Dräger hand pump and tube apparatus 148, 149*f*
 flow kinetics (FKT 1DP1A-SV) 149–150
 mercury analyzer 148–149
 pitot instrumentation 150*f*
 pitot tube 149–150
 RA-915+ mercury analyzer 149*f*
- Interdepartmental Committee on the Redevelopment of
 Contaminated Land (ICRCL) 89
- Internal standard 181, 184
- International Centre for Diffraction Data 158
- Inundation methods 20, 275
- Ion chromatograms 198–201
- Isochemical mineralization 136
 alunogen/coquimbite/voltaite/undefined phase 137*f*
 condensation 136–137

- Isochemical mineralization (*Continued*)
 crystallization 136–137
 exothermic reaction 137
 gas-liquid solidification (GLS) 138
 scanning electron microscope (SEM) images 137–138
 sublimation 137
 products of coal-fire gas 137–138
 supercooling 137
- Isothermal remanent magnetization 215
- J**
- Jharia coalfield (JCF), *See* Catastrophic coal fires
- K**
- Kaolinite 50
 Kuderna Danish apparatus 178
- L**
- Land-cover (coal area) mapping 243
 Landsat Thematic Mapper (TM) 109
 Laurel Run coal fire 223
 Life and human health 85
 direct exposure to coal smoke 87
 fires in coal seams and from burning spoil
 harmful substances 87
 near-surface room and pillar mining 87*f*
 pyrometamorphic rocks 87
 red-shale or clinker products 87
 shallow mines 87
 types of fumes 87
 Lignin 6–7, 48, 55–56
 Lignite 187*f*
 Linear anomaly surface transect (LAST) function 226
 Liptinite 48–49, 54, 60
 Liptite 54
 Lithotypes 13, 54–55
 classification of bituminous coal 58*t*
 macropetrographic classification of brown coal 57*t*
 megascopic classification 55
 black coal lithotypes 55
 brown coal lithotypes 55
 Locating abandoned mine fires 282
 Long-term smoldering 84–85
 Longwall-mining method 33–36
 Loss-on-ignition 89
- M**
- Maceral composition 50*f*, 49*t*,
 inertinite maceral group 49
 fusinite 49
 macrinite 49
 micrinite 49
 semifusinite 49
 liptinite group 48–49
 alginite 48–49
 bituminite 48–49
 vitrinite/huminite 48
 detrovitrinite 48
 gelovitrinite 48
 telovitrinite 48
 Macrinite 14, 49
 Magnetic anomalies 212
 active coal-seam fire 214*f*
 coal fires or clinker 212
 coal-seam-outcrop fires 213
 magnetic field readings 212*f*, 213*f*
 “surface burn” 213
 surveys over paleoclinkers 213
 Magnetic field readings 213*f*
 Magnetic properties 214
 chemical analyses 215
 fine-grained pseudo-single domain grains
 214–215
 Koenigsberger ratios 215
 measured in paleomagnetism laboratories 214
 natural remanent magnetization (NRM) 214
 paleomagnetic study 215
 isothermal remanent magnetization (IRM) 215
 thermal demagnetization 215
 paramagnetic or superparamagnetic phases 214
 parent lithology 215
 pyrometamorphism 214–215
 pyrrhotite and titanomagnetites assemblage 215
 rock magnetism 214–215
 siltstones 215
 volatiles 215
 Magnetic signatures of rocks and soils **209–218**,
 anomalies 212
 edge effect of clinker half-space 216*f*
 field work 211
 cesium vapor magnetometer 211
 geophysics 211
 GPS positioning 211
 ground magnetic surveys 211
 magnetic surveys over burning coal 211
 nanoteslas 211
 proton precession base station magnetometer 211
 temporal diurnal variation 211
 tertiary lignite coal-seam fires 211
 properties 214
 Magnetic susceptibility 210, 214–215, 288–289
 Magnetometry 98, 211, 288, 289, 289*f*
 Mass discrimination 181, 184
 Mass spectrometry 2, 180, 184
 detector 184
 Mass transfer mineralization 136, 138
 gas-altered substrate (GAS) 138
 gas-liquid-altered substrate (GLAS) 138–139
 gas-liquid precipitation (GLP) 140–141
 gas reaction+liquid-solidification (GRLS) 141–142
 Mass transport mechanisms 311
 Medium-volatile bituminous coal 181–184, 187*f*, 188
 Membrane separation plant 329
 Mercury analyzer 148–149
 Meta-anthracite 55
 Metagenesis 175
 Metallurgical furnace or crematorium 66
 copper slags 66
 Tschudi burn 66
 Metamorphism 9
 Methane system 129–130
 Micrinite 14, 49
 Micro-Dumas carbon–nitrogen method (MDCN) 157
 Microlithotypes 54
 bimaceral microlithotypes 54
 clarite or durite 54
 carbominerites, mineral matter 54
 classification and composition 55*t*
 monomaceral microlithotypes 54
 liptite or vitrite 54
 trimaceral microlithotypes 54
 duroclarite/clarodurite/vitrinertoliptite 54
 Microwave region 237
 active remote sensing 237
 Interferometric Synthetic Aperture Radar (InSAR) 237
 map mining-induced subsidence 237
 sensor-target distance 237
 subtle elevation changes 237

- Midvale waste bank 288*f*, 290
 cryogenic injection 291–292
 map of 291*f*
 temperature surface from temperature data 292*f*
 temperature surveys 290–291–292
 vertical thermocouple (TC) wells 290–291
- Mine atmosphere 40
 rate of heat loss and rate of heat gain versus temperature 41*f*
- Mine fire control 268
 abandoned mined land (AML) program 268–269
 conversion factors 270*t*
 extinguishment 41
 fatalities due to ignition and explosions 269*f*
 fire-control research and fire work 269
 inactive or abandoned mines 268
 isolation 41
 Office of Surface Mining, Reclamation, and Enforcement (OSM) 268–269
 Surface Mine Control and Reclamation Act (SMCRA) 268–269
 underground fatalities 269*f*
- Mine-fire diagnostics (MFD) 282
 carbondale 283
 anomalous snow melt 285*f*, 283
 drillers' logs 283
 location of two large and five small heated areas 285*f*
 methane emission 283–284
 noncontiguous combustion zones 284
 use of MFD, nonideal conditions 283–284
 cold boundary 283
 hot and cold subsurface zones 283
 hydrocarbons, definition 282–283
 Large (Allegheny County) 285
 hydrocarbon concentrations 286
 L-shaped combustion zone 286
 Pennsylvania mine-fire site 286*f*
 risk factors 287
 subsurface fires 286
 Percy 287
 Renton 287
 long-term changes in MFD ratio 287*f*
 US Bureau of Mines MFD system 284*f*, 284*f*
 values of diagnostic ratio (R1) for bituminous coal 283*t*
- Mine fires, initiation of 277
 forced ignition 277
 sources 277–278
 rate of heat gain versus rate of heat loss 278*f*
 spontaneous combustion 278
 adiabatic-type calorimeter 278
 coal rank 278
 crossing point method 279
 exothermic or heat-generating reactions 278
 ignition temperature for coal 279
 self-heating behavior 279
 thermophilic bacteria 278
 wasted-coal fires, elements for 277
- Mineral-and rock-collecting techniques 145
 chemical division of Los Alamos National laboratory 146*f*
 collecting coal-fire minerals 146*f*
 quartzofeldspathic sandstone substrate 145–147
 unglazed ceramic tiles 145–147
 X-ray diffraction and electron probe analysis 145–147
- Minerals characterization, analytical methods 165
 electron micrographs 166
 gas chromatograph 165
 infrared spectroscopy 165
 nuclear magnetic and electron spin resonance spectroscopy 165
 optical spectroscopy 165
 Raman spectroscopy 165
 rotating multisample dropper 165*f*
 thermal gravimetric analysis 165
 X-ray fluorescence spectroscopy 165
- Mineral-forming processes 136
 isochemical mineralization 136
 mass transfer mineralization process 136
- Mineral matter 11–13, 50–52, 54–55, 60, 195, 279
 free 11, 12–13, 17
- Mining hazards
 coal gas 104
 carbon dioxide concentrations 104
 coal-fire detector gases 104
 condensation products 104–105
 environmental P–T indicators 105
 P–T stability diagram 104–105
 thermodynamic loop analysis 104–105
 wood-fire detector gases 104
 origin of coal fires 103
 abandoned workings or workings of coal mine 104
 coal mine-related fires 103
 exothermic oxidation reactions 103
 spontaneous combustion, reaction for 104
 spontaneous fires 104
 steam explosion 104
- Ministry of Coal and Mines (MCM) 107
- Mobile steam turbine/generator system 294
- Modern-foam-injection technology 327–333,
 compressed foam 331
 “roofing out” 331
 experimental fires 329
 CO₂ gas inertization techniques 330–331
 compressed air foam systems (CAFS) 329–330
 membrane separation plant 329, 330*f*
 fire science 331
 coal-mine fire fighting 332
 pyrolyze 331
 foam generation, new method 329
 “T” fitting 329
 high-expansion foam 328
 new developments 331
 encapsulated CO₂, use of 331
 subterranean cavity 331
 waste fly ash/bottom ash 331–332
 quality control 331
 weak or inferior foam 331
 water-based foam 328
- Modern legislators 262
- Moisture and mineral matter free (mmmf) 11
- Moisture content 40–41, 60, 84, 85–86–87, 90, 94–95, 99, 177, 180,
 237, 278, 318
- Monomaceral microlithotypes 54
- Montmorillonite 50
- Mountain top removal 38
- Movement conservatism ideology 257
- N**
- Nanometer 157
- Nanoteslas 211
- National Abandoned Land Inventory System 106–107
- National Aerial Photographic Program CIR photos 225
- National Agricultural Imagery Program (NAIP) 226*f*
- National Center for Atmospheric Research Nomhice (NCAR-Nomhice) team 133
- National Institute for Occupational Safety and Health (NIOSH) 329
- National Land Policy and Management Act 263
- Natural barriers 280
 boundary pillars 280
 medium-volatile bituminous coal 280
 roof coal and carbonaceous shale 280
 water table 280

- n*-Dodecane (*n*-C₁₂) 174–175
 Neogene coals 9
 Newlands Act (1902) 261–262
n-Nonane (*n*-C₉) 174
 NOAA Status and Trends Program methods 179
 Non fuel materials 77
 Nonmethane hydrocarbon intercomparison experiment (Nomhice) study 128
 Nonmethane hydrocarbons (NMHCs) 128
 Norhopane (NH) 191
 Northern Peru 65
 ancient Peruvians 65
 small scale 65
 Noxious gases 84–85, 87, 102–103, 105
n-Tetratetracontane (*n*-C₄₄) 174
- O**
 Office of Surface Mining Reclamation and Enforcement's Inventory (OSMRE,2005) 16
 Off-road haulage trucks 32
 Oil-bearing formations 174–175
 On-board thermal infrared scanner 39–40
 One-dimensional smoldering 310–311, 310*f*
 forward, and opposed propagation 310*f*
 Opencast (surface) mines 88, 93
 extinguishing fires, water and bitumen compound 89*f*, 89
 fire fighting units 89
 Shirebrook Colliery spoil tip in Nottinghamshire, England 95–96
 “above-ambient” temperatures 98
 discrete zone of combustion 98
 electrical imaging method 98
 electro magnetic (EM) method 98
 geophysical surveys 98
 geostatistical analysis of sampling 96
 infrared thermal scanning systems 98
 magnetic surveys 87
 predawn infrared thermal image 97*f*, 98
 “Red Shale Tip” 95–96
 resistivity plot 98*f*
 site investigation drilling programs 96
 steep thermal gradients 98
 typical ground-temperature 97*f*
 underground temperatures 98
 slope failure at El Cerrejon Zona Norte, Colombia 93–94
 coal seams burning 95*f*
 large-scale landslide 94*f*
 slope failure in Singrauli coalfield, India 90, 92*t*,
 accumulation of meteoric water 93
 blue–gray clouds of carbon monoxide 90
 burning coal pillars 92*f*
 burning controlled by principal joints 93*f*
 opencast extraction 91*f*
 pillar failure 92*f*
 rate of fire advance 91
 residual ash 90
 smoldering and burning coal 92*f*
 violent burning 91*f*
 visual inspections of pillar fires 93
 spontaneous combustion and spoil heap in Barnsley, England 94–95
 drains 95
 earthmoving equipment 96*f*
 larger/smaller spoil heap 95
 leveling and reprofiling of spoil heap 97*f*
 old colliery spoils heaps 94–95
 restoration work 95
 Optical spectroscopy 165
 Outcrop fires 16
- Overburden 30–31
 area mining 38
 conduction or radiation 280
 depth of 17, 279, 285
 dragline removing 30
 drilling programs 39
 mountain top removal 38
 nature and thickness of 31
 permeable 271–272
 pressure 7, 9,34
 ratio 37
 removal of 31, 37
 served as insulator 17
 stripping ratio 38
 weight of 30–31, 33–34, 175
 Oxidation reaction 17, 40, 56, 84–85, 90, 103–104, 277, 280–281, 308–309–310, 311–312
 Oxides 12, 50, 52, 68–69, 104, 122, 165, 175–176, 214–215
 trace element data 69
 ash compositions 69
 charcoal ash and peat ash 69–73
 coal ash samples 70*t*
 coal burning, or ashing 69
 coal formation 69
 compound potash (K₂O) 73
 fuel at Tschudi burn 69
 known/unknown ash compositions, comparison 72*t*
 mineral zircon (ZrSiO₄) 73
 refractory compounds 69
 zirconium in plants 73–74
 Oxidizer flow 309–310
 Oxygen-depleted gas 311
- P**
 Paleointensity 216
 Paleomagnetism 214
 Palmer's seminal work 308
 Panel 34–35
 Paramagnetic 214
 Parent coal 198
 Parent PAHs 184, 188
 Parr formula 50–52
 Peat fires 308
 Peat formation 6
 Pennsylvania Department of Environmental Protection (PDEP) 64–65
 Pentacyclic triterpanes 201
 Permeability 9, 38, 95, 312, 318–319, 320–321
 Peru 64
 modern brick from Trujillo 65*f*
 Petrogenic four-ring 195–198
 Petrogenic PAH 184
 Phenanthrene (P0) 197*f*
 Phenol theory 85
 Pitch 18, 31, 33, 36–37, 42, 279
 Pitot tube 149–150
 Pittsburgh seam, fire in (1765-1846) 15
 Plant wax signature 190*f*
 Pleistocene coal fires 64
 Pneumatic injection 21
 Polar organics 179
 Policy cycle, phases in 257
 other than monopoly 258
 coal fires in policy 259
 collapsing monopoly 258
 greenhouse gases 259
 monopoly formation 258
 policy consolidation 258
 policy innovation 258
 policy replacement 258

- policy monopoly 257
 bureaucratic agency 258
 classic textbook iron triangle 258
 electoral consensus 257
 nonpermeable subgovernment 258
 policy making 258
 political commodity 258
 predictability 258
 policy phases 258
 Policy innovation in nineteenth century 259
 J.W. Powell: public lands 259
 policy collapse (1980–2008) 263
 policy of pragmatic agriculture 263
 sagebrush rebellion 263
 steady policy decisions 263
 policy consolidation (1902–1934) 261
 conveyance of public lands into private ownership 263
 “modern legislators” 262
 1902 Newlands Act 261–262
 progressive coalition, 1901 261–262
 Taylor Grazing Act in 1934 262–263
 US election results from (1860–2008) and policy phases 262*f*
 policy setting (1876–1904) 264
 cadastral survey, arid lands 261
 collective water usage 261
 congressional elections 260–261
 contentious election results or assassinations 260
 institutional arrangements 261
 Powell’s policy recommendations 261
 President Harrison’s administration 260–261
 United States Geological Survey (USGS) 261
 Policy setting for coal fires 255–266, 256
 coal-geosciences community 258
 government response to policy problems 257
 lessons for coal fires 264
 phases in policy cycle 257
 nineteenth century 259
 1994 United States congressional elections 257
 Polio vaccine 257
 Pollutants 116
 Polycyclic aromatic hydrocarbons (PAHs) 122, 175, 184
 alkylated 184
 analytes 185*t*
 benzo[*b*]fluoranthene and benzo[*k*]fluoranthene 184
 benzo[*g,h,i*]perylene 184
 coelution 184
 diagenetic 184
 EPA method 8270D 184
 ionization 184
 mass spectrometry 184
 parent 184
 petrogenic 184
 profiles of coal and natural coal tars, Breathitt Formation
 naphthalene (N0) 197*f*
 phenanthrene (P0) 197*f*
 unweathered pyrogenic LPAH 197*f*
 weathered pyrogenic HPAHs 197*f*
 See also Polycyclic aromatic hydrocarbons (PAHs)
 profiles of extractable hydrocarbons 184–188, 187*f*
 anthracite 187*f*, 188
 dibenzothiophenes 187*f*
 high-volatile bituminous coal 187*f*, 188
 lignite 187*f*
 medium-volatile bituminous coal 181–184, 187*f*, 188
 petrogenic two-ring PAHs 187*f*
 semivolatile hydrocarbon signatures 187*f*, 188
 subbituminous coal 187*f*
 pyrogenic 184
 selected ion monitoring mode (GC/MS SIM) 184
 transformations
 alkylated homologs 195–198
 aromatic hydrocarbon signatures 195–198
 Breathitt Formation 197*f*
 coal cracking process 198
 composition of carbonization residues 198
 concentrations 198
 GC/FID fingerprints of high-volatile bituminous coal 196*f*
 parent coal 198
 RET 198
 Ruth Mullins coal fire 195–198
 thermal instability 195–198
 See also Polycyclic aromatic hydrocarbons (PAHs)
 Polymers 311
 Poor heat transfer 321
 Porosity 312
 Porous layer open tubular (PLOT) capillary column 131–132
 Porous material/matrix 308–309
 Powder Diffraction File (PDF) 158
 Powder River Basin (PRB) 7
 Powell’s policy recommendations 261
 Pragmatic agriculture, policy of 263
 Predawn and postdusk thermal imagery 85
 Premium house coal 319
 Primary fuel, wood 2
 Proton precession magnetometer surveys 98, 211, 289
 Proximate composition 11
 Pseudo-single domain 214–215
 P–T stability diagram 104–105
 Pulse-based radar system 290
 Pyrite content 60, 84, 90
 Pyrite theory 85
 Pyrogenic PAHs 184
 Pyrolysate 310
 Pyrolysis 11, 175–176, 309–310, 311–312
 front 311
 Pyrolytic condensation 6–7
 Pyrolyze 175, 331
 Pyrometamorphic rocks 87, 210, 214–215–216

Q
 Quadrupole mass spectrometer detector (MSD) 128
 Quartz 12, 50, 69, 156

R
 Radiation 308–309–310
 Raman spectroscopy 165
 Rate of oxidation 85–86
 Reconofax IV instrument 223
 Red dog 21
 Red shale 84–85, 87, 95–96, 98
 Reflection–aureole mapping 242
 Jharia coalfield, India 243*f*, 242
 reflection aureoles/barrenness aureoles 242
 Regimes of combustion of solid fuels 310*f*
 Remnant magnetization 288–289
 Remote sensing methods 225, 231–253,
 aircraft 232
 coal-fire parameter extraction
 crack-density mapping 242
 fire-area estimation 244
 fire-depth estimation 245
 greenhouse-gas emissions 247
 land-cover mapping 243
 reflection–aureole mapping 242
 subsidence mapping 246
 Google Earth™ 232
 Microsoft Virtual Earth™ 232
 NASA World Wind™ 232

- Remote sensing methods (*Continued*)
 platforms and sensors 239
 coal-mining and coal-fire research 239, 240*t*
 Heat Capacity Mapping Mission (HCMM) 239
 imaging systems 239
 thermal infrared (TIR) 239
 TIROS-1 239
 remote sensing, principles
 electromagnetic energy and spectrum 233
 microwave region 237
 shortwave and thermal infrared regions 235
 visible and near-infrared regions 234
 satellites 232
 sensor 232
 time series analysis and integrated interpretation in GIS 248
*Report on the Lands of the Arid Region of the United States, with a
 Detailed Account of the Lands of Utah, 259*
- Residual deposits 84–85
 Retreat longwall mining 34–35
 Rock magnetism 214–215
 Roof coals 17, 280, 290, 297
 Roofing out 331
 Room-and-pillar mining system 17, 32–34
 Rothiemurchus peat fire 313*f*
 Ruth Mullins coal fire 193, 195–198
 Rutile 50
- S**
- Safety precautions, sample collecting 143
 coal-fire minerals and gas collection, hazards 144*f*, 144*f*
- Sagebrush rebellion 263
- Sample analysis, coal and coal tar 129, 181, 184, 180
 EPA method 9060A 180
 See also US Environmental Protection Agency (USEPA)
 geochemical biomarkers 191
 high-resolution hydrocarbon scan 181
 hydrocarbon patterns 180
 mass spectrometry (GC/MS) 180
 petrogenic PAHs 184
 total organic carbon 180
- Sandstones 5
- Saturated hydrocarbon residues 177, 179, 180–181, 188, 198
 coal fires in Breathitt Formation 200*f*
 coal matrix 201
 coke 201
 devolatilization 198–201
 distillate range hydrocarbons (n -C₉ to n -C₂₃) 201
 geochemical biomarker analytes 189*t*
 high-resolution hydrocarbon fingerprint (GC/FID)
 198–201
 high-volatile bituminous coal, thermal exposure 199*f*
 ion chromatograms 198–201
 plant wax patterns 188–191
- “Sea coal” 30, 64
- Secondary electrons 161
- Sedimentary cycle, types of 6
- Sedimentation theories 6
- Seismic characterization 289
 seismic refraction survey 289
 tomographic imaging 289
- Seismic refraction survey 289
- Self-ignition 87, 321
- Self-sustaining 85, 277–278
- Semifusinite 14, 49
- Semivolatile hydrocarbon residues of coal and coal tar **173–208**
 carbonization 175
 cleanup 179
 coal-fire residues 193
 collection 178
 copper solid-phase cleanup of sulfur 179
 extraction 178
 fossil fuels 175
 lines of evidence 175
 sample analysis 180
 sample preparation 178
 source signatures 174
- Shafts 31
- Shallow mines 87
- Shearing machines 32
- Shortwave and thermal infrared regions 235
 blackbody 235
 digital numbers (DNs) 236–237
 emission spectra 235
 emissivity values 236, 237*t*
 high-temperature 235
 kinetic temperature, T_K 237*t*
 Planck’s emission-spectral curves 235, 236*f*
 Planck’s law 235
 radiant temperature, T 237*t*
 satellite-image metadata 236–237
 spectral emissivity, λ 236
 spectral radiance, $B_\lambda \epsilon$ 236–237
 thermal equilibrium 235
 wavelength regions of the electromagnetic spectrum 238,
 238*t*
- Short-wave infrared spectroscopy (SWIR) 163
 crystal vibration theory 163
 of gas-vent minerals 164*f*
 molecular vibrations in chemical groups 163
 portable field-based 163*f*
 of salammoniac 164*f*
 very near infrared range (VNIR) 163
- Shower 321
- Siderite 50
- Signatures, semivolatile hydrocarbon 174, 187*f*, 188, 193
- Silica gel 179
- Silicates 12, 50, 54, 214–215
- Single domain 214–215
- Single point injection 321
- Slopes 31
- Slurry 318
- Smectite 50
- Smelting and working metals 30
- Smoldering 17, 19–20, 64, 84–85, 88, 282
 charcoal briquettes 308
 coal fires 312
 controlling mechanisms of subsurface fires 312
 effects of smoldering fires, factors 312–313
 heat losses 312
 mass loss 312–313
 oxygen flow 312
 porosity 312
 potential structural collapse 312–313
 subsurface smoldering fires 312
 combustion 318
 combustion phenomena and coal fires **307–315**
 propagation 309–310
 wildfires 313
 carbon emissions 313
 largest peat fire, Indonesia 313
 organic soils 313
 peat 313
 recent case of smoldering fire 313
 Rothiemurchus peat fire 313, 313*f*
 thick fuels 313
- Smoldering and combustion **307–315**,
 artistic rendition of fire 309*f*
 burning piles of dust 308

- char 311
- conduction 309–310
- configurations in one-dimensional 310*f*
- controlling mechanisms of subsurface fires 312
- convection 309–310
- convective heat transport 311
- CO,toxic factor 309
- diffusion 309–310
- effects 312–313
- fire safety engineering 308
- flaming combustion 308–309
- heterogeneous chemical reactions 308
- oxidation reaction 308–309
- oxygen-depleted gas 311
- Palmer's seminal work 308
- peat fires 308
- porosity 312
- radiation 309–310
- regimes of combustion of solid fuels 310*f*
- thermal time 309
- Smoldering front, structure 311
 - char or coke 311
 - chemical kinetics 311
 - decomposition process 311
 - discernable regions 311
 - burning region 311
 - char and ash region 311
 - evaporation 311
 - polymers 311
 - preheating of undisturbed fuel 311
 - pyrolysis front 311
 - endothermic reaction 311
 - exothermic reaction 311
 - forward propagation 311
 - mineral 311
 - one-dimensional reaction
 - front in forward smoldering 312*f*
 - peak temperature 311
 - polyaromatic hydrocarbons 311
 - pyrolysis 311
 - self-sustained smoldering 311
 - smoldering kinetics 311
 - water evaporation 311
- Smolder zone 311
- Sodium silicate 179
- Soil
 - calcium in 67
 - explanation (La Rosa) 68
 - induced coupled plasma (ICP) analysis 67
 - soil data 67
 - soil geochemical traverse 67*t*
 - sulfur in 68
 - acid rain 68
 - metallurgy 68
 - pyrite (FeS₂) in coal 68
 - sulfuric acid (H₂SO₄) 68
 - synthetic gypsum (CaSO₄·2H₂O) 68
- Solid by-products of combustion 119
 - coal fire gas 119
 - concentrated elements 119
 - mineral species (33) 120–121
 - study of 120–121
- Solid fuels, combustion of 310*f*,
 - oxidation reactions 310*f*
- Source signatures 174
 - coalification 174
 - gas chromatograph (GC) 174
 - industrial carbonization 175
 - macromolecules 174
 - n*-dodecane (*n*-C₁₂) 174–175
 - n*-nonane (*n*-C₉) 174
 - nonpolar silicone capillary column 174
 - n*-tetratetracontane (*n*-C₄₄) 174
 - oil-bearing formations 174–175
 - PAHs 175
 - semivolatile hydrocarbons 174
 - thermal decomposition 175
- Spall 279
- Sphalerite 50
- Spontaneous combustion 36, 84
 - of coal 56, 84*f*
 - coal petrology 47–62, 56
 - coal oxidation 60
 - coal rank 55
 - coal type influences 60
 - fractured and faulted thick coal seams 60
 - inorganic matter in coal 50
 - lithotypes 54
 - maceral composition of coal 48
 - microlithotypes 54
 - properties 60
 - coal seam and colliery spoil heap fires 86
 - control and prevention 86
 - colliery waste 88
 - opencast sites 88
 - underground coal fires 87
 - examples 89
 - opencast (surface) mines 93
 - underground mines 89
 - exothermic reaction 86
 - heat of reaction 85
 - ignition points 85
 - life and human health 85
 - optimum air flow velocity 86
 - origin 85
 - rate of oxidation 86
 - run-of-mine coal 86
 - theories for causes of 85
 - bacteria theory 85
 - coal-oxygen complex theory 85
 - phenol theory 85
 - pyrite theory 85
- Spray 321
- Stainless steel canisters 128, 147
- Steam engine 2
- Steep-pitch mining 36
- Stereoisomers 191
- Stinkdamp 104
- Stoichiometric 158–159
- Stressed vegetation at “cemetery front” 226*f*
- Strip (open pit) or deep mined coal 143
- Subbituminous coal 187*f*, 190*f*, 223–224
- Sublimation 136–137–138, 141–142
- Suboxic or anoxic nature 175, 179
- Subsidence mapping 246
 - coal pillars 246–247
 - digital remote sensing methods 247
 - InSAR 247
- Subsurface cavities 84–85, 88
- Subterranean cavity 296, 328, 330–331
- Sulfides 12, 19, 50, 54, 85–86, 214
- Sulfur-containing PAHs (SPAHS) 185*t*
- Superparamagnetic 214–215
- Suppression experiments
 - global evaporation 321
 - hand operated atomizer 321
 - mechanisms 318, 321
 - methods, comparison of 324*f*

- Suppression experiments (*Continued*)
 poor heat transfer 321
 shower 321
 single point injection 321
 spray 321
 water application method 324*f*
- Surface coal mining
 area mining 38
 auger mining 38
 contour mining 37
 mountain top removal 38
 surface mining 37
- Surface mining operations
 borehole drilling machines 32
 bucket-wheel excavators 32
 bulldozers 31
 draglines, giant mining machines 32
 front-end loaders 32
 hydraulic backhoes 32
 off-road haulage trucks 32
 scrapers 32
- Surface sealing 22, 107, 109, 271, 273
- Surface wild fires 85
- Surrogate 178–179
- Syngenetic 5, 12, 50, 210
- Synthetic aperture radar (SAR) 105
- T**
- Taylor Grazing Act in 1934 262–263
- Technical Innovation and Professional Services 222
- Tedlar[®] gas bag 147
- Teflon-lined cap 178–179
- Telovitrinite 48
- Temperature monitoring 290
 Centralia mine fire 290
 Midvale waste bank 290
- Tennessee Valley Authority 257
- Terrain conductivity 288–289
- Terrestrial plants 4
- Terrestrial volcanic vents 156–157
- Texas Instruments RS14A scanner 223–224
- Thermal conductivity detector (TCD) 128
- Thermal demagnetization 214–215
- Thermal gravimetric analysis 165
- Thermal imagery 85, 98
- Thermal inertia 318–319
- Thermal infrared imaging (TIR) 39, 220
 forward looking infrared (FLIR) imaging 222
 Star SAFIRE III camera 222
 instantaneous field of view (IFOV) 221
 predawn surveys 221–222
 radiant flux 221
 scanner and its operation 221*f*
 surface factors 220
 instrumentation 221
 topography 220
- Thermal insulation 309–310
- Thermal properties of coal and water 322
- Thermal time 309
- Thermocouples (TC) 144, 290, 319
- Thermodynamic loop analysis 104–105
- Thermoremanent magnetization (TRM) 210, 215
- Time–temperature index (TTI method) 10
- Tomographic imaging 289
- Total extractable hydrocarbons (TEHs) 177
- Total extractable material (TEM) 177
 gravimetric measurements 180–181
 high-resolution hydrocarbon scan 180–181
- Total organic carbon (TOC) 177, 180
- Toxic elements 116, 122
- Toxic gases 94, 107, 116, 118, 121–122, 329–330
- Trench barrier 273
- Tricyclic triterpanes 201–205
- Trimacerol microlithotypes 54
- Triterpane biomarker patterns 192*f*
- Triterpane fingerprints
 coal fires in the Breathitt 203*f*
 thermal exposure 204*f*
- Tschudi burn
 bone fragment 76
 calcined bone 76
 calcined cranial vault fragment (B0502) 76*f*
 calcium and phosphorus content in soil 76
 cremation at 76
 destructive process 76
 “human origin” 77
 modern cremation 76
 protein radioimmuno assay (pRIA) 76, 77*t*
 temperature of 66
 anthracite 66–67
 controlled burning temperatures 66
Tillandsia latifolia 66
 X-ray diffraction patterns 77, 78*f*
- U**
- Ultimate composition 12
- Ultra high purity (UHP) hydrogen 130
- Uncontrolled coal fires 117–118
- Underground coal fires 64, 87
 burning coal seams 88–89
 China coal mine fires 89
 coal-producing regions 64
 controlled directional blasting 88*f*
 fuel ash 88
 “Paso Diablo” in Venezuela 64
 reignition 88
 unreactive gases 89
- Underground coal mining 33
 methods of coal mining 34
 special case of anthracite mining 36
 ventilation 36
- Underground mines 89
 spontaneous combustion in Witbank Coalfield, South Africa 89
 bord and pillar method 89
 burning coal seam 90*f*
 construction of cutoff trenches 90
 pyrite content 90
 surface tension cracks 89
- Unit cell 157–158
- United States Bureau of mines **267–306**,
 characteristics of fires 277
 discontinuous fire propagation 281
 geologic and mining factors 279
 initiation of coal-mine fires 277
 natural barriers 280
 controlling abandoned mine fires
 burnout control 293
 cryogenic slurry injection 297
 foam injection 297
 water injection 295
 fire-control projects 271
 anthracite coalfields 273
 Eastern bituminous region 271
 Western US and Alaska 272
 locating abandoned mine fires 282
 geophysical methods 288
 mine-fire diagnostics 282
 temperature monitoring 290
 mine-fire control 268
- United States congressional elections (1994) 257

- United States Geological Survey (USGS) 261, 262–263
 Unresolved complex mixture (UCM) 181–184
 Uranium–thorium/helium ratios 85
 US Environmental Protection Agency (USEPA) 178
 US presidential and congressional election results (1876–1904) 256
- V**
- Vacuum tube 157
 Ventilation 36
 Visual effects 118
 Barren turf 118
 coal fire of uncertain origin 120^f
 deforestation and bituminous coal 119^f
 emission of toxic coal-fire gas 119^f
 forest and range fires 118
 Internet article by Stein 118
 mining equipment ignited by coal fire 121^f
 piles of burning coal waste 118
 route 61 through Centralia 120^f
 Vitrinertoliptite 54
 Vitrinite 48
 reflectance 8–10, 55
 Vitrite 54
 Volatile content 11, 14, 55, 60, 85–86, 94
 Volatile organic compound (VOC) system 122, 128, 130
 chromatogram, electron capture detector 132^f
 columns in various GC ovens 131^f
 Volcanic gas vents 136
 Volcanic rocks 158–159
 Volcanic vent mineralization 156–157
 Voltage 87, 118, 120–121–122, 136, 137–138, 156–157, 285
 Voltaite 87, 156
- W**
- Waste bank fires 16
 Wasted-coal fires
 control extinguishing subsurface fires
 excavating hot coal 20^f
 hot material and toxic fumes, hazards 20^f
 pneumatic injection through boreholes 21^f
 use of grout with concrete 22^f
 formation of coal
 coal composition 10
 coalification 6
 coal swamps 5
 cyclothems 5
 geologic distribution 3
 ignition and propagation 16
 factors favoring propagation 17
 fire triangle 16^f
 Glenburn anthracite waste bank 18^f
 hazards 19
 mine showing emission of smoke and fumes 18^f
 sources of ignition 17
 incidence 16
 origin of wasted-coal fires
 control 19
 ignition and propagation 16
 incidence 16
 Water application method 324^f, 321
 Water-based foam 328
 Water curtain 275
 Water-gas 88, 90
 Water injection 89, 271–272, 287, 296, 295
 calamity hollow 296
 Renton mine fire 296
 Wavelength dispersive spectrometers 161–162, 165
 Western United States and Alaska 272
 surface seal methods
 Colorado River basin 273
 Missouri River drainage region 273
 Wild fires 85
 Wood 30
 Wood-fire detector gases 104
 World coal consumption (2005) 2
 World Coal Institute (WCI) 64
 World Resources Institute (WRI) 106
 World War II 257
- X**
- X-ray fluorescence spectrometry 215
 X-ray powder diffraction (XRD) 157
 angstroms and nanometers 157
 atomic planes 157
 Bragg's law 158
 crystal motifs (unit cells) 157
 crystal structure 157
 diffraction pattern 157–158
 electromagnetic radiation 157
 electromagnetic spectrum 157
 electronic detector 157
 “monochromatic” source 157
 Powder Diffraction File (PDF) 158
 “reflected beam” 158
 sulfur-bearing mineral assemblages 160^t
 vacuum tube 157
 voltage 157
 X-ray diffractogram of minerals 159^f
 X-ray diffractometer arrangement 158^f
 X-ray goniometer 157
 X-ray spectrum 162
- Z**
- Zircon 12, 50, 73, 85

This page intentionally left blank